UNIVERSITY OF CALIFORNIA,
IRVINE

Isolated Quantum Systems

Dynamics and Phase Structure Far From Equilibrium

DISSERTATION

submitted in partial fulfillment of the requirements
for the degree of

DOCTOR OF PHILOSOPHY
in Physics

by

Aaron Joseph Friedman

Dissertation Committee:
Professor Alexander Chernyshev, Chair
Professor Siddharth A. Parameswaran
Professor Steven R. White

December 2019

In loving memory of

Barbara Rose

and

Arlene Friedman

Contents

List of Figures

List of Tables

ACKNOWLEDGMENTS

There are many people who have inspired, encouraged, influenced, and supported me along the way to this thesis. Before I thank the various physicists who have been kind enough to offer their encouragement, insight, and support in ways that helped me with specific aspects of my research, my overall understanding of physics, and my experience as a doctoral student, I would like to thank all of my friends and family, and particularly, my parents, Ava and Jim. I would not be where I am now without their support and encouragement.

As they will presumably read this thesis, I should start by thanking the members of my committee, Sasha Chernyshev, Sid Parameswaran, and Steve White, for all that I have learned from them through coursework and conversations, and for being kind and supportive people in general. I am especially grateful to my research advisor, Sid Parameswaran, for introducing me to the area of physics that became the subject of this thesis, for being extremely supportive in all matters, and for providing me incredible opportunities to travel the world and meet and work with new people over the years. While this has not been the most conventional trajectory, I feel I have benefitted from this experience substantially, and am better off for it. I am also indebted to Sasha Chernyshev for taking on the various responsibilities of formally advising me following Sid's relocation to Oxford, and for more interesting conversations than I can count. I also want to thank Tim Tait and James Bullock for their interest in my welfare throughout.

I wish to thank my undergraduate advisors, Dan Arovas and John McGreevy, for teaching me most of the physics I use and care about today, and for inspiring my interest in condensed matter theory and encouraging my pursuit thereof. I would also like to thank John Chalker, Romain Vasseur, and Sarang Gopalakrishnan for acting as advisors in various capacities (especially in my time away from UC Irvine), for taking an interest in my career, and for generally being really great physicists to work with and giving me the opportunity to contribute to their projects. I am very happy with our work, and I have learned a great deal.

I would like to thank all of my coauthors: Sid Parameswaran, Romain Vasseur, Drew Potter, Austen Lamacraft, Sarang Gopalakrishnan, John Chalker, Andrea De Luca, and Amos Chan. I am very thankful for all of our discussions, all that I have learned, and the work we have done.

I am extremely grateful to Sthitadhi Roy and Brayden Ware for numerous and lengthy discussions of physics, support, and advice during my time in Oxford and Amherst. I am also indebted to Andrea De Luca, Adam Nahum, Yang-Zhi Chou, Yuan Wan, Michele Fillipone, Wen-Wei Ho, Tibor Rakovszky, Curt von Keyserlingk, Adam Smith, Ehud Altman, Joel Moore, Thierry Giamarchi, David Huse, Tom Iadecola, Dima Abanin, Sagar Vijay, Nicolas Macé, Marko Žnidarič, Steven Thompson, Pablo Sala, Stefan Groha, Fabien Alet, Frank Pollmann, Francesco Serafin, Kush Saha, Miles Stoudenmire, Rahul Nandkishore, Vedika Khemani, Maksym Serbyn, Jonathan Ruhman, Philipp Dumitrescu, Anya Goremykina, Seth Whitsitt, Marco Schiró, Ruben Verresen, and Will Berdanier for various discussions of physics over the years that have been helpful to me. Additionally, I thank Dima Kovrizhin, Fabian Essler, Eric Vernier, Paul Fendley, Dung Nguyen, and Steve Simon for numerous interesting chats about physics and all manner of subjects, and Sam Garratt, Raphael Kozlovsky, Glenn Wagner, Aleksandra Ziolkowska, Richard Fern, Saeed Mahdisoltani, Yuri van Nieuwkerk, and Tunrayo Adeleke-Larodo for lively conversations and generally making me feel welcome in my time at Oxford. I am similarly grateful to Carlos Duque, Javier Lopez, and Utkarsh Agarwal for helping to make my time in Amherst interesting and productive. I want to thank Drew Potter for past collaborations, help with my recent postdoctoral applications, and for hiring me as a postdoc when my anticipated source of funding vanished. I look forward to working together again.

I am humbled to have had several opportunities to visit the Kavli Institute for Theoretical Physics (KITP), and wish to thank the various program organizers and staff who made this happen. I am thankful to have attended numerous summer schools, conferences, and workshops, and would like to thank all the organizers of these events for their hard work and for allowing me to benefit therefrom. I want to thank the organizers of the Boulder school, "*Frustrated and Disordered Systems*," where I learned about the classical analogies to the contents of this thesis, and from Leticia Cugliandolo in particular. I am also grateful to have met and had wonderful discussions with Davide Facoetti, Jonathan Chun-Cheong Lam, Carlos Duque, and Chris Baldwin while there, among many kind and talented physicists. I am likewise grateful to the organizers of the 2019 Les Houches summer school, "Dynamics and Disorder in Quantum Many Body Systems Far from Equilibrium," Dima Abanin, Marco Schiró, and Laurent Sanchez-Palencia, and to all of the lecturers and other attendees—all of whom I have learned from and look forward to meeting at future conferences—and to have lost many table football games with Will Berdanier, won several more with Fabien Alet, and to have had Marco Schiró exclaim, "that is impossible," literally every time I scored a goal.

I also wish to acknolwedge the various lectures, talks, and notes of Leticia Cugliandolo, David Huse, Dan Arovas, and John McGreevy, which have been exceptionally helpful both in my academic development and in writing this thesis. These physicists' interests and point of view have greatly shaped my own.

I would be remiss not to give a shout out to my friends and fellow graduate students at UC Irvine. I am particularly grateful to Jeff Wingo, Pavel Maksimov, Ben Lillard, and my many friends from student government for making my time at Irvine so fun. I am separately grateful to Ben Lillard for letting me use his thesis template. Finally, I would like to thank Lori Greene, Karl Hujsak, Anna Kwa, and Justin Smith for helping me successfully apply for the NSF Graduate Research Fellowship.

On the subject of funding, the work presented in this thesis has been directly supported by the Chancellor's Fellowship at UC Irvine, NSF Grant DGE-1321846 (Graduate Research Fellowship Program), NSF Grant DMR-1455366 (via Sid Parameswaran), NSF Grant PHY-1748958 (via the KITP), the UC Office of the President's California Institute for Quantum Emulation, and a Departmental Dissertation Fellowship (UC Irvine Physics). Other aspects of the work that appears in this thesis has been supported indirectly through the funding sources of my various coauthors; these sources are acknowledged in the corresponding publications. Additionally, many parts of this thesis also appear—often in modified form—in publications by this author; in such cases, the corresponding publication will be references, and the publishing entity of the corresponding paper retains any relevant copyright on the materials that appear in their journal, including, e.g. many figures. Other figures have been borrowed from open access journals, such as *Physical Review X*, in which case this will be indicated in the figure's caption; in these cases, those images are the property of whatever entity is named on the usage guidelines of the American Physical Society for *Physical Review X*, defaulting to the corresponding authors. Finally, Fig. 1.2(a) is reused with permission from the authors and the American Physical Society, which holds the relevant copyright.

CURRICULUM VITAE

Aaron J. Friedman

EDUCATION

Doctor of Philosophy in Physics and Astronomy — **2019**
University of California Irvine — *Irvine, CA*

Bachelor of Science in Physics and Applied Mathematics — **2013**
University of California San Diego — *La Jolla, CA*

RESEARCH EXPERIENCE

Visiting Scholar — **2018–2019**
University of Massachusetts, Amherst — *Amherst, MA*

Recognised Student — **2017–2018**
Oxford University — *Oxford, U.K.*

Graduate Student — **2014–2017**
University of California, Irvine — *Irvine, CA*

Laboratory Assistant — **2012–2014**
University of California, San Diego — *La Jolla, CA*

TEACHING EXPERIENCE

Teaching Assistant — **2014–2016**
University of California, Irvine — *Irvine, CA*

Instructor – COSMOS — **July 2015**
University of California, Irvine — *Irvine, CA*

AWARDS AND FELLOWSHIPS

Departmental Dissertation Fellowship — **Dec. 2019**
Department of Physics and Astronomy, University of California, Irvine — *Irvine, CA*

Graduate Research Fellow — **2016–2019**
National Science Foundation, at the University of California, Irvine — *Irvne, CA*

Chancellor's Fellow — **2014–2016**
University of California, Irvine — *Irvne, CA*

Malcom R. Stacey Memorial Scholarship — **2010–2013**
University of California, San Diego — *La Jolla, CA*

ABSTRACT OF THE DISSERTATION

ISOLATED QUANTUM SYSTEMS

Dynamics and Phase Structure
Far From Equilibrium

AARON JOSEPH FRIEDMAN

Doctor of Philosophy in Physics

University of California, Irvine, 2019

Prof. Alexander Chernyshev, Chair

Statistical mechanics characterizes systems in or near equilibrium using a handful of "state" variables, e.g. temperature, rather than 10^{23} degrees of freedom. Statistical physics describes the expansion of the early universe, aspects of black holes, and most fruitfully, phases of matter and their properties. Quantum considerations have improved this understanding over time and revealed new phenomena, especially in complicated "strongly correlated" systems. *Topological* phases of matter, e.g., are of both fundamental and practical interest: these phases cannot be distinguished locally, unlike ice and water, which also allows them to store and process quantum information in a "fault-tolerant" manner, recently proposed for application to quantum computation. However, above zero temperature, thermal effects can overwrite this information.

Recent experiments on *isolated* systems have raised fundamental questions and revealed new routes to quantum computing. We now know that entanglement, generated dynamically as a quantum state evolves, "hides" local information about the past, producing familiar equilibrium states, described by a temperature. However, many systems do not thermalize: strong disorder can lead to MBL, which supports numerous phenomena *forbidden* in equilibrium and can protect quantum information at infinite temperature. In particular, both MBL and thermal systems are robust phases of matter, with a novel, athermal phase transition between them.

This thesis begins with an overview of MBL and thermalization, followed by an overview of exactly soluble quantum systems. We then turn to an important result in the field by this author: we introduce the first nontrivial example of an integrable Floquet model and comment on its solution and salient features. We then discuss how integrable models can provide insight into quantum thermalization, e.g. in terms of entanglement growth and demonstrating that conserved charges diffuse. We then investigate thermalization away from the integrable limit, also known as "quantum chaos." We review the standard techniques in this field and, briefly, several important results, before reproducing work by this author establishing definitively the long-conjectured result that the onset of thermalization in the presence of a conserved charge is governed by diffusion of said charge. We then investigate the interplay of conventional and topological order with nonequilibrium phase structure, with applications to quantum computation in mind. We review localization-protected quantum order in several models. We then investigate two models with non-Abelian symmetry, and show that MBL in such models can only realize if the symmetry breaks spontaneously to an Abelian subgroup. Finally, we conclude by examining open quantum systems, where we find several counterintuitive results that show that baths can, in some cases, enhance localization in certain systems, which may have use in realizing quantum computation.

Chapter 1

Introduction

1.1 Equilibrium and Thermodynamics

Most of our understanding of physical systems relies on the concept of equilibrium. From expansion of the early universe to classifying phases of matter, most techniques and theories in some manner invoke the notion that a system is in equilibrium with its "environment," a mysterious entity that may represent the immediate surroundings of a particular experiment or the entire rest of the universe. Even theories of dynamics and many out-of-equilibrium systems rely on some notion of proximity to equilibrium, or the existence of "local equilibrium," e.g. a temperature $T(x,t)$ that varies in space and time, rather than being globally uniform; however, local or otherwise, thermodynamic quantities like temperature are only well-defined in equilibrium.

The subject of thermodynamics developed the concept of equilibrium to explain certain phenomena that now fall under the umbrellas of physics, chemistry, and various aspects of engineering. Thermodynamics describes various "thermal cycles," e.g. engines and refrigerators (which are also "engines"), and requires the existence of an external thermal reservoir with which the system may exchange heat or volume, e.g., throughout the cycle. Thermodynamics established several types of equilibria that can exist between two systems: if, on average, the two systems do not exchange *energy*, they are said to be in *thermal equilibrium*; if, on average, the two systems do not exchange *particles*, they are said to be in *chemical equilibrium*; if, on average, the systems do not exchange *volume*—i.e., changes in their interface maintain the average volume of each—the systems are in *mechanical equilibrium*. Additionally, thermodynamics establishes a handful of laws, which bear the subject's namesake, for example that if two systems, $\mathcal{A}$ and $\mathcal{B}$, are each in thermal equilibrium with a third system, $\mathcal{C}$, then so too must $\mathcal{A}$ and $\mathcal{B}$ be in thermal equilibrium with one another.

A key feature of thermodynamics is the associated reduction of variables: a classical system with a "typical" number of particles—i.e. a mole, or 10^{23} particles—is well described not by the positions and momenta of this absurd number of particles, but by the total number of particles, N, the pressure, P, volume, V, and temperature, T. This is captured by the ideal gas law, $PV = Nk_BT$, where k_BT has units of energy, and k_B is the deservedly named *Boltzmann constant*. Such laws were first derived using thermodynamic principles, rather than microscopic scrutiny, and are quite valid in describing simple physical scenarios, e.g. gases inside containers. Thermodynamics also introduced a number of useful quantities that do not have such an obvious microscopic utility, e.g. entropy (which generally relates to the number of available states), and by extension, free energy.

In addition to their admission of a description in terms of an ensemble of similar systems parametrized by a handful of state variables, systems in thermal equilibrium have several other salient features. Chief among these is the existence of a *steady state*: at late times, after which

the system has thermalized, it should reach a time-independent state. Additionally, this state should not be dependent on the system's history, e.g. details of how and why the system was not originally in equilibrium, or its configuration in the distant past.

The subset of dynamical systems that can achieve thermal equilibrium is further restricted to systems that are Poincaré recurrent [1]. Poincaré recurrence applies to certain dynamical systems for which the volume of phase space is conserved, and essentially notes that a given configuration realized at some time, t, will recur if one waits long enough; hence, recurrent systems are arbitrarily close to periodic in time, at sufficiently long time scales. However, thermalization requires the additional property of *ergodicity*, which derives from the ability of the system to explore the entirety of a constant-energy hypersurface in configuration space. Ergodic systems are a subset of recurrent systems, and the main implication of ergodicity is that averages of measurable quantities over time should agree with averages taken over ensembles of similar systems [2, 3].

The framework of classical statistical mechanics justifies thermodynamics, deriving the familiar properties of thermodynamics—and particularly, statistical ensembles—from microscopic considerations. In general, many aspects of the statistical treatment of open classical systems—i.e. those in equilibrium with an external thermal reservoir—can be shown to realize when one treats the system and an explicit bath in isolation: the system and bath indeed thermalize for suitable models of the latter [2]. In fact, there are only a handful of classical systems that do not thermalize: glassy systems have slow dynamics and do not thermalize on experimentally relevant time scales, but they are thermal in the infinite-time limit; "active matter" systems are associated with driving forces that maintain the system in a nonequilibrium state, such that tuning the driving terms to zero results in equilibration; finally, the class of classical systems that do not thermalize in *any* limit is that of *integrable* models, for which the equations of motion can be solved exactly. Because of this, information about the initial configuration is always accessible at late times. The quantum analogy of integrability will be discussed in Ch. 2, and is more nuanced. Although neither classical nor quantum integrable models are thermal in the usual sense, they both relax to a steady state described by a modified statistical ensemble, and have other features in common with systems that do thermalize.

A classical system in isolation evolves according to complicated, coupled nonlinear equations of motion, which derive from the Hamiltonian, $H(\{\vec{q}_j\}, \{\vec{p}_j\}, t)$. For an isolated classical system, one expects H to be time-independent, corresponding to global conservation of energy, $E = H$. The positions and momenta of the constituent particles—given respectively by $\{\vec{q}_j\}$ and $\{\vec{p}_j\}$—depend on time in a manner determined by the form of H. Strictly speaking, an isolated classical system evolves from its initial configuration at $t = 0$ to its configuration at time t in a completely deterministic manner [2, 3]. However, the resulting set of coupled nonlinear partial differential equations of the dN (where d is the dimension of space and N the number of particles) coordinates and momenta are generally not tractable for $N > 2$.

Hence, it is useful to describe these systems probabilistically, motivated by the success of thermodynamics and justified by the concept of chaos, which will be discussed shortly. The system is therefore described by a time-dependent probability density, ϱ, which is a function of the dN-dimensional phase space coordinates, i.e. positions $\vec{Q} = (\vec{q}_1, \vec{q}_1, \ldots, \vec{q}_{N-1}, \vec{q}_N)$ and momenta $\vec{P} = (\vec{p}_1, \vec{p}_1, \ldots, \vec{p}_{N-1}, \vec{p}_N)$. The probability that the system's phase space coordinates, $\vec{Q}$ and $\vec{P}$, at time t are within a differential phase space volume element $d\Gamma = d\vec{Q}\, d\vec{P}$ of the true trajectory given by the initial conditions is given by

$$\varrho\left(\vec{Q}, \vec{P}; t\right) d\Gamma \ , \tag{1.1.1}$$

where $d\Gamma$ is a dN-dimensional phase space measure, and Γ represents a manifold of possible phase

space trajectories at a given energy.

Because ϱ is positive semidefinite and integrates to unity, it is a probability density [2, 3]. A key feature is that ϱ behaves like the density of a fluid: any change at a given point in phase space at some time must be accompanied by a corresponding and conserving change elsewhere, and this must happen in a continuous manner. Hence, ϱ has an associated *continuity equation*, and conservation law related to the incompressibility of phase space [2, 3].

By Liouville's theorem, one has that this phase-space probability distribution function ϱ must be constant in time along the allowed, constant-energy trajectories of the system, which are solutions to Hamilton's equations. This means that a *convective* time derivative of ϱ, evaluated along the trajectories, must be zero. We then demand that at late times, the system reach a steady state; for time-independent Hamiltonians, this corresponds to the demand that $\partial_t \, \varrho = 0$. The remainder of the continuity equation is automatically satisfied if ϱ depends on the phase space coordinates only through the Hamiltonian, and thus one has some phase space probability density $\varrho(H)$.

It is therefore natural to suppose that, at late times, the system and its dynamics have no preference for any particular region of the hypersurface of phase space corresponding to fixed energy, E. The corresponding form of ϱ is the simplest possible solution to the Liouville equation that describes it, which is $\varrho = \varrho_0(E)\, \delta(H - E)$, where H is the Hamiltonian. The overall prefactor must satisfy a normalization condition. This choice corresponds to the microcanonical ensemble (μCE), which is due to the observation by Gibbs [2] that the surface of all configurations with energy E, a constant of motion, can be interpreted as an *ensemble* of similar systems. This is the simplest thermodynamic ensemble, and is a valid ensemble for computing the averages of various functions of phase space coordinates in the thermodynamic limit [2, 3].

For an ergodic system to reach a steady state at late times requires the concept of "mixing" [3]. Systems that satisfy this property are inherently ergodic—just as ergodic systems are inherently recurrent—but the converse need not hold. Essentially, mixing amounts to the observation that a dynamical system more-or-less evenly distributes itself in phase space. For a simple example, a system with two types of particles, a and b, with fractions ν_a and ν_b (with $\nu_a + \nu_b = 1$) will, at late times, have the property that any choice of subregion of the system delineated in real space will, on average, feature the same ratios of the two particles as does the system as a whole.

The mechanism for reaching the history-independent steady state associated with ergodicity and mixing in classical dynamical systems is *chaos*. Additionally, this requires some uncertainty in the initial (or distant past) configuration of the system. A feature of nonlinear coupled differential equations—such as the equations of motion of many-body classical systems—is exponential sensitivity to initial conditions. Any small change in the initial configuration of a system with chaotic dynamics typically results in wildly different configurations at later times.

As an example, consider a system of classical spins living on the sites of a one-dimensional lattice, with classical coordinates $S(x,t)$, which have some associated classical dynamics. We consider an initial configuration of the system given by $S(x,0)$, along with another configuration that differs from $S(x,0)$ only at $x = 0$, by an infinitesimal amount, $dS(0,0)$. Evolving these two states under identical nonlinear classical dynamics, this infinitesimal uncertainty will spread through the system, and we define $dS(x,t)$ as the difference between the two states at each site, x, at times $t > 0$. If the system is chaotic, one expects $dS(x,t)$ to grow in time, although it may have a random sign. Therefore, we quantify the extent of this discrepancy via the out-of-time-ordered correlation function (OTOC),

$$C\,(x,t) \equiv \left\langle \left(\frac{dS(x,t)}{dS(0,0)} \right)^2 \right\rangle \sim e^{t\,\lambda(v)} \ , \tag{1.1.2}$$

where the OTOC is evaluated along rays $x = vt$, and $\lambda(v)$ is the velocity-dependent "Lyapunov exponent," and the average is taken over initial configurations at a given energy. The Lyapunov exponent quantifies the rate of separation of infinitesimally proximal classical trajectories.

For chaotic systems, one has $\lambda(v) > 0$ for $v < v_{LR} = v_B$, where the threshold velocity is the Lieb-Robinson velocity or "butterfly velocity," which defines a light cone for the spread of information about discrepancies in initial conditions: along the light cone, one has $\lambda(v_B) = 0$. Inside the light cone, differences in initial configurations grow exponentially in time, which is perhaps the most notable feature of chaotic systems. Along the light cone, information about the discrepancies spreads through the system, with the same magnitude discrepancy. Outside the light cone, differences decay in time, with $\lambda < 0$.

For classical integrable systems, one has $\lambda = 0$. Considering the interpretation of the Lyapunov exponent in terms of nearby trajectories, we note that integrable models have an extensive set of conserved quantities, which stem from the fact that the bare degrees of freedom can be "rotated" amongst one another to produce as many decoupled equations of motion as there are microscopic degrees of freedom (i.e., "N"). Correspondingly, any initial difference between two states will simply modify the various independent trajectories affected by said change, and there is no "growth" in this discrepancy. Any initial discrepancy between two systems can be recovered at arbitrarily late times. Thus, it *is* possible to recover statistical ensembles of classical integrable models [2]; however, integrable models remember details of their past, and fail to be ergodic due to the independent nature of their phase space trajectories.

Certain models of quantum systems with well-defined classical limits (e.g. "large-N" models and, relatedly, the Sachdev-Ye-Kitaev model [4–8]) are chaotic in the classical sense described above, as can be seen from scrutiny of their classical limits [7–9]. However, generic and very quantum models, e.g. interacting two-state degrees of freedom, cannot be described as above: there is no sense in which one can prepare *small* local deviations from a given configuration, and correspondingly, there is no $\lambda > 0$ regime. Therefore, other means are required to diagnose quantum chaos, which will be the subject of Ch. 5.

For nonintegrable many-body classical systems, by providing for some slight uncertainty in the initial configuration of a chaotic system, the evolution will magnify this uncertainty exponentially in time. Hence, a system with a tiny but finite amount of initial uncertainty will develop macroscopic uncertainty due to chaos, saturating over time to some steady state for which the uncertainty realizes a statistical ensemble of equivalent systems, e.g. the configurations comprising the constant energy surface of the μCE. Additionally, information about the precise initial configuration is "scrambled" under the chaotic dynamics: this growth in uncertainty is not generally invertible; therefore, given some late time set of possible configurations, it is not generally possible to undo dynamical growth of uncertainty to recover the initial state (within the light cone). However, some initial uncertainty is essential for *isolated* classical systems to thermalize. Statistical mechanics becomes valid at late times, after which the system has reached such an ensemble under its chaotic dynamics; due to ergodicity, averages over the ensemble will be equivalent to averages over time, which are highly predictive owing to the steady-state property.

So far, this discussion has described classical systems in isolation. However, statistical mechanics typically uses ensembles to describe classical systems in contact with a thermal reservoir, including the aforementioned μCE. In classical systems, the primary purpose of the thermal reservoir (which will also be referred to as the "bath," "environment," or "outside") is to exchange extensive conserved quantities with the system of interest to facilitate mixing, which allows the latter to reach a history-independent steady state well-described by ensembles. The standard set of conserved quantities are energy, E, particle number, N, and volume, V. In addition to the

microcanonical ensemble, in which N is implicitly fixed for isolated systems, statistical mechanics commonly uses a number of others, each of which should produce identical results in the thermodynamic limit (for thermal systems), due to the "equivalence of ensembles." Thus, the ensembles realize generic distributions of similar classical configurations that in some way fix any quantities that are conserved under the dynamics and scale with the number of particles, N, or volume, V (i.e., *extensive* conserved quantities).

There exist several alternatives to the μCE, all of which require the existence of a thermal reservoir. These ensembles replace the energy parameter of the μCE with temperature, which requires that the system be in thermal equilibrium with something else. In general, each ensemble fixes precisely one extensive, conserved quantity, and assigns to all others *Lagrange multipliers*—e.g. β for energy. For example, the Gibbs directly fixes particle number, N, and fixes the Lagrange multipliers β and p—inverse temperature and pressure, respectively—rather than energy, E, and volume, V. If there are more extensive conserved quantities, there should be correspondingly more Lagrange multipliers. In calculating expectation values and other quantities, one averages over *all* phase space configurations—i.e., not merely constant energy surfaces—with the appropriate Gibbs-Boltzmann weights, e.g. $\exp(-\beta H - \nu N - pV)$. Other ensembles include the ordinary canonical ensemble (OCE), which is a T, V, N ensemble, and the grand canonical ensemble (GCE), a T, μ, V ensemble. The OCE corresponds to the standard Gibbs-Boltzmann distribution, where one sums over configurations with the correct number of particles, volume, and so on, but samples configurations at all energies with the weight $\exp(-\beta H)$. These ensembles and their corresponding partition functions can be derived from basic probabilistic considerations in which a particular quantity is held fixed [3].

Again, these ensembles necessarily lead to equivalent predictions in the thermodynamic limit, and the various partition functions, "free energies," susceptibilities, and similar quantities are related by "Maxwell relations" [3]. In general, a given model will be more easily resolved using a particular ensemble, and that is the primary motivation for considering different ensembles. As an example, one can derive the ideal gas law from microscopics quite straightforwardly in the OCE or Gibbs ensemble. Regarding the equation $pV = k_B NT$, depending on the ensemble, either p *or* V will be an "independent" variable (i.e. a parameter of the ensemble), with the other defined by a Maxwell relation, or generally speaking, in terms of the ensemble in question and its parameters.

These ensembles are readily extended to describe *quantum* systems by replacing integrals over classical phase space with traces over the many-body Hilbert space, and replacing classical "numbers" with the corresponding quantum "operators." Generally speaking, the Gibbs-type ensembles are more useful in quantum systems, as it is easier to introduce Lagrange multipliers than perform restricted sums. As an example, consider a system of free fermions that live on a lattice. There is no notion of volume in this problem, merely energy and particle number. This problem is most easily treated in the GCE, which introduces a temperature $T = 1/k_B\beta$ and chemical potential, μ, but the trace over the many-body Hilbert space is not restricted. Defining the fermion modes in Fourier space, the energies are given by $\varepsilon(k)$, for $k \in \{1, 2, \ldots, L-1, L\}$, and the total energy is given by $\hat{H} = \sum_k \varepsilon(k) c_k^\dagger c_k$, where $n_k = c_k^\dagger c_k \in \{0, 1\}$ is the occupation of the kth mode. The total particle number is given by $\hat{N} = \sum_k c_k^\dagger c_k$, so the grand canonical weight acts on a quantum state as $\exp[-\beta\hat{H} + \beta\mu\hat{N}] = \exp[-\beta \sum_k (\varepsilon(k) - \mu) n_k]$ in this case. The trace is given by summing over all combinations of $n_k = 0, 1$, which factorizes nicely for noninteracting models, giving a useful form for the partition function, free energy, and other thermodynamic quantities. For bosons, the n_k factors sum over all nonnegative integers, which realizes a geometric series.

However, in this treatment, the bath remains a mystery as in the classical case, and is also

fully classical: there are no operators that act on the bath, nor is there a defined Hilbert space for the bath. There is therefore no means for the bath and system to entangle (in the strict quantum sense of the word). As we will see in Sec. 1.3, this is actually an important point. For classical systems, the mystery baths are on firmer ground, as they lead to results equivalent to those that obtain from full consideration of a classical system coupled to a classical reservoir with an explicit microscopic model [2]. While this form of quantum statistical mechanics has been quite effective in describing numerous quantum phenomena, in contrast to the classical case, it has not been fully established under what circumstances quantum systems thermalize with quantum baths, the regimes of violation and their stability, and related physics. However, some of this has been hashed out in very recent years, and will be discussed in the remainder of the introduction.

1.2 Isolated Quantum Systems

The following sections draw heavily from notes taken by the author from various lectures given by Prof. David Huse of Princeton University, and particularly Ref. [9].

Recent progress in the experimental preparation of quantum systems well isolated from their environments has raised fundamental questions about how quantum systems thermalize, and if there are other possibilities. The importance of these questions extends beyond cold atom experiments: the universe is an isolated quantum system. Although isolated systems were originally investigated by the likes of Boltzmann (for classical systems) and von Neumann (quantum systems) [2, 3, 9], interest in these systems has been renewed by the combination of substantial advances in experiments in the field of atomic, molecular, and optical physics (AMO)—and cold atom systems in particular—along with knowledge of the physics of localization developed since Anderson's seminal work on *localization* [10].

In fact, at the time of the initial publication, Anderson noted that sufficiently disordered models of noninteracting electrons would not be able to equilibrate; however, this insight was largely overlooked during the next half century of research on localized systems. In 2006, Basko, Aleiner, and Altschuler showed that single-particle Anderson-localization is stable to weak interactions [10, 11]. Around this time, David Huse and collaborators revived Anderson's insight: they noted that equilibrium statistical mechanics is not the right language in which to consider *many-body* localization (MBL)[1] [9, 12–14].

This led to the discovery that MBL is actually a robust, nonequilibrium *phase of matter* that does not thermalize in any sense [9, 12–14]. Intriguingly, this phase is entirely beyond the conventional, equilibrium theory of phases of matter, and there exists a phase transition between the nonequilibrium MBL phase and a thermal phase, to which the conventional theory of phases and phase transitions applies. As we shall see, the unconventional nature of the MBL phase allows it to host a number of phenomena *forbidden* in equilibrium; some of these have intriguing potential for application, e.g. to quantum computation [15].

We now review various types of isolated quantum systems, and introduce some basic ideas for their study. These quantum systems are many-body, which is to say that their fundamental degrees of freedom interact with one another; those degrees of freedom may be spins, cold atoms, q-bits, etc. Of paramount importance is the fact that these systems are *closed*: they are not in contact

[1] The acronym "MBL" will be used interchangeably to denote both "many-body localization" and "many-body localized."

with a bath, environment, or any external degrees of freedom capable of acting as a reservoir in any sense. We will, however, allow for the study of "driven" systems, which are distinct from systems coupled to external baths in a manner that will be made precise.

There exist a number of well-defined questions that one can address for a given system; for a handful of cases, these questions have known answers. In general, problems in this setting are quite difficult to tackle, as they require knowledge of highly excited states throughout the entire many-body spectrum and the presence of strong—which is often to say, nonperturbative—interactions and spatial inhomogeneity (a.k.a. "disorder"), among other complications. This and subsequent sections are devoted to addressing the following for an appropriate system of interest [9]:

Question 1.1. *Does a given system successfully act as a bath for its constituent subsystems?*

If the answer to the Question 1.1 is yes, then the quantum system thermalizes; the best understood case for which the answer is "no" that is "generic" in some sense is MBL. This is because MBL is stable and not fine-tuned, which is to say it is robust to small perturbations of fairly arbitrary nature. While there exist other athermal states that can realize in isolated quantum systems, they are less established, and may not be stable phases of matter. Some possible examples include quantum critical glasses, many-body quantum scars, and certain kinetically constrained systems.

For many models in one spatial dimension, it is possible to tune parametrically between between the "yes" and "no" answers to Question 1.1; when "no" corresponds to MBL, there is an unconventional phase transition between these two options.

1.2.1 Types of systems

Broadly speaking, there are three classes of systems of interest:

1. **Hamiltonian** systems, which here refers specifically to time-independent Hamiltonians. From an experimental or physical point of view, this describes systems that are fully and properly isolated and quantum, or describes systems that are *well* isolated at times sufficiently short that the outside world has not yet had any effect, but long enough for interactions to have taken effect. The relevant equation is the Schrödinger equation, diagonalized by many-body energy eigenstates $|n\rangle$ satisfying

$$\hat{H}|n\rangle = E_n|n\rangle \ . \tag{1.2.1}$$

   Dynamically, a given system is prepared in some initial state $|\psi(0)\rangle$ at time $t = 0$, which is a linear superposition of energy eigenstates with weight c_n on the nth eigenstate, $|n\rangle$. The state at time t is given by

$$|\psi(t)\rangle = \sum_{n=1}^{\mathcal{D}} e^{-iE_n t} c_n |n\rangle \ , \tag{1.2.2}$$

   where $\mathcal{D}$ is the total many-body Hilbert space dimension. While Eq. (1.2.2) is quite simple, the energies and eigenstates $|n\rangle$ are not simple in any sense for generic many-body systems; correspondingly, the dynamics may be quite complicated to diagnose despite the apparent solubility of Eq. (1.2.2).

2. **Driven** systems, which differ from Hamiltonian systems as defined above in that $\hat{H} \to \hat{H}(t)$ is time dependent. Such driving is classical, in that only the coefficients of various terms in the Hamiltonian vary in time, but there is no explicit coupling to external [quantum] degrees

of freedom. Driven systems of this type are still considered closed because no entanglement can be generated between the system and the drive source (there is no "back action"). This applies to systems in which the drive corresponds to classical degrees of freedom, or is coherent (in which case it will not entangle with the system degrees of freedom). The relevant equation is the *time-dependent* Schrödinger equation,

$$i\frac{d}{dt}|\psi(t)\rangle = \hat{H}(t)\,|\psi(t)\rangle \ , \tag{1.2.3}$$

and the unitary operator that evolves a many-body state $|\psi\rangle$ from time t_0 to time t is given by

$$\hat{\mathcal{U}}(t,t_0) = \hat{\mathcal{T}}\,\exp\left\{-\frac{i}{\hbar}\int_{t_0}^{t} dt'\,\hat{H}(t')\right\} \ , \tag{1.2.4}$$

where $\hat{\mathcal{T}}$ is the time-ordering operator.

3. **Floquet** systems, which are a special case of driven systems that satisfy a *discrete* time translation symmetry[2]:

$$\hat{H}(t+T) = \hat{H}(t) \ , \tag{1.2.5}$$

where T is the period of the drive, not to be confused with temperature. For these models, we restrict our attention to discrete times, which are integer multiples of drive period, i.e., $t_n = nT$ for $n \in \mathbb{N}$. The dynamics are then captured by the Floquet unitary,

$$\hat{F} = \hat{\mathcal{U}}(T,0) \ , \tag{1.2.6}$$

which evolves the system by a single period, where $\hat{\mathcal{U}}$ is defined by Eq. (1.2.4). The discrete-time dynamics are given by an analogue of the Schrödinger equation,

$$|\psi(t_n)\rangle = \hat{F}|\psi(t_{n-1})\rangle \ , \tag{1.2.7}$$

and one can study eigenstates of the Floquet operator $\hat{F}$ directly. In general, we will not study the physics within the drive period, as this reduces to the previous driven case: the physics unique to the Floquet setting is associated with these discrete time steps. Additionally, one can define Floquet models without recourse to time-dependent Hamiltonians, and directly define the single-period unitary operator, $\hat{F}$; dynamics are generated by repeated application of $\hat{F}$. The eigen*values* of $\hat{F}$ have the form $e^{-i\varepsilon_n}$, where ε_n are *pseudoenergies*, only define modulo $2\pi/T$. Unlike true energies, which are eigenvalues of the Hamiltonian, the pseudoenergy does not correspond to an extensive conserved quantity.

Note that all three of the above systems evolve unitarily. This will be a requirement for the discussion to follow, but does not apply to certain open systems, e.g. those coupled to baths in the Lindblad formalism, or systems in which an external observer makes "measurements" during the evolution. These scenarios are interesting, but largely unrelated to the contents of this thesis.

In the Floquet case, one has discrete time translation invariance—i.e., an additional symmetry, which compared to a general drive (the second case above), implies that there exist eigenstates and eigenvalues of the evolution operator. The existence of such an eigenspectrum for the evolution will be important, as many results for both thermalization and localization derive from *spectral properties*.

[2]In contrast to the continuous temporal translation symmetry of Hamiltonian systems.

In the Hamiltonian case, one has continuous time translation invariance. As in the Floquet case, one has eigenstates and eigenvalues of the evolution operator, and the ability to diagnose spectral properties. Unlike the Floquet case, Hamiltonian systems have a conserved energy. The existence of an *extensive* conserved quantity provides additional insight from *transport*. Note that the pseudoenergy eigenvalues of the Floquet evolution do not correspond to an extensive conserved quantity, and thus cannot "be transported."

We will also consider models with additional symmetry structure on top of the "symmetries" defined above. If the symmetries correspond to an extensive conserved quantity, one can have transport of said quantity. However, any such features will be in addition to the basic case in which there is no additional structure, and the results from the latter case still ought to hold in general, though as we shall see there are some notable caveats, e.g. the incompatibility of non-Abelian symmetries and MBL.

We will essentially ignore the second case (driven systems) in the discussion that follows. These systems are generally hard to treat, and the fact that the evolution does not have a spectrum and one cannot study transport without explicitly imbuing the system with a symmetry does not help. Additionally, these systems probably cannot be many-body localized; nonetheless, by considering *random* evolution, i.e. by constructing $\hat{\mathcal{U}}(t, t_0)$ in Eq. (1.2.4) directly out of random unitary matrices, one can learn quite a bit about thermalization, as will be discussed in Ch. 5. In that treatment, there is no associated time-dependent Hamiltonian.

As a final comment before proceeding, the results of the following sections can be thought of as applying to a conventional "open system," if one considers the combined system and bath [environment] to be a single closed system. The key distinction is that Question 1.1 refers to *all* valid choices of subsystems[3], while for the aforementioned case, one need only consider a specific bipartition of the whole, closed system into the subsystem of interest (i.e., the system that is open) and bath, provided all other conditions apply.

1.2.2 Quantum quenches

In general, it is not physically tractable to prepare a quantum system in an eigenstate of the operator that governs the system's evolution. Broadly speaking, isolated quantum systems are analyzed from one of two perspectives: the first is to consider the properties of eigenstates of the evolution (provided the latter has continuous or discrete time translation invariance), and the second is to consider the dynamical and late time properties of systems prepared in some physical state that is not an eigenstate of the evolution, also known as a "quantum quench."

Definition 1.1. A quantum quench refers to preparing a system in some experimentally realizable initial state that crucially is *not* an eigenstate of the evolution operator, $\hat{\mathcal{U}}$, and allowing the system to evolve therefrom. The number of eigenstates of $\hat{\mathcal{U}}$ with which the initial state has nonzero overlap scales exponentially in the size of the system. Specifically, the term "quench" refers to the preparation of the system in this state.

Note that the system is necessarily not closed during the quenching procedure, though it is closed immediately thereafter, and remains so. In general, the initial states have low entanglement: they are generally unentangled product states in the naïve physical basis, but may have entanglement between regions that scales with the boundary of the region. The motivation for this stipulation

[3]This validity will be defined in the next section.

is twofold: firstly, such states are the most reasonable to prepare in the laboratory setting, and secondly, such states are the furthest from being thermal, as will soon be explained.

Following the quench, the system is allowed to evolve under its own dynamics. One then measures various quantities, e.g. expectation values of local observables, $\langle\psi(t)|\hat{\mathcal{O}}|\psi(t)\rangle$, correlation functions of such observables, $\langle\hat{\mathcal{O}}(x,t)\hat{\mathcal{O}}(0,0)\rangle$, and other quantities as a function of time. Restricting to Hamiltonian systems, the quench deposits an extensive amount of energy, E, into the system relative to the ground system. The same can be said for other extensive conserved quantities, which allows for the study of transport following a quench, and leads to a hydrodynamic picture of thermalization, as will be discussed in Ch. 4 and Ch. 5. Because the initial state has overlap with eigenstates throughout the spectrum, the dynamics following a quench probes physics of highly excited states, and has little to do with the physics of ground states commonly addressed in more conventional areas of strongly correlated condensed matter physics.

1.3 Quantum Thermalization

We begin by defining thermalization of an isolated quantum system:

Definition 1.2. An isolated quantum system is thermal if, as a whole, it is able to act as a proper bath for all valid choices of constituent subsystems.

The terms "proper" and "valid" will be elucidated shortly.

Classically, the role of the bath is to exchange extensive conserved quantities with the system; secondarily, it helps generates entropy and allows the system to explore its phase space. Quantumly, the most important function of the bath is the dynamical generation of entanglement between the system and bath degrees of freedom. For a *sub*system of an isolated quantum system to reproduce equilibrium thermodynamics, it must "forget" the details of its initial conditions and eventually reach a time-independent steady state.

In each of the three cases noted in Section 1.2, the many-body state of the full system at time t is *completely determined* by the initial conditions. Thus, the only way for the state of the subsystem [on its own] to be independent of these conditions is for the details of the subsystem's initial state to be hidden nonlocally. The mechanism for this is quantum entanglement: as the system becomes entangled under its own dynamics, it becomes impossible to recover any information about the past by making measurements solely on the subsystem's degrees of freedom. As the system evolves, more and more of these details are encoded in the inaccessible bath degrees of freedom. In quantum systems, the exchange of conserved quantities, e.g. energy, is a secondary role of the bath.

Classical thermal systems maximize entropy, which constrains the "ensembles" one uses to describe these systems. In quantum systems, one finds that entanglement entropy plays the usual role of thermodynamic entropy, which is itself an extensive quantity. Thus, if a quantum system is thermal, then the entanglement must be maximal, and the entanglement entropy must scale with the volume of the relevant subsystem, e.g. $S_A = \alpha \mathrm{Vol}(A)$; because entanglement is maximized, the coefficient α must saturate the maximal value.

1.3.1 Valid subsystems

To be more precise, let us denote by $\mathcal{S}$ all of the degrees of freedom in a given, closed system. The system $\mathcal{S}$ is further divided into a subsystem of interest, which we denote $\mathcal{A}$, and its complement,

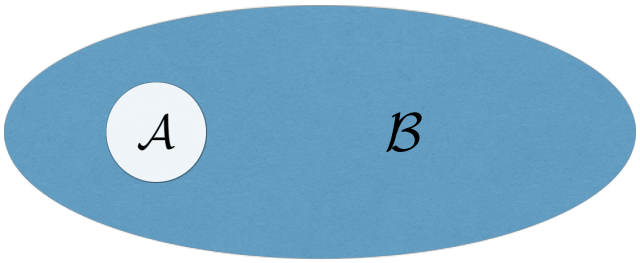

Figure 1.1: Schematic depiction of the system $\mathcal{S} = \mathcal{A} \cup \mathcal{B}$, where $\mathcal{A}$ is the subsystem of interest, in which all measurements will be made, and $\mathcal{B} = \overline{\mathcal{A}}$ is its complement, which acts as a bath for $\mathcal{A}$.

$\mathcal{B} = \overline{\mathcal{A}}$, such that $\mathcal{S} = \mathcal{A} \cup \mathcal{B}$. The former, $\mathcal{A}$, is analogous to the "system" in the usual, open setting, and is the thing we care about. A useful mnemonic is "$\mathcal{B}$ for bath," the role of the complement of $\mathcal{A}$ is to entangle with $\mathcal{A}$ itself so as to conceal information about the latter's past, in the finest tradition of baths.

There are some constraints on the identification of a subset of degrees of freedom $\mathcal{A} \subset \mathcal{S}$ if $\mathcal{A}$ is to correspond to a "valid choice of subsystem," per Definition 1.2 of quantum thermalization. A typical picture is given by Fig. 1.1, in which the subsystem $\mathcal{A}$ is a connected subregion of the full system $\mathcal{S}$: such "real space" delineations are always valid, and generally need not be connected.

Though such choices are most common, it is not necessary for $\mathcal{A}$ to be defined in real space. The main constraint on whether or not a subsystem is valid is locality, which is automatically satisfied by defining $\mathcal{A}$ in real space. While we do not require $\mathcal{A}$ be defined explicitly in real space, we *do* assume that the naïve degrees of freedom in $\mathcal{S}$ admit a local description of some kind. In other words, there must be *some* means of describing the definition of $\mathcal{A}$ that does not require knowledge of the entire system $\mathcal{S}$ at once. For example, a definition of $\mathcal{A}$ in momentum space—defined via Fourier transform—is also perfectly valid, as the Fourier transform merely constitutes a sum over terms in real space with the same locality (i.e., one-body operators map to the sum over one-body operators, and thus remain one-body).

To make this more precise, let us consider the many-body Hilbert space $\mathcal{H}$ and Hamiltonian $\hat{H}$ describing $\mathcal{S}$[4]. We decompose the full Hilbert space via

$$\mathcal{H} = \mathcal{H}_A \otimes \mathcal{H}_B \ , \tag{1.3.1}$$

where $\mathcal{H}_A = \text{span}\left(\{|a\rangle\}\right)$, where the set $\{|a\rangle\}$ denotes a complete orthonormal basis for $\mathcal{A}$ (and likewise for $\mathcal{B}$). As an aside, it is possible that strictly speaking the full Hilbert space $\mathcal{H}$ of $\mathcal{S}$ is a subset of $\text{span}\left(\{|a\rangle\}\right) \otimes \text{span}\left(\{|b\rangle\}\right)$, e.g. due to constraints that make it impossible to form a separate basis for the configurations of $\mathcal{A}$ and $\mathcal{B}$ independently; attempting to do so results in over counting. However, this detail is unimportant to the discussion at hand.

For notational simplicity, let us suppose that the evolution of the full system $\mathcal{S}$ in time is described by a Hamiltonian, $\hat{H}$, which may be time-dependent. We then decompose the Hamiltonian into three parts, one acting nontrivially only on degrees of freedom in $\mathcal{A}$, another acting nontrivially only on degrees of freedom in $\mathcal{B}$, and a boundary term that couples the two:

$$\hat{H} = \hat{H}_A \otimes \hat{\mathbb{1}}_B + \hat{\mathbb{1}}_A \otimes \hat{H}_B + \hat{H}^{\text{int}}_{AB} \ , \tag{1.3.2}$$

where $\hat{\mathbb{1}}$ is the identity. In standard equilibrium statistical mechanics, one defines $\mathcal{A}$ in real space, à la Fig. 1.1, and takes its size to infinity; since energy is extensive, the interaction term coupling

[4]Here "Hamiltonian" is used imprecisely to mean any of the three cases enumerated in Section 1.2, and does not imply time-independence.

regions $\mathcal{A}$ and $\mathcal{B}$ scales with the boundary of $\mathcal{A}$, while the other terms scale with the volume of their respective regions, and the interaction term is therefore negligible by comparison. In this case, we will not take $\mathcal{A}$ to be infinitely large at the outset, and this approximation will generally be incorrect: to determine whether or not $\mathcal{S}$ is thermal, we must determine that it is so for *all* valid choices of $\mathcal{A}$, including small ones.

In the real world, physics is local. For $\mathcal{A}$ to constitute a valid subsystem, the Hamiltonian describing it, given by $\hat{H}_A$ in Eq. (1.3.2) must be local in terms of some basic degrees of freedom. This locality is defined in the quantum information sense, which is to say, the number of degrees of freedom involved in determining the elements of $\hat{H}_A$ must be finite. All of the systems considered in this thesis will have a natural description in terms of degrees of freedom—e.g., spins—defined in real space. This is true of most models one would naturally consider; however, it is worth noting that the procedure being outlined herein is not limited in scope to such models, but extends to generic models that are sufficiently local.

It is perhaps most illustrative to give an example of an invalid choice of subsystem $\mathcal{A}$. For example, imagine that the eigenbasis, $\{|n\rangle\}$ of the full many-body Hamiltonian $\hat{H}$ in Eq. (1.3.2) is known. We can define a Pauli $\hat{Z}$ operator by choosing half the energy eigenstates, and assigning them to the state $|\uparrow_j\rangle$, and assigning the other half to the state $|\downarrow_j\rangle$, where $\hat{Z}_j|\uparrow_j\rangle = +|\uparrow_j\rangle$ and $\hat{Z}_j|\downarrow_j\rangle = -|\downarrow_j\rangle$. In terms of operators, Z_j is the sum of projectors onto eigenstates associated to $\uparrow_j$ minus all projectors associated to $\downarrow_j$. We define a new spin 1/2 at site j' by choosing a different assignment of half the eigenstates as before. All such operators commute with the Hamiltonian $\hat{H}$ by construction[5] Any choice of $\mathcal{A}$ using degrees of freedom defined by this mapping will not result in thermalization, which can be seen from the fact that the Hamiltonian is completely trivial and no entanglement between these degrees of freedom can be generated by the dynamics, precisely because they are defined in terms of eigenstates of the dynamics. The reason this is not generic is that, for many-body systems, the energy eigenstates necessarily require information about all degrees of freedom in any basic, physical basis.

Before proceeding, it is worth reviewing a few basic principles from quantum mechanics. First, we define an observable,

Definition 1.3. An **observable** is a Hermitian operator that is sufficiently low order in the sense of locality or number of degrees of freedom involved in a physical—or experimentally motivated—basis.

The notion of "low order" is entirely dependent on the choice of basis; this is difficult to define in an abstract sense, but it is extremely difficult to find actual physical models where this definition remains elusive. In general, there should exist some basis that captures the most local aspects of a system that can be resolved experimentally, which are the "fundamental" or "basic" degrees of freedom, in some sense. For example, for spins on a lattice, this would correspond to the orientation of a single spin along a given axis. Low order is then defined in this language, and refers to the number of fundamental degrees of freedom. Note that not all Hermitian operators are observable: in fact, if one were to define random Hermitian operators in the many-body Hilbert space, such operators in general will not be observable, unless the system is so small that nothing can be nonlocal.

[5] All of the projectors onto eigenstates necessarily commute with one another, as the eigenstates define an orthonormal basis; the Hamiltonian is merely a sum over these projectors, each weighted by the corresponding energy eigenvalue.

1.3.2 Thermal states

Understanding thermalization of quantum systems requires some notion of a thermal state. There are two types of states in quantum systems: pure states and mixed states. The former are convenient theoretical constructs, represented by a vector, $|\psi\rangle$, in the many-body Hilbert space. Any superposition of a pure state is also a pure state by linearity of Hilbert spaces. The corresponding density matrix of any pure state is $\hat{\rho} = |\psi\rangle\langle\psi|$.

In the laboratory, all states are mixed states: a mixed state is given by a density matrix $\hat{\rho}$ that is the sum of density matrices corresponding to pure states

$$\hat{\rho}_{\text{mixed}} = \sum_{\alpha=1}^{\mathcal{D}} p_\alpha |\alpha\rangle\langle\alpha| \ , \tag{1.3.3}$$

where p_α are the probabilities associated to the pure states indexed α. Like probabilities, these must sum to unity, i.e. $\text{Tr}[\,\hat{\rho}\,] = 1$ is a property of density matrices. Additionally, since $|\alpha\rangle\langle\alpha|$ is a projector, density matrices satisfy $\hat{\rho}^2 = \hat{\rho}$. Finally, the quantum expectation values of observables are given in terms of the density matrix via

$$\langle\hat{\mathcal{O}}\rangle = \text{Tr}[\,\hat{\mathcal{O}}\,\hat{\rho}\,] = \text{Tr}[\,\hat{\rho}\,\hat{\mathcal{O}}\,] \ , \tag{1.3.4}$$

and when $\hat{\rho}$ corresponds to a pure state, this reproduces the usual form of expectation values

$$\hat{\rho} = |\psi\rangle\langle\psi| \implies \langle\hat{\mathcal{O}}\rangle = \text{Tr}[\,\hat{\mathcal{O}}\,\hat{\rho}\,] = \langle\psi|\hat{\mathcal{O}}|\psi\rangle \ . \tag{1.3.5}$$

Finally, the density matrix evolves from its initial form $\hat{\rho}(t_0)$ at some specified time t_0 [which one generally refers to as $t = 0$] according to

$$\hat{\rho}\,(t) = \hat{\mathcal{U}}\,(t,0)\ \hat{\rho}\,(0)\,\hat{\mathcal{U}}^\dagger\,(t,0) \ , \tag{1.3.6}$$

where $\hat{\mathcal{U}}\,(t,0)$ is the same unitary that evolves many-body states, as defined in Section 1.2, e.g. in Eq. (1.2.4). This is easy to see for a pure state, $\hat{\rho} = |\psi\rangle\langle\psi|$, where $\hat{\rho}(t)$ is given by taking $|\psi\rangle \to |\psi(t)\rangle = \hat{\mathcal{U}}(t,0)\,|\psi(0)\rangle$.

Density matrices are useful compared to standard states $|\psi\rangle$ because they encode a probability distribution straightforwardly; we will also make use of standard properties of the reduced density matrix for the subsystem $\mathcal{A}$,

Definition 1.4. For a system $\mathcal{S} = \mathcal{A} \cup \mathcal{B}$ described by the full density matrix $\hat{\rho}_{AB}$, the **reduced** density matrix, $\hat{\rho}_A$, describing the degrees of freedom in $\mathcal{A}$ is given by $\hat{\rho}_A = \underset{B}{\text{Tr}}\,[\,\hat{\rho}_{AB}\,]$.

The reduced density matrix is particularly useful because, for any observable $\hat{\mathcal{O}}_A$ whose support lies entirely in the subsystem $\mathcal{A}$, the expectation value $\langle\hat{\mathcal{O}}_A\rangle$ can be computed using the reduced density matrix $\hat{\rho}_A$, rather than that of the full system. Thermal states are then defined in terms of density matrices as follows:

Definition 1.5. A thermal system $\mathcal{S}$ dynamically evolves to a **thermal state** under its own dynamics that is in thermal equilibrium in the following sense: For any bipartition of the system $\mathcal{S} = \mathcal{A} \cup \mathcal{B}$ into a subextensive subsystem $\mathcal{A}$ and an extensive subsystem $\mathcal{B}$, as the thermodynamic limit $\text{Vol}\,(\mathcal{S}) \to \infty$ is taken with $\text{Vol}\,(\mathcal{A})\,/\text{Vol}\,(\mathcal{S}) \to 0$, one recovers a sequence of density matrices $\hat{\rho}^{\text{eq}}_{AB}$, which are *thermal* if

$$\hat{\rho}_A(t) = \underset{B}{\text{Tr}}\,[\,\hat{\rho}_{AB}(t)\,] \to \hat{\rho}^{\text{eq}}_A\,(T,\mu,\dots) = \underset{B}{\text{Tr}}\,[\,\hat{\rho}^{\text{eq}}_{AB}\,] \ , \tag{1.3.7}$$

at suitably late times, t, as this limit is taken, where $\hat{\rho}_A^{\text{eq}}(T, \mu, \dots)$ only depends upon a handful of state variables as in standard thermodynamics, corresponding to *any* relevant thermodynamic ensemble.

Note that the notion of a "thermal state" is only sharply defined in the thermodynamic limit, in which the number of degrees of freedom in the full system, $\mathcal{S}$, is taken to infinity. Correspondingly, all extensive quantities describing $\mathcal{S}$—e.g. volume, energy, etc.—diverge in this limit. We require that the volume of $\mathcal{A}$ grow slower than $\mathcal{B}$, and vanishingly so as the thermodynamic limit is taken on the full system. As this limit is taken, one recovers a sequence of states, which converge to a specific state—independent of the microscopic details and initial conditions of $\mathcal{A}$—as the thermodynamic limit is taken for $\mathcal{S}$, in which case that state is the thermal state.

Any standard ensemble from statistical mechanics should result in the *same* reduced density matrix for the subsystem $\mathcal{A}$ at late enough times for $\mathcal{A}$ to have equilibrated. However, because the full system $\mathcal{S}$ evolves unitarily from its initial state, these choices will result in different density matrices for the full system $\mathcal{A} \cup \mathcal{B}$. In general, $\hat{\rho}_{AB}^{\text{eq}} = \exp(-\beta \hat{H}_{AB})$ should be a valid choice, though in contrast standard equilibrium statistical mechanics, this is not the only choice or a even a necessary one *a priori*. As a reminder, Definition 1.5 should apply for all valid choices of $\mathcal{A}$ using the same choice of $\hat{\rho}_{AB}^{\text{eq}}$ (or sequence thereof in the thermodynamic limit); this may breakdown for extremely inhomogeneous systems, and we will ignore such systems.

In the presence of conservation laws, including temperature, the ensemble must either specify directly the values of each of the system's extensive conserved quantities, as in the standard microcanonical ensemble, or their conjugate quantities, which are Lagrange multipliers for the conserved quantities (i.e. the coolness [inverse temperature] $\beta \propto 1/T$ is conjugate to energy, chemical potential μ is conjugate to particle number, N, pressure p to volume, and so on), as in the general statistical ensembles. Note that noncommuting conserved quantities are not a problem, as the noncommutativity is expected to vanish in the thermodynamic limit.

A special case and notable exception is integrability. Quantum integrable models have an extensive number of extensive conserved quantities, and relax to a "generalized" equilibrium described by a Generalized Gibbs Ensemble (GGE) featuring infinitely many Lagrange multipliers for its infinitely many conserved quantities. These will be discussed separately in Ch. 2.

For a quantity to be conserved, it must commute with the evolution of the system, e.g. $[\hat{H}, \hat{\mathcal{O}}] = 0$. To be extensive, these quantities must have a nonvanishing local density. Examples include quantities that can be expressed as the sum of local terms, such as energy (the Hamiltonian is generally the sum of local terms), magnetization $\hat{S}_{\text{tot}}^z = \sum_j \hat{S}_j^z$ in models of spins, and so on. On the other hand, there is no local density for the pseuoenergies of Floquet systems, or for projectors onto particular Hamiltonian eigenstates, which necessarily commute with the Hamiltonian itself, but for which one cannot define a density that is nonvanishing in the thermodynamic limit.

Further, it is essential that the *uncertainty* of an extensive conserved quantity be *subextensive*. An example in which this is not the case is a system prepared in superposition of two different energy eigenstates with very different energies. This is problematic because it complicates or even precludes the definition of a temperature. While there may be theoretical scenarios in which macroscopic superpositions of this type can nonetheless correspond to well-defined state variables with particular values, these are unlikely to be realized in any experimental setting. A typical case is for the uncertainty—or variance—in energy, e.g., to scale as $\Delta E \sim \sqrt{V}$, where V is the volume.

To summarize: The thermal state $\hat{\rho}_{AB}^{\text{eq}}$ is defined for the full system $\mathcal{S} = \mathcal{A} \cup \mathcal{B}$ without refer-

ence to dynamics, and may be chosen to correspond to any of a number of statistical ensembles, all of which should result in the same physical properties and satisfy the same criteria. In particular, the ensemble should account for each of the system's extensive conserved quantities, if any, either by fixing their value directly, or assigning them a corresponding Lagrange multiplier. For *any* choice of sub-extensive subsystem $\mathcal{A}$, upon tracing out the degrees of freedom in $\mathcal{B} = \overline{\mathcal{A}}$, and taking the limit $\mathrm{Vol}(\mathcal{B}) \to \infty$, one recovers a reduced density matrix for $\mathcal{A}$ alone that is produces the correct expectation values for local observables (at suitably late times for the system to have reached equilibrium and thermalized). For a given identification of $\mathcal{A}$, *all* [valid] choices of ensembles should result in the same reduced density matrix for $\mathcal{A}$, a property also known as the "equivalence of ensembles." Additionally, the choice of $\hat{\rho}_{AB}^{\mathrm{eq}}$ must be valid for all choices of $\mathcal{A}$, when the thermodynamic limit is taken on the system as a whole with $\mathcal{A}$ finite.

In principle, one can extract thermodynamic quantities from the equilibrium state $\hat{\rho}_{AB}^{\mathrm{eq}}$, although this may be impractical from a theoretical standpoint. As an example, one could imagine affixing to the system $\mathcal{S}$ some extra degrees of freedom—e.g., a narrow tube filled with mercury—which collectively act as a thermometer. All of the above discussion should apply equally to the choice of $\mathcal{A}$ corresponding precisely to the auxiliary thermometric degrees of freedom. One can then make a measurement using the reduced density matrix for $\mathcal{A}$ to measure the temperature, and thereby extract this information from the full system's equilibrium thermal state, $\hat{\rho}_{AB}^{\mathrm{eq}}$. In general, the difficulty lies in "calibrating" such thermometers.

Some final notes:

- This applies to pure states equally as well as to mixed state density matrices.
- One can take $\hat{\rho}_{AB}^{\mathrm{eq}}$ to be the standard Boltzmann weight for the full system. However, the usual practice in conventional equilibrium statistical mechanics of fixing the *reduced* density matrix for $\mathcal{A}$ to be given by $\exp\left(-\beta \hat{H}_A\right)$ is not valid, as it ignores the interaction terms coupling $\mathcal{A}$ to the rest of the system, which we cannot take to be negligible without taking $\mathrm{Vol}(\mathcal{A}) \to \infty$. In an average sense, and in that limit, this may be true, but strictly speaking the point is to describe internal thermalization of $\mathcal{S}$ as a whole, which requires consideration of finite subsystems $\mathcal{A}$, which must be completely and correctly described by the equilibrium state $\hat{\rho}_{AB}^{\mathrm{eq}}$ of the whole system.
- A single energy eigenstate, $|n\rangle$, is also a valid microcanonical ensemble. Note that if there are extensive conserved quantities other than energy, these must be fixed as well, if not already fixed by $|n\rangle$.

1.3.3 Thermalization following a quench

In the laboratory, a system is initialized in a given state at time $t = 0$, and allowed to evolve under its own dynamics thereafter. If the system is thermal, we expect the system to evolve to the thermal state described in Section 1.3.2. This is also known as a quantum quench, as discussed in Sec. 1.2.2. As previously noted, the full density matrix evolves according to

$$\hat{\rho}_{AB}(t) = \hat{\mathcal{U}}(t,0)\ \hat{\rho}_{AB}(0)\hat{\mathcal{U}}^{\dagger}(t,0)\ , \tag{1.3.6}$$

and if the system thermalizes, then as $t \to \infty$, the full density matrix approaches the equilibrium density matrix, $\hat{\rho}_{AB}^{\mathrm{eq}}$, which can take the form of any of a number of density matrices corresponding to equivalent ensembles—described by only a handful of parameters, e.g. T and μ—to reproduce

fully the correct results for all observables made in the subregion $\mathcal{A}$, for any valid, subextensive choice of $\mathcal{A} \subset \mathcal{S}$.

As $t \to \infty$, the only information about the initial conditions that can one can observe locally is encoded in the state variables that parametrize $\hat{\rho}_{AB}^{\text{eq}}$, e.g. temperature, T, and chemical potential, μ. All other details are otherwise "hidden" nonlocally in $\mathcal{S} = \mathcal{A} \cup \mathcal{B}$. For example, the apparent temperature of the equilibrium state that the system approaches as $t \to \infty$ is fixed by the energy density of the initial state. Hence, if the system is in a macroscopic superposition of states with very different energies, temperature will not be well defined if and/or when the system equilibrates, as discussed in Section 1.3.2. Whether or not this temperature can be measured in any sense is unimportant; rather, if the system thermalizes, then the properties of all subsystems $\mathcal{A}$ should follow from choosing $\hat{\rho}_{AB}^{\text{eq}}$ to be the standard Gibbs-Boltzmann distribution with a temperature that is fixed by the initial energy density, e.g. The same applies to all other parameters of the ensemble, associated to other extensive conserved quantities as applicable.

A special case is a system with time-dependent evolution $\hat{H}(t)$ and no other extensive conserved quantities. In this case, there are no thermal parameters, and $\hat{\rho}_{AB}^{\text{eq}}$ must be proportional to the identity, appropriately normalized:

$$\hat{\rho}_{AB}^{\text{eq}} = \mathcal{D}^{-1} \hat{\mathbb{1}}_{AB} \ , \tag{1.3.8}$$

where $\mathcal{D}$ is the many-body Hilbert space dimension, ensuring that the density matrix has unit trace. In this case, the reduced density matrix is also proportional to the identity operator for the reduced Hilbert space. This is the equilibrium density matrix for random, time-dependent, and Floquet evolution in the absence of any other conserved quantities.

1.3.4 The eigenstate thermalization hypothesis

The Eigenstate Thermalization Hypothesis (ETH) refers to specific conditions under which an isolated quantum system may be thermal. These conditions are sufficient, but known not to be necessary: ETH is simply one scenario under which thermalization occurs, and its constraints are, in fact, too strong. Due to the fact that it has only been realized recently that one can relax some of these constraints, in later parts of the thesis, "ETH" will be used as a shorthand for general thermal quantum systems.

Historical Remarks The history of ETH spans many years and some contributions are often overlooked, due to the fact that widespread interest in quantum thermalization has only taken hold very recently. Any historical review would be remiss to neglect Landau, who made a statement in a footnote in one of the volumes on theoretical physics that captures the essence of ETH. From experience, ignoring this detail during a talk will provoke a Russian member of the audience to interject, "Not so much question but historical comment: since you say it is just a 'hypothesis,' I should point out that Landau actually was first to note this." Not surprisingly, this is true. The 1980s saw a surge of interest in quantum chaos, and some of these concepts appear in a numerical study of a noninteracting spin chain in work by Jensen and Shankar [16]. At the tail end of this, Deutsch and Srednicki respectively published papers [17, 18] in 1991 and 1994 that are widely credited as establishing ETH. These were widely neglected until cold atom experimentation saw incredible advances and became popular among condensed matter theorists; interest was revived by Rigol and collaborators in a paper studying the Bose-Hubbard model [19], at which point the subject took off. And for most if not all topics that appear in this thesis, Tomaž Prosen probably wrote a paper on the subject 5 to 20 years before it became popular.

Diagonal ETH The Eigenstate Thermalization Hypothesis necessarily requires eigenstates of the evolution operator, and so we restrict to Hamiltonian and Floquet systems. For notational convenience, let us use the language of Hamiltonians, though the analogous equations for Floquet are basically the same, with energies replaced by pseudoenergies. We start from the Schrödinger equation

$$\hat{H}|n\rangle = E_n|n\rangle \ , \tag{1.2.1}$$

and initialize the system in a pure state at time $t = 0$ given by

$$|\psi(0)\rangle = \sum_{n=1}^{\mathcal{D}} c_n|n\rangle \ , \tag{1.3.9}$$

so that the state at time t is given simply by

$$|\psi(t)\rangle = \sum_{n=1}^{\mathcal{D}} e^{-iE_n t}c_n|n\rangle \ . \tag{1.2.2}$$

Consider the expectation value of an observable $\hat{\mathcal{O}}$ at time t,

$$\langle\hat{\mathcal{O}}\rangle(t) = \langle\psi(t)|\hat{\mathcal{O}}|\psi(t)\rangle \tag{1.3.10}$$

$$= \sum_{n=1}^{\mathcal{D}} |c_n|^2 \langle n|\hat{\mathcal{O}}|n\rangle + \sum_{\substack{n,m=1 \\ n\neq m}}^{\mathcal{D}} e^{i(E_m-E_n)t}c_n^* c_m \langle n|\hat{\mathcal{O}}|m\rangle \ , \tag{1.3.11}$$

and as $t \to \infty$, the coefficients multiplying the off-diagonal terms $\langle n|\hat{\mathcal{O}}|m\rangle$ are randomly distributed about the unit circle, as are the matrix elements themselves, and as $L, t \to \infty$, the second term in Eq. (1.3.11) vanish if the system thermalizes. This is known as *dephasing*, and implies that for thermal systems, the late-time expectation values of observables are given by the *diagonal ensemble*, i.e. the diagonal elements of the observable in a basis that diagonalizes the evolution operator. Thus, we have at late times

$$\langle\hat{\mathcal{O}}\rangle(t) = \sum_{n=1}^{\mathcal{D}} |c_n|^2 \langle n|\hat{\mathcal{O}}|n\rangle \ , \tag{1.3.12}$$

which is notably time-independent, consistent with the steady state condition of thermal equilibrium.

However, recall that in equilibrium, the expectation values of observables must be independent of the initial conditions, encoded by the coefficients c_n in Eq. (1.3.12). Since $\sum_n |c_n|^2 = \langle\psi(0)|\psi(0)\rangle = 1$, this is obviously accomplished if $\langle n|\hat{\mathcal{O}}|n\rangle$ is independent of the eigenstate $|n\rangle$, in which case

$$\langle\hat{\mathcal{O}}\rangle(t) \to \langle\hat{\mathcal{O}}\rangle_{\text{eq}} \stackrel{!}{=} \langle n|\hat{\mathcal{O}}|n\rangle \ , \quad \forall \ |n\rangle \ , \tag{1.3.13}$$

which means *any eigenstate of the Hamiltonian [or evolution operator] is a perfectly valid microcanonical ensemble*. Even for nonequilibrium initial states where the off-diagonal terms in Eq. (1.3.11) are not remotely negligible at $t = 0$ one will find that said terms vanish at late times, and owing to the normalization condition constraining the coefficients c_n, the result Eq. (1.3.13) recovers.

Definition 1.6. The Eigenstate Thermalization Hypothesis *is* the statement $\langle n|\hat{\mathcal{O}}|n\rangle \to \langle\hat{\mathcal{O}}\rangle_{\text{eq}}$, $\forall \ |n\rangle$, with $\langle\hat{\mathcal{O}}\rangle_{\text{eq}}$ independent of the eigenstate, $|n\rangle$. From this and dephasing, the result $\langle\hat{\mathcal{O}}\rangle(t) \to \langle\hat{\mathcal{O}}\rangle_{\text{eq}}$ as $t \to \infty$ follows automatically.

Some additional comments:

- Occasionally in conventional thermodynamics the order of limits can be important. That is also true here: the $t \to \infty$ limit should be taken prior to—or rather, faster than—the limit of infinite volume.

- The various statements made about observables only apply to those that are sufficiently local. To be sufficiently local, an observable's support must be limited to a valid, subextensive choice of $\mathcal{A} \subset \mathcal{S}$.

- The constraints noted in Section 1.3.2 still apply to the coefficients c_n. To wit, any uncertainty in the expectation value of extensive conserved quantities must be subextensive to make for a nice ensemble. For temperature, e.g., to be well defined, one should restrict to an initial state $|\psi(0)\rangle$ with the majority of its weight on eigenstates $\{|n\rangle\}$ in some window of energy. The average energy density will set the temperature.

- Any finite-size system will have small deviations from the result Eq. (1.3.13) that vanish in the thermodynamic limit. There will be slight variations between $\langle n|\hat{\mathcal{O}}|n\rangle$ from state to state, and the off-diagonal term in Eq. (1.3.11) will vary a bit around zero at different times, t. This vanishes in the large time limit.

- The statement "$\forall\ |n\rangle$" in Definition 1.6 of ETH is overkill, and responsible for making ETH "too strong" a statement. One could imagine a system containing one or several eigenstates $|n\rangle$ for which Eq. (1.3.13) fails to hold, but the effect of these states, both in terms of the overall fraction of the eigenstates they represent, and the extent to which they violate ETH, vanishes in the thermodynamic limit. Additionally, the strong version of ETH seems to hold valid even for numerical studies on small systems.

- Degeneracies in the energy spectrum are not a problem, unless the degeneracy of a given energy is extensive, which is highly nongeneric. For subextensive degeneracy, any effect in the off-diagonal terms in Eq. (1.3.11) will be cancelled by other degeneracy effects with opposite sign, and this all vanishes as $L, t \to \infty$.

- There are swaths of systems for which ETH is false, including many-body localized systems, quantum scars, etc. Note that a modified version of ETH holds for integrable systems that accounts for their infinite set of conserved quantities, but there is no meaningful distinction between ETH and its modified counterpart at the level of this discussion.

- All of these results are for interacting systems, free systems are different, and generally fall into the category of integrability. Disordered free systems can instead be similar to many-body localized systems, to be discussed, depending on dimension and disorder strength.

Off-diagonal ETH Srednicki showed that for thermalization to occur, it is sufficient for the off-diagonal terms in Eq. (1.3.11) to satisfy

$$\langle n|\hat{\mathcal{O}}|m\rangle = e^{-S(\overline{E})/2}\, f\left(E_n, E_m\right)\, R_{n,m}\ , \tag{1.3.14}$$

where S is the thermodynamic entropy of the whole system $\mathcal{S} = \mathcal{A} \cup \mathcal{B}$, evaluated at the mean energy $\overline{E} = (E_n + E_m)/2$, and f is an arbitrary function that falls off for large $\Delta E = |E_n - E_m|$, and

may depend on $\overline{E}$ as well; the coefficients $R_{n,m}$ look like elements of a random matrix, and if R is a random matrix, then the system is definitely thermal. The matrix R encodes ingredients like locality, and model-dependent details. Both f and R should be $O(1)$; the entropy S is extensive, and thus the leading factor in Eq. (1.3.14) suppresses the off-diagonal matrix elements of $\hat{\mathcal{O}}$ in the eigenbasis of the evolution operator in the thermodynamic limit. It is not settled what conditions are necessary to ensure the validity of Eq. (1.3.14).

Note that Eq. (1.3.14) implies Eq. (1.3.13). The eigenstates $\{|n\rangle\}$ are eigenstates of the evolution, and therefore have no dynamics. This also means that they already satisfy the steady-state condition for thermal states, but to be truly thermal, must also reproduce thermal equilibrium expectation values. This is captured by Eq. (1.3.13). Since eigenstates do not evolve, if an eigenstate is thermal, it is thermal from $t = 0$. Together, Eq. (1.3.14) and Eq. (1.3.13) provide that "all eigenstates are thermal" $\implies$ "all initial pure states thermalize," which is somewhat intuitive, but also unnecessary, as previously explained.

Volume-law entanglement entropy The von Neumann entanglement entropy is a measure of entanglement between a subsystem $\mathcal{A}$ and its complement, $\mathcal{B}$, given in terms of the reduced density matrix for subsystem $\mathcal{A}$, $\hat{\rho}_A$ via

$$S_{A|B} = -\mathrm{Tr}[\,\hat{\rho}_A \ln \hat{\rho}_A\,] \ , \tag{1.3.15}$$

and one recovers the same value using instead the reduced density matrix for $\mathcal{B}$. Note that there are other measures of entanglement, e.g. Rényi entropies, and similar quantities, e.g. mutual information, that may be of use.

For systems that thermalize, the thermodynamic entropy is equal to the entanglement entropy. This is best understood for systems with no conserved quantities, as in the context of those systems it is clearest that entanglement is the mechanism for equilibration and thermalization in quantum systems. Because entropy is extensive, one must therefore have

$$S_{A|B} = s_A(T, \mu, \dots)\ \mathrm{Vol}(\mathcal{A}) \ , \tag{1.3.16}$$

where the coefficient $s_A(T, \mu, \dots)$ is the equilibrium entropy density as a function of the relevant state variables. Because thermal states maximize entropy, quantum thermal states maximize s_A and therefore entanglement in general. As we will see in briefly in Sec. 1.5—as well as Ch. 4 and Ch. 5—for a system prepared in a product state at $t = 0$ (i.e. a state with no entanglement and $S_{A|B} = 0$ at $t = 0$), entanglement entropy grows *linearly* in time until saturating to the value given by Eq. (1.3.16). The time required for the system to thermalize is given by this time for systems with no conserved quantities; in the presence of such conserved charges, thermalization may be further delayed by transport of that charge, as we will see in Ch. 5. While thermalization implies volume-law entanglement entropy, the converse does not hold.

Finally, note that ETH is merely one scenario by which thermalization *can* occur, but it is not the only one. However, it does seem to be fairly generic, supported even by exact numerics for very small systems. These arguments are even more successful in the context of random evolution, for which provable results exist in certain limits, as will be discussed in Ch. 5. Rigorous proofs are otherwise rare, if even possible; ETH should be regarded as a conjecture supported by experimental and general observation, along with various numerical studies and other arguments.

1.4 Many-Body Localization

Anderson published his seminal work on localization in 1958, and was interested in nonergodic behavior, particularly in the context spins in Silicon experiments [10]. That paper, and most work following it, related to noninteracting systems, but was contemporaneously conjectured to survive weak interactions. The insight into nonergodicity was not appreciated until half a century later, when people began considering nonperturbative interactions in such systems more seriously. For the purposes of this section, there will be no need to delve into the rich history of Anderson localization[6], and the noninteracting physics will recover as a simple limit of the general results.

However, it is worth noting that numerous phenomena from single-particle localization or localization in low-temperature systems do not exist in the general setting of MBL. For example, "weak localization" of noninteracting particles subject to low disorder—characterized by a localization length that is large compared to the mean free path—does not seem to have a many-body analogue. While knowledge of single-particle localization has helped shape our present understanding of MBL, it is unwise to assume that aspects of single-particle localization—especially those concerning ground state physics—port over to the nonequilibrium study of MBL.

1.4.1 General formulation

Localization can be understood in a fairly general sense in the following way. Begin by choosing a *local* basis in which the Hamiltonian, $\hat{H}$, is *mostly* diagonal, e.g.

$$\hat{H} \to \hat{H}_{\text{diag}} + \hat{H}_{\text{off}} \quad , \quad \text{such that} \quad \left\|\hat{H}_{\text{diag}}\right\| \gg \left\|\hat{H}_{\text{off}}\right\| \ . \tag{1.4.1}$$

For most of the models studied in the literature, $\hat{H}$ is written in the basis of lattice sites, and is already mostly diagonal in that basis. However, the results for those systems can be extended to slightly more generic systems by a local rotation of basis that brings the Hamiltonian into the form Eq. (1.4.1).

The diagonal term can be regarded as an on-site potential, and may encode diagonal interactions as well. The off-diagonal term corresponds to hopping in the one-body case, and can be viewed as hopping in the rotated basis, or in Fock space. In general, if a system localizes, the correct choice of this basis and decomposition in Eq. (1.4.1) will be obvious. Dynamically, the diagonal term gives phases to the components of $|\psi\rangle$ in the local basis, and the off-diagonal term generates transitions between these basis states.

Suppose that $\hat{H}_{\text{diag}}$ has eigenvalues V_n^0, which for noninteracting $\hat{H}_{\text{diag}}$ correspond to the potential on the generalized site n. The off-diagonal terms "hop" between the $\hat{H}_{\text{diag}}$ eigenstates $|m\rangle$ and $|n\rangle$ [with respective eigenvalues V_m^0 and V_n^0] with coupling $t_{m,n}$,

$$\hat{H}_{\text{diag}} = \sum_{n=1}^{\mathcal{D}} V_n^0 |n\rangle\langle n| \tag{1.4.2}$$

$$\hat{H}_{\text{off}} = \sum_{m \neq n} t_{m,n} |m\rangle\langle n| \ . \tag{1.4.3}$$

For $t_{m,n} \gtrsim |V_n^0 - V_m^0|$, the eigenstates of the diagonal part are strongly mixed, resulting in a delocalized state when $\hat{H}_{\text{diag}}$ is many-body. In the other limit $t_{m,n} \ll |V_n^0 - V_m^0|$, there is minimal

[6]This term is commonly used to refer to localization in noninteracting systems, but many-body localization could easily be called many-body Anderson localization.

mixing, and perturbation theory in the off-diagonal term converges, resulting in "localization" to the corresponding local basis used to recover the diagonal part, with exponentially vanishing tails away from this configuration.

In this case, the eigenstates are localized to a handful of basis states. In this case, blocks of eigenstates of $\hat{H}_{\text{diag}}$ are "detuned," as the energy difference between various local configurations far exceed the coupling strengths of any dynamical process(es) that connect them. Strong spatial disorder can lead to such localization, as can "deterministic" potentials that are incommensurate to the lattice, e.g. quasiperiodic potentials $V(r) = V_0 \cos(k \cdot r)$ for k an irrational multiple of the lattice spacing, destroying *any* translation invariance. Thus, detuning, and not randomness, is the essential feature for many-body localization.

Note that the case where $\hat{H}$ is noninteracting has been studied at length, and differs from the above discussion in some important ways. For example, in one dimension, disordered non-interacting models of spinless fermions, spins 1/2, q-bits, etc., are always localized, although the localization length may be quite large. However, noninteracting models are easier to solve, have been studied at length in the literature, and are not automatically robust to the inclusion of interactions, and therefore not necessarily generic or stable. Thus, we will not worry about them.

Finally, this discussion also applies to the Floquet setting, as the evolution still has eigenstates. For the Floquet case, one ought to compare the difference in eigenphases $|e^{i\theta_n} - e^{i\theta_m}|$ to the coupling $t_{m,n}$, which will only be meaningfully defined modulo $2\pi/T$.

1.4.2 A more specific formulation

More concrete results can be obtained by restricting to two-state systems, e.g. q-bits, spins 1/2, or spinless fermions. Let us work in the spin language, and define the diagonal part of the Hamiltonian

$$\hat{H}_{\text{diag}} = \hat{H}_0 = \sum_{\vec{n}} h_{\vec{n}} \hat{Z}_{\vec{n}} \ , \tag{1.4.4}$$

where $\vec{n}$ are some site-like index, which may have multiple components, and $\hat{Z}_n$ is the Pauli matrix measuring the component of the nth spin along the z direction[7], and

$$h_{\vec{n}} > 0 \, , \quad \text{with} \quad h_{\vec{n}} \neq h_{\vec{m}} \quad \text{if} \quad \vec{m} \neq \vec{n} \ , \tag{1.4.5}$$

are any set of coefficients that do not repeat in any regular pattern as a function of $\vec{n}$, e.g. independently drawn random numbers, or a quasiperiodic function of $\vec{n}$ that is incommensurate to the "lattice." Note that $\vec{n}$ may describe real sites, single-particle orbitals, or any other sensible parametrization of degrees of freedom that is either strictly local or decays exponentially in real space. In general, it is easiest to regard $\vec{n}$ as indexing sites. Whatever the choice of $\vec{n}$, the corresponding Pauli operators must satisfy the usual relation that Pauli matrices on different "sites" commute, i.e. $[Z_{\vec{n}}, Z_{\vec{m}}] = 0$. Also note that this discussion can be extended to Floquet systems as in Section 1.4.1.

The eigenstates of the Hamiltonian given in Eq. (1.4.4) are unentangled, classical product states: letting $\hat{Z}_j|n\rangle = z_j|n\rangle$ for an eigenstate $|n\rangle$, the eigenstates are then enumerated by the various configurations of these local eigenvalues, $\{z_j = \pm 1\}$. Because they are eigenstates of the Hamiltonian, and therefore the evolution operator, these states have no dynamics, and remain unentangled classical product states for all time. No entanglement is generated under the evolution,

[7]This notation is more common in the Quantum Information community. To quote one of my mentors, John McGreevy, "Sight is a valuable commodity. In order not to waste it, let us use $\hat{Z}$ instead of $\hat{\sigma}^z$."

and it is therefore not possible for this model to thermalize in the sense described in previous sections[8], and the system remains localized in the eigenbasis of $\hat{H}_0$. The next step is to address stability to generic perturbations, which must include interactions.

However, localization in Hilbert space [or "Fock" space, as it is often termed in the context of many-body systems], or to any of the basis states, does not give a correct picture of MBL in generic systems. For single-particle localization, one can understand the many-body problem entirely in terms of single-body physics, and single-particle wave functions *can* be localized to a site, $\vec{n}$, but this does not hold for many-body states like $|n\rangle$. Truly, MBL corresponds to localization in the coordinate space $\vec{n}$, and the thing that is localized are the *eigenoperators* $\{\hat{Z}_{\vec{n}}\}$. For $\hat{H}_0$ as defined in Eq. (1.4.4), these operators are *strictly* local in the $\vec{n}$ basis, and possibly exponentially localized in some lattice basis; these operators are *conserved* in the sense that $[\hat{H}_0, \hat{Z}_{\vec{n}}] = [\hat{Z}_{\vec{n}}, \hat{Z}_{\vec{m}}] = 0$, and they are *complete* in the sense that the eigenvalues of all $\{\hat{Z}_{\vec{n}}\}$ fully specify the many-body energy E.

Note that many-body wavefunctions cannot be "local" in any specific or general sense, with the exception of cases where the wavefunction is "separable." However, generally speaking, many-body wavefunctions can only be separable if the problem is not truly many-body, and the many-body wavefunction is merely a [Slater determinant] product of single-body wavefunctions, which can be localized in real space. The more general way to phrase localization is in terms of localization of *operators*, as above; for single-body problems, the operators that are localized measure the occupation of a localized single-body orbital.

While the eigenstates of $\hat{H}_0$ do not have dynamics for trivial reasons, general initial states will not be eigenstates of this Hamiltonian. The dynamics of a general initial state simply involve Larmor precession of the various $\hat{Z}_{\vec{n}}$, with each degree of freedom—indexed by $\vec{n}$—precessing at a different frequency. There is no generation of entanglement as these spins independently precess, nor is there transport, e.g. of energy, for the model defined in Eq. (1.4.4).

To make things many-body, we add weak interactions to $\hat{H}_0$. For the definition of $\hat{H}_0$ in Eq. (1.4.4) to remain sensible, we should only include interaction terms that involve operators acting on two or more sites [or pseudo-sites] $\vec{n}$. In general, we will restrict to the case of two-body interactions, and generally speaking, the terms we add to $\hat{H}_0$ correspond to nearest-neighbor, two-body interactions of degrees of freedoms on the bare, physical sites. One would next rotate the full Hamiltonian to diagonalize all single-body terms—including any such terms that arise from the bare interactions—and these single-particle terms are cast into the form $\hat{H}_0$ in Eq. (1.4.4). This process will rotate a given interaction term into terms that flip one or more of the eigenvalues of a given $\hat{Z}_{\vec{n}}$, and likely also result in interactions between these operators, e.g. of the form $J_{mn}\hat{Z}_{\vec{n}}\hat{Z}_{\vec{m}}$.

Provided there are no degeneracies, this many-body localized structure is perturbatively stable to interactions, provided the strength of interactions is weak compared to the overall scale of the coefficients h in Eq. (1.4.4). When this happens, the terms that flip the values of the local operators $\hat{Z}_{\vec{n}}$ can be treated using perturbation theory to modify the single-body $\{\hat{Z}_{\vec{n}}\}$, and the perturbation series converges. This was a primary result of the work of Basko, Aleiner, and Altschuler [11], and was also posited by Anderson in ref. 10. The vanishing of transport in the single-body case will prove generic to many-body localized systems, but other dynamical properties, e.g. the generation of entanglement, will be modified in the presence of interactions.

[8] As a minor caveat, if the ground state of $\hat{H}_0$ [or of $-\hat{H}_0$] is unique—i.e., nondegenerate—then that particular state will obey ETH because of this uniqueness, according to David Huse.

1.4.3 The many-body localized phase

For models with short-range interactions, there are a number of cases where MBL is fairly well understood. To clarify,

Definition 1.7. For interactions or hopping terms in many-body quantum systems to be *short-ranged*, the coupling strengths for terms connecting distant points in real space must decay exponentially in the distance, and sufficiently rapidly for this decay to be evident on reasonable—i.e. subextensive—scales.

Nearest-neighbor and next-nearest neighbor interactions are the most common examples. Such short-ranged models have the same general structure as $\hat{H}_0$, as defined in Eq. (1.4.4). The key feature that gives rise to the properties of the MBL phase is the existence of a complete set of local integrals of motion (or "LIOMs," also referred to as "ℓ-bit," in contrast to the naïve, physical degrees of freedom, which are "p-bits") [20]. In general, the LIOM is associated to the *operator* $\hat{\tau}_n^z$, which is conserved by the dynamics, while the ℓ-bit is the degree of freedom that is *measured* by $\hat{\tau}_n^z$. The LIOMs are defined by:

Definition 1.8. A complete set of local integrals of motion (LIOMs) is defined by a set of operators acting on psuedo-spin degrees of freedom, $\{\hat{\tau}_n^z\}$. These objects are *local* in the sense that the support of the nonidentity component(s) of $\hat{\tau}_n^z$ decays exponentially in the distance from some primary locus in real space, e.g. site n. The term "integral of motion" denotes that these quantities are *conserved*:

$$[\hat{\tau}_n^z, \hat{\mathcal{U}}] = [\hat{\tau}_n^z, \hat{\tau}_m^z] = 0 \ , \tag{1.4.6}$$

where $\hat{\mathcal{U}}$ is the unitary evolution operator, corresponding to Hamiltonian or Floquet dynamics. This set of operators is "complete" in that the eigenvalues—and eigenstates—of the evolution $\hat{\mathcal{U}}$ are fully and uniquely specified by enumerating all possible configurations of the ℓ-bits in the basis of the operators $\{\hat{\tau}_n^z\}$.

In the MBL phase, the Hamiltonian can be expressed purely in terms of the operators $\{\hat{\tau}_n^z\}$, and operators such as $\hat{\tau}_n^x$ do not appear, as in Eq. (1.4.7): there are no "dynamics" of the ℓ-bits. The MBL phase therefore has an extensive number of conserved quantities, i.e. an *emergent integrability*; unlike proper integrable systems, here the conserved quantities are *localized* 2. Note that this framework applies equally well to single-particle Anderson localization [10], where the ℓ-bits correspond to localized single-particle orbitals, and the LIOMs are the "occupancies" of those orbitals. In that case, the ℓ-bit is a two-state degree of freedom; in general cases, the ℓ-bit will always have the same dimension as the p-bits, i.e. the local Hilbert space dimension in real space. In the literature, it is common to default to q-bits (i.e., a two-state local Hilbert space), but the generalization to q-dits (i.e., a d-state local Hilbert space) is trivial.

Regarding the diagonal Hamiltonian, $\hat{H}_0$, from Eq. (1.4.4), one notes that this Hamiltonian has already been cast into the ℓ-bit language by construction, with $\{\hat{Z}_{\vec{n}}\}$ the corresponding LIOMs. The important point is that, in the best understood version of the MBL phase, turning on a weak interaction term $\hat{H}_{\text{int}}$ "dresses" these LIOMs (and corresponding ℓ-bits) via perturbation theory in the interaction terms, in a manner analogous to the dressing of noninteracting electrons to form effectively free quasiparticles with dressed properties in Landau's Fermi liquid. In contrast to the Fermi liquid, where the quasiparticle lifetime is infinite only precisely at the Fermi surface, the "quasiparticles" of the MBL phase have an infinite lifetime, and are therefore perfectly stable.

Note that there may be other types of MBL beyond this description, e.g. in models with long-range interactions, or other scenarios. However, this point remains largely speculative and unresolved at the time of writing.

In one spatial dimension and for a particular Hamiltonian model, there exists a proof due to John Imbrie [21] that MBL exists in the above described form. This proof accounts for nonperturbative effects, and makes the assumption that there is limited attraction between energy levels so that eigenenergies do not accumulate at certain values and cause the denominators that arise in perturbation theory to diverge. While this assumption has led some to regard Imbrie's work as a derivation and not a proof, it is worth noting that while there does not exist a rigorous proof of Imbrie's assumption, there are few if any models that are not fine-tuned and known not have this property. Given the physical reasonability of this assumption, Imbrie's work can be regarded as a rigorous proof of the stability of a particular $\hat{H}_0$ to sufficiently weak interactions $\hat{H}_{\text{int}}$ of a particular form. The form of $\hat{H}_0$ and $\hat{H}_{\text{int}}$ considered should be fairly generic, implying the procedure may be replicated for other models.

In terms of the ℓ-bits, the full Hamiltonian $\hat{H}$ given by Eq. (1.4.1) takes the generalized Ising form

$$\hat{H} = \sum_{n=1}^{L} \tilde{h}_n \hat{\tau}_n^z + \sum_{\substack{m,n=1 \\ m>n}}^{L} \tilde{J}_{m,n} \hat{\tau}_m^z \hat{\tau}_n^z + \dots \ , \tag{1.4.7}$$

where the omitted terms $\dots$ above contain higher-order terms involving only the z component of the ℓ-bit operators. Additionally, these terms decay exponentially quickly in the largest separation between any two ℓ-bits involved, and terms acting on a greater number of ℓ-bits generally have smaller coefficients. All such terms are *diagonal* in the ℓ-bit basis, and these terms arise from rotating away all off-diagonal terms in $\hat{H}_{\text{off}}$. Since the $\dots$ terms contain interactions between the ℓ-bits involving arbitrary numbers of bodies, this model is local because it is diagonalized by a set of local operators. If this prescription works, in the one dimensional MBL phase, the single-particle terms must be dominant.

Note that the definitions of the ℓ-bits are *not unique*. This is rarely mentioned in the literature, but actually recovering an ℓ-bit description for a given model is generally not an easy task. However, in general, the ℓ-bits are local: the rotations that diagonalize $\hat{H}_{\text{off}}$ should be local, and it may be possible to get a fairly accurate version of the LIOMs by truncating to some specified order in perturbation theory or, somewhat equivalently, using a shallow-depth unitary circuit of finite depth.

1.5 Localized vs. Thermal Phases

Both thermal phases, described in Section 1.3, and many-body localized phases, described in Section 1.4, are proper phases of matter, with an unconventional, nonequilibrium, nonthermodynamic phase transition between the two. This transition can be regarded as a transition of the *eigenstates*, or relatedly, a dynamical transition: whereas thermodynamic phase transitions correspond to singularities in thermodynamic quantities, e.g. free energies, the many-body [de-]localization transition may be observed in the resulting dynamics, e.g. vanishing transport in the MBL phase. Studying this nonequilibrium phase structure will be the subject of Ch. 6, but this section will cover some introductory aspects. An early overview comparing the thermal (ergodic, ETH) phase, the MBL phase, and single-particle Anderson localization—taken from Ref. 12—is given in Table 1.1. These results will be explained in this section.

Thermal	Single-particle localized	Many-body localized
Memory of initial conditions 'hidden' in global operators at long times	Some memory of local initial conditions preserved in local observables at long times	Some memory of local initial conditions preserved in local observables at long times
ETH true	ETH false	ETH false
May have nonzero dc conductivity	Zero dc conductivity	Zero dc conductivity
Continuous local spectrum	Discrete local spectrum	Discrete local spectrum
Eigenstates with volume-law entanglement	Eigenstates with area-law entanglement	Eigenstates with area-law entanglement
Power-law spreading of entanglement	No spreading of entanglement	Logarithmic spreading of entanglement
Dephasing	No dephasing	Dephasing
Dissipation	No dissipation	No dissipation

Table 1.1: Comparison of thermal (ETH), single-particle (Anderson) localized, and many-body localized (MBL) phases, taken from Ref. [12].

1.5.1 The "standard model" for MBL-ETH

Unlike the model of high energy particle physics bearing the same moniker, the "standard model" of MBL is not so-named for any physical reason. It is not even necessarily a "good" model, merely one that was utilized during the first studies of MBL as a strictly nonequilibrium phenomenon. The model is the isotropic spin-1/2 Heisenberg chain with antiferromagnetic couplings[9] and on-site disordered magnetic fields, given by

$$\hat{H}_{\text{std}} = \frac{J}{4}\sum_{j=1}^{L-1}\left(\vec{\sigma}_j\cdot\vec{\sigma}_{j+1}-\hat{\mathbb{1}}\right) + \frac{1}{2}\sum_{j=1}^{L}h_j\hat{\sigma}_j^z \tag{1.5.1}$$

$$= \underbrace{\frac{J}{2}\sum_{j=1}^{L-1}\left(\hat{\sigma}_j^+\hat{\sigma}_{j+1}^- + h.c.\right)}_{\text{hopping}} + \underbrace{\frac{J}{4}\sum_{j=1}^{L-1}\hat{\sigma}_j^z\hat{\sigma}_{j+1}^z}_{\text{interactions}} + \underbrace{\frac{1}{2}\sum_{j=1}^{L}h_j\hat{\sigma}_j^z}_{\text{disorder}}\ , \tag{1.5.2}$$

where $\vec{\sigma}_j = \left(\hat{\sigma}_j^x,\hat{\sigma}_j^y,\hat{\sigma}_j^z\right)$, $\hat{\sigma}_j^+ = |\uparrow_j\rangle\langle\downarrow_j|$, $\hat{\sigma}_j^- = |\downarrow_j\rangle\langle\uparrow_j|$, and the fields $\{h_j\}$ are independently drawn (i.i.d.) random numbers, sampled equiprobably from the interval $[-h,h]$, where the parameter h controls the overall strength of disorder. The model is clearly strictly local, involving only on-site and nearest-neighbor terms, and has an overall $U(1)$ symmetry corresponding to conservation of $\hat{S}^z = \sum_j\hat{\sigma}_j^z$, where it is typical to restrict to an even number of sites, L, and half filling, $\hat{S}^z = 0$. Being Hamiltonian, this model has a conserved energy, $\hat{H}$. It is also standard to consider open boundaries: there is neither computational nor analytical advantage to periodic boundaries—usually invoked to construct momentum eigenstates—due to disorder, which breaks translation invariance; additionally, it is easier to measure numerically the bipartite entanglement entropy on an open chain; finally, compared to periodic boundaries, one can meaningfully measure correlation functions to twice the distance for a chain of size L on an open chain (nothing can be farther than $L/2$ from anything else on a ring).

[9]For highly excited states and in the presence of sufficiently strong disorder, these signs don't appear to matter. This includes repulsive versus attractive interactions, which I checked numerically at one point.

One subideal feature of the Hamiltonian given in Eq. (1.5.2) is that, in the limit $h \to 0$, the Hamiltonian is both non-Abelian and integrable. In the limit of no disorder, this model becomes the Heisenberg ferromagnet, which has a more complicated $SU(2)$ symmetry in which all components of spin, $\hat{S}^x$, $\hat{S}^y$, and $\hat{S}^z$, are conserved, and do not commute with one another. Such complications are not generic. A better choice of "standard model" would have been a Floquet model with no extensive conserved quantities, well away from any integrable point, even in the limit of vanishing disorder, to better and more independently probe various physics.

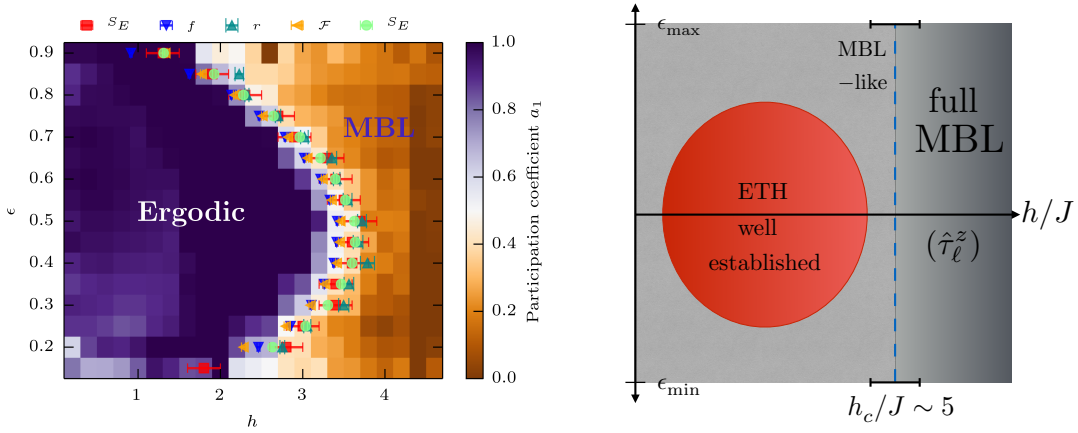

(a) Numerics. (b) Theory.

Figure 1.2: Figure (a)—reprinted with permission from Ref. 22 [David J. Luitz, Nicolas Laflorencie, and Fabien Alet, *Phys. Rev. B*, **91**, 081103(R), Feb. 2015] Copyright (2015) by the American Physical Society—shows numerical evidence for the MBL phase diagram for the "standard model" out to $L = 22$ sites using a variety of measures. Figure (b) represents Sketch of the phase diagram for the "standard model," representing a combination of numerical studies of finite systems and other analytical results, which should hold in the thermodynamic limit $L \to \infty$. Note the error bars on the location of the MBL transition. The vertical axes in both represent the energy density, ϵ, normalized in the full range from the ground state to most excited state; the horizontal axis, h/J, is the strength of disorder normalized by that of interactions (and hopping terms).

Nonetheless, the "standard model" has been studied at length numerically: a phase diagram based on state-of-the-art numerics is reproduced in Fig. **??**(a) from Ref. 22. In these numerical studies, one fixes the symmetry sector—i.e. total magnetization, $\hat{S}^z_{\text{tot}}$—generally focusing on the largest sector, which has equal numbers of up and down spins. One then varies the ratio of the parameters h and J, often working at infinite temperature, in which case all energies are equiprobable. In this case, the expectation value of an observable is given by the expectation value in an eigenstate of the Hamiltonian, averaged over all eigenstates with equal weight. In practice, to reproduce such spectral averages it is sufficient to use Lanczos algorithms and study a handful of states (say, 50) from the middle of the spectrum.

However, other studies sample throughout the spectrum, as shown in Fig. **??**(a), motivated by the notion of mobility edges from single-particle localization. In the latter case, eigenstates at the "edges" of the energy band are localized, while a window of states in the middle of the spectrum are delocalized. However, the "fully" many-body localized phase is characterized by a *complete* set of local integrals of motion, which can only be reconciled with localization throughout the entire many-body spectrum. The full MBL phase is the only one known to exist in the thermodynamic limit. However, as depicted in Fig. 1.2b(b), there may exist "weak" MBL phases, or MBL-like

phases, that do feature such phenomena, and hence we have allowed for such a many-body mobility edge beneath the full MBL transition, where states at the outer edges of the spectrum may be MBL, but not in the sense of having a complete set of LIOMs (i.e. $\{\hat{\tau}^z_\ell\}$ operators). However, the current expectation is that the thermal (i.e. ergodic, or ETH) region of Fig. 1.2b(b) may in fact grow in extent in the thermodynamic limit.

Definition 1.9. The *strong*—or *full*—MBL phase is characterized by a complete set of LIOMs, which characterize the entire spectrum of eigenstates of the evolution operator. Therefore, this phase is only well-defined in the Hamiltonian and Floquet settings, and by construction precludes a "mobility edge," e.g. of the type found in single-particle localized systems in $d > 1$. The strong or full MBL phase is a robust phase of matter, and the only type of MBL known to exist in the thermodynamic limit. This phase is essentially known to be limited to one spatial dimension ($1d$).

The strong MBL phase should be contrasted with another type of localization, which we refer to as "weak MBL."

Definition 1.10. *Weak* MBL refers to systems that appear to show all of the properties of strong MBL. They are "weak" in the sense that they are not "strong." Systems realizing weak-MBL may differ from strong MBL in that: they are not robust to generic perturbations; the localization physics is only dynamically realized on short time scales (also known as "pre-thermal" regimes); the localization physics is limited to finite sizes and does not survive upon taking the thermodynamic limit; the system does not feature a complete set of local integrals of motion that satisfy Definition 1.8; and possibly other points of comparison. Compared to strong MBL, weak MBL is far more accessible both experimentally and numerically, and therefore should not be discounted. However, it does not share the most impressive feature of strong MBL, which is to say that it is generally not a phase of matter.

Whether there exist versions of MBL that differ from the definition of strong MBL (Def. 1.9) but still manage to realize a phase of matter remains an open question. Note that the numerical phase diagram in Ref. 22 must be taken with a grain of salt because of the existence of weak MBL. While most numerical studies report a critical disorder strength of roughly $h_c/J \approx 3.5$, the theoretical phase diagram in Fig. 1.2b—meant to capture the thermodynamic limit—extends the critical value out to five to be safe, and includes error bars to emphasize the fact that it is presently unclear the extent to which the numerical studies of Ref. 22 are capturing full MBL, as opposed to its weaker variants.

Note that a phase diagram of the form given in Fig. 1.2b should hold roughly for a model that is quasiperiodic, rather than disordered, likely with a different value of h_c/J, where h refers to the strength of the deterministic spatial potential, which should be incommensurate with the lattice. The main difference between quasiperiodicity versus disorder should be sample-to-sample variations, especially in the properties of eigenstates and the various measures of thermalization versus localization.

1.5.2 Comment on techniques

Due to the complicated and generic nature of these systems, most of studies rely upon exact or nearly exact numerics for extremely small systems. A number of studies have focused on

dynamical aspects of ETH/MBL, which allows for the study of roughly 30 spins 1/2 by using Krylov spaces [23]. Others examine the properties of eigenstates—which were shown in Sec. 1.3.4 to be valid ensembles—generally sampled from the middle of the spectrum. Other studies use the infinite temperature ensemble (as $T \to \infty$—i.e., $\beta \to 0$—the standard Gibbs-Boltzmann weight $e^{-\beta \hat{H}} \to \hat{\mathbb{1}}$), which is also what happens in systems with neither symmetries nor continuous time translation invariance. In most cases, such spectral averages are well approximated by sampling a handful of states (i.e. roughly 50) from the middle of the spectrum, allowing for the use of Lanczos diagonalization methods. Such techniques can describe roughly 25 spins 1/2.

In general, progress is made in solving a given quantum system using some simplifying assumptions. For example, in studying equilibrium systems at $T = 0$, one can restrict to the ground state, and possibly low-lying excitations, and use procedures such as the density matrix renormalization group (DMRG) [24, 25] to target the lowest energy state in each "update," and restrict to a manifold of states with extremely low entanglement. For translation invariant model, it is possible to use the "infinite" version, iDMRG, and find the ground state of an infinite system by studying a handful of sites. In the setting of MBL versus ETH, one is interested in arbitrarily excited states of interacting, disordered models (i.e. those without translation invariance and for which the Hilbert space does not factorize), which may not have any simplifying symmetries, and are known—in the thermal phase—to have an entanglement entropy that scales with the volume of a given region. Each of these individually is enough to kill most techniques. Additionally, most perturbative techniques rely on perturbing about a noninteracting and homogenous part of the Hamiltonian, i.e. a hopping term. However, such techniques treat *both* interactions and disorder perturbatively, yet it is now well established that these two terms determine whether a system is MBL or thermal, and that there exist a number of nonperturbative instabilities that must be considered. Therefore, perturbing in either—let alone both—of these quantities is not a reliable way to study nonequilibrium phase structure.

However, one phenomenological property of MBL phases is that their highly excited states have most or all of the properties of quantum ground states, i.e. area-law entanglement and the ability to host quantum order and quantum phase transitions. This insight has led to the adaptation of several techniques used to study ground-state physics to the MBL setting, but these techniques are generally not useful on the thermal side, or near the many-body delocalization transition, which is theorized to be governed by Griffiths—or "rare region"—effects.

The first example is the strong disorder renormalization group (SDRG), also known as the real space renormalization group (RSRG), sometimes written as RSRG-X in the literature when applied to excited states in the context of MBL. These techniques coarse-grain the Hamiltonian in real space, diagonalizing the strongest terms first, and fixing their state, and generating new couplings between neighboring degrees of freedom at lowest order in perturbation theory. For certain systems, e.g. the disordered Ising chain, each step results in a Hamiltonian of the same form, with a single site fixed in a particular state, i.e. $|\uparrow\rangle$, and the sites on either side are coupled perturbatively, and the site that was fixed is "frozen in." However, this theory requires the assumption of strong disorder: if there are nearby terms—especially those that do not commute—with comparable couplings, the technique is no longer valid. Assuming strong disorder, each step of the RG only strengthens the disorder distribution: if the technique is valid, the model flows to infinite disorder (and associated infinite disorder critical points / fixed points), and is asymptotically exact in that limit. However, there are conjectures that certain transitions only hold in the infinite disorder limit. These properties and several implementations of RSRG-X will appear in Ch. 6. It is worth noting that RSRG ignores a lot of "quantumness" as it fixes the wavefunction into a classical product state in certain cases. In other cases, e.g. those characterized by "random-singlets," some

entanglement is generated, but the maximal scaling with the size of a region is $\log L$, short of the volume law entanglement of thermal phases. Therefore, RSRG-X of this type essentially cannot resolve thermal eigenstates.

Another technique that works deep in the [full] MBL phase is an adaptation of DMRG to excited states, DMRG-X [26]. This technique relies on the fact that MBL eigenstates have area-law entanglement, and are therefore amenable to the entanglement-truncation procedure exploited by DMRG-X. However, this technique necessarily breaks down near the transition, and is therefore not capable of answering most of the outstanding questions surrounding nonequilibrium phases. Without being overly dismissive, it is also unlikely that DMRG-X can provide insight beyond that afforded by a knowledge of the existence of local integrals of motion. Additionally, the technique may not be valid outside the MBL regime that is characterized by a complete set of LIOMs.

Finally, other techniques, such as the numerical linked-cluster expansion (NLC), are often only truly useful on the thermal side of the transition, and only provide access to larger systems when considering particular quantities, e.g. entanglement entropy. For this technique in particular, it is possible to measure the entanglement entropy of a generic system out to twice as many sites as one could study using exact numerics (and not Lanczos methods). However, a mere doubling (i.e. $L = 30$ instead of $L = 15$) is not justified compared even to Lanczos and shit-invert methods considering the inexact nature.

1.5.3 Spectral properties

A particularly transparent heuristic of "quantum chaos" or thermalization is afforded by spectral properties. As systems without any time-translation invariance do not have an eigenspectrum for their evolution, such systems cannot be diagnosed in this way, and we restrict to Floquet and [time-independent] Hamiltonian systems. A key fingerprint of chaos is given by *level repulsion*: the energy levels of a thermal system know about one another and repel. This is related to "avoided crossings" from standard perturbation theory: thermal quantum systems constitute a phase of matter, and are therefore robust to perturbations, and so weakly perturbing the model will adjust the levels, which will not "cross" but rather "repel." Other intuitive pictures may be presented in the literature.

In contrast, integrable models and MBL systems have an extensive set of local conserved quantities. Thus, the *many-body* spectrum is recovered from populating an extensive number of independent quantum numbers. Because these quantities are independent, albeit for different reasons, the distribution of levels of integrable and MBL systems realizes the *Poisson* distribution. Thermal systems, on the other hand, realize Wigner-Dyson distributions corresponding to the symmetries present in the model. Much of our understanding of this matter comes from random matrix theory (RMT), and in fact, an intuitive picture is that thermal systems ought to have the properties of random matrices. This will be explored and utilized more explicitly in Ch. 5.

In Hamiltonian [Floquet] systems, the "spectrum" refers respectively to the set of energies [pseudoenergies]. A useful diagnostic is the "r ratio" [27], defined by

$$r = \sum_{n=2}^{\mathcal{D}} \frac{\min\left(E_{n+1} - E_n, E_n - E_{n-1}\right)}{\max\left(E_{n+1} - E_n, E_n - E_{n-1}\right)} , \tag{1.5.3}$$

where $n \in \{1, 2, \ldots, \mathcal{D}-1, \mathcal{D}\}$ labels the energy [pseudoenergy] eigenvalues in ascending order. It is also typical to average r over an ensemble of similar systems; at infinite temperature it often suffices to sample a finite set of eigenvalues from the middle of the spectrum. The r-ratio is used as a diagnostic of the ETH-MBL transition in the "standard model," as can be seen in Fig. 1.2a.

In both MBL and integrable models, there are many levels that are unrelated to one another: in the former case, because the model is localized, and the eigenvalues of LIOM operators that are well separated in real space are unrelated and do not repel (i.e. this can be derived directly from the ℓ-bit formalism, but also follows generally from the notion of localization); in the latter case, there are extensively many symmetry sectors that are independent, and thus do not repel. For general models with a symmetry, the r ratio should be computed within a symmetry sector to avoid spuriously Poisson values. The value in the Poisson case (uncorrelated spectrum) is known

$\langle r \rangle$	Orthogonal	Unitary	Symplectic
Gaussian	0.535898	0.602658	0.676168
Circular	0.526922	0.596543	0.671921
Poisson	0.386294		

Table 1.2: Expected values of the r statistic, defined in Eq. (1.5.3), for various ensembles, quoted from Ref. [27].

exactly, corresponding to $r = 2\ln 2 - 1 \approx 0.38$. For the Wigner-Dyson ensembles, the values are known theoretically but only to numerical accuracy. The expected values can be found in Table 1.2. Hamiltonian systems fall into one of the Gaussian ensembles: those with time reversal symmetry correspond to the Gaussian orthogonal ensemble (GOE), those without time reversal symmetry (i.e. chiral Hamiltonians) correspond to the Gaussian unitary ensemble (GUE), and symplectic ensembles (GSE) refer to systems with time-reversal but no other "rotational" symmetries, and are less common. Circular ensembles are the equivalent of Gaussian ensembles for unitary matrices, and hold for Floquet systems, falling into the same three categories with the same relation to symmetry.

In addition to the r ratio, another simple measure of spectral rigidity is the spectral form factor, to which much of Ch. 5 is devoted. The spectral form factor probes two point-correlations of the density of eigenvalues of the evolution operator, and provides a coarse-grained snapshot of the system that can appear to favor quantum chaos, especially in numerical simulations [28]. However, it can be used to extract other useful information. This quantity will be discussed in more detail in Ch. 5.

1.5.4 Entanglement entropy

As discussed in Sec. 1.3, for quantum systems in a thermal phase, both eigenstates and late-time states following a quench are expected to show volume-law entanglement. Specifically, this means that the von Neumann entropy associated with a bipartition of isolated quantum degrees of freedom, $\mathcal{S}$, into a system, $\mathcal{A}$, and bath, $\mathcal{B}$—defined in Eq. (1.3.15)—scales with the volume of $\mathcal{A}$[10]. For a one dimensional system this implies for the entanglement entropy

$$S_{A|B} = -\mathrm{Tr}\,\hat{\rho}_A \ln \hat{\rho}_A \ = \alpha\,\mathrm{Vol}\,(\mathcal{A}) \propto L_A^d \ , \tag{1.5.4}$$

where d is the spatial dimension. Additionally, thermal systems maximize entropy, and thus the coefficient of proportionality, α, should be the maximal one. As an aside, there will be variations between eigenstates and realizations of disorder in any given measurement.

[10] In general, the entanglement entropy is limited by the smaller of the two components; however, per the formalism used in Sec. 1.3, this must always be $\mathcal{A}$.

In localized phases, one expects area law entanglement, much like one expects in quantum ground states. In single-body and many-body localized phases, this is easily understood as a direct consequence of the existence of exponentially localized eigenoperators (i.e. the LIOMs, $\{\hat{\tau}^z\}$). The entanglement across a bipartition of the system scales with the extent to which information about the state—encoded entirely in the LIOMs themselves—crosses the cut. Since the ℓ-bits upon which the LIOMs act are exponentially localized in real space, as are the LIOMs themselves, the amount of entanglement of the region $\mathcal{A}$ of the system falls off exponentially with the distance from the entanglement cut. Hence, for all practical purposes, the entanglement entropy scales with the size of the cut itself, which is one dimension lower than the system itself, and thus, an "area law" (in the typical setting of $d = 1$, this corresponds to a constant independent of the system's length) [29].

In some sense, volume-law scaling of entanglement with system size is a defining feature of the thermal phase, and area-law entanglement away from the ground state is a feature of localized phases. Additionally, systems described by a model that sits exactly at a quantum phase transition—also known as "critical systems"—are expected to show logarithmic scaling of entanglement entropy [30]. This is a natural result of having correlations on all length scales, and in equilibrium, is closely connected to conformal field theory. Whether or not nonequilibrium critical *phases* exist is an interesting and largely open question [31–33], which will appear in Ch. 6. As a final note, in $d = 1$, it is extremely difficult to differentiate between area-law, logarithmic, and volume-law dependence on subregion size, which generally is limited to roughly fourteen sites in the best cases.

An interesting feature of the ETH-MBL transition is that the entanglement entropy changes between volume- and area-law scaling across the transition. In contrast, quantum phase transitions—which occur at $T = 0$ in quantum models as one tunes another parameter (e.g. magnetic field)—are between two phases with area-law entanglement. Thermal phase transitions, which are the most familiar and common, are between two phases with volume-law entanglement (i.e. both phases are thermal). At the time of its discovery, the MBL-ETH transition was the first of this type; since then, additional such transitions have been uncovered. For example, the highly entangled state of an otherwise thermal system can be reduced to an area-law state by repeated local measurements, which "collapse" the corresponding degrees of freedom, spoiling any entanglement they may have had with their surroundings [9].

1.5.5 Entanglement production

For thermal systems, mechanisms for the production of entanglement evolving from an initial product state (i.e. a quench from an unentangled initial state) will be discussed in Ch. 4, using insights from integrability, and Ch. 5, using random circuits and the technology of "quantum chaos." The general expectation is that entanglement entropy in thermal—as well as integrable—systems following a quench should grow linearly in time [9, 19, 34].

The fact that eigenstates of the evolution operator in the full MBL phase have area-law (i.e., constant for the standard $1d$ setting) entanglement might lead one to believe that entanglement is uninteresting in the MBL phase. While this is true in the single-body case, where the lack of interactions limit substantially the spread of entanglement, the MBL phase is actually more interesting, and grows logarithmically in time. Although this was brought to the general attention of the community by Ref. 35, as with many matters related to the various areas of physics that appear in this thesis, this was pointed out several years before by Prosen and collaborators in Ref. 36. This was also shown directly from the LIOM picture in Ref. 29. Eventually, the entanglement entropy grows to a maximal late-time value with volume-law scaling; this late-time value

may have a lower coefficient of proportionality than one expects for thermal systems.

Let us consider a quantum quench in an MBL phase from an initially unentangled state. Consider the phenomenological model of an MBL phase, given by the ℓ-bit Hamiltonian defined in Eq. (1.4.7),

$$\hat{H} = \sum_{n=1}^{L} \tilde{h}_n \hat{Z}_n + \sum_{\substack{m,n=1 \\ m>n}}^{L} \tilde{J}_{m,n} \hat{Z}_m \hat{Z}_n + \dots \ , \tag{1.4.7}$$

where, as a reminder, the coefficient of higher n-body terms generally have smaller coefficients than fewer-body terms, which also necessarily fall off more quickly on average. In this basis, the eigenstates of the Hamiltonian are at most area-law entangled in the naïve basis (i.e. the real space "p-bits"), and are unentangled in the basis of ℓ-bits upon which the LIOMs, $\{\hat{Z}_n\}$ (or $\{\hat{\tau}^z_n\}$ in the literature), act.

For the initial state, $|\psi(0)\rangle$, we choose a physically preparable pure state that is an unentangled tensor product over configurations physical sites, i.e., a product state in the p-bit basis. States of this type will have area-law entanglement in the basis of ℓ-bits; crucially, the initial state is not an eigenstate of $\hat{H}$ in Eq. (1.4.7). We will also consider other initial states that are not in a local eigenstate of *any* of the LIOMs that fully specify $\hat{H}$. For example, the eigenstates of $\hat{H}$ are given by enumerating the eigenvalues of the LIOMs, $\{\hat{Z}_n\}$; we allow for initial states that are product states of $\{\hat{X}_n\}$, where $\{\hat{Z}_n, \hat{X}_n\} = 0$. The LIOM operator $\hat{Z}_n$ is conjugate to $\hat{X}_n$: each operator flips back and forth between the eigenstates of the others, as with the corresponding Pauli matrices.

We now imagine replacing all many-body terms in Eq. (1.4.7) with an "effective" two-body interaction,

$$\sum_{m,n} J^{\text{eff}}_{mn} \hat{Z}_m \hat{Z}_n = \sum_{m,n} \left[J^{(2)}_{mn} \hat{Z}_m \hat{Z}_n + \sum_p \left[J^{(3)}_{mnp} \hat{Z}_m \hat{Z}_n \hat{Z}_p + \sum_q \left[J^{(4)}_{mnpq} \hat{Z}_m \hat{Z}_n \hat{Z}_p \hat{Z}_q + \dots \right] \right] \right] \ , \tag{1.5.5}$$

which encodes all higher-body terms in a mean-field sense. The precise details will not be important to this analysis. However, we do expect

$$J^{\text{eff}}_{m,n} \sim J_0 \exp\left(-|n-m|/\zeta_z\right) \ , \tag{1.5.6}$$

where ζ_z need not be the same as the decay length associated with $J^{(2)}_{mn}$ or any other length scale in Eq. (1.4.7). It is expected to be $O(1)$. The effective Hamiltonian is then given by

$$\hat{H} = \sum_{n=1}^{L} \tilde{h}_n \hat{Z}_n + \sum_{\substack{m,n=1 \\ m>n}}^{L} J^{\text{eff}}_{mn} \hat{Z}_m \hat{Z}_n \ , \tag{1.5.7}$$

which is Ising-like, but nonetheless acts nontrivially on the states we will consider.

Our initial states are unentangled in some basis, and we now address how the Hamiltonian given in Eq. (1.5.7) generates entanglement. While it is possible for one-body terms close to the entanglement cut to generate entanglement when acting on a product state of p-bit configurations, such terms cannot generate entanglement in the bulk of either region, $\mathcal{A}$ or $\mathcal{B}$, and are therefore not the dominant process. such terms do not generate entanglement acting on product states prepared in the $\{\hat{X}_n\}$ basis.

The dominant contribution to entanglement production is the two-body term, and in particular, the terms in which $\hat{Z}_m$ acts in the bulk of $\mathcal{A}$ and $\hat{Z}_n$ acts in the bulk of $\mathcal{B}$ or vice versa. Because the Hamiltonian is strictly local, the number of such terms that have $O(1)$ coefficients scales with the boundary delineating $\mathcal{A}$ and $\mathcal{B}$. For the $1d$ system of interest, this is an $O(1)$ number. Of

course, there are $O(L^2)$ terms with vanishing coefficients, which are negligible. The ability of any such term to entangle $\mathcal{A}$ and $\mathcal{B}$ can be rigorously bounded in such local models by

$$\frac{dS(\mathcal{A})}{dt} \leq c \left\| J^{\text{eff}}_{mn} \hat{\tau}^z_m \hat{\tau}^z_n \right\| \ , \tag{1.5.8}$$

where c is a constant that can be computed numerically [29]. Essentially, the maximum entanglement entropy that can be generated in $\mathcal{A}$ by a unitary operator of the form $\exp\left(-i\hat{O}_{AB}t\right)$ acting notrivially on both $\mathcal{A}$ and $\mathcal{B}$ is bounded by the logarithm of the local Hilbert space dimension (in region $\mathcal{A}$) on which it acts. In general, the maximum is saturated when $t\hat{O}_{AB} \sim 1$ is order unity. This occurs when

$$t\, J_0 \exp\left(-|n-m|/\zeta_z\right) \approx 1 \ , \quad \text{i.e.} \quad r_{\text{ent}}(t) = \zeta_z \log\left[J_0 t\right] \ , \tag{1.5.9}$$

is the distance over which ℓ-bits are entangled. Essentially, all spins within $r_{\text{ent}}(t)$ of the cut at time t are entangled. Physically, entanglement is generated because the physical state at a given time is a product over ℓ-bits not oriented directly along the z axis, and the Hamiltonian causes the ℓ-bits to precess about the z axis at a rate dependent on the orientation of other ℓ-bits, some of which are on the other side of the entanglement cut.

The size of the entangled subregion of $\mathcal{A}$ grows logarithmically in time until it spans the entirety of $\mathcal{A}$, at which point it will be proportional to L_A, i.e. volume-law. However, as previously mentioned, it is generally expected that the coefficient of proportionality, α, in the volume law $S(\mathcal{A}) = \alpha L_A$, will generally be less than the thermal coefficient. However, initial states corresponding to $\{\hat{X}_n\}$ eigenstates are a notable exception, due to dephasing. In general, there may be other states that are weird, though it is worth noting that the $\{\hat{X}_n\}$ states may not be experimentally feasible.

1.5.6 Operator spreading

The general understanding of information propagation in many-body quantum systems relies heavily either on concepts from transport or the existence of well-defined quasiparticle excitations. However, recent scrutiny of quantum systems with neither particle-like excitations nor extensive conserved quantities that can be transported has motivated the development of other means to study the propagation of information, motivated by ideas from the quantum information and quantum computation communities. Operator spreading captures many universal features of other measures of information spreading, and is more generic than entanglement spreading, e.g.

Operator spreading for thermal systems will be discussed in Ch. 4, which describes the transport of extensive conserved quantities using broken integrability, and Ch. 5, which will briefly address operator spreading in generic chaotic systems, which need not have any notion of a quasiparticle or any extensive conserved quantities.

In localized systems it is natural to expect that there exist many operators that do not spread at all, and that generic operators may spread slowly. For example, the LIOM operators, $\{\hat{Z}_n\}$ ($\{\hat{\tau}^z_n\}$ in the literature), commute with the evolution operator, and therefore do not spread. In fact, they do not do anything under the dynamics generated by the Hamiltonian given in Eq. (1.4.7). Since the Hamiltonian—and by extension, the unitary time evolution operator—can be expressed purely in the $\{\hat{Z}_n\}$ basis, operators that do not commute with these LIOMs have a chance of spreading. The LIOM cycle operators, $\{\hat{X}_n\}$, which "flip" or "cycle" between eigenstates of the LIOM operators, $\{\hat{Z}_n\}$, likely have the best chance of spreading (amongst single-body operators).

The time evolution of the operator $\hat{\tau}_n^x$ is given by

$$i\frac{d}{dt}\hat{X}_n = [\hat{H}, \hat{X}_n] = \hat{X}_n + \sum_m J_{nm}^{(2)} \hat{Y}_n \hat{Z}_m + \sum_{m,p} J_{nmp}^{(3)} \hat{Y}_n \hat{Z}_m \hat{Z}_p + \dots \ , \tag{1.5.10}$$

where $\hat{H}$ is given by Eq. (1.4.7), and note that the righthand side of the above expression does not commute with $\hat{H}$. In fact, there is one operator in each of the above terms that does not commute with $\hat{H}$: in the very first term, this is $\hat{X}_n$, and in all other terms it is $\hat{Y}_n$. Taking another commutator will turn the $\hat{Y}$ operators into $\hat{X}$ operators and vice versa, and multiply them with other $\hat{Z}$ operators (which commute with $\hat{H}$). Dynamically, in generic states (those that are not eigenstates of $\hat{H}$), the nth ℓ-bit therefore precesses at a rate determined by the configuration of other spins, as noted in Sec. 1.5.5 in the context of entanglement entropy.

Additionally, the support of the operator $\hat{X}_n(t)$ grows in time under the dynamics. In this context, "support" refers to the number of sites upon which a given operator does not act as the identity. Because the Hamiltonian given in Eq. (1.4.7) connects all terms, the support of $\hat{X}_n$ immediately extends to all sites after an infinitesimal evolution, however the corresponding coefficients decay exponentially. As a direct consequence, the region in which $\hat{X}_n(t)$ has $O(1)$ support (i.e. acts on a site as a nonidentity with magnitude $\|\hat{X}_n(t)\| \sim 1$) grows *logarithmically* in time away from site n, much like entanglement entropy.

Thus, information about operators and entanglement entropy in generic states in the MBL phase both spread from an initial locus (i.e. the $t = 0$ support of the operator or the entanglement cut) according to $\zeta_z \ln t$. Operator spreading is the fundamental quantity, and entanglement growth follows therefrom [9]. Note that the coefficient ζ_z is a decay length that can be extracted from the scale on which two-body LIOM-LIOM interaction terms in the Hamiltonian—written in the form of Eq. (1.4.7)—decay. From the spreading of ℓ-bit operators, one can extract information about operator spreading in the basis of p-bits by superposing the ℓ-bit operators with exponential tails. In general, off-diagonal components will spread, while diagonal components of operators are likely static.

Chapter 2

Integrability

2.1 What Is Integrability?

"If you gotta ask, you'll never know."
-Louis Armstrong, asked to define "Jazz"[1]

Quantum integrable models possess exact quasiparticle solutions, which can be understood in principle even in the thermodynamic limit without recourse to the use of statistical ensembles. The term "integrability" refers to the fact that the set of coupled differential equations for classical integrable systems are soluble, and thus one can "integrate" these equations using the initial conditions at $t = 0$ to recover the behavior at arbitrary times. However, due to the fact that such a direct relationship between the configuration of an integrable system at late times $t \gg 0$ and its initial configuration at $t = 0$ exists, integrable systems cannot thermalize in the usual sense. Analogous properties hold for quantum integrable systems, which also possess exact solutions and an extensive set of conserved quantities (or integrals of motion). Both classical and quantum integrable models do relax and admit a description in terms of "Generalized Gibbs Ensemble," which will be discussed in Sec. 2.5.

Although the first quantum integrable model was solved back in 1931, the subject remains very much alive and interesting nearly a century later. In fact, only in the last two decades was it realized that an entire, infinite family of conserved quantities had been unaccounted for in the very same model that was solved in the 1930s. One of the most promising features of integrable models is their description using generalize hydrodynamics (GHD), the subject of Sec. 2.6, which describes transport, correlation functions, and more in terms of a hydrodynamic variables, providing a valuable reduction in complexity and number of degrees of freedom. However, early on, it was thought that this theoretical framework was invalid as it was unable to reproduce the correct Drude weights for particle transport in the XXZ model. Subsequently, and perhaps while doing something entirely different, Tomaž Prosen unearthed an infinite number of additional conserved quantities for that model; upon accounting for these extra charges, GHD produced the Drude weights correctly.

In addition, until the publication of Ref. 37 by this author—which is reproduced in greater detail in Ch. 3—it was not known whether there existed models that were interacting, integrable, quantum, and unique to the Floquet setting. Of course, free theories are technically integrable,

[1] I got the idea to use this quote from *Wikipedia* (The Free Encyclopedia), whose article on integrability quotes Nigel Hitchin, who quotes Louis Amstrong. So already integrability is a multidisciplinary pursuit.

and free Floquet quantum systems have been known for some time. Additionally, Tomaž Prosen established [38] a means of constructing integrable Floquet models using the "R matrix"—which will be introduced in Sec. 2.3—of an integrable Hamiltonian, but these models can be smoothly deformed to Hamiltonian evolution, and cannot possess interesting features unique to the Floquet setting such as chiral quasiparticles in the bulk of a system.

Finally, it is common in theoretical models of condensed matter systems to use free theories as a starting point and add new ingredients, such as interactions and disorder, using the machinery of perturbation theory. However, interacting integrable models already possess exact quasiparticle solutions, making them a superior starting point from which to perturb to general models. For most integrable models, the utility of these exact solutions is offset by the complexity or impossibility of solving the quantization condition on the momenta of the constituent particles; however, in most—if not all—cases, this complexity is actually alleviated in the thermodynamic limit, where one can invoke the thermodynamic Bethe Ansatz (TBA), described in Sec. 2.4.

2.2 The Coordinate Bethe Ansatz

The coordinate Bethe Ansatz (CBA), also known as the nested Bethe Ansatz (acronym unnecessary) [39–42], was the original technique used by Hans Bethe[2] in 1931 [39] to solve the so-called Heisenberg model, which was one of the first quantum models put forth to describe the behavior of quantum degrees of freedom (in this case, spins in a magnet). The field of integrability has since expanded, and generally speaking, the Algebraic Bethe Ansatz (ABA), which will be covered briefly in Sec. 2.3, is much more generic and powerful. However, the CBA is nonetheless worthy of study, and many other properties of integrable models follow directly therefrom. It is worth noting that the CBA is probably only applicable in one dimension.

In this section, we will treat the the canonical example of an integrable quantum system, and the first historical example: the XXX Heisenberg ferromagnet, given by

$$\hat{H}_{\mathrm{XXX}} = -\frac{J}{4}\sum_{j=1}^{L-1}\left(\vec{\sigma}_j\cdot\vec{\sigma}_{j+1} - \hat{\mathbb{1}}\right) \ , \tag{2.2.1}$$

where $\vec{\sigma}_j = \left(\hat{\sigma}_j^x, \hat{\sigma}_j^y, \hat{\sigma}_j^z\right)$ are spin-1/2 operators acting on a local two-state Hilbert space $\mathbb{C}^2$. The spins 1/2 are arranged in a one dimensional ring (i.e. with periodic boundaries, site $j+L$ is site j), and the term "ferromagnet" refers to the sign of J being positive. This model has an $SU(2)$ symmetry, corresponding to rotations

$$\hat{U}_\alpha = \exp\left(-i\theta_\alpha\sum_{j=1}^{L}\hat{\sigma}_j^\alpha\right) \ , \tag{2.2.2}$$

for $\alpha = x, y, z$, all of which commute with $\hat{H}_{\mathrm{XXX}}$ as defined in Eq. (2.2.1). The exponentiated quantities in Eq. (2.2.2) above are examples of conserved quantities, the most familiar being the z-axis magnetization

$$\hat{S}^z_{\mathrm{tot}} \equiv \frac{1}{2}\sum_{j=1}^{L}\hat{\sigma}_j^z \ , \tag{2.2.3}$$

[2]Bethe did not call his solution method the "Bethe Ansatz."

which commutes with the Hamiltonian. A slightly more generic form with only $U(1)$ symmetry—corresponding to conservation of $\hat{S}^z_{\text{tot}}$ as defined in Eq. (2.2.3)—is given by the XXZ model,

$$\hat{H}_{\text{XXZ}} = -\frac{J}{2}\sum_{j=1}^{L-1}\left(\hat{\sigma}^+_j\hat{\sigma}^-_{j+1} + \hat{\sigma}^-_j\hat{\sigma}^+_{j+1}\right) - \frac{J\Delta}{4}\sum_{j=1}^{L-1}\left(\hat{\sigma}^z_j\hat{\sigma}^z_{j+1} - \hat{\mathbb{1}}\right) + h\sum_{j=1}^{L}\hat{\sigma}^z_j \ , \tag{2.2.4}$$

which realizes $\hat{H}_{\text{XXX}}$ for $\Delta = 1$ and $h = 0$. In principle, it would be easiest to derive the general solutions for the XXZ model defined in Eq. (2.2.4), and take the appropriate limits to recover the XXX results, with such a derivation provided in Ref. 40. However, we will have no use for the XXZ model, and will restrict to XXX from the outset to avoid having superfluous variables floating about (the XXX model will make an appearance in Ch. 5 in the context of many-body quantum chaos in the presence of conserved charges).

The first consideration in treating the XXX Hamiltonian defined in Eq. (2.2.1) is symmetry. We work in the local z basis, and begin by divvying the various many-body states into sectors labelled by total magnetization along the z axis, i.e. $\hat{S}^z_{\text{tot}}$ as defined in Eq. (2.2.3). The sectors with $\hat{S}^z_{\text{tot}} = \pm L/2$ correspond to all spins either up or down, and have precisely one state. These states are annihilated by the $\hat{H}_{\text{XXX}}$, which can be seen perhaps most readily by regarding the form given by Eq. (2.2.4) with $h = 0$ (the value of Δ is unimportant for these states). These two states have eigenvalue 0; in fact, one can derive from the $SU(2)$ symmetry that *each* $\hat{S}^z_{\text{tot}}$ sector has exactly one state with Hamiltonian eigenvalue 0. That state will be the unique ground state in the corresponding sector (the many-body ground state therefore has $(L+1)$-fold degeneracy).

Let us denote the vacuum by

$$|0\rangle \equiv |\uparrow\uparrow\uparrow\ldots\uparrow\uparrow\rangle \ , \tag{2.2.5}$$

i.e. the state with all spins up, corresponding to $\hat{S}^z_{\text{tot}} = +L/2$. The fundamental excitations above this vacuum states, $|0\rangle$, are given by flipping a single spin. Such flipped-spin excitations correspond to a change in the total spin by one, and are known as *magnons*. We now define the sector ladder operators

$$\hat{S}^\pm = \sum_{j=1}^{L}\hat{\sigma}^\pm_j \ , \tag{2.2.6}$$

where, as always, $\hat{\sigma}^+_j = |\uparrow_j\rangle\langle\downarrow_j|$ and $\hat{\sigma}^\pm_j = \left(\hat{\sigma}^\mp_j\right)^\dagger$. Starting from the state $|0\rangle$, we recover the ground state in subsequent $\hat{S}^z_{\text{tot}}$ sectors—starting with $\hat{S}^z_{\text{tot}} = (L-1)/2$—by acting with $\hat{S}^\pm$. In a sector with $\hat{S}^z_{\text{tot}} = S$, corresponding to $N = N_\downarrow = L/2 - S$ magnons, the ground state is given by

$$|S\rangle = \left(\hat{S}^-\right)^N|0\rangle \ , \tag{2.2.7}$$

and the low-lying excitations above $|S\rangle$ are plane-wave superpositions of magnons, e.g. of the form

$$|S,k\rangle = \frac{1}{\sqrt{L}}\sum_{j=1}^{L}e^{ikj}\hat{\sigma}^-_j|S+1\rangle \ , \tag{2.2.8}$$

with $|S+1\rangle$ being the ground state of the sector with one fewer magnon, defined by Eq. (2.2.7).

2.2.1 Single-magnon solution

The simplest starting point is to examine the sector containing single-magnon excitations. In fact, the general premise of the Bethe Ansatz techniques is that the full spectrum of the Hamiltonian

is given by the sum of dispersions corresponding to single-particle dispersions, $\varepsilon(k)$, with the quantization of the allowed momenta, k, governed by complicated equations. Thus, the first step in trying to solve an integrable model must be identifying the single-particle excitations, which we have already done. Here, we find their dispersion.

There are L single particle states on a chain with L sites, corresponding to the L different places to flip a spin from $|0\rangle$ in the physical z-basis. We can label these states by the real-space position of the particle. The available states are then $|j\rangle$ for $j \in \{1, 2, \ldots, L-1, L\}$. Because our system is on a ring, all labels j are defined modulo L, such that $|j+L\rangle \cong |j\rangle$. Acting on such a basis state, the Hamiltonian $\hat{H}_{\mathrm{XXX}}$, whose many-body form is given by Eq. (2.2.1), takes the form

$$\hat{H} = -\frac{J}{2}\sum_{j=1}^{L}\left(|j+1\rangle\langle j| + |j-1\rangle\langle j| - 2|j\rangle\langle j|\right) \ , \tag{2.2.9}$$

where the final term comes from the the fact that precisely two of the interaction terms in Eq. (2.2.1) give $-J/2$ (the interaction term is zero for aligned spins and $-J/2$ for misaligned spins; there are precisely two misalignments for any position of the magnon), as depicted in Fig. 2.1.

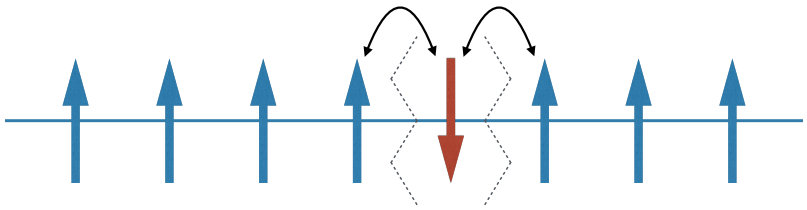

Figure 2.1: Representation of the single-body problem: regardless of where the flipped spin is on the lattice, there are precisely two bonds along which $\hat{\sigma}^z_j\hat{\sigma}^z_{j+1}$ gives -1, indicated by the zig-zag lines above; the flipped spin is free to hop to the site to the left or right.

We next construct plane waves via Fourier transformation:

$$|k\rangle = \frac{1}{\sqrt{L}}\sum_{j=1}^{L} e^{ikj}|j\rangle \quad , \quad |j\rangle = \frac{1}{\sqrt{L}}\sum_{k} e^{-ikj}|k\rangle \ , \tag{2.2.10}$$

where the quantization of k is fixed by the condition $|j+L\rangle = |j\rangle$, which dictates $e^{ikL} = 1 \implies k = 2\pi n/L$ for $n \in \{1, 2, \ldots, L-1, L\}$. Inserting this definition of $|j\rangle$ in terms of plane waves, $|k\rangle$ into Eq. (2.2.9) recovers

$$\begin{aligned}
\hat{H} &= -\frac{J}{2}\sum_{j=1}^{L}\left(|j+1\rangle\langle j| + |j-1\rangle\langle j| - 2|j\rangle\langle j|\right) \\
&= -\frac{J}{2L}\sum_{j=1}^{L}\sum_{k,k'} e^{ikj}\left(e^{-ik'(j+1)}|j+1\rangle + e^{-ik'(j-1)} - 2e^{-ik'j}\right)|k'\rangle\langle k| \\
&= \frac{J}{2L}\sum_{k,k'}\left(2 - e^{-ik'1} - e^{ik'1}\right)|k'\rangle\langle k|\sum_{j=1}^{L} e^{i(k-k')j} \\
&= \frac{J}{2L}\sum_{k,k'}\left(2 - 2\cos\left[k'\right]\right)|k'\rangle\langle k|\left(L\delta_{k,k'}\right) \\
&= J\sum_{k}\left(1 - \cos\left[k\right]\right)|k\rangle\langle k| = \sum_{k}\varepsilon_k|k\rangle\langle k| \ ,
\end{aligned} \tag{2.2.11}$$

where $\varepsilon_k \in [0, 2J]$. In particular, the low energy physics is captured by small momentum $k \ll 1$, in which case $\varepsilon_k \approx Jk^2/2$ corresponding to the standard ballistic kinetic energy of free particles.

In the anisotropic case, given by Eq. (2.2.4), the linear term $h\sum_j \hat{\sigma}_j^z = 2hS$ has a fixed value dependent only on the $\hat{S}_{\text{tot}}^z$ sector, labelled by eigenvalue S, and not the configuration within the sector; it can therefore be ignored. However, taking the strength of the $\hat{\sigma}_j^z\hat{\sigma}_{j+1}^z$ term to be $\Delta J/4$ modifies the dispersion, given by Eq. (2.2.11), to the general form

$$\varepsilon_k = J\left(\Delta - \cos\left[k\right]\right) \ . \tag{2.2.12}$$

2.2.2 Two-magnon solution

We now consider the sector with two magnons, which has "L choose 2" states, i.e. $L(L-1)/2$ configurations corresponding to all possible ways to flip two spins. The magnons are indistinguishable, and there is no meaning to labelling them separately. We define a real-space basis $\{|j_1, j_2\rangle\}$ subject to the condition $j_2 > j_1$, with $j_{1,2} \in \{1, 2, \ldots, L-1, L\}$. When the magnons are well separated, as depicted in Fig. 2.2(a), the action of the Hamiltonian on a given state $|j_1, j_2\rangle$ is given by

$$\begin{aligned}\hat{H}_{\text{XXX}}|j_1, j_2\rangle &= \varepsilon\,|j_1, j_2\rangle \\ &= -\frac{J}{2}\left[|j_1 - 1, j_2\rangle + |j_1 + 1, j_2\rangle + |j_1, j_2 - 1\rangle + |j_1, j_2 - 2\rangle - 4\Delta|j_1, j_2\rangle\right] \ ,\end{aligned} \tag{2.2.13}$$

where the anisotropy $\Delta \to 1$ in the Heisenberg XXX case, but is included here for convenience. For the special case where the magnons are on neighboring sites, i.e. $|j, j+1\rangle$, as depicted in Fig. 2.2(b), we demand that

$$\varepsilon\,|j, j+1\rangle = -\frac{J}{2}\left[|j-1, j+1\rangle + |j, j+2\rangle - 2\Delta|j_1, j_2\rangle\right] \ , \tag{2.2.14}$$

with the *same* energy ε in both cases. This can also be satisfied by plane waves, as in the single-magnon sector, with some adjustments. We can extend the formula given by Eq. (2.2.13) to capture the special cases given by Eq. (2.2.14) for some two-magnon state

$$|\Psi_{k_1,k_2}\rangle = \sum_{j_1<j_2} \Psi_{k_1,k_2}\left(j_1, j_2\right)|j_1, j_2\rangle \ , \tag{2.2.15}$$

if we also insist that the "boundary condition"

$$\Psi_{k_1,k_2}\left(j, j\right) + \Psi_{k_1,k_2}\left(j+1, j+1\right) - 2\Delta\Psi_{k_1,k_2}\left(j, j+1\right) = 0 \ , \tag{2.2.16}$$

in which case Eq. (2.2.13) is solved everywhere by the Bethe Ansatz wavefunction

$$\Psi_{k_1,k_2}\left(j_1, j_2\right) = e^{ik_1j_1}e^{ik_2j_2} + S\left(k_2, k_1\right)e^{ik_2j_1}e^{ik_1j_2} \ , \tag{2.2.17}$$

where $S\left(k_2, k_1\right) = S_{21}$ is the *scattering matrix*.

Using this Ansatz wave function, we recover

$$\varepsilon_2\left[k_1, k_2\right] = \varepsilon_1\left[k_1\right] + \varepsilon_1\left[k_2\right] = J\left(2 - \cos\left[k_1\right] - \cos\left[k_2\right]\right) \ , \tag{2.2.18}$$

where the two-body dispersion, ε_2, is the sum of the one-body dispersions ε_1.

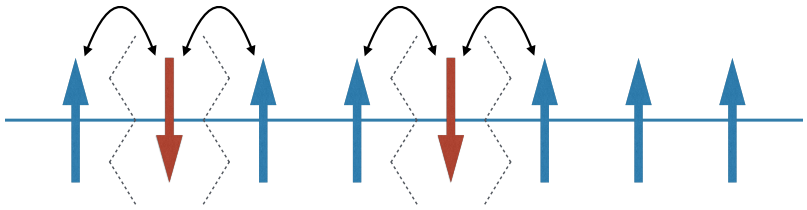

(a) Standard two-body case.

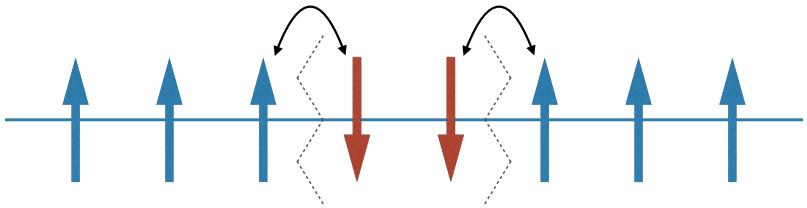

(b) Special two-body case.

Figure 2.2: Representation of the two-body problem. Figure (a) corresponds to the standard case in which the magnons are sufficiently well separated that the Hamiltonian acts on each independently, as in the one body case, e.g. as depicted in Fig. 2.1. Figure (b) corresponds to the special case in which the magnons are on neighboring sites. In this case, there are only two violated bonds ($\hat{\sigma}^z_j \hat{\sigma}^z_{j+1} = -1$), and the magnons can only hop outward, since no site can be doubly occupied.

Inserting the Ansatz defined by Eq. (2.2.17) into the boundary condition given by Eq. (2.2.16) gives an explicit form to the scattering matrix,

$$S(k_2, k_1) = -\frac{1 + e^{i(k_1+k_2)} - 2\Delta e^{ik_2}}{1 + e^{i(k_1+k_2)} - 2\Delta e^{ik_1}} \ , \tag{2.2.19}$$

which also implies that $\Psi_{k_1,k_2}(j_1, j_2)$ is zero if $k_1 = k_2$. Thus, each momentum mode can be occupied at most once. This feature holds for all integrable models; however, aside from having a maximum occupancy of one, the quasiparticle states that arise in general integrable models have no other properties of [free] fermions.

We also have the properties

$$S(k_1, k_2) = [S(k_2, k_1)]^* = [S(k_2, k_1)]^{-1} \ , \tag{2.2.20}$$

as one would expect for a unitary scattering matrix.

The remaining task to complete the solution of this sector is to determine the allowed values of $k_{1,2}$. As in the single-magnon case, we have the property that translation by L leaves states invariant. Thus, we the conditions

$$\Psi_{k_1,k_2}(j_1, j_2) = \Psi_{k_1,k_2}(j_2, j_1 + L) = \Psi_{k_1,k_2}(j_1 + L, j_2 + L) \ , \tag{2.2.21}$$

and the latter constraint, in which both particles are translated by L, dictates that $e^{iL(k_1+k_2)} = 1$, and as usual, the total momentum $k_1 + k_2 = K$ is quantized according to $K = 2\pi N/L$ with $N \in \{1, 2, \ldots, L-1, L\}$. The other conditions are given by

$$e^{ik_2 L} = e^{-ik_1 L} = S(k_2, k_1) \ , \tag{2.2.22}$$

which constitutes a Bethe Ansatz equation (BAE). In general, these equations are not easy to solve, as we will shortly see. It is also worth noting that there exist solutions to these equations with complex momenta given by $k_j = K/2 \pm iu/2$, such that the total momentum K is real, but the relative momentum iu is complex. This corresponds to a *bound state* of the two particles.

2.2.3 Many-magnon solution

We have now solved the XXX model for one and two magnon sectors. Much as the many-body states of free systems can be expressed in terms of single-body solutions, the key feature of quantum integrable systems is that many-body states can be expressed in terms of two-body solutions.

Definition 2.1. Quantum integrable models are distinguished by an extensive number of local conserved quantities (i.e. equal in number to the number of degrees of freedom or system size, each being defined as the sum of strictly local terms), and exact solutions that are two-body reducible. All events that the integrable dynamics (Hamiltonian or Floquet unitary) can beget on a given many-body state can be factorized into two-body processes (i.e. collisions). In contrast, free systems have exact solutions that are one-body reducible, and the occupation of each single-body mode is a local conserved quantity. Free quantum systems are a subset of integrable quantum systems.

For N particles states, one has many-body states of the form

$$\Psi_{\{k_n\}}\left(\{j_n\}\right) = \sum_{\text{perm.}} A_{i_1,\ldots,i_N} \exp\left\{i\left(k_{i_1} j_1 + \cdots + k_{i_N} j_N\right)\right\} \ , \tag{2.2.23}$$

which is a sum over all permutations of assignments of momenta to the positions.

In most cases, one picks a site on the lattice to call "1," numbering all sites that follow going clockwise in increasing order until reaching site L, directly counterclockwise of 1. One then assigns the "reference" state to the configuration $j_1 < j_2 < \cdots < j_L$, with the momentum k_n matched to j_n. Compared to this reference state, any state that differs by having swapped momenta k_m and k_n picks up a factor of $S\left(k_n, k_m\right)$ for $x_n > x_m$ (in the other case, simply swap the labels m and n, e.g.).

For concreteness, the three-body wave function is given by

$$\begin{aligned}\Psi_{k_1,k_2,k_3}\left(j_1,j_2,j_3\right) = {} & e^{ik_1j_1}e^{ik_2j_2}e^{ik_3j_3} + S\left(k_2,k_1\right)e^{ik_2j_1}e^{ik_1j_2}e^{ik_3j_3} \\ & + S\left(k_2,k_1\right)S\left(k_3,k_1\right)e^{ik_2j_1}e^{ik_3j_2}e^{ik_3j_2} \\ & + S\left(k_2,k_1\right)S\left(k_3,k_1\right)S\left(k_3,k_2\right)e^{ik_3j_1}e^{ik_2j_2}e^{ik_1j_2} \\ & + S\left(k_3,k_1\right)S\left(k_3,k_2\right)e^{ik_3j_1}e^{ik_1j_2}e^{ik_2j_2} + S\left(k_3,k_2\right)e^{ik_1j_1}e^{ik_3j_2}e^{ik_2j_2} \ ,\end{aligned} \tag{2.2.24}$$

which corresponds to an eigenstate of $\hat{H}_{\text{XXX}}$ given by

$$\left|\Psi_{k_1,k_2,k_3}\right\rangle = \sum_{j_1<j_2<j_3} \Psi_{k_1,k_2,k_3}\left(j_1,j_2,j_3\right)\left|j_1,j_2,j_3\right\rangle \ , \tag{2.2.25}$$

with dispersion

$$\varepsilon_3\left(k_1,k_2,k_3\right) = \sum_{n=1}^{3} \varepsilon_1\left(k_n\right) \ , \tag{2.2.26}$$

and each of the above equations generalized trivially to more than three bodies. Hence, by solving the two-body sector, we have the solution for all sectors.

Due to additional particles, there are now extra boundary condition relations for the wavefunction Ψ, e.g.

$$\begin{aligned}\Psi_{\{k_n\}}\left(\{j_n\}\right) &= \Psi\left(j_1, j_2, \ldots, j_L\right) \\ &= \Psi\left(j_2, \ldots, j_L, j_1 + L\right) \\ &= \Psi\left(j_3, \ldots, j_L, j_1 + L, j_2 + L\right) \\ &= \ldots \\ &= \Psi\left(j_1 + L, j_2 + L, \ldots, j_L + L\right) \ , \end{aligned} \tag{2.2.27}$$

resulting in the N-body Bethe Ansatz equations (BAE)

$$e^{ik_n L} = \prod_{\substack{m=1 \\ m\neq n}}^{N} S\left(k_n, k_m\right) \ , \tag{2.2.28}$$

which has an interpretation as the number of phases acquired as a particle is dragged through the entire system. For most interacting integrable models, solving the BAE is not possible by hand, requiring recourse to numerical evaluation for finite numbers of particles. However, the quantization condition is relaxed as $L \to \infty$, where the continuum limit can be taken for the allowed momenta. This is the spirit of the thermodynamic Bethe Ansatz, which will be discussed in Sec. 2.4.

In a trivial extension of Eq. (2.2.26) for three magnons, the energy eigenvalues of general integrable models are given by

$$E\left(k_1, \ldots, k_N\right) = \sum_{n=1}^{N} \varepsilon_1\left(k_n\right) \ , \tag{2.2.29}$$

and for general models, we may generalize the momentum to a "rapidity." In the Floquet model considered in Ch. 3, the energy will be replaced by the Floquet pseudoenergy, with many other details remaining the same.

2.3 The Algebraic Bethe Ansatz

This section is partially reproduced from Ref. [43] by this author—and especially the Supplementary Material associated with that work—and is the result of substantial contributions from coauthor Andrea De Luca.

2.3.1 General formulation of the inhomogeneous algebraic Bethe Ansatz

In the *coordinate* Bethe Ansatz [39–42]—outlined for the Heisenberg model, $\hat{H}_{\mathrm{XXX}}$, in Sec. 2.2—one seeks multiparticle eigenfunctions—i.e. multimagnon plane waves—along with a scattering matrix describing the exchange of the excitations' momenta. However, this approach suffers from technical complications in generic models, and especially so in Trotterized evolutions, $\hat{M}$, consisting of a "circuit" of two-site gates, which we will encounter in Ch. 5. A more direct approach to treat these

models is instead based on the equivalent *algebraic* Bethe Ansatz formulation [44, 45]. Restricting to the case of spins 1/2—i.e. a local Hilbert space given by $\mathbb{C}^2$—we introduce the R-matrix

$$\hat{\mathcal{R}}_{a,b}(\lambda) = \frac{\lambda}{\lambda + 2i}\hat{\mathbb{1}}_{ab} + \frac{2i}{\lambda + 2i}\hat{\mathbb{P}}_{ab} \ , \tag{2.3.1}$$

which acts on spins 1/2 labelled a and b, and is standard to systems with $SU(2)$ symmetry. The exchange operator $\hat{\mathbb{P}}_{a,b}$ is defined by

$$\hat{\mathbb{P}}_{a,b}|s_a, s_b\rangle = |s_b, s_a\rangle \ . \tag{2.3.2}$$

The key feature of the R matrix is that is satisfies the Yang-Baxter identity [42].

Going forward, for clarity, indices of the form $i, j, k, \ldots$ will indicate sites in the real spin lattice, while indexes of the form $a, b, c, \ldots$ will indicate the auxiliary spaces, all of which are spins 1/2. The Yang-Baxter identity can be written as an operator identity in $\mathbb{C}^2_a \otimes \mathbb{C}^2_b \otimes \mathbb{C}^2_i$, and we have

$$\hat{\mathcal{R}}_{a,b}(\lambda - \mu)\hat{\mathcal{R}}_{i,a}(\lambda)\hat{\mathcal{R}}_{i,b}(\mu) = \hat{\mathcal{R}}_{i,b}(\mu)\hat{\mathcal{R}}_{i,a}(\lambda)\hat{\mathcal{R}}_{a,b}(\lambda - \mu) \tag{2.3.3}$$

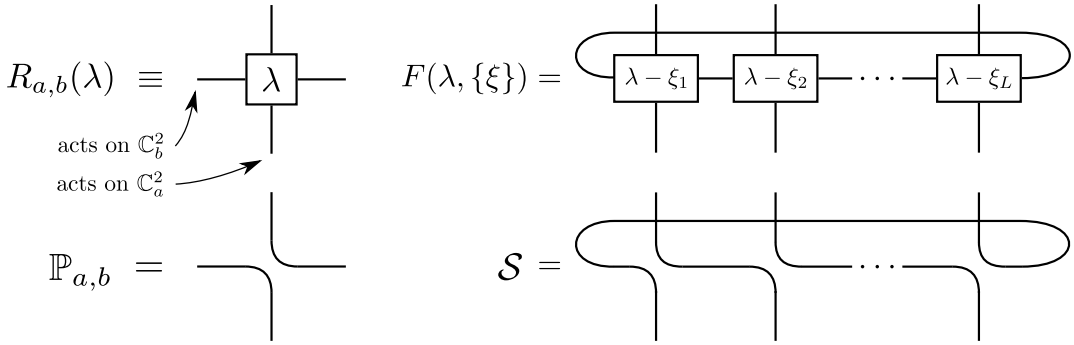

Figure 2.3: Diagrammatic representations of $\hat{\mathcal{R}}_{a,b}(\lambda - \mu)$, $\hat{F}(\lambda, \{\xi\})$, $\hat{\mathbb{P}}_{a,b}$ and $\hat{\mathcal{S}}$. Note that in the current convention, $\hat{\mathcal{R}}_{a,b}(\lambda - \mu)$ acts in the top right direction.

We next introduce the transfer matrix (or T-matrix), which acts jointly on all L physical spin degrees of freedom and an auxiliary spin degree of freedom, labelled a:

$$\hat{\mathcal{T}}_{L,a}(\lambda, \{\xi\}) = \hat{\mathcal{R}}_{1,a}(\lambda - \xi_1)\hat{\mathcal{R}}_{2,a}(\lambda - \xi_2)\ldots\hat{\mathcal{R}}_{L,a}(\lambda - \xi_L) \ , \tag{2.3.4}$$

where the *rapidity* λ and *inhomogeneities* ξ's are arbitrary complex numbers. Note that the subscripts in Eq. (2.3.4) label Hilbert spaces, as is customary in the Bethe Ansatz literature (see also Figure 2.3). Schematically, λ parameterizes the quasimomentum $k(\lambda)$ carried by the auxiliary particle while traversing the chain.

A crucial result is that employing Eq. (2.3.3) many times, one can prove the so-called RTT relation

$$\hat{\mathcal{R}}_{a,b}(\lambda - \mu)\hat{\mathcal{T}}_{L,a}(\lambda, \{\xi\})\hat{\mathcal{T}}_{L,b}(\mu, \{\xi\}) = \hat{\mathcal{T}}_{L,b}(\mu, \{\xi\})\hat{\mathcal{T}}_{L,a}(\lambda, \{\xi\})\hat{\mathcal{R}}_{a,b}(\lambda - \mu) \tag{2.3.5}$$

From this relation it follows that if we set $F(\lambda, \{\xi\})$ as the trace over the auxiliary space, i.e. $F(\lambda, \{\xi\}) = \operatorname{Tr}_a[\hat{\mathcal{T}}_{L,a}(\lambda, \{\xi\})]$, as illustrated in Figure 2.3, we have that

$$[F(\lambda, \{\xi\}), F(\lambda', \{\xi\})] = 0 \ , \qquad \lambda, \lambda' \in \mathbb{C} \ . \tag{2.3.6}$$

In the auxiliary space, $\hat{\mathcal{T}}(\lambda)$ can be written as a 2×2 matrix of operators acting on the *physical* spins,

$$\hat{\mathcal{T}}(\lambda) = \begin{pmatrix} \hat{A}(\lambda) & \hat{B}(\lambda) \\ \hat{C}(\lambda) & \hat{D}(\lambda) \end{pmatrix} . \tag{2.3.7}$$

This construction is useful because the fact that the R-matrix in Eq. (2.3.1) satisfies the Yang-Baxter relation, given by Eq. (2.3.3), implies a set of algebraic relations between the coefficients in Eq. (2.3.7), computed at the same inhomogeneities [46].

With this notation it is clear that $F(\lambda,\{\xi\}) = A(\lambda,\{\xi\}) + D(\lambda,\{\xi\})$ and, moreover, Eq. (2.3.5) can be interpreted as a set of commutation relations for the operators A, B, C, D. Those relevant for us are

$$[B(\lambda,\{\xi\}), B(\mu,\{\xi\})] = 0 \tag{2.3.8}$$

$$A(\lambda,\{\xi\})B(\mu,\{\xi\}) = f_+(\lambda-\mu)B(\mu,\{\xi\})A(\lambda,\{\xi\}) + g_+(\lambda-\mu)B(\lambda,\{\xi\})A(\mu,\{\xi\}) \tag{2.3.9}$$

$$D(\lambda,\{\xi\})B(\mu,\{\xi\}) = f_-(\lambda-\mu)B(\mu,\{\xi\})D(\lambda,\{\xi\}) + g_-(\lambda-\mu)B(\lambda,\{\xi\})D(\mu,\{\xi\}) \tag{2.3.10}$$

where the functions

$$f_\pm(\lambda) = \frac{\lambda \mp 2i}{\lambda} , \qquad g_\pm(\lambda) = \pm\frac{2i}{\lambda} \tag{2.3.11}$$

are independent of the inhomogeneities $\{\xi\}$. We fix the vacuum state $|\Omega\rangle = |\uparrow\uparrow\ldots\uparrow\rangle$; this is an eigenstate of $F(\lambda,\{\xi\})$, since

$$A(\lambda,\{\xi\})|\Omega\rangle = \mathfrak{a}(\lambda,\{\xi\})|\Omega\rangle; \qquad D(\lambda,\{\xi\})|\Omega\rangle = \mathfrak{d}(\lambda,\{\xi\})|\Omega\rangle; \qquad C(\lambda,\{\xi\})|\Omega\rangle = 0 , \tag{2.3.12}$$

and in the current normalization scheme, one has

$$\mathfrak{a}(\lambda,\{\xi\}) = 1 , \tag{2.3.13}$$

$$\mathfrak{d}(\lambda,\{\xi\}) = \prod_i \left(\frac{\lambda-\xi_i}{\lambda-\xi_i+2i}\right) . \tag{2.3.14}$$

One can then check [46] that the operators $B(\lambda,\{\xi\})$ can be used to build eigenstates of $F(\lambda,\{\xi\})$

$$F(\lambda,\{\xi\})|\{\lambda\}\rangle = \Lambda(\lambda,\{\lambda\},\{\xi\})|\{\lambda\}\rangle , \tag{2.3.15}$$

$$|\{\lambda\}\rangle \equiv B(\lambda_1,\{\xi\})\ldots B(\lambda_N,\{\xi\})|\Omega\rangle \tag{2.3.16}$$

if the Bethe Ansatz equations (BAE), given by

$$\prod_{b\neq a}\frac{f_-(\lambda_a-\lambda_b)}{f_+(\lambda_a-\lambda_b)} = \frac{\mathfrak{a}(\lambda_a,\{\xi\})}{\mathfrak{d}(\lambda_a,\{\xi\})} , \tag{2.3.17}$$

are satisfied, where $a, b = 1,\ldots,N$. The eigenvalue $\Lambda(\lambda,\{\lambda\},\{\xi\})$ is given by

$$\Lambda(\lambda,\{\lambda\},\{\xi\}) = \mathfrak{a}(\lambda,\{\xi\})\prod_a f_+(\lambda-\lambda_a) + \mathfrak{d}(\lambda,\{\xi\})\prod_a f_-(\lambda-\lambda_a) . \tag{2.3.18}$$

Note that each application of $B(\lambda,\{\xi\})$ decreases by 1 the total magnetization along z:

$$[B(\lambda), \hat{S}^z] = B(\lambda) \quad \Longrightarrow \hat{S}^z|\{\lambda\}\rangle = (L/2-N)|\{\lambda\}\rangle . \tag{2.3.19}$$

2.3.2 Trotterized XXX

To avoid repetition, let us restrict to a single example, which will be of use in Ch. 5, and appears in Ref. 43 by this author. The model of interest is a discrete-time Floquet model featuring a circuit construction (depicted in Fig. 2.4, which does not correspond to unitary evolution, but rather Hermitian evolution. This can be regarded either as evolution of a quantum model in imaginary time $\tau = it$, or perhaps more reasonably, as a formalism for the real-time evolution of a classical lattice gas in one dimension with two-state degrees of freedom on each site. Both of these formulations are equivalent, as will be elucidated in Ch. 5.

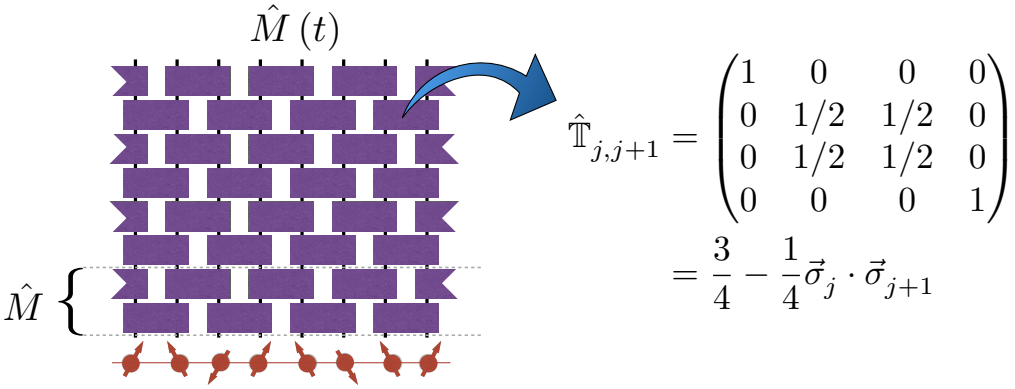

Figure 2.4: Depiction of the brick-wall circuit geometry corresponding to the Trotterized XXX "evolution." The system is evolved by a single time step by application of the single period evolution operator, $\hat{M}$, a two-layer circuit with the first and second layers—composed of two-site Hermitian gates, $\hat{\mathbb{T}}$—acting respectively on odd and even bonds. The individual gates, $\hat{\mathbb{T}}_{j,j+1}$ can be rewritten as $\hat{\mathbb{1}}_{j,j+1} - \hat{H}_{j,j+1}$, where $\hat{H}_{j,j+1}$ is the local two-site term that appears in the Heisenberg XXX Hamiltonian in Eq. (2.2.1). Hence, $\hat{M}$ describes a *Trotterized* version of the XXX model, evolved in imaginary time: interpreting the time t as an inverse temperature, $t \to \beta = 1/k_B T$, $\hat{M}(\beta)$ can be regarded as a Trotterization of the XXX partition function.

Referring to Fig. 2.4, the evolution to time t is given by $\hat{M}(t) = \hat{M}^t$, with the single-period evolution operator, $\hat{M} \equiv \hat{M}_2 \cdot \hat{M}_1$, a depth-two circuit comprised of local two-site gates: assuming even L, the two layers correspond respectively to odd and even bonds, with $\hat{M}_1 = \hat{\mathbb{T}}_{1,2} \otimes \hat{\mathbb{T}}_{3,4} \otimes \ldots$ and $\hat{M}_2 = \hat{\mathbb{T}}_{2,3} \otimes \hat{\mathbb{T}}_{4,5} \otimes \ldots$. The full evolution operator, $\hat{M}$, along with the individual layers, $\hat{M}_{1,2}$ and their constituent gates $\hat{\mathbb{T}}_{j,j+1}$, are Hermitian.

The matrix $\hat{\mathbb{T}}_{j,j'}$ acts only on sites j, j' as

$$\hat{\mathbb{T}}_{j,j'} = \frac{1}{2}(\hat{\mathbb{1}}_{j,j'} + \hat{\mathbb{P}}_{j,j'}), \tag{2.3.20}$$

where $\hat{\mathbb{P}}_{j,j'} = \frac{1}{2}(\hat{\hat{\mathbb{1}}}_{j,j'} + \vec{\sigma}_j \cdot \vec{\sigma}_{j'})$ is the "swap operator," defined in Eq. (2.3.2). In terms of classical lattice gases, the evolution $\hat{M}(t) = \hat{M}^t$ describes a discrete-time symmetric simple exclusion process (SSEP) for a classical lattice gas [40].

Noting that

$$\hat{\mathbb{T}}_{j,j+1} \equiv \hat{\hat{\mathbb{1}}}_{j,j+1} - \hat{\mathbb{H}}_{j,j+1} \ , \tag{2.3.21}$$

where the "Hamiltonian" can be written

$$\hat{\mathbb{H}}_{j,j+1} = -\frac{1}{4}(\vec{\sigma}_j \cdot \vec{\sigma}_{j+1} - \hat{\hat{\mathbb{1}}}_{j,j+1}) \ , \tag{2.3.22}$$

takes the form of the local Hamiltonian term of the spin-1/2 Heisenberg ferromagnet, defined in Eq. (2.2.1). Thus, $\hat{M}$ has an interpretation as a Trotterization of the time-evolution operator for $\hat{H}_{\mathrm{XXX}}$ in imaginary time. This can also be viewed as the *density matrix* $\exp\left(-\beta \hat{H}_{\mathrm{XXX}}\right)$ evaluated at inverse temperature $\beta = t$, and without proper normalization.

We now fix the values of the inhomogeneities that appear in the general Bethe Ansatz equations, i.e. Eq. (2.3.17) in Sec. 2.3.1, according to

$$\xi_j = i + (-1)^j \delta \ , \tag{2.3.23}$$

and for clarity, we refer to the transfer matrix for the Trotterized problem as $F_\delta(\lambda) \equiv F(\lambda, \{\xi\})$ with the ξ_j's given by Eq. (2.3.23). We also assume L to be an even integer. We then define the evolution operator as

$$\hat{M}_\delta = F_\delta(i-\delta)^{-1} F_\delta(i+\delta) \ . \tag{2.3.24}$$

Inspecting Eq. (2.3.4), we see that the transfer matrix involves the matrices

$$\hat{\mathcal{R}}_{a,b}(0) = \mathbb{P}_{a,b} \ , \quad \hat{\mathcal{R}}_{a,b}(\pm\delta) \equiv \hat{\mathcal{R}}^{\pm}_{a,b} \ , \tag{2.3.25}$$

and we next introduce the shift operator

$$\mathcal{S}|s_1, s_2, \ldots, s_L\rangle = |s_2, s_3, \ldots s_L, s_1\rangle \ , \qquad \mathcal{S}^\dagger \mathcal{S} = \mathbf{1}, \tag{2.3.26}$$

which can be rewritten as a trace over the auxiliary space

$$\mathcal{S} = \operatorname*{Tr}_a \left[\mathbb{P}_{1,a} \mathbb{P}_{2,a} \ldots \mathbb{P}_{L,a}\right] \ . \tag{2.3.27}$$

We then write

$$\mathcal{S}^\dagger F_\delta(i+\delta) = \check{R}^{+}_{1,2} \check{R}^{+}_{3,4} \ldots \check{R}^{+}_{L-1,L} \ , \tag{2.3.28a}$$

$$\mathcal{S}^\dagger F_\delta(i-\delta) = \check{R}^{-}_{L,1} \check{R}^{-}_{2,3} \ldots \check{R}^{-}_{L-2,L-1} \ , \tag{2.3.28b}$$

where we introduced

$$\check{R}^{\pm}_{ab} = \hat{\mathbb{P}}_{ab} \hat{\mathcal{R}}^{\pm}_{ab} \ . \tag{2.3.29}$$

Note that the relations of Eq. (2.3.28) imply that the square of the shift operator belongs to the set of commuting operators

$$\mathcal{S}^2 = F_\delta(i+\delta) F_\delta(i-\delta) \ , \tag{2.3.30}$$

as expected from the two-site translation invariance of the Trotterized model. Moreover, from Eq. (2.3.28b) one can immediately read off the expression for $F(i/2-\delta/2)^{-1}$ as

$$F_\delta(i-\delta)^{-1} = (\check{R}^{-}_{L-2,L-1})^{-1} (\check{R}^{-}_{L-4,L-3})^{-1} \ldots (\check{R}^{-}_{2,3})^{-1} (\check{R}^{-}_{L,1})^{-1} S^\dagger \ . \tag{2.3.31}$$

Furthermore, from the definition of the R matrix, i.e. Eq. (2.3.1), one can show that

$$(\hat{\mathcal{R}}^{\pm}_{a,b})^{-1} = \hat{\mathcal{R}}^{\mp}_{a,b} \ . \tag{2.3.32}$$

Therefore, we conclude that

$$\hat{M}_\delta = \check{R}^{+}_{L-2,L-1} \check{R}^{+}_{L-4,L-3} \ldots \check{R}^{+}_{L,1} \check{R}^{+}_{1,2} \check{R}^{+}_{3,4} \ldots \check{R}^{+}_{L-1,L} \ . \tag{2.3.33}$$

Thus, inserting Eq. (2.3.23) into the general Bethe Ansatz equations Eq. (2.3.17), one obtains

$$\left(\frac{\lambda_a+(\delta+i)}{\lambda_a+(\delta-i)}\right)^{L/2}\left(\frac{\lambda_a-(\delta-i)}{\lambda_a-(\delta+i)}\right)^{L/2}=\prod_{\substack{b=1\\b\neq a}}^{N}\left(\frac{\lambda_a-\lambda_b+2i}{\lambda_a-\lambda_b-2i}\right)\,. \tag{2.3.34}$$

The eigenvalue of $\hat{M}_\delta$ corresponding to the state $|\{\lambda\}\rangle$ is then given by

$$\hat{M}_\delta|\{\lambda\}\rangle=\prod_a\frac{f_+(i+\delta-\lambda_a)}{f_+(i-\delta-\lambda_a)}|\{\lambda\}\rangle\,, \tag{2.3.35}$$

where we used the relation $\mathfrak{d}(\frac{i\pm\delta}{2})=0$. We now observe that for $\delta=i$, $\check{R}^+=\frac{1}{2}(\hat{\mathbb{1}}+\hat{\mathbb{P}})$ and thus

$$\hat{M}=\lim_{\delta\to i}\hat{M}_\delta\,. \tag{2.3.36}$$

In general, by setting $\hat{F}(\lambda)\equiv\hat{A}(\lambda)+\hat{D}(\lambda)$, one finds that $[\hat{F}(\lambda),\hat{F}(\lambda')]=0\,,\ \forall\ \lambda,\lambda'$. The presence of a one-parameter family of commuting quantities establishes integrability for any choice of $\{\xi_j\}$, but only *particular* choices give rise to interesting local models. By varying the parameter $\delta\in[0,i]$, one can interpolate between the standard XXX spin chain, given by Eq. (2.2.1), and its Trotterized cousin, $\hat{M}$, given by a circuit comprising the T-matrices defined in Eq. (2.3.20). The isotropic Heisenberg spin chain is recovered for the homogeneous case, $\xi_j=i/2$, while the brick-wall geometry relevant to $\hat{M}$ is realized via $\xi_j=i\,(1+(-1)^j)$, from which it follows that

$$\hat{M}=\lim_{\delta\to i}\hat{F}\,(i-\delta)^{-1}\,\hat{F}\,(i+\delta)\,, \tag{2.3.37}$$

where the limit is needed to account for the noninvertibility of $\hat{\mathbb{T}}_{j,j'}$ in Eq. (2.3.20).

The common eigenstates of the conserved quantities $\hat{F}(\lambda)$ (and thereby $\hat{M}$) can be obtained via algebraic properties as described above. Thus $\hat{M}$ has eigenstates

$$\hat{M}|\lambda_1,\ldots,\lambda_N\rangle_S=e^{-\sum_j\varepsilon(\lambda_j)}|\lambda_1,\ldots,\lambda_N\rangle\,, \tag{2.3.38}$$

where $|\lambda_1,\ldots,\lambda_N\rangle_S=\hat{B}(\lambda_1)\ldots\hat{B}(\lambda_N)|S\rangle$. The integer N encodes the magnetization eigenvalue via $\hat{S}^z|\lambda_1,\ldots,\lambda_N\rangle_S=(S-N)|\lambda_1,\ldots,\lambda_N\rangle$. Due to interactions, the parameters $\lambda_1,\ldots,\lambda_N$ are not free, but satisfy Bethe Ansatz equations—given generally in Eq. (2.3.34)—which for $\hat{M}$ take the form

$$\left(\frac{\lambda_j+2i}{\lambda_j-2i}\right)^{L/2}=\prod_{\substack{j'=1\\j'\neq j}}^{N}\left(\frac{\lambda_j-\lambda_{j'}+2i}{\lambda_j-\lambda_{j'}-2i}\right)\,, \tag{2.3.39}$$

the solution of which provides the full spectrum of $\hat{M}$.

The eigenvalues in Eq. (2.3.35) can be written as

$$\hat{M}B(\lambda_1)\ldots B(\lambda_N)|\Omega\rangle=e^{\sum_a-\varepsilon(\lambda_a)}|\Omega\rangle\,,\qquad\varepsilon(\lambda)=-\log\frac{\lambda^2}{\lambda^2+4} \tag{2.3.40}$$

where $\varepsilon(\lambda)$ plays the role of an effective magnon energy. Using Eq. (2.3.30) recovers the spectrum of the shift operator

$$\mathcal{S}^2|\{\lambda\}\rangle=e^{2i\sum_a k(\lambda_a)}|\{\lambda\}\rangle\,,\qquad e^{2ik(\lambda)}=\left(\frac{\lambda+2i}{\lambda-2i}\right) \tag{2.3.41}$$

which coincides with the relation $k(\lambda)=\operatorname{arccot}(\lambda/2)\in[-\pi/2,\pi/2]$ that recovers for $\hat{M}$. In terms of this rapidity-dependent momentum, the dispersion relation in Eq. (2.3.40) can be rewritten as

$$\varepsilon(\lambda)=2\ln\cos k(\lambda). \tag{2.3.42}$$

2.4 The Thermodynamic Bethe Ansatz

2.4.1 Roots of the Bethe equations

The thermodynamic Bethe Ansatz (TBA) is a powerful tool for describing one-dimensional integrable quantum models in the thermodynamic limit, $L \to \infty$, where, e.g., L is the number of spins in a Heisenberg chain. We begin by sketching the TBA formalism, and then apply it to the Trotterized XXX example used in the previous section.

The starting point is the coupled set of Bethe Ansatz equations (BAE), i.e. Eq. (2.2.28) for the XXX model, which take the general form

$$e^{ik_n L} = \prod_{\substack{m=1 \\ m \neq n}}^{N} S\left(k_n, k_m\right) \ , \tag{2.2.28}$$

where S is the scattering matrix, N is the number of particles, and L the number of sites, or the equivalent generalization. Taking the logarithm of both sides gives a more standard version of the BAE,

$$L k_n = 2\pi I_n - i \sum_{m \neq n} \ln\left[S\left(k_n, k_m\right)\right] \ , \tag{2.4.1}$$

where I_n is integer, which may be zero, and it is typical to rename the logarithm of the scattering matrix

$$\Theta\left(k_n, k_m\right) = -i \ln\left[S\left(k_n, k_m\right)\right] \ . \tag{2.4.2}$$

As a quick note, the total momentum is given by summation over n of Eq. (2.4.1),

$$K = \sum_n k_n = \frac{2\pi}{L} \sum_n I_n + \sum_{\substack{m,n=1 \\ m \neq n}}^{N} \Theta\left(k_n, k_m\right) = \frac{2\pi}{L} \sum_n I_n \ . \tag{2.4.3}$$

Note that in certain models, e.g. XXZ and its variants, one must also account explicitly for *string solutions* to the BAE, corresponding to multiparticle bound states. Additionally, there are minor caveats for continuum models, e.g. Lieb-Liniger. These cases are well understood and extensive literature exists on the subject, so we will not devote any consideration to such matters.

The next step in the TBA formalism is to replace the integer quantum numbers, $\{I_n\}$, which completely label a state, by "counting functions" for the corresponding rapidity or momentum, according to $I_n = L\, c(\lambda_n)$, where λ_n is a rapidity variable, related to momentum. In this case Eq. (2.4.1) becomes

$$c\left(\lambda_n\right) = \frac{1}{2\pi} k\left(\lambda_n\right) - \frac{1}{2\pi L} \sum_{\substack{m=1 \\ m \neq n}}^{N} \Theta\left(\lambda, \lambda_m\right) \ , \tag{2.4.4}$$

where, in the case $L\, c(\lambda) = I_n$, if the momentum (or rapidity) mode corresponding to I_n is occupied, one has a "particle," and if it is unoccupied, one has a "hole."

We now define root solutions to the BAE, which correspond to the particle and hole densities, $\rho_{\mathrm{p}}\left(\lambda\right)$ and $\rho_{\mathrm{h}}\left(\lambda\right)$, and their sum, the total density of states, $\rho_{\mathrm{s}}\left(\lambda\right)$, given by

$$\rho_{\mathrm{s}}\left(\lambda\right) = \rho_{\mathrm{p}}\left(\lambda\right) + \rho_{\mathrm{h}}\left(\lambda\right) = \frac{d\, c}{d\lambda} \ , \tag{2.4.5}$$

where $L \rho_{\mathrm{p}}\left(\lambda\right) d\lambda$ is the number of particles with rapidity between λ and $\lambda + d\lambda$, and $L \rho_{\mathrm{h}}\left(\lambda\right) d\lambda$ is the density of holes in the same rapidity interval.

Returning to Eq. (2.4.4), clearly the sum over $m \neq n$ is not particularly compatible with the continuum notation, and we convert the sum to an integral to recover the expression for $c(\lambda)$, writing

$$\frac{1}{L}\sum_{\substack{m=1\\m\neq n}}^{N}\ln\left[S\left(\lambda_n,\lambda_m\right)\right]\to\sum_{\substack{m=1\\m\neq n}}^{N}\ln\left[S\left(\lambda_n,\lambda_m\right)\right]\frac{\lambda_m-\lambda_{m+1}}{L\left(\lambda_m-\lambda_{m+1}\right)}\to\int d\lambda\ln S\left(k\left(\lambda_n\right),k\left(\lambda\right)\right)\rho_{\mathrm{p}}\left(\lambda\right)\ , \tag{2.4.6}$$

and we have

$$c\left(\lambda\right)=\frac{1}{2\pi}k\left(\lambda\right)+\frac{1}{2\pi i}\int d\lambda'\ln S\left(\lambda,\lambda'\right)\rho_{\mathrm{p}}\left(\lambda'\right)\ , \tag{2.4.7}$$

and we can take the rapidity derivative of the counting function in Eq. (2.4.5) explicitly using Eq. (2.4.7) to recover

$$\rho_{\mathrm{s}}\left(\lambda\right)=\rho_{\mathrm{p}}\left(\lambda\right)+\rho_{\mathrm{h}}\left(\lambda\right)=\frac{1}{2\pi}\frac{dk}{d\lambda}+\left[\hat{\mathcal{K}}\rho_{\mathrm{p}}\right]\left(\lambda\right)\ , \tag{2.4.8}$$

where the operator $\hat{\mathcal{K}}$ denotes convolution against the differential scattering kernel K,

$$\left[\hat{\mathcal{K}}g\right]\left(\theta\right)=\int\frac{d\phi}{2\pi}K\left(\theta,\phi\right)g\left(\phi\right)\ ,\quad\text{where}\quad K\left(\theta,\phi\right)=\frac{1}{i}\frac{d}{d\theta}\ln S\left(\theta,\phi\right)\quad , \tag{2.4.9}$$

where in many models, S is symmetric in θ,ϕ, and many TBA references use the opposite sign convention, whereas this notation is more consistent with the generalized hydrodynamics literature.

2.4.2 Yang-Yang free energy

To proceed, we next define the *entropy* as the logarithm of the number of available states, given by

$$dS\left(\lambda\right)=\log\frac{\left(L\rho_{\mathrm{s}}\left(\lambda\right)d\lambda\right)!}{\left(L\rho_{\mathrm{p}}\left(\lambda\right)d\lambda\right)!\left(L\rho_{\mathrm{h}}\left(\lambda\right)d\lambda\right)!}\ , \tag{2.4.10}$$

where for multiple species of particles the argument of the logarithm becomes a product over species. Using $L\to\infty$ and Stirling's approximation for $\log n!$, one has

$$dS\left(\lambda\right)=L\,d\lambda\left[\rho_{\mathrm{s}}\left(\lambda\right)\ln\rho_{\mathrm{s}}\left(\lambda\right)-\rho_{\mathrm{p}}\left(\lambda\right)\ln\rho_{\mathrm{p}}\left(\lambda\right)-\rho_{\mathrm{h}}\left(\lambda\right)\ln\rho_{\mathrm{h}}\left(\lambda\right)+\ldots\right]\ , \tag{2.4.11}$$

and integrating over λ one defines the *entropy density* as a functional of the TBA root densities,

$$s=\int d\lambda\left[\rho_{\mathrm{s}}\left(\lambda\right)\ln\rho_{\mathrm{s}}\left(\lambda\right)-\rho_{\mathrm{p}}\left(\lambda\right)\ln\rho_{\mathrm{p}}\left(\lambda\right)-\rho_{\mathrm{h}}\left(\lambda\right)\ln\rho_{\mathrm{h}}\left(\lambda\right)\right]\ , \tag{2.4.12}$$

also known as the Yang-Yang entropy [45, 47].

Denoting by $\varepsilon(\lambda)$ the energy dispersion as a function of rapidity, the *energy density* is given by

$$e=\int d\lambda\,\varepsilon\left(\lambda\right)\,\rho_{\mathrm{p}}\left(\lambda\right)\ , \tag{2.4.13}$$

which bears an obvious resemblance to the continuum limit of the second quantized energy for free fermions.

Combining these two, one recovers the free energy density $f=e-Ts$, such that expectation values in the thermodynamic limit are given by a partition function $Z=\exp\left(-Lf/T\right)$,

$$f=\int d\lambda\left[\varepsilon\left(\lambda\right)\,\rho_{\mathrm{p}}\left(\lambda\right)+\rho_{\mathrm{p}}\left(\lambda\right)\ln\rho_{\mathrm{p}}\left(\lambda\right)+\rho_{\mathrm{h}}\left(\lambda\right)\ln\rho_{\mathrm{h}}\left(\lambda\right)-\rho_{\mathrm{s}}\left(\lambda\right)\ln\rho_{\mathrm{s}}\left(\lambda\right)\right]\ . \tag{2.4.14}$$

2.4.3 TBA equations

As in nonintegrable settings, we seek root densities $\rho_{\rm p}$ and $\rho_{\rm h}$ that minimize the Yang-Yang free energy given by Eq. (2.4.14). We vary the free energy with respect to the quasiparticle density $\rho_{\rm p}$, subject to the constraint given by Eq. (2.4.5), i.e. variations in the hole density are given by

$$\delta\rho_{\rm h} = -\delta\rho_{\rm p} + \hat{\mathcal{K}}\delta\rho_{\rm p} \ , \tag{2.4.15}$$

and introducing the TBA pseudoenergy ϵ, by analogy to free fermion problems,

$$\frac{\rho_{\rm h}(\lambda)}{\rho_{\rm p}(\lambda)} = e^{\epsilon(\lambda)/T} \ , \tag{2.4.16}$$

and doing some functional differentiation, one recovers the *TBA equation*

$$\epsilon(\lambda) = \varepsilon(\lambda) - T\log\left[1+e^{-\epsilon/T}\right]\hat{\mathcal{K}}^{\dagger} \ , \tag{2.4.17}$$

where the † has the same meaning as in linear algebra: the convolution operator acts from the right.

Using a few manipulations, one can massage the free energy given by Eq. (2.4.14) into the form

$$f = -T\int\frac{d\lambda}{2\pi}\log\left[1+e^{-\epsilon/T}\right] \ , \tag{2.4.18}$$

expressed in terms of the pseudoenergy solution ϵ to the TBA equation, i.e. Eq. (2.4.17).

2.4.4 String hypothesis for Trotterized XXX

Returning to the example of the Trotterized XXX model, more work is required to deal with the complicated quantization conditions for the spectrum of $\hat{M}$. Continuing this analysis, the other solutions to the Bethe Ansatz equations (BAE), given by Eq. (2.3.39), are recovered via application of the "string hypothesis [41]. One assumes that standard strings can be used, since the scattering matrix—given by the right-hand side of Eq. (2.3.39)—is unchanged compared to the standard XXX spin chain. Therefore, one can assume that the roots of the BAE are arranged as

$$\lambda_\alpha^{(n,m)} = \lambda_\alpha^{(n)} + i(2m-n+1) \ , \qquad m = 0,\ldots,n-1 \ , \tag{2.4.19}$$

where n is the number of roots contained in the n-string. The index α labels the string "type" and $\lambda_\alpha^{(n)} \in \mathbb{R}$ is the string "center," corresponding to the real part of the momentum, in analogy to the discussion of two-magnon bound states at the end of Sec. 2.2.2. Deviations with respect to Eq. (2.4.19) are expected to be exponentially suppressed in the system size, L. Here, we assume that the string hypothesis is valid at least for generic values of the parameter δ, which we retain as a regularizer, to be sent to i.

Inserting the string Ansatz into the BAE (i.e. Eq. (2.3.39)), we recover the string form of the Bethe Ansatz equation which involves only the string centers. The derivation follows as a trivial analogy to the derivation for the XXX spin chain, e.g. in Ch. 8 of Ref. 45.

One then obtains the logarithmic form of the BAE for the string centers

$$L\,\theta_n^{(\delta)}(\lambda_\alpha^{(n)}) = 2\pi I_\alpha^{(n)} + \sum_{(m,\beta)\neq(n,\alpha)}\Theta_{n,m}(\lambda_\alpha^n - \lambda_\beta^m) \ . \tag{2.4.20}$$

The above equation is nearly identical to that corresponding to the standard XXX spin chain, which recovers upon replacing $\theta(\lambda) \to \theta^{(\delta)}(\lambda)$, where for an arbitrary function $g(\lambda)$ we define

$$g^{(\delta)}(\lambda) = \frac{1}{2}\left(g(\lambda+\delta) + g(\lambda-\delta)\right) \ , \tag{2.4.21}$$

and set

$$\theta_n(\lambda) = 2\arctan(\lambda/n) \ . \tag{2.4.22}$$

We then take the thermodynamic limit, $L \to \infty$, of Eq. (2.4.20) in the standard sense, by introducing the density of roots and holes for each string length n, respectively $\rho_n(\lambda)$ and $\rho_n^h(\lambda)$, defined in Eq. (2.4.5) in Sec. 2.4.1 with a different notation[3]. For the present discussion, the ensemble of root densities characterizes each eigenstate in the thermodynamic limit as the density of the string centers,

$$\rho_n(\lambda) = \frac{1}{L}\sum_\alpha \delta(\lambda - \lambda_\alpha^{(n)}) \ , \qquad n = 1, \ldots, \infty \ . \tag{2.4.23}$$

From this it follows that the eigenvalues of $\hat{M}$ and the total magnetization $\hat{S}^z_{\rm tot}$ converge to

$$\langle\{\lambda\}|\hat{M}|\{\lambda\}\rangle \overset{L\to\infty}{=} \exp\left[L\sum_{n=1}^\infty \varepsilon_n(\lambda)\rho_n(\lambda)\right] \tag{2.4.24}$$

$$\langle\{\lambda\}|S^z|\{\lambda\}\rangle \overset{L\to\infty}{=} \frac{L}{2} - L\sum_{n=1}^\infty n\rho_n(\lambda) \ , \tag{2.4.25}$$

where we define the effective energy of the n-string magnon according to

$$\epsilon_n(\lambda) \equiv \sum_{m=0}^{n-1} \epsilon\big(\lambda + i(2m-n+1)\big) = \ln\left(\frac{\lambda^2+(n-1)^2}{\lambda^2+(n+1)^2}\right) \ . \tag{2.4.26}$$

The Bethe Ansatz equations, given by Eq. (2.4.20), translate into a functional relation between the density of roots and the density of holes

$$a_n^{(\delta)}(\lambda) = \rho_n(\lambda) + \rho_n^h(\lambda) + \sum_{m=1}^\infty (T_{nm}\circ\rho_m)(\lambda) \ , \qquad n = 1, \ldots, \infty \ , \tag{2.4.27}$$

where we denote the convolution as

$$(g\circ h)(\lambda) = \int d\lambda' g(\lambda-\lambda')h(\lambda') \ , \tag{2.4.28}$$

and we defined the quantities

$$a_n(\lambda) = \frac{1}{2\pi}\frac{d}{d\lambda}\theta(\lambda/n) = \frac{1}{\pi}\frac{n}{\lambda^2+n^2} \tag{2.4.29}$$

$$T_{nm}(\lambda) = a_{|n-m|}(\lambda)(1-\delta_{n,m}) + a_{n+m}(\lambda) + 2\sum_{\ell=|n-m|+1}^{n+m-1} a_\ell(\lambda) \ . \tag{2.4.30}$$

[3]The notation of Sec. 2.4.1 will be used in future sections, the notation has been altered for the present discussion to account for multiple particles species.

2.4.5 TBA for Trotterized XXX

As a particular example, consider the evaluation of the function $\phi(t,s)$ defined by

$$\phi(t,s) = -\lim_{L\to\infty} L^{-1} \ln \mathrm{Tr}_s(\hat{M}^t) \ , \tag{2.4.31}$$

and recognizing $\hat{M}^t \approx \exp\left(-t\hat{H}_{\mathrm{XXX}}\right)$, the trace above represents a Trotterized analogue to the partition function of the XXX model at inverse temperature $\beta = t$, and thus ϕ has an interpretation as a *free energy density* in the Trotterized model.

To account for the projection onto the subspace $S = sL$, we make use of the Legendre transform, namely

$$\phi(t,s) = \max_h[\psi(t,h) - 2hs] \ , \qquad \psi(t,h) = -\lim_{L\to\infty} L^{-1} \log \mathrm{Tr}\left[\hat{M}^t e^{2hS^z}\right] \tag{2.4.32}$$

where the trace in Eq. (2.4.32) is unrestricted vis a vis magnetization sector. We now compute $\psi(t,h)$ exactly using the formalism of the TBA. The standard procedure is to rewrite the trace as a functional integral over the root/holes densities

$$\mathrm{Tr}\left[M^t e^{-2hS^z}\right] = \sum_{\{\lambda\}} \langle\{\lambda\}|M^t e^{2hS^z}|\{\lambda\}\rangle = \int \mathcal{D}\rho_n \mathcal{D}\rho_n^h \, \delta(\mathrm{BAE}) e^{-L\mathcal{F}[\rho,\rho^h]} \ , \tag{2.4.33}$$

where the $\delta(\mathrm{BAE})$ enforces the relation that appears in Eq. (2.4.27). The functional $\mathcal{F}(\rho,\rho^h)$ takes the form

$$\mathcal{F}[\rho,\rho^h] = -h + \sum_n \int dx \rho_n(\lambda)(\epsilon_n(\lambda) + 2hn) + S_{YY}[\rho,\rho^h] \tag{2.4.34}$$

$$S_{YY}[\rho,\rho^h] = -\rho_n(\lambda)\ln\left(1+\frac{\rho_n^h(\lambda)}{\rho_n(\lambda)}\right) - \rho_n^h(\lambda)\ln\left(1+\frac{\rho_n(\lambda)}{\rho_n^h(\lambda)}\right) \ , \tag{2.4.35}$$

where the Yang-Yang entropy $S_{YY}[\rho,\rho^h]$ [47] accounts for the exponentially large number of states described by the same root densities. At large L, the minimization of $\mathcal{F}[\rho,\rho^h]$ leads to the equations for $\eta_n(\lambda) = \rho_n^h(\lambda)/\rho_n(\lambda)$

$$\ln\eta_n(\lambda) = t\epsilon_n(\lambda) + 2hn + \sum_{m=1}^{\infty} T_{nm} \circ \ln(1+\eta_m^{-1}(\lambda)) \ . \tag{2.4.36}$$

Inserting this solution in the expression for $\mathcal{F}[\rho,\rho^h]$ we get its value at the minimum, namely

$$\psi(t,h) = -h - \sum_n \int dx a_n^{(\delta)}(\lambda) \ln\left(1+\eta_n^{-1}(\lambda)\right), \tag{2.4.37}$$

which holds for arbitrary δ, and can be further simplified for $\delta \to i$. Indeed, writing explicitly the case $n = 1$ of Eq. (2.4.36):

$$\ln(1+\eta_1(\lambda)) = tg_1^{(\delta)}(\lambda) + 2h + \sum_{m=1}^{\infty} (a_{m-1} + a_{m+1}) \circ \ln(1+\eta_m^{-1}(\lambda)) \ . \tag{2.4.38}$$

We moreover note that

$$\frac{a_{m-1}(\lambda) + a_{m+1}(\lambda)}{2} = a_m^{(i)}(\lambda) \tag{2.4.39}$$

we obtain

$$\psi(t,h) \equiv \lim_{\lambda\to 0} \frac{t\epsilon_1(\lambda) - \ln\eta_1(\lambda)}{2} \tag{2.4.40}$$

Note that the limiting procedure is required just because both $g_1^{(i)}(\lambda)$ and $\ln\eta_1(\lambda)$ are singular for $\lambda \to 0$, but their difference is not.

2.5 Generalized Thermalization

Classical integrable models do not thermalize in any limit; however, they can nonetheless be described using statistical mechanics. Because their equations of motion can be integrated directly, there is no notion of chaos in classical integrable systems: any finite uncertainty in the initial conditions remains finite as the system evolves—corresponding to a Lyapunov exponent of zero—in contrast to chaotic systems, where such uncertainty is magnified exponentially within a Lieb-Robinson "light cone," allowing the system to approach equilibrium and justifying the use of statistical ensembles. Essentially, integrable models indeed remember *local* details of their past configuration, and this information remains accessible to local measurements.

Additionally, because integrable systems have an infinite number of extensive, local conserved quantities in the thermodynamic limit, they cannot be described in terms of a handful of state variables, unlike typical thermal systems. In fact, if one were not aware of the need to specify the values of these conserved charges, an integrable system would appear athermal, e.g. in terms of spectral properties, due to the existence of infinitely many independent sectors whose eigenvalues do not repel.

However, there are aspects of thermalization that integrable systems do realize. For example, these models generally relax to a steady state that is independent of time, much like thermal systems. Additionally, this steady state can be described by a local density matrix, which may be drawn from a *generalized* ensemble—designed to account for the special properties of integrable models—to reproduce the expectation values of local observables using statistical mechanics.

The reason that integrable models remember details of their initial conditions is that they are translation invariant. Hence, following a quench, the expectation value of the energy density, for example, is given by

$$e(t) = \lim_{t\to\infty} \lim_{L\to\infty} L^{-1} \langle \psi(t)|\hat{H}|\psi(t)\rangle = \lim_{t\to\infty} \lim_{L\to\infty} L^{-1} \langle \psi(t)|\hat{H}_{j,j+1}|\psi(t)\rangle \ , \tag{2.5.1}$$

due to translation invariance of the Hamiltonian and its eigenstates. This translation invariance is built into the model and its eigenstates, and not merely some property that recovers in an average sense. Unlike thermal phases, which are robust to small perturbations, integrability is fine-tuned, and this property would be destroyed by introducing spatial inhomogeneity, e.g.

As can be seen from Eq. (2.5.1), at *any* time t following a quench, one can make a strictly local measurement in a finite subsystem and thereby recover information about the initial energy density, and the initial energy itself. However, as discussed in Ch. 1, this is also expected to hold for nonintegrable quantum systems that *do* thermalize in the standard sense: in such systems, the energy density of the state at $t = 0$ dictates the late-time "temperature" of the system following the quench. If the system is translation invariant, one expects to recover this information locally, per Eq. (2.5.1); for inhomogeneous systems, it may be possible for the choice of subsystem $\mathcal{A}$ to change somewhat the effective temperature, as the subsystem $\mathcal{A}$ may exchange energy with its "environment," $\mathcal{B}$, under the global dynamics.

This is also true of classical thermal systems, and the origin of the microcanonical ensemble: thermal systems forget as much information about the past as is permitted. However, since energy is preserved by the dynamics, this will generally be preserved to late times, and thus the system must remember it. The microcanonical ensemble therefore consists of all states that have the same energy, as these are the set of states that can be realized from the initial configuration. This provides a perfectly valid thermal ensemble.

However, if there exist other extensive, conserved quantities that can be expressed as the sum of local terms, then the expectation value of these conserved quantities in the distant past

will also be accessible at arbitrarily late times, determined by a formula essentially identical to Eq. (2.5.1). In this case, we must generalize the microcanonical ensemble, accounting for these conserved quantities using the *generalized microcanonical ensemble* [48–51], which, like its non-generalized counterpart, fixes directly the value of each conserved quantity, and the partition function is essentially a delta function that selects configurations with precisely the correct values of these quantities. The values of all other observables are free to fluctuate. Denoting by $|n\rangle$ the various eigenstates of an integrable Hamiltonian, the expectation value of an observable $\hat{\mathcal{O}}$ in the generalized microcanonical ensemble is given by

$$\langle\hat{\mathcal{O}}\rangle_{\mathrm{G}\mu\mathrm{E}} = \sum_n{}' \langle n|\hat{\mathcal{O}}|n\rangle \ , \tag{2.5.2}$$

where the $'$ denotes a restriction of the sum over eigenstates to those that agree on the values of charges. This can be generalized sensibly to describe systems with any number of translation invariant, extensive, local conserved quantities.

However, integrable systems in the thermodynamic limit have an infinite number of such quantities. In the special case of free systems, fixing the eigenvalues of each of these charges fixes the eigenstate of the evolution, and forms a complete many-body basis; for general, interacting integrable systems, it is natural to expect that no two eigenstates agree exactly on every single charge. Thus, to recover a valid statistical ensemble, one can use a truncated generalized microcanonical ensemble that agrees only on a limited set of the charges that are of interest, and/or simply demand that the expectation values of these charges are *close* to one another. Considering the standard case of post-quench dynamics, in analogy to Sec. 1.3.3, one restricts to eigenstates $|n\rangle$ for which the expectation values of the charges are parametrically *close* to their initial values, i.e.

$$\left|\langle n|\hat{Q}_j|n\rangle - \langle\psi(0)|\hat{Q}_j|\psi(0)\rangle\right| < \delta_{Q_j} \ , \tag{2.5.3}$$

which defines a valid statistical ensemble to which integrable models relax following a quench [48, 52, 53].

However, it is more common to use Gibbs ensembles, where instead of specifying the values of conserved quantities, one assigns to each conserved quantity a Lagrange multiplier—e.g. inverse temperature $\beta = 1/T$ to energy, E, chemical potential μ to particle number, N, and so on—and fixes instead the value of the Lagrange multiplier. In a direct extension of the standard Gibbs ensemble for thermal systems with finitely many conserved quantities, the Generalized Gibbs Ensemble (GGE) [48, 48–51] assigns an infinite number of Lagrange multipliers, $\{\beta_j\}$ to the expectation values of the each of the infinitely many charges $\overline{Q}_j = \langle\hat{Q}_j\rangle$. In particular, one has the partition function

$$Z_{\mathrm{GGE}} = \sum_n \exp\left(-\sum_j \beta_j \langle n|\hat{Q}_j|n\rangle\right) \ , \tag{2.5.4}$$

and the expectation values of observables are given by

$$\langle\hat{\mathcal{O}}\rangle_{\mathrm{GGE}} = \frac{\sum_n \langle n|\hat{\mathcal{O}}|n\rangle\, e^{-\sum_j \beta_j \langle n|\hat{Q}_j|n\rangle}}{\sum_n e^{-\sum_j \beta_j \langle n|\hat{Q}_j|n\rangle}} \ , \tag{2.5.5}$$

and by equivalence of ensembles, one should have

$$\overline{\hat{\mathcal{O}}} = \langle\hat{\mathcal{O}}\rangle_{\mathrm{GGE}} = \langle\hat{\mathcal{O}}\rangle_{\mathrm{G}\mu\mathrm{E}} \ , \tag{2.5.6}$$

and as in the microcanonical case, it is common practice to truncate the generalized Gibbs ensemble to fix only finitely many of the $\{\beta_j\}$. In contrast to the GμE, in the GGE this is mathematically quite simple, as one simply sets $\beta_j = 0$ for any charge not part of the truncated set. From the perspective of the partition function, this amounts to omitting Lagrange multipliers for any quantity one does not care to fix, which in practice will be the vast majority.

As a final note, there is no good reason to call these "generalized" Gibbs ensembles, as nothing about Gibbs' original formulation was contingent on there being exactly three—or even finitely many—Lagrange multipliers (or conserved quantities). However, it has become common nomenclature to preface standard techniques with the word "generalized" in the context of quantum integrability. However, the generalized microcanonical ensemble does in fact generalize the μCE of thermal systems, which historically only accounted for energy.

2.6 Generalized Hydrodynamics

2.6.1 Semiclassical approximation: Bethe-Boltzmann

Generalized hydrodynamics (GHD) proceeds in much the same fashion as regular hydrodynamics, which apply to conserved quantities in general. There are two equivalent formulations, in terms of the infinitely many conserved quantities themselves, and relatedly, in terms of the quasiparticle density, which corresponds to the root densities that appear in the TBA equations, i.e. Eq. (2.4.17) in Secs. 2.4.1 and 2.4.3. In previous sections, all quantities were strictly global, and to use the hydrodynamic framework (as is standard practice for instance in the treatment of kinetic theory that recovers the Boltzmann equation, and other semiclassical procedures), one trades global equilibrium—or general globally defined quantities—for locally varying counterparts [54–56].

Considering a generalized Gibbs ensemble (GGE) of the type defined in Sec. 2.5, one can capture this local structure (i.e. x dependence) by sending $\beta_j \to \beta_j(x)$. It is also possible to formulate the derivation of the Boltzmann equation using a physically motivated, but perhaps less rigorous method, outlined in Ref. 54. In this case, one divides the system into M cells, with the ith cell having length L_i, and further supposes that

- The system is quantum mechanical on length scales comparable to L_i, but semi-classical on length scales comparable to the size of the full system, L. This provides for the specification, e.g., of the particle number, $N_i(t)$, of cell i at time t, but not particle positions within cell i.
- The constituent particles of the ith cell are in an eigenstate $|\psi_i(t)\rangle$ of the $N_i(t)$-body Hamiltonian of cell i.
- The thermodynamic limit can be taken on L_i and $N_i(t)$ in the ith cell, i.e. $L_i, N_i(t) \to \infty$ with their ratio, $\rho_i(t) = N_i(t)/L_i$ finite. This density is directly related to root densities of the TBA equations.
- The full system size $L \gg L_i$, and there are many cells, i. In this case, $\rho_i(t) \to \rho(i,t) \to \rho(x,t)$, and similarly for the densities of other relevant quantities. However, the infinitely many densities of conserved charges, q_i, can be recovered from the quasiparticle density that comes from TBA.
- This also requires that quantities like $\rho_i(t)$ and the density of states in cell i vary sufficiently slowly with i and t that they may be treated as continuous and differentiable functions $\rho(x,t)$.

- Finally, this requires that the full wavefunction for the entire system is a tensor product of the wavefunctions in the individual cells.

2.6.2 Insights from TBA

Here we consider the physics of a quantum quench in an integrable model using the TBA formalism. We use the generalized μCE outlined in Sec. 2.5 that does not fix exactly the expectation values of all conserved quantities, but rather, requires that they be within some threshold of their expectation value as calculated at $t = 0$. Essentially, this amounts to relaxing the usual δ function associated to the microcanonical partition function to a distribution of small but finite width. In this case, if we consider the eigenstates within this microcanonical window, in the thermodynamic limit, this collection of eigenstates defines a single macrostate, $|\rho_{\rm p}, \rho_{\rm h}\rangle$, due to the nature of the TBA formalism[4], which acts like the steady state of thermal systems.

Note that we are generally interested in working with quenches, rather than in direct eigenstates of the integrable model, as the hydrodynamic regime is expected to describe the relaxation from local equilibrium to the global equilibrium steady-state described by the thermodynamic macrostate $|\rho_{\rm p}, \rho_{\rm h}\rangle$. In general, one can extract from the $t = 0$ state the appropriate expectation values of all conserved quantities, which generally can be expressed in terms of $\rho_{\rm p}$, as shown below. Thus, one can recover the macrostate $|\rho_{\rm p}, \rho_{\rm h}\rangle$ and introduce local structure—in the form of spatiotemporal dependence, $\rho_{\rm p}(\theta) \to \rho_{\rm p}(\theta; x, t)$—to calculate all local properties as one approaches the steady state, following local equilibration as described by the semi-classical picture of the previous section.

Thus, one has a spatially and temporally varying root density $\rho_{\rm p}(\theta; x, t)$, where θ is a generic rapidity index. For relativistic models, e.g. XXZ and Sinh-Gordon, θ is actually a rapidity. For Galilean-invariant models, e.g. free fermions and Lieb-Liniger, θ is proportional to momentum itself, $\theta = v^{\rm group}(\theta) = p/m$. It will also prove convenient to define the occupation factor (or "Fermi factor," so-called because the quasiparticle modes can be at most singly occupied),

$$n(\theta; x, t) = \frac{\rho_{\rm p}(\theta; x, t)}{\rho_{\rm s}(\theta; x, t)} \ , \tag{2.6.1}$$

where $\rho_{\rm s}(\theta)$ is the locally varying density of states, defined globally in the TBA formalism via Eq. (2.4.5). It will also be important to recall the operator, $\hat{\mathcal{K}}$, denoting convolution against the differential scattering kernel:

$$[\hat{\mathcal{K}} g](\theta) = \int \frac{d\phi}{2\pi} K(\theta, \phi)\, g(\phi) \ , \quad \text{where} \quad K(\theta, \phi) = \frac{1}{i}\frac{d}{d\theta} \ln S(\theta, \phi) \quad . \tag{4.3.4}$$

With some manipulations, one can prove from TBA the relation

$$2\pi\rho_{\rm s}(\theta) = p'(\theta) + 2\pi[\hat{\mathcal{K}}\rho_{\rm p}](\theta) \ , \tag{2.6.2}$$

where $p'(\theta) = dp/d\theta$ is the derivative of the momentum with respect to rapidity (a constant in Galilean invariant models). This can be re-written as

$$\rho_{\rm s}(\theta) = \frac{1}{2\pi}\left(1 - \hat{\mathcal{K}} n\right)^{-1}(p') = \frac{1}{2\pi}(p')^{\rm dr}(\theta) \ , \tag{2.6.3}$$

[4]This assumes a particular notion of the generalized microcanonical ensemble and the "window," which is intertwined with the thermodynamic Bethe Ansatz itself and well formulated in the literature.

where n is the occupation factor defined in Eq. (2.6.1) and the "dressing operation" is defined for arbitrary functions of rapidity via

$$(g)^{\mathrm{dr}}(\theta) = \left[\left(1 - \hat{\mathcal{K}}\hat{\mathcal{N}}\right)^{-1} g\right](\theta) \ , \tag{2.6.4}$$

where $\hat{\mathcal{N}}$ denotes convolution against a diagonal operator with kernel $n(\theta)\,\delta(\theta - \phi)$, and is equivalent to multiplication by the occupation factor, n. Note that the inverse operator above may be evaluated by expressing the above as a geometric series in $\hat{\mathcal{K}}\hat{\mathcal{N}}$, or using an alternate formulation:

$$(g)^{\mathrm{dr}}(\theta) = g(\theta) + \int \frac{d\phi}{2\pi} K(\theta,\phi)\, n(\phi)\, (g)^{\mathrm{dr}}(\phi) \ , \tag{2.6.5}$$

and in general, these must be computed numerically. For Lieb-Liniger, such numerical computation converges extremely rapidly as one iterates Eq. (2.6.5).

We must also define the effective velocity, $v^{\mathrm{eff}}(\theta)$ of a quasiparticle with rapidity θ. Compared to the group velocity,

$$v^{\mathrm{group}}(\theta) = \frac{\varepsilon'(\theta)}{p'(\theta)} \ , \tag{2.6.6}$$

the effective velocity is the actual propagation velocity of quasiparticles, accounting for collisions between particles of different rapidities, which dresses the group velocity in analogy to the dressing defined in Eq. (2.6.5),

$$v^{\mathrm{eff}}(\theta) = v^{\mathrm{group}}(\theta) + \int d\phi \frac{1}{p'(\theta)} K(\theta,\phi)\, \rho_{\mathrm{p}}(\phi) \left(v^{\mathrm{eff}}(\phi) - v^{\mathrm{eff}}(\theta)\right) \ , \tag{2.6.7}$$

and using some manipulations of Eq. (2.6.1), Eq. (2.6.3), and the above, one has

$$\rho_{\mathrm{p}}(\theta) = \frac{n(\theta)}{2\pi} (p')^{\mathrm{dr}}(\theta) \ , \quad \rho_{\mathrm{p}}(\theta)\, v^{\mathrm{eff}}(\theta) = \frac{n(\theta)}{2\pi} (\varepsilon')^{\mathrm{dr}}(\theta) \ , \tag{2.6.8}$$

and dividing these relations recovers

$$v^{\mathrm{eff}}(\theta) = \frac{(\varepsilon')^{\mathrm{dr}}(\theta)}{(p')^{\mathrm{dr}}(\theta)} \ , \tag{2.6.9}$$

which is similar to the group velocity definition, Eq. (2.6.6).

An important takeaway from Eq. (2.6.8) is that the spacetime dependence of *all* quantities that one might consider can be regarded as inherited from the occupation function $n(\theta; x, t)$. Regarding Eq. (2.6.8), the only quantities that appear on the righthand side of the two expressions are the occupation factor, n, and direct functions of rapidity, e.g. the differential scattering kernel, K, and rapidity derivatives of the momentum, p, and single-particle energy, ε. Such quantities do not inherit local structure from the procedure of divvying the system into hydrodynamic "cells" that imbues densities and related quantities with semiclassical, local structure. This is standard to such semiclassical techniques, where rapidity-dependent quantities are associated to quantum numbers, which are uniform across hydrodynamic cells, and by construction do not have local variations. All spatiotemporal variations are acquired solely through *functional* dependence on quantities related to the density, all of which can be expressed in terms of the "bare" quantities above (i.e. momentum- or rapidity-like quantities) and n. One could equivalently regard the quasiparticle density ρ_{p} as being the fundamental source of local structure. However because it is n and not ρ_{p} that appears in the dressing operator $\left(1 - \hat{\mathcal{K}}n\right)^{-1}$, and because—unlike ρ_{p}—the hydrodynamic equation for n are diagonal in rapidity (and therefore a hydrodynamic eigenmode), we regard n as the fundamental quantity.

2.6.3 Quasiparticle continuity equation

In the quasiparticle language, the hydrodynamics of the quasiparticles with density $\rho_{\rm p}(\theta;x,t)$ is given simply by the *continuity equation*

$$\partial_t \rho_{\rm p}(\theta;x,t) + \partial_x \left[v^{\rm eff}(\theta;x,t)\, \rho_{\rm p}(\theta;x,t) \right] = 0 \ , \tag{2.6.10}$$

where $v^{\rm eff}(\theta;x,t)\,\rho_{\rm p}(\theta;x,t)$ is the *current* of quasiparticles with rapidity θ. We can make use of the definitions in Eq. (2.6.8), defining

$$\hat{\mathcal{U}} = \hat{\mathcal{N}} \left(1 - \hat{\mathcal{K}} \hat{\mathcal{N}} \right)^{-1} \ , \tag{2.6.11}$$

we have $2\pi\,\rho_{\rm p} = \hat{\mathcal{U}}(p')$ and $2\pi\, v^{\rm eff}\,\rho_{\rm p} = \hat{\mathcal{U}}(\varepsilon')$, and we note that

$$\partial_{x,t} \hat{\mathcal{U}}\, f = \left(1 - n\hat{\mathcal{K}} \right)^{-1} \partial_{x,t} n \left(1 - \hat{\mathcal{K}} n \right)^{-1} f = \left(1 - n\hat{\mathcal{K}} \right)^{-1} \partial_{x,t} n\, f^{\rm dr} \ , \tag{2.6.12}$$

and Eq. (2.6.10) becomes

$$0 = \frac{1}{2\pi} \left(1 - n\hat{\mathcal{K}} \right)^{-1} \left\{ (p')^{\rm dr}\, \partial_t n + (\varepsilon')^{\rm dr}\, \partial_t n \right\} \tag{2.6.13}$$

$$= \left(1 - n\hat{\mathcal{K}} \right)^{-1} \frac{(p')^{\rm dr}}{2\pi} \left\{ \partial_t n + \frac{(\varepsilon')^{\rm dr}}{(p')^{\rm dr}} \partial_t n \right\} \tag{2.6.14}$$

$$= \left(1 - n\hat{\mathcal{K}} \right)^{-1} \rho_{\rm s} \left\{ \partial_t n + v^{\rm eff} \partial_x n \right\} \ , \tag{2.6.15}$$

which we include in detail so the extension to a nonzero righthand side of Eq. (2.6.10) is clear. In the integrable case, the continuity equation becomes

$$\partial_t n(\theta;x,t) + v^{\rm eff}[\theta;n]\, \partial_x n(\theta;x,t) = 0 \ , \tag{2.6.16}$$

which is diagonal. Thus, the occupation factor, n, diagonalizes the GHD equation in the quasiparticle language, Eq. (2.6.10).

We can also rewrite Eq. (2.6.10) using similar manipulations. Defining the convolution operator

$$\hat{A} = \left(1 - n\hat{\mathcal{K}} \right)^{-1} v^{\rm eff} \left(1 - n\hat{\mathcal{K}} \right) \ , \tag{2.6.17}$$

we can partially "undo" the diagonalization that produced Eq. (2.6.16) to recover

$$\partial_t \rho_{\rm p}(\theta;x,t) + \left[\hat{A} \partial_x \rho_{\rm p} \right](\theta;x,t) = 0 \ , \tag{2.6.18}$$

which is not diagonal in rapidity, but does simplify the derivative situation.

In all of the equations above, it is clear that a key feature of integrable hydrodynamics is *ballistic transport*. This can be seen by solving Eq. (2.6.16) using the method of characteristics.

2.6.4 Ballistic transport of quasiparticles

The Fermi factor equation, Eq. (2.6.16), is quasilinear, and therefore soluble in principle (and practice) via characteristic coordinates [57]. We make the Ansatz for the solution

$$n(\theta;x,t) = \int d\phi \int dy\, \mathcal{K}[\theta,x,t;\phi,y,0]\; n_0(\phi;y) \ , \tag{2.6.19}$$

where the initial condition at $t = 0$, $n(\theta; x, t) = n_0(\theta; x)$, which implies $\mathcal{U}[\theta, x, 0; \phi, y, 0] = \delta(x - y)\,\delta(\theta - \phi)$. The occupation factor equation, Eq. (2.6.16), is

$$0 = \left\{\partial_t + v^{\text{eff}}[\theta, n]\,\partial_x\right\} n(\theta; x, t) \ , \tag{2.6.20}$$

which is solved by

$$0 = \left\{\partial_t + v^{\text{eff}}[\theta, n]\,\partial_x\right\} \mathcal{U}[\theta, x, t; \phi, y, 0] \ . \tag{2.6.21}$$

We define some function $X_\theta(t)$ such that

$$\frac{dX_\theta}{dt} = v^{\text{eff}}[\theta, \tilde{n}] \ , \tag{2.6.22}$$

where the velocity is allowed to depend on the solution $\tilde{n}(\theta; t) \equiv n(\theta; X_\theta(t), t)$, and therefore the kernel (or "propagator") $\mathcal{U}$.

We make an Ansatz for the propagator, $U[\theta, t; \phi, y] \equiv \mathcal{U}[\theta, X_\theta(t), t; \phi, y]$, where $x \to X_\theta(t)$. Since X satisfies Eq. (2.6.22), the righthand side of Eq. (4.3.15) becomes a total derivative of U with respect to t, i.e. $d/dt = \partial_t + v^{\text{eff}}[\theta, n]\,\partial_x$, and Eq. (4.3.15) is solved if

$$\frac{dU}{dt} = \partial_t U + v^{\text{eff}}[\theta, n]\,\partial_x U = 0 \ , \tag{2.6.23}$$

which combined with Eq. (2.6.22), turns the partial differential equation (PDE), Eq. (4.3.15), into two coupled ordinary differential equations (ODEs), if one regards of the arguments θ, ϕ, y of U as labels and not independent variables. Unlike PDEs, nonlinear ODEs are often soluble, which makes the method of characteristics generally powerful. This case is particularly easy, since the equation $dU/dt = 0$ simply implies that U is constant, equal to its $t = 0$ value,

$$U[\theta, t; \phi, y] = U[\theta, 0; \phi, y] \ , \tag{2.6.24}$$

where the time zero version is given by

$$U|_{t=0} = \lim_{t \to 0} \mathcal{U}[\theta, X_\theta(t), t; \phi, y] = \delta(\theta - \phi)\,\delta(X_\theta(0) - y) \ , \tag{2.6.25}$$

and the full solution recovers from expressing $X_\theta(0)$ in terms of $x \leftrightarrow X_\theta(t)$ and t itself. Thus, the solution for n is given by

$$\tilde{n}(\theta; t) = n_0(\theta; X_\theta(0)) \ , \tag{2.6.26}$$

which as written is independent of t, and both sides of Eq. (2.6.22) can be integrated directly over time, from 0 to t, to obtain

$$X_\theta(t) - X_\theta(0) = t v^{\text{eff}}[\theta, n_0(\cdot; X_\cdot(0))] \ , \tag{2.6.27}$$

and solving for $X_\theta(0)$ provides the full solution

$$n(\theta; x, t) = \tilde{n}_{\text{int}} = n_0\left(\theta; x - t v^{\text{eff}}[\theta, n]\right) \ , \tag{2.6.28}$$

which is slightly complicated only because the effective velocity is both a function of rapidity, θ, and a functional of the occupation factor, n.

2.6.5 Euler hydrodynamics of charges

Because hydrodynamics is associated with conservation laws, it is also natural to consider GHD in the languages of the charges, rather than the "Bethe-Boltzmann" formalism treated thus far [54, 56, 58, 59]. However, the average value of the charges in terms of a given GGE are given straightforwardly using the root densities, i.e. $\rho_{\rm p}(\theta)$. In particular, associated to the nth charge, $\mathfrak{q}_n$ is the rapidity-dependent single-particle eigenvalue $h_n(\theta)$, and the set of all functions h_n form a complete set that can fully specify any smooth function of rapidity. Because of this, there is a direct mapping from the space of densities as a function of rapidity, $\rho_{\rm p}(\theta)$, and the space of charges, $q_n = \langle \mathfrak{q}_n \rangle$. The latter are defined by

$$q_n(x,t) = \int d\theta\, h_n(\theta)\, \rho_{\rm p}(\theta;x,t) = \int \frac{d\theta}{2\pi}\frac{dp}{d\theta}\, h_n^{\rm dr}(\theta)\, n(\theta;x,t) \ , \tag{2.6.29}$$

and the corresponding *currents*, $j_n = \langle \mathfrak{j}_n \rangle$, are given by

$$j_n(x,t) = \int d\theta\, h_n(\theta)\, v^{\rm eff}(\theta)\, \rho_{\rm p}(\theta;x,t) = \int \frac{d\theta}{2\pi}\frac{dE}{d\theta}\, h_n^{\rm dr}(\theta)\, n(\theta;x,t) \ , \tag{2.6.30}$$

where the latter expressions in the preceding equations show that the currents and charges are essentially integrals of the occupation factor over momentum and energy, respectively, weighted by the dressed spectral function h. The latter equation, Eq. (2.6.30), is only valid at the level of Euler hydrodynamics; at the level of Navier-Stokes hydrodynamics, we must allow for the possibility that the expectation values of local observables are sensitive to the gradient of the quasiparticle density. However, this correction can simply be added to the hydrodynamic equations later on, and we will address it separately.

At the level of Euler hydrodynamics, the continuity equation for the nth charge is given by

$$\partial_t q_n(x,t) + \partial_x j_n(x,t) = 0 \ , \tag{2.6.31}$$

where the nth current should be considered as a functional of *all* charges $\{q_m\}$. This is given approximately by

$$\partial_x j_n(x,t) = \sum_m A_{nm}\partial_x q_m(x,t) \ , \tag{2.6.32}$$

where

$$A_{nm} = \frac{\delta j_n}{\delta q_m} = \int d\theta h_n(\theta)\left[\hat{A}h_m\right](\theta) = \int d\theta h_n^{\rm dr}(\theta)\, v^{\rm eff}(\theta)\left(h_m - n(\theta)\left[\hat{\mathcal{K}}h_m\right](\theta)\right) \ , \tag{2.6.33}$$

where $\hat{A}$ is the *same* matrix defined in Eq. (2.6.17).

2.6.6 Navier-Stokes hydrodynamics of charges

There are also corrections to Eq. (2.6.30) at the *Navier-Stokes* scale [58–60],

$$\begin{aligned} j_{{\rm Nav},n}(x,t) &= j_{{\rm Eul},n}(x,t) \\ &\quad - \frac{1}{2}\int d\theta h_n(\theta)\int d\phi \mathcal{D}\left[\theta,\phi;\rho_{\rm p}(\cdot)\right]\partial_x\rho_{\rm p}(\phi) \ , \end{aligned} \tag{2.6.34}$$

where $j_{{\rm Eul},n}$ is the Euler version, Eq. (2.6.30). The form of the diffusion matrix is constrained by various physical properties, and depends on the GGE in question.

It is worth noting that this correction necessarily vanishes for any charge for which the corresponding current is itself a conserved charge, including the total particle density in Lieb-Liniger and free fermion (i.e. Galilean-invariant) models, or the energy density in XXZ or Sinh-Gordon (i.e. relativistic) models. In both cases, the current corresponds to momentum density.

Chapter 3

Floquet Integrability

This Chapter is largely drawn from Ref. 37 by this author.

3.1 Introduction

Periodically driven (or "Floquet") quantum systems have become a major theme in many-body physics [61–75]: driving enables one to engineer exotic states of matter experimentally [76–79] to realize phases that are absent in equilibrium [67–69, 80–88]. Floquet dynamics are captured by a unitary, $\hat{F}$, which evolves the system by a single period; when $\hat{F}$ is not smoothy connected to the identity, the resulting dynamics are distinct from those of any "static" Hamiltonian ($e^{i\hat{H}t}$ is always deformable to the identity). This is particularly transparent in noninteracting Floquet systems: their band structure is compactified in both quasimomentum *and* quasienergy, which allows for band structures that wind nontrivially in quasienergy (Figure 3.1a), which cannot be realized in local lattice Hamiltonians [66–70, 80, 81]. Thus, Floquet systems can host unpaired chiral modes, while Hamiltonian dynamics only admit chiral modes on the boundaries of higher-dimensional systems [66, 68, 89, 90]. In systems with nontrivial quasienergy winding, each single-particle state has a quantized time-averaged current; protocols that accomplish such adiabatic particle transfer are called "Thouless pumps" [66, 91, 92].

These topological features remain long-lived in certain interacting models [92–94]; however, interactions generally heat a system up to infinite temperature, unless it is integrable or many-body localized (MBL) [11, 12, 14, 95–99]. Although MBL can protect Floquet topological phases [15, 82, 99–112], such *localized* phases do not host chiral modes. *Interacting* integrable systems are another broad class of systems that do not thermalize [19, 113–115]; whether distinctively Floquet versions exist has been less discussed [38, 116–119].

This Chapter presents an interacting integrable Floquet model that hosts quasiparticles with a nontrivial winding number, i.e. an integrable Thouless pump. Unlike previously proposed interacting integrable Floquet systems, this model is not smoothly connected to any Hamiltonian, and is thus inherently Floquet, rather than an "integrable Trotterization" [38]. This model is a fully quantum extension of an integrable cellular automaton known as Rule 54, or the Floquet Fredrickson-Andersen (FFA) model [120–122]. FFA's simplicity has elucidated various puzzles concerning hydrodynamics and operator growth in generic interacting integrable systems [121–128]. FFA can be written as a Floquet unitary comprising local gates, but it is classical in that it

maps computational-basis product states to one another. Although FFA has chiral quasiparticles, they do not disperse, but instead all have one of two group velocities, ±1. The dispersing FFA (DFFA) generalization we introduce here alternates the FFA dynamics with that of a particular strictly local Hamiltonian, making the model fully quantum by restoring dispersion while preserving integrability. This generalization remains simple enough that the Bethe equations can be solved analytically—a remarkable feature for an interacting model. This model is simple because the quantization of either quasiparticle species depends only on the total number of quasiparticles of each species, and *not* on their rapidities. This simplicity also manifests in the existence of special local operators that remain lightly entangled at all times, as in FFA [125, 128]. This model is the first representative of a class of interacting integrable models specific to the Floquet setting, featuring stable chiral quasiparticles.

3.2 The Dispersing Floquet Frederickson-Andersen Model

The model is defined on a chain of $2L$ q-bits (i.e. spins 1/2) with dynamics generated by the repeated application of the Floquet operator, the unitary evolution operator that evolves the system by a single period. The Floquet unitary comprises a sequence of three unitaries, the first two corresponding to the nondispersing model, and the latter to a "Hamiltonian" evolution term $e^{-i\lambda\hat{H}}$ responsible for the dispersion,

$$\hat{F}(\lambda) = e^{-i\lambda\hat{H}} \prod_{j \text{ even}} \hat{U}_{j-1,j,j+1} \prod_{j \text{ odd}} \hat{U}_{j-1,j,j+1}, \tag{3.2.1}$$

with gates

$$\hat{U}_{j-1,j,j+1} \equiv \text{CNOT}(1 \to 2)\,\text{CNOT}(3 \to 2)\,\text{Toff.}(1,3 \to 2), \tag{3.2.2}$$

in terms of controlled NOT (CNOT) and Toffoli gates [129], and $\hat{H}$ is a Hamiltonian specified below. In simpler terms, $\hat{U}_{j-1,j,j+1}$ is the instruction "flip spin j if one or both of its nearest neighbors is up." The two layers of the FFA unitary in terms of spin-1/2 operators each have the form

$$\hat{F}_{\text{sites}} = \bigotimes_{j \in \text{sites}} \hat{U}_{j-1,j,j+1} \tag{3.2.3}$$

$$\equiv \bigotimes_{j \in \text{sites}} \left[\sigma_j^x \left(\hat{\mathbb{1}} - \hat{d}_{j-1}\hat{d}_{j+1}\right) + \hat{d}_{j-1}\hat{d}_{j+1}\right], \tag{3.2.4}$$

where "sites" are even or odd, and $\hat{d}_j = \frac{1}{2}\left(\hat{\mathbb{1}}_j - \sigma_j^z\right)$ is the projector onto $\downarrow$ on site j in the σ^z basis. Analogously, we define the projector onto $\uparrow$ as $\hat{u}_j = \frac{1}{2}\left(\hat{\mathbb{1}}_j + \sigma_j^z\right)$ for later use. For $\lambda = 0$, the third step of the drive vanishes, and this model reduces to FFA, $\hat{F}(0) = \hat{F}_0$. In principle, $\hat{F}_0$ is applied first, however by construction $[\hat{H}, \hat{F}_0] = 0$, and thus the Hamiltonian and FFA have simultaneous eigenstates.

3.2.1 Nondispersing limit

On its own, $\hat{F}_0$ hosts two species of chiral quasiparticle excitations above the vacuum state $|0\rangle = |\downarrow\downarrow\ldots\downarrow\rangle$, indexed $\nu = +1$ for "right-movers" and $\nu = -1$ for "left-movers." We regard the $2L$ physical sites as L unit cells: the nth unit cell contains the A site $2n-1$ and B site $2n$. If both of these sites are $\uparrow$, then there is a $\nu = +1$ right-moving doublon in cell n; if the B site of cell $n-1$

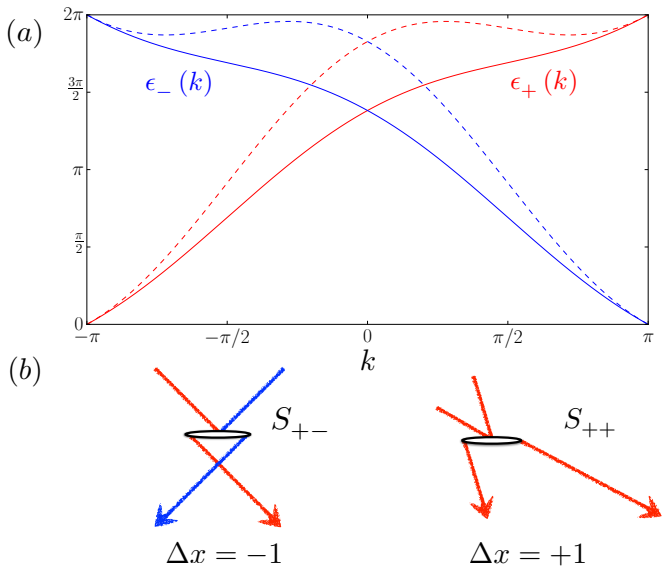

Figure 3.1: Chiral quasiparticles in the DFFA model. (a) Dispersion relations showing the (bare) single-particle Floquet quasienergies $\varepsilon(k)$ for both + and − quasiparticles, for $\lambda = 0.3$ (solid lines) and $\lambda = 0.65$ (dashed lines). Both bands are topological (chiral) as they wrap around the periodic quasienergy direction, and can only exist in a periodically driven system. Note that for $\lambda = 0.65$, the ±-particles can be left(right)-moving for some range of momenta. (b) Soliton gas picture. The scattering events in the DFFA model factorize onto simple two-body processes, which semi-classically correspond to a displacement $\Delta x = \pm 1$ after a collision, independently of the momenta of the quasiparticles.

and A site of n are both ↑, there is a $\nu = -1$ left-moving doublon in cell n. Additionally, we refer to isolated ↑'s as *molecules*, which contain one of each mover: a molecule on the A site of cell n corresponds to both $\nu = \pm 1$ movers in cell n; a B molecule in cell n corresponds to a + at n and − at $n+1$. The molecule states ↓↑↓ arise during collisions between the two species. Apart from these collisions, $\hat{F}_0$ acts by changing the positions of the ± particles by ±1 unit cell, and conserves independently the number of each, $N_\pm$.

In the FFA model all quasiparticle excitations have two possible velocities and no dispersion. The structure of conservation laws in this model differs from that of generic interacting integrable models, in which a generalized Gibbs ensemble (GGE) [50] can be fully specified through the distribution of quasiparticle velocities. In the FFA model, there are only two velocities, which do not fully specify a state. The remaining conservation laws correspond to asymptotic "spacings" between adjacent quasiparticles of the same species [122]. In the zero-density limit, the bare spacings between same-species quasiparticles are conserved, since all such quasiparticles have the same velocity. At nonzero densities, one can define an asymptotic spacing by accounting for interaction effects: e.g., suppose we have two + quasiparticles that are n steps apart; the quasiparticle on the right collides first with a − quasiparticle and is time delayed by one step: therefore, while there is a − quasiparticle between them, the two + quasiparticles will be exactly $n-1$ steps apart if their asymptotic spacing is n. Given a spin configuration, its asymptotic spacings can be found numerically by simulating its free expansion into vacuum [122].

3.2.2 Adding dispersion

We now construct $\hat{H}$, the Hamiltonian part of Eq. (3.2.1), to generate dispersion while maintaining integrability. Conservation of particle number automatically precludes many simple terms, i.e. most single spin processes. Even a pair-hopping term like $\hat{\sigma}^+_i\hat{\sigma}^+_{i+1}\hat{\sigma}^-_{i+2}\hat{\sigma}^-_{i+3}$ will not conserve $N_\pm$: it can bring two + doublons to neighboring unit cells, producing a − doublon on the intervening bond. The simplest $N_\pm$-conserving operator that disperses quasiparticles is $\hat{h}_j \equiv \hat{d}_{j-1}\hat{\sigma}^+_j\hat{\sigma}^+_{j+1}\hat{\sigma}^-_{j+2}\hat{\sigma}^-_{j+3}\hat{d}_{j+4}$, where $\hat{d}_j \equiv \frac{1}{2}(1-\hat{\sigma}^z_j)$ [analogously, $\hat{u}_j \equiv \frac{1}{2}(1+\hat{\sigma}^z_j)$]. This term "checks" that it would not create any new quasiparticles before moving one. Setting $\hat{H} = \sum_j(\hat{h}_j + \hat{h}^\dagger_j)$ would give a simple dispersive extension of FFA; however, we cannot confirm that this preserves integrability, so we add other terms:

$$\begin{aligned}\hat{H} \;=\; \sum_i \big(&\hat{d}_i\hat{\sigma}^+_{i+1}\hat{\sigma}^+_{i+2}\hat{\sigma}^-_{i+3}\hat{\sigma}^-_{i+4}\hat{d}_{i+5} + \hat{d}_i\hat{\sigma}^+_{i+1}\hat{\sigma}^-_{i+2}\hat{d}_{i+3}\\ &+\hat{d}_i\hat{\sigma}^+_{i+1}\hat{\sigma}^+_{i+2}\hat{u}_{i+3}\hat{d}_{i+4} + \text{refl.}\\ &+\hat{d}_i\hat{\sigma}^+_{i+1}\hat{\sigma}^+_{i+2}\hat{\sigma}^-_{i+3}\hat{u}_{i+4}\hat{u}_{i+5} + \text{refl.}\\ &+\hat{d}_i\hat{u}_{i+1}\hat{\sigma}^+_{i+2}\hat{u}_{i+3}\hat{u}_{i+4} + \text{refl.}\\ &+\hat{u}_i\hat{u}_{i+1}\hat{\sigma}^+_{i+2}\hat{\sigma}^-_{i+3}\hat{u}_{i+4}\hat{u}_{i+5}\big) + \text{h.c.},\end{aligned} \tag{3.2.5}$$

where "refl." indicates that one should reverse the sequence of indices in the previous term. In the quasiparticle language, $\hat{H}$, given by Eq. (3.2.5), maps a configuration σ to a uniform superposition of all configurations σ' with a single quasiparticle moved by one unit cell, provided $N_\pm$ are preserved.

The Hamiltonian given by Eq. (3.2.5) commutes with $\hat{F}_0$, but nevertheless acts nontrivially because $\hat{F}_0$ has exponentially degenerate eigenstates: for a given $N_\pm$ in a system of size L, there are only $O(L^2)$ eigenvalues, but exponentially many basis states, corresponding to different quasiparticle positions. The Hamiltonian defined in Eq. (3.2.5) lifts the degeneracy in this subspace, and thus makes the dynamics fully quantum. This perturbation cures many pathological features of the FFA model that are due to these degeneracies, such as its failure to equilibrate to the diagonal ensemble [122].

3.3 The Coordinate Bethe Ansatz for FFA

3.3.1 Vacuum state

The DFFA model has a "vacuum" state given by $|0\rangle = |\downarrow\downarrow\ldots\downarrow\downarrow\rangle$ upon which $\hat{F}_0$ acts as the identity. The elementary excitations are "doublons", or pairs of neighboring flipped spins $\uparrow\uparrow$, and come in two flavors, depending on whether the first spin is on an even or odd site. Thus, we regard the lattice of consisting of L two-site unit cells, labelled A and B, corresponding respectively to odd and even sites in the original enumeration. From the vacuum, we create a $\nu = L$ (-1) doublon in the nth unit cell by flipping the sites $2n-2$ and $2n-1$, or a $\nu = R$ $(+1)$ doublon in the nth unit cell by flipping sites $2n-1$ and $2n$.

In isolation, $\hat{F}_0$ will act by moving the $\nu = -1$ doublons one unit cell to the left, and the $\nu = +1$ doublons one unit cell to the right, and hence we refer to these respectively as left- and right-movers, or more commonly, by their displacement $\delta x = \pm 1$ under FFA. FFA conserves the total momentum, as well as the respective numbers of left and right movers [1].

[1] In a sense, FFA itself acts like a "chiral translation" symmetry; unlike the standard translation symmetry, FFA

3.3.2 Single-body sectors

The single particle excitations of this model are given by plane wave superpositions of these excitations:

$$|k,\nu\rangle = L^{-1/2}\sum_{n=0}^{L} e^{ikn}\sigma^x_{2n-1}\sigma^x_{2n+\nu-1}|0\rangle \quad \text{s.t.} \quad \hat{F}_0|k,\nu\rangle = e^{-i\epsilon_\nu(k)}|k,\nu\rangle, \quad \text{with} \quad \epsilon_\nu(k) = \nu k, \tag{3.3.1}$$

where k is the momentum. Note that the unit cell translation operator $\hat{T}$ commutes with both $\hat{F}_0$ and $\hat{H}$; its eigenvalues are e^{-ik} for $k = 2\pi q/L$ for integer $q \in \{1,2,\ldots,L\}$. From the above expression, we see that $\hat{F}_0$ has the same action as $\hat{T}$ on right movers and $\hat{T}^{-1} = \hat{T}^\dagger$ on left-movers.

Looking to more-body sectors, if only one species is present, $\hat{F}_0$ acts as a translation operator (or its inverse, depending on $\nu = \pm 1$). There are never collisions between particles of the same species under FFA, only those of opposite species. Unlike a conventional translation operator, FFA is special in that it has its own S matrix associated with this scattering of left and right movers, which we will observe in sectors containing both species $\nu = \pm 1$.

3.3.3 Counting excitations

To describe sectors with additional movers, we must understand the counting of the number of movers in a given configuration. When one of each movers is present, at some point $\hat{F}_0$ will cause them to collide, realizing one of two "molecule" states, which are special configurations with a single, isolated up spin. One obtains an A or B molecule in the nth unit cell when, respectively, the spin on the A or B site of that unit cell is up, with both of its neighbors down ($\downarrow_{2n-2}\uparrow_{2n-1}\downarrow_{2n}$ or $\downarrow_{2n-1}\uparrow_{2n}\downarrow_{2n+1}$). In the former case ($A$), both the left- and right-mover are taken to be in unit cell n (i.e. they have the same position), in the latter, the right mover is still at cell n, but the left-mover is in cell $n+1$.

Thus, we say there is a $\nu = +1$ right-mover in unit cell n if both spins in the unit cell are up (in which case the mover is a doublon; this is independent of the neighboring spins), or if *either* spin in the unit cell is up, with both neighbors down. The condition for a $\nu = -1$ left-mover is *shifted to the left by one physical spin compared to the right*: if the B site of cell $n-1$ and the A site of cell n are up, there is a left-moving doublon in cell n (again, independent of neighboring spins); if *either* of these spins is up and both its neighbors down, then there is a left-mover in site n that is part of a molecule. With this, rather than label states by the configurations of the physical spin half degrees of freedom, we will do so by the positions of the various movers and their form (i.e. doublons vs. molecules).

3.3.4 Two-body sectors

Let us now consider $\hat{F}_0$ when $N_+ = N_- = 1$, which will provide insight into generic many-body sectors. Acting on the majority of configurations, $\hat{F}_0$ moves the left and right movers one site in their namesake direction, however when the two are nearby, we obtain the following collisions in the $|x_+, x_-\rangle$ basis for doublons and $|\alpha, x\rangle$ basis for molecules, with $\alpha = A, B$:

$$\begin{array}{ccccccc} \downarrow\overset{+}{\uparrow}\uparrow\downarrow\overset{*}{\downarrow}\downarrow\uparrow\overset{-}{\uparrow}\downarrow & \longrightarrow & \downarrow\overset{+}{\uparrow}\overset{*}{\uparrow}\overset{-}{\uparrow}\downarrow & \longrightarrow & \downarrow\overset{B}{\overset{*}{\uparrow}}\downarrow & \longrightarrow & \downarrow\uparrow\overset{-}{\uparrow}\overset{*}{\downarrow}\overset{+}{\uparrow}\uparrow\downarrow \\ |n-1,n+2\rangle & \longrightarrow & |n,n+1\rangle & \longrightarrow & |B,n\rangle & \longrightarrow & |n+1,n\rangle \end{array} \tag{3.3.2}$$

by itself constitutes an integrable model, and is associated with its own S matrix. Hence, we do not reduce FFA to the status of a symmetry in our treatment of this model.

$$\begin{array}{ccccccc} \downarrow\overset{+}{\uparrow}\uparrow\overset{*}{\downarrow}\overset{-}{\uparrow}\uparrow\downarrow & \longrightarrow & \downarrow\overset{*}{\underset{A}{\uparrow}}\downarrow & \longrightarrow & \downarrow\uparrow\overset{*}{\uparrow}\uparrow\downarrow & \longrightarrow & \downarrow\uparrow\uparrow\downarrow\overset{*}{\downarrow}\uparrow\uparrow\downarrow \\ |n-1,n+1\rangle & \longrightarrow & |A,n\rangle & \longrightarrow & |n,n\rangle & \longrightarrow & |n+1,n-1\rangle \end{array}, \tag{3.3.3}$$

where in Eq. (3.3.2) the $*$ site is $2n$, and in Eq. (3.3.3) the $*$ site is $2n-1$. As in the single-particle (or single-species) sectors, $\hat{F}_0$ acts by cycling through the states in a closed "orbit", much like the eigenstates of the translation operator, $\hat{T}$.

For $N_+ = N_- = 1$, $\hat{F}_0$ changes the separation of the movers $\delta \equiv x_- - x_+$ by two (excepting a "delay" step which leaves both in place) (3.3.2–3.3.3). Hence if L is even, $\hat{F}_0$ preserves δ modulo 2, yielding two distinct orbits with degenerate eigenvalues under FFA, distinguished by δ mod 2; if L is odd, then both types of collisions must occur before we return to the initial configuration. Much of this discussion will apply to sectors with more movers, and the general method for constructing eigenstates will be the same.

Let us now construct eigenstates of $\hat{F}_0$ for $N_+ = N_- = 1$ and even $L = 2\ell$. As noted, there are two degenerate orbits of $\ell+1$ states under $\hat{F}_0$, corresponding respectively to the collision processes given in Eq. (3.3.3) and Eq. (3.3.2), or equivalently, A vs. B molecules, or δ even vs. odd. The fact that the orbits are closed follows from the identity $\hat{F}_0^{\ell+1}\hat{T}^{\pm\ell} = \hat{\mathbb{1}}$, which immediately dictates the eigenvalues of $\hat{F}_0$,

$$\hat{F}_0|n,k,\alpha\rangle = e^{-i\theta_{n,k}}|n,k,\alpha\rangle\,, \quad \theta_{n,k} = \frac{2\pi n - \ell k}{\ell+1} = \frac{4\pi n - Lk}{L+2}, \tag{3.3.4}$$

where $\alpha = A, B$ designates the orbit based on its molecule, as depicted in (3.3.2–3.3.3). The eigenvalue $\theta_{n,k} = \sum_\pm \pm k_\pm$ is the *relative momentum* and $k = \sum_\pm k_\pm$ is the total momentum, set by translation invariance as usual.

We now formulate the eigenstates of $\hat{F}_0$ explicitly: we will first define a natural basis for this sector, which will allow us to conveniently express the allowed orbits, and finally, massage these eigenstates into the traditional plane-wave form common to integrable systems. The first step is the definition of a translation-invariant basis for this sector, indexed by the separation δ

$$|\delta,k\rangle = L^{-1/2}\sum_{j=1}^{L} e^{ikj}|x_+ = j, x_- = j+\delta \bmod L\rangle \tag{3.3.5}$$

for the doublon configurations, and for the molecules $\alpha = A, B$:

$$|\alpha,k\rangle = L^{-1/2}\sum_{j=1}^{L} e^{ikj}|\alpha,j\rangle, \tag{3.3.6}$$

though in this sector, one can also interpret the molecules as additional values of δ. We define the eigenstates of $\hat{F}_0$ with respect to some "reference configuration", which we choose to be the corresponding molecule states $|\alpha,k\rangle$ for notational convenience, i.e. the eigenstates are formed as

$$|n,k,\alpha\rangle \equiv (\ell+1)^{-1/2}\sum_{m=0}^{\ell} e^{-im\theta_{n,k}}\hat{F}_0^{-m}|\alpha,k\rangle,. \tag{3.3.7}$$

For clarity, we can write out these orbits as

$$|n,k,A\rangle = (\ell+1)^{-1/2}\left\{|A,k\rangle + e^{i\theta_{n,k}}|\delta=0,k\rangle + \sum_{m=1}^{\ell-1} e^{im(k-\theta_{n,k})}|\delta=2m,k\rangle\right\} \tag{3.3.8a}$$

$$|n,k,B\rangle = (\ell+1)^{-1/2}\left\{|B,k\rangle + e^{-i\theta_{n,k}}|\delta=1,k\rangle + e^{-i\theta_{n,k}}\sum_{m=1}^{\ell-1} e^{im(k-\theta_{n,k})}|\delta=2m+1,k\rangle\right\}, \tag{3.3.8b}$$

and note that a different choice of "reference configuration" will result in an overall factor of $e^{i\theta_{n,k}}$ to some power compared to the above.

We can massage Eq. (3.3.8) into a form that looks like plane waves by rotating the A/B eigenstates into symmetric or anti-symmetric linear combinations, parametrized by $\eta = \pm 1$ (unrelated to $\nu = +/- = R/L$):

$$|n,k,\eta\rangle = \frac{1}{\sqrt{2}}\left(|n,k,A\rangle + \eta e^{i\psi}|n,k,B\rangle\right),, \tag{3.3.9}$$

and consideration of the action of the Hamiltonian in Section 3.4.2 dictates that $\psi = \left(k+\theta_{n,k}\right)/2 = k_+$. Expanding this we have

$$|k_+,k_-\rangle \propto \sum_{x=1}^{L} e^{i(k_++k_-)x}\left(|A,x\rangle + e^{ik_+}|B,x\rangle\right) + \sum_{\substack{x_\pm=1\\ x_+\neq x_-}}^{L} e^{ik_+x_+}e^{ik_-x_-}|x_+,x_-\rangle \;+\; e^{i(k_+-k_-)}\sum_{x=1}^{L} e^{i(k_++k_-)x}|x\,,\,x\rangle, \tag{3.3.10}$$

where η from Eq. (3.3.9) has been eliminated in favor of extending the allowed values of (k_+,k_-) from the quantization of k and $\theta_{n,k}$ to include π-shifted pairs $(k_++\pi, k_-+\pi)$. Although these states will be degenerate under $\hat{F}_0$, this distinction is necessary for the counting of states, and $\hat{H}$ will lift these degeneracies in 3.4.2.

Recalling that the molecules also correspond to particular configurations of the two movers, the coefficient of the A molecule terms are also of the same plane wave form $e^{ik_+x_+}e^{ik_-x_-}$ as most of the doublon terms; however, the B-molecule at cell n now corresponds to a right-mover at n and a left-mover at $n+1$, so its coefficient is in fact $e^{i(k_+-k_-)}e^{ik_+x_+}e^{ik_-x_-}$, and we note that the same extra factor of $e^{i(k_+-k_-)}$ has been applied to the same-cell doublon terms $|x,x\rangle$. These states are the respective "delay" states (i.e. the movers are in the same positions as in the preceding state under FFA) in the orbits defined in Eq. (3.3.2) and Eq. (3.3.3), respectively. Thus, we have identified the S *matrix* for FFA:

$$\widetilde{S}\left(k_+,k_-\right) = +e^{i(k_+-k_-)}\ , \tag{3.3.11}$$

where, compared to the S matrices of other known integrable systems, here we have an overall sign of +1 rather than −1 due to the *distinguishability* of the two particles. Because these particles are distinguishable, we ascribe no meaning to swapping the order of the momentum arguments.

Note the fact that this S matrix multiplies only two of the configurations in Eq. (3.3.10) is an artifact of our choice of reference configuration, i.e., Eq. (3.3.8). In general, the S matrix defined in Eq. (3.3.11) appears on all post-collision configurations until the end of the "orbit", which for our choice was rather immediate. One could also make the natural choice that all terms with $x_- \le x_+$ (and the B molecule) get an S matrix, and all others do not. The quantization condition on θ ensures that there is no mismatch.

To complete our treatment of this sector, when the number of unit cells, $L = 2\ell+1$, is *odd*, by analogy to Eq. (3.3.4) we have

$$\hat{F}_0|m,k\rangle = e^{-i\theta_m}|m,k\rangle, \quad \theta_m = \frac{2\pi m}{L+2} \cong \frac{2\pi m' - L\,k}{L+2}, \tag{3.3.12}$$

where here θ need not depend on k since $\hat{F}_0^{L+2} = \hat{\mathbb{1}}$, and compared to Eq. (3.3.4) we allow twice as many values of the integer m. We construct eigenstates as before as orbits under $\hat{F}_0$ starting from the A molecule states for concreteness, and again recover a state of the general form of Eq. (3.3.9), with the explicit value of $\psi = \pi\left(m + Lk/2\pi\right) + \left(k+\theta_m\right)/2$, where m is the index of θ_m. Unlike Eq. (3.3.9), we have a single sector of size $L+2$, and here there is no parameter η, and the overall sign of the B terms relative the A terms is set by ψ. The placement of the S matrices is the same as for even L eigenstates.

3.3.5 More-body sectors

In sectors with *arbitrary* numbers of particles, the eigenstates of $\hat{F}_0$ continue to be orbits constructed in a similar fashion, and based on the results for small sectors, we can guess the pattern for the quantization, which we have confirmed numerically. In general, one has

$$K = \sum_{\pm} K_{\pm} = \frac{2\pi N_k}{L} \qquad N_k \in \{1, 2, \ldots, L-1, L\} \tag{3.3.13a}$$

$$\Theta = \sum_{\pm} \pm K_{\pm} = \frac{2\pi N_\theta + (N_+ - N_- - L)\, K}{L + N_+ + N_-} \qquad N_\theta \in \{1, \ldots, L + N_+ + N_-\}, \tag{3.3.13b}$$

provided that $L + N_+ + N_-$ is *odd*. If $L + N_+ + N_-$ is even, then we have

$$\Theta = \sum_{\pm} \pm K_{\pm} = \frac{4\pi N_\theta + (N_+ - N_- - L)\, K}{L + N_+ + N_-} \qquad N_\theta \in \left\{1, \ldots, \frac{1}{2}(L + N_+ + N_-)\right\}, \tag{3.3.13c}$$

which comes from operator identities of the form $\hat{F}_0^{\left[\frac{1}{2}\right](L+N_+ +N_-)} \hat{T}^m = \hat{\mathbb{1}}$ (for some m). These equations also fully determine the total momentum of all right-movers, K_+, and the total momentum of all left-movers, K_-. However, without a Hamiltonian term, it is not clear that there is a means to extract the allowed momenta of the *individual* movers, or re-write linear combinations of the various degenerate orbits as plane-waves in general many-body sectors, as one expects for integrable systems. As for the placement of S matrices in these eigenstates, one need only choose a reference state as the "default" ordering of the movers, and for each configuration with a different order of movers (due to collisions), apply corresponding S matrices as in the $N_+ = N_- = 1$ sector.

3.4 The Hamiltonian Perturbation

To generalize FFA, we will now include a dispersing Hamiltonian term in the evolution

$$\hat{F}(\lambda) = e^{-i\lambda \hat{H}} \cdot \hat{F}_0, \tag{3.4.1}$$

where $\hat{H}$ is a local Hamiltonian that acts on a given configuration σ of $\pm$ particles by mapping them with unit weight to all other configurations σ' such that exactly one of the movers has been moved by a single unit cell, while preserving the number of movers of each type $N_\pm$. In cases where there are two states corresponding to a particular configuration of movers, the Hamiltonian will map to the configuration σ' that is closest to σ under bare FFA, thereby preserving the phase delays of the latter.

In fact, the action of this Hamiltonian is quite straightforward, however owing to the complicated nature of defining the locations of the movers, the form of $\hat{H}$ on the physical spins will *appear* quite complicated and nongeneric. Writing $\hat{H}$ as the sum over local terms $\hat{H}_n$, we have

$$\begin{aligned}\hat{H}_n = &\underbrace{\hat{d}_n \hat{\sigma}^+_{n+1} \hat{\sigma}^+_{n+2} \sigma^-_{n+3} \hat{\sigma}^-_{n+4} \hat{d}_{n+5}}_{\text{doublon hopping}} + \underbrace{\hat{d}_n \hat{\sigma}^+_{n+1} \hat{\sigma}^-_{n+2} \hat{d}_{n+3}}_{\text{molecule hopping}} + \underbrace{\hat{d}_n \hat{\sigma}^+_{n+1} \hat{\sigma}^+_{n+2} \hat{u}_{n+3} \hat{d}_{n+4} + \text{refl.}}_{\text{molec.} \leftrightarrow \text{doublons}} \\ + &\underbrace{\hat{d}_n \hat{\sigma}^+_{n+1} \hat{\sigma}^+_{n+2} \hat{\sigma}^-_{n+3} \hat{u}_{n+4} \hat{u}_{n+5} + \text{refl.}}_{\text{doublon absorption}} + \underbrace{\hat{d}_n \hat{u}_{n+1} \hat{\sigma}^+_{n+2} \hat{u}_{n+3} \hat{u}_{n+4} + \text{refl.}}_{\text{molecule absorption}} + \underbrace{\hat{u}_n \hat{u}_{n+1} \hat{\sigma}^+_{n+2} \hat{\sigma}^-_{n+3} \hat{u}_{n+4} \hat{u}_{n+1}}_{\text{exchange}} + h.c.,\end{aligned} \tag{3.4.2}$$

where '+ refl.' indicates that one should also include the same term with the operators in reverse order, and the Hermitian conjugate of each term above should also be included; as before, $\hat{d}$ projects onto $\downarrow_z$, and $\hat{u}$ projects onto $\uparrow_z$.

3.4.1 Single-species sectors

In the single-particle sector, and single-species sector in general, only the first term in Eq. (3.4.2) acts nontrivially. This term takes the form $\hat{d}_n\hat{\sigma}^+_{n+1}\hat{\sigma}^+_{n+2}\sigma^-_{n+3}\hat{\sigma}^-_{n+4}\hat{d}_{n+5} + h.c.$, and hops a doublon (of either type) by one unit cell, provided no other particles are nearby, and hence adds to the purely chiral pseudo-energies of bare FFA, $\varepsilon = \pm k$ a more typical cosine dispersion[2]. For the single particle eigenstates of FFA, one has

$$\hat{F}(\lambda)|k,\pm\rangle = e^{-i\varepsilon}|k,\pm\rangle, \quad \text{with} \quad \varepsilon = \pm k + 2\lambda\cos(k), \tag{3.4.3}$$

where the cosine term is independent of the species index, $\nu = \pm 1$, as $\hat{H}$ does not differentiate between the two.

We now consider the two-body sector; when necessary for concreteness, let us take them to be + particles (right movers). Since the particles are indistinguishable and cannot be placed in adjacent unit cells, this gives $\frac{1}{2}L(L-3)$ states $|x_1,x_2\rangle$ with $x_2 > x_1 + 1$. The action of $\hat{F}_0$ on these states is trivial: $\hat{F}_0|x_1,x_2\rangle = |x_1 \pm 1, x_2 \pm 1\rangle$, and amounts to translation. Since $[\hat{F}_0,\hat{H}] = 0$, eigenstates of $\hat{H}$ will automatically be eigenstates of $\hat{F}_0$. These eigenstates will take the standard coordinate Bethe Ansatz (CBA) form

$$|k_1,k_2\rangle \propto \sum_{x_2>x_1+1}\left(e^{i(k_1x_1+k_2x_2)} + S(k_2,k_1)\,e^{i(k_1x_2+k_2x_1)}\right)|x_1,x_2\rangle, \tag{3.4.4}$$

where $S(k_2,k_1)$ is the same-species S matrix corresponding to the swapping of momenta k_1 and k_2. Unlike the S matrix for FFA that applies to particles of opposite species, the order of the momenta are important here, however the form of S is the same for both $\nu = \pm 1$.

The corresponding wave function is given – up to an overall normalization constant – by

$$\Psi_{k_1,k_2}(x_1,x_2) \equiv \langle x_1,x_2|k_1,k_2\rangle \propto \left(e^{i(k_1x_1+k_2x_2)} + S(k_2,k_1)\,e^{i(k_1x_2+k_2x_1)}\right). \tag{3.4.5}$$

From this follows the "Schrödinger equation"

$$e^{-i\varepsilon_\pm(k_1,k_2)}\langle x_1,x_2|k_1,k_2\rangle = \langle x_1,x_2|e^{-i\lambda\hat{H}}\hat{F}_0|k_1,k_2\rangle = e^{\mp i(k_1+k_2)}\langle x_1,x_2|e^{-i\lambda\hat{H}}|k_1,k_2\rangle. \tag{3.4.6}$$

Because this system is integrable, one expects $\varepsilon_\pm(k_1,k_2) = \varepsilon_\pm(k_1)+\varepsilon_\pm(k_2) = \pm(k_1+k_2)+2\lambda\cos(k_1)+2\lambda\cos(k_2)$, and factoring this out, one has $e^{-i\lambda E(k_1,k_2)}\langle x_1,x_2|k_1,k_2\rangle = \langle x_1,x_2|e^{-i\lambda\hat{H}}|k_1,k_2\rangle$, where $E(k_1,k_2) = 2\cos(k_1) + 2\cos(k_2)$. However, clearly $|k_1,k_2\rangle$ is an eigenstate of $\hat{H}$, independent of λ, and we can write the preceding equalities in the more familiar form

$$E(k_1,k_2)\,\Psi_{k_1,k_2}(x_1,x_2) = \Psi_{k_1,k_2}(x_1-1,x_2)+\Psi_{k_1,k_2}(x_1+1,x_2)+\Psi_{k_1,k_2}(x_1,x_2-1)+\Psi_{k_1,k_2}(x_1,x_2+1), \tag{3.4.7}$$

with

$$E(k_1,k_2) = 2\cos(k_1) + 2\cos(k_2) = E_1(k_1) + E_1(k_2). \tag{3.4.8}$$

The Ansatz embodied in Eq. (3.4.4) already satisfies Eq. (3.4.7) when $x_2 - x_1 > 2$ for any choice of $S(k_2,k_1)$. The form of the latter factor may be determined in the usual fashion by ensuring that Eq. (3.4.7) holds—with the same eigenvalue $E(k_1,k_2)$, given by Eq. (3.4.8)—when $x_2 = x_1 + 2$, which gives

$$S(k_2,k_1) = -e^{i(k_2-k_1)}, \tag{3.4.9}$$

[2]One might expect this term to be sufficient, and indeed a Hamiltonian comprising only this term may well be integrable, but we are unable to solve for its eigenstates and spectrum.

which resembles the FFA S matrix $\widetilde{S}$, excepting the overall factor of -1 and meaning of the order of the momentum arguments, both of which derive from indistinguishability. We finish our solution of the two body problem by figuring out the quantization of the momenta k_1 and k_2. Their sum $K = k_1 + k_2$ is constrained by translation invariance, an generally a quantity we will fix by hand. Additionally, one has the Bethe Ansatz Equations (BAE), obtained by bringing one of the particles around the system, i.e. demanding $\Psi_{k_1,k_2}(x_1, x_2) = \Psi_{k_1,k_2}(x_2, x_1 + L)$

$$e^{-ik_1 L} = S(k_2, k_1) = e^{ik_2 L}, \tag{3.4.10}$$

although because $e^{i(k_1+k_2)L} = 1$, this is only truly a single relation. As in other integrable models, we also have

$$S(k_2, k_1) = S(k_1, k_2)^* = S(k_1, k_2)^{-1} . \tag{3.4.11}$$

These BAE admit straightforward solutions

$$k_2 = K - k_1 , \quad k_1 = \frac{(2m+1)\,\pi}{L-2} - \frac{K}{L-2} , \tag{3.4.12}$$

for $m \in \{1, 2, \ldots, L-2\}$, which we have confirmed with exact numerical diagonalization.

With any number of movers of the same type, the wave functions take the form

$$\Psi_{k_1,\ldots,k_{N_\nu}}(x_1, \ldots, x_{N_\nu}) = \sum_{\text{perm}} A_{j_1,\ldots,j_{N_\nu}} \exp\left(ik_{j_1}x_1 + \cdots + ik_{j_{N_\nu}}x_{N_\nu}\right), \tag{3.4.13}$$

where a given permutation that exchanges the momenta k_n and $k_{m>n}$ is accompanied by an S matrix $S(k_m, k_n)$ as usual. For example, for *three* particles of the same species, ν, one has wave functions

$$\begin{aligned}\Psi_{k_1,k_2,k_3}(x_1, x_2, x_3) = {} & e^{ik_1x_1}e^{ik_2x_2}e^{ik_3x_3} + S_{21}e^{ik_2x_1}e^{ik_1x_2}e^{ik_3x_3} + S_{21}S_{31}e^{ik_2x_1}e^{ik_3x_2}e^{ik_1x_3} \\ & + S_{21}S_{31}S_{32}e^{ik_3x_1}e^{ik_2x_2}e^{ik_1x_3} + S_{31}S_{32}e^{ik_3x_1}e^{ik_1x_2}e^{ik_2x_3} + S_{32}e^{ik_1x_1}e^{ik_3x_2}e^{ik_2x_3},\end{aligned} \tag{3.4.14}$$

where S_{32} is a temporary shorthand for $S(k_3, k_2)$. As more particles of the same species are added, one includes additional permuted terms to the wave function, accompanied by S matrices for the corresponding permuted momenta.

These wave functions correspond to eigenstates of both $\hat{F}_0$ and $\hat{H}$, with eigenvalue under the latter

$$\hat{H}|k_1, \ldots, k_{N_\nu}\rangle = E(k_1, \ldots, k_{N_\nu})\,|k_1, \ldots, k_{N_\nu}\rangle = \sum_{m=1}^{N_\nu} E_1(k_m)\,|k_1, \ldots, k_{N_\nu}\rangle \tag{3.4.15}$$

and as for the two-body sector, the quantization condition obtains by bringing one particle around the system:

$$e^{ik_m L} = \prod_{\substack{n=1 \\ n\neq m}}^{N_\nu} S(k_m, k_n) , \tag{3.4.16}$$

which also reduces to Eq. (3.4.10) for $N_\nu = 2$. As in that case, one also has the quantization of total momentum $\sum_m k_m = K = 2\pi q/L$ for $q \in \{1, 2, \ldots, L\}$. Together, these equations admit *exact solutions*, in contrast to most known integrable models, which we can see by noting

$$e^{ik_j L} = \prod_{\substack{j'=1 \\ j'\neq j}}^{N_\nu} S_{\nu\nu}(k_j, k_{j'}) = -\prod_{j'=1}^{N_\nu}\left(-e^{i(k_j - k_{j'})}\right) = e^{i(\pi(N_\nu-1)+N_\nu k_j)}\prod_{j'=1}^{N_\nu} e^{-ik_{j'}} = e^{i(\pi(N_\nu-1)+N_\nu k_j)}e^{-iK}, \tag{3.4.17}$$

which implies $1 = e^{-i(\pi(N_\nu-1)-K+(L-N_\nu)k_j)} = e^{2\pi i m_j}$, from which we extract the solutions for $N_\nu - 1$ of the momenta

$$k_j = \frac{1}{L-N_\nu}\left(\pi\left(2m_j + N_\nu - 1\right) - K\right), \tag{3.4.18}$$

where $m_j \in \{1, 2, \ldots, L-N_\nu\}$, and the final momentum given by $k_{N_\nu} = K - \sum_{m=1}^{N_\nu-1} k_m$. Additionally, one has the constraint that no two particles can have the same momentum. Lastly, Eq. (3.4.18) reduces to Eq. (3.4.12) for $N_\nu = 2$.

3.4.2 Sectors with both species

We now consider the full Floquet drive $\hat{F}(\lambda)$ in sectors with both $\pm$ particles. The smallest such sector has $N_\pm = 1$, and we already found eigenstates for this sector in the context of $\hat{F}_0$. Re-visiting this sector will help explain many of the terms in $\hat{H}$ beyond the doublon hopping term, which was the only nontrivial term in the single-species sectors discussed in Section 3.4.1.

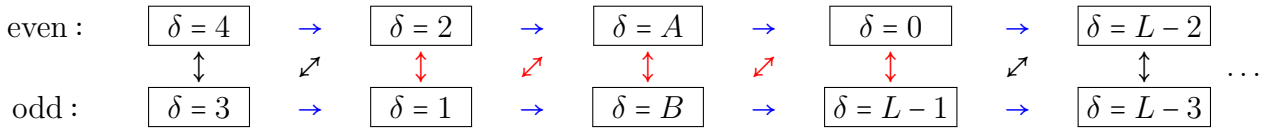

Figure 3.2: There are two types of collision processes under the bare FFA dynamics, corresponding to even or odd separations, and respectively, the appearance of A or B molecules. The FFA unitary evolution operator $\hat{F}_0$ cycles between the states in these orbits, reproduced diagramatically above, with blue arrows indicating the action of the FFA model, black arrows indicating processes produced by the doublon hopping term, and red arrows indicating processes corresponding to all other Hamiltonian terms.

The full Hamiltonian acts as follows on position basis states $|x_+, x_-\rangle$, $|A, x\rangle$, $|B, x\rangle$; starting with the "general" case (the black arrows in Figure 3.2), and then listing "exceptions" (red arrows in Figure 3.2), we have

$$\hat{H}|x_+, x_-\rangle = |x_+ + 1, x_-\rangle + |x_+ - 1, x_-\rangle + |x_+, x_- + 1\rangle + |x_+, x_- - 1\rangle \tag{3.4.19a}$$
$$\hat{H}|x, x+1\rangle = |A, x\rangle + |A, x+1\rangle + |x-1, x+1\rangle + |x, x+2\rangle \tag{3.4.19b}$$
$$\hat{H}|A, x\rangle = |x, x+1\rangle + |x-1, x\rangle + |B, x\rangle + |B, x-1\rangle \tag{3.4.19c}$$
$$\hat{H}|B, x\rangle = |A, x\rangle + |A, x+1\rangle + |x, x\rangle + |x+1, x+1\rangle \tag{3.4.19d}$$
$$\hat{H}|x, x\rangle = |B, x\rangle + |B, x-1\rangle + |x+1, x\rangle + |x, x-1\rangle \tag{3.4.19e}$$
$$\hat{H}|x+1, x\rangle = |x, x\rangle + |x+1, x+1\rangle + |x+2, x\rangle + |x+1, x-1\rangle, \tag{3.4.19f}$$

where if not specifically listed above, the action of $\hat{H}$ on a state defaults to Eq. (3.4.19a).

To see that $\hat{H}$ and $\hat{F}_0$ have simultaneous eigenstates, consider $N_+ = N_- = 1$ with $L = 2\ell$ is even, in which case the eigenstates of $\hat{F}_0$ are $|n, k, \alpha\rangle$ for $\alpha = A, B$, corresponding to the type of molecule that obtains (or even/odd separations, respectively). We rotate to form eigenstates as symmetric or anti-symmetric combinations of these two,

$$|n, k, \eta\rangle = \frac{1}{\sqrt{2}}\left(|n, k, A\rangle + \eta e^{i\psi}|n, k, B\rangle\right), \tag{3.3.9}$$

with $\eta = \pm 1$ (unrelated to the species index $\nu = \pm 1$). Using equations Eq. (3.4.19), we find that

$$\hat{H}|n,k,A\rangle = 4\cos\left(\frac{k}{2}\right)\cos\left(\frac{\theta_{n,k}}{2}\right)e^{i(k+\theta_{n,k})/2}|n,k,B\rangle, \tag{3.4.20}$$

explaining why we chose $\psi = (k+\theta_{n,k})/2 = k_+$ in Section 3.3. We also note that

$$4\cos\left(\frac{k}{2}\right)\cos\left(\frac{\theta_{n,k}}{2}\right) = 2\cos(k_L) + 2\cos(k_R) = E(k_L,k_R) = E_1(k_L) + E_1(k_R), \tag{3.4.21}$$

as expected, apart from the factor of η multiplying the contents of Eq. (3.4.21). We absorb the overall sign $\eta = \pm 1$ into the definition of the allowed momenta k_+ and k_- by noting that $\cos(k \pm \pi) = -\cos(k)$, and that shifting both k_+ and k_- by π preserves both $k = k_+ + k_-$ and $\theta = k_+ - k_-$ modulo 2π. Finally, when L is odd, these two degenerate orbits merge into one, eliminating the free parameter η, which is replaced by the factor $(-1)^{m+Lk/2\pi}$ where m indexes the allowed eigenvalues θ, per Eq. (3.3.12). It is also worth noting that $\hat{H}$ lifts degeneracies of $\hat{F}_0$, such as that of the sector with $N_\pm = 1$ with L even; because of this, the full, dispersing model has spectral properties more reminiscent of conventional integrable systems.

As we add more movers of either type, not much changes compared to the above, with a few notable exceptions. The first is that new collision processes emerge: for example with $N_+ = 1$ and $N_- = 2$, $\hat{F}_0$ factorizes into its action on an isolated left-mover, and its action as in the $N_\pm = 1$ sector, with the singular exception that $\hat{F}_0|B,x\rangle \otimes |x_- = x+2\rangle = |A,x+1\rangle \otimes |x_- = x\rangle$. However, no knowledge of these new processes is necessary to form eigenstates, since the eigenstates of $\hat{H}$ will also be eigenstates of $\hat{F}_0$. Second, we have the possibility of "cluster states" with three or more physical spins up. Looking at the same $N_+ = 1$ and $N_- = 2$ sector, $\hat{F}_0|A,x\rangle \otimes |x_- = x+2\rangle = |x_+ = x; x_- = x, x+2\rangle$, where the latter looks like $\ldots \downarrow\uparrow_{2x-2}\uparrow_{2x-1}\uparrow_{2x}\uparrow_{2x+1}\downarrow \ldots$. For each additional mover (of alternating type), we have the possibility of a cluster with one additional up spin. In the $N_+ = 1$ and $N_- = 2$ sector, the two left-movers can only be in adjacent unit cells if the right-mover is in the same position as the first left-mover. Therefore, the right-mover is stuck: it cannot be moved by $\hat{H}$ without moving one of the left-movers at the same time. Since $\hat{H}$ can only act by moving one quasiparticle, only the outer left-movers can be moved, and they must be moved out of the cluster. This property holds for larger, generic clusters as well.

In fact, the action of $\hat{H}$ on these "cluster" configurations explains all the remaining terms not accounted for by Figure 3.2. In general, all of the doublons in the cluster are locked in place, and $\hat{H}$ can only act by bringing movers into or out of the cluster at the edges, either in the form of molecules or two-body clusters ($\uparrow\uparrow$). Lastly, there is a term allowing for one mover to hop between adjacent clusters. It is also worth noting that the same-species S matrix $S(k_2,k_1)$ is designed to give zero weight to a state with movers of the same type on adjacent sites. One might then worry that these cluster configurations will have zero weight; fortunately, these states are also "delay states", i.e. two (or more) of the movers will be in the same place if one acts with $\hat{F}_0^{-1}$, and therefore they will also have a factor of $\widetilde{S}$ that will prevent the weight on these states from vanishing.

3.4.3 Form of the solution

For generic many-body sectors, the eigenstates are constructed from plane waves (solutions to the single-particle sector) as in Hamiltonian integrable systems. First, we write the "naïve" wave

function for a given configuration as the product of the wave functions within the two sectors given by Eq. (3.4.13), i.e.

$$\Psi_{k_1^+,\ldots,k_{N_+}^+;k_1^-,\ldots,k_{N_-}^-}\left(x_1^+,\ldots,x_{N_+}^+;\,x_1^-,\ldots,x_{N_-}^-\right)=\Psi_{k_1^+,\ldots,k_{N_+}^+}\left(x_1^+,\ldots,x_{N_+}^+\right)\Psi_{k_1^-,\ldots,k_{N_-}^-}\left(x_1^-,\ldots,x_{N_-}^-\right)\,, \tag{3.4.22}$$

each of which is the sum over permutations of the momenta in that sector. Unlike the single-species sectors, we will also have molecule configurations, for which the form of the wave-function is identical to the doublon configurations: plane waves evaluated at the prescribed positions of the molecules' constituent movers. We then identify a "reference" configuration, i.e. an ordering of all the ± movers, starting from the first unit cell, and compared to this configuration, any configuration in which the order of a + and − is interchanged picks up an S matrix for that collision, $\widetilde{S}\left(k_n^+,k_m^-\right)$.

This is most easily seen in sectors with sufficiently low density to admit a state where all − particles are to the right of all + particles; in this case, every state with the mth − left of the nth + will be multiplied by $\widetilde{S}\left(k_{i_n}^+,k_{i_m}^-\right)$. Since the wave function is a superposition over different assignments of the momenta $\{k_n^+,k_m^-\}$ to the various movers, each individual term in the sum will have a different momentum appearing in any particular factor of $\widetilde{S}$, as $\widetilde{S}$ is associated to the movers. In summary:

$$\begin{gathered}\Psi_{k_1^+,\ldots,k_{N_+}^+;k_1^-,\ldots,k_{N_-}^-}\left(x_1^+,\ldots,x_{N_+}^+;\,x_1^-,\ldots,x_{N_-}^-\right)=\\ \sum_{\text{perm}}A^+_{n_1,\ldots,n_{N_+}}A^-_{m_1,\ldots,m_{N_-}}\varsigma\left(k_{n_1}^+,\ldots,k_{n_{N_+}}^+;k_{m_1}^-,\ldots,k_{m_{N_-}}^-\right)e^{ik_{n_1}^+x_1^++ik_{m_1}^-x_1^-+\cdots+ik_{n_{N_+}}^+x_{N_+}^++ik_{m_{N_-}}^-x_{N_-}^-}\,,\end{gathered} \tag{3.4.23}$$

where the coefficients A are unity for unpermuted labels, and acquire factors S_{21} if the momenta of the first and second mover (of a given species) are swapped. The factor ς is a place-holder for the product of necessary $+-$ S matrices, $\widetilde{S}\left(k_{n_j}^+,k_{m_i}^-\right)$, relative some "default" configuration of the movers.

The structure of these eigenstates gives rise to the quantization of the momenta. Recall that the quantization of $\hat{F}_0$, which is independent of $\hat{H}$, constrains $\Theta=K_+-K_-=\sum_\pm \pm K_\pm$, and as always, translation invariance dictates the quantization of total momentum $K=K_++K_-=\sum_\pm K_\pm$, per Eq. (3.3.13). Even in a trivial limit wherein we omitted $\hat{F}_0$ from our Floquet drive, the fact that $[\hat{F}_0,\hat{H}]=0$ would still lead to the same quantization condition. Since a quantization condition exists for both the sums and differences of $K_\pm$, the two are both independently fixed. What remains is a formula of the form Eq. (3.4.16) for scenarios in which both movers are present. As in that case, these conditions obtain from moving one quasiparticle around the entire system, and correspondingly, contains S matrices corresponding to all of the resultant collisions. Thus, compared to Eq. (3.4.16), one expects the full quantization condition to contain S matrix factors corresponding to collisions between quasiparticles of *opposite* chirality as well. Indeed, those equations are

$$e^{ik_j^\nu L}=\prod_{\substack{n=1\\n\neq j}}^{N_\nu}S\left(k_j^\nu\,,\,k_n^\nu\right)\prod_{m=1}^{N_{\bar{\nu}}}\widetilde{S}^{\bar{\nu}}\left(k_j^\nu\,,\,k_m^{\bar{\nu}}\right) \tag{3.4.24a}$$

where again, there is no meaning to switching the order of the momenta for $\widetilde{S}$. For right-movers with momenta p_j, this takes the form

$$e^{ip_jL} = \prod_{\substack{n=1\\n\neq j}}^{N_+} S\left(p_j\,,\,p_n\right) \prod_{m=1}^{N_+} \widetilde{S}^{-1}\left(p_j\,,\,q_m\right), \tag{3.4.24b}$$

$$= -\prod_{n=1}^{N_+}\left[-e^{i(p_j-p_n)}\right] \prod_{m=1}^{N_-}\left[e^{i(q_m-p_j)}\right] \tag{3.4.24c}$$

$$= (-1)^{N_+-1}\, e^{i(N_+\,p_j-K_+)} e^{i(K_--N_-p_j)}, \tag{3.4.24d}$$

and for left-movers with momenta q_j, the form

$$e^{iq_jL} = \prod_{\substack{n=1\\n\neq j}}^{N_-} S\left(q_j\,,\,q_n\right) \prod_{m=1}^{n_+} \widetilde{S}\left(p_m\,,\,q_j\right) \tag{3.4.24e}$$

$$= -\prod_{n=1}^{N_-}\left[-e^{i(q_j-q_n)}\right] \prod_{m=1}^{N_+}\left[e^{i(p_m-q_j)}\right] \tag{3.4.24f}$$

$$= (-1)^{N_--1}\, e^{i(N_-\,q_j-K_-)} e^{i(K_+-N_+q_j)}. \tag{3.4.24g}$$

In either case, one then has

$$e^{ik_j^\pm L} = (-1)^{N_\pm-1}\, e^{i\left(N_\pm\,k_j^\pm-K_\pm\right)} e^{i\left(K_\mp-N_\mp k_j^\pm\right)} \tag{3.4.24h}$$

which implies

$$e^{2\pi i m_j^\pm} = 1 = e^{i(L-N_\pm+N_\mp)k_j^\pm} e^{i(K_\pm-K_\mp)}\,(-1)^{N_\pm-1}, \tag{3.4.24i}$$

from which we can easily extract the solutions

$$k_j^+ = \frac{\pi\left(2m_j^+ + N_+ - 1\right) - \Theta}{L - N_+ + N_-} \qquad m_j^+ \in \{1,2,\ldots,L-N_++N_-\} \tag{3.4.25a}$$

$$k_j^- = \frac{\pi\left(2m_j^- + N_- - 1\right) + \Theta}{L - N_- + N_+} \qquad m_j^- \in \{1,2,\ldots,L-N_-+N_+\}\,. \tag{3.4.25b}$$

The solutions to this model consist of all $\left\{k_j^\pm\right\}$ of the form Eq. (3.4.25) where K and Θ satisfy Eq. (3.3.13), and $\sum_{j=1}^{N_\pm} k_j^\pm = K_\pm = \frac{1}{2}\left(K \pm \Theta\right)$. Additionally, no two movers of the same type may have the same momentum. These BAE have been tested against exact numerics for small systems, and appear to hold for all accessible sizes (roughly 22 physical spins and $N_\pm \sim L/2$, and out to larger L for lower filling fractions). The corresponding eigenvalues under the combined action are given by

$$e^{-i\lambda\hat{H}}\hat{F}_0|k_1^+,\ldots,k_{N_+}^+\,;\,k_1^-,\ldots,k_{N_-}^-\rangle = e^{-i\varepsilon\left(k_1^+,\ldots,k_{N_+}^+\,;\,k_1^-,\ldots,k_{N_-}^-\right)}|k_1^+,\ldots,k_{N_+}^+\,;\,k_1^-,\ldots,k_{N_-}^-\rangle, \tag{3.4.26}$$

with

$$\varepsilon\left(k_1^+,\ldots,k_{N_+}^+\,;\,k_1^-,\ldots,k_{N_-}^-\right) = \sum_\pm \sum_{j=1}^{N_\pm}\left\{\pm\,k_j^\pm + 2\lambda\cos\left(k_j^\pm\right)\right\}. \tag{3.4.27}$$

3.5 Summary of the Bethe Ansatz Solution

For clarity, here is a concise summary of the coordinate Bethe Ansatz solution, which applies both to FFA and its dispersing counterpart, DFFA.

Single-quasiparticle sectors We first find eigenstates of Eq. (3.2.1) for a single ± quasiparticle, $|j,\pm\rangle = \sigma^x_{2j}\sigma^x_{2j\pm1-1}|0\rangle$. The Fourier transform is an eigenstate of $\hat{F}(\lambda)$,

$$\hat{F}(\lambda)\,|k,\nu\rangle = \mathrm{e}^{-i\nu k - 2i\lambda\cos k}|k,\nu\rangle, \tag{3.5.1}$$

where $\nu = \pm1$, with $+1$ corresponding to right-movers and -1 to left-movers. Here, λ controls the strength of the dispersing term, and $k = 2\pi m/L$ for integer m, with L the system size in unit cells (each containing two sites). This model thus has two chiral bands, as shown in Figure. 3.1. For $\lambda < 1/2$, all + (−) quasiparticles have right- (left-) moving group velocities, but for $\lambda > 1/2$, both species have left- and right-moving quasiparticles. The group velocities of ± quasiparticles are given by $v^0_{\pm,k} = \pm1 - 2\lambda\sin k$. These chiral bands are characterized by a quantized winding number $\nu = \int_{-\pi}^{\pi}\frac{dk}{2\pi}v^0_{\pm,k} = \pm1$, which is the invariant characterizing Thouless pumping [66, 91, 92].

Bethe Ansatz solution We now move on to multi-particle sectors. We note, first, that in the absence of left-movers, the FFA evolution is just a trivial global translation. In this purely right-moving sector, the dynamics of + quasiparticles consists of hopping and hardcore nearest-neighbor repulsion. The scattering phase shift between particles of the same species is thus

$$S_{++}(k_2,k_1) = S_{--}(k_2,k_1) = \mathcal{S}(k_2,k_1) = -\mathrm{e}^{i(k_2-k_1)}\ . \tag{3.5.2}$$

Meanwhile, the scattering between left and right movers is engineered to retain the FFA form such that the phase shift after a collision is $S_{-+}(k_+,k_-) = \tilde{\mathcal{S}}(k_+,k_-) = +e^{i(k_+-k_-)}$, and no meaning is ascribed to the order of the arguments. Higher-body collisions factorize onto the two-body scattering processes, ensuring integrability. For a many-body state with fixed (N_+,N_-), where $\{k^\pm_j\}$ refer to the momenta of the ±-quasiparticles, we find the following quantization condition

$$\begin{aligned} e^{ik^+_jL} &= \prod_{\substack{n=1\\n\neq j}}^{N_+}\mathcal{S}\left(k^+_j\,,\,k^+_n\right)\prod_{m=1}^{N_-}\tilde{\mathcal{S}}^*\left(k^+_j\,,\,k^-_m\right), \\ e^{ik^-_jL} &= \prod_{\substack{n=1\\n\neq j}}^{N_-}\mathcal{S}\left(k^-_j\,,\,k^-_n\right)\prod_{m=1}^{N_+}\tilde{\mathcal{S}}\left(k^-_j\,,\,k^+_m\right). \end{aligned} \tag{3.5.3}$$

These quantization conditions have the same form as Bethe equations in Hamiltonian systems. Translational invariance and the recurrence properties of the FFA model (with which the Hamiltonian defined in Eq. (3.4.2) commutes) impose two further constraints. We require, first, that $\sum_j k^+_j + \sum_j k^-_j = K$, where $K = 2\pi m/L$ with m is one of the allowed global momenta, and second, that the relative momentum $\sum_j k^+_j - \sum_j k^-_j = \Theta$, where

$$\Theta = \frac{2\pi N_\theta + (N_+ - N_- - L)K}{L + N_- + N_+}, \tag{3.5.4}$$

with $1 \le N_\theta \le (L + N_- + N_+)$ an integer, unless $L + N_- + N_+$ is even, in which case N_θ must be as well. Finally, no two quasiparticles of the same species may occupy the same momentum

state, as in general integrable systems. With these constraints the solutions given by Eq. (3.5.3) fully characterize the eigenstates in a finite system, and the corresponding quasienergy $e^{-i\varepsilon}$ of the Floquet unitary, given by Eq. (3.2.1), reads $\varepsilon = \sum_{\nu=\pm}\sum_{n=1}^{N_\nu}(\nu k_n^\nu + 2\lambda\cos k_n^\nu)$.

Remarkably, these equations are simple enough that they can be solved exactly for any finite system. The set of allowed momenta for either species, ν is

$$k_j^\nu = \frac{\pi(2m_j^\nu + N_\nu - 1) - \nu\Theta}{L - N_\nu + N_{\bar{\nu}}}, \tag{3.5.5}$$

with $\bar{\nu} = -\nu$ and $1 \le m_j^\nu \le L - N_\nu + N_{\bar{\nu}}$. The number of available $m_j^\pm$ decreases with the total number of $\pm$ movers because neighboring unit cells cannot both host $\pm$'s without a $\mp$ between them. We also note that the quantization condition depends on the total number and momentum of the $\pm$ quasiparticles, not on the details of their distribution. Relatedly, Eq. (3.5.3) and Eq. (3.5.5) do not depend on λ, and thus also apply to $\hat{F}_0$, though in that model, the phase shift between quasiparticles of the same species is ill-defined as they move in unison and never collide.

The DFFA model corrects several pathological features of FFA. We show this numerically by analyzing the quasienergy level statistics using exact diagonalization (ED), finding that the levels do not repel, as plotted in Figure 3.3), consistent with integrability. We also confirm using ED that the value of the "r-ratio" [95] is consistent with a Poisson distribution for all $\lambda > 0$, as expected for integrable models.

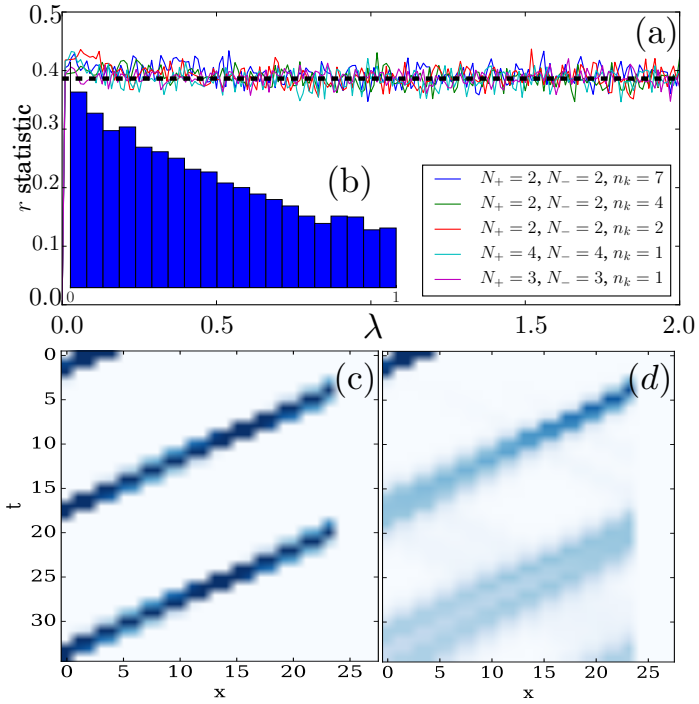

Figure 3.3: Numerical results. Quasi-energy level statistics as a function of λ, for several values of $N_\pm$ and K at $L = 9$: (a) the r ratio shows good agreement with a Poisson distribution (dashed line) for all $\lambda > 0$; (b) the distribution of r for $\lambda = 1.0$ (inset) does not show level repulsion, consistent with integrability. Plot of the OTOC $C(t)$ for $L = 14$ unit cells with $N_+ = 1$ and $N_- = 2$, for (c) $\lambda = 0$, corresponding to FFA, and (d) $\lambda = 0.05$, where we see that the OTOC does not "fill in" behind the front except through the dispersion of the perturbed quasiparticle. All data obtained from exact diagonalization.

3.6 Operator Dynamics

The rapidity-independent scattering kernels in the DFFA model have important consequences for operator spreading, which is simpler here than in generic integrable models [125]. In the generic case, any operator creates a "light cone" that fills in at late times: a spatially local operator has a spread of momenta and thus of group velocities, and the velocity-dependence of the scattering kernel implies that perturbing the velocity of one quasiparticle will affect the trajectories of all the others. This does not happen either in the hard rod gas or in the DFFA model, since the scattering kernel in these models is velocity-independent and consequently, any perturbation that preserves $N_\pm$ will only affect the state of one quasiparticle. Thus the butterfly cone, measured via the out-of-time-order correlator [130–133] (OTOC) $C(x,t) \equiv \frac{1}{2}\left|\mathrm{Tr}\left\{[\hat{h}_{j=2}, \hat{\sigma}^z_x(t)]^2\right\}\right|$ does not "fill in" except through the dispersion of the perturbed quasiparticle, as depicted in Figure 3.3. This property can also be seen from the coordinate Bethe ansatz: an operator that changes the velocity of a + quasiparticle does not alter the quantization condition for any other quasiparticles, and thus does not force a global rearrangement, in contrast to the generic case.

3.7 The Thermodynamic Bethe Ansatz for FFA

The Bethe Ansatz equations given by Eq. (3.4.24) admit exact and simple solutions, as seen in Eq. (3.4.25). Although these equations and solutions remain simple even as $L \to \infty$, it is nonetheless useful to go through the standard procedure of the thermodynamic Bethe Ansatz (TBA), which has been successfully applied to other integrable models [45]. In particular, the exceptionally simple nature of this model's S matrices will translate into simple results in the TBA formalism. As well, this will provide access to statistical mechanics of this model and generalized Gibbs ensembles (GGE), which stand apart from known interacting integrable models not only due to their simplified form, but the Floquet nature of the model requires that one forego the use of the standard Yang-Yang "free energy' [47], as this model has neither an extensive conserved energy nor a corresponding notion of temperature. We will find it convenient to introduce the following function:

$$\mathcal{S}_0(k_2 - k_1) = e^{i(k_2 - k_1)}, \tag{3.7.1}$$

such that $\mathcal{S}(k_2, k_1) = -\mathcal{S}_0(k_2 - k_1) = \mathcal{S}^*(k_1, k_2)$ for either $\nu = \pm 1$, and $\tilde{\mathcal{S}}(k^+_m, k^-_n) = \tilde{\mathcal{S}}(k^-_n, k^+_m) = +\mathcal{S}_0(k^+_m - k^-_n)$.

3.7.1 Bethe equations in the thermodynamic limit

We begin with quantization condition given by Eq. (3.4.25),

$$2\pi m^\nu_j = L k^\nu_j + i \sum_{\substack{n=1 \\ n\neq j}}^{N_\nu} \ln -\mathcal{S}_0\left(k^\nu_j - k^\nu_n\right) + i \sum_{m=1}^{N_{\bar{\nu}}} \ln \mathcal{S}_0\left(k^{\bar{\nu}}_m - k^\nu_j\right), \tag{3.7.2}$$

and replace the quantum numbers m^ν_j with counting functions $L c_\nu(k)$, as in the standard application of the TBA in Section 2.4 of Chapter 2, where the index ν labels species (as is the case in the presence of string excitations in the Trotterized XXX model). When $L c_\nu(k) = m^\nu_j$, if the momentum mode corresponding to m^ν_j is occupied, this corresponds to the presence of a particle;

otherwise, there is a hole. The counting function for FFA (or DFFA) satisfies

$$c_\nu(k) = \frac{k}{2\pi} + \frac{i}{2\pi L}\left\{ i\pi N_\nu + \sum_{n=1}^{N_\nu} \ln \mathcal{S}_0\left(k_j^\nu - k_n^\nu\right) - \sum_{m=1}^{N_{\mp}} \ln \mathcal{S}_0\left(k_m^{\bar\nu} - k_j^\nu\right)\right\} . \tag{3.7.3}$$

Note that due to the comparatively simple structure of the DFFA model, it is possible to simplify Eq. (3.7.3) substantially; however, to maintain consistency with other works on TBA, we proceed without doing so. The total density of states, $\rho_{\mathrm{s},\nu}$, which is the sum of the densities of particles and holes,

$$\rho_{\mathrm{s},\nu} = \rho_{\mathrm{p},\nu} + \rho_{\mathrm{h},\nu} \ , \tag{3.7.4}$$

obtains by differentiating the counting function, $c_\nu(k)$, with respect to its momentum argument:

$$\rho_{\mathrm{p},\nu}(k) + \rho_{\mathrm{h},\nu}(k) = \rho_{\mathrm{s},\nu}(k) = \frac{d\,c_\nu}{dk}(k) \ . \tag{3.7.5}$$

Note that we will use implicitly the relation

$$\frac{1}{L}\sum_{\substack{n=1\\ n\neq m}} f\left(k_{(m)} - k_n\right) \to \int_{-\pi}^{\pi} dk'\, f\left(k_{(m)} - k'\right)\rho_{\mathrm{p},\nu}(k') \ . \tag{3.7.6}$$

To match other references on integrable systems, we define the S matrix in the space of species labels via

$$S_{\nu\nu'}(q_2,q_1) = \delta_{\nu\nu'}\mathcal{S}(q_2,q_1) + (1-\delta_{\nu\nu'})\,\tilde{\mathcal{S}}^{\nu'}(q_2,q_1)\,, \tag{3.7.7}$$

where in the second term ν' is an *exponent*, not a superscript, and these objects are also defined in Eq. (3.7.1). The differential scattering kernel K is then given by

$$K_{\nu\nu'}(q,q') \equiv \frac{1}{i}\frac{d}{dq}\ln S_{\nu\nu'}(q-q') = \frac{1}{i}\left(i\delta_{\nu\nu'} - i\left(1-\delta_{\nu\nu'}\right)\right) = \left(2\,\delta_{\nu\nu'} - 1\right) = \nu\nu', \tag{3.7.8}$$

when both ν,ν' take the values ±1 ($+1$ for right-movers and -1 for left-movers). The convolution operator $\hat{\mathcal{K}}$ is therefore

$$[\hat{\mathcal{K}}\,f]_\nu(q) = \sum_{\nu'}\int_{-\pi}^{\pi}\frac{dq'}{2\pi}\,K_{\nu,\nu'}(q,q')\,f_{\nu'}(q') = \sum_{\nu'}\nu\,\nu'\,\langle f_{\nu'}(q)\rangle_q \ , \tag{3.7.9}$$

which is notably independent of momentum.

Given the above, the density of states, $\rho_{\mathrm{s},\nu}$ is therefore

$$\rho_{\mathrm{s},\nu}(p) = \frac{1}{2\pi}\left\{1 - \int_{-\pi}^{\pi} dp'\,\rho_{\mathrm{p},\nu}(p') + \int_{-\pi}^{\pi} dq\,\rho_{\mathrm{p},\bar\nu}(q)\right\} = \frac{1}{2\pi}\left(1 + \frac{N_\nu - N_{\bar\nu}}{L}\right) = \frac{1}{2\pi}\left(1 - \varrho_\nu + \varrho_{\bar\nu}\right), \tag{3.7.10a}$$

where $\bar\nu = -\nu$ is the other label, and $\varrho_\nu = \frac{N_\nu}{L} = \int_{-\pi}^{\pi} dk\,\rho_{\mathrm{p},\nu}(k)$. Summarizing these results:

$$\rho_{\mathrm{p},\nu}(k) + \rho_{\mathrm{h},\nu}(k) = \rho_{\mathrm{s},\nu}(k) = \frac{d\,c_\nu}{dk}(k) = \frac{1}{2\pi}\left(1 + \varrho_{\bar\nu} - \varrho_\nu\right) = \frac{1}{2\pi}\left\{1 + \int_{-\pi}^{\pi} dk'\,\left[\rho_{\mathrm{p},\bar\nu}(k') - \rho_{\mathrm{p},\nu}(k')\right]\right\}, \tag{3.7.11}$$

which means that $\rho_{\mathrm{p},\nu}$ is independent of k, as are $\rho_{\mathrm{s},\nu}$ and $\rho_{\mathrm{h},\nu}$. Since all densities are k-independent, as is the differential scattering kernel and occupation factor, all dressing operations will be completely trivial, which will substantially simplify the use of TBA and generalized hydrodynamics (GHD).

3.7.2 Effective TBA partition function

We now construct an effective partition function with respect to which one can compute thermodynamic expectation value via the generalized Gibbs ensemble (GGE). The partition function is the exponential of an effective "free energy," which is a poor choice of name for a Floquet system. Instead, we will refer to the analogous object as the "[generalized] Gibbs potential" (GGP), or symbolically: $G = L\,\mathcal{G}$. Because the model is Floquet, there is no extensive conserved energy, nor a definition of temperature, T; correspondingly, we do not insist other quantities inherit units of energy, and the need for β and other quantities does not arise:

$$\mathcal{Z} = e^{-G} = \int \mathcal{D}\left[\rho_+, \rho_-\right] e^{-L\mathcal{G}[\rho_+,\rho_-]} \tag{3.7.12}$$

$$= \int \mathcal{D}\left[\rho_+, \rho_-\right] e^{-\mu_+ N_+} e^{-\mu_- N_-} e^{L\,S_{YY}[\rho_+,\rho_-]}, \tag{3.7.13}$$

where S_{YY} is the Yang-Yang entropy function corresponding to the densities of states $\rho_{\mathrm{s},\nu}$ that correspond to the TBA equations, Eq. (3.7.11). For concreteness, we restricted to a GGE specified by two chemical potentials $\mu_\pm$ for the two-quasiparticle species. Correspondingly, the above becomes

$$\mathcal{G}\left[\rho_+, \rho_-\right] = \mu_+ \varrho_+ + \mu_- \varrho_- - S_{YY}\left[\rho_+, \rho_-\right] \tag{3.7.14}$$

$$= \sum_{\nu=\pm 1} \int_{-\pi}^{\pi} dk\, \left\{\mu_\nu \rho_{\mathrm{p},\nu} - \left[\rho_{\mathrm{s},\nu} \ln \rho_{\mathrm{s},\nu} - \rho_{\mathrm{p},\nu} \ln \rho_{\mathrm{p},\nu} - \rho_{\mathrm{h},\nu} \ln \rho_{\mathrm{h},\nu}\right]\right\}. \tag{3.7.15}$$

Since the partition function has the form $\mathcal{Z} = \int \mathcal{D}\rho e^{-L\mathcal{G}[\rho]}$ as $L \to \infty$, we can compute this integral by saddle point, i.e. finding extrema of $\mathcal{G}$. Thus, we will use a functional variation, sending $\rho_{\mathrm{p},\nu} \to \rho_{\mathrm{p},\nu} + \delta\rho_{\mathrm{p},\nu}$ and $\mathcal{G} \to \mathcal{G} + \delta\mathcal{G}$, and then choose $\rho_{\mathrm{p},\nu}$ such that $\delta\mathcal{G} \to 0$. We will also make use of the fact that the variations of the particle and hole densities are related by the TBA Bethe equations, Eq. (3.7.11), and derive a variational relation therefrom:

$$\delta\rho_{\mathrm{s},\nu}(k) = \delta\rho_{\mathrm{p},\nu}(k) + \delta\rho_{\mathrm{h},\nu}(k) = \frac{1}{2\pi} \int_{-\pi}^{\pi} dk' \left[\delta\rho_{\mathrm{p},\bar{\nu}}(k') - \delta\rho_{\mathrm{p},\nu}(k')\right] \tag{3.7.16}$$

and with this, we are ready to extremize the GGP:

$$\delta\mathcal{G} = \sum_{\nu=\pm 1} \int_{-\pi}^{\pi} dk\, \{\mu_\nu \delta\rho_{\mathrm{p},\nu} - [\delta\rho_{\mathrm{p},\nu} \ln \frac{\rho_{\mathrm{s},\nu}}{\rho_{\mathrm{p},\nu}} + \delta\rho_{\mathrm{h},\nu} \ln \frac{\rho_{\mathrm{s},\nu}}{\rho_{\mathrm{h},\nu}}]\}, \tag{3.7.17}$$

where so far, all ρ's have been functions of k. We now invoke Eq. (3.7.16) and must be explicit about this. After a few standard manipulations [45] one has

$$\delta\mathcal{G} = \sum_{\nu=\pm 1} \int_{-\pi}^{\pi} dk\, \delta\rho_{\mathrm{p},\nu}(k) \left\{\mu_\nu - \left[\ln \frac{\rho_{\mathrm{h},\nu}}{\rho_{\mathrm{p},\nu}} - \int_{-\pi}^{\pi} \frac{dq}{2\pi} \ln\left(1 + \frac{\rho_{\mathrm{p},\nu}(q)}{\rho_{\mathrm{h},\nu}(q)}\right) + \int_{-\pi}^{\pi} \frac{dq}{2\pi} \ln\left(1 + \frac{\rho_{\mathrm{p},\bar{\nu}}(q)}{\rho_{\mathrm{h},\bar{\nu}}(q)}\right)\right]\right\}, \tag{3.7.18}$$

which is zero if the quantity in curly braces above is zero. Writing $\frac{\rho_{\mathrm{h},\nu}(k)}{\rho_{\mathrm{p},\nu}(k)} = e^{\epsilon_\nu(k)}$, the extremization is guaranteed by the TBA equations:

$$\epsilon_\nu(k) = \mu_\nu + \int_{-\pi}^{\pi} \frac{dq}{2\pi} \ln \frac{1 + e^{-\epsilon_\nu(q)}}{1 + e^{-\epsilon_{\bar{\nu}}(q)}}. \tag{3.7.19}$$

These equations imply that ϵ_ν does not depend on momentum, so that

$$\epsilon_\nu = \mu_\nu + \ln \frac{1 + e^{-\epsilon_\nu}}{1 + e^{-\epsilon_{\bar{\nu}}}}, \tag{3.7.20}$$

In the case where $N_+ = N_-$, whence one has $\mu_+ = \mu_- = \mu$, the equations simplify even further to $\epsilon_\nu = \mu$ for both $\nu = \pm 1$.

3.7.3 Summary of thermodynamics

In the thermodynamic limit, one defines densities of quasiparticles at a given species and rapidity, $\rho_\pm(k)$, as well as total densities of states $\rho_\pm^{\text{tot}}(k)$, related via the Bethe equations

$$2\pi\rho_{\text{s},\pm}(q) = 2\pi\rho_{\text{p},\pm}(q) + 2\pi\rho_{\text{h},\pm}(q) = 1 + \varrho_\mp - \varrho_\pm, \tag{3.7.21}$$

where

$$\varrho_\pm \equiv \int_{-\pi}^{\pi} dq\, \rho_{\text{p},\pm}(q) = N_\pm/L\ . \tag{3.7.22}$$

These equations follow from the continuum limit of Eq. (3.5.3), with the scattering kernels

$$\mathcal{K}_{\nu\nu'} = \frac{1}{2\pi i}\frac{d}{dk}\ln S_{\nu\nu'}\ , \tag{3.7.23}$$

with $\nu, \nu' \in \{+, -\}$, i.e.

$$\mathcal{K}_{++} = \mathcal{K}_{--} = 1/(2\pi)\ , \qquad \mathcal{K}_{+-} = \mathcal{K}_{-+} = -1/(2\pi)\ . \tag{3.7.24}$$

Starting with these equations, one can straightforwardly construct generalized equilibrium states of this Floquet system. We emphasize that since the DFFA model is integrable, its dynamics lead to nontrivial steady states that are distinct from featureless infinite temperature states that would be expected for generic interacting Floquet systems. For concreteness we focus on generalized equilibrium states characterized by a given density of ± quasiparticles via the partition function $\mathcal{Z} = \sum_{\{\sigma\}} e^{-\mu_- N_- - \mu_+ N_+}$, but our discussion extends naturally to arbitrary GGEs for this model. In terms of quasiparticle densities, the partition function reads $\mathcal{Z} \sim \int \mathcal{D}\rho e^{L\int dk S_{\text{YY}}} e^{-L\mu_+\int dk \rho_{k,+} - L\mu_-\int dk \rho_{k,-}}$ where S_{YY} is the so-called Yang-Yang entropy [45, 47] associated with the occupation of quasiparticle states. In the thermodynamic limit these integrals are dominated by their saddle point, giving rise to thermodynamic Bethe Ansatz (TBA) equations analogous to Hamiltonian integrable systems [45]. This leads to the following equations for the occupation numbers (Fermi factors)

$$n_\nu(k) \equiv \frac{\rho_{\text{p},\nu}(k)}{\rho_{\text{s},\nu}(k)} \equiv (1 + e^{\epsilon_\nu(q)})^{-1}\ , \tag{3.7.25}$$

which turn out to be independent of k:

$$\epsilon_\pm = \mu_\pm + \log\left(\frac{1 + e^{-\epsilon_\pm}}{1 + e^{-\epsilon_\mp}}\right). \tag{3.7.26}$$

Together with Eq. (3.7.21) this forms a complete characterization of the generalized Gibbs ensemble. For $\lambda = 0$ (i.e. the FFA model), the properties of this ensemble can also be derived by a transfer-matrix calculation [125]; these approaches give equivalent results. These TBA solutions allow one to probe the physics of Thouless pumps in an *interacting* model even in the limit $L \to \infty$, and generalize the formalism to the Floquet setting.

3.8 Generalized Hydrodynamics

3.8.1 General results

Coarse-grained dynamics in the FFA and DFFA models can be described using the recently developed theory of generalized hydrodynamics (GHD) [54–56, 59, 134–149]. GHD treats the system semiclassically as a soliton gas [136]. There are two species of solitons, labelled by $\nu = \pm 1$, whose bare group velocities v_k^0 follow from the dispersion relation, Eq. (3.5.1). When solitons collide, each pick up a semi-classical displacement $\Delta x = 2\pi\mathcal{K}$ in the direction of motion, as depicted in Figure 3.1. Like-species (unlike-species) collisions speed up (slow down) solitons by one step. Collisions lead to a dressing of the velocities [52, 55, 56], with the effective velocities in a state with quasiparticle densities $\rho_{\mathrm{p},\pm}(k)$ given by

$$v_\pm(k) = v_\pm^0(k) + \int dq (v_\pm(k) - v_\pm(q))\rho_{\mathrm{p},\pm}(q) - \int dq (v_\pm(k) - v_\mp(q))\rho_{\mathrm{p},\mp}(q) \ . \tag{3.8.1}$$

The generalized hydrodynamics [55, 56] of the DFFA model follows immediately from the TBA equations derived in Sec. 3.7. Let us consider a (generalized) equilibrium state with filling $n = \frac{1}{1+e^\mu}$, corresponding to $\mu_+ = \mu_- = \mu$. The effective (dressed) velocities of the quasiparticles in this simple GGE follow from the equation given in the main text, and they are given by

$$v_{\pm,k} = \pm\frac{1}{1+2\varrho} - 2\lambda \sin k. \tag{3.8.2}$$

As in generic interacting integrable models, the quasiparticle trajectories broaden diffusively due to the random collisions with other quasiparticles. The variance of the position of a given quasiparticle at time t is given by [58, 125]

$$\delta x_{\nu,k}^2(t) = t\frac{1}{[\rho_{\mathrm{s},\nu}(k)]^2}\sum_{\nu'}\int dk' \, |v_\nu(k) - v_{\nu'}(k')| \, [\mathcal{K}_{\nu\nu'}^{\mathrm{dr}}(k,k')]^2 \rho_{\mathrm{p},\nu'}(k')\,(1 - n_{\nu'}(k'))\,, \tag{3.8.3}$$

where

$$\mathcal{K}_{\nu\nu'}^{\mathrm{dr}}(k,k') = \mathcal{K}_{\nu\nu'}(k,k') - \sum_{\nu''}\int dk'' \mathcal{K}_{\nu\nu''}(k,k'')\mathcal{K}_{\nu''\nu'}^{\mathrm{dr}}(k'',k')n_{\nu''}(k'')\,, \tag{3.8.4}$$

is the "dressed kernel", and $n_\nu(k) = \rho_{\mathrm{p},\nu}(k) \,/\, \rho_{\mathrm{s},\nu}(k)$ is the filling fraction (or "Fermi factor"). We evaluate these formulae in an equilibrium state with chemical potential μ, corresponding to a given filling

$$\varrho_\nu = \int dk \, \rho_{\mathrm{p},\nu}(k) \ , \tag{3.8.5}$$

and when the chemical potentials for left- and right-movers are both μ, the fillings ϱ are equal. The equations for the dressed Kernels become

$$\mathcal{K}_{++}^{\mathrm{dr}} = \frac{1}{2\pi} - \varrho\left(\mathcal{K}_{++}^{\mathrm{dr}} - \mathcal{K}_{+-}^{\mathrm{dr}}\right), \tag{3.8.6}$$

$$\mathcal{K}_{+-}^{\mathrm{dr}} = -\frac{1}{2\pi} - \varrho\left(\mathcal{K}_{+-}^{\mathrm{dr}} - \mathcal{K}_{++}^{\mathrm{dr}}\right), \tag{3.8.7}$$

so that

$$\mathcal{K}_{++}^{\mathrm{dr}} = \mathcal{K}_{--}^{\mathrm{dr}} = \frac{1}{2\pi(1+2\varrho)}, \ \mathcal{K}_{+-}^{\mathrm{dr}} = \mathcal{K}_{-+}^{\mathrm{dr}} = -\frac{1}{2\pi(1+2\varrho)}. \tag{3.8.8}$$

These explicit expressions for the dressed kernels combined with the dressed velocities, Eq. (3.8.2), fully determine the quasiparticle broadening using Eq. (3.8.3). This expression simplifies even further in the case of the pure FFA model ($\lambda = 0$). Focusing on a right-mover, the effective velocity reads $\pm v_\pm = 1 - \frac{2\varrho}{1+2\varrho} = \frac{1}{1+2\varrho}$. This yields

$$\delta x^2(t) = t(2\pi)^2 \left(\int_{-\pi}^{\pi} dk' \right) |2v_+| \, (\mathcal{K}_{+-}^{\mathrm{dr}})^2 \frac{1}{2\pi} \varrho(1-\varrho) = t \frac{2\varrho(1-\varrho)}{(1+2\varrho)^3}. \tag{3.8.9}$$

This coincides with the formula found in Ref. 125 using a more elementary transfer matrix approach.

3.8.2 Charge and current formalism

Let us restrict to the bare FFA model, sans dispersion for the remainder of our hydrodynamic treatment. One useful feature of this model is that the hydrodynamic equations for the two most physically relevant conserved quantities, the densities of left and right movers, decouple from the infinitely many other conserved quantities, which relate to asymptotic spacing. Additionally, both the group and effective velocities without dispersion are extremely simple ($v_R^{\mathrm{grp}} = 1, v_L^{\mathrm{grp}} = -1$), and in working in a GGE with $\mu_L = \mu_R = \mu$, we find that no quantities depend on momentum.

The important conserved charges correspond to the total density of left [right] movers, integrated over rapidity, which we denote $\varrho_\nu = \int d\theta \rho_{\mathrm{p},\nu}(\theta; x, t) = 2\pi \rho_{\mathrm{p},\nu}(\cdot; x, t)$, as the densities are rapidity independent. Importantly, we will use $\nu = L, R$ explicitly, to avoid confusion with a different meaning of the $\pm$. We can solve for the effective velocities as functionals of these quantities,

$$v_R = 1 - \frac{2\varrho_L}{1 + \varrho_R + \varrho_L} \tag{3.8.10a}$$

$$v_R = -1 + \frac{2\varrho_R}{1 + \varrho_R + \varrho_L} \ , \tag{3.8.10b}$$

and the corresponding hydrodynamic equations without perturbations are

$$\partial_t \varrho_\nu + \partial_x \left[v_\nu \varrho_\nu \right] = 0 \ , \tag{3.8.11}$$

for $\nu = L, R$.

However, a superior notation is afforded by defining hydrodynamic charges via a rotation of the quantities ϱ_ν:

$$q_\pm = \varrho_R \pm \varrho_L \ , \tag{3.8.12}$$

in terms of which the GHD equations are

$$\partial_t q_+ + \partial_x j_+ = 0 \tag{3.8.13}$$

$$\partial_t q_- + \partial_x j_- = 0 \ , \tag{3.8.14}$$

where

$$j_+ = q_- \ , \quad j_- = \frac{q_-^2 + q_+}{1 + q_+} \ , \tag{3.8.15}$$

in this GGE, as can be seen by expressing v_ν in terms of $q_\pm$,

$$v_R = \frac{q_- + 1}{q_+ + 1} \ , \quad v_L = \frac{q_- - 1}{q_+ + 1} \ . \tag{3.8.16}$$

The ability to express currents directly in terms of charges without approximation does not appear to extend to other interacting integrable models, and depends crucially on the fact that in this GGE none of the relevant quantities depend on rapidity.

Inserting these definitions for the currents, we obtain two coupled GHD equations in terms of $q_\pm$ only:

$$0 = \partial_t q_+ + \partial_x q_- \tag{3.8.17}$$

$$0 = \partial_t q_- + \frac{2q_-}{q_+ + 1}\partial_x q_- + \frac{1 - q_-^2}{(q_+ + 1)^2}\partial_x q_+ \ , \tag{3.8.18}$$

and the latter expression can be re-written in terms of the bare velocities,

$$0 = \partial_t q_- + (v_R + v_L)\,\partial_x q_- - v_R v_L \partial_x q_+ \ . \tag{3.8.19}$$

3.8.3 Ballistic hydrodynamics

Taking an extra time derivative of Eq. (4.5.9) and Eq. (4.5.10), one can insert the latter into the former, i.e.

$$\partial_t^2 q_+ = -\partial_x \partial_t q_- \ , \tag{3.8.20}$$

where the righthand side is equal to a spatial derivative of the other terms in Eq. (4.5.10). By reinserting Eq. (4.5.9), we can replace all spatial derivatives of q_- with time derivatives of q_+, the result is:

$$\begin{gathered}\left(\partial_t^2 + (v_L + v_R)\,\partial_x\partial_t + v_L v_R \partial_x^2\right) q_+ = \\ (v_R - v_L)\,(\partial_t q_+ + v_L \partial_x q_+)\,(\partial_t q_+ + v_R \partial_x q_+) \ ,\end{gathered} \tag{3.8.21}$$

and noting that

$$(\partial_t + v_{\bar\nu}\partial_x)\, v_\nu = 0 \tag{3.8.22}$$

is equivalent to Eq. (4.5.10) for $\Gamma = 0$, we can rewrite the lefthand side of Eq. (4.5.13) as $(\partial_t + v_R\partial_x)\,(\partial_t + v_L\partial_x)\,q_+$, in which case both the left and right sides of Eq. (4.5.13) are zero if *either*

$$(\partial_t + v_\nu \partial_x)\, q_+ = 0 \ , \tag{3.8.23}$$

for either choice $\nu = L, R$, demonstrating that q_+ is exactly ballistic.

Choosing a solution for q_+ corresponding to the same ν as in Eq. (4.5.16), one can then rewrite Eq. (4.5.10) as

$$0 = \partial_t q_- + (v_R + v_L)\,\partial_x q_- - v_R v_L \partial_x q_+ \tag{3.8.24}$$

$$0 = \partial_t q_- - v_R \partial_t q_+ - v_L \partial_t q_+ + v_{\bar\nu}\partial_t q_+ \tag{3.8.25}$$

$$0 = \partial_t q_- - v_\nu \partial_t q_+ \tag{3.8.26}$$

$$0 = \partial_t q_- + v_\nu \partial_x q_- \ , \tag{3.8.27}$$

which shows that q_- satisfies the same equation as q_+ and propagates ballistically with the same velocity. This means that the sum and difference of $q_\pm$, i.e. $\varrho_{L,R}$, also propagate ballistically, e.g. with their corresponding velocity, $v_{L,R}$,

$$\left(\partial_t + v_{L,R}\partial_x\right) \varrho_{\nu=L,R} = 0 \ , \tag{3.8.28}$$

and it seems that these modes can propagate with the velocity of the other mover.

We can also express the individual charges ϱ_ν in terms of the Fermi factors and show that the latter propagate ballistically, as one expects in general integrable models. The occupation factor is defined by

$$n_\nu(k) = \frac{\rho_{\mathrm{p},\nu}(k)}{\rho_{\mathrm{s},\nu}(k)} = \frac{\varrho_\nu/2\pi}{(1+\varrho_{\bar\nu}-\varrho_\nu)/2\pi} = \frac{\varrho_\nu}{1+\varrho_{\bar\nu}-\varrho_\nu} = n_\nu \ , \tag{3.8.29}$$

and with some simple iterations one can recover

$$\varrho_\nu = \frac{n_\nu(1+2n_{\bar\nu})}{1+n_\nu+n_{\bar\nu}} \ , \tag{3.8.30}$$

and one can insert this into any of the relations for the charges to find the exact relation

$$(\partial_t + v_\nu \partial_x)\, n_\nu(x,t) = 0 \ , \tag{3.8.31}$$

which agrees with the general result for hydrodynamics of integrable models: they are diagonalized by the occupation factor.

Note that in certain ensembles, it may be more complicated to demonstrate certain results for the charges, though the occupation factor results should always hold. In fully general scenarios, it may be possible to see diffusion of q_-, e.g., at the level of Navier-Stokes hydrodynamics. However, one should always find that q_+ propagates ballistically—as long as it is conserved—as it has the special property that its current, $j_+ = q_-$, is itself a conserved charge. Thus, the hydrodynamic equations, e.g. Eq. (4.5.9), for q_+ do not receive corrections at the level of Navier-Stokes hydrodynamics, compared to the Euler equations provided above.

3.9 Summary and Outlook

In summary, we present and solve exactly a Floquet model that is the first of its kind in a number of respects. It is the first example of an interacting integrable Floquet model that is neither smoothly deformable to Hamiltonian dynamics [38] nor classically simulable (FFA). Our solution of the dispersing model has provided insight into the physics of FFA, which prior to this work was not confirmed to be integrable in the Yang-Baxter sense; the dispersing model regularizes several pathological features of FFA. Our model nonetheless preserves the chiral quasiparticle excitations of FFA, which realize topological Thouless pumping. Despite the complicated nature of the Hamiltonian terms, the resulting Bethe equations, Eq. (3.5.3), and TBA equations, Eq. (3.7.26), are the simplest of any interacting integrable model as far as we are. This model shows the existence of interacting Floquet models with stable chiral quasiparticles, and suggests a route to finding others, building on integrable cellular automata [120, 124, 150, 151].

Finally, we briefly discuss the experimental implications of this work. The FFA model itself is simple to implement on extant "noisy intermediate-scale quantum computers" [152] based on ion traps, cold atoms, or superconducting qubits, since the CNOT and Toffoli gates are basic, well-developed gates. The Hamiltonian, given by Eq. (3.2.5), is more challenging, although a Trotterized version that preserves integrability can be implemented on small gate-based quantum simulators; transport, operator growth [153], and even level statistics [154] have been measured in this setting. There might also be simpler-to-realize deformations of FFA that retain integrability (e.g., models that only contain the doublon hopping term). Exploring such deformations is an interesting topic for future work.

Chapter 4

Quantum Thermalization from Integrability Breaking

Parts of this Chapter are drawn from Ref. 155 by this author.

4.1 Introduction

In one dimension, many paradigmatic models of quantum many-body physics—such as the Hubbard, Heisenberg, and Lieb-Liniger models—are integrable. These models approximately describe a variety of experiments, in contexts ranging from quasi-one-dimensional materials to ultracold atomic gases. Thus, approximate integrability is of wide experimental relevance. In nearly integrable systems, the short-time dynamics are integrable, feature infinitely many conservation laws, and are described by the recently developed framework of generalized hydrodynamics (GHD) outlined in Ch. 2; at long enough times, however, the dynamics are chaotic, feature a finite set of conservation laws, and are presumably described by conventional hydrodynamics [54–56, 58–60, 148, 156].

In addition, while a number of properties of integrable systems are not generic to thermal systems, other properties may well be. Other aspects of thermal systems may be recovered by perturbing about fine-tuned integrable Hamiltonians (or Floquet unitaries), which explicitly break the extensive set of conserved quantities to a mere handful, and remove other pathological features of integrable models. When such perturbations are sufficiently weak to admit perturbative treatment, they can be regarded as introducing a finite lifetime to the absolutely stable quasiparticles of integrable models. The existence of such quasiparticle solutions of the unperturbed integrable model—which may include nonperturbative interactions—provides a useful platform from which to investigate thermalization.

Many early studies of thermal systems relied upon integrable models and their exact solutions to gain insight into more general systems [19, 157]. For example, in Ref. 19, numerous aspects of thermal systems, including spectral properties, are confirmed via consideration of generalized Gibbs ensembles, and has been extended since [158]. Additionally, using integrability, one can show analytically how the ideal conductivity of metals arises from microscopics [135]. Finally, as previously mentioned, various systems—including truly integrable and nearly integrable models—

that are relevant to experiments have been studied using integrability as a starting point, e.g. the quantum Newton's cradle [146, 159].

4.2 Entanglement Dynamics

The fact that integrable models have well-defined quasiparticle solutions lends itself to an intuitive picture of the dynamical spread of entanglement following a global quantum quench [34, 160–163]. Importantly, the quasiparticle modes that delimit the eigenstates of integrable models behave like free particles, albeit with complicated quantization conditions owing to the fact that they secretly encode interactions. However, for all intents and purposes, these particles are perfectly stable, parametrized by a "rapidity" label related to the momentum—each of which can be at most singly occupied—and the set of occupations delimits a "microstate." In the thermodynamic limit, the quantization relaxes as the allowed rapidities are continuous; the system is then described by a "macrostate," specified by the roots of the Bethe equations that arise from the thermodynamic Bethe Ansatz (TBA). These roots correspond to the densities of quasiparticles and "holes" in rapidity space, denoted ρ_{p} and ρ_{h}, respectively. Associated to the macrostate is an entropy of configuration, corresponding to the number of equivalent microstates (i.e. microscopic eigenstates), quantified by the Yang-Yang entropy, which is analogous to thermodynamic entropy for integrable models.

We then consider a global quantum quench of an integrable system, in which the entire system is prepared in some states at time $t = 0$ that is not an eigenstate of the evolution. For standard thermal systems, although the global system never reaches a steady state that is in any way independent of the $t = 0$ state, local subsystems can do so. Unlike standard thermal systems, integrable models possess an extensive set of local (and quasilocal) conserved quantities, which prevents this from happening even locally, as explained in Ch. 2 and Sec. 2.5 in particular. However, integrable models *can* be described by statistical ensembles, as detailed in Sec. 2.5, though they will not have several properties of thermal ensembles.

Consider now the generalized microcanonical ensemble outlined in Sec. 2.5, and consider ensembles that do not exactly fix the values of all conserved quantities, but rather insist that they be within some threshold of their expectation value at $t = 0$. Essentially, this amounts to relaxing the usual δ function associated to the microcanonical partition function to a distribution of small but finite width. In this case, if we consider the eigenstates within this microcanonical window, in the thermodynamic limit, these eigenstates give rise to a single macrostate, $|\rho_{\mathrm{p}}, \rho_{\mathrm{h}}\rangle$, due to the nature of the TBA formalism[1]. If one is able to extract from the state at $t = 0$ the appropriate expectation values of all conserved quantities (which generally can be expressed in terms of ρ_{p}, as noted in Sec. 2.6), then one can recover the macrostate $|\rho_{\mathrm{p}}, \rho_{\mathrm{h}}\rangle$ and calculate all local properties of the steady state—given by $|\rho_{\mathrm{p}}\rangle$—at all times following the quench. It is from this picture that generalized hydrodynamics (GHD) emerges.

The same semiclassical picture that gives rise to GHD also admits a picture of the spreading of entanglement. We assume the initial state at $t = 0$ is a product state in the real space basis, and therefore unentangled, with $S = 0$. In particular, we note that the thermodynamic entropy of a given subsystem, $\mathcal{A}$, at very late times must be equal to the entanglement entropy accumulated dynamically during that time [34, 160, 162]. The quantitative results for the spread of entanglement entropy in integrable models was sketched in Ref. 160, and has been established quite rigorously

[1] This assumes a particular notion of the generalized microcanonical ensemble and the "window," which is intertwined with the thermodynamic Bethe Ansatz itself and well formulated in the literature.

by subsequent works, e.g. Refs. 162 and 34. That argument is based on "light cone spreading of entanglement" by quasiparticles created by the quench; the original work relied heavily on conformal field theory [160], with later works showing that this picture is, in fact, quite generic to integrable models.

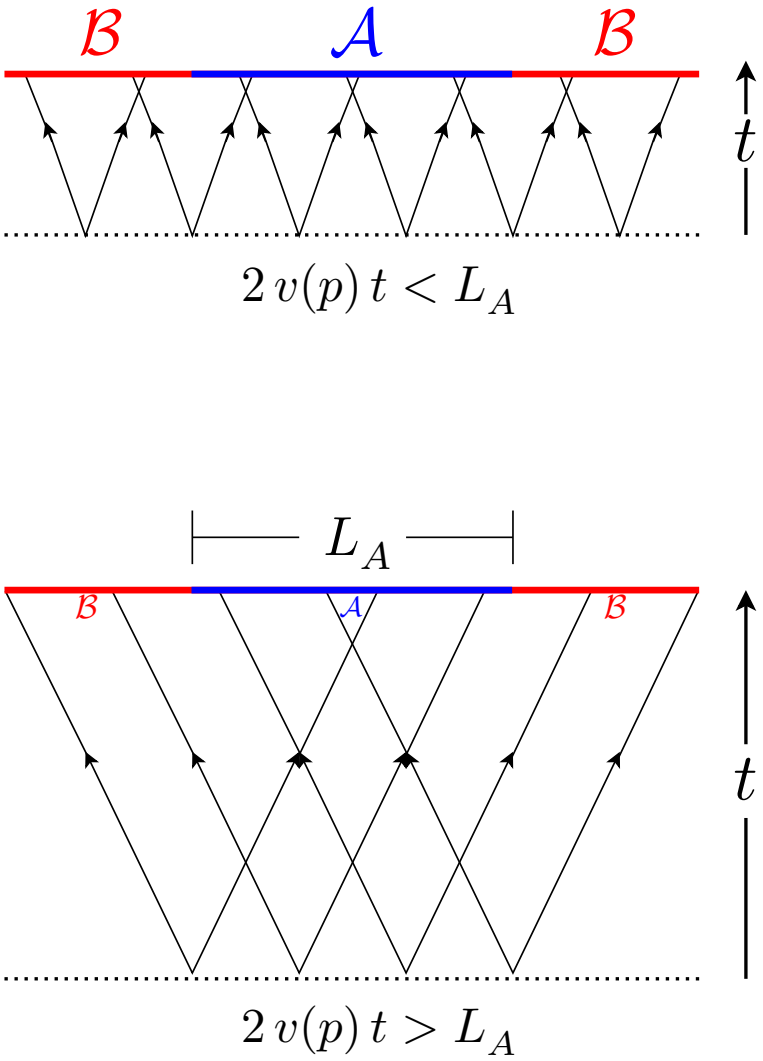

Figure 4.1: A sketch of the semiclassical pictures used in Ref. 160. The figure depicts the semiclassical propagation of quasiparticles created in pairs following a global quench in an integrable system. The entanglement entropy between two regions, $\mathcal{A}$ and $\mathcal{B}$, at time $t > 0$ is related to the number of quasiparticles pairs created at $t = 0$ where one of the quasiparticles ended up in $\mathcal{A}$ and the other in $\mathcal{B}$. The entanglement entropy grows linear until it saturates $\mathrm{Vol}\,(\mathcal{A}) = L_A$, in agreement with results for thermal systems.

Restricting to the standard case of Hamiltonian systems, a generic quench deposits an extensive amount of energy into the system relative its ground state (or steady state). The only means by which the system can relax to a steady state is for this excess of energy to create quasiparticle pairs. From a different point of view, the action of the Hamiltonian on generic states that are not eigenstates will necessarily involve the creation of quasiparticle pairs above some TBA macrostate. For initial states that are not terribly inhomogeneous, in general, quasiparticle pairs will be created

fairly uniformly throughout the system [160], and the key feature is that only quasiparticles created at the same point (or within some relevant distance of one another) are entangled. Therefore, at late times, $t > 0$, the entanglement between regions $\mathcal{A}$ and $\mathcal{B}$ is given precisely by the number of quasiparticles currently in $\mathcal{B}$ for which their counterpart, created by the quench, is in $\mathcal{A}$. Thus, for a given entanglement cut at some time, t, one recovers the entanglement entropy by retracing the semiclassical quasiparticle trajectories to $t = 0$, as depicted in Fig. 4.1

Since the particles propagate semiclassically, it is possible to trace them back to their starting point at time $t = 0$. In particular, the points x and y can only be entangled at time $t > 0$ if a left-moving quasiparticle arriving at x is entangled with a right-moving particle arriving at y, both at time t, which can only happen if $x \pm v(p)t \sim y \mp v(p)t$, where p is the quasiparticle momentum, which relates directly to the rapidity. In practice, we will be interested in the entanglement between two regions, and therefore an exact equality will not be necessary. Assuming that particles pairs with momenta $p, -p$ are created with some probability $f(p)$, this leads to the simple formula

$$S_{A|B}(t) \approx \int_{x_a \in \mathcal{A}} dx_a \int_{x_b \in \mathcal{B}} dx_b \int_{x_0 \in \mathcal{S}} dx_0 \int dp\, f(p)\, \delta(x_a - x_0 - v(p)\, t)\, \delta(x_b - x_0 + v(p)\, t) \tag{4.2.1}$$

$$\propto t \int dp\, f(p)\, 2v(p)\, \Theta(L_A - 2v(p)\, t) + L_A \int dp\, f(p)\, \Theta(2v(p)\, t - L_A)\ , \tag{4.2.2}$$

where $f(p)$ depends on the quench protocol, the velocities are determined from TBA, and we have taken $L_A < L_B$ as usual. Note that this requires taking the limit $L_A, t \to \infty$ with their ratio fixed. These limits are taken *after* taking the full length of the system, L, to be infinite. The first term above shows the linear growth of entanglement in time, which is precisely waht one expects for standard thermal systems; the second terms captures the saturation to a final value that scales linearly in the volume of $\mathcal{A}$, also as expected for thermal systems. This formalism is exact for noninteracting integrable models, and has been refined and extended in numerous ways, but retains the same overall structure and leads to the same qualitative results [34, 161, 162].

4.3 Hydrodynamics of Thermal Systems

In GHD, transport is generically ballistic—with some quantities exhibiting diffusive broadening depending on the generalized Gibbs ensemble (GGE) of choice—although there are various limits featuring more exotic behavior; in conventional hydrodynamics, one expects conserved quantities to diffuse, unless the system possesses Galilean invariance. The timescales governing this crossover from ballistic to diffusive hydrodynamics have recently been explored both experimentally and numerically, and have been shown to match a Fermi golden rule (FGR) prediction, with matrix elements that are evaluated numerically via exact diagonalization on small systems. However, except in noninteracting and weakly interacting models, the nature of relaxation, and the coefficients governing the long-time hydrodynamics, have not been computed. The existing perturbative results do not apply to many of the experimentally relevant settings, such as the Heisenberg and Hubbard models, which are, in general, strongly interacting integrable systems.

Here, we develop a framework for computing relaxation and diffusion in nearly integrable systems, building on the formalism of GHD. A central result is a compact formula for the diffusion constant in nearly integrable systems with one (or a few) residual conservation laws. The specifics of the integrability-breaking mechanism enter this formula through a set of microscopic rates that govern the decay of the approximately conserved quantities. In general, these rates depend on the

microscopic mechanism of integrability-breaking. However, for integrability-breaking perturbations that are spatially slowly varying (e.g., smooth potentials and long-range interactions), these rates can themselves be expressed in terms of GHD data; in these cases the diffusion constant can be fully expressed in terms of GHD data. Having introduced these general results, we apply them to some specific systems in which the physics is particularly transparent, and finally comment on the case in which the integrable dynamics is itself nontrivial.

4.3.1 Hydrodynamic equations

The quasi-particle picture of GHD consists of an equation for the density, $\rho_{\rm p}(\theta;x,t)$, which is related to roots of the TBA equations for an integrable system divvied up into fluid cells, but with some caveats. We use the notation of the GHD literature for comparison, but this should not be construed as an endorsement. The density equation is

$$\partial_t\rho_{\rm p}(\theta;x,t)+\partial_x\left[v^{\rm eff}_\theta\rho_{\rm p}\right](\theta;x,t)=\Gamma\left[\theta;\rho_{\rm p}(\theta;x,t)\right]\ , \tag{4.3.1}$$

where θ is a "rapidity." In the integrable case, $\Gamma=0$.

It will be convenient to use the "dressing" operator, defined by

$$g^{\rm dr}(\theta)=\left[\left(1-\hat{\mathcal{T}}\hat{\mathcal{N}}\right)^{-1}g\right](\theta)\ , \tag{4.3.2}$$

where $\hat{\mathcal{N}}$ denotes multiplication by the Fermi [occupation] factor, $n(\theta)=\rho_{\rm p}(\theta)/\rho_{\rm s}(\theta)$, where $\rho_{\rm s}(\theta)$ is the total density of states, which also derives from TBA; $\hat{\mathcal{K}}$ denotes convolution with the differential scattering kernel, i.e.,

$$\left[\hat{\mathcal{N}}g\right](\theta)=\int d\phi\,\delta(\theta-\phi)\,n(\phi)\,g(\phi) \tag{4.3.3}$$

$$\left[\hat{\mathcal{K}}g\right](\theta)=\int d\phi\,\frac{\varphi(\theta,\phi)}{2\pi}\,g(\phi)\ , \tag{4.3.4}$$

where $\varphi(\theta,\phi)=-i\partial_\theta S(\theta,\phi)$[2]. For many models of interest, we generally have

$$\varphi(\theta,\phi)=\varphi(\phi,\theta)=\varphi(\theta-\phi)\ . \tag{4.3.5}$$

We also define a *pseudo-dressing* operator

$$\hat{\mathcal{D}}=\frac{1}{\rho_{\rm s}(\theta)}\left(1-\hat{\mathcal{N}}\hat{\mathcal{K}}\right)\ . \tag{4.3.6}$$

Using these relations, Eq. (4.3.1) can be written

$$\partial_t\rho_{\rm p}(\theta;x,t)+\left[\hat{A}\,\partial_x\rho_{\rm p}\right](\theta;x,t)=\Gamma\left[\theta;\rho_{\rm p}(\theta;x,t)\right]\ , \tag{4.3.7}$$

where

$$\hat{A}=\hat{\mathcal{D}}^{-1}\,v^{\rm eff}\,\hat{\mathcal{D}}\ . \tag{4.3.8}$$

The lefthand side of Eq. (4.3.1) is diagonalized by mapping to the Fermi factor, $n(\theta;x,t)$:

$$\partial_t n(\theta;x,t)+v^{\rm eff}(\theta;x,t)\,\partial_x n(\theta;x,t)=\hat{\mathcal{D}}\,\Gamma[\theta,n]\ , \tag{4.3.9}$$

where $v^{\rm eff}$ depends on x,t solely through its dependence on n:

$$v^{\rm eff}(\theta;x,t)=\frac{(\varepsilon')^{\rm dr}}{(p')^{\rm dr}}\ , \tag{4.3.10}$$

where $p(\theta)$ and $\varepsilon(\theta)$ are, respectively, the rapidity-dependent momentum and energy[3]; for Galilean

[2]For multi-species models, there are subtleties related to transpose, etc., but these seem to work out.

[3]These are independent of x and t and follow from Bethe Ansatz.

invariant models, $p = m\theta$, $\varepsilon = m\theta^2/2$. In this sense, the effective velocity is a function of θ and a functional of n.

Note that Eq. (4.3.1) and Eq. (4.3.9) are *quasilinear* expressions. While there are few techniques for nonlinear equations, one of them—the method of characteristics—applies to such equations. Even for $\Gamma = 0$, this does not seem to work for Eq. (4.3.1) or Eq. (4.3.7), only for n, i.e., Eq. (4.3.9). Particular forms of Γ admit such a solution for Eq. (4.3.1), and one such example will be considered in Sec. 4.3.3: one finds exact ballistic propagation in the integrable case; for the simple case $\Gamma \to n(\theta;x,t)/\tau(\theta)$—which manifestly breaks *all* conserved quantities—we find a similar solution with an overall exponential damping.

By integrating the equations for $\rho_{\rm p}(\theta)$ over θ, weighted by appropriate functions, $h_n(\theta)$, one obtains equations involving the conserved charges, q_n. There is a direct correspondence between the space of these objects, the space of densities $\rho_{\rm p}(\theta;x,t)$, and the space of occupation factors, n. The average charges and currents are respectively defined by

$$q_n(x,t) \equiv \int d\theta\, h_n(\theta)\, \rho_{\rm p}(\theta;x,t) \tag{4.3.11a}$$

$$j_n(x,t) \equiv \int d\theta\, h_n(\theta)\, v^{\rm eff}[\theta;x,t]\, \rho_{\rm p}(\theta;x,t)\ . \tag{4.3.11b}$$

The definitions in Eq. (4.3.11) are valid for any integrable model on the *Euler scale*, including those with multiple quasiparticle species.

4.3.2 Integrability breaking term

For systems in which the integrability-breaking perturbation term is much smaller in magnitude than the couplings corresponding to the underlying integrable theory, the former can be treated perturbatively, and the formalism of generalized hydrodynamics can still be used. In general, details of the integrability-breaking term should be accounted for in the GGE used to compute various quantities in the thermodynamic and hydrodynamic picture, since these quantities will determine the steady state to which the system relaxes at late time, e.g. in the linear response regime. The integrability-breaking term on the righthand side of Eq. (4.3.1) can be recovered using the standard Fermi golden rule calculation for the rate that appears in collision integrals in kinetic theory [54–56, 59, 60].

For interacting integrable systems, the quasiparticle solutions are essentially free, as the Hamiltonian (or Floquet unitary) can be expressed purely in terms of the occupations of these quasiparticle modes and their corresponding dispersion. However, the quasiparticles do scatter elastically with one another under unitary evolution of a typical state (i.e., a state that is not an eigenstate) and in the hydrodynamic picture. However, this scattering is accounted for entirely by using the dressed velocity, defined in Eq. (4.3.10). Therefore, there is no need for a collision integral in the GHD equations, and any scattering events must be induced by terms that break integrability.

Thus, the integrability-breaking term is directly analogous to impurity scatterers and other physics that appear in the standard Boltzmann equation for thermal systems. This term, which we denote Γ, will be a function of rapidity, and a functional of the quasiparticle density, $\rho_{\rm p}$, and will derive from matrix elements in the same way that decay rates are derived from FGR. An important point is that, for certain reasonable integrability-breaking perturbations—e.g., certain power-law two-body interactions in the interacting Bose gas and general continuous spatial potentials coupled to the density—the corresponding matrix elements for the FGR terms, and thus the function Γ, can be evaluated using GHD. This is because, in contrast to standard hydrodynamics, which

provides equations for one-point functions, the GHD formalism actually provides information about certain types of n-point functions, and in particular, those corresponding to correlations among the integrable model's charges and currents. Hence, perturbations that are related directly to charges, currents, or two-point operators involving these objects, are likely possible to evaluate using GHD.

For more general terms, these can be recovered perturbatively to low order using *form factor expansions*, which evaluate the matrix elements of generic processes that create particle-hole pairs over a given TBA macrostate. For concreteness, consider a system of interacting particles with a conserved density $q(x)$, i.e. $\int d\theta \rho_{\mathrm{p}}(\theta; x, t)$ (e.g., the z component of magnetization in the XXZ model or the particle density in the Lieb-Liniger model). Now we consider integrability breaking due to a long-range density-density interaction of the form $V(x-y)q(x)q(y)$. Long-range interactions are well-suited to hydrodynamic treatment because they involve small momentum transfer: hydrodynamics only applies to systems that can be understood by truncating to at most two spatiotemporal derivatives, and thus must be well-described by truncation to second order in momentum. However, we must also restrict to interactions that fall off sufficiently rapidly (i.e. faster than $|x-y|^{-2}$) that the small-k limit of the Fourier transform $V(k)$ is well-defined. An ideal situation would be, e.g., two weakly coupled integrable "tubes," separated by a distance d that is large compared to microscopic length scales. In that case, one can partition the system into hydrodynamic cells of size $\gtrsim d$, yielding local GHD at long distances, but also restricting the integrability-breaking collisions to small momentum transfer.

In this case, one uses the form factor expansion of arbitrary operators given in Ref. 60. This expansion is presented in detail in that reference, and will not be reproduced here. For certain operators outlined above, this expansion is exact and can be computed purely in terms of GHD data and the GGE in question. For more general perturbations, one should perform an expansion in terms of processes that create particle-hole pairs, and those that create two particle-hole pairs. In general, one can regard processes that necessarily involve higher order processes as beyond the scope of perturbation theory [60]. However, for higher-order operators that can be expressed directly in terms of the charges and currents, this may be possible using various results for n-point functions [56, 59, 59, 60, 156, 164]. Thus, it is generally quite feasible to evaluate the Fermi golden rule term to leading and even subleading order in perturbation theory.

4.3.3 Simple case: Fully broken integrability

The hydrodynamic equation in terms of the Fermi factor, i.e. Eq. (4.3.9), can be solved exactly via characteristics in a simplified case, where we have only a diagonal term from the Fermi golden rule. We start with the demand that

$$n(\theta; x, t) = \int d\phi \int dy \, \mathcal{K}[\theta, x, t; \phi, y, 0] \, n_0(\phi; y) \ , \tag{4.3.12}$$

where the initial condition at $t = 0$, $n(\theta; x, t) = n_0(\theta; x)$, which implies

$$\mathcal{K}[\theta, x, 0; \phi, y, 0] = \delta(x-y)\,\delta(\theta-\phi) \ . \tag{4.3.13}$$

The occupation factor equation, Eq. (4.3.9), in the limit $\Gamma \to 0$ becomes

$$0 = \left\{ \frac{1}{\tau(\theta)} + \partial_t + v^{\mathrm{eff}}[\theta, n]\,\partial_x \right\} n(\theta; x, t) \ , \tag{4.3.14}$$

which is solved by

$$0 = \left\{ \frac{1}{\tau(\theta)} + \partial_t + v^{\mathrm{eff}}[\theta, n]\,\partial_x \right\} [\theta, x, t; \phi, y, 0] \ . \tag{4.3.15}$$

We define some function $X_\theta(t)$ such that

$$\frac{d\,X_\theta}{dt} = v^{\text{eff}}[\theta, \tilde{n}] \ , \tag{4.3.16}$$

where the velocity is allowed to depend on the solution $\tilde{n}\,(\theta; t) \equiv n\,(\theta; X_\theta(t), t)$, and therefore the kernel/propagator $\mathcal{K}$.

We make an Ansatz for the propagator, $U\,[\theta, t; \phi, y] \equiv \mathcal{K}\,[\theta, X_\theta(t), t; \phi, y]$, where $x \to X_\theta(t)$. Since X satisfies Eq. (4.3.16), the righthand side of Eq. (4.3.15) contains the diagonal τ term along with a total derivative of U with respect to t, i.e. $d/dt = \partial_t + v^{\text{eff}}\,[\theta, n]\,\partial_x$, and Eq. (4.3.15) is solved if

$$-\frac{U}{\tau} = \frac{d\,U}{dt} \ , \tag{4.3.17}$$

which combined with Eq. (4.3.16), turn the PDE, Eq. (4.3.15), into two coupled ODEs, if we think of the arguments θ, ϕ, y of U as labels. Unlike PDEs, nonlinear ODEs are often soluble, in this case, it's unimportant because the hard ODE, Eq. (4.3.17), is actually linear; it is solved if U by

$$U\,[\theta, t; \phi, y] = e^{-t/\tau(\theta)}\,U\,[\theta, 0; \phi, y] \ , \tag{4.3.18}$$

where the time zero version is given by

$$U|_{t=0} = \lim_{t\to 0} \mathcal{K}\,[\theta, X_\theta(t), t; \phi, y] = \delta\,(\theta - \phi)\,\delta\,(X_\theta\,(0) - y) \ , \tag{4.3.19}$$

and now, to return to the full solution, we must express $X_\theta\,(0)$ in terms of $x \leftrightarrow X_\theta(t)$ and t itself.

This is a bit more difficult than the integrable case treated in Ch. 2, where, instead, we have

$$\tilde{n}_{\text{easy}}\,(\theta; t) = e^{-t/\tau(\theta)}\,n_0\,(\theta; X_\theta(0)) \ , \tag{4.3.20}$$

which, in contrast to the integrable case, depends on t. However, the righthand side is independent of $X(t)$, allowing for the formal integration of both sides of Eq. (4.3.16) from 0 to t, leading to

$$X_\theta\,(t) - X_\theta\,(0) = \int_0^t dt'\,v^{\text{eff}}[\theta, \tilde{n}_{\text{easy}}\,(\cdot; t')] \ , \tag{4.3.21}$$

which still allows for the replacement of $X_\theta\,(0)$ with expressions involving t and $x \leftrightarrow X_\theta\,(t)$. Finally, we have

$$n_{\text{easy}}\,(\theta; x, t) = e^{-t/\tau(\theta)} n_0\,(\theta; x - X_\theta\,(t)) \ , \tag{4.3.22}$$

which is a bit more convoluted, but shows that one clearly recovers decay of n.

Note that this diagonal form corresponds to

$$\hat{\mathcal{D}}\,\Gamma\,[\theta, n] = \frac{n(\theta; x, t)}{\tau(\theta)} \ , \tag{4.3.23}$$

in Eq. (4.3.9). Such a term *is* present for a reasonable form of Γ—e.g. corresponding to a perturbation that preserves only particle number of the form used in Sec. 4.6—and without linearization. However, this term by itself breaks all conservation laws, and so one expects all of the charges to decay. This seems to be consistent with Eq. (4.3.22). Any diffusion due to this simple form of Γ will be subleading to the overall decay.

4.3.4 Linearized hydrodynamics of quasiparticles

Since the full, nonlinear hydrodynamics, given by Eq. (4.3.9), are generally not tractable, we work in the "linear response" regime. Essentially, we regard the solution for the Fermi factor, e.g., as taking the form

$$n(\theta;x,t) \to \overline{n}(\theta) + \delta n(\theta;x,t) \ , \tag{4.3.24}$$

where the first term gives the "background," which does not vary locally and relates to the TBA steady-state values. The second term is the response of the system to the perturbation and local variations, truncated to linear order in δ. We define the analogous quantities:

$$\rho_{\rm p}(\theta;x,t) \to \overline{\rho}_{\rm p}(\theta) + \delta\rho_{\rm p}(\theta;x,t) \tag{4.3.25}$$

$$\rho_{\rm s}(\theta;x,t) \to \overline{\rho}_{\rm s}(\theta) + \delta\rho_{\rm s}(\theta;x,t) \ , \tag{4.3.26}$$

where the second term in each will be considered small, and the limit $\delta \to 0$ can be taken to recover various relations: one can think of δ as a parameter that can be tuned to zero to obtain trivial solutions, though we also use δn to refer to the varying part.

To wit, taking $\delta \to 0$ in Eq. (4.3.1) and Eq. (4.3.9) gives the long-time "background" solution(s), i.e. the respective conditions

$$0 = \lambda\,\Gamma\left[\overline{\rho}_{\rm p}(\theta);\theta\right] \tag{4.3.27a}$$

$$0 = \frac{\lambda}{\overline{\rho}_{\rm s}(\theta)}\left(1-\overline{n}(\theta)\hat{\mathcal{K}}\right)\Gamma\left[\overline{n}(\cdot);\cdot\right] \ , \tag{4.3.27b}$$

where the functional dependence of Γ on the first argument is different in the two lines above, and $\cdot$ is a placeholder for a θ-type parameter, to be convolved. The first relation, Eq. (4.3.27a), suggests that the nonvarying part of Γ ought to be zero (in the TBA steady state), and renders the latter redundant.

We have another condition from the fact that the microscopic integrability-breaking terms preserve the total number of particles (by assumption):

$$0 = \int d\theta\,\Gamma\left[n(\theta;x,t);\theta\right] = \int d\theta\,\Gamma\left[\overline{n}(\theta);\theta\right] \ , \tag{4.3.28}$$

which is trivially satisfied as $\delta \to 0$, since the integrand is null in this case.

Note that $\overline{\rho}_{\rm p}$ and $\overline{\rho}_{\rm s}$ are related to the background occupation factor, $\overline{n}$ by the usual relations,

$$\overline{\rho}_{\rm s}(\theta) = \frac{1}{2\pi}\left(1-\hat{\mathcal{K}}\,\overline{n}\right)^{-1}\left(\frac{dp}{d\theta}\right) \ , \tag{4.3.29}$$

and from this,

$$\overline{\rho}_{\rm p}(\theta) = \overline{n}(\theta)\,\overline{\rho}_{\rm s}(\theta) \ . \tag{4.3.30}$$

As it happens, we will have no need for the quantity $\delta\rho_{\rm s}(\theta;x,t)$. However, the nontrivial part of the quasiparticle density, $\delta\rho_{\rm p}(\theta;x,t)$, can be recovered from the relation

$$2\pi\rho_{\rm s}(\theta) = \frac{dp}{d\theta} + 2\pi\hat{\mathcal{K}}\hat{\mathcal{N}}\rho_{\rm s} \ , \tag{4.3.31}$$

by multiplying from the left by $n(\theta)$, which recovers

$$\delta\rho_{\rm p}(\theta;x,t) = \left(1-\overline{n}(\theta)\hat{\mathcal{K}}\right)^{-1}\overline{\rho}_{\rm s}(\theta)\,\delta n(\theta;x,t) \ . \tag{4.3.32}$$

We now linearize the righthand side of Eq. (4.3.9), by taking a Taylor series with respect to the occupation factor, and retaining only $O(\delta)$ terms. In particular, we note straightaway that differentiation of $\rho_{\mathrm{s}}(\theta)$ will result in a term that goes like $-1/\overline{\rho}_{\mathrm{s}}(\theta)$ times the original righthand side of Eq. (4.3.1) evaluated at $\delta = 0$, which is zero by Eq. (4.3.27b). Hence, we can replace the $\rho_{\mathrm{s}}(\theta)$ denominator with its average, $\overline{\rho}_{\mathrm{s}}(\theta)$. There is also a factor of $n(\theta)$ encoded by $\hat{\mathcal{N}}$; because $\overline{\Gamma} = 0$, when we take the $\delta = 0$ limit of the equation for $\rho_{\mathrm{p}}(\theta; x, t)$, Eq. (4.3.1), as seen in Eq. (4.3.27a), this term vanishes as well.

Hence, we need only expand Γ itself in terms of the occupation factors, and Eq. (4.3.9) becomes

$$\partial_t \delta n + v_\theta^{\mathrm{eff}} \partial_x \delta n = \frac{\lambda}{\overline{\rho}_{\mathrm{s}}(\theta)} \left(1 - \overline{n}(\theta)\hat{\mathcal{K}}\right) \int d\beta \frac{\delta\Gamma}{\delta n(\beta)} \delta n(\beta) \tag{4.3.33}$$

$$= \frac{\lambda}{\overline{\rho}_{\mathrm{s}}(\theta)} \int d\alpha\, d\beta\, \left(\delta(\alpha - \theta) - \overline{n}(\theta)\varphi(\theta, \alpha)\right) \frac{\delta\Gamma\left[\overline{n}(\alpha); \alpha\right]}{\delta n(\beta)} \delta n(\beta) \tag{4.3.34}$$

$$\partial_t \delta n(\theta; x, t) + v_\theta^{\mathrm{eff}} \partial_x \delta n(\theta; x, t) = \lambda \int d\beta\, \gamma(\theta, \beta)\, \delta n(\beta; x, t) \tag{4.3.35}$$

and the lefthand side is diagonal in every sense, but the righthand side remains to be diagonalized in rapidity space. We can imagine doing perturbation theory in the off-diagonal terms of Eq. (4.3.35), using the fact that the integrability-breaking perturbation terms Γ are small, as parametrized by λ, which we can take to be strictly less than one if needed to ensure convergence, and invoking hydrodynamics as required.

Starting from Eq. (4.3.35),

$$\partial_t \delta n(\theta; x, t) + v_\theta^{\mathrm{eff}} \partial_x \delta n(\theta; x, t) = \lambda \int d\beta\, \gamma(\theta, \beta)\, \delta n(\beta; x, t) \ , \tag{4.3.35}$$

we assert a perturbative solution δn of the form

$$\delta n(\theta; x, t) = \sum_{\ell=0}^{\infty} \lambda^\ell \delta n^{(\ell)}(\theta; x, t) \ , \tag{4.3.36}$$

and then we evaluate Eq. (4.3.35) order-by-order in λ.

At order λ^0, we have the "bare" equation

$$\partial_t \delta n^{(0)}(\theta; x, t) + v_\theta^{\mathrm{eff}} \partial_x \delta n^{(0)}(\theta; x, t) = 0 \ , \tag{4.3.37}$$

which has a straightforward solution in terms of the initial, $t = 0$, profile of the occupation factor. Demanding for the full solution

$$\delta n(\theta; x, t = 0) = \eta_0(\theta; x) \ , \tag{4.3.38}$$

where η is a known/given function (because η looks like n?), the solutions to Eq. (4.3.37) are given by

$$\delta n^{(0)}(\theta; x, t) = \eta_0^{(0)}\left(\theta; x - v_\theta^{\mathrm{eff}} t\right) \ , \tag{4.3.39}$$

which is pretty easy, and we have included the notation $\eta_0^{(0)}$ to allow for the fully generic possibility of λ-dependent initial condition(s).

From this, we can obtain all the corrections at higher order in λ by noting

$$\partial_t \delta n^{(\ell)}(\theta; x, t) + v_\theta^{\mathrm{eff}} \partial_x \delta n^{(\ell)}(\theta; x, t) = \int d\beta\, \gamma(\theta, \beta)\, \delta n^{(\ell-1)}(\beta; x, t) \ , \tag{4.3.40}$$

which has a solution of the form

$$\delta n^{(\ell)}(\theta;x,t) = \eta_0^{(\ell)}\left(\theta;x-v_\theta^{\rm eff}t\right) + \int_{x-v_\theta^{\rm eff}t}^{x}\frac{dy}{v_\theta^{\rm eff}}\int d\beta\,\gamma(\theta,\beta)\,\delta n^{(\ell-1)}\left(\beta;y,t+\frac{y-x}{v_\theta^{\rm eff}}\right), \tag{4.3.41}$$

where there is a good chance we will absorb all of the initial condition into the $\ell = 0$ term, eliminating the first term above for all $\ell > 0$.

We define the more complicated convolution operator $\hat{\mathcal{G}}$: $f(\theta;x,t) \to g(\theta;x,t)$ (i.e. this operator acts on the spatial and temporal arguments, and not merely the rapidity), via

$$g(\theta;x,t) = \hat{\mathcal{G}}\,f(\theta;x,t) = \int_{x-v_\theta^{\rm eff}t}^{x}\frac{dy}{v_\theta^{\rm eff}}\int d\beta\,\gamma(\theta,\beta)\;f\left(\beta;y,t+\frac{y-x}{v_\theta^{\rm eff}}\right), \tag{4.3.42}$$

and we take $\eta^\ell(x) = 0$ for $\ell > 0$, and write the initial condition as $\delta n(\theta;x,t=0) = \eta_0(\theta;x)$. In this case, the full solution for δn, given by Eq. (4.3.36), is

$$\delta n(\theta;x,t) = \sum_{\ell=0}^{\infty}\lambda^\ell\hat{\mathcal{G}}^\ell\eta_0\left(\theta;x-v_\theta^{\rm eff}t\right) \tag{4.3.43}$$

$$= \left(\hat{1}-\lambda\hat{\mathcal{G}}\right)^{-1}\eta_0\left(\theta;x-v_\theta^{\rm eff}t\right), \tag{4.3.44}$$

which looks nice, but a lot of ugliness is hidden in $\hat{\mathcal{G}}$. Of course, we always have the option to use the series expansion, truncated to some order λ^ℓ, but this doesn't seem to be helpful given that convolution with γ is...convoluted and equally foreboding equations define other quantities—e.g. the effective velocity—for generic models

Using Eq. (4.3.32), we can obtain the full answer for the quasi-particle density from the linearized solution for the Fermi factor:

$$\delta\rho_{\rm p}(\theta;x,t) = \left(1-\overline{n}(\theta)\hat{\mathcal{K}}\right)^{-1}\left(\hat{1}-\lambda\hat{\mathcal{G}}\right)^{-1}\overline{\rho}_{\rm s}(\vartheta)\;\eta_0\left(\vartheta;x-v_\vartheta^{\rm eff}t\right), \tag{4.3.45}$$

where ϑ is simply a dummy variable of the θ-type, and after all convolution has been taken care of the righthand side should be a function of θ. We could also replace $\overline{\rho}_{\rm s}(\vartheta)\,\eta_0(\vartheta;x)$ with the initial condition for the varying part of the quasiparticle density, $\rho_{\rm p}(\vartheta;x,t=0)$, i.e. $\rho_0(\vartheta;x)$.

Note that this can be evaluated directly for initial conditions corresponding to any continuously integrable function, including generic analytic functions, the Dirac δ function, and so on. Although it is difficult to look at this form and see that it corresponds to diffusion of particles (which we have taken to be preserved by $\Gamma \neq 0$), this solution closely resembles the diffusive propagators that recover from kinetic theory. As in that case, in the setting of broken integrability, the particles propagate ballistically between collisions, which randomly scatter their propagation velocities to new values; however, the principle difference, which complicates the overall form of the solution, is the fact that dressing and undressing operators act on particle density (or propagator) in between scattering events and ballistic propagation. Although this is likely tractable for a specific choice of model and form of Γ, it is difficult to proceed in generality, and we therefore turn to the charge and current formulation of GHD.

4.3.5 Soliton gas techniques

In addition to the solutions provided herein, largely in the linear response regime, another important feature of generalized hydrodynamic is that it is possible to simulate actual integrable

systems numerically and at scale. This involves the use of classical soliton gases, outlined in Ref. 164. Essentially, the insight is that the important physics of relaxation, scattering, and other hydrodynamic features is well captured by viewing the quasiparticles of the quantum model as classical solitons (i.e. hard rods), and imbuing them with the appropriate velocities, scattering matrices, and other properties of the quantum model. The reasoning is the same that leads to the semiclassical picture of kinetic theory in the first place. Hence, the theoretical predictions presented herein are supplemented by the ability to simulate them precisely, e.g. for the sake of comparison to experiment.

4.4 Diffusive Hydrodynamics of Conserved Charges from Integrability Breaking

We generally have to linearize, as explained previously, but in the language of currents and charges, we can recover exact diffusion—along with the diffusion constant—without further approximation. We consider the case where the conservation of all but one of the charges $\{q_n\}$ is spoiled by the integrability breaking term. Let us label the charge that remains conserved q_n.

The general equation for the mth charge is

$$\partial_t q_m + \partial_x j_m = \Gamma_m \left[\{q_j\}\right] \ , \tag{4.4.1}$$

where Γ_m is the integral over rapidity of the function $h_m(\theta)$ times $\Gamma\left[\theta; \rho_{\mathrm{p}}(\cdot)\right]$ from the righthand side of the quasiparticle density of equation. For $m = n$, the special charge, we have $\Gamma_n = 0$. However, we want to write everything in terms of charges, and so we expand the above quantities using functional derivatives:

$$\partial_t q_m + \sum_{m'} A_{m,m'} \partial_x q_{m'} = \sum_{m'} \Gamma_{m,m'} q_{m'} \ , \tag{4.4.2}$$

where $A_{m,m'}$ is the functional derivative of the current j_m with respect to charge $q_{m'}$. Aussi, on a

$$\Gamma_{m,m'} = \frac{\delta \Gamma_m}{\delta q_{m'}} \ , \tag{4.4.3}$$

analogously, and we will not make reference to single-indexed Γ again in this section.

Donc, avec quelques massages, on a pour la $m$ième charge:

$$\left(\partial_t + A_{m,m}\partial_x - \Gamma_{m,m}\right) q_n = \sum_{m' \neq m} \left(\Gamma_{m,m'} - A_{m,m'}\partial_x\right) q_{m'} \ , \tag{4.4.4}$$

et pour le cas particulier de $m = n$, on a

$$\left(\partial_t + A_{n,n}\partial_x\right) q_n = -\sum_{m \neq n} A_{n,m}\partial_x q_m \ , \tag{4.4.5}$$

et on peut mettre la première équation, Eq. (4.4.4), en la deuxième, et on trouve

$$\begin{aligned} \left(\partial_t + A_{n,n}\partial_x\right) q_n &= -\sum_{m \neq n} A_{n,m}\partial_x q_m \\ &= -\sum_{m \neq n} A_{n,m}\partial_x \left(\partial_t + A_{m,m}\partial_x - \Gamma_{m,m}\right)^{-1} \sum_{m' \neq m} \left(\Gamma_{m,m'} - A_{m,m'}\partial_x\right) q_{m'} \ , \end{aligned} \tag{4.4.6}$$

et on définit

$$[\hat{\Gamma}]_{m,m'} = \Gamma_{m,m'} = \gamma_m \delta_{m,m'} + \left(1 - \delta_{m,m'}\right) \widetilde{\Gamma}_{m,m'} \tag{4.4.7}$$

$$[\hat{A}]_{m,m'} = A_{m,m'} = a_m \delta_{m,m'} + \left(1 - \delta_{m,m'}\right) \widetilde{A}_{m,m'} \ , \tag{4.4.8}$$

and I'll use this convention of twiddles for offdiagonal pieces and lowercase for diagonal pieces, with

$$\hat{\Gamma} = \widetilde{\Gamma} + \hat{\gamma} \tag{4.4.9}$$

$$\hat{A} = \widetilde{A} + \hat{a} \ , \tag{4.4.10}$$

just as a reminder that we can define these things as matrices in the space of charge indices. We will also use the operators

$$\hat{g} = \left(\partial_t + \hat{a}\partial_x - \hat{\gamma}\right)^{-1} \tag{4.4.11}$$

$$[\hat{g}]_{m,m'} = \left(\partial_t + A_{m,m}\partial_x - \Gamma_{m,m}\right)^{-1} \delta_{m,n} \tag{4.4.12}$$

$$\widetilde{\Delta} = \widetilde{\Gamma} - \widetilde{A}\partial_x \tag{4.4.13}$$

$$[\widetilde{\Delta}]_{m,n} = \left(\Gamma_{mn} - A_{mn}\partial_x\right)\left(1 - \delta_{m,n}\right) \ , \tag{4.4.14}$$

où—et Je l'écris en anglais parce que c'est important—all internal sums over m and n skip $m, n = 0$, and only include this if explicitly evaluated at the 0 index. Otherwise, all the indices are fair game. To avoid confusion, and ensure invertibility of various operators, we will use projectors P_n onto the nth index (the special one), and $\overline{P}_n$ onto all other states, with $P_n + \overline{P}_n = \hat{\mathbb{1}}$. We now insert these handy definitions into Eq. (4.4.6), et on a

$$\left(\partial_t + A_{n,n}\partial_x\right) q_n = -\left[\widetilde{A}\,\partial_x\,\overline{P}_n\,\hat{g}\,\widetilde{\Delta} P_n\right]_{n,n} q_n - \sum_m \left[\tilde{A}\,\partial_x\,\overline{P}_n\,\hat{g}\,\widetilde{\Delta}\,\overline{P}_n\right]_{n,m} q_m \ , \tag{4.4.15}$$

and as an aside, many of these restrictions are enforced automatically (i.e. with the projectors lots of twiddles matrices are equal to their regular forms). On a maintenant,

$$\begin{aligned}\left(\partial_t + A_{n,n}\partial_x\right) q_n = &-\left[\hat{A}\,\partial_x\,\overline{P}_n\,\hat{g}\,\widetilde{\Delta}\,P_n\right]_{n,n} q_n - \left[\hat{A}\,\partial_x\,\overline{P}_n\,\hat{g}\,\widetilde{\Delta}\,\overline{P}_n\,\hat{g}\,\widetilde{\Delta} P_n\right]_{n,n} q_n \\ &- \left[\hat{A}\,\partial_x\,\overline{P}_n\,\hat{g}\,\widetilde{\Delta}\,\overline{P}_n\,\hat{g}\,\widetilde{\Delta}\,\overline{P}_n\,\hat{g}\,\widetilde{\Delta}\right]_{n,n} q_n - \ldots \end{aligned} \tag{4.4.16}$$

$$\partial_t q_n + A_{n,n}\partial_x q_n = -\left[\hat{A}\,\partial_x\,\overline{P}_n \sum_{\ell=1}^{\infty}\left[\hat{g}\,\widetilde{\Delta}\overline{P}_n\right]^\ell\right]_{n,n} q_n \tag{4.4.17}$$

$$\partial_t q_n + A_{n,n}\partial_x q_n = -\sum_{\ell=0}^{\infty}\left[\hat{A}\,\partial_x\,\overline{P}_n\left[\hat{g}\,\widetilde{\Delta}\overline{P}_n\right]^\ell \hat{g}\,\widetilde{\Delta} P_n\right]_{n,n} q_n \ , \tag{4.4.18}$$

which we can further simplify by being clever.

We note the following:

$$\widetilde{\Delta} = \widetilde{\Gamma} - \widetilde{A}\partial_x = \hat{\Gamma} - \hat{\gamma} - \hat{A}\partial_x + \hat{a}\partial_x \tag{4.4.19}$$

$$= -\left(\hat{A}\partial_x - \hat{\Gamma}\right) + \hat{a}\partial_x - \hat{\gamma} = -\left(\partial_t \hat{A}\partial_x - \hat{\Gamma}\right) + \partial_t + \hat{a}\partial_x - \hat{\gamma} \tag{4.4.20}$$

$$= -\hat{G}^{-1} + \hat{g}^{-1} \tag{4.4.21}$$

$$\hat{G} = \left(\partial_t \hat{A}\partial_x - \hat{\Gamma}\right)^{-1} \ , \tag{4.4.22}$$

from which we can see that

$$\hat{F} \equiv \sum_{\ell=0}^{\infty} \overline{P}_n \left[\hat{g}\, \widetilde{\Delta} \overline{P}_n \right]^{\ell} = \sum_{\ell=0}^{\infty} \overline{P}_n \left[\left(1 - \hat{g}\hat{G}^{-1}\right) \overline{P}_n \right]^{\ell} = \overline{P}_n \frac{1}{\overline{P}_n \left[1 - \left(1 - \hat{g}\hat{G}^{-1}\right)\right] \overline{P}_n} \overline{P}_n \ , \tag{4.4.23}$$

which includes redundant projectors. Since the inverse of $\hat{G}$ is only even defined in the projected subspace, this becomes

$$\hat{F} = \overline{P}_n \frac{1}{\hat{g}\hat{G}^{-1}} \overline{P}_n = \overline{P}_n \left[\hat{g}\hat{G}^{-1}\right]^{-1} \overline{P}_n = \overline{P}_n \hat{G}\, \hat{g}^{-1} \overline{P}_n \ , \tag{4.4.24}$$

which we insert into Eq. (4.4.18) to obtain

$$\begin{aligned} \partial_t q_n + A_{n,n} \partial_x q_n &= -\sum_{\ell=0}^{\infty} \left[\hat{A}\, \partial_x \overline{P}_n \left[\hat{g}\, \widetilde{\Delta} \overline{P}_n \right]^{\ell} \hat{g}\, \widetilde{\Delta} P_n \right]_{n,n} q_n \\ &= -\left[\hat{A}\, \partial_x \overline{P}_n \hat{G}\, \hat{g}^{-1}\, \hat{g}\, \widetilde{\Delta} P_n \right]_{n,n} q_n \qquad (4.4.25) \\ &= -\left[\hat{A}\, \partial_x \overline{P}_n \hat{G}\, \widetilde{\Delta} P_n \right]_{n,n} q_n \qquad (4.4.26) \\ &= -\left[\hat{A}\, \partial_x \overline{P}_n \left(\partial_t + \hat{A}\partial_x - \hat{\Gamma}\right)^{-1} \overline{P}_n \left(\widetilde{\Gamma} - \widetilde{A}\partial_x\right) P_n \right]_{n,n} q_n \ , \qquad (4.4.27) \end{aligned}$$

and since the rightmost term is flanked by projectors onto different states, these terms are necessarily off-diagonal, and we can replace the twiddled guys with the regular ones:

$$\partial_t q_n + A_{n,n} \partial_x q_n = -\left[\hat{A}\, \partial_x \overline{P}_n \left(\partial_t + \hat{A}\partial_x - \hat{\Gamma}\right)^{-1} \overline{P}_n \left(\hat{\Gamma} - \hat{A}\partial_x\right) P_n \right]_{n,n} q_n \ , \tag{4.4.28}$$

and now we factor out a $\hat{\Gamma}$ of the inverse term, and expand it—fully legitimately—as a geometric series, noting that the order of the operators is due to the fact that $(AB)^{-1} = B^{-1} A^{-1}$, and we can write

$$\begin{aligned} \left(\partial_t + \hat{A}\partial_x - \hat{\Gamma}\right)^{-1} &= -\left(1 - \hat{\Gamma}^{-1}\partial_t + \hat{\Gamma}^{-1}\hat{A}\partial_x\right)^{-1} \hat{\Gamma}^{-1} \qquad (4.4.29) \\ &= -\sum_{\ell=0}^{\infty} \left(\hat{\Gamma}^{-1}\partial_t + \hat{\Gamma}^{-1}\hat{A}\partial_x\right)^{\ell} \hat{\Gamma}^{-1} \ , \qquad (4.4.30) \end{aligned}$$

which we insert into Eq. (4.4.28) to recover

$$\partial_t q_n + A_{n,n} \partial_x q_n = \sum_{\ell=0}^{\infty} \left[\hat{A}\, \partial_x \overline{P}_n \left(\hat{\Gamma}^{-1}\partial_t + \hat{\Gamma}^{-1}\hat{A}\partial_x\right)^{\ell} \hat{\Gamma}^{-1} \overline{P}_n \left(\hat{\Gamma} - \hat{A}\partial_x\right) P_n \right]_{n,n} q_n \ , \tag{4.4.31}$$

and regarding the $\Gamma^{-1}\Gamma$ (where the latter term is the first in the rightmost parenthetical), we note that

$$\overline{P}_n \left[\hat{\Gamma}^{-1} \overline{P}_n \hat{\Gamma} \right] P_n = \overline{P}_n \left[\overline{P}_n \right] P_n = 0 \ , \tag{4.4.32}$$

which is to say that Γ^{-1} is only defined in the $\overline{P}_n$ subspace, and therefore $\Gamma^{-1} = \Gamma^{-1}\overline{P}_n$ and $\Gamma^{-1}\Gamma = \overline{P}_n$ and the above expression vanishes. Et voilà, l'équation complète (par Eq. (4.4.31)) est

$$\partial_t q_n + A_{n,n} \partial_x q_n = -\sum_{\ell=0}^{\infty} \left[\hat{A}\, \partial_x \overline{P}_n \left(\hat{\Gamma}^{-1}\partial_t + \hat{\Gamma}^{-1}\hat{A}\partial_x\right)^{\ell} \hat{\Gamma}^{-1} \overline{P}_n \hat{A} \partial_x P_n \right]_{n,n} q_n \ , \tag{4.4.33}$$

, and it is worth pointing out that any term with $\ell > 0$ has more than two derivatives. To hydrodynamic order, there are no time derivatives.

As a reminder, the only approximation made here was to linearize the equations for charge and current, and relatedly, to decompose of the currents and Γ_m onto charges. In general, functional differentiation allows this. However, such steps seem to be necessary simply to treat the diffusive corrections that enter at the level of Navier-Stokes hydrodynamics, even in the *fully integrable* case. To make Eq. (4.4.33) more aesthetically pleasing and physically informative, we expand in spatiotemporal derivatives to second order. We can then use another recursion procedure to eliminate time derivatives of q_n on the righthand side in favor of higher-order terms by plugging the lefthand side into the righthand side and repeating. As a reminder, such higher-order derivatives strictly cannot be included at the level of hydrodynamics; indeed, if such terms are necessary, then hydrodynamics does not apply at all.

At the level of hydrodynamics, the full expression is then

$$\partial_t q_n + A_{n,n}\partial_x q_n = -\left[\hat{A}\,\partial_x\,\hat{\Gamma}^{-1}\hat{A}\partial_x\right]_{n,n} q_n \ , \tag{4.4.34}$$

where the overall minus sign is fine, since in general $\Gamma \sim -\tau^{-1}$, where $\tau > 0$, and there are implicit projectors $\overline{P}_n$ between $\hat{\Gamma}^{-1}$ and its friends. Note that if $A_{n,n} = 0$, the drift term goes away, and if this quantity is nonzero we actually expect this term to be present, since somehow the current of q_n is proportional to a conserved charge, which is q_n itself. There are particular scenarios in which one might expect this to be the case; in more general scenarios, the GGE should dictate that $A_{n,n} = 0$, producing ordinary diffusion as one would expect.

4.5 Hydrodynamics in FFA

The FFA model is characterized by two species of chiral quasiparticle excitations, which we term left and right movers. Note that we work here with the nondispersing variant of FFA in the interest of simplicity. Most of this model's conserved quantities are unimportant, save the respective numbers of each movers. Throughout, we work in a GGE in which both movers' densities are coupled to the same chemical potential. In this ensemble, and without dispersion, the quasiparticle densities and group velocities do not depend on rapidity ($v_R^{\mathrm{grp}} = 1, v_L^{\mathrm{grp}} = -1$).

The important conserved charges correspond to the total density of left [right] movers, integrated over rapidity, which we denote $q_\nu(x,t) = \int d\theta \rho_{\mathrm{p},\nu}(\theta;x,t) = 2\pi\rho_{\mathrm{p},\nu}(\cdot;x,t)$, as the densities are rapidity independent. As for Galilean models, when integrability is preserved, the total number of particles $\int dx q_\nu(x,t) = N_\nu$ is time independent.

We can solve for the velocities as functionals of these quantities,

$$v_R = 1 - \frac{2q_L}{1+q_R+q_L} \tag{4.5.1a}$$

$$v_R = -1 + \frac{2q_R}{1+q_R+q_L} \ , \tag{4.5.1b}$$

and the corresponding hydrodynamic equations without perturbations are

$$\partial_t q_\nu + \partial_x\left[v_\nu q_\nu\right] = 0 \ , \tag{4.5.2}$$

for $\nu = L, R$.

4.5.1 Integrability breaking

We will be interested in terms that preserve the total number of movers, $q_R + q_L$, but do not conserve q_ν individually, i.e.

$$\partial_t q_\nu + \partial_x \left[v_\nu q_\nu \right] = \Gamma \left[q_\nu, q_{\overline{\nu}} \right] \left(q_{\overline{\nu}} - q_\nu \right) \ , \tag{4.5.3}$$

for arbitrary functional Γ. We will find it more convenient to work with the quantities

$$q_\pm = q_R \pm q_L \ , \tag{4.5.4}$$

in terms of which the GHD equations are

$$\partial_t q_+ + \partial_x j_+ = 0 \tag{4.5.5}$$

$$\partial_t q_- + \partial_x j_- = -2\Gamma \left[q_+, q_- \right] q_- \ , \tag{4.5.6}$$

where

$$j_+ = q_- \ , \quad j_- = \frac{q_-^2 + q_+}{1 + q_+} \ , \tag{4.5.7}$$

in this GGE, as can be seen by expressing v_ν in terms of $q_\pm$,

$$v_R = \frac{q_- + 1}{q_+ + 1} \ , \quad v_L = \frac{q_- - 1}{q_+ + 1} \ . \tag{4.5.8}$$

The ability to express currents directly in terms of charges does not extend to other interacting integrable models as far as we are aware, and depends crucially on the fact that in this GGE none of the relevant quantities depend on rapidity.

Inserting these definitions for the currents, we obtain two coupled GHD equations in terms of $q_\pm$ only:

$$\partial_t q_+ + \partial_x q_- = 0 \tag{4.5.9}$$

$$\partial_t q_- + \frac{2q_-}{q_+ + 1} \partial_x q_- + \frac{1 - q_-^2}{\left(q_+ + 1 \right)^2} \partial_x q_+ = -2\Gamma \left[q_+, q_- \right] q_- \ , \tag{4.5.10}$$

and the latter expression can be re-written in terms of the bare velocities,

$$\partial_t q_- + \left(v_R + v_L \right) \partial_x q_- - v_R v_L \partial_x q_+ = -2\,\Gamma\, q_- \ . \tag{4.5.11}$$

Note that we do not consider breaking of N_+ (and conservation of N_-) as this case has numerous pathological features, for example that the current j_- depends on q_-, and will therefore exhibit biased diffusion. Additionally, it is difficult to imagine perturbations that break the conservation of total charge but preserve relative charge that do not eventually see the system relax to $N_+ = 0$, in which case $N_- = 0$ as well. Hence, we restrict only to breaking of N_- in the remainder.

4.5.2 Reminder: Integrable case

Note that in the integrable case, $\Gamma = 0$, one expects exact ballistic transport of q_+ because its corresponding current is the conserved charge q_-, as can be seen in terms of the Fermi factor. Additionally, taking an extra time derivative of Eq. (4.5.9) and Eq. (4.5.10), one can insert the latter into the former, i.e.

$$\partial_t^2 q_+ = -\partial_x \partial_t q_- \ , \tag{4.5.12}$$

where the righthand side is equal to a spatial derivative of the other terms in Eq. (4.5.10). By reinserting Eq. (4.5.9), we can replace all spatial derivatives of q_- with time derivatives of q_+, the result is:

$$\begin{aligned}\left(\partial_t^2 + (v_L + v_R)\,\partial_x\partial_t + v_L v_R \partial_x^2\right) q_+ = \\ (v_R - v_L)\,(\partial_t q_+ + v_L \partial_x q_+)\,(\partial_t q_+ + v_R \partial_x q_+) \ ,\end{aligned} \tag{4.5.13}$$

and noting that

$$(\partial_t + v_{\overline{\nu}}\partial_x)\, v_\nu = 0 \tag{4.5.14}$$

is equivalent to Eq. (4.5.10) for $\Gamma = 0$, we can rewrite the lefthand side of Eq. (4.5.13) as

$$(\partial_t + v_R \partial_x)\,(\partial_t + v_L \partial_x)\, q_+ \ , \tag{4.5.15}$$

in which case both the left and right sides of Eq. (4.5.13) are zero if *either*

$$(\partial_t + v_\nu \partial_x)\, q_+ = 0 \ , \tag{4.5.16}$$

for either choice $\nu = L, R$, demonstrating that q_+ is exactly ballistic.

Choosing a solution for q_+ corresponding to the same ν as in Eq. (4.5.16), one can then rewrite Eq. (4.5.10) for $\Gamma = 0$ as

$$\partial_t q_- + (v_R + v_L)\,\partial_x q_- - v_R v_L \partial_x q_+ = 0 \tag{4.5.17}$$

$$\partial_t q_- - v_R \partial_t q_+ - v_L \partial_t q_+ + v_{\overline{\nu}} \partial_t q_+ = 0 \tag{4.5.18}$$

$$\partial_t q_- - v_\nu \partial_t q_+ = 0 \tag{4.5.19}$$

$$\partial_t q_- + v_\nu \partial_x q_- = 0 \ , \tag{4.5.20}$$

which proves that q_- satisfies the same equation as q_+ and is ballistic with the same velocity.

4.5.3 Recovering diffusion

We note straightaway that the linearized version of Eq. (4.5.10) with $\Gamma \neq 0$ should correspond to decay of q_-. Linearizing that equation recovers precisely decay, with a "source" determined by q_+, which of course will, strictly speaking, depend on q_-. We will be interested in the behavior of q_+, and to see this, we repeat the procedure of taking an extra time derivative that gives rise to exact ballistic hydrodynamics in the integrable case. The result is a modification of Eq. (4.5.13),

$$\begin{aligned}\left(\partial_t^2 + (v_L + v_R)\,\partial_x\partial_t + v_L v_R \partial_x^2 + 2\Gamma\partial_t\right) q_+ = \\ (v_R - v_L)\,(\partial_t q_+ + v_L \partial_x q_+)\,(\partial_t q_+ + v_R \partial_x q_+) \\ +2q_- \left(\frac{\partial\Gamma}{\partial q_+}\partial_x q_+ - \frac{\partial\Gamma}{\partial q_-}\partial_t q_+\right) \ ,\end{aligned} \tag{4.5.21}$$

which is a bit more complicated.

However, at late times, we expect q_- to have decayed substantially compared to other terms, and also that the $\partial_t^2 q_+$ term is small compared to $2\Gamma\partial_t q_+$. Approximating $q_- \to 0$, referring to the definitions of the velocities, we now write $v_R = v_0$, $v_L = -v_0$, where

$$v_0 = (1 + q_+)^{-1} \ , \tag{4.5.22}$$

and at late times, Eq. (4.5.21) becomes

$$\left(2\,\Gamma\partial_t - v_0^2\partial_x^2\right) q_+ = 2v_0\left\{\left(\partial_t q_+\right)^2 - v_0^2\left(\partial_x q_+\right)^2\right\} \ , \tag{4.5.23}$$

and if we ignore these nonlinear terms at late times, we get diffusion,

$$\partial_t q_+ = D\partial_x^2 q_+ \ , \tag{4.5.24}$$

where the diffusion "constant" is given by

$$D = \frac{v_0^2}{2\Gamma} = \frac{1}{2\Gamma\left(1+q_+\right)^2} \ , \tag{4.5.25}$$

and a more careful treatment may be possible, e.g. writing the righthand side of Eq. (4.5.24) in the form $\partial_x D\left[q_+\right]\partial_x q_+$, corresponding to nonlinear diffusion.

Note that had we included a diffusive correction to the Euler equation for q_-, Eq. (4.5.10), this would result in a term of order ∂_x^3 in the final equation for q_+, which would therefore be dropped as such terms play no role at the level of hydrodynamics. Since q_- decays to zero, it is not important if it also diffuses while decaying.

Repeating the procedure more carefully, one has

$$\partial_t^2 q_+ = -\partial_t\partial_x q_- = \partial_x\left(-\partial_t q_-\right) \tag{4.5.26}$$

$$= \partial_x\left[2\Gamma q_- + \frac{2q_-}{q_+ + 1}\partial_x q_- + \frac{1-q_-^2}{\left(q_+ + 1\right)^2}\partial_x q_+\right] \tag{4.5.27}$$

$$= -2\Gamma\partial_t q_+ + 2q_-\left[\frac{\partial\Gamma}{\partial q_+}\partial_x q_+ - \frac{\partial\Gamma}{\partial q_-}\partial_t q_+\right]$$

$$+ \partial_x\left[\frac{2q_-}{q_+ + 1}\partial_x q_-\right] + \partial_x\left[\frac{1-q_-^2}{\left(q_+ + 1\right)^2}\partial_x q_+\right] \ , \tag{4.5.28}$$

and now we drop $\partial_t^2 q_+$ compared to $2\Gamma\partial_t q_+$ at late times, and writing

$$\tilde{\Gamma} = \Gamma + q_-\frac{\partial\Gamma}{\partial q_-} \ , \tag{4.5.29}$$

and

$$\tilde{v} = 2q_-\frac{\partial\Gamma}{\partial q_-} \ , \tag{4.5.30}$$

we have

$$2\tilde{\Gamma}\partial_t q_+ - \tilde{v}\partial_x q_+ = \partial_x\left[\frac{2q_-}{q_+ + 1}\partial_x q_- + \frac{1-q_-^2}{\left(q_+ + 1\right)^2}\partial_x q_+\right] \ , \tag{4.5.31}$$

which has the form of nonlinear diffusion with drift given by $\tilde{v}$. At late times, $\tilde{v} \to 0$ and $\tilde{\Gamma} \to \Gamma$ as $q_- \to 0$. The second term on the righthand side has the exact form of nonlinear diffusion, the first term results from the fact that the effective "diffusion constant" in general models will not be of the form $\partial_x D\left[q_\cdot\right]\partial_x q_\nu$, but rather $\sum_{\overline{\nu}}\partial_x D_{\nu,\overline{\nu}}\partial_x q_{\overline{\nu}}$.

Examining the term in Eq. (4.5.31) containing $\partial_x q_-$, we can expand this as $2\left(1+q_+\right)^{-1}\left(\partial_t q_+\right)^2$ plus terms proportional to q_-, which therefore vanish on the same timescale that justified ignoring $\partial_t^2 q_+$ at late times. Finally, we can justify ignoring $\left(\partial_t q_+\right)^2$ for precisely the same reason as $\partial_t^2 q_+$ at late times, and justify ignoring this term, to recover Eq. (4.5.24) with nonlinear diffusion constant

$$D = \frac{1-q_-^2}{2\left(\Gamma + q_-\frac{\partial\Gamma}{\partial q_-}\right)\left(1+q_+\right)^2} \ , \tag{4.5.32}$$

which reduces to Eq. (4.5.25) for $\Gamma t \gg 1$.

4.5.4 Linearized solution

Although it was possible to recover diffusion in FFA with only q_+ conserved without recourse to linear response using only a handful of approximations, it will be useful to examine the resulting equations in the linear response regime for comparison. In particular, we can repeat the calculation of Sec. 4.4 for the special case where the current of the conserved charge, $j_+ = q_-$ is itself a conserved charge, and there are no other charges present, corresponding to FFA. We also note that the $\delta = 0$ limit of the linear response equations seem to require that $\overline{q}_- = 0$, i.e. at late times, the relative charge decays to zero in this GGE (which is indeed globally true for $\mu_L = \mu_R$). Regarding Eq. (4.4.33),

$$\partial_t q_+ + A_{+,+}\partial_x q_+ = -\sum_{\ell=0}^{\infty}\Big[\hat{A}\,\partial_x\,P_-\left(\hat{\Gamma}^{-1}\partial_t + \hat{\Gamma}^{-1}\hat{A}\partial_x\right)^{\ell}\hat{\Gamma}^{-1}P_-\,\hat{A}\partial_x\,P_+\Big]_{+,+} q_+ \ , \quad , \tag{4.4.33}$$

and we net use the fact that $A_{+,-} = 1$ and $A_{+,+} = 0$, with $A_{-,\cdot}$ arbitrary. We also use the fact that $\Gamma_{+,\pm} = 0$. In this case, the leading A's on the left get evaluated with their first index as 0, which requires that their second index be one. In that case, the above simplifies to

$$\partial_t q_+ = -\hat{A}_{+,-}\,\partial_x \sum_{\ell=0}^{\infty}\Big[\left(\hat{\Gamma}^{-1}\partial_t + \hat{\Gamma}^{-1}\hat{A}\partial_x\right)^{\ell}\hat{\Gamma}^{-1}\Big]_{-,-}\,\hat{A}_{-,+}\partial_x q_+ \ , \tag{4.5.33}$$

and recalling that all internal indices in the matrix multiplication in the square braces above are only defined in the subspace that does not include +. Since all charges other than q_- decouple from q_+, this means that only diagonal elements can appear above, and using $A_{+,-} = 1$ and

$$\overline{A}_{-,+} = \frac{1-\overline{q}_-^2}{\left(1+\overline{q}_+\right)^2} = \frac{1}{\left(1+\overline{q}_+\right)^2} = v_0^2 \ , \tag{4.5.34}$$

and noting that $\hat{\Gamma}_{-,-} = -2\overline{\Gamma}$ and $A_{-,-} \propto \overline{q}_- = 0$, we then have

$$\partial_t q_+ = \partial_x \sum_{\ell=0}^{\infty}\left(\hat{\Gamma}^{-1}\partial_t\right)^{\ell}\,\frac{v_0^2}{2\overline{\Gamma}}\partial_x q_+ \ , \tag{4.5.35}$$

$$\partial_t q_+ = \frac{v_0^2}{2\overline{\Gamma}}\partial_x^2 q_+ + O\left(\partial^3\right) \ , \tag{4.5.36}$$

which agrees exactly with the diffusion constant computed without linearization, given in Eq. (4.5.25). Additionally, had we chosen a different GGE, for example one for which $\overline{q}_- \neq 0$, we would instead recover the result given in Eq. (4.5.32), which is equivalent upon taking $\overline{q}_- \to 0$. In that case, it must be the case that $\overline{\Gamma} \to 0$; however, this is not a problem as $\overline{\Gamma}$ would not appear in Eq. (4.5.35), but would instead be replaced by the quantities that appear in Eq. (4.5.32). Although FFA fails to be generic in numerous ways, this seems to suggest that linear response is an excellent approximation, in that the resulting equations capture most or all of the physics of the nonlinear equations.

4.6 Hydrodynamics in Bose Gases

4.6.1 Basics of the Lieb-Liniger model

Other than FFA, the simplest interacting integrable model—in terms of the complexity of its quantization condition and solutions—corresponds to a Bose gas in the continuum with a repulsive

δ-function interaction, also known as the Lieb-Liniger model. The corresponding Hamiltonian is generally written in the form

$$\hat{H} = -\sum_j \frac{1}{2m}\frac{\partial^2}{\partial x_j^2} + c\sum_{i<j}\delta\left(x_i - x_j\right) \ , \tag{4.6.1}$$

where $\{x_j\}$ labels the positions of the bosons. In the limit $c \to \infty$, at remotely low energies there can be at most one boson in a given position; correspondingly, in this limit, the excitations behave like free fermions [56, 59, 165]. In general, we can take the mass, m, to be unity for convenience.

The differential scattering kernel is given by

$$\varphi\left(\theta, \phi\right) = \frac{4c}{\left(\theta - \phi\right)^2 + 4c^2} \ , \tag{4.6.2}$$

and the charges, q_n, and currents, j_n, recover from integration against the single-particle eigenvalues, which are the rapidity-dependent functions $h_n(\theta)$,

$$h_n\left(\theta\right) = m\frac{\theta^n}{n!} \ , \tag{4.6.3}$$

and thus $n = 0$ corresponds to particle number—or mass—density, $n = 1$ to momentum, $n = 2$ to energy, and so on. Other relations exist as well, for example, the interpretation of the current of momentum as a generalized "pressure."

We also note that $q_1 = j_0$, as can be seen by integrating the effective velocity against the quasiparticle density. Because $p'(\theta) = m$ is independent of rapidity and the scattering kernel φ is symmetric in its arguments, this becomes

$$\int d\theta\, \rho_{\rm p}\left(\theta\right)\, v^{\rm eff}\left(\theta\right) = \int d\theta\, \rho_{\rm p}\left(\theta\right)\, v^{\rm grp}\left(\theta\right) + \int d\theta \int d\phi\, \rho_{\rm p}\left(\theta\right)\, \varphi\left(\theta, \phi\right)\, \rho_{\rm p}\left(\phi\right)\left[v^{\rm eff}\left(\phi\right) - v^{\rm eff}\left(\theta\right)\right]/m \ , \tag{4.6.4}$$

where the second term vanishes by a simple change of variables, $\phi \leftrightarrow \theta$ in one of the two terms in square braces under the double integral, and noting that $v^{\rm grp}\left(\theta\right) = \varepsilon'(\theta)/p'(\theta) = \theta = h_1(\theta)$, we see this is the case.

Except for the specific form of the Hamiltonian, given by Eq. (4.6.1), and differential scattering kernel, given by Eq. (4.6.2), all other features are not merely properties of the Lieb-Liniger model, but all Galilean-invariant integrable models.

4.6.2 Hydrodynamic equations

In particular, we will be interested in perturbations that preserve only particle number, q_0. Thus, for the quasiparticle density, $\rho_{\rm p}\left(\theta; x, t\right)$, we have

$$\partial_t \rho_{\rm p}\left(\theta; x, t\right) + \partial_x\left[v_\theta^{\rm eff}\rho_{\rm p}\right]\left(\theta; x, t\right) = \Gamma\left[\theta; \rho_{\rm p}\left(\theta; x, t\right)\right] \ , \tag{4.6.5}$$

where, in the integrable case, $\Gamma = 0$. This can also be written

$$\partial_t \rho_{\rm p}\left(\theta; x, t\right) + \left[\hat{A}\,\partial_x \rho_{\rm p}\right]\left(\theta; x, t\right) = \Gamma\left[\theta; \rho_{\rm p}\left(\theta; x, t\right)\right] \ , \tag{4.6.6}$$

where the operator $\hat{A}$ is the same operator defined in previous sections.

We can also integrate the equations for $\rho_{\rm p}(\theta)$ over θ with appropriate functions, $h_n(\theta)$ to obtain equations involving the charges, q_n, which will be addressed in Sec. 4.6.4. The average charges and currents are respectively defined by

$$q_n(x,t) \equiv \int d\theta\, h_n(\theta)\ \rho_{\rm p}(\theta;x,t) = \int \frac{d\theta}{2\pi} p'(\theta)\, n(\theta;x,t)\, h_n^{\rm dr}(\theta) \tag{4.6.7a}$$

$$j_n(x,t) \equiv \int d\theta\, h_n(\theta)\ v^{\rm eff}[\theta;x,t]\ \rho_{\rm p}(\theta;x,t) = \int \frac{d\theta}{2\pi} \varepsilon'(\theta)\, n(\theta;x,t)\, h_n^{\rm dr}(\theta)\ , \tag{4.6.7b}$$

where $p(\theta)$ and $E(\theta)$ are respectively the momentum and energy, whose derivatives with respect to rapidity appear above; for Galilean invariant models, $p = m\theta$, $E = m\theta^2/2$. The definitions, Eq. (4.3.11), are valid for any integrable model on the *Euler scale*, including multiple quasiparticle species.

4.6.3 Relaxation time approximation

For particle number, we have the exact relation

$$\partial_t q_0 + \partial_x q_1 = 0\ , \tag{4.6.8}$$

which means that

$$\begin{aligned} -\int d\theta\, \partial_t \rho_{\rm p}(\theta;x,t) &= \int d\theta\, \partial_x \left[v^{\rm eff}(\theta;x,t)\, \rho_{\rm p}(\theta;x,t) \right] \\ &= \int d\theta\, \theta \partial_x \rho_{\rm p}(\theta;x,t) = \int d\theta\, \left[\hat{A} \partial_x \rho_{\rm p}(\cdot;x,t) \right](\theta)\ , \end{aligned} \tag{4.6.9}$$

and for the first charge, q_1, which happens to be the zeroth current j_0, we have

$$\partial_t q_1 + \partial_x j_1 = \Gamma_1 + \dots\ , \tag{4.6.10}$$

where $\dots$ represent a Navier-Stokes correction that is strictly zero for Eq. (4.6.8), and we will find this is not important to this equation either. Note that Γ_1 is some semiarbitrary functional of the charges and currents, given by

$$\Gamma_1 = \int d\theta\, \theta\, \Gamma[\theta] \tag{4.6.11}$$

$$= \int d\theta\, \theta \left\{ \int d\phi W[\theta,\phi;\dots]\, \rho_{\rm p}(\phi;x,t) - \rho_{\rm p}(\theta;x,t) \int d\phi W[\phi,\theta;\dots] \right\}\ , \tag{4.6.12}$$

where W is allowed to be a functional of the quasiparticle density, and $W[\theta,\phi] = W[\phi,\theta]$ must hold, independent of any sense in which W is a functional of $\rho_{\rm p}$. Writing

$$\frac{1}{\tau(\theta)} \equiv \int d\phi W[\theta,\phi] = \int d\phi W[\phi,\theta]\ , \tag{4.6.13}$$

we have

$$\Gamma[\theta] = -\frac{\rho_{\rm p}(\theta;x,t)}{\tau(\theta)} + \int d\theta W[\theta,\phi]\, \rho_{\rm p}(\phi;x,t)\ , \tag{4.6.14}$$

which automatically satisfies

$$\Gamma_0 = \int d\theta\, \Gamma[\theta] = 0\ , \tag{4.6.15}$$

due to the structure of W, and for the RHS of the q_1 equation we have

$$\Gamma_1 = -\int d\theta\, \theta \frac{\rho_{\rm p}(\theta; x, t)}{\tau(\theta)} + \int d\theta \int d\phi\, \theta W[\theta, \phi]\, \rho_{\rm p}(\phi; x, t) \ , \tag{4.6.16}$$

and we can imagine Taylor expanding W about $\theta, \phi = 0$, and in its functional dependence if needed, i.e.

$$W[\theta, \phi; \dots] = W_0 + W_1(\theta + \phi) + W_{1,1}\theta\phi + \frac{1}{2}W_2\left(\theta^2 + \phi^2\right) + \dots \ , \tag{4.6.17}$$

and keeping only the lowest order term for now, as is standard practice in the usual application of kinetic theory, we take W to be independent of rapidities, etc., and we take

$$W \to \frac{1}{\tau}\frac{1}{\int d\theta 1} \ , \tag{4.6.18}$$

for normalization, with τ independent of rapidity, and to lowest order, we recover the general formula

$$\Gamma_n = -\frac{1}{\tau}\int d\theta h_n(\theta)\, \rho_{\rm p}(\theta) + \frac{1}{\tau}\frac{\int d\theta h_n(\theta)}{\int d\theta 1}\int d\phi \rho_{\rm p}(\phi) \ , \tag{4.6.19}$$

due to the normalization condition for W. Note that the second term on the righthand side above vanishes unless n is even, because h_n integrates to h_{n+1} and h_{2n} are even functions of rapidity. In general, we must use standard techniques for complete bases that are not orthonormal, which involves division by a two-point function. For simplicity, we can assume that $\int d\theta h_{2n}(\theta) = \int d\theta h_0(\theta)$, but this is unimportant since we are only interested in the $n = 1$ case, where this term vanishes, and we have

$$\Gamma_1 = -\frac{1}{\tau}\int d\theta h_1(\theta)\, \rho_{\rm p}(\theta) = -\frac{q_1}{\tau} \ , \tag{4.6.20}$$

which gives a nice decay equation for q_1:

$$\partial_t q_1 + \partial_x j_1 = -\tau^{-1} q_1 \ , \tag{4.6.21}$$

where we have ignored higher order corrections. Note that the version of Γ_n given in Eq. (4.6.19) to lowest order satisfies the constraint $\Gamma_0 = 0$, and if we wanted to expand to include higher order corrections, we would have to ensure that this was still the case. However, given standard practices in kinetic theory, it is probably fine to make the approximation that W scatters all rapidities into one another with equal probabilities (i.e., the standard relaxation time approximation).

To proceed, we take a spatial derivative of Eq. (4.6.21) and a time derivative of Eq. (4.6.8), recovering

$$\partial_t^2 q_0 = -\partial_t \partial_x q_1 = \partial_x\left(-\partial_t q_1\right) \tag{4.6.22}$$

$$= \partial_x\left(\partial_x j_1 + \tau^{-1} q_1\right) \tag{4.6.23}$$

$$= \partial_x^2 j_1 + \tau^{-1}\partial_x q_1 \tag{4.6.24}$$

$$= \partial_x^2 j_1 - \tau^{-1}\partial_t q_0 \ , \tag{4.6.25}$$

which we obtained by using the original relation, Eq. (4.6.8). We now drop $\partial_t^2 q_0$, as it is dominated at late times by $\tau^{-1}\partial_t q_0$, to recover a nice expression

$$\partial_t q_0 = \tau \partial_x^2 j_1 \ , \tag{4.6.26}$$

which already looks diffusive. However, we can improve upon this. As a brief aside, note that had we included the Navier-Stokes diffusive correction for q_1, it would appear in Eq. (4.6.26) at order ∂_x^3, which is therefore negligible at the level of hydrodynamics. As for q_1, since we have established that it decays to zero, it is unimportant whether or not this charge also diffuses while decaying, since we evaluate the diffusion constant in the long-time limit, at which point any diffusive broadening of q_1 will be unimportant (this limit is captured by ignoring $\partial_t^2 q_0$ in favor of $\tau^{-1}\partial_t q_0$).

We now massage the righthand side of Eq. (4.6.26):

$$\tau \partial_x^2 j_1 = \tau \partial_x^2 \int d\theta \, \theta \, v_\theta^{\rm eff} \rho_{\rm p}(\theta; x, t) \tag{4.6.27}$$

$$= \tau \partial_x \int d\theta \, \theta \, \partial_x \left[v_\theta^{\rm eff} \rho_{\rm p}(\theta; x, t) \right] \tag{4.6.28}$$

$$= \tau \partial_x \int d\theta \, \theta \left[\hat{A} \partial_x \rho_{\rm p}(\cdot; x, t) \right](\theta) \ , \tag{4.6.29}$$

which already resembles the expected form corresponding to nonlinear diffusion, and would be of exactly the correct form if, instead of $\partial_x \rho_{\rm p}$, we had $\partial_x q_0$. While we *could* perform an expansion of $\hat{A}$, but this would neglect infinitely many terms, and it is not actually clear at this stage that those terms are small. We now proceed

$$= \tau \partial_x \int d\theta \, \theta \left(1 - n\hat{\mathcal{K}}\right)^{-1} v_\cdot^{\rm eff} \left(1 - n\hat{\mathcal{K}}\right) \partial_x \rho_{\rm p} \tag{4.6.30}$$

$$= \tau \partial_x \int d\theta \, \theta \sum_{\ell=0}^{\infty} \left(n\hat{\mathcal{K}}\right)^\ell v_\cdot^{\rm eff} \left(1 - n\hat{\mathcal{K}}\right) \partial_x \rho_{\rm p} \tag{4.6.31}$$

$$= \tau \partial_x \int d\theta_0 \, \theta_0 \sum_{\ell=0}^{\infty} \left\{ \prod_{k=1}^{\ell} \int \frac{d\theta_k}{2\pi} n(\theta_{k-1}) \, \varphi(\theta_{k-1}, \theta_k) \right\} v_{\theta_\ell}^{\rm eff}$$
$$\times \int \frac{d\theta_{\ell+1}}{2\pi} \left\{ 2\pi \delta(\theta_\ell - \theta_{\ell-1}) - n(\theta_\ell) \, \varphi(\theta_\ell, \theta_{\ell+1}) \right\} \partial_x \rho_{\rm p}(\theta_{\ell+1}; x, t) \ , \tag{4.6.32}$$

and putting the terms in different places and numbering them in reverse order—which is the trick one uses to recover similar identities, e.g. for q_n in terms of dressed h functions vs. undressed ones—one writes

$$= \tau \partial_x \sum_{\ell=0}^{\infty} \int d\alpha_0 \, \partial_x \rho_{\rm p}(\alpha_0; x, t) \left[\prod_{k=1}^{\ell+1} \int \frac{d\alpha_k}{2\pi} \right] \left\{ 2\pi \delta(\alpha_0 - \alpha_1) - n(\alpha_1) \, \varphi(\alpha_0, \alpha_1) \right\}$$
$$\times \, v_{\alpha_1}^{\rm eff} \left[\prod_{k=1}^{\ell} n(\alpha_{k+1}) \, \varphi(\alpha_{k+1}, \alpha_k) \right] \alpha_{\ell+1} \ , \tag{4.6.33}$$

and we can put these terms in a more useful ordering, and reverting from α to θ for convenience,

$$= \tau \partial_x \int d\theta_0 \, \partial_x \rho_{\rm p}(\theta_0; x, t) \int \frac{d\theta_1}{2\pi} \left\{ 2\pi \delta(\theta_0 - \theta_1) - \varphi(\theta_0, \theta_1) \, n(\theta_1) \right\}$$
$$\times \, v_{\theta_1}^{\rm eff} \sum_{\ell=0}^{\infty} \left\{ \prod_{k=2}^{\ell+1} \int \frac{d\theta_k}{2\pi} \varphi(\theta_{k-1}, \theta_k) \, n(\theta_k) \right\} \theta_{\ell+1} \ , \tag{4.6.34}$$

which, in terms of operators, is given by

$$\partial_t q_0 = \tau \partial_x^2 j_1 \tag{4.6.35}$$

$$= \tau \partial_x \int d\theta \partial_x \rho_{\rm p}(\theta) \left(1 - \hat{\mathcal{K}}^T n\right) v_{\cdot}^{\rm eff} \left(1 - \hat{\mathcal{K}}^T n\right)^{-1} \theta \ , \tag{4.6.36}$$

where the last θ is merely a dummy rapidity index. Note that, for Lieb-Liniger, $\hat{\mathcal{K}}$ is its own transpose, and for generic models, this actually works out. Thus, the above becomes

$$\partial_t q_0 = \tau \partial_x \int d\theta \partial_x \rho_{\rm p}(\theta) \left(1 - \hat{\mathcal{K}} n\right) v_{\cdot}^{\rm eff} \ (\theta)^{\rm dr} \tag{4.6.37}$$

$$= \tau \partial_x \int d\theta \partial_x \rho_{\rm p}(\theta) \left(1 - \hat{\mathcal{K}} n\right) v_{\cdot}^{\rm eff} \, h_1^{\rm dr}(\cdot) \tag{4.6.38}$$

$$= \tau \partial_x \int d\theta \partial_x \rho_{\rm p}(\theta) \left(1 - \hat{\mathcal{K}} n\right) v_{\cdot}^{\rm eff} \, \frac{(\varepsilon'(\theta))^{\rm dr}}{m} \ , \tag{4.6.39}$$

where $m = p'(\theta)$ can be taken to unity, but we will keep track of it for now. We can relate the dressed derivative of the energy to the velocity, $(\varepsilon'(\theta))^{\rm dr} = (p'(\theta))^{\rm dr} v_\theta^{\rm eff}$, to recover

$$\partial_t q_0 = \tau \partial_x \int d\theta \partial_x \rho_{\rm p}(\theta) \left(1 - \hat{\mathcal{K}} n\right) \frac{(p')^{\rm dr}(\cdot)}{p'(\cdot)} \left(v_{\cdot}^{\rm eff}\right)^2 \tag{4.6.40}$$

$$= \tau \, \partial_x \int d\theta \, \partial_x \rho_{\rm p}(\theta) \ \left(1 - \hat{\mathcal{K}} n\right) (1)^{\rm dr} \left(v_{\cdot}^{\rm eff}\right)^2 \tag{4.6.41}$$

$$\partial_t q_0 = \tau \, \partial_x \int d\theta \, \partial_x \rho_{\rm p}(\theta) \ \left(1 - \hat{\mathcal{K}} n\right) h_0^{\rm dr}(\cdot) \left(v_{\cdot}^{\rm eff}\right)^2 \ , \tag{4.6.42}$$

which now very closely resembles the answer recovered for FFA, i.e. $D \sim \tau v^2$.

A lazy route would be to pretend that the undressing operator, $\left(1 - \hat{\mathcal{K}} n\right)$, acted only on $(1)^{\rm dr}$ to turn it back into a 1, leaving just v^2. In fact, this term is truly present, and is the lowest order term present in an expansion in $\hat{\mathcal{K}}$ operators. Steaming ahead, we can rewrite the righthand side of Eq. (4.6.42) as

$$\tau \partial_x \int d\theta \partial_x \rho_{\rm p}(\theta) \left(1 - \hat{\mathcal{K}} n\right) \left(v_{\cdot}^{\rm eff}\right)^2 \left(1 - \hat{\mathcal{K}} n\right)^{-1} (h_0) \ , \tag{4.6.43}$$

where $h_0 = 1$. We then take the naïve step of performing an expansion of the two dressing operators to recover terms of the form

$$v^2 + \left[v^2, \hat{\mathcal{K}} n\right] + \dots \ , \tag{4.6.44}$$

which is only justified if the scattering kernel, φ, is small. However, for moderate interaction strengths, $c \gg 1$, this is in fact the case.

We now pursue another route, defining the undressing operator $\hat{U}$ with kernel

$$\mathcal{U}(\theta, \phi) = \delta(\theta - \phi) - \frac{1}{2\pi} \varphi(\theta, \phi) \, n(\phi) \ , \tag{4.6.45}$$

and we can write Eq. (4.6.42) as

$$\partial_t q_0 = \tau \, \partial_x \int d\theta \, \partial_x \rho_{\rm p}(\theta) \int d\phi \mathcal{U}(\theta, \phi) \left[v^{\rm eff}(\phi)\right]^2 (1)^{\rm dr}(\phi) \tag{4.6.46}$$

$$= \partial_x \int d\theta \, \mathcal{D}\left[\theta; \rho_{\rm p}\right] \partial_x \rho_{\rm p}(\theta) \ , \tag{4.6.47}$$

which is very close to having the right form we want, and seems to agree with FFA. To wrap this up, we shift ϕ by θ in the integral to recover

$$= \tau\,\partial_x \int d\theta\,\partial_x \rho_{\rm p}(\theta) \int d\phi \left\{\delta(\phi) - \frac{1}{2\pi}\varphi(\phi)\,n(\phi+\theta)\right\} \left[v^{\rm eff}(\phi+\theta)\right]^2 (1)^{\rm dr}(\phi+\theta) \ , \tag{4.6.48}$$

and now we can justify expanding everything except $\rho_{\rm p}(\theta)$ about $\theta = 0$. This expansion is of precisely the same type that was used previously for the integrability breaking term, Γ, and is therefore connected to the relaxation time approximation. Because the single-particle eigenfunctions for the charges in Lieb-Liniger correspond to a Taylor series in rapidity, this can also be viewed as related to hydrodynamic projection, i.e. onto the slowest modes. To lowest order, we have

$$\partial_t q_0 = \tau\,\partial_x \int d\theta\,\partial_x \rho_{\rm p}(\theta) \int d\phi \left\{\delta(\phi) - \frac{1}{2\pi}\varphi(\phi)\,n(\phi)\right\} \left[v^{\rm eff}(\phi)\right]^2 (1)^{\rm dr}(\phi) \ , \tag{4.6.49}$$

along with possible $O(\theta)$ terms. That expansion will add terms that involve q_n for n corresponding to the order of the expansion in θ. It is possible that these fall off in strength, or that much of the θ dependence is actually washed out by the ϕ integral in the first place, resulting in small couplings. Lastly, all q_n for $n > 0$ decay, so regardless, these corrections will vanish on the timescale τ that allowed us to ignore the $\partial_t^2 q_0$ term earlier on (i.e. an argument based on relevant time scales). To lowest order, this is

$$\partial_t q_0 = \tau\,\partial_x\,\overline{\mathcal{D}} \int d\theta\,\partial_x \rho_{\rm p}(\theta) = \tau\,\partial_x \left[\overline{\mathcal{D}}\,\partial_x q_0\right] \ , \tag{4.6.50}$$

corresponding to nonlinear diffusion; to lowest order, the diffusion constant—which is a functional of the density (or charges and currents)—is given by

$$\overline{\mathcal{D}} = \int d\phi \left\{\delta(\phi) - \frac{1}{2\pi}\varphi(\phi)\,n(\phi)\right\} \left[v^{\rm eff}(\phi)\right]^2 (1)^{\rm dr}(\phi) \ , \tag{4.6.51}$$

which seems to agree with all other results, i.e.

$$\mathcal{D} \propto \tau \langle v^2 \rangle \ , \tag{4.6.52}$$

and did not involve explicit linearization. However, in practice, there is no way to recover the dressing operator, effective velocity, or other quantities without linearizing. Therefore, we should compare to the results that recover from linearization.

4.6.4 Linear response

Starting from Eq. (4.4.33), i.e.,

$$\partial_t q_n + A_{n,n}\partial_x q_n = -\sum_{\ell=0}^{\infty} \left[\hat{A}\,\partial_x\,\overline{P}_n \left(\hat{\Gamma}^{-1}\partial_t + \hat{\Gamma}^{-1}\hat{A}\partial_x\right)^{\ell} \hat{\Gamma}^{-1}\overline{P}_n\,\hat{A}\partial_x\,P_n\right]_{n,n} q_n \ ,$$

we note that for the case of interest, $A_{0,m} = \delta_{m,1}$, in which case the above becomes

$$\partial_t q_0 = -\partial_x \sum_{\ell=0}^{\infty} \sum_{n>0} \left[\left(\hat{\Gamma}^{-1}\partial_t + \hat{\Gamma}^{-1}\hat{A}\partial_x\right)^{\ell} \hat{\Gamma}^{-1}\right]_{1,n} \hat{A}_{n,0}\,\partial_x\,q_0 \ , \tag{4.6.53}$$

and limiting to two derivatives as required by hydrodynamics, we have

$$\partial_t q_0 = -\sum_{n>0} \left[\hat{\Gamma}^{-1}\right]_{1,n} \hat{A}_{n,0}\, \partial_x^2 q_0 \ , \tag{4.6.54}$$

and using the standard expansion of Γ, with $\Gamma_{1,1} = -1/\tau_1$, we have

$$\partial_t q_0 = \tau_1 \hat{A}_{1,0}\, \partial_x^2 q_0 \ - \ -\sum_{n>1} \left[\hat{\Gamma}^{-1}\right]_{1,n} \hat{A}_{n,0}\, \partial_x^2 q_0 \ , \tag{4.6.55}$$

where the terms in the sum are expected to be less significant in the limit corresponding to the relaxation time approximation. Note that $A_{1,0} \propto \langle (v^{\text{eff}})^2 \rangle$, and hence we find

$$D \sim \frac{\langle v^2 \rangle}{\Gamma} = \tau \langle v^2 \rangle \ , \tag{4.6.56}$$

in agreement with the previous derivation and FFA.

4.7 Summary and Outlook

In summary, we have showcased a number of scenarios in which integrability can be used to gain insight into more generic systems. In particular, interacting integrable models represent an advantageous starting point for any perturbative treatment compared to free systems, as the former includes interactions from the outset. The existence of exact quasiparticle solutions makes integrable models particularly convenient to study, and they can de described—both directly and via statistical ensembles—in the thermodynamic limit.

In addition to diagnosing spectral properties and the spread of entanglement, integrable systems are ideal for consideration of transport, due largely to their well-developed hydrodynamic description. We examined at length how one can start from an integrable model and break all but one of its conservation laws to recover a hydrodynamic description of a thermal (ergodic) system with a single conserved quantity. As one would expect, this charge diffuses, and the formalism of generalized hydrodynamics allows for the evaluation of the diffusion constant both for general models with generic perturbations, and for a number of specific cases. In all cases, we find that the diffusion constant, $D \propto v^2 / \Gamma$, as one would expect, where Γ is the decay rate of the nonconserved quantities, determined by Fermi's golden rule. A key feature is the ability to compute this quantity entirely in the framework of integrability, i.e. using GHD data.

Such techniques are expected to be useful going forward, e.g. in computing transport, the expectation values of local observables, and correlation functions in near-integrable systems. For example, this technique should be directly applicable to quantum Newton's cradle experiments [146,159], Bose gases in general, and a number of cold atom experiments that are nearly integrable.

There may be other applications of particular integrable models going forward as well. For example, the Hamiltonian that defines the dispersing Floquet Frederickson-Andersen model (DFFA) is highly constrained, and has excitations that are not one-body in the underlying degrees of freedom defining the model. By removing certain terms and adding other generic terms, it may be possible to realize many-body quantum scars in the intuitive setting of an integrable model, which has well-defined symmetries and quasiparticle excitations. It is also worth noting that, in the limit $L \to \infty$, with $N_R/L - N_L/L = O(1/L)$ and $N_R/L = N_L/L$ finite, the quantization condition for the allowed momenta in DFFA becomes $k_j = 2\pi n_j/L + \delta$, which is the same as Fourier transforms. Thus, the excitations resemble free fermions in a manner that may be possible to exploit—this is

not the case in other interacting integrable models, save the trivial $c \to \infty$ limit of Lieb-Liniger. By alternating the DFFA dynamics with on-site disorder (in the physical basis of qubits), it may be possible to find another concrete example of many-body localization in the thermodynamic limit. Finally, because DFFA has topologically nontrivial quasiparticle excitations and nonperturbative interactions, it may be a useful platform for scrutinizing thermal systems with topological properties. This may be extended by unearthing new Floquet integrable models, e.g. starting from classical cellular automata and adding dispersion. We relegate these topics to future research.

Chapter 5

Quantum Chaos

5.1 Introduction

Integrability is a useful platform for investigating aspects of thermal systems by adding perturbations that violate most or all of their infinitely many conservation laws and imbue a finite lifetime to their quasiparticle excitations. However, it is also worthwhile to understand quantum thermalization, also known as "quantum chaos," away from the integrable limit so as to separate fully the physics associated with conservation laws and well-defined quasiparticles from the most generic aspects of thermalization, which should hold for general evolution (i.e. Hamiltonian, Floquet, and typical driven systems), even in the absence of *any* extensive conserved quantities or any notion of quasiparticle excitations, as can certainly be realized in the laboratory. Additionally, the classical analogues to quantum integrable versus quantum chaotic models stand directly opposed: classical integrable systems are the only classical systems that do not exhibit chaos or thermalize in *any* sense, which further motivates the scrutiny of quantum chaos in a setting unrelated to integrability.

In classical terms, chaotic systems are generally described by a coupled set of nonlinear equations of motion, which render them highly sensitive to their initial conditions. For classical systems, this is central to the use of statistical ensembles: acknowledging even a tiny amount of uncertainty in the initial conditions of a classical system, the notion of chaos ensures that as the system approaches its late-time steady state this uncertainty will be exponentially magnified, producing an ensemble of possible configurations for the system to explore, with no "memory" of the particular initial state. However, quantum systems are, by definition, perfectly sensitive to their initial conditions: a given initial state always evolves to a single, specific state, which is completely determined by its initial conditions. The quantum system cannot globally "forget" its initial state, nor is there an exactly corresponding notion of exponential growth of uncertainty: a quantum system can be prepared in some initial state with macroscopic uncertainty in the expectation values of numerous observables and subsequently evolved under its own dynamics to a single state.

However, as was discussed in Ch. 1, quantum systems do not require this exponential growth in uncertainty to provide a valid ensemble: uncertainty is built into quantum states. Any physically preparable initial state will not be an eigenstate of the evolution (for any models worth considering), and will thus entangle as it evolves forming an ensemble. Alternatively, a system in an eigenstate of the evolution will not be in an eigenstate of generic local observables, and thus eigenstates of the evolution, which are already steady states by construction, also provide perfectly valid ensembles. So despite the apparent paradox that quantum systems have perfect memory of their initial states, due to entanglement generated associated to the evolution of a quantum system (either generated dynamically evolving from a product state or encoded directly into eigenstates of the evolution),

the initial state is completely inaccessible to *any* local measurements. Additionally, compared to classical systems, quantum systems have uncertainty built in.

In the strict sense of the classical phenomenon, there is no such thing as quantum chaos. Some definitions of quantum chaos are formulated for models with well-defined classical limits [4–8]: for such models, quantum chaos is associated with the realization of classical chaos in the classical limit of the quantum model. Efforts to extend quantities such as Lyapunov exponents to quantum systems have revealed the need for special care, and that in general this may not necessarily be a reasonable procedure [133]. Hence, more recently, those studying quantum chaos have sought to define the phenomenon separately from its classical counterpart.

5.2 Random Unitary Circuits

The notion of quantum chaos—or quantum ergodicity, as often phrased in the context of the eigenstate thermalization hypothesis (ETH)—is intertwined with *random matrix theory* (RMT): first, quantum chaotic systems are characterized by an RMT eigenvalue distribution [166, 167]; second, their eigenfunctions can be understood as random vectors [168–171]. One consequence is that quantum thermalization (or chaos) is always associated with *level repulsion* between energy eigenvalues. In practice, this *spectral rigidity* has often been used as an efficient means to pinpoint quantum ergodicity breaking [14, 158, 172–174].

The validity and possible regimes of violation of ETH have been scrutinized in different types of chaotic systems [175–180]; however, numerical tests of ETH are challenging as they require the diagonalization of Hamiltonians where the total number of elements scales exponentially with the number of microscopic degrees of freedom [176, 181–183]. An obvious limitation is that, while RMT captures several aspects of quantum chaos, replacing the microscopic time evolution by a colossal random matrix acting on the full many-body Hilbert space overlooks a key facet of the former, namely locality.

Recent efforts have endeavored to establish and improve upon minimal models of chaotic many body quantum systems starting from RMT, and enforcing locality via random *local* unitary gates to form "circuits" [180, 184–193]. Such models generally display quantum chaos, as characterized by entanglement entropy, the decay of local observables, and out-of-time-ordered correlation functions [184, 186, 187].

Unitary circuits were initially used in the quantum information community in relation to quantum computation, but have also seen recent use in the context of quantum information of black holes. More recently, these models have been adapted to investigate many-body quantum chaos. In particular, there are three main categories of circuit models, all of which use n-site unitary gates drawn from a distribution of Haar masure, defaulting to two-site gates absent any particular reason to do otherwise, and act on q-dimensional spins (also known as "qudits") arranged on a lattice, which may be in one dimension or higher. The first type of circuit model evolves the system by applying two-site gates at random: all gates are drawn independently, and at each time step, a bond is selected at random and its constituent sites acted upon by the unitary gate. The second type of model features a "brick wall" geometry: all gates at all points in spacetime are drawn independently, and a single time step involves a depth-two circuit, with the first layer acting on even bonds and the second layer acting on odd bonds or vice versa. The third type of model features the same brick wall geometry, but gates are only drawn randomly in space: these models are "Floquet" random unitary circuits (FRUCs): the gates comprising the two layers that make up a single time step (or period) are chosen at random, and the system is evolved thereafter by

repeated application of precisely the same gates. There are also many models used in the study of quantum chaos that are not of the random circuit type, however these models are not of immediate or direct interest.

The primary reason for using random unitary circuits is that they are simple. Simply from their geometry, it is easy to see how information about local operators or entanglement propagates in these systems. One can also immediately establish a "speed of light" and associated "light cone" that bound the spreading of information, which arises directly from the circuit geometry and local structure. However, the speed of propagation of information and entanglement generally falls short of such bounds. More importantly, referring to the three types of models enumerated in Ch. 1, the first two circuit models fall into the category of "driven" systems, and the FRUCs are manifestly Floquet. In all three cases, these systems do not have an extensive conserved energy, and unless one puts them in by hand, these models may have no extensive conserved quantities of any kind. Additionally, they have no obvious quasiparticle excitations. Thus, these models are able to probe the most basic and structureless aspects of quantum chaos, and separate the roles of extensive conserved quantities, and other "typical" features of general thermal systems from the basic mechanism for chaos. These models are also as far as possible from the limit of integrability.

The purpose of randomness is to model generic systems. Consider a generic quantum system that is robust to small perturbations and has no extensive conserved quantities or well-defined quasiparticles: there is no reason to expect that any such model (i.e. any generic) can be solved, and the only conceivable means to learn anything would be to consider an ensemble of similar systems. Such an ensemble is most easily captured by using random matrices, which also provide analytic control in certain limits, making it possible to learn things about generic systems. The randomness is thus a tool for describing generic systems. The degree of difficulty of performing the ensemble average depends on which type of circuit structure is being used and the observable or physical quantity being measured. In general, the Floquet circuit is the most challenging to use, and in all cases, taking q to be large provides simplifications[1].

A circuit model of the first type was used to characterize the spread of entanglement in quantum chaotic systems [184]. Models of the second type are most frequently employed in the literature—having a more appealing and consistent structure than models of the first type while being less complicated than models of the third type—to characterize operator spreading and related physics, including in the presence of certain symmetries [185, 186, 189, 190, 193].

Models of the third type—i.e. Floquet random circuits—allow for the analytical derivation of RMT spectral rigidity, in the limit of large local Hilbert space dimension [187, 188] or at fine-tuned solvable points [192, 194]. More precisely, these works demonstrated that RMT behavior only appears for eigenvalue separations small on the scale of the inverse of the Thouless time, t_{Th}, named in analogy with single-particle disordered conductors [195, 196]. The value of t_{Th} depends on the linear system size L and characterizes the time scale for the onset of quantum chaos. It remains an open question to understand which mechanisms control the scaling of t_{Th} with L. In the remainder, we will restrict to circuits of the third type and the study of spectral properties.

[1]Note that q, the local Hilbert space dimension, is the only free "parameter" once one decides on a particular circuit format and restricts to a particular gate size and the Haar ensemble.

5.3 Chaotic Dynamics of Quantum Information

5.3.1 Entanglement growth

The spread of entanglement was first studied using random unitary circuits in Ref. 184, to which the reader is referred for a more complete analysis, along with a treatment of higher dimensions. Here, we briefly review a particular and illustrative calculation from that work, and comment on other work.

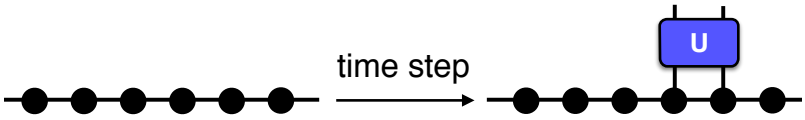

Figure 5.1: Figure from Ref. 184 (open access). Action of the circuit, $\hat{W}$, in a single time step. An independently drawn two-site Haar random unitary gate is applied to a bond selected at random in each time step.

Ref. 184 employs random unitary circuits of the first type: at each step, a two-site gate is randomly drawn from a distribution of Haar measure and applied to a bond selected at random, as depicted in Fig. 5.1. The local degrees of freedom are qudits, i.e. q-state colors, and the model has no symmetries of any kind. To measure entanglement, we consider a system of finite length, L, and imagine bipartitioning the system somewhere in real space, and evaluating the entanglement entropy at some time, t, to recover the entanglement entropy, $S(x,t)$. Although this technique works in higher dimensions, let us restrict to one dimension, and imagining placing the entanglement cut immediately to the right of site x. Using the standard practice for entanglement growth, we take the initial density matrix for this system is at $t = 0$ to be a pure product state, from which the density evolves according to

$$\hat{\rho}_{AB}(t) = \hat{W}(t)\,|\psi\rangle\langle\psi|\,\hat{W}^{\dagger}(t)\ , \tag{5.3.1}$$

where $\hat{W}(t)$ is the random unitary evolution operator realized by the circuit. The reduced density matrix, $\hat{\rho}_A(t) = \mathrm{Tr}_B\left[\hat{\rho}_{AB}(t)\right]$, is formed by tracing over configurations of degrees of freedom in "B," i.e. tracing over all qudits at sites $y > x$. Because the von Neumann entropy defined in Ch. 1 is generally difficult to evaluate for generic and random systems, owing to the its dependence on the trace of the logarithm of $\hat{\rho}_A(t)$, we instead make use of a family of Rényi entropies, with the αth Rényi entropy defined in terms of the reduced density matrix via

$$q^{-(\alpha-1)S_\alpha(t)} = \mathrm{Tr}[\hat{\rho}_A^{\alpha}(t)]\ , \tag{5.3.2}$$

which recovers the von Neumann entanglement entropy in the limit $\alpha \to 1$[2], and q appears on the lefthand side (rather than e) due to the standard practice in information theory of taking base-q logarithms, which accurately encodes the number of "bits."

Measuring general Rényi entropies can be quite convoluted, and most studies simply examine S_2, which provides a valuable measure of entanglement, but does not necessarily give any insight

[2]In practice, it is uncommon to measure various Rényi entropies, extract the α dependence, and extrapolate to $\alpha = 1$. The Rényi entropies already provide a useful measure of entanglement.

into the von Neumann entanglement entropy. What should be clear is that we can establish an *upper bound* on the entanglement entropy via

$$S_\alpha(t) \leq S_0(t) = \log_q \mathrm{Tr}[\,(\hat{\rho}_A(t))^0\,]\,, \tag{5.3.3}$$

and this bound applies to the von Neumann limit ($\alpha \to 1$) as well. The trace over $\hat{\rho}_A^0$ essentially accounts the number of nonzero diagonal elements (or eigenvalues) of the reduced density matrix at time t. Since the eigenvalues of the reduced density matrix sum to unity, the number of nonzero eigenvalues will always bound from above the trace of any power of $\hat{\rho}_A$.

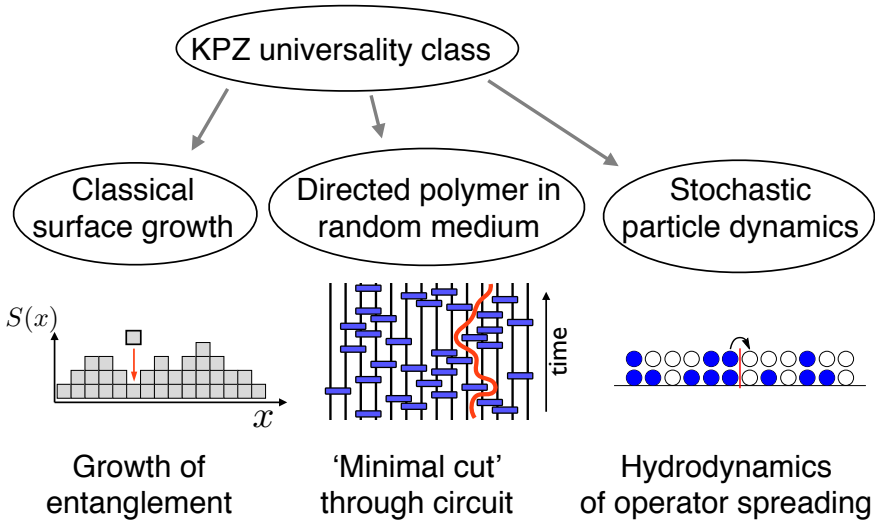

Figure 5.2: Figure from Ref. 184 (open access). Depiction of the "KPZ triumverate," the three models principally associated to the KPZ universality class, and depicts how notions of information spreading in chaotic systems in $D = 1 + 1$ can be mapped onto each of these three.

Concerned with an upper bound on entanglement growth, Ref. 184 investigated the zeroth Rényi entropy, or equivalently, the rank of the reduced density matrix, for a given time, t, and choice of entanglement cut. The primary result of this study was the finding that the growth and fluctuations of this entanglement measure obey the Kardar-Parisi-Zhang (KPZ) equation, a well-studied and exactly soluble nonlinear model from classical statistical mechanics. Associated with the equation is the KPZ universality class, which consists of three distinct types of problems, all described by the KPZ equation, as depicted in Fig. 5.2, and any problem that can be mapped onto a problem in the KPZ universality class therefore inherits the known, universal features of models in this class.

Referring to Fig. 5.2, the first two questions relate to the growth of entanglement, and the latter to operator growth. In the remainder, we will consider the "minimal cut" picture of entanglement in one spatial dimension, which maps onto the problem of a directed polymer in a random medium. In this formulation of the problem, the entanglement measure, $S(x,t)$, given by the zeroth Rényi entropy, is determined entirely by the geometry of the random circuit in spacetime, depicted in Fig. 5.3. Recall that gates are applied essentially randomly in space and time. After t time steps, one chooses a site x, and partitions (i.e. "cuts") the system in two, with region $\mathcal{A}$ corresponding to sites $\{1, 2, \ldots, x-1, x\}$ and region $\mathcal{B}$ to sites $\{x+1, x+2, \ldots, L-1, L\}$.

Since the initial state is unentangled, if—for a particular instance of the circuit—at time t no two-site unitary gates have been applied to the bond joining sites x and $x+1$, then the many-body

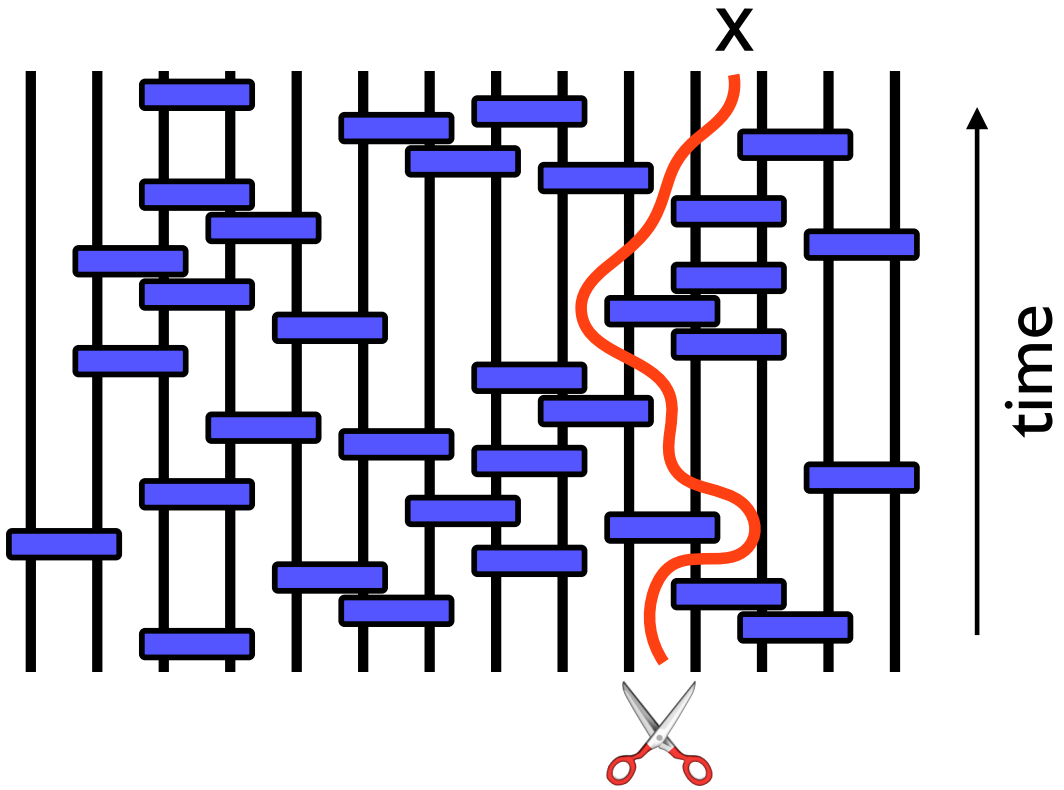

Figure 5.3: Figure from Ref. 184 (open access). Any cut through the circuit starting at the entanglement partition point, x, at time t, which separates the legs to the left and right of x, provides an upper bound on the entanglement entropy, $S(x,t)$.

wavefunction can be factorized as a direct product of wavefunctions for regions $\mathcal{A}$ and $\mathcal{B}$. For the regions to entangle, at least one unitary gate must be applied to the bond straddling the cut. When that happens, other gates can then help spread entanglement into $\mathcal{A}$ and $\mathcal{B}$.

Several simplification arise because we are only interested in establishing an upper bound on the entanglement entropy, rather than quantifying it precisely. This is further simplified by the fact that this bound, the zeroth Rényi entropy, is simply equal to the number of number of nonzero diagonal elements of $\hat{\rho}_A$. In particular, an upper bound for S_0 is given by actually making an entanglement cut, starting at x,t, and continuing the line until either the bottom or sides are reached, as depicted in Fig. 5.3, and we define S_{cut} in terms of the number of gates and vertical lines crossed. Note that the value of S_{cut} for *any* choice of cut provides an upper bound for all Rényi entropies; the best bound is provided by the minimal cut. In particular,

$$S_{\text{cut}} = \#\text{ lines crossed} \quad + 2 \times \#\text{ gates crossed}\ , \tag{5.3.4}$$

and one can restrict to cuts that never cross gates without loss of generality (this also explains the factor of two on the second term above: avoiding a gate requires crossing a vertical line twice).

Such "cut-based" measures of entanglement draw from literature in other areas of physics [184]. The reasoning is as follows: the rank of the reduced density matrix corresponding to a cut at x,t is bounded from above by $q^{S_{\text{cut}}}$ because one can evaluate the wave function at time t as the sum over unentangled wavefunctions that factorize across the cut, and the number of terms in the sum is equal to the rank of the reduced density matrix; this number depends on the number of

intermediate links—generated by $\hat{W}(t)$—which can be no more than the number of vertical lines crossed as depicted in Fig. 5.3. For example, if no gates are applied at the bond $x, x+1$, then a vertical line suffices, giving $S_{\text{cut}} = 0$, which is consistent with the fact that no entanglement has been generated across the cut. If a single cut is necessary, this means that, on one or both sides of the cut, only one spin has been entangled across the cut. The formulation of the reduced density matrix (for the subsystem with only one spin entangled across the cut) as a sum over factorized wavefunctions then requires summing at most over the possible configurations of this entangled spin, which is at most q. This provides an upper bound on every Rényi entropy, with S_0 potentially saturating this bound, $S_{\text{cut}} = \log_q q = 1$. Scenarios requiring additional cut vertical legs follow accordingly.

While any choice of cut provides an upper bound, the best bound is provided by the best—or *minimal*—cut. The problem of finding the minimal cut falls in the KPZ universality class: this problem maps to the problem of finding the ground states of directed polymers in random media. In the classical problem, the polymer there moves laterally in x and vertically in t (using the labels of the circuit), just like the entanglement cut; there exists an energy penalty for bending the polymer, which corresponds to S_{cut} here; there is a random spatial potential that obstructs the polymer, manifested here by the random structure of the gates, e.g. as depicted in Fig. 5.3. There is a large body of literature on the polymer problem that can be imported here, and in particular, one has the KPZ equation

$$\partial_t S(x,t) = \nu \partial_x^2 S(x,t) - \frac{\lambda}{2} \left(\partial_x S(x,t)\right)^2 + \eta(x,t) + c \ , \tag{5.3.5}$$

which can be viewed as diffusive propagation in the presence of noise, η—which comes from the random placement of unitary gates—placement, along with a nonlinear term that generates the interesting physics, and a constant that implies steady growth of entropy in time. In particular, the constant C controls the growth behavior of the entropy, which is clearly linear in time if one ignores the other terms; the other terms describe *fluctuations* of $S(x,t)$.

While the finding that the fluctuations of S are described by the KPZ equation is an important result, in the remainder, we will focus on understanding the growth of entanglement in the circuit setting. In particular, ignoring the noise and spatial fluctuations of $S(x,t)$ in Eq. (5.3.5), which are universally subleading, with

$$\langle S(x,t) \rangle = v_E \, t + B t^{1/3} \ , \tag{5.3.6}$$

where $\langle \ldots \rangle$ denotes averaging over ensembles (gate realizations), and the exponent $1/3$ in the second term derives from the KPZ universality class. The validity of KPZ exponents have been confirmed through extensive numerical study. This equation highlights the linear growth of entanglement, as observed in small systems numerics and predicted from integrability (e.g. in Ch. 4). This can also be understood through coarse-grained, ensemble-averaged consideration of the circuit.

We ignore the specific details of gate placement in any particular realization of the circuit, and consider only what happens in an average sense. At very short times, one expects on average that there is a probability t/L that a gate will be applied across a particular choice of cut, x; rescaling our definition of time so that $L/2$ applications of gates corresponds to a single unit of time, one expects on average to have to cross exactly one leg of the circuit per time step. Thus, at early times, one expects linear growth of S with t. However, we must also recall that one has the option to terminate the cut at the chain's side.

At intermediate times, this can be difficult to diagnose for cuts near the chain's center. Instead, let us consider a cut near the edge of the chain. For example, considering a cut between sites n

and $n+1$, one expects that after nL applications of gates, on average, the minimal cut will be given by making a cut that goes directly out the side of the chain; prior to this time, it is, on average, optimal to make a cut that goes straight down. Combining these pictures, one expects entanglement to grow linearly in time, i.e., $S(x,t) = \alpha(x)\,t$, and plateau at a value determined by the growth rate, i.e. $S_{\max}(x,t) = \alpha(x)\,x$ for $t \geq x$, in the previously detailed units. Thus, one concludes that

$$\langle S\,(x,t)\rangle = \begin{cases} v_E\,t & \text{for } x \geq v_E\,t \\ x & \text{for } x < v_E\,t \end{cases}, \tag{5.3.7}$$

when we neglect the subleading terms in Eq. (5.3.5). This picture is fully consistent with numerical studies on small systems, direct simulations of circuits, predictions from integrability, and thermodynamic principles.

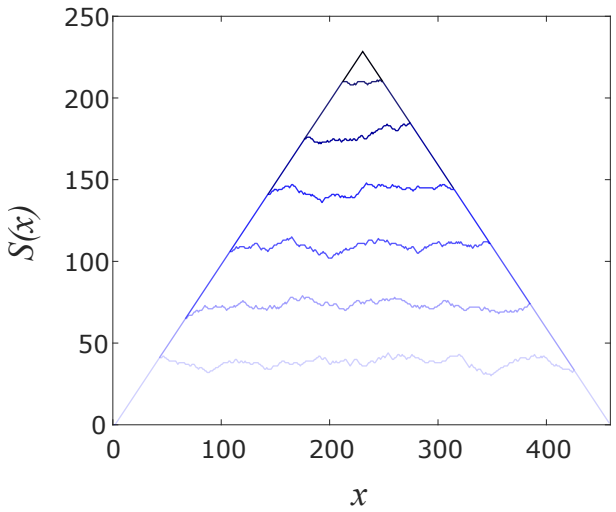

Figure 5.4: Figure from Ref. 184 (open access). Numerical simulation of the von Neumann entanglement entropy, $S(x,t)$, using Clifford gates on a system with $L = 459$ spins 1/2, evaluated for successive times $t = 340$, 690, 1024, 1365, 1707, 2048, and 4096. The overall pyramid shape is associated with the times at which entanglement across a cut at x saturates to the maximal value: in the circuit language, this is the time after which it becomes more effective (on average) to draw the cut from x to the side of the circuit, rather than the bottom. The maximal entanglement entropy is realized at the center of the chain after $t \approx L/2$, as expected.

For different circuit geometries, including Trotterizations of Hamiltonian dynamics, the expected number of "crossed legs" changes, but the intuition that, after some amount of time, the minimal cut corresponds to one exiting the side of the circuit still holds. Thus, the picture of linear growth followed by a plateau ought to be quite generic, with different evolutions realizing different coefficients of linear growths, i.e., different values of v_E. For maximally chaotic systems, this will approach the light cone velocity, which is the maximum speed of information propagation, dictated by the geometry of the circuit; for actual physical systems, the entanglement velocity will be lower. The validity of the above results have been confirmed using a $1/q$ expansion in non-Floquet circuits with brick-wall geometry [185, 186] and Floquet circuits with brick-wall geometry [187]; additionally, this is supported by direct numerical study of standard circuits (e.g. Clifford circuits, used to generate Fig. 5.4) [184] and numerical and analytical study of numerous other chaotic models [9].

5.3.2 Operator growth

As was seen in Ch. 1, in the Heisenberg picture of time evolution, the complexity of generic operators grows in time to involve increasing numbers of degrees of freedom. The support of an operator—defined as the number of degrees of freedom upon which the operator acts nontrivially (i.e. not as the identity, $\hat{\mathbb{1}}$)—grows with each time step, due to the fact that the chaotic dynamics connects (and entangles) degrees of freedom. At late times, i.e. timescales associated with thermalization, the operator $\hat{W}^\dagger(t)\,\hat{\mathcal{O}}(0)\,\hat{W}(t)$ will involve so many degrees of freedom that direct measurement is essentially impossible. Of course, in the Schrödinger picture, operators are constant in time, and states evolve in complexity. However, what this picture tells us is that given a measurement outcome for a local observable, the result of the same measurement at the initial time, $t = 0$, corresponding to $\hat{W}(t)\,\hat{\mathcal{O}}\,\hat{W}^\dagger(t)$, is so much more complex and nonlocal as to be nonrecoverable. This provides a useful means to understand how information in chaotic many-body quantum systems—e.g. about the system in the distant past—is "hidden" nonlocally by the dynamics, so that at sufficiently late times, the outcome of any measurement of a local observable acting on a particular subsystem is insensitive to initial conditions.

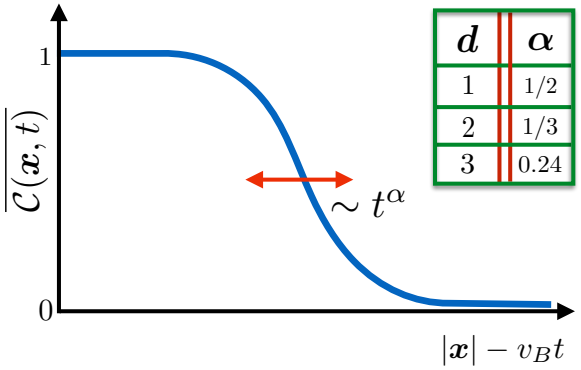

(a) Results for OTOCs.

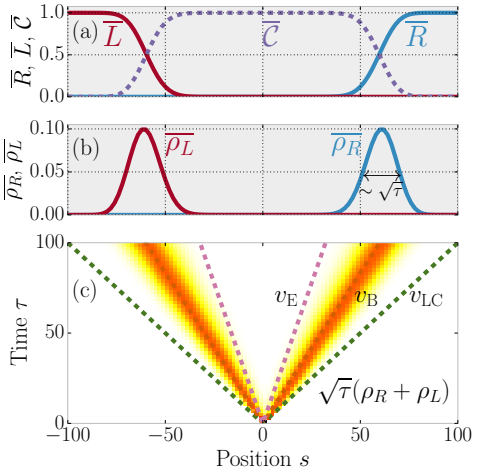

(b) General operator spreading.

Figure 5.5: Figure a is from Ref. 185 (open access). Here, d is the spatial dimension, and $\overline{\mathcal{C}(x,t)}$ is the ensemble-averaged OTOC corresponding to generic observables sampled from a generalization of the Pauli $\hat{X}$ and $\hat{Z}$ matrices to qudits (with local Hilbert space dimension q). The finding is that propagates ballistically at the "butterfly velocity," v_B, which derives its name from the butterfly effect associated with classical chaos; the operator "front" broadens as t^α as the front propagates. In one dimension, this corresponds to biased diffusion: ballistic propagation of the operator front in space, with diffusive broadening of the front itself. In two dimensions, the broadening is described by the KPZ equation, which is unrelated to the recovery of KPZ for entanglement growth in one dimension. Figure b is from Ref. 186 (open access). Numerical study of the growth of generic single-site operators with time in one spatial dimension. The result is ballistic propagation of the operator front with diffusive broadening, in agreement with Fig. a.

In contrast to the situations that one can access by perturbing about integrable models, here we are particularly interested in the spread of operators unrelated to any conservation laws, although we will address conservation laws as well. As in the previous section, we will limit our consideration to one dimension, although Ref. 185 provides results for out-of-time-ordered correlation functions

(OTOCs) in $d = 1, 2, 3$ spatial dimensions, summarized in Fig. 5.5(a). The correlation function, $\mathcal{C}$[3], in Ref. 185 is defined by

$$\mathcal{C}(x,t) = \frac{1}{2}\,\mathrm{Tr}\left\{\hat{\rho}\,[\hat{\mathcal{O}}_0(t), \hat{Y}_j]^\dagger\,[\hat{\mathcal{O}}_0(t), \hat{Y}_j]\right\}\ , \tag{5.3.8}$$

where $\hat{\mathcal{O}}_0$ acts only on site 0 at time $t = 0$, and evolves according to $\hat{\mathcal{O}}_0(t) = \hat{W}^\dagger(t)\,\hat{\mathcal{O}}_0(0)\,\hat{W}(t)$. Under the evolution, the number of sites upon which $\hat{\mathcal{O}}_0(t)$ acts grows with time; in this example, the "size" of $\hat{\mathcal{O}}_0(t)$ is taken to be the region of sites in which $\hat{\mathcal{O}}_0(t)$ fails to commute with *typical* operators, $\hat{Y}_j$ with $O(1)$ strength on site j. Since there are no conserved quantities, including energy, the standard choice of equilibrium density matrix, $\hat{\rho}$, is the identity, $\hat{\mathbb{1}}$. The OTOC is averaged over ensembles of circuits and choices of the typical operator.

Going forward, we follow the discussion of Ref. 186, but note that the methodology and results are essentially the same as those of Ref. 185. To describe generic observables, it is most convenient to define a basis of all possible operators in the many-body Hilbert space, which has dimension q^{dL}. We restrict to one spatial dimension, $d = 1$, and consider only generic systems with no "special" states, i.e. neither symmetries nor constraints, so that all q^L states can be connected dynamically. We enumerate a basis of q^{2L} unique operators in analogy to the Pauli matrices, $\hat{\mathbb{1}}_j, \hat{X}_j, \hat{Y}_j, \hat{Z}_j$, defined on each site, j, which for two-level systems enumerate all 4^L unique operators that can act on the many-body system. Local operators will act as the identity on most degrees of freedom. This operator basis is particularly useful due to its local construction: each basis operator is a *string* of operators that act on individual sites; local operators are those that act as the identity on all but a handful of sites. Any given operator, $\hat{\mathcal{O}}$, will be a linear superposition of the basis operators: this basis enumerates a vector space in which all operators live, and we assign to this vector space the symmetric inner product

$$\langle \hat{A}|\hat{B}\rangle \equiv \frac{1}{q^L}\,\mathrm{Tr}\,[\hat{A}^\dagger \hat{B}]\ , \tag{5.3.9}$$

which defines the norm of an operator $\hat{\mathcal{O}}$ as $\sqrt{\langle \hat{\mathcal{O}}|\hat{\mathcal{O}}\rangle}$.

Consider a generic operator of interest, $\hat{\mathcal{O}}_0$, which at time $t = 0$ acts as the identity on all but one site, which we call "0," upon which $\hat{\mathcal{O}}_0$ realizes any linear combination of the basis operators for site 0. We note that the basis operators, $\{\hat{\sigma}^\mu\}$ evolve according to

$$\hat{\sigma}^\mu(t) = \hat{W}^\dagger(t)\,\hat{\sigma}^\mu\,\hat{W}(t) = \sum_\nu c_\nu^\mu(t)\,\hat{\sigma}^\nu\ , \tag{5.3.10}$$

where the time-dependent coefficient $c_\nu^\mu(t)$ gives the overlap of the operator string labelled ν with the time-evolved string μ. Using standard completeness relations, this is given by

$$c_\nu^\mu(t) = \langle \hat{\sigma}^\nu|\hat{\sigma}^\mu(t)\rangle = \frac{1}{q^L}\,\mathrm{Tr}\left\{(\hat{\sigma}^\nu)^\dagger\,\hat{W}^\dagger(t)\,\hat{\sigma}^\mu\,\hat{W}(t)\right\}\ . \tag{5.3.11}$$

For convenience, one can take $\hat{\mathcal{O}}_0$ to correspond to a particular choice of $\hat{\sigma}^\mu$, which acts as the identity except on site 0, rather than a linear combination of such operators. In this case, at $t = 0$, $c_\nu^\mu(0) = \delta_{\mu,\nu}$, and because the basis operators generalize Pauli matrices, $\hat{\mathcal{O}}_0$ has unit norm. Since

[3]The OTOC is actually given by $1 - \mathcal{C}$, which also recovers from $\mathcal{C}$ if one drops the factor of 1/2 and the commutator brackets.

the dynamics are unitary, for $t > 0$, the norm of $\hat{\mathcal{O}}_0$ must be preserved; for this constrains the coefficients, c, to satisfy

$$\langle\hat{\mathcal{O}}|\hat{\mathcal{O}}\rangle = 1 = \sum_\nu |c_\nu^\mu(t)|^2 \ , \tag{5.3.12}$$

as with standard vector spaces. Thus, the coefficients $|c|^2$ are like probabilities: they are positive semi-definite and sum to unity.

For short times, there is little or no weight, c_ν^μ, on strings $\hat{\sigma}^\nu$ with nonidentity components far from site 0. In general, the goal of this exercise is to understand how the strings that contribute to Eq. (5.3.10) get longer with time under the dynamics generated by $\hat{W}$. To analyze the extent to which the support of $\hat{\mathcal{O}}_0$ spreads in time t, it is convenient to introduce the concepts of right [left] weights, which we interpret as a density. The right weight of $\hat{\sigma}^\mu$ evolved to time t is given by

$$\rho_R^\mu(j,t) = \sum_\nu{}' |c_\nu^\mu(t)|^2 \ , \tag{5.3.13}$$

where the prime indicates restriction to strings ν for which the rightmost nonidentity operator acts on site j. An analogous equation defines the left weight. Because the sum over j of $\rho_R^\mu(j,t) = 1$, this quantity can be interpreted as a density.

To understand the dynamics of the right weight, we need only consider the action of a single two-site unitary gate, i.e. corresponding to sites j, $j+1$, which takes the system from time t to time $t+1$. Consider strings with right weights at sites j and $j+1$ at time t and $t+1$. Of the q^4-1 nonidentity operators that act on the Hilbert space corresponding to these two sites, q^2-1 of these act nontrivially only on $\rho_R^\mu(j,t)$, with the remaining q^4-q^2 operators acting on $\rho_R^\mu(j+1,t)$ (including operators that act on both). The Haar random unitary generates all possible transitions between these q^4-1 operators, and with roughly the same probability (after averaging). Thus, the probability for a right weight at site j to stay in place is given by the fraction of operators that act only on site j, i.e. $p = (q^2-1)/(q^4-1) = 1/(q^2+1)$. The ensemble-averaged probability for the right weight to move from site j to site $j+1$ under this gate is given by $1-p = q^2/(q^2+1)$.

Consideration of the ensemble-averaged effect of subsequent layers of the circuit leads straightforwardly to the conclusion that the right weight performs a biased random walk under the action of the circuit, $\hat{W}$, moving to the right with probability $p_R = q^4/(q^2+1)^2$ and to the left with probability $p_L = 1/(q^2+1)^2$, and stays put with probability $1-p_L-p_R = 2q^2/(q^2+1)^2$. In the limit $q\to\infty$, $p_R \to 1$, and the probability to stay put or go back vanish. The result of this random walk is that the front propagates from $x = 0$ ballistically, with $\langle x\rangle = v_B t$, with the butterfly velocity given by

$$v_B = p_+ - p_- = \frac{q^4}{(q^2+1)^2} - \frac{1}{(q^2+1)^2} = \frac{q^2-1}{q^2+1} \ , \tag{5.3.14}$$

where p_+ is the probability with which the right [left] weight moves to the right [left], and p_- the probability the front moves in the direction opposite its namesake. For $q\to\infty$, the butterfly velocity approaches the light cone velocity, 1. For physical systems, the butterfly velocity will be less than the light cone velocity.

The corresponding stochastic evolution equation for the ensemble-averaged right [left] weight[4] is

$$\overline{\rho_R}(x,t+1) = 2p(1-p)\overline{\rho_R}(x,t) + (1-p)^2\overline{\rho_R}(x-1,t) + p^2\overline{\rho_R}(x+1,t) \ , \tag{5.3.15}$$

[4]Technically, the right weight is relaxed from $\rho_R^\mu(j,t)$ to $\rho_R^\mu(x,t)$, where x corresponds to the bonds upon which the first layer of the circuit acts, rather than specific sites.

which is a lattice version of biased diffusion, which has solution

$$\overline{\rho_R}(x,t) = \frac{q^{2(t+x)}}{(1+q^2)^{2t}} \binom{2t}{t+x} , \tag{5.3.16}$$

and taking $t, x \to \infty$ with $x/t \approx v_B$ fixed, one can invoke Stirling's approximation to recover the [biased] diffusive kernel

$$\overline{\rho_R}\big(x = v_B t + O(\sqrt{t})\big) = \frac{1}{\sqrt{\pi(1-v_B^2)t}} \exp\left\{-\frac{(x-v_B t)^2}{(1-v_B^2)\,t}\right\} , \tag{5.3.17}$$

so that the operator front propagates ballistically with velocity v_B, and the front itself broadens diffusively.

Similar considerations can be used to characterize OTOCs as well, and are in agreement with Ref. 185. In particular, the OTOC grows sharply after the light cone arrives, but does not exhibit an exponential growth—i.e. related to the Lyapunov exponent—as one might expect from classical chaos. Details of the OTOC are unimportant to the considerations of this thesis. In addition to their specific results, these works [185,186]—along with results from integrability breaking—paint a clear picture that at intermediate-to-late times, thermal (or chaotic) systems are well-described by hydrodynamics, even in the absence of conserved quantities (i.e. hydrodynamics of information).

The above procedure can be repeated in the presence of an extensive conserved quantity, e.g. a $U(1)$ symmetry corresponding to the conservation of the z-component of spin, appropriately generalized to q-state degrees of freedom. This procedure is outlined in contemporary Refs. 189 and 190. In the presence of a conserved charge, we must consider separately operators that overlap with the conserved charge, and the nonconserved component of a given operator. One then finds that the conserved part of the operator diffuses, as one expects for conserved charges. Additionally, the weight of the operator corresponding to the conserved part is transferred at some rate under the dynamics to nonconserved operators, which spread ballistically, as described above. The nonconserved components propagate much more quickly and become nonlocal, providing a "reservoir" that allows for dissipation, as one generally expects to find in thermal systems.

5.4 Spectral Statistics in a Minimal Model

A minimal model of many-body quantum chaos is given by a brick-wall Floquet unitary circuit comprising two-site gates, which acts on q-state "colors" that live on a lattice. Because the model is Floquet, all times are discrete, $t \in \mathbb{N}$, and evolution by t time steps is given by t applications of the single period evolution operator, $\hat{W}$. The brick-wall structure of $\hat{W}$ is depicted in Fig. 5.6. Using this model, Ref. 187 obtained analytic expressions for the spectral form factor (SFF), decay of local observables, out-of-time-ordered commutators (OTOCs), and the second Renyi entropy. Excepting the SFF, these results agree with previous studies on non-Floquet circuits, but are more difficult to obtain than in the latter setting; the SFF is a measure of spectral rigidity, and has no meaning in non-Floquet circuits, which do not have a spectrum.

Thus, while dynamics are more difficult to tackle in the Floquet setting, the primary advantage of the latter is the ability to access *spectral* properties. There exist several common probes of spectral signatures of quantum chaos, another being the r ratio that measures the ratio of level spacings, and thereby level repulsion. The spectral form factor, $K(t)$, is the Fourier transform of

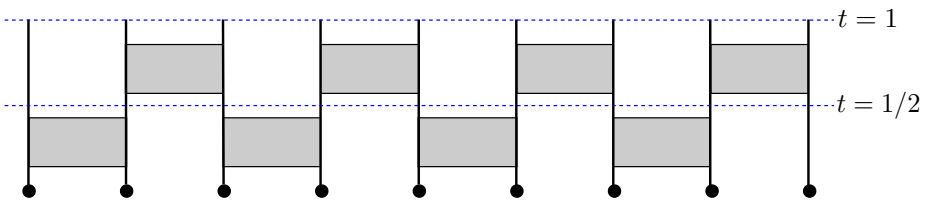

Figure 5.6: A depiction of the Floquet unitary circuit.

the two-point correlation function of the density of eigenvalues of the evolution, i.e.

$$K(t) \equiv \sum_{m,n=1}^{\mathcal{D}} \langle e^{i(\theta_m - \theta_n)t} \rangle = \langle \left| \mathrm{Tr}\left[\hat{W}(t)\right] \right|^2 \rangle \ , \tag{5.4.1}$$

where $\{\theta_m\}$ are the eigenphases of $\hat{W}$, $\mathcal{D}$ is the many-body Hilbert space dimension, $\hat{W}(t)$ is equivalent to the tth power of $\hat{W}$ due to the Floquet structure, and $\langle \ldots \rangle$ denotes the average over an ensemble of statistically similar systems. The SFF is the Fourier transform of the two-point correlation function of eigenphases. Clearly for $t = 0$ one has $K(0) = \mathcal{D}^2$, and going forward we will only refer to $K(t)$ for $t > 0$.

For $t \ll \mathcal{D}$, $K(t)$ probes correlations between levels with a separation far greater than the mean level spacing, $\propto \mathcal{D}^{-1}$. In chaotic systems, one expects $K(t)$ to be linear in t due to "Coulombic suppresion" of long-wavelength fluctuations in the density of eigenvalues of $\hat{W}$. For uncorrelated eigenphases, $K(t) = \mathcal{D}$ for all times, as can be demonstrated exactly for free fermions on a lattice with a disordered on-site potential, e.g. For $t \sim \mathcal{D}$, $K(t)$ captures correlations between eigenvalues with separations comparable to the mean level spacing. It is therefore expected that for $t \geq t_{\mathrm{Heis}}$ one has $K(t) = \mathcal{D}$, where the Heisenberg time, $t_{\mathrm{Heis}} = \mathcal{D}$ is equal to the many-body Hilbert space dimension, or inverse mean level spacing. In a naïve sense, once this threshold has been met, $K(t)$ reflects eigenvalues $\{\theta_m\}$ that are in an average sense closer to θ_n than the mean level spacing, which gives only the $m = n$ terms in the sum in Eq. (5.4.1).

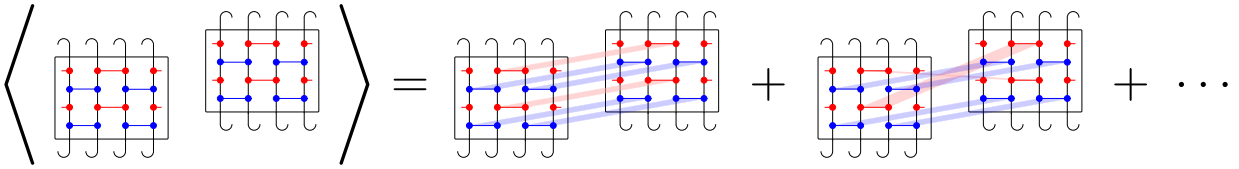

Figure 5.7: A schematic illustration of the diagrammatic representation of $K(t)$ according to Ref. 187.

According to Ref. 187, the evaluation of the ensemble average in Eq. (5.4.1), which defines $K(t)$, amounts to generating all diagrams by pairing two-site unitary gates with their Hermitian conjugates at each bond, as schematically illustrated in Fig. 5.7. However, for a given t, there are $(t!)^{2(L-1)}$ diagrams in total, making further approximation necessary. The only parameter at our disposal is q, and the situation becomes far more tractable as $q \to \infty$. Although this limit can be problematic when considering operator spreading, it does not appear to afflict the SFF in quite the same way.

In the large-q limit, the leading contributions consist of t different diagrams—where $t \in \mathbb{Z}$ is the time measured in Floquet periods—each of which has an identical "cyclical" pairing at *all* sites (or

bonds, perhaps more accurately) as illustrated in Figs. 5.7 and 5.8. A rigorous derivation can be found in Ref. 187. These t diagrams are "Gaussian," in the sense that they can be evaluated using

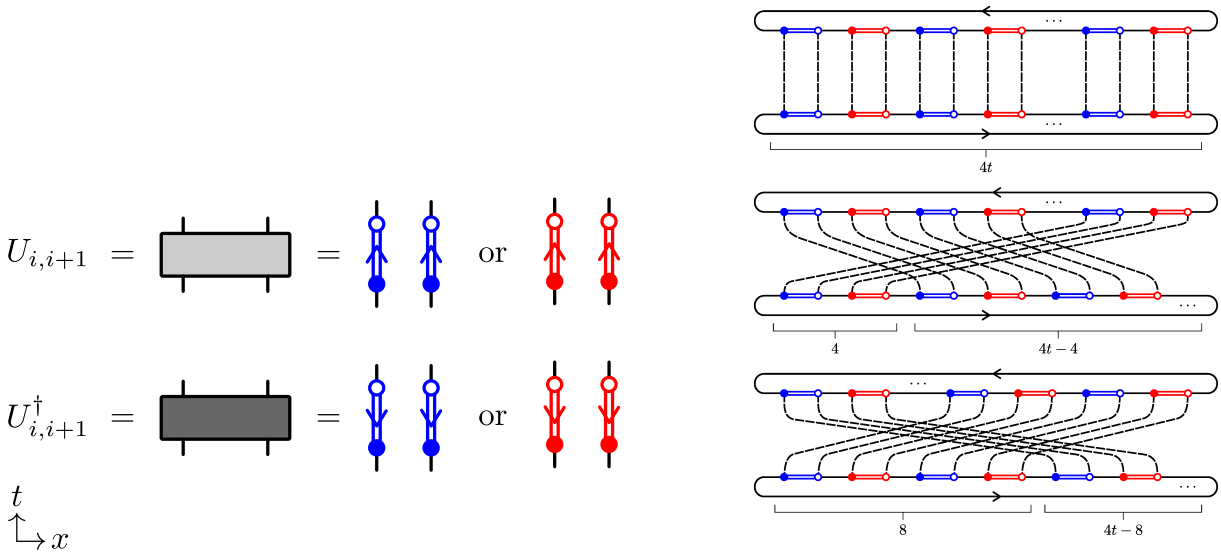

(a) Diagrammatic notation. (b) Leading t diagrams.

Figure 5.8: Figure from Ref. 187 by collaborators (open access). Figure (a) represents a convenient notation for performing the diagrammatic expansion, as appears in [187]. Figure (b) considers the Haar averaging of unitaries (and their conjugates) corresponding to a single bond, $i, i+1$. There are t leading diagrams: the upper diagram corresponds to pairing the first $\hat{U}$ with the first $\hat{U}^\dagger$ and so on; the next diagrams correspond to cyclic pairings, which due to cyclic invariance of the trace—represented by the closed outer loop—are all equivalent to one another. This produces an overall factor of t, which is the expected behavior for chaotic systems.

the Wick contraction of a random unitary and its conjugate. The diagrams depicted in Fig. 5.8b, contribute factors

$$\overline{U^{k,l}_{i,j} U^{*\,k',l'}_{i',j'}} = \frac{1}{q^2} \delta_{i,i'} \delta_{j,j'} \delta_{k,k'} \delta_{l,l'} \ , \tag{5.4.2}$$

to leading order. Other diagrams have more complicated prefactors, and are subleading in q^{-1}. Additionally, while Fig. 5.8b depicts a single bond, note that the evaluation of the Haar contractions of the indices of that bond constrain the indices that feed into the unitaries connected to neighbors on either side, fixing the contraction of those indices to match *exactly* the contractions of the first bond considered, i.e. as shown in Fig. 5.8b. This is referred to as the "bond constraint" in Ref. 187, and gives the leading terms contributing to $K(t)$ from consideration of a single bond. Any deviations from the bond constraint carry a penalty of q^{-2} at minimum, and generally q^{-4} or higher, and are thus strongly subleading.

While the $q \to \infty$ limit may seem drastic, and partially problematic as $\mathcal{D}, t_{\text{Heis}} \to \infty$, it is worth noting a few things. As previously mentioned, for a given t, there are $(t!)^{2(L-1)}$ diagrams in total, which make even the task of collecting only the subleading diagrams for some arbitrary time untenable. Additionally, it is well known that for finite q, L, no expansion in $1/q$ can capture the transition from the linear ramp to the post-Heisenberg plateau, which would be the only benefit to having t_{Heis} finite. There does not appear to be an established means to move away from the $q \to \infty$ limit while retaining both generality and analytic control.

However, taking $q \to \infty$, tracing over expressions of the type that appear in Eq. (5.4.2) will cancel the factor of q^{-2}, and the result of the ensemble averaging, to leading order, is unity. The factor of t corresponding to the cyclically equivalent diagrams in Fig. 5.8b is all that remains: this is precisely the linear ramp regime that indicates quantum chaos. Additionally, this result depends crucially on the gate structure: if sites are decoupled in particular ways, $K(t)$ grows much more quickly, corresponding to less chaotic dynamics. For example, if $\hat{W}$ consists only of single-site unitary gates, then $K(t) = t^L$ out to the Heisenberg time, q. If $\hat{W}$ consists only of one of the two layers, i.e. only even bonds, then $K(t) = t^{L/2}$ out to the Heisenberg time q^2. This pattern holds for any dynamics involving disconnected blocks of n sites. One way to think about the finite q limit is to imagine that, at early times, interactions have not yet had adequate time to couple the system, which therefore behaves initially as L decoupled blocks. As the system evolves and entangles through interactions, these sites merge into chaotic blocks of size ξ, each of which has $K_\xi(t) = t$, with the overall SFF scaling as $t^{L/\xi}$, until all blocks have merged into a single block that spans the entire system, after which $K(t) = t$, unless $K(t)$ for the whole system saturates to $\mathcal{D}$ before the system can thermalize, in which case, which would indicate that the system is not chaotic. The time required to reach the linear ramp regime is known as the Thouless time, t_{th}. In Sec. 5.5, we investigate the Thouless time in models with symmetries, where it is expected that even in the most chaotic of systems, the system's thermalization is delayed by the need for information about the conservation law to spread through the system.

5.5 Spectral Statistics in Models with Conserved Charges

This Sec. is largely drawn from Ref. 43 by this author.

5.5.1 Overview

In this Section, we investigate the effect of a local conserved quantity $\hat{Q}$ on the behavior of t_{Th} and, more generally, on the spectral properties of the evolution operator, $\hat{W}$, of a Floquet system. In particular, we consider the two-point spectral form factor (SFF) $K(t)$, defined in Eq. (5.4.1) in Sec. 5.4,

$$K(t) \equiv \sum_{m,n=1}^{\mathcal{D}} \langle e^{i(\theta_m - \theta_n)t} \rangle = \langle \left| \text{Tr}\left[\hat{W}(t)\right] \right|^2 \rangle \,.$$

For spatially extended one-dimensional ($1d$) systems without a conserved density [188,197], $K(t) \simeq t^{L/\xi(t)}$ for $t \ll t_{\text{Th}}$: the system can be seen as partitioned into $L/\xi(t)$ chaotic blocks, with a length $\xi(t)$ that grows with t. RMT behavior is recovered for $t \gtrsim t_{\text{Th}}$ with $\xi(t = t_{\text{Th}}) \sim L$. In the presence of a conserved quantity with diffusive transport, it is natural to expect $t_{\text{Th}} \sim L^2/D$, where D is the diffusion constant. The idea that the timescale L^2/D controls the onset of RMT spectral correlations was proposed on a heuristic basis in [193], with support from a variety of estimates and numerical studies. Here we establish this result in an exact treatment of a minimal model. We also set out the scaling behavior of $K(t)$ in the time interval $1 \ll t \lesssim t_{\text{Th}}$ and show that this holds for a numerical simulation of an actual Floquet system with a conserved charge.

To probe $K(t)$ we build on a Floquet circuit model introduced in [187] and introduced in Sec. 5.4, consisting of a chain with q-state "spins" (or "colors") at each site. The model has a time-evolution operator $\hat{W}$ constructed from unitary gates that act on neighboring pairs of sites. Gates are randomly selected in space but repeated periodically in time. Using a diagrammatic method to average over the individual matrices [198], to leading order at large q, one finds $K(t) = K_{\mathrm{CUE}}(t)$ for any $t \neq 0$, so that $t_{\mathrm{Th}} \to 0$ as $q \to \infty$. In the following, we formulate and characterize an extension of this model that hosts a $U(1)$ symmetry corresponding to a local, conserved operator $\hat{Q}$ that commutes with $\hat{W}$. In this way, the limit $q \to \infty$ has a twofold convenience: first, it allows controlled diagrammatic calculations; second, it washes out any effect on $K(t)$ not due to $\hat{Q}$.

5.5.2 Model

The model we use is a Floquet random unitary circuit (FRUC) defined on a chain of L sites with local Hilbert space $\mathcal{H}_{\mathrm{loc}} \equiv \mathbb{C}^q \otimes \mathbb{C}^2$, the on-site tensor product of a q-dimensional *color* and a spin 1/2. The former degree of freedom facilitates Haar averaging [187,188,190], and we encode a $U(1)$ symmetry using the latter, following [190], corresponding (in standard notation) to conservation of $\hat{Q} = \hat{S}^z = \frac{1}{2}\sum_{j=1}^{L} \hat{\sigma}_j^z$. This model with its single symmetry is expected to capture the spectral properties of generic models with a single, extensive conserved quantity.

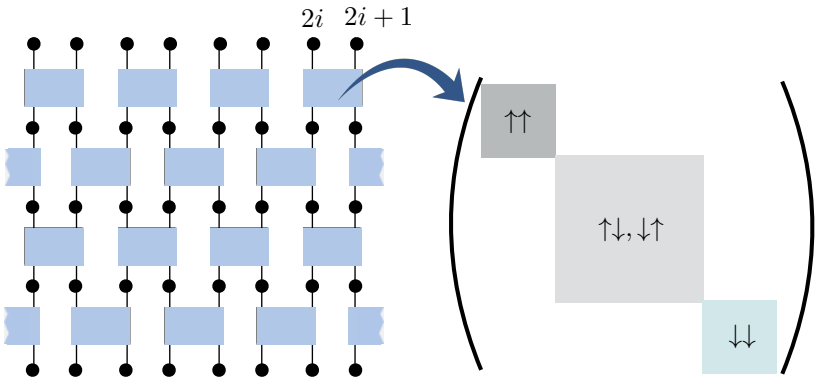

Figure 5.9: Figure from Ref. 190 (open access). Overall structure of the $U(1)$ conserving circuit and local gates. The individual $4q^2 \times 4q^2$ two-site unitary gates, $\hat{U}_{j,j+1}$, are block diagonal in the z basis of the spins 1/2 due to the conservation of local magnetization $S^z_{j,j+1} = \left(\hat{\sigma}^z_j + \hat{\sigma}^z_{j+1}\right)/2$. If the spins j and $j+1$ are jointly in the $\uparrow\uparrow$ or $\downarrow\downarrow$ states, the gate acts nontrivially only on the q-state colors as a $q^2 \times q^2$ unitary. If the j and $j+1$ spins are in either of the states $\uparrow\downarrow$ or $\downarrow\uparrow$, the gate may mix them, acting as a $2q^2 \times 2q^2$ unitary. Each of the three unitary blocks are independently drawnly drawn from a distribution of Haar measure, indicated by their different colors.

The single-period—or Floquet—evolution operator $\hat{W} \equiv \hat{W}_2 \cdot \hat{W}_1$ is given here by a depth-two circuit comprised of local two-site gates: assuming even L, the two layers correspond respectively to odd and even bonds, with $\hat{W}_1 = \hat{U}_{1,2} \otimes \hat{U}_{3,4} \otimes \ldots$ and $\hat{W}_2 = \hat{U}_{2,3} \otimes \hat{U}_{4,5} \otimes \ldots \hat{U}_{L,1}$. We require that each $\hat{U}_{j,j+1}$ preserves the local magnetization $S^z_{j,j+1} = \frac{1}{2}\left(\hat{\sigma}^z_j + \hat{\sigma}^z_{j+1}\right)$ [189, 190]. Thus $\hat{U}_{j,j+1}$ is a $4q^2 \times 4q^2$ block diagonal matrix, acting as a $q^2 \times q^2$ matrix in each of the $\uparrow\uparrow$ and $\downarrow\downarrow$ subspaces, and as a $2q^2 \times 2q^2$ matrix in the $\uparrow\downarrow$, $\downarrow\uparrow$ subspace, with all three blocks independently drawn Haar random unitaries, as depicted in Fig. 5.9.

To characterize spectral correlations in this quantum circuit, we compute the SFF as defined in Eq. (5.4.1). Since $[\hat{W}, \hat{S}^z] = 0$, $\hat{W}$ is block-diagonal, levels from different $\hat{S}^z$ sectors do not repel; thus, we define

$$K(t,s) \equiv \langle \underset{s}{\mathrm{Tr}}[\hat{W}(t)] \underset{s}{\mathrm{Tr}}[\hat{W}^\dagger(t)] \rangle \tag{5.5.1}$$

where 's' indicates restriction to the subspace $\hat{S}^z = S = L\,s$ and $\langle \cdots \rangle$ denotes Haar averaging, which can be performed diagrammatically as depicted in Fig. 5.7. Note that for finite L, only a discrete set of values of s are allowed.

5.5.3 Effective spin-1/2 calculation

The ensemble averaging in Eq. (5.5.1) maps $K(t,s)$ to the partition function of a Trotterized Heisenberg ferromagnet. Evaluating this average amounts to generating all diagrams [187] by pairing unitaries $\hat{U}_{j,j+1}$ with their complex conjugates $\hat{U}^\dagger_{j,j+1}$ at each bond, as depicted in Sec. 5.4, but now with additional spin degrees of freedom involved.

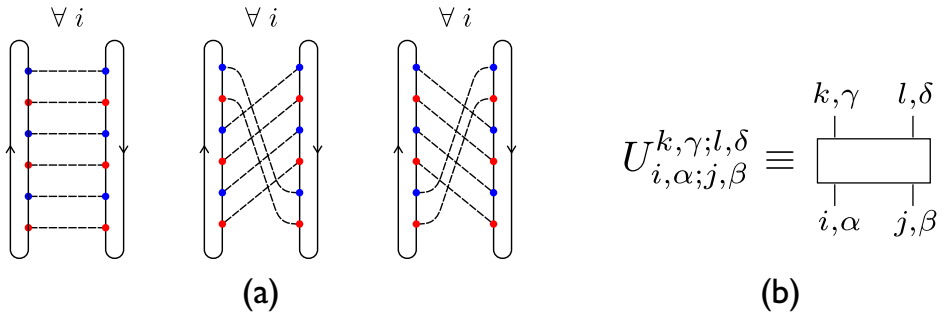

Figure 5.10: (a): The three leading diagrams of $K(t)$ at $t = 3$ in the large-q limit [187]. For each diagram, every site i takes the *same* configuration. (b): The diagrammatical representation of $U^{k,\gamma;l\delta}_{i,\alpha;j,\beta}$, where the Roman [Greek] indices correspond to color [spin] degrees of freedom.

As in the case without auxiliary spin 1/2 degrees of freedom, the evaluation of the ensemble average in Eq. (5.5.1), which defines the restricted spectral form factor, $K(t,s)$, amounts to generating all diagrams by pairing unitary gates with their Hermitian conjugates at each bond, as schematically illustrated in Figs. 5.7 and 5.10a. As $q \to \infty$, the leading contributions come from t diagrams, each of which has an identical 'cyclical' pairing at all sites [187]. These t diagrams are 'Gaussian', in the sense that they can be evaluated using the Wick contraction of a random unitary and its conjugate (Fig. 5.10b),

$$\begin{aligned} \overline{U^{k,\alpha;l,\alpha}_{i,\alpha;j,\alpha} U^{*\,k',\alpha;l',\alpha}_{i',\alpha;j',\alpha}} &= \frac{1}{q^2}\delta_{i,i'}\delta_{j,j'}\delta_{k,k'}\delta_{l,l'} \\ \overline{U^{k,\alpha;l,\beta}_{i,\alpha;j,\beta} U^{*\,k',\alpha;l',\beta}_{i',\alpha;j',\beta}} &= \frac{1}{2q^2}\delta_{i,i'}\delta_{j,j'}\delta_{k,k'}\delta_{l,l'} \qquad \text{if } \alpha \neq \beta \end{aligned} \quad , \tag{5.5.2}$$

where Roman [Greek] indices correspond to color [spin] degrees of freedom, in an extension of Eq. (5.4.2). Using Eq. (5.5.2), we translate each of these t diagrams into an algebraic term by summing over the color and spin degrees of freedom.

The sum over the "color" degrees of freedom will cancel out all factors of q that appear in Eq. (5.5.2), as seen in Sec. 5.4 [187]. This leaves a sum over the spin degrees of freedom, subject to the constraint $S^z = \sum_{j=1}^{L} \hat{\sigma}^z_j = s\,L$. Observe that the choice of spin degrees of freedom in $\hat{W}$ fixes

those in $\hat{W}^\dagger$ due to Eq. (5.5.2). Consequently, the sum over configurations of the spins 1/2 can be computed by enumerating all possible ways to assign spins in the diagrammatic representation of $\underset{s}{\mathrm{Tr}}[\hat{W}]$—as illustrated in Fig. 5.11—such that (i) the global magnetization satisfies $S^z = Ls$ along any horizontal fixed-time slice of the diagram, and (ii) the local magnetization $S^z_{j,j+1} \equiv \hat{\sigma}^z_j + \hat{\sigma}^z_{j+1}$ is preserved across each two-site gate.

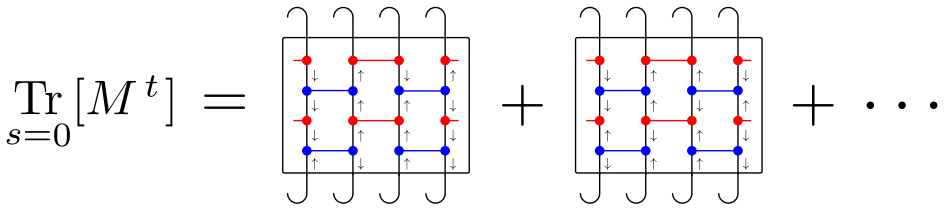

Figure 5.11: The sum over spins can be computed by finding all possible configurations of the spins 1/2 allowed in the diagrammatic representation of $\underset{s}{\mathrm{Tr}}[\hat{W}]$, such that the global magnetization satisfies $S^z = sL$ ($s = 0$ as depicted above), and the local magnetization is conserved by each gate.

This allows for the sum over spins to be reproduced by an equivalent expression,

$$\lim_{q\to\infty} K(t,s) = |t|\,\underset{s}{\mathrm{Tr}}[\hat{M}^t]\,, \tag{5.5.3}$$

where the factor of $|t|$ comes from there being t such leading diagrams. The trace over the *effective* spin-1/2 evolution operator, $\hat{M}$, accounts for the sum over the color and spin degrees of freedom in a given leading diagram. Like $\hat{W}$, $\hat{M} \equiv \hat{M}_2 \cdot \hat{M}_1$ consists of two layers: $\hat{M}_1 = \hat{\mathbb{T}}_{1,2} \otimes \hat{\mathbb{T}}_{3,4} \otimes \ldots$ and $\hat{M}_2 = \hat{\mathbb{T}}_{2,3} \otimes \hat{\mathbb{T}}_{4,5} \otimes \ldots$, as depicted in Fig. 5.12. $\hat{M}$ is hermitian, owing to contraction of a unitary and its conjugate, and is invariant under a shift by two sites due to ensemble averaging. The matrix $\hat{\mathbb{T}}_{j,j'}$ acts only on sites j, j' as

$$\hat{\mathbb{T}}_{j,j'} = \frac{1}{2}(\hat{\mathbb{1}}_{j,j'} + \hat{\mathbb{P}}_{j,j'}) = \begin{pmatrix} 1 & 0 & 0 & 0 \\ 0 & 1/2 & 1/2 & 0 \\ 0 & 1/2 & 1/2 & 0 \\ 0 & 0 & 0 & 1 \end{pmatrix}, \tag{5.5.4}$$

where the factor of $\frac{1}{2}$ in $\hat{\mathbb{T}}_{j,j'}$ originates from the $\frac{1}{2q^2}$ term in Eq. (5.5.2), and the "swap operator," $\hat{\mathbb{P}}$ is given by

$$\hat{\mathbb{P}}_{j,j'} = \frac{1}{2}(\hat{\mathbb{1}}_{j,j'} + \vec{\sigma}_j \cdot \vec{\sigma}_{j'})\ . \tag{5.5.5}$$

We note that $\hat{M}$ describes a discrete-time symmetric simple exclusion process (SSEP) for a classical lattice gas [40]. Although the original FRUC featured a $U(1)$ symmetry, after Haar averaging and taking $q \to \infty$, $K(t,s)$ exhibits an enlarged $SU(2)$ invariance in the remaining spin-1/2 variables; we believe this is specific to the large-q limit. Additionally, as we clarify below, $\hat{M}$ belongs to a family of commuting transfer matrices, unveiling an emergent integrability, and the possibility of computing $K(t,s)$ exactly [38].

This model leads to a Thouless time that scales diffusively. To see this, note that

$$\hat{\mathbb{T}}_{j,j+1} \equiv \hat{\hat{\mathbb{1}}}_{j,j+1} - \hat{\mathbb{H}}_{j,j+1}\ , \tag{5.5.6}$$

where the two-site "Hamiltonian term,"

$$\hat{\mathbb{H}}_{j,j+1} = -\frac{1}{4}(\vec{\sigma}_j \cdot \vec{\sigma}_{j+1} - \hat{\hat{\mathbb{1}}}_{j,j+1})\ , \tag{5.5.7}$$

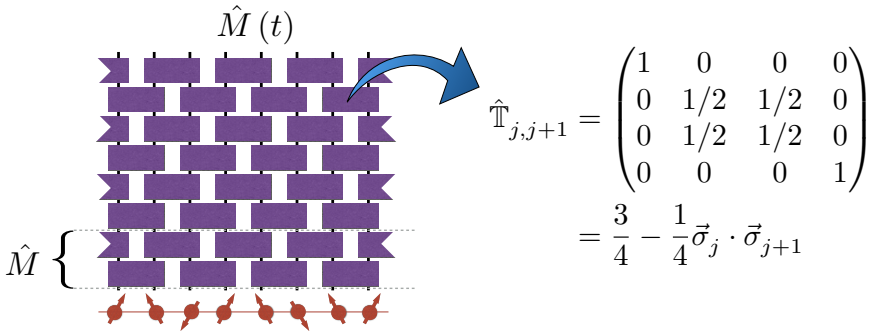

Figure 5.12: Figure 2.4 from Ch. 2 included here for convenience. On the left is a depiction of the brick-wall circuit geometry corresponding to the Trotterized XXX "evolution" operator, $\hat{M}$. On the right are the individual two-site gates, $\hat{\mathbb{T}}_{j,j+1}$, which comprise the circuit, expressed in terms of $\hat{H}_{j,j+1}$, which is the local two-site term that appears in the Heisenberg XXX Hamiltonian in Eq. (2.2.1) in Ch. 2.

describes the spin 1/2 Heisenberg ferromagnet, i.e. the XXX model discussed in Ch. 2. Thus, we can interpret $\mathrm{Tr}[\hat{M}^t]$ in Eq. (5.5.3) as a Trotterization of the partition function of the XXX model at inverse temperature $\beta = t$, i.e.

$$\operatorname*{Tr}_s [\hat{M}^t] \simeq \operatorname*{Tr}_s [e^{-tH_{\mathrm{XXX}}}] \ , \quad \text{with} \quad H_{\mathrm{XXX}} = \sum_j \hat{\mathbb{H}}_{j,j+1} \ . \tag{5.5.8}$$

Hence, the behavior of $K(t,s)$ at late times reflects the low-temperature properties of the Heisenberg ferromagnet, H_{XXX}, which has $(L+1)$-fold degenerate ground states with vanishing energy. Each S^z sector has a unique ground state, $|S\rangle \equiv (\hat{S}^-)^{N_\downarrow}|\uparrow \ldots \uparrow\rangle$ with $\hat{S}^\pm \equiv \sum_j \hat{\sigma}_j^\pm$ and $N_\downarrow = L/2 - S = L\,(1/2 - s)$. Low-lying excitations above each $|S\rangle$ are *magnons*, i.e. plane-wave superpositions of spin flips

$$|S,k\rangle = \frac{1}{\sqrt{L}} \sum_{j=1}^{L} e^{ijk} \hat{\sigma}_j^- |S+1\rangle \ , \quad k = \frac{2\pi p}{L} \ , \tag{5.5.9}$$

characterized by a quadratic dispersion relation $\varepsilon(k) \propto k^2$ at small k. Expanding in $t \gg L^2$, one expects only the lowest energy magnon contributes and

$$\lim_{q\to\infty} K(t,s) \underset{t\gg L^2}{=} |t| \left(1 + e^{-\frac{4\pi^2 t}{L^2}} + \ldots \right) . \tag{5.5.10}$$

This suggests diffusive scaling of the Thouless time, $t_{\mathrm{Th}} \propto L^2$; a similar correspondence with H_{XXX} was established in [193] for random unitary circuits with a conserved density, lending support for the generality of this result. However, to investigate the regime $1 \ll t \ll L^2$, we must consider states with extensive numbers of magnons, and many-body effects.

5.5.4 Solution via integrability

Many of the details of this calculation can be found in Ch. 2, where the model of interest to the analysis of Eq. (5.5.3) is the "Trotterized XXX" model, which can be studied using Bethe Ansatz techniques. The computation of $\mathrm{Tr}_s[\hat{M}^t]$ would be simplified by knowledge of the full eigenspectrum of $\hat{M}$. Following the *coordinate Bethe Ansatz* for H_{XXX} [41, 42], one seeks multi-magnon eigenfunctions, i.e. plane-waves, along with a scattering matrix describing the exchange

of the excitations' momenta. However, this approach suffers from technical complications due to the circuit construction of $\hat{M}$. A more direct approach is instead based on the equivalent *algebraic Bethe Ansatz* formulation [44], detailed in Sec. 2.3 of Ch. 2.

The result of that calculation is the dispersion relation for $\hat{M}$, given by

$$\varepsilon(\lambda) \equiv -2 \ln \cos k(\lambda). \tag{5.5.11}$$

At small k, a quadratic dispersion relation is recovered, $\varepsilon \to k^2$, as is expected since the discrepancies between $\hat{M}^t$ and $e^{-tH_{\mathrm{XXX}}}$ become irrelevant at long wavelengths. However, it is worth noting that the coefficient of the dispersion is markedly different in these two cases, and the exact dispersion should be used. Although knowledge of the dispersion and the quantization conditions of the allowed momenta, k, simplify substantially the evaluation of Eq. (5.5.3), the main bottleneck remains the exponential growth in L of the Hilbert space dimension, and the difficulty in solving the Bethe Ansatz equations that constrain the allowed momentum values.

However, in the thermodynamic limit $L, S \to \infty$ with $s = S/L$ fixed, the solutions of the Bethe Ansatz equations acquire a simple structure, as explained in Sec. 2.4 of Ch. 2. Using the thermodynamic Bethe Ansatz formalism, as detailed in Sec. 2.4, we can compute a quantity analogous to the free energy of the Trotterized partition function, from which the relevant scaling properties can be extracted.

5.5.5 Scaling form

We define the function

$$\phi(t, s) = -\lim_{L \to \infty} L^{-1} \ln \left[K(t, s) / |t| \right] \ , \tag{5.5.12}$$

which can be computed exactly for any integer t, either by solving an infinite set of coupled integral equations—i.e. the Thermodynamic Bethe Ansatz (TBA) [45, 47]—or, perhaps more efficiently, via the 'quantum transfer matrix method' [199, 200], which requires the solution of an algebraic equation in $2|t|$ variables (see also Appendix A). While the latter is better suited to calculating $K(t)$ at a *particular* time t, the former affords analytic insight into behavior at large times. Since the limit $L \to \infty$ implies $t_{\mathrm{Heis}} \to \infty$, we expand Eq. (5.5.12) about large t using TBA,

$$\phi(t, s) = -\frac{C}{\sqrt{t}} + \frac{1}{2(2s+1)t} + \dots \ , \tag{5.5.13}$$

where the constant $C = \zeta(3/2)/\sqrt{4\pi}$, where $\zeta(z)$ is the Riemann Zeta function, and $q \to \infty$ is taken implicitly. Ignoring the Trotterized structure of $\hat{M}$ and taking $\hat{M} \sim e^{-H_{\mathrm{XXX}}}$ relates Eq. (5.5.13) to the low-temperature expansion of the specific heat close to the ferromagnetic ground state of H_{XXX} [201, 202].

The form of Eq. (5.5.13) implies diffusive scaling even for $t \ll DL^2$. From the behavior $\phi(t, s) \sim (Dt)^{-1/2}$ it is apparent that the value of D is independent of s, a consequence of the emergent $SU(2)$ symmetry at $q \to \infty$. However, the scaling limit relevant for $K(t)$ in the regime $1 \ll t \lesssim t_{\mathrm{Th}}$ is *distinct* from that recovered from TBA, i.e. Eq. (5.5.13): the former requires $t, L \to \infty$ with $x \equiv t/L^2$ *fixed*, while the latter requires the thermodynamic limit $L \to \infty$ at fixed t. Nevertheless, these results suggest a scaling form

$$\lim_{t, L \to \infty} \ln \left[K(t, s)/t \right] = \kappa(x, s) \ . \tag{5.5.14}$$

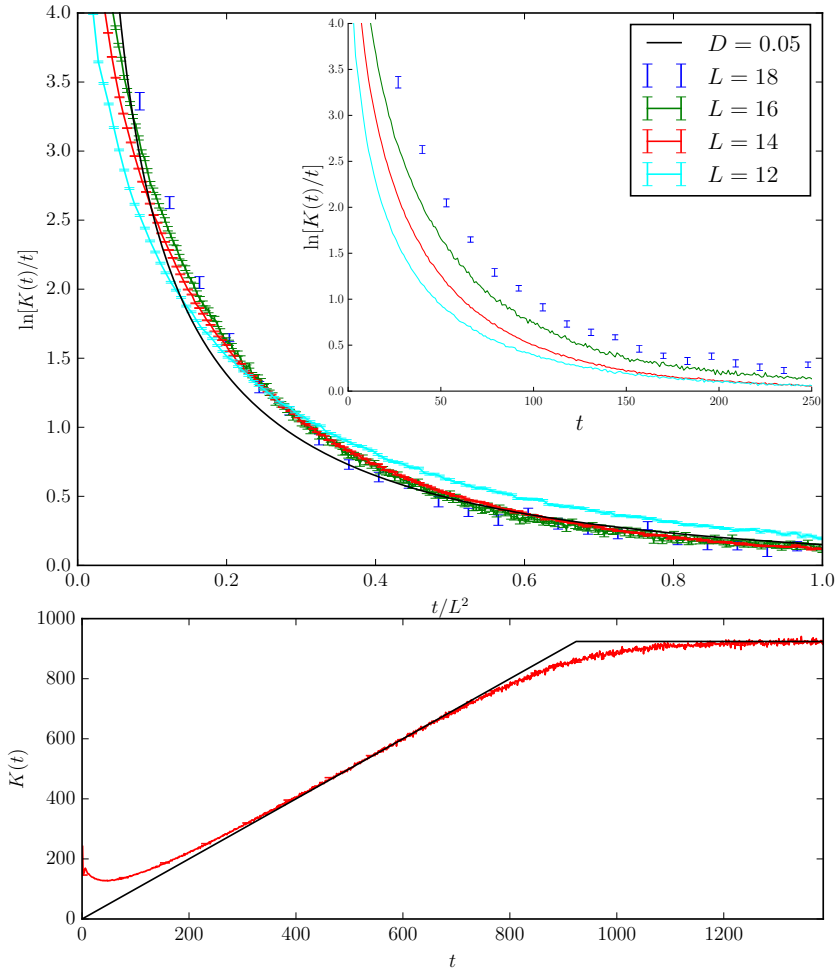

Figure 5.13: Behavior of $K(t)$. Upper figure (main panel): $\ln K\,(t)\,/t$ vs t/L^2. The scaling collapse of data for $L = 14$, 16, and 18 indicates that the Thouless time $t_{\rm Th}$ is controlled by diffusion; small deviations for $L = 12$ are presumably a finite-size effect. The full line is a fit to the scaling function given by Eq. (5.5.16) with $D = 0.05$. Inset: same data vs t for comparison. Lower panel: $K(t)$ for $L = 12$; the small system size narrows the relative extent of the ramp regime $K(t) = t$, highlighting the short-time, pre-RMT behavior.

Despite the inherent integrability, exact calculation of $\kappa(x,s)$ is a challenging task. Nevertheless, its asymptotic behavior can be read off from Eq. (5.5.10) and Eq. (5.5.13): for early times ($x \ll 1$) one inserts Eq. (5.5.12) into Eq. (5.5.13); for late times ($x \gg 1$) one expands the logarithm on the righthand side of Eq. (5.5.10). Thus

$$\kappa(x,s) \underset{x\ll 1}{\sim} Cx^{-1/2} \quad \text{and} \quad \kappa(x,s) \underset{x\gg 1}{\sim} e^{-4\pi^2 x}\,. \tag{5.5.15}$$

By treating the magnons as noninteracting bosons, using $\mathrm{Tr}[\hat{M}^{\,t}\,] \approx \mathrm{Tr}[e^{-tH}]$, we recover

$$\kappa\,(x,s) = -\sum_{n\neq 0} \ln\left[1 - e^{-xD(2\pi n)^2}\right]\,, \tag{5.5.16}$$

which precisely agrees with Eq. (5.5.15) if one uses the diffusion constant $D = 1$ associated to the true dispersion, Eq. (5.5.11), at small k. Although these predictions are obtained for $q \to \infty$, we

expect their qualitative features to be valid for generic chaotic many-body systems with conserved charges. More details are provided in Appendix A.

5.5.6 Numerical evidence

We now turn to numerical simulation to test Eq. (5.5.14) in chaotic quantum systems at finite q. At $q = 1$, the FRUC considered above exhibits a numerically small diffusion constant that makes it difficult to avoid finite-size effects at the accessible values of L. Instead, we use a model adapted from [189], defined by

$$\hat{W} = e^{-it_4\hat{H}_4}e^{-it_3\hat{H}_3}e^{-it_2\hat{H}_2}e^{-it_1\hat{H}_1}, \tag{5.5.17}$$

where

$$\begin{aligned}\hat{H}_1 &= \sum_j \left(J_z^1\,\hat{\sigma}_j^z\hat{\sigma}_{j+1}^z + h_j^1\,\hat{\sigma}_j^z\right)\\ \hat{H}_3 &= \sum_j \left(J_z^2\,\hat{\sigma}_j^z\hat{\sigma}_{j+2}^z + h_j^2\,\hat{\sigma}_j^z\right)\\ \hat{H}_2 &= \hat{H}_4 = J_{xy}\sum_j \left(\hat{\sigma}_j^x\hat{\sigma}_{j+1}^x + \hat{\sigma}_j^y\hat{\sigma}_{j+1}^y\right),\end{aligned} \tag{5.5.18}$$

with periodic boundary conditions. We take $J_z^1 = \left(\sqrt{3}+5\right)/6$, $J_z^2 = \sqrt{5}/2$, and $J_{xy} = \left(2\sqrt{3}+3\right)/7$, with $h_n^{1,2}$ drawn independently from the uniform distribution $[-1.0, 1.0]$ for ensemble averaging. We choose $t_1 = 0.4$, $t_2 = 0.1$, $t_3 = 0.3$, and $t_4 = 0.2$ to avoid time-reversal symmetry around any instant in the period (we check that nearest-neighbor level statistics are CUE). In contrast to a recent study [203], we did not investigate $K(t)$ at strong disorder, as our concern is with the behavior of ergodic systems.

5.5.7 Discussion

We have presented analytical and numerical evidence showing the significance of the Thouless time $t_{\text{Th}} = L^2/D$ for spectral correlations in systems with a conserved charge. These results are consistent with a scaling form $K(t) \sim |t|\exp\left[\kappa(t/L^2)\right]$. We believe this form to be generic in describing the onset of chaos in quantum systems with a conserved quantity. We also provide a form, Eq. (5.5.16), of the scaling function, κ, defined in Eq. (5.5.14), by neglecting the interactions between magnons in our FRUC, which is in good agreement with our numerical simulations. The question of the exactness and universality of Eq. (5.5.16) is an interesting topic for future study.

5.6 Summary and Outlook

In summary, we have demonstrated how one can use random unitary evolution to study quantum thermalization away from the limit of integrability, i.e. quantum chaos. This technique draws from the fact that thermal systems should have the properties of an ensemble of similar systems, captured by random matrices, along with particular ingredients, such as the Haar measure and diagrammatic averaging, which provide analytic control. Particularly, we have seen how evolving under a random unitary *circuit*—which enforces locality—gives rise to specific and expected results relating to the dynamical spread of quantum information, e.g. the spreading of entanglement and information about generic operators. Although for certain quantum models it is possible to define

sensible Lyapunov exponents, the results discussed above provide a more generic notion of quantum chaos, e.g., as distinct from athermal and/or integrable quantum systems.

Additionally, we note that early work using this technique sought to probe minimal models of many-body quantum chaos, i.e. those without symmetries, and notion of quasiparticles, or other nongeneric features. However, subsequent works have shown that one can systematically include such ingredients into circuits of interest to probe more particular and even—in the cases of circuits with conserved quantities—more generic systems. However, it remains to be seen how much more utility can be extracted from the use of circuits. The primary advantage of using circuits is the ability to study the thermodynamic limit and still recover analytical results. Often times, this is facilitated via a "classical" expansion, i.e. large q. In such cases, much of the quantumness of a true system is essentially overlooked, and the results correspond only to the most chaotic of systems, with typical systems showing less chaos (i.e., slower scrambling times, slower propagation of information, and so on).

However, in some cases, e.g. the spectral form factor calculation in the presence of conserved quantities, this can actually work out quite well. Referring to the latter case, discussed in detail in Sec. 5.5, the calculation of the spectral form factor is generally only tractable at very short times, or in the limit $q \to \infty$. In general, it is not even possible to enumerate all terms that recover at first order in $1/q$. The SFF is then diagnosed in several limits, though in the thermodynamic limit, it remains possible to recover answers in most regimes. Despite the use of $q, L, t \to \infty$, the analytic prediction of the circuit calculation is in remarkably good agreement with numerical data corresponding to the opposite: $q = 1, L \lesssim 18, t \gtrsim 1$. Additionally, by approximating the magnons of the resulting spin-1/2 calculation as free bosons with the same dispersion—expanded to lowest order in momentum—we recovered a scaling function that interpolates precisely between the two limiting forms recovered from the exact calculation. More surprisingly, this same function displays excellent agreement with numerical data for small systems, merely by taking the coefficient of the ballistic dispersion, $\varepsilon(k) = Dk^2$, to be a free parameter. Understanding why this free boson calculation is so effective remains an open question for future work [43].

One possibly interesting direction for future research, currently underway by this author, is the consideration of spectral properties (i.e. $K(t)$) in models with kinetic constraints. These systems are generally expected to be less chaotic than conventional systems, and their classical counterparts are used to model dynamics in nonergodic classical glasses. At the level of the circuits, there is little distinction between a symmetry and a constraint: in fact, the $U(1)$ conserving circuit can also be regarded as encoding the constraint of simple exclusion, i.e. that no two magnons (spin flips) can occupy the same site. In the $U(1)$ case, we found that $K(t) = t\,\mathrm{Tr}\,[\hat{M}^t]$, where $\hat{M}$ encodes a symmetric simple exclusion process. Viewing the $U(1)$ conservation of the z-component of spin in each two-site gate as a constraint, rather than the local enforcement of a global symmetry, we note that putting in the constraint of symmetric simple exclusion in the quantum circuit leads to a form of $K(t)$ that is directly related to the sum of return probabilities in the classical circuit with the *same* constraint. This property will extend to generic constraints that one may wish to put in the circuit, which leads to surprising results. For example, the nonconserving East circuit results in $K(t) = t\,\mathrm{Tr}\,[\hat{M}^t]$, with $\hat{M}$ a Trotterized classical East circuit. At late times, K is dominated by the gap between the trivial eigenstate of $\hat{M}$ with eigenvalue unity, and the lowest excited state. For the classical East model, this is known to scale as L^-2, corresponding to *diffusion*. However, there is no obvious local conserved quantity to be diffused. For models with both symmetries and constraints, we find subdiffusion. This same method may be applied to circuits with dipole symmetries, building off recent work [204] to analyze fracton models. From the above, absent degeneracies and other complications, one generally expects diffusion or subdiffusion.

In particular, this anomalous diffusion is likely associated to symmetry-like objects that can be identified in constrained systems, which was recently the subject of Ref. 204.

Chapter 6

Order in Non-Equilibrium Phases

6.1 Introduction

One of the interesting properties of MBL is its ability to support quantum orders at energy densities corresponding to large or infinite temperatures, among other phenomena that are forbidden in equilibrium systems. One useful view on MBL phases is that highly excited states of MBL systems have many properties of ground states of equilibrium systems, e.g. in terms of the protection of quantum information.

6.2 Localization-Protected Order

The simplest model that hosts localization-protected quantum order in its excited state phase structure is essentially the transverse field Ising model [205]. This is the same model that gives the simplest picture of quantum order in the equilibrium setting. To extend this model to the nonequilibrium setting, we consider the Hamiltonian

$$\hat{H}_{\text{Ising}} = -\sum_j \left(J_j \hat{Z}_j \hat{Z}_{j+1} + h_j \hat{X}_j + J'_j \left(\hat{Z}_j \hat{Z}_{j+2} + \hat{X}_j \hat{X}_{j+1} \right) \right) , \tag{6.2.1}$$

where the J'_j terms are self-dual and destroy the mapping of the first two terms (the standard Ising/Kitaev chain) to spinless free fermions (a p-wave superconductor). Additionally, each coupling is an independently drawn random number from the interval $(0, W]$ with $W > 0$ characterizing overall disorder strength, although we also should regard these couplings as having a knob that tunes the strength of the interactions, i.e. $\{J'_j\}$. Note that these couplings should be drawn from different distributions on the aforementioned interval.

In equilibrium and at zero temperature, the "clean" version of the Hamiltonian given in Eq. (6.2.1) (i.e. $J_i = J$, $h_i = h$, and $J'_i = J$), exhibits a well known quantum phase transition of the equilibrium variety (i.e. in the ground state) between a $J \gg h$ ferromagnet (FM) with a pair of degenerate ground states and $J \ll h$ paramagnet (PM) with a unique ground state. Mapping the model to fermions via Jordan-Wigner, the FM (PM) phase corresponds to a topological (trivial) phase with (without) zero-energy Majorana edge modes. As one moves to finite temperature, $T > 0$, the excitations above the ground state play a role: In the FM phase, these excitations are *domain walls* between the two degenerate ground states. The choice of clean couplings ensures translation invariance, which allows the domain walls to move freely across the system with no additional energy penalty. Thus, at any finite temperature, the penalty of creating domain walls

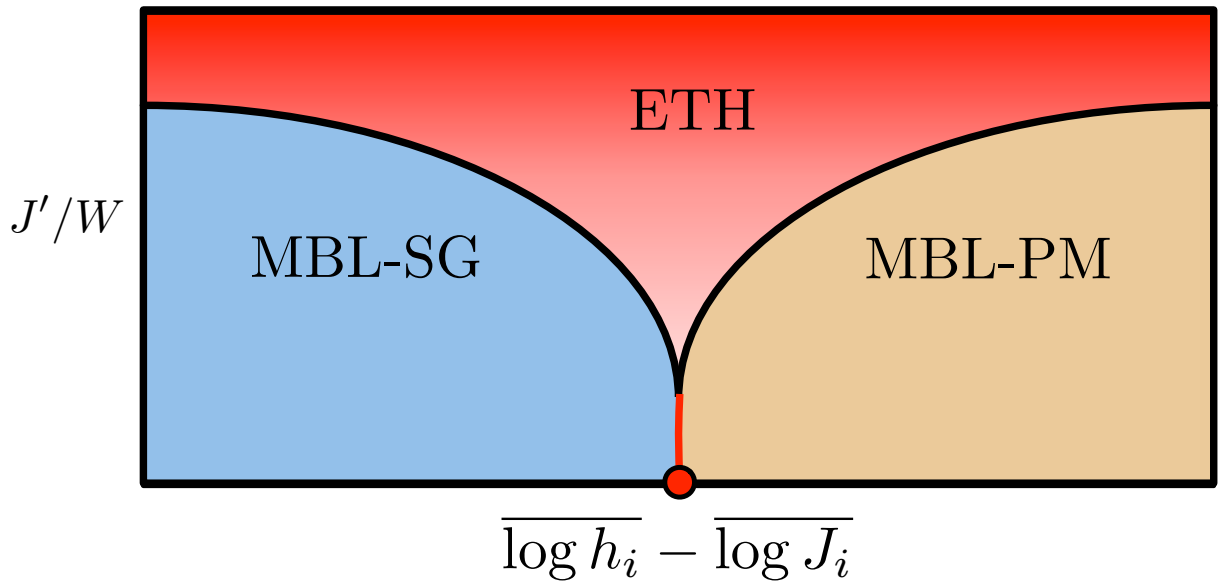

Figure 6.1: Nonequilibrium, eigenstate phase diagram for the modified Ising chain given by Eq. (6.2.1). A similar figure appears in Ref. 205. The eigenstates in the "Spin Glass" (SG) MBL phase are "cat states," i.e., macroscopic superposition of two different states that are related by the *global* $\mathbb{Z}_2$ symmetry operator, $\prod_j \hat{X}_j$. The eigenstates in the "paramagnet" (PM) MBL phase have the structure of simple products of eigenvalues of the *local* $\mathbb{Z}_2$ symmetry operator, $\hat{X}_j$. The thermal phase (ETH) is symmetry-preserving, and therefore a standard paramagnet. Note that the real space renormalization group for excited states (RSRG-X) predicts a direct transition between the MBL-PM and MBL-SG phases, separated by an infinite-randomness critical point (at the self-dual point). It is unclear if a direct transition between two MBL phases with different symmetries can exist at finite disorder; thus, a red line separates these phases at strong but finite disorder.

can be afforded by the system, and the domain walls sweep through the system with no energy penalty, destroying the order. Thus, in equilibrium and at finite temperature, the translation-invariant Ising chain has a crossover—rather than a transition—as the ratio h/J is tuned across the putative critical value from $T = 0$.

In the limit of strong disorder, W, or weak interactions, $\{J_j'\}$, the system can realize an MBL phase, as described in Ch. 1. When the system is in the MBL phase, the domain wall excitations on the ferromagnetic side are *pinned* (i.e. localized) by disorder, even when the density of such excitations is appreciably greater than zero. By mapping the problem to Majoranas, both single spin flips and domain walls are characterized by Majorana bilinears: the pinning of domain walls therefore amounts to localization of a finite density of quasiparticle excitations. For strong disorder, when the *typical* bond strength, $\overline{\log J_j}$, is large compared to the typical field strength, $\overline{\log h_j}$, the system is said to have "spin glass order" [15, 206, 207], which is analogous to the ferromagnetic phase of clean, equilibrium systems, in that the object $\langle \hat{Z}_i \hat{Z}_j \rangle \neq 0$, even as $|i - j| \to \infty$. However, in contrast to the homogeneous, low-temperature, equilibrium counterpart, not all spins or domains will be aligned, and although the z component of distant spins ought to be correlated, they can be antialigned, e.g., resulting in an algebraic sign that depends on i and j. However, it is nonetheless the case that the spins are effectively "frozen" in some configuration, defined along the z axis, which depends on the eigenstate in question. Hence, it is typical to define an order parameter that is the square of the above quantity, summed over sites, averaged over eigenstates, and appropriate

normalized, as will be done in Secs. 6.4 and 6.5.

In the opposite limit of bond strength relative field strength, i.e. $\overline{\log J_j} \ll \overline{\log h_j}$, the system can still realize an MBL phase for sufficiently strong disorder. However, in this limit there is no spin-glass order, e.g. as measured by correlations of the above-described form: rather, this limit realizes an MBL *paramagnet*. In terms of Majoranas, compared to the spin glass phase, in the paramagnet spin flips are localized; the spin-flip is also a Majorana bilinear defined on the dual sites, and the spin-flip excitation is dual to the domain wall. An interesting fact is that, for sufficiently strong disorder, both the spin glass and paramagnet appear to exist across the entire eigenspectrum, as one varies the relative strengths of typical bonds and fields, and both phases have been verified numerically [207].

By decreasing the strength of disorder or increasing the strength of interactions, one finds a delocalization transition from the MBL phase to a thermal phase in which only the paramagnet seems to survive. Thus, the spin glass phase is said to be "protected" by localization; this phenomenon is referred to as "localization-protected order" [15]. The [eigenstate] phase diagram for the Hamiltonian given in Eq. (6.2.1) is sketched in Fig. 6.1. It remains unsettled whether or not there is a direct transition from the MBL paramagnet to the MBL spin glass, or if instead there is an intervening thermal phase that is not visible in small-systems numerics or using infinite-disorder techniques [9, 15, 208]. Studies employing the latter technique seem to find evidence that such transitions exist, at least at infinite disorder—to which these methods flow asymptotically—[31, 206, 208–213]; however, there are reasons to suspect that such transitions are not possible for systems with finite disorder in the thermodynamic limit [9]. Additionally, there are indications that the transition (or crossover) between the MBL paramagnet and spin glass is governed by an infinite-randomness fixed point, which arises naturally in the setting of strong-disorder (or real space) renormalization group methods [32, 33, 205, 213, 214].

6.3 Disordered Clock Models

6.3.1 Introduction

The $\mathbb{Z}_2$ Ising model has a special place amongst lattice spin models because it lies at the intersection between standard spin-1/2 models (and by extension models of q-bits and spinless fermions), and $\mathbb{Z}_n$ clock models, models with onsite dihedral symmetry, D_n, and S_n Potts models. The latter three are related, and reduce to the same model for $n = 2$. The spin s models have local Hilbert space dimension $d = 2s + 1$, and $d = n$ for the $\mathbb{Z}_n$, D_n, and S_n models. In each case, there is an operator associated with measurement, and is typically expressed as a diagonal operator in the local basis: this is typically denoted $\hat{S}^z$ for general spin models, and $\hat{\sigma}^z$ or $\hat{Z}$ for spin 1/2; for the clock and Potts models, this is simply denoted $\hat{sigma}$ by convention. Additionally, there exist operators that shift or 'cycle' through the states: for general spin models these are raising and lowering operators $\hat{S}^{\pm}$, and for spin 1/2 one can also define the spin flip operator $\hat{\sigma}^x = \hat{X} = \hat{\sigma}^+ + \hat{\sigma}^-$; in the clock-type models the cycle operators are denoted $\hat{\tau}$ and $\hat{\tau}^\dagger$. In the special case of $n = 2$, one has $\hat{Z} = \hat{\sigma}$ and $\hat{X} = \hat{\tau} = \hat{\tau}^\dagger$, since $\hat{\tau}^2 = \hat{\mathbb{1}}$.

A key distinction is that there is a "highest" state in a spin model that is annihilated by the raising operator, given by $|+s\rangle$ in the $\hat{S}^z$ basis, along with a lowest state that is annihilated by the lowering operator, given by $|-s\rangle$ in the $\hat{S}^z$ basis. However, the key feature of clock models is that their raising and lowing operators are *cyclic*, much like the hands on a clock: the raising operator $\hat{\tau}$ acts on the highest state under the weight operator, $\hat{\sigma}$, by cycling it around the "clock" back to

the lowest state. For an n state clock or Potts model, one has $|n\rangle = |0\rangle$, and all related quantities are only defined modulo n.

6.3.2 The generic $\mathbb{Z}_n$ model

It is convenient to define the nth root of unity,

$$\omega = \exp\left(\frac{2\pi i}{n}\right) \tag{6.3.1}$$

to streamline notation. The default basis corresponds to the on-site eigenstates of the weight operator, $\hat{\sigma}_j$:

$$\hat{\sigma}|m\rangle = \omega^m|m\rangle \ , \quad \hat{\sigma}^\dagger|m\rangle = \omega^{-m}|m\rangle \ , \quad \hat{\sigma}^n = (\hat{\sigma}^\dagger)^n = \hat{\mathbb{1}} \ , \quad \hat{\sigma}^\dagger = \hat{\sigma}^{n-1} \tag{6.3.2}$$

$$\hat{\tau}|m\rangle = |m+1\rangle \ , \quad \hat{\tau}^\dagger|m\rangle = |m-1\rangle \ , \quad \hat{\tau}^n = (\hat{\tau}^\dagger)^n = \hat{\mathbb{1}} \ , \quad \hat{\tau}^\dagger = \hat{\tau}^{n-1} \tag{6.3.3}$$

These two operators do not have a straightforward [anti-]commutation relation, only the multiplication rule:

$$\hat{\sigma}\hat{\tau} = \omega\hat{\tau}\hat{\sigma}. \tag{6.3.4}$$

The three remaining relations are easy to find:

$$\hat{\sigma}^\dagger\hat{\tau}^\dagger = \omega\hat{\tau}^\dagger\hat{\sigma}^\dagger \ , \quad \hat{\sigma}\hat{\tau}^\dagger = \omega^{-1}\hat{\tau}^\dagger\hat{\sigma} \ , \quad \hat{\sigma}^\dagger\hat{\tau} = \omega^{-1}\hat{\tau}\hat{\sigma}^\dagger \tag{6.3.5}$$

The shift and weight operators are dual to one another: in the basis of eigenstates of the shift operators $\hat{\tau}_j$, the weight operator ω_j acts by shifting $\hat{\tau}$ states. We will denote eigenstates of the shift operator $\hat{\tau}$ by $|q\rangle$, defined via

$$|q\rangle = \frac{1}{\sqrt{n}}\sum_m \omega^{-qm}|m\rangle \tag{6.3.6}$$

$$\hat{\tau}|q\rangle = \omega^q|q\rangle \tag{6.3.7}$$

$$\hat{\sigma}|q\rangle = |q-1\rangle \tag{6.3.8}$$

Generic Hamiltonians with $\mathbb{Z}_n$ symmetry feature two types of terms, which are dual to one another, as in the $n = 2$ Ising model. The first is the nearest-neighbor interaction term—or "topological" term—which compares the states of neighboring sites j, $j+1$ in the $\hat{\sigma}$ basis,

$$\hat{H}_{\text{top}} = -J\sum_{j=1}^{L-1}\sum_{m=1}^{n-1} a_m\left(\hat{\sigma}_j^\dagger\hat{\sigma}_{j+1}\right)^m, \tag{6.3.9}$$

with the condition

$$a_{n-m} = a_m^* \ , \tag{6.3.10}$$

for Hermiticity. Note that if n is even, $a_{n/2}$ must be purely real.

The other term is the "transverse field" or "trivial" (i.e. non-topological) term,

$$\hat{H}_{\text{triv}} = -f\sum_{j=1}^{L-1}\sum_{m=1}^{n-1} b_m\left(\hat{\tau}_j\right)^m, \tag{6.3.11}$$

where $b_{n-m} = b_m^*$ for Hermiticity.

The above describes "clean" systems without spatial disorder, but generally we will be interested in the case in which all of the above coefficients vary from site to site, and we can dispense with the overall sign without loss of generality. Additionally, by further constraining the coefficients $a_{m,j}$ and $b_{m,j}$, for $n > 2$ the symmetry can be enlarged: the dihedral group

$$D_n = \mathbb{Z}_n \rtimes \mathbb{Z}_2 \ , \tag{6.3.12}$$

corresponding to the dihedral symmetries of regular n-sided polygons, where the $\mathbb{Z}_n$ discrete rotation and the "chiral" $\mathbb{Z}_2$ reflection symmetry do not commute, or the permutation group S_n, which includes the cyclic group $\mathbb{Z}_n$ as a proper subset, and where $S_2 = \mathbb{Z}_2$, $S_3 = D_3 = \mathbb{Z}_3 \rtimes \mathbb{Z}_2$, and for $n > 2$ is non-Abelian and finite, consisting of all cycles and permutations of n objects. The Potts model arises if all coefficients a are equal to one another (for a given bond), and the same for b (for a given site).

In a sense, the clock models are "chiral" Potts models. Additionally, it is likely possible to realize more complicated on-site symmetries in models with larger n. The $n = 3$ Potts model is of particular interest because S_3 is the smallest finite non-Abelian group. All of the models described above have the property that they are self-dual.

We can exchange the measurement and cycle operators for a description in terms of "parafermion" operators, which extend the construct of the Majorana fermion used to understand the Ising model. The local Hilbert space of each site is represented by two parafermion modes. The on-site cycle operator is a bilinear involving the two modes on the same site, and the nearest-neighbor interaction term is also a bilinear consists of the two parafermions joined by the link (one from each site). These two parafermion types can be thought of as a single type of parafermion that lives on a lattice with twice as many sites as the original model. In this case the Hamiltonian takes on the form:

$$\hat{H} = -\sum_{x=1}^{2L-1} \omega^{1/2} \sum_{m=1}^{n-1} K_x^{(m)} \left(\alpha_x^\dagger \alpha_{x+1}\right)^n \ , \tag{6.3.13}$$

and we now explain this mapping in greater detail.

6.3.3 Parafermion description

The two terms in the Clock/ Potts Hamiltonian may each be expressed using two species of *parafermion* operators, defined by

$$\chi_j \equiv \left(\prod_{k=1}^{j-1} \hat{\tau}_k\right) \hat{\sigma}_j \quad , \quad \tilde{\chi}_j \equiv -\omega^{-1/2} \chi_j \hat{\tau}_j = -\omega^{+1/2} \left(\prod_{k=1}^{j} \hat{\tau}_k\right) \hat{\sigma}_j \ , \tag{6.3.14}$$

and obey the relations

$$\left(\chi_j\right)^n = \left(\chi_j^\dagger\right)^n = 1 \ , \quad \left(\chi_j\right)^{n-1} = \chi_j^\dagger \tag{6.3.15}$$

$$\left(\tilde{\chi}_j\right)^n = \left(\tilde{\chi}_j^\dagger\right)^n = 1 \ , \quad \left(\tilde{\chi}_j\right)^{n-1} = \tilde{\chi}_j^\dagger \tag{6.3.16}$$

The multiplication rules for these operators are interesting in that they depend on the site. For $k > j$:

$$\chi_j \chi_k = \omega \chi_k \chi_j \ , \quad \chi_j^\dagger \chi_k^\dagger = \omega \chi_k^\dagger \chi_j^\dagger \ , \quad \chi_j^\dagger \chi_k = \omega^{-1} \chi_k \chi_j^\dagger \ , \quad \chi_j \chi_k^\dagger = \omega^{-1} \chi_k^\dagger \chi_j \tag{6.3.17}$$

$$\tilde{\chi}_j \tilde{\chi}_k = \omega \tilde{\chi}_k \tilde{\chi}_j \ , \quad \tilde{\chi}_j^\dagger \tilde{\chi}_k^\dagger = \omega \tilde{\chi}_k^\dagger \tilde{\chi}_j^\dagger \ , \quad \tilde{\chi}_j^\dagger \tilde{\chi}_k = \omega^{-1} \tilde{\chi}_k \tilde{\chi}_j^\dagger \ , \quad \tilde{\chi}_j \tilde{\chi}_k^\dagger = \omega^{-1} \tilde{\chi}_k^\dagger \tilde{\chi}_j \tag{6.3.18}$$

and for $k \geq j$:

$$\chi_j \tilde{\chi}_k = \omega \tilde{\chi}_k \chi_j \ , \quad \chi_j^\dagger \tilde{\chi}_k^\dagger = \omega \tilde{\chi}_k^\dagger \chi_j^\dagger \ , \quad \chi_j^\dagger \tilde{\chi}_k = \omega^{-1} \tilde{\chi}_k \chi_j^\dagger \ , \quad \chi_j \tilde{\chi}_k^\dagger = \omega^{-1} \tilde{\chi}_k^\dagger \chi_j \tag{6.3.19}$$

We can invert these definitions to obtain expressions for the two terms of the original Hamiltonian:

$$\hat{\sigma}_j^\dagger \hat{\sigma}_{j+1} = -\omega^{1/2} \tilde{\chi}_j^\dagger \chi_{j+1} \tag{6.3.20}$$

$$\hat{\tau}_j = -\omega^{1/2} \chi_j^\dagger \tilde{\chi}_j \tag{6.3.21}$$

We see above that there are two modes per site, and we know from the duality that we can also define the same theory between the sites. Thus, it is convenient to think of the mode $\tilde{\chi}_j$ as acting to the right of mode χ_j on site j. We define a "comprehensive" parafermion mode, α as follows:

$$\alpha_{2j-1} \equiv \chi_j \ , \quad \alpha_{2j} \equiv \tilde{\chi}_j . \tag{6.3.22}$$

Using this convention, both terms in the Hamiltonian have the same form,

$$\sum_x \sum_m K_x^{(m)} \left(\alpha_x^\dagger \alpha_{x+1} \right)^m , \tag{6.3.23}$$

where the weight necessarily depends on the pseudo-site, even for the clean system (where it amounts to perfect dimerization between the f and J terms).

The on-site multiplication rules for the α operators are given by

$$\left(\alpha_j\right)^n = \left(\alpha_j^\dagger\right)^n = 1 \ , \quad \left(\alpha_j\right)^{n-1} = \alpha^\dagger \ , \quad \left(\alpha_j^\dagger\right)^{n-1} = \alpha \ , \tag{6.3.24}$$

and the multiplication rules for $k > j$ are

$$\alpha_j \alpha_k = \omega \alpha_k \alpha_j \ , \quad \alpha_j^\dagger \alpha_k^\dagger = \omega \alpha_k^\dagger \alpha_j^\dagger \ , \quad \alpha_j^\dagger \alpha_k = \omega^{-1} \alpha_k \alpha_j^\dagger \ , \quad \alpha_j \alpha_k^\dagger = \omega^{-1} \alpha_k^\dagger \alpha_j \ . \tag{6.3.25}$$

6.3.4 Real space renormalization group for $n = 3$ parafermions

The $n = 3$ clock model is described by the Hamiltonian

$$\hat{H} = \sum_{j=1}^{L-1} J_j \left(e^{i\phi_j} \hat{\sigma}_j^\dagger \hat{\sigma}_{j+1} + h.c. \right) + \sum_{j=1}^{L} f_j \left(e^{i\theta_j} \hat{\tau}_j + h.c. \right) \ , \tag{6.3.26}$$

which can be cast into the parafermion language via

$$\hat{\sigma}_j^\dagger \hat{\sigma}_{j+1} = -\omega^{1/2} \tilde{\chi}_j^\dagger \chi_{j+1} = \omega^{-1} \tilde{\chi}_j^\dagger \chi_{j+1}$$
$$\hat{\tau}_j = -\omega^{1/2} \chi_j^\dagger \tilde{\chi}_j = \omega^{-1} \chi_j^\dagger \tilde{\chi}_j \ .$$

Using the α operators, one defines new weights and phases (this can be done with a single expression by using a factor of $(-1)^x$),

$$\left(K_x \ , \ \varphi_x\right) = \begin{cases} \left(J_j \ , \ \phi_j\right) & \text{if } x = 2j \\ \left(f_j \ , \ \theta_j\right) & \text{if } x = 2j-1 \end{cases} \ ,$$

in terms of which the Hamiltonian given in Eq. (6.3.26) takes the simple form

$$\hat{H} = \sum_{x=1}^{2L-1} \omega^{-1} K_x \left(e^{i\varphi_x} \alpha_x^\dagger \alpha_{x+1} + e^{-i\varphi_x} \alpha_x \alpha_{x+1}^\dagger \right) . \tag{6.3.27}$$

The real space renormalization group (RSRG) [31–33, 206, 209, 213, 215, 216] is a coarse graining procedure that resolves the eigenstates and energy eigenvalues of the Hamiltonian in real space, by constructing diagonalizing Hamiltonian terms in descending order of strength, and obtaining corrections due to overlapping terms via second order [degenerate] perturbation theory. Additional details can be found in Appendix B.1, along with the references cited above. In scenarios where this technique works, the distribution of couplings is modified as the RG runs, and flows toward infinite disorder, where the RSRG is asymptotically exact.

Suppose we find the strongest bond on some [pseudo-]site x, with strong coupling $K_x = \Omega$. Writing $\phi_x \to \Phi$, we then diagonalize

$$\hat{H}_0 = \Omega\omega^{-1}\left(e^{i\Phi}\alpha_x^\dagger\alpha_{x+1} + e^{-i\Phi}\alpha_x\alpha_{x+1}^\dagger\right), \tag{6.3.28}$$

and note that the operator $\omega^{-1}\alpha_x^\dagger\alpha_{x+1}$ recovers either $\hat{\tau}_j$ or $\hat{\sigma}_j^\dagger\hat{\sigma}_{j+1}$, and therefore has eigenvalues ω^{q_x}, where q_x is some book-keeping integer with value $0, 1, 2$. Thus, the unperturbed energy for $\hat{H}_0$ is

$$\mathcal{E}_0 = 2\Omega\cos\left(\Phi + \frac{2\pi q_x}{3}\right). \tag{6.3.29}$$

The perturbation, V, consists of couplings to nearest neighbors. To treat this problem requires consideration of four pseudosites: we denote the two pseudosites corresponding to the strong bond, Ω, by $x, x{+}1$, and the two pseudosites flanking this strong bond on the left and right will be denoted L and R, respectively, as depicted in Fig. 6.2. The dashed red line in Fig. 6.2 indicates the strongest

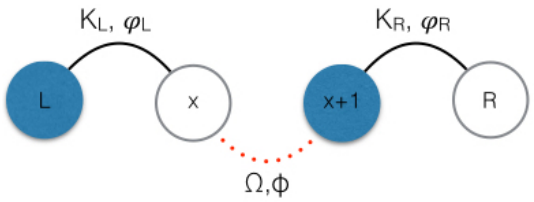

Figure 6.2: Representation of a given step in the RSRG procedure for the $\mathbb{Z}_3$ clock model.

bond, with coupling Ω; the two solid lines on top represent terms associated with the perturbing potential, V,

$$V \equiv \Omega\ \omega^{-1}\{K_L(\underbrace{e^{i\varphi_L}\alpha_L^\dagger\alpha_x}_{\hat{u}_L} + \underbrace{e^{-i\varphi_L}\alpha_L\alpha_x^\dagger}_{\hat{u}_L^\dagger}) + K_R(\underbrace{e^{i\varphi_R}\alpha_{x+1}^\dagger\alpha_R}_{\hat{u}_R} + \underbrace{e^{-i\varphi_R}\alpha_{x+1}\alpha_R^\dagger}_{\hat{u}_R^\dagger})\}, \tag{6.3.30}$$

so that the full Hamiltonian is given by

$$\hat{H} = \hat{H}_0 + \lambda\hat{V}\ , \quad \lambda = \Omega^{-1}. \tag{6.3.31}$$

After fixing the state of the strong bond—i.e. choosing a particular value of the "unperturbed" energy $\mathcal{E}_0$ by fixing the state of the strong bond, $q_x \in \{0, 1, 2\}$—the next step is to resolve the terms $\hat{V}$ to lowest order using degenerate perturbation theory about $\hat{H}_0$, i.e.

$$\langle\psi_\alpha|\widetilde{V}|\psi_\beta\rangle = \Omega^{-2}\sum_{|\gamma\rangle\notin\mathcal{H}_d}\frac{\langle\psi_\alpha|V|\gamma\rangle\langle\gamma|V|\psi_\beta\rangle}{\mathcal{E}_0 - \langle\gamma|H_0|\gamma\rangle}, \tag{6.3.32}$$

and for each of the four terms, $\{\hat{u}_i\}$, in Eq. (6.3.30), one takes $|\gamma\rangle = \hat{u}_{L/R}|\psi_\beta\rangle$ or $\hat{u}_{L/R}^\dagger|\psi_\beta\rangle$, as the case may be, and denotes the energy eigenvalue of the intermediate state (under the unperturbed

Hamiltonian) $\mathcal{E}_\gamma$. For each u term acting on the ket $|\psi_\beta\rangle$, there are two other $\hat{u}$ terms that may contribute from the next operation of $\hat{V}$. The first is the conjugate of the original, which will yield a term proportional to the identity overall. This term is trivial, and the resulting term is proportional to the identity, and therefore a constant that is unimportant physically. For a given choice of u, there is precisely one other term that can return the state $\hat{u}_i|\psi\rangle$ to the same configuration of the strong bond, $x, x+1$, while acting as nonidentity operators on all other parafermion modes. Thus, there are four possible terms that can be generated, which take the form

$$\langle\psi_\alpha|\tilde{V}_1|\psi_\beta\rangle = \frac{K_L K_R}{\omega^2}\sum_{u_i\in V}\langle\varphi_\alpha|\hat{u}_{i^*}\frac{1}{\mathcal{E}_0-\hat{H}_0}\hat{u}_i|\varphi_\beta\rangle. \tag{6.3.33}$$

The four possible configurations of $\hat{u}_{i^*}\hat{u}_i$ are:

$$\begin{aligned} &e^{i(\varphi_L+\varphi_R)}\alpha_L^\dagger\alpha_x\alpha_{x+1}^\dagger\alpha_R && e^{i(\varphi_L+\varphi_R)}\alpha_{x+1}^\dagger\alpha_R\alpha_L^\dagger\alpha_x \\ &e^{-i(\varphi_L+\varphi_R)}\alpha_L\alpha_x^\dagger\alpha_{x+1}\alpha_R^\dagger && e^{-i(\varphi_L+\varphi_R)}\alpha_{x+1}\alpha_R^\dagger\alpha_L\alpha_x^\dagger \end{aligned} \tag{6.3.34}$$

For each of the two possible phases, both terms carrying that phase are equivalent in total, but the intermediate state, and denominator in Eq. (6.3.33) are different. Going through the two terms, and realizing they act on a q_x state:

$$\alpha_L^\dagger\alpha_x\alpha_{x+1}^\dagger\alpha_R = \alpha_{x+1}^\dagger\alpha_R\alpha_L^\dagger\alpha_x = \alpha_L^\dagger\alpha_R\alpha_x\alpha_{x+1}^\dagger = \alpha_L^\dagger\alpha_R\left(\omega^{1-q_x}\right) \tag{6.3.35}$$

$$\alpha_L\alpha_x^\dagger\alpha_{x+1}\alpha_R^\dagger = \alpha_{x+1}\alpha_R^\dagger\alpha_L\alpha_x^\dagger = \alpha_L\alpha_R^\dagger\alpha_x^\dagger\alpha_{x+1} = \alpha_L\alpha_R^\dagger\left(\omega^{1+q_x}\right) \tag{6.3.36}$$

To calculate the energy differences, the action of each quadratic parafermion term on an H_0 eigenstate will be useful:

$$\begin{aligned} \alpha_{x+1}^\dagger\alpha_R &: q_x \to q_x+1 \\ \alpha_{x+1}\alpha_R^\dagger &: q_x \to q_x-1 \\ \alpha_L^\dagger\alpha_x &: q_x \to q_x-1 \\ \alpha_L\alpha_x^\dagger &: q_x \to q_x+1 \end{aligned}$$

These four terms can be written as follows:

$$\widetilde{V} = \frac{K_L K_R}{2\Omega}\sum_{\pm}\frac{\omega^{-2}\left(e^{i(\varphi_L+\varphi_R)}\omega^{1-q_x}\alpha_L^\dagger\alpha_R + e^{-i(\varphi_L+\varphi_R)}\omega^{1+q_x}\alpha_L\alpha_R^\dagger\right)}{\cos(\Phi+\frac{2\pi q_x}{3})-\cos(\Phi+\frac{2\pi}{3}(q_x\pm 1))},$$

and writing $\cos(2\pi/3) = -1/2$, some manipulations recover

$$= \omega^{-1}\left\{\frac{K_L K_R}{\Omega}\frac{\cos\left(\Phi+\frac{2\pi q_x}{3}\right)}{\cos 2\left(\Phi+\frac{2\pi q_x}{3}\right)+\frac{1}{2}}\right\}\left\{e^{i(\varphi_L+\varphi_R-\frac{2\pi q_x}{3})}\alpha_L^\dagger\alpha_R + e^{-i(\varphi_L+\varphi_R-\frac{2\pi q_x}{3})}\alpha_L\alpha_R^\dagger\right\} \tag{6.3.37}$$

$$= \omega^{-1}\tilde{K}_{LR}\left\{e^{i\tilde{\varphi}_{LR}}\alpha_L^\dagger\alpha_R + e^{-i\tilde{\varphi}_{LR}}\alpha_L\alpha_R^\dagger\right\}, \tag{6.3.38}$$

which has the same form as original Hamiltonian, but the parafermion modes on sites $x, x+1$ have *both* dropped out, creating an effective bond between sites $L = x-1$ and $R = x+2$, with coupling $\tilde{K}_{LR}$ and chiral phase $\tilde{\varphi}_{LR}$. As a special aside, for the Ising case $n = 2$, q_x disappears completely from the bond renormalization (and there are no phases).

The important equations from the RG fusion are:

$$\tilde{K}_{LR} = \frac{K_L K_R}{\Omega} \frac{\cos\left(\Phi + \frac{2\pi q_x}{3}\right)}{\cos 2\left(\Phi + \frac{2\pi q_x}{3}\right) + \frac{1}{2}} \tag{6.3.39a}$$

$$\tilde{\varphi}_{LR} = \varphi_L + \varphi_R - \frac{2\pi q_x}{3} \tag{6.3.39b}$$

6.3.5 Discussion

Regarding the renormalization that occurs from decimating (i.e. diagonalizing) a strong parafermion pair, and fusing its neighbors, i.e. Eq. (6.3.39), it is clear that this has the same general form as the $n = 2$ Ising case. The main new ingredient is the existence of phases, renormalized according to Eq. (6.3.39b). As in the Ising case, with each step, exactly two parafermion modes "drop out" of the Hamiltonian, and a new, effective Hamiltonian forms that has the same form as the original, with modified couplings straddling the decimated parafermions. Also as in the Ising case, this RG flows to infinite disorder.

If, on average, more bonds are decimated than fields, the system will be in the $\mathbb{Z}_n$ spin glass phase, analogous to the $\mathbb{Z}_2$ spin glass described in Sec. 6.2. On the other hand, if more fields are decimated, the system flows to a $\mathbb{Z}_n$ paramagnet. At infinite disorder (to which the RG flows), both phases are MBL, as they are strongly localized. The former, spin glass phase, features topological edge modes, realized by $\mathbb{Z}_n$ parafermions. The latter is, paramagnet, corresponds to a trivial phase. Note that at weak disorder, where one expects thermal phases, the RSRG procedure invoked above is likely not valid, as one will have too many nearly-degenerate couplings when starting the RG, all of which must be accounted for in a given step. This can result in nonlocal mixing of terms, generating extra entanglement and leading to a breakdown of the technique, but also suggesting thermalization due to strong repulsion of many-body levels and entanglement production.

In particular, the $\mathbb{Z}_3$ clock model is expected to have the *same* nonequilibrium eigenstate phase structure as its $\mathbb{Z}_2$ cousin, the transverse field Ising chain. One note is that, compared to the Ising Hamiltonian defined in Eq. (6.2.1), the "integrability-breaking" terms are not necessary for $n > 2$: While these theories are bilinear in the parafermion language, they are not integrable in the same sense, because parafermions cannot be counted. The integrability of the Ising case is due largely to a mapping from Majorana to Dirac (or "regular") fermions, for which bilinearity is significant. Nonetheless, all of the richness of equilibrium phase diagrams of $\mathbb{Z}_3$ clock models relies crucially on certain ratios between the various couplings, including the phases, and the absence of disorder. For generic models of the form Eq. (6.3.26), none of these phases will be realizable with any nonzero disorder. Thus, the phase diagram for the $\mathbb{Z}_3$ clock model should be described by Fig. 6.1.

Finally, for precisely the same reasons that the $\mathbb{Z}_3$ clock model has the same phase diagram as the $\mathbb{Z}_2$ Ising model, we predict that *all* $\mathbb{Z}_n$ clock models have the same phase structure. Although these models have extra terms with increasing n, randomness prevents the type of fine-tuning required to realize more complicated phase structure in clean systems in equilibrium (and usually at $T = 0$). In particular, whether the system is MBL or thermal is determined entirely by the relative strength of interactions versus disorder (or, if preferable, simply the overall strength of disorder). If the system is thermal, it must be a paramagnet; however, at strong disorder, it may be possible to realize either a paramagnet or a spin glass. Because the disorder is strong, one can invoke the RSRG used for $\mathbb{Z}_{2,3}$, and independent of n, on average one either decimates more fields or more bonds. In the latter case, it is possible to realize a spin glass, with the glassy structure of domains given by fixing the various bonds under the RG.

However, this procedure and result are complicated if we allow the model to have a different symmetry, e.g. the dihedral symmetries or permutation symmetries mentioned previously. This will be the subject of Sec. 6.4.

6.4 The Disordered S_3 Potts Model

This Section is largely drawn from Ref. 33 by this author.

6.4.1 Introduction

Little is known about the generic properties and possible phases of quantum systems out of equilibrium, where even a basic understanding at the level of Landau theory has remained elusive. Many-body systems can reach an effective equilibrium state under their own dynamics even in isolation, a process encoded in the properties of individual eigenstates via a set of criteria collectively termed the eigenstate thermalization hypothesis (ETH) [169, 170]. A distinct class of many-body localized (MBL) systems [11, 12], usually with quenched randomness, violate these criteria and cannot self-thermalize. As they need not satisfy the stringent requirements imposed by ETH, even highly excited eigenstates of MBL systems can exhibit properties usually associated with quantum ground states [15, 101]. This permits the classification of out-of-equilibrium MBL systems into distinct *eigenstate phases* separated by *eigenstate phase transitions* [208], echoing the classification of ground states and critical points in equilibrium systems, and providing a window into nonequilibrium quantum order.

As ETH systems conform to the expectations of equilibrium statistical mechanics, at infinite effective temperature ($T \to \infty$) they exhibit the eigenstate phase structure of a thermal paramagnet, with trivial spatial and temporal correlations. In contrast, MBL systems can exhibit richer behavior — for instance, an MBL Ising model can exhibit both broken-symmetry (spin glass) and paramagnetic phases even for $T \to \infty$ [15, 206, 207, 210]. In this regime — that is dominated by properties of highly-excited eigenstates — a particularly sharp distinction emerges for *non-Abelian* symmetries. While ETH systems with such symmetries are again thermal paramagnets as $T \to \infty$, a fully MBL phase is inconsistent with non-Abelian symmetry [217]. This indicates that the onset of full MBL must coincide with breaking of the symmetry, and that any symmetry-preserving phase is either (i) thermal, in the sense of ETH; or (ii) an athermal 'quantum critical glass' [31] that does not admit the local tensor product description of a fully MBL phase. In recent work [32], we illustrated the former scenario in fermion chains with $U(1) \rtimes \mathbb{Z}_2$ symmetry, whose non-Abelian semi-direct product structure (denoted '$\rtimes$') reflects the nontrivial action of a $\mathbb{Z}_2$ particle-hole symmetry (PHS) on a conserved $U(1)$ charge. As disorder is increased, PHS is spontaneously broken in highly excited eigenstates whenever they are fully MBL. This rules out the possibility of using PHS in conjunction with MBL to stabilize a topological phase — corresponding to class AIII in the usual taxonomy [218, 219] of symmetry-protected topological (SPT) phases — as $T \to \infty$. Similar considerations [217] limit MBL-protected SPT phases [100, 220–222], and rule out many phases that host non-Abelian anyons.

Some $1d$ topological phases host non-Abelian parafermionic edge modes *independent* of any protecting symmetries [223], and are therefore apparently more amenable to localization protection. However, such 1D parafermionic chains are still inextricably linked to symmetry, although indirectly: they are related, via the Fradkin-Kadanoff mapping [224], to $\mathbb{Z}_n$ quantum clock models, with the topological (trivial) phases of the parafermions corresponding to ordered (disordered)

phases of the spins [223]. The question of MBL protection of parafermion edge modes then turns on the interplay of localization with the symmetry of the spin chain. Though $\mathbb{Z}_n$ itself is Abelian, for special *achiral* parameter values, $\mathbb{Z}_n$ clock models with $n \geq 3$ acquire an additional $\mathbb{Z}_2$ reflection symmetry, enhancing the global symmetry to that of the non-Abelian dihedral group $D_n \cong \mathbb{Z}_n \rtimes \mathbb{Z}_2$. For $n = 3$, since $D_3 = S_3$, this is equivalent to the 3-state quantum Potts model. Our focus here is on understanding how the non-Abelian symmetry of this model influences its nonequilibrium phase structure.

This question is interesting for several reasons, explored in the remainder of this paper. First, while superficially similar to the previously-studied $U(1) \rtimes \mathbb{Z}_2$ example, the D_3 model has a richer phase diagram — intuitively, $U(1)$ symmetry constrains possible phases more strongly than D_3 symmetry. Second, since breaking $U(1)$ symmetry is impossible even with MBL in $d = 1$, the *only* possibility for an MBL phase in a $U(1) \rtimes \mathbb{Z}_2$ system breaks the $\mathbb{Z}_2$ symmetry; in the clock model, the $\mathbb{Z}_3$ subgroup of D_3 may also be broken. This means that at strong disorder it may be possible to tune between distinct MBL phases via an unusual critical point. Third, there is the intriguing possibility of an athermal, symmetry-preserving quantum critical glass phase [case (ii) discussed above]. Finally, to return to our original motivation, $\mathbb{Z}_3$ breaking in highly excited eigenstates translates via duality [225] to the existence of a nonequilibrium topological phase that hosts edge parafermion modes relevant to fault-tolerant quantum computing.

Before proceeding, we mention that related work by Prakash *et al.* [226], also considered the role of non-Abelian symmetries in the excited states of a somewhat distinct model. The results presented here are consistent with that work—where they overlap—though their emphasis was not on the nature of the critical behavior between MBL phases. Their work also speculates as to the existence of a QCG phase, a question on which we remain for the moment agnostic.

6.4.2 Model and symmetries

We now turn to the $\mathbb{Z}_3$ quantum clock—or Potts—model, described by the Hamiltonian

$$H = -\sum_{j=1}^{L-1} J_j e^{i\phi_j} \hat{\sigma}_j^\dagger \hat{\sigma}_{j+1} - \sum_{j=1}^{L} f_j e^{i\theta_j} \hat{\tau}_j + \text{h.c.}, \tag{6.4.1}$$

where J_j, f_j, θ_j, ϕ_j are all real, and discussed below. The operators commute on different sites and satisfy

$$\hat{\sigma}_j^3 = \hat{\tau}_j^3 = 1, \ \hat{\sigma}_j \hat{\tau}_j = \omega \hat{\tau}_j \hat{\sigma}_j, \tag{6.4.2}$$

on a single site, where $\omega = e^{\frac{2\pi i}{3}}$.

In the eigenbasis of the *weight* operator, $\hat{\sigma}$, defined by: $\hat{\sigma}|m\rangle = \omega^m |m\rangle$, $\hat{\tau}$ is a *shift* operator: $\hat{\tau}|m\rangle = |m+1\rangle$, with ket labels taken modulo 3 henceforth. The conjugate $\hat{\tau}$-eigenbasis $|q\rangle$ interchanges these roles: $\hat{\tau}|q\rangle = \omega^q |q\rangle$, $\hat{\sigma}|q\rangle = |q-1\rangle$. Viewed as a 3-state quantum rotor, $-i \ln \hat{\sigma}$ represents the angle of the rotor, and the $\hat{\tau}$ measures its angular momentum (modulo 3).

For generic parameter choices, Eq. (6.4.1) has a global $\mathbb{Z}_3$ rotation symmetry generated by $\hat{\mathcal{Q}} = \prod_j \hat{\tau}_j$, with $\hat{\mathcal{Q}}^3 = 1$. For $\phi_j, \ \theta_j \equiv 0 \bmod \pi/3$, there is also a $\mathbb{Z}_2$ mirror symmetry: $\hat{\mathcal{X}} \equiv \prod_j \hat{\mathcal{X}}_j$, where $\hat{\mathcal{X}}_j$ exchanges the $|1\rangle$, $|2\rangle$ eigenstates of *either* $\hat{\sigma}_j$, $\hat{\tau}_j$, and $\hat{\mathcal{X}}^2 = 1$. Together, $\hat{\mathcal{Q}}, \hat{\mathcal{X}}$ generate the group $D_3 = S_3 \cong \mathbb{Z}_3 \rtimes \mathbb{Z}_2$, where the semidirect product structure reflects the fact that $\hat{\mathcal{Q}}$, $\hat{\mathcal{X}}$ do not commute. Consequently, in the $\hat{\sigma}_j$ basis there are two additional $\mathbb{Z}_2$ symmetries $\hat{\mathcal{X}}\hat{\mathcal{Q}}$, $\hat{\mathcal{X}}\hat{\mathcal{Q}}^2$, which respectively leave $|1\rangle$, $|2\rangle$ invariant, while exchanging the other states. When they are viewed as 3-state quantum rotors in the xy-plane, $\hat{\mathcal{Q}}$ is a $2\pi/3$ rotation, and $\hat{\mathcal{X}}$ is a mirror reflection of the rotor about one of its 3 directions (which also inverts the angular momentum, $\hat{\tau}$).

In the clean limit of the $\mathbb{Z}_3$ Hamiltonian Eq. (6.4.1), the ground state has an ordered phase that spontaneously breaks $\hat{\mathcal{Q}}$ for $J \gg f$, and a disordered phase for $J \ll f$. These correspond respectively to parafermionic phases with and without edge zero modes [223]. The chiral couplings explicitly break $\mathbb{Z}_2$, and the ground states in both limits break two of the $\mathbb{Z}_2$ reflection symmetries $\hat{\mathcal{X}}, \hat{\mathcal{X}}\hat{\mathcal{Q}}, \hat{\mathcal{X}}\hat{\mathcal{Q}}^2$. This model also possesses a sequence of incommensurate phases [227,228]. Extensive recent work [229–233] has focused on the clean case; we shall instead study the situation when the couplings are disordered, i.e. J_j and f_j on each site are i.i.d. random variables, while keeping $\phi_j, \theta_j \equiv 0 \bmod \pi/3$, so that the symmetry group is D_3. We wish to understand whether highly excited eigenstates of Eq. (6.4.1) satisfy ETH, or are instead MBL; and if the latter, whether and how they break the non-Abelian D_3 symmetry. We note that previous analysis [234] of low-energy excited-states of clock models focused on edge zero modes in clean systems, a setting quite distinct from the nonequilibrium disordered case studied here. For the non-Abelian XXZ chain [32], the excited-state real-space renormalization group [206] (RSRG-X) provides useful insights; here, the reduced D_3 symmetry complicates matters, as explained in Appendix B.1. Since RSRG-X is inconclusive, we turn instead to a numerical analysis, which we now describe.

6.4.3 Numerics

We investigate the random D_3 chain via numerical exact diagonalization of Eq. (6.4.1). Since we have three states per site, only a discrete global symmetry, and study highly excited eigenstates, we are limited to systems of length $L \leq 10$. Therefore, we must perform finite-size scaling analysis of our data in order to extract the phase diagram and conjectured critical behavior. It is convenient to parametrize couplings as $J_j = \lambda_j \frac{(1+\delta)}{2}$ and $f_j = \lambda'_j \frac{(1-\delta)}{2}$; with this choice, $\delta = \pm 1$ are trivial limits corresponding to idealized fixed-point Hamiltonians for the ordered (spin glass) and paramagnetic phases respectively. (In the parafermionic language, δ is the dimerization, i.e. the bias in strength between odd and even couplings.) The random coefficients λ, λ' are drawn from the distribution $P(\lambda) = \frac{1}{W}\lambda^{1-1/W}$, where disorder is stronger for larger W, with $W = 1.0$ equivalent to a uniform distribution on $(0, 1]$. For each realization of disorder we use the shift-invert method [22] to obtain $\mathcal{N} = 50$ eigenstates from approximately the middle of the many-body spectrum, and average our data over $10^3 - 10^4$ such realizations. We use open boundary conditions, and slightly reduce the Hilbert space size by restricting to eigenstates of both $\hat{\mathcal{Q}}$ and $\hat{\mathcal{X}}$ with eigenvalue unity. Although $\hat{\mathcal{Q}}$ and $\hat{\mathcal{X}}$ do not commute, states constructed in the $\hat{\tau}$ basis have eigenvalue ω^Q under $\hat{\mathcal{Q}}$, where $Q = \sum_j q_j \bmod 3$, and if $Q = 0$ for some such state, then the $\mathbb{Z}_2$ partner of this state also has $Q = 0$. In this way, we can construct a basis of simultaneous eigenstates of $\hat{\mathcal{Q}}$ and $\hat{\mathcal{X}}$ from states with $\hat{\mathcal{Q}}|\psi\rangle = |\psi\rangle$ by superposing such states with their $\mathbb{Z}_2$ partner.

6.4.4 Observables

To map out the ergodic and localized regions in the transverse field-disorder plane (here parametrized by δ, W respectively), we numerically measure several indicative quantities. We study the energy level statistics via the 'r-ratio' [14], defined in terms of gaps $\delta_n = E_n - E_{n-1}$ between successive energy eigenvalues as $r = \min(\delta_n, \delta_{n-1})/\max(\delta_n, \delta_{n-1})$. Once all symmetries have been taken into account, for ETH systems energy level repulsion results in $r \approx 0.53$, characteristic of the Gaussian orthogonal random matrix ensemble, whereas for MBL systems $r \approx 0.38$, reflecting the Poisson statistics when level repulsion is absent [14,95]. It is crucial that we consider only eigenstates within a given symmetry sector, as pairing between different sectors will artificially suppress r [15, 32] in broken-symmetry states, and our auxiliary $\mathbb{Z}_2$ order parameter is only valid when evaluated with

eigenstates of the $\mathbb{Z}_3$ cycle. We do not show level statistics data for $|\delta| \gtrsim 0.7$ as they show unphysically small r-ratios due to 'fragmentation' of the spectrum in the vicinity of perfect dimerization. We also study the scaling of the half-chain entanglement entropy $S_E^{(n)} = -\mathrm{Tr}\hat{\rho}_n \ln \hat{\rho}_n$, computed in the nth eigenstate from the reduced density matrix $\hat{\rho}_n \equiv \mathrm{Tr}_{i>\lceil L/2 \rceil} |n\rangle\langle n|$.

6.4.5 Order parameters

Glassy breaking of the $\mathbb{Z}_3$ symmetry may be diagnosed by an Edwards-Anderson-type order parameter,

$$\hat{\tau} Pottseq : s3opm_3 = \frac{1}{\mathcal{N} L^2} \sum_{n=1}^{\mathcal{N}} \sum_{i \neq j} \left| \langle n | \hat{\sigma}_i^\dagger \hat{\sigma}_j | n \rangle \right|^2, \tag{6.4.3}$$

where n labels eigenstates. This is analogous to the order parameter used to analyze MBL phases in the Ising [207] and XXZ [32] chains, and will be nonzero in an eigenstate only if $\mathbb{Z}_3$ symmetry is broken. The square average ensures that quenched site-to-site and eigenstate-to-eigenstate variations do not cancel, a standard strategy employed for spin-glass order. Breaking $\mathbb{Z}_3$ automatically breaks $\mathbb{Z}_2$; we verify this explicitly in our numerics, and will justify analytically in Appendix 6.4.7. We term a phase with $m_3 \neq 0$ a $\mathbb{Z}_3$ *spin glass*. In the parafermion language, this $\mathbb{Z}_3$ spin glass corresponds to the topological phase with parafermionic edge states.

In addition, there is a $\mathbb{Z}_2$ chiral symmetry, $\hat{\mathcal{X}}$, in the transverse-field phase $f \gg J$, in which $\mathbb{Z}_3$ is *preserved*. To detect glassy chiral ordering, we examine

$$m_\chi = \frac{1}{\mathcal{N} L^2} \sum_{n=1}^{\mathcal{N}} \sum_{i \neq j} \left| \langle n | \hat{\mathcal{J}}_i \hat{\mathcal{J}}_j | n \rangle \right|^2, \tag{6.4.4}$$

where the operator $\hat{\mathcal{J}}_j = \frac{1}{i\sqrt{3}} \left(\hat{\tau}_j - \hat{\tau}_j^\dagger \right) = \frac{2}{\sqrt{3}} \mathrm{Im}(\hat{\tau}_j)$ measures the chirality on a single site and anticommutes with $\hat{\mathcal{X}}\hat{\mathcal{Q}}^n$. We term a phase with $m_\chi \neq 0$ but $m_3 = 0$ a chiral $\mathbb{Z}_3$ paramagnet since it preserves $\mathbb{Z}_3$ but breaks the chiral $\mathbb{Z}_2$ symmetry. In the parafermionic representation, the chiral paramagnet corresponds to a topologically trivial MBL phase without edge states. Observe that D_3 symmetry is broken in both the $\mathbb{Z}_3$ spin glass and the chiral paramagnet: completely in the former, and down to an Abelian $\mathbb{Z}_3$ subgroup in the latter. Note however that $m_\chi = 0$ in the $\mathbb{Z}_3$ spin glass even though $\mathbb{Z}_2$ is broken, as we have defined m_χ in the dual basis, which we elucidate below, e.g. in Section 6.4.7.

6.4.6 Scaling exponents

In the strongly disordered limit $W \gg 1$, we conjecture that a direct transition between an MBL spin glass and a chiral MBL paramagnet occurs at the self-dual point $\delta = 0$, and is characterized by "random singlet" critical exponents. In particular, we expect this transition to share the universal properties of the $T = 0$ disordered Ising chain [235] , including a *true* correlation length with mean scaling exponent $\nu \geq 2$, consistent with Harris and Chayes-Chayes-Fisher-Spencer bounds [236], where $\xi \sim \Delta^{-\nu}$ and Δ is a disorder-dependent logarithmic measure of distance from criticality [215, 216].

Additionally, the *mean critical correlations* behave like $\bar{C}_{ij} = \left| \langle \hat{\sigma}_i^z \hat{\sigma}_j^z \rangle \right| \sim |i-j|^{-\beta}$. For the random Ising case [215,216], the exponent β has a known value of $\beta_{\mathrm{Ising}} = 2 - \varphi$, where φ is the golden ratio $\left(1+\sqrt{5}\right)/2$. A quick calculation reveals that the Edwards-Anderson-type order parameters used to detect full D_3 symmetry breaking should then scale as $L^{-\beta}$ as well, viz. $m_3 = \frac{1}{L^2} \sum_{i \neq j} \bar{C}\left(|i-j|\right) \approx$

$\frac{1}{L^2}\int_0^L \mathrm{d}x \int_0^L \mathrm{d}y\, |x-y|^{-\beta} \propto L^{-\beta}$, and one expects the same value of $\beta = \beta_{\text{Ising}}$ only if the D_3-breaking transition is in the same universality class as the random Ising transition.

Thus, in performing finite size scaling for strong disorder, we multiply the order parameters by L^β to obtain a quantity with scaling dimension zero. We display figures for the values of β and ν that produce the best quality fit, and take the quality of this collapse as good evidence in favor of an infinite randomness critical point at $\delta_c = 0$. However, we do *not* claim to extract numerically precise values of either ν or β; we only demonstrate that the data obtained are consistent with the values of these exponents one would expect from the Ansatz of infinite randomness criticality. This scaling behavior is relevant only near criticality and at strong disorder (large W, $\delta \sim 0$). We find that the expected value of $\nu = 2$ produces a good quality fit, but so too do all $\nu \in [2,3]$. As these also satisfy the Harris bound, we cannot rule them out conclusively.

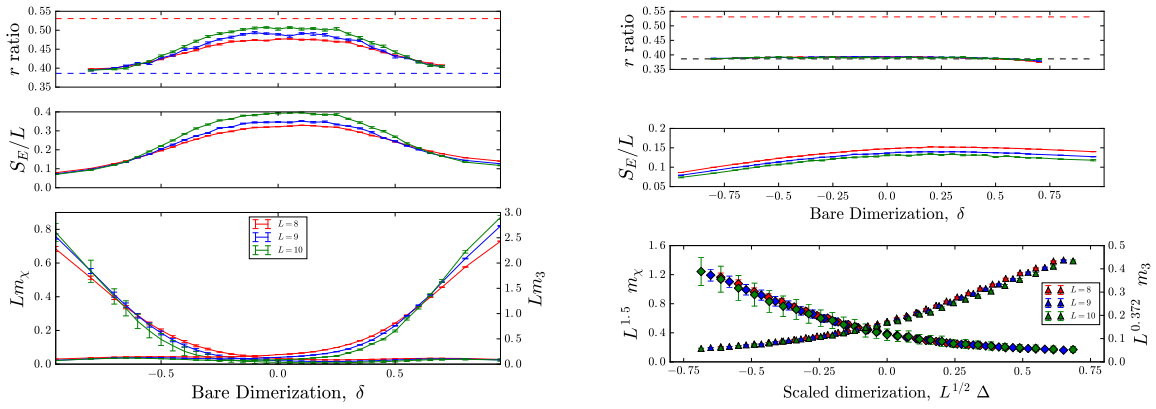

(a) Weak disorder, $W = 0.5$.

(b) Strong disorder, $W = 2.0$.

Figure 6.3: Figure (a): Random D_3 chain at weak disorder, $W = 0.5$. (Top) Level statistics measured by r-ratio display two transitions: for $|\delta_c| \lesssim 0.5$, r tends to the ETH value $r \approx 0.53$ characteristic of the Gaussian orthogonal ensemble with increasing L, whereas outside this region $r \to 0.38$, indicating Poisson statistics of MBL. (Center) Half-chain entanglement entropy density $S_{\text{E}}(L)/L$ is consistent with volume (area) law scaling in the ETH (MBL) regions. (Bottom) Spin-glass order parameters of $\mathbb{Z}_3$ and chiral symmetry (scaled by L, see text) also show crossings at $|\delta_c| \approx 0.5$, showing that MBL coincides with the onset of symmetry-breaking. Figure (b): Random D_3 chain at strong disorder, $W = 2.0$. (Top) Since $r \approx 0.38$ for all values of δ, we infer that the system is always MBL. (Center) Entanglement entropy density is consistent with area-law scaling as $L \to \infty$, again consistent with MBL. (Bottom) Scaling collapses of m_3 ($\triangle$) and m_χ ($\diamond$), both consistent with a direct transition at $\delta_c = 0$ between distinct broken-symmetry MBL phases. Here $\nu = 2$, and $\Delta = \frac{\overline{\ln J} - \overline{\ln f}}{\mathrm{var} J + \mathrm{var} f} = \frac{1}{2W^2} \ln \frac{1+\delta}{1-\delta}$ is a rescaled tuning parameter. [The point where the two collapsed curves cross has no physical significance.]

6.4.7 Subsidiary $\mathbb{Z}_2$ breaking in the $\mathbb{Z}_3$ spin glass

For the parameter space we investigate, the model Eq. (6.4.1) has a global $D_3 = S_3$ symmetry generated by the action of a $\mathbb{Z}_3$ cycle $\hat{\mathcal{Q}} = \prod_j \hat{\tau}_j$ and a $\mathbb{Z}_2$ swap $\hat{\mathcal{X}} \equiv \prod_j \hat{\mathcal{X}}_j$, where $\hat{\mathcal{X}}_j$ interchanges local eigenstates $|1\rangle \leftrightarrow |2\rangle$ of *either* σ_j or τ_j, while leaving $|0\rangle$ invariant. In the $\mathbb{Z}_2$ Ising model, spin glass order is detected using an Edwards-Anderson order parameter. The Ising chain has only a global $\mathbb{Z}_2$ symmetry generated by $\hat{\mathcal{S}} = \prod_j \hat{\sigma}_j^x$, and the corresponding eigenstate-averaged order

parameter is

$$m_{\text{Ising}} = \frac{1}{\mathcal{N}L^2}\sum_{n=1}^{\mathcal{N}}\sum_{i\neq j}\left|\langle n|\hat{\sigma}_i^z\hat{\sigma}_j^z|n\rangle\right|^2, \tag{6.4.5}$$

where $\hat{\sigma}_j^z$ anticommutes with the local symmetry generator, $\hat{\sigma}_j^x$. For D_3, the analogous operator $\hat{\mathcal{J}}_j = \frac{1}{i\sqrt{3}}\left(\hat{\tau}_j - \hat{\tau}_j^\dagger\right)$ anticommutes with the chiral $\mathbb{Z}_2$ generator $\hat{\mathcal{X}}_j$, as evinced by their matrix representations in the $\hat{\tau}_j$-basis:

$$\hat{\mathcal{X}}_j = \begin{pmatrix}1&0&0\\0&0&1\\0&1&0\end{pmatrix}_j, \quad \hat{\mathcal{J}}_j = \begin{pmatrix}0&0&0\\0&1&0\\0&0&-1\end{pmatrix}_j, \tag{6.4.6}$$

which have the appropriate Pauli matrix structure. We therefore use the conjugate operator $\hat{\mathcal{J}}$ to construct the chiral Edwards-Anderson order parameter for $\hat{\mathcal{X}}$-breaking,

$$m_\chi = \frac{1}{\mathcal{N}L^2}\sum_{n=1}^{\mathcal{N}}\sum_{i\neq j}\left|\langle n|\hat{\mathcal{J}}_i\hat{\mathcal{J}}_j|n\rangle\right|^2. \tag{6.4.7}$$

As previously stated, $\hat{\mathcal{X}}_j$ has the same matrix form in the σ-basis; one may also construct the conjugate in that basis, $\hat{\mathcal{K}}_j = \frac{1}{i\sqrt{3}}\left(\hat{\sigma}_j - \hat{\sigma}_j^\dagger\right)$, whereupon the order parameter becomes

$$\tilde{m}_\chi = \frac{1}{\mathcal{N}L^2}\sum_{n=1}^{\mathcal{N}}\sum_{i\neq j}\left|\langle n|\hat{\mathcal{K}}_i\hat{\mathcal{K}}_j|n\rangle\right|^2 \tag{6.4.8}$$

$$= \frac{1}{9\mathcal{N}L^2}\sum_{\substack{n\\ i\neq j}}\left|\langle n|\left(\hat{\sigma}_i^\dagger\hat{\sigma}_j + \hat{\sigma}_i\hat{\sigma}_j^\dagger - \hat{\sigma}_i^\dagger\hat{\sigma}_j^\dagger - \hat{\sigma}_i\hat{\sigma}_j\right)|n\rangle\right|^2. \tag{6.4.9}$$

However, the energy eigenstates $|n\rangle$ are constructed as eigenstates of $\hat{\mathcal{Q}} = \prod_j \hat{\tau}_j$, and therefore correspond to states with a fixed $\mathbb{Z}_3$ charge $Q = \sum_j q_j \bmod 3$. The latter two terms in Eq. (6.4.9) both change the total $\mathbb{Z}_3$ charge by ± 1, and therefore have a trivially zero expectation value. The σ-basis order parameter then becomes $\tilde{m}_\chi = \frac{1}{9\mathcal{N}L^2}\sum_{n=1}^{\mathcal{N}}\sum_{i\neq j}\left|\langle n|\left(\hat{\sigma}_i^\dagger\hat{\sigma}_j + \hat{\sigma}_i\hat{\sigma}_j^\dagger\right)|n\rangle\right|^2 = \frac{4}{9}m_3$, i.e, proportional to the Edwards Anderson order-parameter for $\mathbb{Z}_3$-breaking. As an aside, using either of the other two $\mathbb{Z}_2$ symmetry operators $\hat{\mathcal{X}}\hat{\mathcal{Q}}$, $\hat{\mathcal{X}}\hat{\mathcal{Q}}^2$ and constructing the corresponding order parameters in the σ-basis has the same result: the only respective changes are factors of ω and ω^2 multiplying the trivial $\hat{\sigma}_i^\dagger\hat{\sigma}_j^\dagger$ term. Hence, the $\mathbb{Z}_3$-breaking spin glass necessarily breaks chiral $\mathbb{Z}_2$, and so D_3 is fully broken in this phase.

6.4.8 Details of the auxiliary $\mathbb{Z}_2$ order parameter

The $\mathbb{Z}_2$ order parameter defined in Eq. (6.4.4) measures chiral order in the τ-basis – i.e., breaking of D_3 to a $\mathbb{Z}_3$-preserving paramagnet. This order parameter is designed for use only in a paramagnetic phase, wherein $\mathbb{Z}_3$ is preserved, and is not a useful measure of $\mathbb{Z}_2$ breaking when evaluated with states that are *not* eigenstates of the $\mathbb{Z}_3$ generator. Although the derivation from conjugacy to the $\mathbb{Z}_2$ generator derived in the preceding subsection is sufficient, we also performed several sanity checks to confirm this quantity is reasonable. To wit, it has the appropriate action on generic states constructed specifically to preserve or break the $\mathbb{Z}_2$ symmetry. Additionally, it is everywhere zero when computed in *ground states* of the D_3 model, where the quantum phase transition at $T = 0$

only admits either a fully D_3-preserving paramagnet or a spin glass that breaks D_3 completely. Lastly, it shows chiral ordering when calculated in eigenstates of the chiral $\mathbb{Z}_3$ Hamiltonian, which breaks explicitly the $\mathbb{Z}_2$ subgroup of D_3 (provided $\bar{f}_j > \bar{J}_j$). The fact that this quantity is zero even in D_3 ground states and all $\mathbb{Z}_3$ eigenstates for $\bar{J}_j > \bar{f}_j$ confirms that it is only meaningful on the putatively paramagnetic side of the phase diagram, $\delta \leq 0$.

6.4.9 Results

Armed with these measures of ergodicity and symmetry breaking, we now study their behavior at weak and strong disorder.

Weak Disorder For a representative choice of weak disorder, $W = 0.5$ (Figure 6.3a), we identify a pair of transitions both in level statistics and entanglement. For $|\delta| \lesssim 0.5$, the r-ratio increases towards the ETH value of 0.53 with increasing system size, whereas outside this region it decreases towards the MBL value of 0.38. This is also consistent with the change from area-law to volume-law scaling observed in the eigenstate-averaged entanglement entropy ($S_E = \sum_{n=1}^{\mathcal{N}} S_E^{(n)}/\mathcal{N}$). We conclude that an ETH region for $|\delta| \lesssim 0.5$ is flanked by a pair of MBL phases. We next study symmetry-breaking, by considering the scaled quantities Lm_3, Lm_χ: these scale $\sim L$ in a phase with spin-glass order, and vanish in a symmetry preserving phase. Crossings of curves of either Lm_3 or Lm_χ corresponding to different system sizes approximately locate transitions between a paramagnetic and broken-symmetry phase. Within the accuracy of our numerics, these appear to coincide with the crossings in level statistics, with the $\delta \gtrsim 0.5$ ($\delta \lesssim 0.5$) phase breaking the D_3 ($\mathbb{Z}_2$) symmetry in a spin glass sense. We track similar behavior up to $W \approx 1.0$, whereupon the ETH phase disappears; we therefore identify $W > 1.0$ with strong disorder. Fig. 6.4 shows the extent of the ETH phase and approximate locations of the crossings in r, m_3 and m_χ. Crucially, a fully D_3 symmetric MBL phase is absent, in accord with general symmetry restrictions [217].

Strong Disorder For strong disorder (e.g. $W = 2.0$, see Figure 6.3b) we find no evidence for an ETH phase in either level statistics or entanglement: with increasing L, $r \to 0.385$ and S_E/L decreases, consistent with either MBL or eigenstate criticality [31], for all δ. Extrapolating from weak disorder, we see that the two MBL-ETH transition lines appear to converge at around $W \approx 1.0$. Recall that the two MBL phases have distinct broken symmetries. At strong disorder, as the ETH phase is absent and an MBL paramagnet is inconsistent with D_3 symmetry [217], there must be either a direct transition between the two broken-symmetry MBL phases, or an intervening symmetry-preserving quantum critical glass phase. [A third possibility, namely that a narrow sliver of ETH phase persists to strong disorder [237,238], is not evident in our numerics but we cannot rule it out for $L \to \infty$.] Although it is challenging to distinguish these scenarios given our limited range of system sizes, we find some support for the former via finite-size scaling analysis, as follows. First, we argue that self-duality of Eq. (6.4.1) implies symmetry under reflection of δ, fixing a single direct transition to occur at $\delta_c = 0$ (we ignore small finite-size corrections to duality from the open boundary conditions; note that the weak disorder MBL-ETH transitions are at roughly $\pm\delta_c$, consistent with duality). Second, we assume that a direct transition between MBL phases is controlled by an infinite-randomness fixed point, with length-time scaling $\ell^\psi \sim \ln t$. We fix $\psi = 1/2$, characteristic of a random singlet critical point, the generic scenario [235] in systems with Abelian global symmetries (as both phases lack full non-Abelian D_3 symmetry), and use the scaling form

$$m(\delta, L) = L^{-\beta} \Phi\left[L^{1/\nu}\Delta\right], \tag{6.4.10}$$

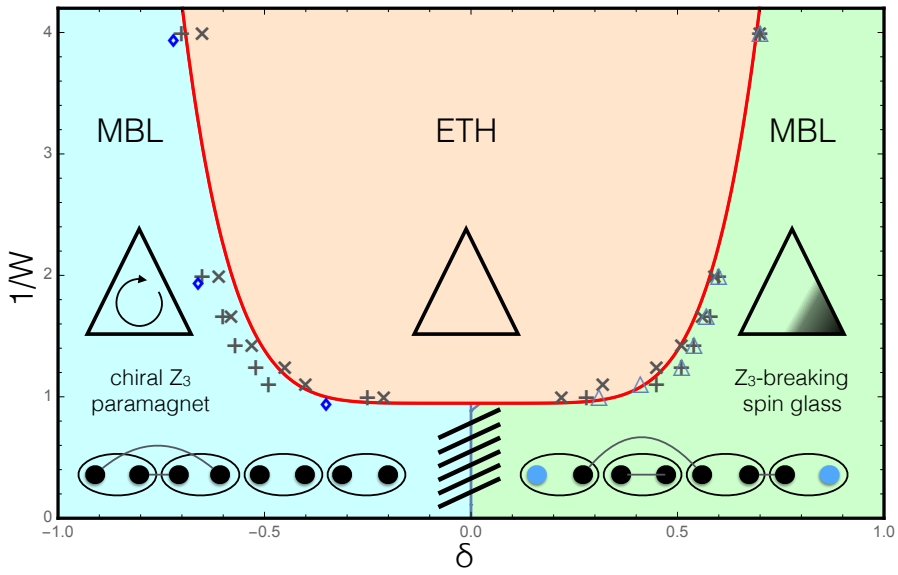

Figure 6.4: Non-equilibrium global phase diagram of random D_3 chain. The MBL-ETH boundary (red line) is an estimate based on crossings in level statistics and scaled entanglement entropy (denoted $\times$, † respectively). For weak disorder we also indicate crossings in the $\mathbb{Z}_3$ ($\triangle$) and chiral ($\diamond$) order parameters. At strong disorder, we find scaling collapse consistent with an infinite-randomness critical point at $\delta_c = 0$; however, we cannot conclusively rule out a nonergodic quantum critical glass in the transition region (hatched). (Inset) schematic of the symmetry-breaking pattern and the topological/trivial phases of dual parafermions.

where $\nu = 2$, $\Delta = \frac{\overline{\ln J} - \overline{\ln f}}{\mathrm{var} J + \mathrm{var} f} = \frac{1}{2W^2} \ln \frac{1+\delta}{1-\delta}$ tunes across the $\delta_c = 0$ critical point, and Φ is a universal function. For m_3, the exponent $\beta = 0.372$ derives from known results for $\psi = 1/2$ infinite-randomness critical scaling of the random transverse-field Ising model [215, 216], which predict an exponent $\beta_{\mathrm{Ising}} = 2 - \varphi$. The same scaling does not hold for m_χ, where β is not known analytically, and we merely fit these data using the scaling form Eq. (6.4.10). As we see from the bottom panel of Fig. 6.3b, the data for m_3, m_χ show reasonably good collapse when scaled according to Eq. (6.4.10), with the exponent $\beta_\chi = 1.5$ chosen to show that a satisfactory collapse according to Eq. (6.4.10) exists, though we do *not* claim to have extracted a precise value from the data. With no other free parameters, the collapses are at least consistent with a direct infinite-randomness transition between the $\mathbb{Z}_3$ spin glass and the chiral paramagnet (though other exponent choices also give reasonable data collapses). Furthermore, we cannot rule out a possible sliver of a quantum critical glass *phase* rather than a critical point, which might show similar scaling collapse for accessible system sizes. We indicate this ambiguity by the hatched lines marking the transition region in Fig. 6.4.

6.4.10 Discussion

The results for this system are summarized by the global nonequilibrium phase diagram for the random D_3 chain depicted in Figure 6.4. To the extent this can be determined, MBL always appears

to coincide with the breaking of the non-Abelian discrete D_3 symmetry. The MBL $\mathbb{Z}_3$ spin glass completely breaks this symmetry; in a different language, this phase will host parafermionic zero modes stable at finite temperature. The other MBL phase is a $\mathbb{Z}_3$-symmetric paramagnet, which — unlike its ground-state counterpart — breaks the remaining $\mathbb{Z}_2$ chiral symmetry, consistent with the no-go theorem forbidding MBL with non-Abelian symmetry. At $\delta = -1$, the model describes a trivial paramagnet, the eigenstates of which feature extensive degeneracies due to the D_3 symmetry. Our numerics show that for any finite interaction $\delta > -1$, the degeneracy due to the chiral $\mathbb{Z}_2$ component of D_3 is lifted by spontaneous symmetry breaking. This is precisely the instability of the MBL phase to non-Abelian symmetries predicted in a previous work [217]. While an ETH phase intervenes at weak disorder, at strong disorder we find evidence for an infinite-randomness transition between these distinct broken-symmetry MBL phases, although a more exotic possibility, an athermal quantum critical glass, cannot be definitively ruled out. We conjecture that similar features apply, *mutatis mutandis*, to other non-Abelian random spin chains with D_n symmetry. Further investigation of such models, e.g. via matrix product state methods [26, 239–241], would be an interesting avenue for future work.

6.5 The Random-Bond XXZ Model

This Section is largely drawn from Ref. 32 by this author.

6.5.1 Introduction

Many-body localization (MBL) extends the concept of single particle (Anderson) localization due to random chemical potentials [10] to the excited states of isolated interacting quantum systems [11, 242,243]. MBL systems raise the compelling prospect of supporting quantum coherent information storage and processing [13,20,244–247], and nontrivial quantum order [15,100,101,206,220,248,249] in highly excited states far from thermal equilibrium [250]. Moreover, phase transitions between MBL states [31, 206, 210, 251] (or between MBL and thermalizing systems [14, 22, 95, 214, 252, 253]) represent new classes of nonequilibrium quantum critical behavior.

A natural generalization of random potential localization is particle-hole symmetric (PHS) disorder such as that due to random hopping amplitudes (or random vector potentials in dimensions higher than one). In one dimension and in the absence of interactions, PHS disorder does not fully localize single-particle states at zero energy, resulting in a marginally localized random-singlet phase with infinite randomness quantum critical properties [216, 254]. In this paper, we examine the fate of the highly excited states of this marginally localized phase [255] in the presence of interactions by studying an equivalent problem, the random-bond XXZ spin 1/2 chain

$$H = \sum_{i=1}^{L-1} J_i \left(S_i^x S_{i+1}^x + S_i^y S_{i+1}^y + \Delta_i S_i^z S_{i+1}^z \right), \tag{6.5.1}$$

where $S_i^\mu = \frac{1}{2}\sigma_i{}^\mu$, and σ_i^μ with $\mu = x, y, z$ are the standard Pauli matrices. We consider open boundary conditions. In addition to spin conservation, the Hamiltonian defined in Eq. (6.5.1) has an Ising symmetry generated by $\mathcal{C} = \prod_i \sigma_i^x$. A Jordan-Wigner transformation maps Eq. (6.5.1) to a spinless fermion chain with nearest-neighbor interactions (that vanish for $\Delta_i = 0$), with $\mathcal{C}$

now playing the role of PHS. In thermal equilibrium and at zero temperature, interactions are an irrelevant perturbation and do not affect the ground state critical properties [216]. However, in the absence of interactions, the excited states are highly degenerate due to the combination of single-particle integrability and symmetry, and hence even weak interactions can be expected to dramatically modify the dynamical properties of this system.

Using a combination of real-space renormalization group (RSRG) arguments and exact diagonalization we show that arbitrarily weak interactions necessarily destroy the random-singlet critical properties in excited states, either by inducing thermalization (at weak disorder) or by spontaneously breaking PHS (strong disorder). In the latter case, this leads to a counterintuitive scenario wherein the ground state is *less* localized (more entangled) than excited states. In addition, the ground-state random singlet phase can be thought of as a phase transition between a certain 1D symmetry protected topological insulator with chiral symmetry and a trivial insulator, and hence understanding its dynamical behavior will also shed light on questions of extending symmetry-protected topological (SPT) order (and related Floquet SPT orders) to highly excited states in MBL systems. We argue that the spontaneous symmetry breaking inherent at strong disorder presents a fundamental obstacle to achieving this goal.

These results should be contrasted with a prior study of XXZ chains [209] that used a related dynamical RSRG method to argue that the quantum critical behavior of the noninteracting ground state extends to highly excited states. However, as noted in [209], these dynamical RSRG results apply only to the fine-tuned Néel initial state which artificially removes the excited-state degeneracies from the dynamically accessible Hilbert space. We expect that our results reflect the true dynamical properties of generic (*i.e.*, not fine-tuned) states.

6.5.2 RSRG-X

The $T = 0$ low-energy physics of the antiferromagnetic XXZ spin chain Eq. (6.5.1) is well understood in terms of a real-space renormalization group (RSRG) approach valid at strong disorder [216]. The key idea is to focus on the strongest bond of the chain $\Omega = J_i$. Assuming strong disorder, this bond is typically much larger than its neighbors, $\Omega \gg J_R, J_L$ ($J_{R/L} \equiv J_{i\pm1}$), so to leading order we can diagonalize this strong bond by forming a singlet between the spins S_i and S_{i+1}. Quantum fluctuations then induce an effective XXZ coupling between the spins $S_L = S_{i-1}$ and $S_R = S_{i+2}$. Iterating this procedure, the effective disorder strength grows under renormalization so that RSRG becomes asymptotically exact – *i.e.* gives exact results for universal quantities [216]. This approach was recently generalized to construct many-body excited states of random spin chains by observing that at each step, it is possible to project the strong bond onto an excited-state manifold [206, 209]. The resulting excited-state RSRG (RSRG-X [206]) iteratively resolves smaller and smaller energy gaps Ω and allows one to construct, in principle, the full many-body spectrum. Assuming $\Delta \equiv \Delta_i \neq \pm 1$ to avoid resonances, projecting onto the eigenstates $|\uparrow\downarrow\rangle \pm |\downarrow\uparrow\rangle$ of the strong bond preserves the XXZ form of the effective interaction between S_L and S_R with parameters $J_{\text{eff}} = J_L J_R/((1 \mp \Delta)\Omega)$ and $\Delta_{\text{eff}} = \Delta_L \Delta_R(\Delta \mp 1)/2$, respectively. Another possibility would be to project onto the zero-energy states $|+\rangle = |\uparrow\uparrow\rangle$, $|-\rangle = |\downarrow\downarrow\rangle$, where these two degenerate states can be interpreted as components of a new effective superspin S_{eff} with a different $U(1)$ charge $S_z = \pm 1$ than the original UV spins 1/2. Spin conservation implies that S_{eff} cannot be flipped by a first order process like $S^+_{L,R} S^-_{\text{eff}} + \text{h.c.}$ Keeping track of all the symmetry-allowed processes, we find the effective Hamiltonian

$$H_{\text{eff}} = J_L \Delta_L S^z_L S^z_{\text{eff}} + J_R \Delta_R S^z_R S^z_{\text{eff}} + \frac{J_L J_R}{\Omega(\Delta^2 - 1)} \left[\frac{S^+_L S^-_R}{2} + \Delta S^+_L S^+_R S^-_{\text{eff}} + \text{h.c.} \right] + \dots \tag{6.5.2}$$

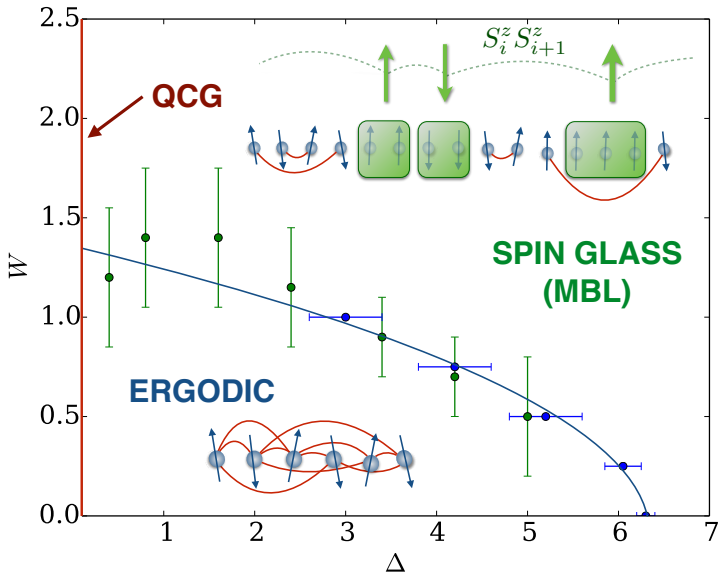

Figure 6.5: Phase diagram of the random-bond XXZ chain at energy density $\epsilon = 0.5$ from exact diagonalization results. The quantum critical behavior of the free model ($\Delta = 0$) is destroyed by interactions, giving rise to either an ergodic phase at weak disorder where all spins are highly entangled, or to a many-body localized phase with spin glass order at strong disorder. The phase boundary is estimated from finite-size crossings at constant W (blue symbols) or constant Δ (green symbols). The excited states in the spin glass phase consist of effective superspins (green spins) showing a random pattern of frozen magnetization varying from eigenstate to eigenstate.

where we have ignored second-order corrections to the Ising $S^z_{L,R}S^z_{\rm eff}$ terms.

In the noninteracting case [256] ($\Delta_i = 0$), the effective Hamiltonian always has the same XX form as the original one so that the procedure can be readily iterated. The sign of the J coupling being essentially irrelevant, the flow equations for the couplings are identical to the groundstate ones. This indicates that the random XX chain at finite energy density is a "Quantum Critical Glass" [31] (QCG), a critical variant of MBL with logarithmic scaling of the entanglement and power-law mean correlation functions. Crucially, the effective spins $S_{\rm eff}$ (created when projecting onto the $S_z = \pm 1$ excited states) completely decouple from the rest of the chain, thereby producing an exponential degeneracy of the many-body eigenstates generated by RSRG-X. This degeneracy is a consequence of the PHS of the single-particle spectrum, that dictates that single-particle energies come in pairs $(\epsilon, -\epsilon)$. The remainder of this paper focuses on investigating the fate of these extensive degeneracies upon the inclusion of interactions.

6.5.3 Interaction-induced spin glass order

From Eq. Eq. (6.5.2), we see that the interactions generate two new types of term: second-order couplings $S^+_L S^+_R S^-_{\rm eff}$ + h.c. flipping the effective spin $S_{\rm eff}$ and more importantly Ising couplings $S^z_{R,L}S^z_{\rm eff}$ generated at first-order in perturbation theory. To leading order, the effective Hamiltonian takes the form of a simple Ising coupling that will dominate over the much weaker second order flip-flop terms involving S_L, S_R. Although it is hard to keep track of all the multi-spin terms emerging after many RSRG-X iterations, the trend is already clear. Namely, superspins made of $n > 2$ aligned UV spins will be eventually generated in the course of the RG. Because of spin conservation, it is increasingly harder to flip these large superspins as this will involve higher-

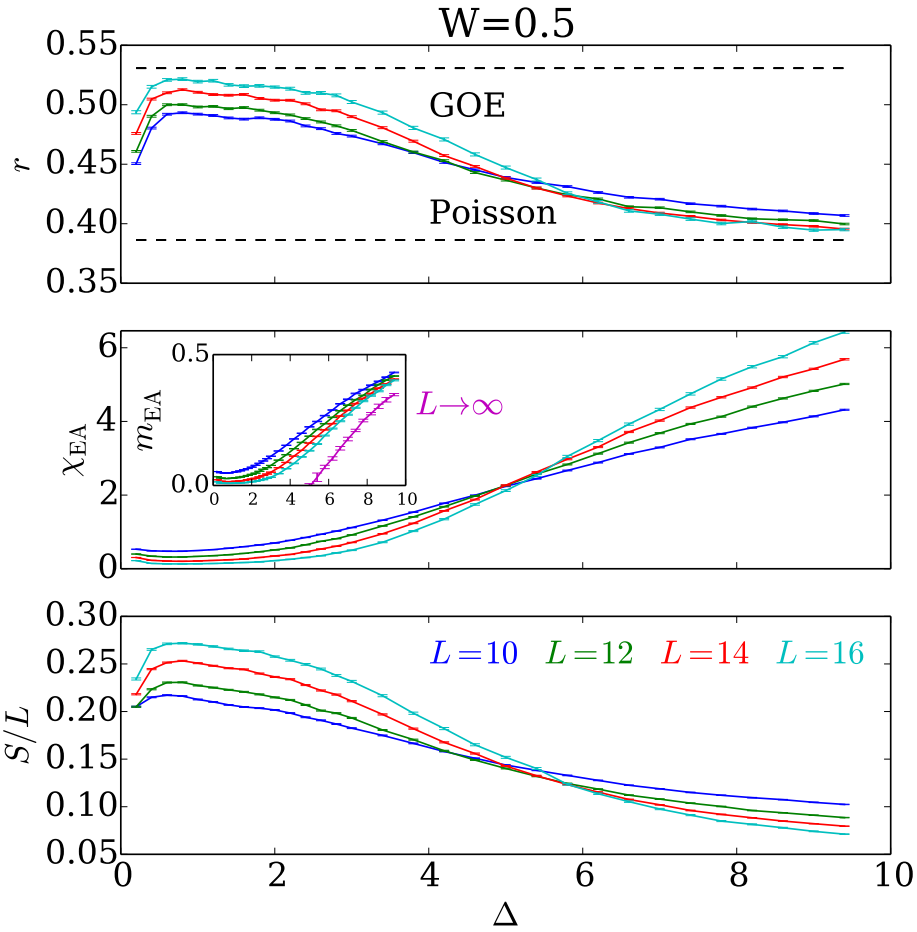

Figure 6.6: Ergodic to spin glass (MBL) transition. At weak disorder ($W = 0.5$), our data are consistent with an ergodic to spin glass (MBL) transition as Δ is increased. *Top:* Ratio of consecutive level spacings showing a transition from GOE to Poisson statistics. *Middle:* Scaling of $\chi_{\rm EA}$ showing a divergence with system size in the localized phase. Inset: Extrapolations of $m_{\rm EA}$ with L^{-1} finite-size corrections (see text) are consistent with spin glass order in the MBL phase. *Bottom:* Finite-size scaling of the entanglement entropy.

order processes in perturbation theory involving many super-spin clusters. This strongly suggests a physical picture of the excited states in terms of almost frozen superspins with strong Ising interactions, very weakly coupled by flip-flop terms generated at higher order in perturbation theory. The eigenstates would then consist of (super)spins showing a random pattern of frozen magnetization — breaking the Ising symmetry — varying from eigenstate to eigenstate.

Such spontaneous breaking of PHS by interactions generates a random chemical potential term $\sum_i \mu_i S_i^z$ (*e.g.* in a mean field treatment $\mu_i = \sum_{j=i-1,i+1} J_j \Delta_j \langle S_j^z \rangle$), which localizes the extended single-particle modes near zero energy and cuts off the quantum critical spin fluctuations at length scales longer than the spin-glass correlation length. Spontaneous PHS breaking appears to be the only route to an MBL phase in this model: in particular, single-spin terms $h_i S_i^{x,y,z}$ acting on the super-spins are forbidden by symmetry. This result implies that whereas the edges of the many-body spectrum are quantum critical with algebraic mean correlations, high energy density eigenstates are *more* localized, in sharp contrast with random-field MBL systems where higher energy densities tend to favor delocalization [11, 22].

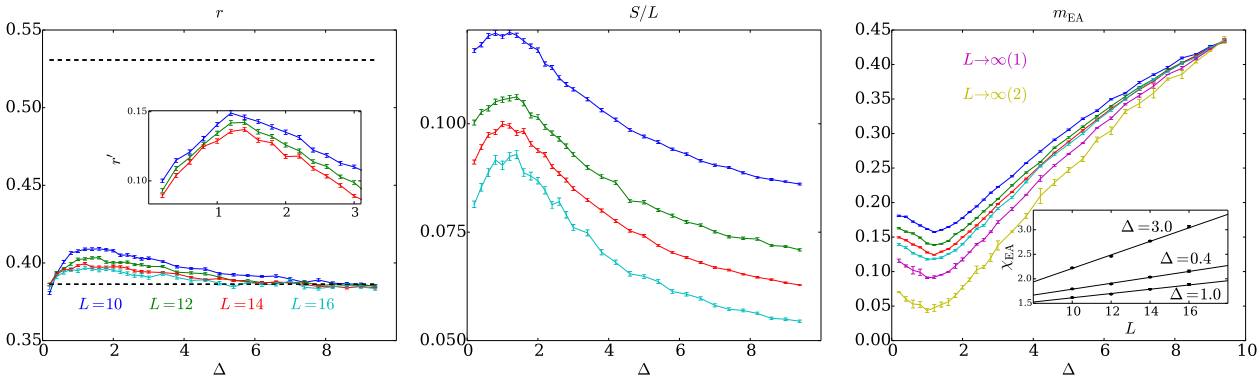

Figure 6.7: Strong disorder spin glass phase ($W = 2.0$). *Left*: Poisson statistics of the level spacings. Inset: when not restricted to a given $\mathbb{Z}_2$ sector, the gap ratio r' decreases with system size (well below the Poisson value), signaling pairing of the excited eigenstates. *Middle*: Sub-extensive scaling of the entanglement entropy. *Right*: Extrapolations of the spin glass order parameter $m_{\rm EA} = \chi_{\rm EA}/L$ are consistent with nonvanishing values in the thermodynamic limit for all values of $\Delta > 0$, indicating spin glass order. Extrapolations are performed using $1/L^2$ (1) and $1/L$ (2) finite-size corrections. We note that the small dip around $\Delta \approx 1$ is naturally accounted for by the enhanced probability of local resonances $\Delta_i \approx 1$ [31] (see text). Inset: Linear scaling of $\chi_{\rm EA}$ with system size, consistent with spin glass order.

6.5.4 Numerical results

Though the above argument based on RSRG-X strongly suggests that even infinitesimally weak interactions will destroy the quantum critical glass behavior of the random XX spin chain and lead to spin glass order instead, it is hard to explicitly track all the higher-order terms generated during the renormalization process that could (in principle) flip the super-spins. In order to clarify this issue, we now turn to numerical exact diagonalization methods to study Eq. (6.5.1). We draw the couplings $J_i \in (0, 1]$ from the power-law distribution $P(J) = \frac{1}{W}\frac{1}{J^{1-1/W}}$ and we choose Δ_i to be uniformly distributed in the interval $[-\Delta, \Delta]$. We also restrict to even L and $\sum_i S^z_i = 0$, and consider the even sector of the $\mathbb{Z}_2$ symmetry $\mathcal{C}$. For each disorder realization, we first calculate the extremal energies $E_{\rm min}$ and $E_{\rm max}$ and define the normalized energy density $\epsilon = (E - E_{\rm min})/(E_{\rm max} - E_{\rm min})$. We then use the shift-invert method [22] to obtain the 50 eigenstates with energy closest to $\epsilon = 0.5$, corresponding to the middle of the many-body spectrum. Results are averaged over at least 2×10^3 disorder realizations.

To distinguish between ergodic and nonergodic phases we measure the level spacing parameter [95]

$$r_n = \min(\delta_n, \delta_{n+1})/\max(\delta_n, \delta_{n+1}) \ , \tag{6.5.3}$$

characterizing the ratio between consecutive level spacings $\delta_n = E_n - E_{n-1}$ averaged over energy levels n. Its disorder-averaged value changes from that characteristic of random matrices in the Gaussian orthogonal ensemble, $r_{\rm GOE} \simeq 0.5307$ [257] in the ergodic phase, to $r_{\rm Poisson} = 2\ln 2 - 1 \simeq 0.3863$ (reflecting absence of level repulsion) in the MBL regime. We also compute the bipartite entanglement entropy $S_n = -{\rm tr}\rho_n \ln \rho_n$, where ρ_n the reduced density matrix in the nth eigenstate after tracing over half of the system. The entanglement scales as $S_n \sim 1, \log L$, and L for MBL, QCG, and thermalizing systems respectively. To characterize the spin glass order, we introduce an Edwards-Anderson-like order parameter,

$$m_{\rm EA} = \frac{1}{L^2}\sum_n \sum_{i\neq j} \left|\langle n|\sigma^z_i \sigma^z_j|n\rangle\right|^2 , \tag{6.5.4}$$

which tends to a constant (zero) in the thermodynamic limit for a spin-glass ordered (disordered) phase. (We also consider the auxiliary quantity $\chi_{\rm EA} \equiv L m_{\rm EA}$ [251], which can in principle distinguish short-range spin glass order from certain types of quasi-long range order.)

6.5.5 Phase diagram

The results are summarized in the phase diagram of Figure 6.5 (see Appendix C for details). For weak disorder ($0 \le W \lesssim 1.5$), and $\Delta < \Delta_c(W)$, we find GOE level statistics, extensive entanglement, and vanishing spin glass order signaling a thermal phase. In this range of W, increasing Δ drives an MBL transition to a spin glass-ordered phase at $\Delta = \Delta_c(W)$, heralded by a crossing in the finite size scaling plots of r, S, and $\chi_{\rm EA}$, per Figure 6.6.

Interestingly, our numerics strongly suggest that for weak enough disorder, arbitrarily weak interactions lift the degeneracies of the noninteracting case and lead to thermalization. This is natural since at weak disorder and $\Delta = 0$, degenerate PHS-conjugate pairs of orbitals that are either doubly occupied or both empty (corresponding to superspins in the RSRG-X language) have large spatial extent and overlap with many other degenerate pairs of orbitals. Then, upon the inclusion of interactions there are many strongly overlapping resonances that lead to thermalization. In other words, at weak disorder each orbital typically overlaps with many others, such that the higher-spin $S^+_L S^+_R \ldots S^-_{\rm eff}$ type flip-flop terms are no longer strongly suppressed by many powers of a small parameter, and the massive degeneracy of the noninteracting case can be lifted by quantum fluctuations which naturally lead to thermalization. For strong disorder however, each degenerate pair of orbitals are sharply localized and interacts mainly with its nearest neighbors through predominantly Ising interactions leading to the spin glass MBL phase discussed above.

6.5.6 Strong disorder regime

For strong disorder ($W \gtrsim 1.5$), we observe a clear finite-size scaling trend towards Poisson level statistics, and sub-extensive entanglement entropy. In this strong-disorder regime, our RSRG-X predictions should apply, and we therefore expect an MBL spin glass phase, as shown in Figure 6.7. To distinguish between QCG and MBL phases, we examine the scaling of the spin glass order parameter with system size. Whereas for an MBL phase with long-range spin glass order $\lim_{L\to\infty} m_{\rm EA} \neq 0$, for a QCG with only algebraic quasi long-range order, $m_{\rm EA} \sim L^{-\alpha}$ ($\chi_{\rm EA} \sim L^{1-\alpha}$). We observe that $\chi_{\rm EA}$ clearly grows with system size, inconsistent with a QCG with $\alpha > 1$. In particular, this observation rules out a QCG in the same universality class as the random XX case ($\Delta = 0$) [209], which would have $\alpha = 2$ [216]. From our RSRG-X scenario, we expect two types of finite size corrections to $m_{\rm EA}$: $1/L$ terms coming from short-range ordered regions , and $1/L^2$ terms from the vestige of random-XX QCG. Extrapolating our data for $m_{\rm EA}$ using fits to either $1/L$ or $1/L^2$ finite-size corrections predicts a nonvanishing limiting value of $m_{\rm EA}$, suggesting spin-glass order for all $\Delta > 0$, as depicted in Figure 6.7. Though our data is perfectly consistent with linear growth of $\chi_{\rm EA} = L m_{\rm EA} \sim L$, we cannot definitively rule out a more exotic QCG phase with $\alpha \ll 1$, distinct from the $\Delta = 0$ XX random singlet phase.

In this spin glass (MBL) phase, the eigenstates for large systems should be cat states $|n\rangle_\pm = (|n\rangle \pm \mathcal{C}|n\rangle)/\sqrt{2}$ that are even/odd under the $\mathbb{Z}_2$ symmetry generated by $\mathcal{C} = \prod_i \sigma^x_i$, where $|n\rangle$ is some eigenstate-dependent pattern of σ^z magnetization (with some background of random-singlet spins). The energy splitting between the two true eigenstates $|n\rangle_\pm$ is exponentially small in system size and scales as $\sim \mathrm{e}^{-L/\xi}$ with ξ the localization length, implying that the broken-symmetry state $|n\rangle$ becomes metastable in the limit of large systems [15]. Meanwhile, the level spacing scales as

$\delta \sim e^{-(\ln 2)L}$ at "infinite temperature" (corresponding to our choice of normalized energy density $\epsilon = 0.5$). At strong disorder, the localization length in the spin glass phase should be small and we therefore expect the eigenstates to be "paired" [15]: the level spacing between each doublet is exponentially small compared to the typical level spacing. This implies that the r ratio should vanish, provided one does not restrict to a given $\mathbb{Z}_2$ sector (recall that up to now, we worked in the even sector of the particle-hole symmetry $\mathcal{C}$). In a quantum critical glass phase (with quasi-long range order), we expect the energy splitting of these quasi-doublets to become stretched-exponential [206, 215], i.e., much larger than the many-body level spacing, thereby forbidding a regime with paired eigenstates. The r ratio thus provides us with a clear way to distinguish true long-range spin glass order from the quasi-long range order of a quantum critical glass in small systems.

We checked that for sufficiently strong disorder ($W = 2.0$ and $W = 2.5$) where there is no sign of an ergodic phase, the r ratio computed in the full spectrum of the $S_z = 0$ sector (denoted by r') indeed decreases with system size, even for small values of $0.2 \leq \Delta \leq 1.0$ (Fig. 6.7) where a quantum critical glass phase was previously predicted [209]. This strongly supports our claim of a spin glass phase extending all the way to infinitesimal Δ.

We also remark that the small dip around $\Delta \approx 1$ in Fig. 6.7 is naturally explained by the enhanced probability of local resonances $|\Delta_i| \approx 1$. Recall that uniform anisotropies $\Delta_i = 1$, $\forall i$ with global SU(2) symmetry are known to lead to thermalization for arbitrary disorder strength [31,209, 220]. In our case of inhomogeneous anisotropies distributed uniformly in $[-\Delta, \Delta]$, the probability of having a resonance $1 - \epsilon < |\Delta_i| < 1 + \epsilon$ for small $\epsilon > 0$ is obviously strictly zero if $\Delta < 1 - \epsilon$, decays as $\sim 1/\Delta$ for $\Delta > 1 + \epsilon$, and therefore exhibits a maximum near $\Delta \approx 1$ (at $\Delta = 1 + \epsilon$).

6.5.7 Constraints on protection of SPT order by MBL

Our RSRG-X arguments and numerical results both show an inherent instability of the XX critical point towards a noncritical MBL spin glass upon the inclusion of interactions. Interestingly, these results imply a related instability of certain symmetry protected topological (SPT) orders, that one might have thought could emerge in highly excited states of MBL systems. Consider Eq. (6.5.1), with an even number of spins, dimerized hoppings $J_i = \frac{1}{2} J_i^{(0)} \left(1 + \delta_i (-1)^i\right)$, and weak interactions ($\Delta_i \ll 1$). Then the ground state is topologically trivial for $\delta = \delta_i > 0$, but exhibits SPT order with symmetry-protected spin 1/2 topological edge states for $\delta < 0$ (see Appendix C.2). This model is dual to a 1D fermion SPT of class AIII [218, 219] via a standard Jordan-Wigner mapping, where the edge states are protected by the symmetry $U(1) \times \mathbb{Z}_2^{\mathcal{S}}$ where $\mathcal{S} = \mathcal{C}K$, with K acting as complex conjugation (see Appendix C.2).

In the perfectly dimerized limit, $\delta = -1$, the ground state consists of singlets on all dimerized bonds, with dangling spin 1/2 degrees of freedom at the left and right ends, and excitations are either nondegenerate $S^z = 0$ triplets, $|\uparrow_i \downarrow_{i+1}\rangle + |\downarrow_i \uparrow_{i+1}\rangle$, or doubly degenerate $S^z = \pm 1$ triplets, $|\uparrow_i \uparrow_{i+1}\rangle, |\downarrow_i \downarrow_{i+1}\rangle$ on a strong bond. Moving away from the perfectly dimerized limit, $\delta \gtrsim -1$, these doubly degenerate $S^z = \pm 1$ bond-triplets weakly interact via virtual excitations of the intervening nondegenerate $S^z = 0$ bonds. These interactions are strongly random, decaying exponentially in distance between the $S^z = \pm 1$ bonds, and symmetry dictates that these interactions be of XXZ form (plus less relevant multi-spin interactions). Thus the $S^z = \pm 1$ excitations form a new effective XXZ chain that, crucially, has no memory of the initial dimerization pattern δ_i. According to the preceding sections of this paper, at finite energy density this effective XXZ chain will either thermalize (weak disorder) or spontaneously break symmetry (strong disorder); in both cases, the underlying SPT order is destroyed.

6.5.8 Discussion

We have argued that the notion of particle-hole symmetric Anderson localization does not extend to the MBL case. Even though interactions are an irrelevant perturbation in the ground state, they drastically affect the structure of excited states leading either to thermalization at weak disorder or to spontaneously broken particle-hole symmetry at strong disorder, thereby destroying in both cases the quantum critical properties of the noninteracting model.

Our results also imply the instability of SPT order with $U(1)\times\mathbb{Z}_2^{\mathcal{S}}$ symmetry. Previous analyses of whether SPT order can extend to highly excited states of MBL systems [220, 248, 249] focused on whether it is possible to construct a locally integrable (commuting projector) "fixed-point" model of the phase for which all excited states are localized with concurrent SPT order. Our present study furnishes an example where such a locally integrable model is possible (the perfectly dimerized state), but for which there are inherent degeneracies in the excitations that, upon weak perturbation away from the strictly integrable limit, result in spontaneous symmetry breaking. Our results also rule out the realization of certain stable Floquet SPT orders [66, 68, 258, 259] with no equilibrium counterparts, such as those in driven systems, that require an MBL setting to avoid catastrophic heating [99, 103, 260]. It would be very interesting to investigate whether our results can be generalized to rule out the existence of PHS many-body localization and related excited state SPT orders in higher-dimensional systems.

6.6 Non-Abelian Symmetry

The studies referred to in Secs. 6.4 and 6.5 by this author and collaborators led to related work, Ref. 217, which established the incompatibility of many-body localization with non-Abelian symmetries. In particular, any system with a global symmetry groups containing multiplets—which is to say irreducible representations ("irreps") with dimension greater than one—is incompatible with MBL. All non-Abelian symmetry groups fall into this category, including those with finite-dimensional representations, e.g. the S_3 Potts model studied in Sec. 6.4, as well as those with continuous representations, e.g. the $U(1)\rtimes\mathbb{Z}_2$ symmetric random-bond XXZ chain detailed in Sec. 6.5. An intuitive explanation is that the ℓ bits that define the fully many-body localized phase must transform independently under the model's symmetry, G, which necessarily implies extensively many local degeneracies in the spectrum if G is non-Abelian.

To illustrate this, suppose a given system with a non-Abelian symmetry G has an MBL phase. The corresponding ℓ bits for this model thus transform as irreps of G, with different states of the ℓ bit (i.e. eigenstates of the LIOM) labeling irreps of G. For G to be non-Abelian and act faithfully on the system, at least some of these irreps must have dimension larger than one, and must therefore result in degenerate eigenvalues of the LIOM operator. Since the full spectrum of eigenstates of the model is completely specified by a configuration of these ℓ bits, correspondingly, the full set of energy eigenvalues, defined in terms of eigenvalues of the LIOMs, will have degeneracies that scale exponentially with the system size. A key facet of the MBL phase is that it is a robust phase of matter, i.e. stable to small but [fairly] arbitrary perturbations; however, the presence of such superextensive degeneracy in the energy spectrum makes the Hamiltonian unstable to perturbations, as can be seen using standard perturbation theory. Further, there is no way to "lift" these degeneracies without breaking the symmetry.

Hence, models with non-Abelian symmetries either realize a thermal phase, or realize MBL by spontaneously breaking the full non-Abelian symmetry down to a discrete symmetry. In the models studied in Secs. 6.4 and 6.5, both of these outcomes were realized. Additionally, it may

be possible to realize more exotic but nonergodic phases in these models. While some evidence of these phases was observed for the S_3 Potts model [33], the limitation of exact numerics and complicated nature of the RSRG made this impossible to diagnose. Whether such physics can be realized in general models or those with non-Abelian symmetries, as well as whether this behavior constitutes a phase of matter, remains an open question [217].

6.7 Summary and Outlook

In conclusion, we have investigated the interplay between both conventional and topological order and nonequilibrium phase structure—namely, thermalization versus localization. In particular, we have seen how various aspects associated to ground states of clean quantum systems, e.g., those in equilibrium with a classical reservoir at $T = 0$, are realized in highly excited states of disordered models. Additionally, we have unearthed certain symmetry constraints on MBL phases, and ruled out the possibility of certain types of MBL-protected topological orders, and shown that the rich phase structure of clean clock models cannot be realized in the nonequilibrium setting. We have also showcased the descriptive power of the real-space renormalization group technique applied to highly excited states. Although this technique presumes strong disorder, it becomes asymptotically exact as it flows to infinite disorder under the RG. We have also found numerical evidence for more exotic, nonergodic regimes, which require scrutiny beyond the scope of RSRG and small systems numerics. While we expect that a wealth of interesting physics may be realized in this setting, the primary limiting factor is the lack of available techniques that do not suffer from one or more serious deficiencies or limitations. In the future, we hope to develop techniques that can access the thermodynamic limit in such nonequilibrium systems, particularly by adapting successful techniques for more conventional strongly correlated quantum systems.

Chapter 7

Open Quantum Systems

7.1 Introduction

The ability to realize quantum systems that are well isolated from their environment has led to new efforts to understand how such systems thermalize. The Eigenstate Thermalization Hypothesis (ETH) [169, 170] provides a mechanism for part of an isolated system to equilibrate with the rest, which acts as a bath (thermal reservoir), to reproduce the familiar results of statistical mechanics. These efforts have also revealed classes of non-ergodic systems that do not thermalize per ETH.

In practice, no experiment can remain isolated forever [261–263], which motivates careful theoretical study of the environment itself [264–267]. As MBL and ETH focus on highly excited eigenstates—and therefore effectively at large or infinite effective temperature, T—baths in this nonequilibrium context are approximated as Markovian, i.e. memoryless on long timescales [265]. In contrast, for $T \to 0$, the bath autocorrelation time can diverge, so that memory effects become significant. Such non-Markovian baths can arise naturally from quantum dissipation, induced, e.g. by coupling to a continuum of gapless excitations [268, 269]. Most studies heretofore have focused primarily on the former, Markovian baths, whose action is history-independent: such baths generally delocalize systems, rendering them more thermal [265].

A fundamental result of ETH is that the mechanism for thermalization of a [sub-]system is *entanglement* between the 'system' and 'bath' [169, 170]. Thus, a Markovian bath—which foregoes any description of the bath itself—necessarily overlooks this key aspect of thermalization. In fact, the failure of quantum systems to thermalize is highly dependent on such details; hence, Markovian baths may not be ideal for understanding possible dynamics beyond outright thermalization.

To gain insight into alternative behavior in the presence of baths, we turn to techniques used to study quantum dissipation; in particular, the model pioneered by Caldeira and Leggett [268, 269] and used in numerous subsequent works [270–275], which we detail in Sec. 7.2. Although Caldeira-Leggett baths are designed to thermalize a system (as can be seen using a standard Keldysh calculation [276]), recent work has shown that it is nonetheless possible for system coupled to these baths to feature dynamical properties reminiscent of localization [271, 274, 275]. A single particle, moving in a harmonic potential landscape in the presence of such dissipation will undergo a dynamical localization transition as the dissipation strength is *increased* [271], and the decohering effect of the bath results in effective Zeno localization [277] to one of the potential wells; recently, it was shown that the inclusion of a second, incommensurate potential will destroy the delocalized phase entirely, for arbitrary non-zero coupling to the bath [275], as detailed in Sec. 7.3.

Most studies of Caldeira-Leggett (CL) baths involve non-interacting systems, or a single particle; despite these simplified settings, such systems can nonetheless exhibit phase transitions

[270, 271, 273, 278–283]. However, exact results for interacting systems have remained largely elusive, and we explore this in Sec. 7.4.

7.2 Caldeira-Leggett Baths

In classical, non-equilibrium statistical physics, Brownian motion of a particle is described by the Langevin equation,

$$m\ddot{q} + \eta\dot{q} + \frac{\partial V}{\partial q} = \xi(t) \ , \tag{7.2.1}$$

where the ensemble averages of the fluctuating, dissipative force satisfy $\langle \xi(t) \rangle = 0$, $\langle \xi(t)\xi(t') \rangle = 2\eta\delta(t - t')$.

For classical systems, this equation can be derived from first principles using the formalism of the "megabath" [2], in which regards the system as consisting of the actual system of interest, and a toy model for a bath. They system and explicit bath are coupled to one another, and the combined system is itself coupled to the conventional mystery bath standard throughout statistical mechanics. The latter exists as a crutch for the calculation, as it is not possible in general to solve the infinitely many coupled nonlinear equations of motion that arise from the Euler-Lagrange equations for the classical system.

Modeling the bath as a collection of harmonic oscillators, one can then establish thermalization between the system and explicit bath. Additionally, the Langevin equation, given by Eq. (7.2.1), recovers directly. There are a number of caveats, of course. For example, the harmonic oscillator bath is integrable, and thus unable to reach an equilibrium distribution, which is a necessary condition for the oscillators to serve as a thermal bath as intended. This can be avoided by assuming that the oscillators had some mysterious interactions in the distant past, and that they equilibrated to a standard Gibbs-Boltzmann ensemble while the interactions were present, and the interactions have been conveniently turned off since then to facilitate calculation. The result shows how dissipation can arise from microscopic considerations of the bath.

The bath model pioneered by Caldeira and Leggett [268, 269, 272, 273] consists of a tower of quantum simple harmonic oscillators. This quantum bath provides for the demonstration of similar results compared to its classical counterpart, e.g. dissipation, in quantum systems in contact with their environment. Note that it is possible to formulate this model in the Keldysh formalism [276], in which case it is unnecessary to employ the "mega bath" necessary for the analogous classical calculation[1]. This calculation is a standard result, and reveals that morally equivalent results obtain for generic configurations of the bath (i.e. in terms of the initial density matrix in the distant past) as obtain for the thermal density matrix. The latter can be shown to be equivalent to the Matsubara formalism, i.e. the mega bath calculation at finite temperature. Hence, we will rely upon the latter as the formalism is simpler.

The simplest examples involving the Caldeira-Leggett formalism describe the dissipative dynamics of a *single* quantum degree of freedom [268, 269, 271, 278–281]. This can be the position of a particle, but similar models arise more generally in 'quantum impurity problems', describing e.g. the phase of a resistively and capacitively shunted Josephson junction, a Kondo spin in a metal, or the scattering phase shift at a quantum point contact or across a mobile impurity in a quantum fluid [284–286]. Despite their simplicity, these models can nevertheless exhibit phase transitions, e.g. as a function of dissipation strength [271, 280, 282, 287], and the results of Sec. 7.3.

[1] It is also worth mentioning that there exists a classical version of Keldysh in which this is also possible, though difficult.

To use a particular example relevant to Sec. 7.3, consider a "system" consisting of a single, quantum particle with position q, in which case the full Hamiltonian for the "system" and Caldeira-Leggett bath is given by

$$H = \frac{p^2}{2m} + V(q) + \sum_a \left(\frac{P_a^2}{2M_a} + \frac{1}{2} M_a \omega_a^2 \left(Q_a + \frac{f_a[q]}{M_a \omega_a^2} \right)^2 \right), \tag{7.2.2}$$

where $V(q)$ is some spatial potential felt by the particle and the rightmost term above is known as a "counter term" (which appears in the classical version as well), which ensures that the effect of the bath is purely dissipative [2]. We will primarily concern ourselves with a linear coupling between the particle and the bath, $f[q] = \lambda_a q$, however it is possible to repeat this procedure for general couplings, but in general these will result in corrections to the potential, V, in Eq. (7.2.2), and will be higher-order in temporal nonlocality. Such scenarios are likely less physical, and generally less soluble.

Under certain conditions, which are sufficiently generic, one can integrate over (i.e. "trace out") the bath degrees of freedom to recover an effective action for the hero particle in terms of its position, q. This procedure relies on the fact that the bath action is Gaussian, and the coupling to the system is linear in the oscillator displacements, as we show below.

Hence, we use the Euclidean time action, which we separate into terms corresponding to the system (i.e. the particle at q), bath, and coupling:

$$S_0[q] = \int_0^{\beta\hbar} \mathrm{d}\tau \left(\frac{m}{2} \dot{q}^2(\tau) + V\left(q(\tau)\right) \right), \tag{7.2.3}$$

and the bare action for the oscillator bath,

$$S_B\left[\{Q_a\}\right] = \int_0^{\beta\hbar} \mathrm{d}\tau \sum_a \frac{m_a}{2} \left(\dot{Q}_a^2(\tau) + \omega_a^2 Q_a^2(\tau) \right), \tag{7.2.4}$$

and finally, the system-bath coupling,

$$S_C\left[q, \{Q_a\}\right] = \int_0^{\beta\hbar} \mathrm{d}\tau \sum_a f_a[q(\tau)] Q_a(\tau) \tag{7.2.5}$$

where at present, we have ignored the "counter-term," which we can be inserted later into $S_0[q]$. We wish to calculate the effective action $S_{\text{eff}}[q]$, which obtains after integrating out the bath degrees of freedom,

$$e^{-S_{\text{eff}}[q]/\hbar} = \frac{\left\langle e^{-S_{\text{tot}}[q,\{Q_a\}]/\hbar} \right\rangle_B}{\left\langle e^{-S_B[\{Q_a\}]/\hbar} \right\rangle_B} \tag{7.2.6}$$

$$e^{-\left(S_0[q] + S'_{\text{eff}}[q]\right)/\hbar} = e^{-S_0[q]/\hbar} \frac{\left\langle e^{-\left(S_C[q,\{Q_a\}] + S_B[\{Q_a\}]\right)/\hbar} \right\rangle_B}{\left\langle e^{-S_B[\{Q_a\}]/\hbar} \right\rangle_B} \tag{7.2.7}$$

$$e^{-S'_{\text{eff}}[q]/\hbar} = \left\langle e^{-S_C[q,\{Q_a\}]/\hbar} \right\rangle_B . \tag{7.2.8}$$

Consider now the quantity

$$F_0\left[q(\tau)\right] = \int \left[DQ\right] \exp\left\{ -\frac{1}{\hbar} \int_0^{\beta\hbar} \mathrm{d}\tau \left(\frac{M}{2} \dot{Q}^2 + \frac{M}{2} \omega^2 Q^2 - \gamma Q q \right) \right\}, \tag{7.2.9}$$

which can be generalized to an arbitrary coupling that is a function of Euclidean time, $\gamma \to -if(\tau)$, for convenience of notation. We then evaluate

$$F\left[f(\tau), x_1, x_2\right] = \int_{Q(0)=x_1}^{Q(\beta\hbar)=x_2} [DQ] \exp\left\{-\frac{1}{\hbar}\int_0^{\beta\hbar} \mathrm{d}\tau \left(\frac{M}{2}\dot{Q}^2 + \frac{M}{2}\omega^2 Q^2 + if(\tau)Q(\tau)\right)\right\} \tag{7.2.10}$$

$$= \left(\frac{2\pi\hbar \sinh\left(\beta\hbar\omega\right)}{M\omega}\right)^{-1/2} e^{-\Phi[q]/\hbar}, \tag{7.2.11}$$

where Φ is an effective action that is written explicitly in equation 3.40 on page 82 of Feynman's book, and will be produced in detail below.

To summarize the procedure: Starting from $F\left[f(\tau), x_1, x_2\right]$, one can use integration by parts to expand about the classical path $x_0(\tau)$, which satisfies the Euler-Lagrange equations for the action represented by F and satisfies the initial and final conditions $x_0(0) = x_1$ and $x_0(\beta\hbar) = x_2$. We then expand the oscillator degree of freedom as $Q = x_0 + y$, where $y(0) = y(\beta\hbar) = 0$. This procedure is unnecessary if $x_1 = x_2$, which is precisely what one demands in the Matsubara formalism.

This function F will only give the top part[2] of the expectation value, which needs to be normalized, i.e.

$$e^{-S'_{\mathrm{eff}}[q]/\hbar} = \left\langle e^{-S_C[q,\{Q_a\}]/\hbar}\right\rangle_B = \frac{\left\langle e^{-(S_C[q,\{Q_a\}]+S_B[\{Q_a\}])/\hbar}\right\rangle_B}{\left\langle e^{-S_B[\{Q_a\}]/\hbar}\right\rangle_B} = \prod_a \frac{\int \mathrm{d}x_a F\left[f(\tau), x_a, x_a\right]}{\int \mathrm{d}x_a F\left[0, x_a, x_a\right]}\ , \tag{7.2.12}$$

where the oscillator path integrals are computed with $Q_a(0) = Q_a(\beta\hbar) = x_a$, and subsequently integrated over possible endpoints x_a.

The resulting expression can be solved via Fourier series for both Q and f,

$$Q(\tau) = \frac{a_0}{2} + \sum_{n=1}^{\infty}\left(a_n \cos\left(\frac{2\pi n\tau}{\beta\hbar}\right) + b_n \sin\left(\frac{2\pi n\tau}{\beta\hbar}\right)\right) \tag{7.2.13}$$

$$f(\tau) = \frac{f_0}{2} + \sum_{n=1}^{\infty}\left(f_n \cos\left(\frac{2\pi n\tau}{\beta\hbar}\right) + g_n \sin\left(\frac{2\pi n\tau}{\beta\hbar}\right)\right), \tag{7.2.14}$$

which already encodes the fact that $Q(0) = Q(\beta\hbar) \equiv x_a$, and we can then replace the path integral over $[Q]$, combined with integration over the constraint x_a, with integration over all the coefficients $\{a_n, b_n\}$. Although this involves some monstrous Jacobean, because of the overall normalization factor in Eq. (7.2.12), this will work out nicely. We have

$$\prod_\alpha \exp\left\{-\frac{f_0^2}{4M_\alpha\omega_\alpha^2} - \frac{\beta}{2M_\alpha}\sum_{n=1}^{\infty}\frac{f_n^2 + g_n^2}{\left(\omega_\alpha^2 + \left(\frac{2\pi n}{\beta\hbar}\right)^2\right)}\right\}, \tag{7.2.15}$$

which can be simplified using the formula

$$\frac{1}{\pi\lambda} + \frac{2\lambda}{\pi}\sum_{n=1}^{\infty}\frac{\cos\left(n\phi\right)}{n^2+\lambda^2} = \frac{\cosh\left(\pi\lambda - \lambda\left|\phi\right|\right)}{\sinh\left(\pi\lambda\right)}, \tag{7.2.16}$$

to obtain the effective action

$$e^{-S'_{\mathrm{eff}}[q]/\hbar} = \prod_a \exp\left[-\frac{1}{4M_a\hbar\omega_a}\int_0^{\beta\hbar}\mathrm{d}\tau\int_0^{\beta\hbar}\mathrm{d}\tau' f(\tau)f(\tau')\frac{\cosh\left(\omega_a\left|\tau-\tau'\right| - \beta\hbar\omega_a/2\right)}{\sinh\left(\beta\hbar\omega_a/2\right)}\right]. \tag{7.2.17}$$

[2] I believe this is called a "numerator."

Recognizing that the function f ought to be periodic in imaginary time on the interval $[0, \beta\hbar]$, Eq. (7.2.17) becomes

$$e^{-S'_{\rm eff}[q]/\hbar} = \prod_a \exp\left[-\frac{1}{4M_a\hbar\omega_a} \int_0^{\beta\hbar} \mathrm{d}\tau \int_{-\infty}^{\infty} \mathrm{d}\tau' f(\tau) f(\tau') e^{-\omega_a|\tau-\tau'|} \right] , \tag{7.2.18}$$

by cleverly extending the bounds of integration over τ' to make Eq. (7.2.17) much more user-friendly.

We now make explicit the function $\gamma = -if(\tau)$, which we take to be linear in the coordinate of the particle, $if(\tau) = \lambda_a q(\tau)$, into Eq. (7.2.18), so that the resulting action is Gaussian, and because the coupling is also linear in the bath coordinate, so this is nice and reciprocal. The result is

$$S'_{\rm eff}[q] = -\sum_a \left\{ \frac{\lambda_a^2}{4M_a\omega_a} \int_0^{\beta\hbar} \mathrm{d}\tau \int_{-\infty}^{\infty} \mathrm{d}\tau' q(\tau) q(\tau') e^{-\omega_a|\tau-\tau'|} \right\}, \tag{7.2.19}$$

and making the substitution $q(\tau)q(\tau') = \left[q^2(\tau) + q^2(\tau') - (q(\tau) - q(\tau'))^2\right]/2$ allows for a nice cancellation with the counter term that we have thus far largely ignored (which is also related to why the counter term is needed), and we recover

$$S'_{\rm eff}[q] = \sum_a \left\{ \frac{\lambda_a^2}{8M_a\omega_a} \int_0^{\beta\hbar} \mathrm{d}\tau \int_{-\infty}^{\infty} \mathrm{d}\tau' \left(q(\tau) - q(\tau')\right)^2 e^{-\omega_a|\tau-\tau'|} \right\} . \tag{7.2.20}$$

We now make the "useful" identification(s)

$$\alpha(s) \equiv \sum_a \frac{\lambda_a^2}{4M_a\omega_a} e^{-\omega_a|s|} = \int_0^{\infty} \frac{\mathrm{d}\omega}{2\pi} J(\omega) e^{-\omega|s|}, \tag{7.2.21}$$

which defines the bath spectral function, $J(\omega)$,

$$J(\omega) = \frac{\pi}{2} \sum_a \frac{\lambda_a^2}{M_a\omega_a} \delta(\omega - \omega_a) , \tag{7.2.22}$$

and results in the effective action

$$S'_{\rm eff}[q] = \frac{1}{2} \int_0^{\beta\hbar} \mathrm{d}\tau \int_{-\infty}^{\infty} \mathrm{d}\tau' \left(q(\tau) - q(\tau')\right)^2 \int_0^{\infty} \frac{\mathrm{d}\omega}{2\pi} J(\omega) e^{-\omega|\tau-\tau'|}. \tag{7.2.23}$$

In general, one can assume $J(\omega)$ is analytic, and possesses either a specific power-law form, $J(\omega) = \eta_\gamma |\omega|^\gamma$, or is the sum over such terms.

We will generally be interested in the specific form of $J(\omega)$ corresponding to *Ohmic* dissipation:

$$J(\omega) = \eta|\omega|. \tag{7.2.24}$$

Calculations for and constraints on other forms of $J(\omega)$ can be found in Appendix D.1.1, as not all of these have finite Fourier transforms, a necessary element for obtaining a useful "free theory."

For the case of Ohmic dissipation, i.e. with J given by Eq. (7.2.24), we obtain the full Euclidean action for the hero particle

$$S_0 = \frac{\eta}{4\pi} \int_0^{\beta\hbar} d\tau \int_{-\infty}^{\infty} d\tau' \left(\frac{q(\tau) - q(\tau')}{\tau - \tau'} \right)^2 + \frac{m}{2} \int_0^{\beta\hbar} d\tau \left(\dot{q}^2(\tau) + V\left[q(\tau)\right] \right), \tag{7.2.25}$$

which amounts to an effective temporally non-local term, in addition to the bare terms present in Eq. (7.2.3).

7.3 Quantum Brownian Motion

This Section is largely drawn from Ref. 275 by this author.

7.3.1 Introduction

Localization has been a subject of interest for over half a century, following Anderson's seminal work on electron propagation in disordered media [10]. Recently, the recognition that the many-body localized (MBL) insulator is a stable state of matter with robust non-equilibrium phase structure has sparked renewed interest in the topic [11,13,14,21,250]. Although much of this effort has focused on isolated systems with uncorrelated disorder, two departures from these prevalent paradigms have emerged as significant. First, studying localization in open quantum systems coupled to an external 'bath' is both intrinsically interesting [264–267] and relevant to many experiments [261–263,288]. Second, quasiperiodic systems can also display localization, but unlike their disordered cousins, may be less susceptible to rare region effects that disrupt MBL in $d > 1$ [237,238,289–293]. Quasiperiodic potentials can be engineered robustly and controllably in cold atom experiments, either by superposing two mutually incommensurate optical lattices, or by 'cut-and-project' techniques. Experiments have now begun to probe the interplay of localization, interactions, and coupling to a bath in quasiperiodic systems [261,262,293–298].

In this Section, we show that the properties of a quasiperiodic system can be altered by coupling to a bath with non-trivial dynamics, even without interactions. In a departure from previous studies [265], we will focus on non-Markovian baths, which arise from models of dissipation, induced, e.g. by coupling to a continuum of gapless excitations [268,269], as detailed in Sec. 7.2. Despite their simplicity, these models can nevertheless exhibit phase transitions, e.g. as a function of dissipation strength [271,280,282,287].

For instance, a particle in a periodic potential can undergo a $T = 0$ phase transition as the strength of Ohmic dissipation α is tuned: for $\alpha > \alpha_c$ the particle is localized in one of the potential minima, while for $\alpha < \alpha_c$ it is delocalized and undergoes quantum Brownian motion over long distances, where α_c is a critical value of dissipation set by the periodicity of the potential [271]. We examine the fate of this $T = 0$ transition for *quasi*periodic potentials. We show that the delocalized phase present at weak dissipation $\alpha < \alpha_c$ for a single periodic potential [271] is destabilized by an additional periodic perturbation, even when the latter has a *higher* critical dissipation strength in isolation. The resulting phase diagram depends on the ratio between the periods of the potentials. In the commensurate case, the delocalized phase survives, but with a lower critical dissipation strength than for either potential in isolation; for the incommensurate (quasiperiodic) case, it is destroyed. Notably, with dissipation the delocalized phase is absent even for infinitesimally weak quasiperiodic perturbations, in striking contrast to the dissipationless case [289] where it survives up to a critical value of the quasiperiodicity. Although the problem formally maps to a 'double-frequency' boundary sine-Gordon model with no exact solution, we can compute an approximate localization length using renormalization-group (RG) techniques. We showcase this approach for examples of commensurate and incommensurate perturbations.

We also find a surprising application of our analysis to the currently more experimentally realizable setting of a mobile impurity moving in a periodic lattice in one dimension, immersed in a quantum fluid that it scatters strongly via contact interactions. Here our model describes the

dissipative dynamics of the scattering phase across the impurity, the relevant commensurability is between the gas density and the lattice, and the transition corresponds to a change in the impurity dispersion (energy-momentum relation $E(P)$), from flat to periodic.

7.3.2 Model

We begin by considering a single quantum particle interacting with a bath of harmonic oscillators [268, 269]. The joint Hamiltonian is

$$H = H_0(q) + \frac{1}{2}\sum_a \frac{p_a^2}{m_a} + m_a\omega_a^2\left(x_a + \frac{f_a[q]}{m_a\omega_a^2}\right)^2, \tag{7.3.1}$$

where a indexes the oscillators, q is the spatial coordinate of the particle, and $H_0 = p^2/2m + V(q)$, with $V(q)$ a local potential. We assume linear particle-bath coupling $f[q] = \lambda_a q$, and characterize the bath via its spectral function $J(\omega) = \frac{\pi}{2}\sum_a \frac{\lambda_a^2}{m_a\omega_a}\delta(\omega-\omega_a)$. We restrict to Ohmic dissipation, $J(\omega) = \eta|\omega|$, which in the classical/high-temperature limit yields Brownian motion described by a Langevin equation [268, 269]. Integrating out the bath in the partition function yields an (imaginary-time) effective action for the particle [299], which for Ohmic dissipation and $V = 0$ is

$$S_0 = \int_0^{\beta\hbar} d\tau\left[\frac{m}{2}\dot{q}^2(\tau) + \frac{\eta}{2\pi}\int_{-\infty}^{\infty} d\tau' \frac{q(\tau)q(\tau')}{(\tau-\tau')^2}\right]. \tag{7.3.2}$$

We scale out a microscopic length q_0 (this will be set by the potential) and take $\theta(\tau) = 2\pi q(\tau)/q_0$. We identify the characteristic energy scale $E_0 = (2\pi\hbar)^2/mq_0^2$ required to confine the particle to q_0, so that $\Lambda = E_0/\hbar$ sets the scale of the bare kinetic energy. Since this is irrelevant under the RG by power counting (compared to the nonlocal bath contribution) we replace it by a cutoff Λ on the bath term [271, 278, 279, 281]

$$S_0[\theta(\omega)] = \frac{\alpha}{4\pi}\int_{-\Lambda}^{\Lambda}\frac{d\omega}{2\pi}\,|\omega|\,|\theta(\omega)|^2\,. \tag{7.3.3}$$

Appropriate choices of $V(q)$ realize a number of interesting scenarios. We will exclusively consider potentials of the form $V(q) = -\sum_\mu V_\mu\cos(\lambda_\mu q)$, with one or two V_μ initially nonzero. In this case, we choose $q_0 = 2\pi/\min[\lambda_\mu]$, and rescale parameters to obtain $V[\theta] = \sum_\mu V_\mu\cos(\lambda_\mu\theta)$, where now $\lambda_\mu \geq 1$ and $V_1 \neq 0$. We will analyze the phase diagram of $S_0 + S_V$, where $S_V = \int d\tau\, V[\theta(\tau)]$, for different choices of λ_μ.

7.3.3 A single harmonic

We first consider a single harmonic, i.e. $V_\mu = 0$ for $\mu \neq 1$, corresponding to a particle in a periodic potential [271, 278–282], with

$$S_V[\theta(\tau)] = -V_1\int d\tau\cos\left[\theta(\tau)\right], \tag{7.3.4}$$

meaning $S_0 + S_v$ is a boundary sine-Gordon model. Therefore, the perturbative effect of the potential to the 'free fixed point' Eq. (7.3.3) can be straightforwardly diagnosed using momentum-shell RG [271, 300], as follows. First, we split the fields into 'slow' and 'fast' modes $\theta(\omega) =$

$\theta_s(\omega)\Theta[\Lambda/b - \omega] + \theta_f(\omega)\Theta[\omega - \Lambda/b]$ where Θ is the unit step function, and $b = e^\ell$. We then integrate out the fast modes, possibly generating new terms, using a cumulant expansion about the Gaussian S_0, and rescale frequencies via $\omega \mapsto b\omega$ to keep S_0 fixed. Finally, we define rescaled fields via $\theta(\tilde{\omega}) = b^{-1}\theta_s(\omega)$. Iterating this transformation, we obtain the RG flow equation for V_1:

$$\frac{dV_1}{d\ell} = \left(1 - \frac{1}{\alpha}\right) V_1 + O(V_1^3). \tag{7.3.5}$$

This shows that the model has a phase transition at $\alpha_c = 1$: for $\alpha < \alpha_c$, V_1 flows to zero under the RG (corresponding to the free phase), whereas for $\alpha > \alpha_c$, V_1 is relevant and the flow is to strong coupling. In this limit, a variational estimate suggests that the localization length ξ^* diverges as $(\alpha - \alpha_c)^{-1/2}$ [271]. The constancy of α under RG follows from two facts. First, note that V_1 is local in time, and coarse-graining preserves locality; in contrast, S_0 is nonlocal in time for $T \to 0$, and so cannot emerge in the perturbative RG. Second, the coefficient of θ is fixed by translational symmetry, $\theta \to \theta + 2\pi\mathbb{Z}$. Thus, α does not flow [271]. Additionally, while V_1 itself does not receive corrections at second order in V_1, a V_2 term *is* generated at $O(V_1^2)$.However, it is less relevant than V_1, which is always the most relevant term generated by the flow to *all* orders. (This will no longer be true if a second harmonic V_γ with $\gamma \notin \mathbb{Z}$ is included.)

7.3.4 Generalized RG flows

We now study the double-frequency (bichromatic) boundary sine-Gordon model,

$$S_V\left[\theta(\tau)\right] = -\int d\tau \left\{V_1 \cos\left[\theta(\tau)\right] + V_\gamma \cos\left[\gamma\theta(\tau)\right]\right\}, \tag{7.3.6}$$

where, without loss of generality, we take $\gamma > 1$. Observe that with this choice, for $\alpha < 1$, both V_1 and V_γ are irrelevant if considered in isolation. For $\gamma \in \mathbb{Z}$, any term generated by the RG has a higher scaling dimension than V_1, and is therefore also irrelevant. For $\gamma \notin \mathbb{Z}$, we must consider the terms generated at second order in the RG equations. Intuitively, this is because 'beating' between two cosines can yield a cosine with a shorter wavelength, potentially relevant even when V_1, V_γ are not. This picture already signals that rational and irrational γ are physically distinct: in the former case, there are finitely many such beats; in the latter there are infinitely many. This is a consequence of the fact that a quasiperiodic potential has no shortest reciprocal lattice vector [3].

To study these effects quantitatively, we determine the RG flow equations. We consider all wavevectors generated by the RG, corresponding to the set $\mathcal{L} = \{\lambda : \lambda = |m + \gamma n|, m, n \in \mathbb{Z}\}$ [4]. While an explicit derivation of RG equations requires a tedious (albeit standard) cumulant expansion [300], their structure is fixed by the operator product expansion of boundary sine-Gordon theory:

$$\frac{dV_\lambda}{d\ell} = \left(1 - \frac{\lambda^2}{\alpha}\right) V_\lambda + \sum_{\lambda',\lambda''} C_\lambda^{\lambda'\lambda''} V_{\lambda'} V_{\lambda''} + \ldots \tag{7.3.7}$$

where $C_\lambda^{\lambda'\lambda''} = \frac{\lambda'\lambda''}{2\alpha}(\delta_{\lambda,\lambda'+\lambda''} - \delta_{\lambda,\lambda'-\lambda''})$, and '…' denotes higher-order terms that we neglect in this perturbative analysis. Evidently, this coupled set of equations Eq. (7.3.7) captures the beat phenomenon described above, since at $O(V^2)$ the RG generates new terms that are absent at the bare level. These in turn generate other terms as the flow proceeds. The absence of $\theta \mapsto \theta + 2\pi$ symmetry may allow additional terms that in principle could affect the RG flows; however, the

[3] Though they are not periodic in space, quasicrystals *do* have a regular structure of Bragg peaks.

[4] In mathematical terms, $\mathcal{L}$ is a $\mathbb{Z}$-module on $\{1, \gamma\}$.

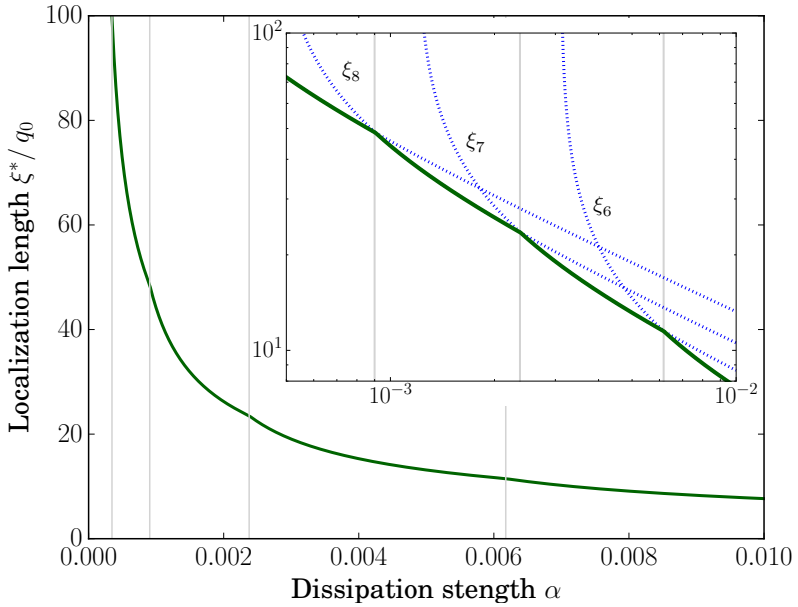

Figure 7.1: Localization length ξ^* as a function of dissipation α for quasiperiodic potential with $\gamma = \varphi$ (solid green). Inset: same plot on log-log scale. As α is decreased, ξ^* is a piecewise function that changes non-analytically for $\alpha \sim \alpha_n = \varphi^{-2n}$ between successive $\xi_n = \frac{q_0}{2\pi}\sqrt{\frac{2\ell_n}{\alpha}}$ (see Eq. (7.3.9)).

set Eq. (7.3.7) remains valid at a perturbative level, and we proceed assuming their validity. To understand their solution, we consider the scenario where $V_1 = u_0, V_\gamma = \epsilon u_0$ at the bare level; for a given α, the question then is to determine (i) the new critical dissipation strength $\alpha_c' < \alpha_c$; (ii) the RG time $\ell^*(\alpha)$ at which, for $\alpha_c' < \alpha < \alpha_c$ a relevant potential generated by these bare values flows to $O(1)$; and (iii) the corresponding localization length associated with this relevant potential. For $\ell \gtrsim \ell^*$ we enter the strong-coupling regime where our perturbative RG is no longer reliable. Unlike in the conventional single-frequency boundary sine-Gordon problem, there is no exact solution or duality to leverage here. Though we have assumed a flow to strong coupling, we cannot rule out the possibility of an intermediate fixed point stabilized by higher-order terms neglected in Eq. (7.3.7); this is a question for future analysis.

Taking $\gamma = m/n \geq 1$ to be an irreducible *rational* number, the minimum non-zero wavevector is given by $\lambda_c = 1/n$, and all V_λ for $\lambda \in \mathcal{L}$ are irrelevant if $\alpha < \alpha_c' \equiv \lambda_*^2$, i.e., the delocalized phase survives, but shrinks in extent. However, for $\alpha_c' < \alpha < 1$, the localization is driven by high-order 'beats': bare V_1, V_γ are irrelevant, but generate other V_λs as they flow to zero; eventually, a relevant term emerges and grows to $O(1)$. The corresponding scale ℓ^* controls the crossover to localization: intuitively, it is the scale at which the particle 'sees' the potential. To understand this, we consider Eq. (7.3.7) for a minimal set of V_λ needed to generate a relevant term. We ignore second-order terms for each unless they help generate the relevant term, which is justified by numerical iteration of Eq. (7.3.7). We then integrate the flows of $V_1(\ell)$ and $V_\gamma(\ell)$ directly [300]. For $\gamma = 3/2$ and $1/4 < \alpha < 1$, since a relevant term ($V_{1/2}$) is generated by these two directly, we find it grows to $O(1)$ in an RG 'time'

$$\ell^* = \frac{\alpha}{\alpha_c' - \alpha} \ln\left[\epsilon u_0^2\right] + \ldots, \tag{7.3.8}$$

where the omitted terms ... do not involve u_0 or ϵ. We can extract from this scale a localization length $\xi^* \propto \sqrt{\langle \theta^2(\tau)\rangle}$, where in evaluating the average we only consider the modes between the

current RG scale $\Lambda e^{-\ell^*}$ and the original cutoff Λ. We find $\xi^* = \frac{q_0}{2\pi}\sqrt{\frac{2\ell^*}{\alpha}} \propto (\alpha - \alpha_c)^{-1/2}$ [300], which mirrors a variational calculation for the single-harmonic problem [271]. A similar relation for ℓ^* may be obtained for generic commensurate γ, but with the difference that higher powers of ϵ and u_0 appear in the logarithm, corresponding to the fact that the relevant operator emerges at a higher order.

7.3.5 Quasiperiodic case

We now turn to the quasiperiodic (incommensurate) problem. For irrational $\gamma \notin \mathbb{Q}$, we see immediately that the minimum non-zero wavevector λ_c in $\mathcal{L}$ is ill-defined. Therefore, the critical dissipation strength for localization is zero, so that arbitrarily weak dissipation leads to localization. Intuitively, for rational $\gamma = m/n$, the combined potential $V(\theta) = V_1 \cos\theta + V_\gamma \cos\gamma\theta$ always contains a periodic set of equally-spaced minima (e.g., at spacing $2\pi n$); if the dissipation is sufficiently weak that coherent tunneling between these minima remains possible, the delocalized phase survives. Conversely, for irrational γ, $V(\theta)$ hosts no such periodic set of minima — indeed, there is no real-space periodicity. Therefore, the coherent tunneling is disrupted on long length scales, so that no matter how small the dissipation, the particle will eventually come to rest in some potential minimum.

For concreteness, we consider the *Fibonacci potential*, given by $\gamma = \varphi = \frac{1}{2}\left(1 + \sqrt{5}\right)$, the Golden mean. Within $\mathcal{L}$, we note that the decreasing sequence $\lambda_n \equiv (-1)^n \left(F_{n+1} - \varphi F_n\right) = \varphi^{-n}$ – where F_n is the n^{th} element of the Fibonacci sequence – goes to zero rapidly as $n \to \infty$. We will refer to these as Fibonacci wave numbers: taking $\lambda_0 = 1$, $\lambda_1 = \varphi - 1$ is the first new term generated by the RG with a smaller wave number than those present at the bare level, and subsequent λ_n are quickly generated by successive RG iterations, $\lambda_n = \lambda_{n-2} - \lambda_{n-1}$. Although for a given α there exist many arbitrary $\mu_{m,n} = m - \varphi n$ such that $\mu_{m,n}^2 < \alpha$, a smaller Fibonacci wave number will always have been generated earlier in the RG, and thus will have had more time to grow in strength and spawn further λ_n. Thus, determining the most relevant wave number is simplified relative to a generic irrational γ (though by analogy to the Fibonacci case, we conjecture they will be generated by successive 'best rational approximants' of γ).

The crossover to localization is controlled by a critical scale ℓ^*, the RG time for *some* relevant term to become $O(1)$. We denote λ_{n^*} as the first relevant term become $O(1)$ when all λ_n are allowed to be non-zero. Each λ_n requires RG time ℓ_n to grow to $O(1)$, and ℓ^* corresponds to the smallest among the ℓ_n for a given α, where ℓ_n are determined by analogy to Eq. (7.3.8):

$$\ell_n = \frac{\alpha}{\varphi^{-2n} - \alpha} \ln\left[V_\gamma^{F_n} V_1^{F_{n+1}}\right], \tag{7.3.9}$$

as may be verified by direct integration of Eq. (7.3.7) [300]. Omitted from Eq. (7.3.9) are subleading corrections that vanish in the limit $\alpha \ll 1$ [300]. As α is decreased, ℓ^* is set by successive ℓ_{n^*} with larger Fibonacci indices: taking $V_1 = -\ln V_\gamma = 1$, we see that $\xi^* = \frac{q_0}{2\pi}\sqrt{\frac{2\ell^*}{\alpha}}$ is determined by successive ℓ_n in a piecewise manner, with ℓ^* changing from ℓ_n to ℓ_{n+1} at $\alpha \sim \varphi^{-2n} = \lambda_n^2$. This leads to non-analyticity in ξ^* (Fig. 7.1). Although there is always a relevant, localizing potential with wave number λ_{n^*}, it requires increasingly long for this term to be generated, corresponding to $\ell^* \to \infty$. Dynamically, it will take increasingly longer for the particle to 'feel' the localization.

7.3.6 Experimental realization in a mobile impurity

So far, we have assumed that our model directly describes a particle in a quasiperiodic landscape. This can be challenging to engineer and observe in cold-atom simulations. We now discuss an alternative route to the same physics in a mobile impurity problem [284–286, 301]. Consider a single mobile impurity, with coordinate X and momentum P, in a periodic optical lattice (spacing $a = 1$ and length L), and immersed in a quantum fluid. Describing the latter as a Luttinger liquid with interaction parameter K and velocity v,

$$H_g = \frac{v}{2\pi} \int_{-L/2}^{L/2} dx \left[K(\partial_x \theta)^2 + \frac{1}{K} (\partial_x \phi)^2 \right] \tag{7.3.10}$$

with $[\phi(x), \partial_y \theta(y)] = i\pi\delta(x-y)$ captures its dynamics. We assume that the optical lattice is sufficiently strong that the impurity has tight-binding dispersion given by $H_i = -t_i \cos(P)$, and that the particle and the gas interact via contact interactions $H_{\text{int}} = u\rho(X)$, where $\rho(X)$ is the density of the gas, and t_i and u are coupling strengths. The full Hamiltonian is $H = H_i + H_g + H_{\text{int}}$. It is convenient to make a unitary transformation $\mathcal{U}_X = e^{iP_g X}$ to the frame co-moving with the impurity, so that $H \mapsto \mathcal{U}_X H \mathcal{U}_X^{-1} = H_g + u\rho(0) - t_i \cos(P - P_g)$. Since X is now absent from H, P is conserved and corresponds to the total momentum. We now take the $u \to \infty$ limit, corresponding to a strongly-scattering impurity, where the leading term at $O(1/u)$ involves the tunneling of gas particles across the impurity. This yields the Josephson-like term $H_r \approx -t_g \cos(\Theta)$, where $\Theta = \theta(0^+) - \theta(0^-)$ describes the phase shift across the impurity. We may relate P_g to Θ by using the usual Luttinger liquid relations for the density $\rho = \pi^{-1}\partial_x \phi$ and momentum $\pi_\phi = \partial_x \theta$:

$$P_g = \int_{|x|>\epsilon} dx \rho \pi_\phi = \frac{1}{\pi} \int_{|x|>\epsilon} dx\, \partial_x \phi \partial_x \theta = -\nu\Theta, \tag{7.3.11}$$

where the integral excludes the origin as there is a break in the fluid at the impurity. We have used the mode expansion $\phi(x) = \phi_0 + \pi \frac{N}{L} x + \tilde{\phi}(x)$, $\theta(x) = \theta_0 + \pi \frac{J}{L} x + \tilde{\theta}(x)$, where N, J are the total particle number and current, respectively, and $\nu = N/L$ is the average density or filling. Finally, we integrate out the gapless sound modes of H_g subject to the boundary condition $\theta(0^+, t) - \theta(0^-, t) = \Theta(t)$; this generates dissipative dynamics for Θ. Working in imaginary time we arrive at the impurity effective action

$$S_i = \int d\tau \left[t_i \cos(P + \gamma\Theta) + t_g \cos\Theta \right] + \frac{\alpha}{4\pi} \int d\omega |\omega| |\Theta_\omega|^2 \tag{7.3.12}$$

with $\alpha = 1/K$ [5], $\gamma = \nu$; $P \neq 0$ does not affect the RG flows, and hence, we see that the impurity is described by the double-frequency sine-Gordon action, with the wavevector of one of the cosines tuned by the gas density. Reinstating the lattice spacing a, we see that $\gamma = \nu a$ corresponds to the number of gas atoms in each unit cell of the potential seen by the impurity; evidently, there is no particular restriction to commensurate γ. In this language, the regime where the cosines are irrelevant corresponds to an impurity that is non-dispersive, i.e. whose energy is independent of P, while the one where the cosines are relevant correspond to a dispersive impurity. When the gas density is commensurate with the impurity potential, the impurity is able to move recoillessly between minima while simultaneously allowing an integer number of gas particles to tunnel across it; for sufficiently weak dissipation this 'dressed' process continues to show quantum Brownian motion. This effect is absent in the quasiperiodic case, but depending on the scale at which the

[5] We take K to be the effective value obtained after eliminating derivative terms of the form $\partial_x \Theta$.

system is probed, the dispersion will show different periodicity set by the potential that controls ξ^*. We defer further investigation of the impurity realization of the quasiperiodic problem to future work.

7.3.7 Discussion

In conclusion, we have shown that a quantum particle moving in a quasiperiodic potential is always localized by a dissipative bath as $T \to 0$. This is in sharp contrast with the well-known quantum phase transition in the periodic case. We also argued that this physics could be realized in the strong-coupling regime of a mobile impurity in a one-dimensional Fermi gas moving in a periodic lattice. On the formal side, we note that while the infrared behavior of the single-frequency boundary sine-Gordon field theory can be studied using instanton expansions and integrability, much less is known about multi-frequency variants. It would be very interesting — and of direct relevance to an experimentally accessible regime of mobile impurity problems — to develop analytic tools to analyze the flow to strong coupling in this theory, and investigate the possibility of a new class of intermediate-coupling fixed points.

7.4 Dissipative Quantum Fluids

This Section is largely drawn from Ref. 302 by this author.

7.4.1 Introduction

Here we consider the effect of such a dissipative bath on an interacting, one-dimensional quantum system, which in various limits may represent any of a number of experiments. Taking the system to be somewhat insulated from its environment, one expects the bath to have a weak, dissipative effect thereupon, motivating the use of the CL formalism. Since the CL bath equilibrates with the system, we exploit standard equilibrium methods to examine the low-temperature properties of the combined system and bath, and also obtain results for arbitrary $T > 0$ using the Matsubara formalism.

At long wavelengths, the physics of fluids comprising either boson or fermion degrees of freedom (degrees of freedom) is captured by the paradigmatic Luttinger liquid [303–309]. The bare action Eq. (7.4.1) for this system is quadratic in a scalar, bosonic 'displacement' field, $\phi(x,\tau)$, related to fluctuations of the density. Depending on microscopic details, there may also be corrections of the form $\cos[m\phi(x,\tau)]$, for various harmonics m, which may correspond to spatial potentials, Umklapp processes, etc. We comment on the physical relevance of these terms using correlation functions and a renormalization group (RG) analysis.

Regarding the partition function of the Luttinger liquid and bath, we can trace out the bath degrees of freedom exactly [268–275, 299] to obtain an effective theory for the Luttinger liquid [274, 310–316]. The primary result will be the creation of a temporally non-local density-density interaction term, which is also quadratic in ϕ. Hence, we are able to compute various two-point correlation functions of ϕ nonperturbatively. Comparing these correlation functions to those of the 'closed' Luttinger liquid, we find that the dissipative bath destroys the perfect metallic conductivity of the Luttinger liquid, and also makes cosine terms far more relevant, in agreement with Ref. 312.

The latter renders the system more sensitive to spatial potentials coupling to the density, as well as back-scattering processes, each of which further localizes the system. Although the CL bath thermalizes with the Luttinger liquid, in surprising contrast to Markovian baths, the decohering effect of the CL bath renders the Luttinger liquid more localized.

7.4.2 Model

The 'system' is a quantum fluid in a one dimensional ring of length L. For concreteness, we take the fluid's microscopic degrees of freedom to be fermions, though our results should hold for bosons as well [308]. In one dimension, the coarse grained theory of either is the Luttinger liquid [303–309], with Euclidean action

$$S_{LL} = \frac{\hbar u}{2\pi K} \int_0^{\beta\hbar} d\tau \int_{-L/2}^{L/2} dx \left(\left(\frac{1}{u} \partial_\tau \phi \right)^2 + (\partial_x \phi)^2 \right), \tag{7.4.1}$$

where the velocity, u, and stiffness, K, are given by

$$u \equiv \left[\left(v_F + g_4 \right)^2 - g_2^2 \right]^{1/2}, \; K \equiv \left[\frac{v_F + g_4 - g_2}{v_F + g_4 + g_2} \right]^{1/2}, \tag{7.4.2}$$

where for spinless fermions, g_2 is the small-q matrix element of the interaction between fermions near opposite Fermi points, and g_4 corresponds to fermions near the same Fermi point [307, 308]. We have taken the usual limit of δ-function interactions, but it is possible to treat any sufficiently short-ranged interaction [307].

The field ϕ is related to the fermion density via

$$\rho(x) = -\frac{1}{\pi} \nabla \phi(x) + \frac{1}{\pi\alpha} \cos\left[2k_F x - 2\phi(x) \right] + \ldots, \tag{7.4.3}$$

where we have omitted higher harmonics of ϕ[6], and α is a vanishing length scale (UV cutoff). The conjugate momentum to ϕ is $\Pi = \pi^{-1} \nabla \theta$, proportional to the *current*. An equivalent action is given by replacing $\phi \leftrightarrow \theta$ and $K \leftrightarrow K^{-1}$ in Eq. (7.4.1).

In general, other terms in Eq. (7.4.1) are possible, e.g. if one considers curvature of the electron dispersion $\varepsilon(k)$, or various potentials that couple to the harmonic parts of the density Eq. (7.4.3). We neglect these at long wavelengths [307, 308] to highlight the *leading* alteration to the Luttinger liquid induced by dissipation. We consider the most relevant of these corrections using perturbative RG in Sec. 7.4.9.

The *full* model consists of the action Eq. (7.4.1) for the 'system', that of the oscillator bath, S_B, and a coupling, S_C, between the two:

$$S_{\text{full}}[\phi, \varphi] = S_{LL}[\phi] + S_B[\varphi] + S_C[\phi, \varphi], \tag{7.4.4}$$

where in the continuum one has [268–270, 272, 273]

$$S_B[\varphi] = \frac{1}{2} \int_0^{\beta\hbar} d\tau \int_{-L/2}^{L/2} dx \left(\left(\frac{1}{c} \partial_\tau \varphi \right)^2 + (\partial_x \varphi)^2 \right), \tag{7.4.5}$$

[6] The explicit form of these terms may depend on the bosonization convention and microscopic details, which are not of central importance in this work. This will also change for the chiral or helical Luttinger liquids.

for some velocity c. The system-bath coupling is linear in both the density, ρ Eq. (7.4.3) and the bath field, φ,

$$S_C[\phi,\varphi] = \int_0^{\beta\hbar} d\tau \int_{-L/2}^{L/2} dx\, \lambda(x)\, \rho(x)\, \partial_x \varphi \ . \tag{7.4.6}$$

for arbitrary λ. Generally, our analysis will not be sensitive to microscopic details of either S_B Eq. (7.4.5) or S_C Eq. (7.4.6), i.e. c and $\lambda(x)$; however some details are essential for the elimination of the bath degrees of freedom to be tractable. To wit, we require S_B Eq. (7.4.5) to be quadratic, and that S_C Eq. (7.4.6) be linear at least in the bath field φ. Both stipulations are inherent to the CL model; and most naturally captured by Eq. (7.4.5) and Eq. (7.4.6).

Regarding the corresponding partition function $\mathcal{Z} = \mathrm{Tr}\{e^{-S_{LL}-S_B-S_C}\}$, we can integrate (or trace) out the bath degrees of freedom, φ, to obtain a modified theory for the Luttinger liquid [268–273, 299]. This results in an "effective" term $S_{\text{eff}}[\phi]$ being added to S_{LL} Eq. (7.4.1), which will also be bilinear in ϕ, to produce the Gaussian action

$$S_0[\phi] = S_{LL}[\phi] + S_{\text{eff}}[\phi]\,. \tag{7.4.7}$$

This relies crucially on the linearity of Eq. (7.4.6) in both φ and $\rho \sim -\frac{1}{\pi}\nabla\phi$, and S_B being quadratic in φ; because this term results from Gaussian integration over $\varphi(x,\tau)$, it will always be *non-local in time* [272–274, 310–316].

In simpler models—where the "system" consists of a single degrees of freedom, e.g. the position of a particle or a two-level system [268–273]—one makes a particular Ansatz for the bath spectral function. Because S_B is Gaussian, this choice corresponds directly to a particular coupling $J(k,\omega)$ (in Fourier space) for the non-local term S_{eff} Eq. (7.4.8). Absent such an Ansatz, S_0 would be sensitive to non-generic microscopic details of the bath; additionally, this choice affects only the ω- and k-dependence of the *coefficient* J of the term(s) in S_{eff}, whereas bilinearity in ϕ and temporal non-locality are jointly guaranteed by the linear and quadratic nature of Eq. (7.4.6) and S_B in φ, respectively. Following this standard practice in the treatment of CL baths [268–273], we assert *some* spectral function (i.e. coupling $J(k,\omega)$ in S_{eff}), and invoke RG relevance to constrain which forms merit consideration.

Thus, in general, one expects a term of the form [274, 312]

$$S_{\text{eff}}[\phi] = J(k,\omega)\,|\phi_{\omega,k}|^2 \ . \tag{7.4.8}$$

Taylor expanding J in ω and k recovers a sum of terms $J_{m,n}|\omega|^m|k|^n$. Terms with $m+n>2$ are *irrelevant* in the RG sense, vanishing at long wavelengths. Terms with $m+n=2$ are *marginal*, i.e. fixed under the RG, and trivially modify the Luttinger liquid's velocity, u, and stiffness, K. Since CL baths generate interactions that are nonlocal in time, there should be at least one power of ω; thus, we restrict to the "Ohmic" form, $J \propto |\omega|$, to capture the relevant, non-trivial physics of the bath[7], as established in Ref. 312. We add to S_{LL} Eq. (7.4.1) the term

$$S_{\text{eff}}[\phi] = \frac{\hbar\,\eta}{2\pi}\int dk \int d\omega\,|\omega|\,|\phi_{k,\omega}|^2\,, \tag{7.4.9}$$

and restrict to $\eta \geq 0$ [268, 269, 271, 274, 275, 312–315].

A quadratic term of the form Eq. (7.4.9) will always be present in the presence of dissipation, however in general other terms in S_{eff} may be realized upon integrating out the bath [274, 312–315].

[7] One can regard the parameters u and K as having been modified to absorb any 'marginal' terms

In particular, for spinless fermions, ρ includes harmonics of ϕ Eq. (7.4.3); if the full form of ρ is coupled to the bath, one expects a temporally non-local term $\propto \csc^2(\tau-\tau')\cos[\phi(x,\tau)-\phi(x,\tau')]$, and possibly higher harmonics [312,313]. However, the important physics of dissipation is already captured by the quadratic term Eq. (7.4.9), and not only can we not treat the cosine term exactly, but its non-local nature complicates slightly the use of RG techniques, which are generally local.

Thus, taking $\beta\hbar$ and L finite for generality, the effective action for the Luttinger liquid with the bath degrees of freedom integrated out takes the form

$$S_0 = \sum_{k,\omega_n} \frac{u^2k^2+\omega_n^2+uKJ(k,\omega_n)}{2\pi\, u\, K\, \beta\, L} |\phi(k,\omega_n)|^2 \ , \tag{7.4.10}$$

as appears in Ref. 312. For analytic J, we invoke RG relevance and the arguments above to restrict our consideration to $J(k,\omega_n)=\eta|\omega_n|$ Eq. (7.4.9) in the remainder.

7.4.3 Two-point correlation functions

The Luttinger liquid's Gaussian action Eq. (7.4.1) allows for the computation of many physical properties directly from two point correlation functions, $\langle\phi(x,\tau)\,\phi(0,0)\rangle$. Thus, most of the calculational "heavy lifting" will be contained in this section, as we recover analytic solutions for the two point function without further approximation, even at non-zero temperature. We define the following:

$$F(x,\tau) = K^{-1}\langle[\phi(x,\tau)-\phi(0,0)]^2\rangle \tag{7.4.11}$$

$$= \frac{2\pi u}{\beta\hbar L}\sum_k\sum_{\omega_n}\frac{1-\cos(kx+\omega_n\tau)}{u^2k^2+\omega_n^2+uKJ(k,\omega_n)} \tag{7.4.12}$$

$$G(x,\tau) = K^{-1}\langle\phi(x,\tau)\,\phi(0,0)\rangle \tag{7.4.13}$$

$$= \frac{\pi u}{\beta\hbar L}\sum_k\sum_{\omega_n}\frac{\cos(kx+\omega_n\tau)}{u^2k^2+\omega_n^2+uKJ(k,\omega_n)}, \tag{7.4.14}$$

such that

$$F(x,\tau) = 2G(0,0) - 2G(x,\tau), \tag{7.4.15}$$

where strictly speaking, $G(0,0)$ is evaluated by first sending $x, u\tau \to \alpha$, and subsequently taking the limit $\alpha \to 0$ where safe [308]. The parameter α is like a lattice spacing, and $\alpha^{-1}=\Lambda$ is a UV cutoff.

We calculate these correlation functions following the same procedure as for the Luttinger liquid without dissipation (i.e. $\eta=0$) [308]. Surprisingly, we find exact solutions for both $G(x,\tau)$ and $F(x,\tau)$ for arbitrary T. Because the calculation is standard, and the results obtained are exact, we relegate the mathematical derivation to Appendix D.3.1. We also confirm that taking $\eta\to 0$ reproduces the known results for the standard case in Appendix D.3.3. Finally, while we do not write them down explicitly, we note that *single particle* correlation functions obtain directly from the results of this section, combined with those for the 'closed' Luttinger liquid [308, Appendix C]. All of the results presented in this section correspond to the $L\to\infty$ limit, with $J(k,\omega)=\eta|\omega|$.

7.4.4 Zero temperature correlation functions

At zero temperature, we send $\beta\to\infty$, simplifying the calculation in Appendix D.3.1, as the sums over Matsubara frequencies in (7.4.11-7.4.14) become integrals. Regarding Eq. (D.3.11), all of the

terms containing factors $e^{-m\beta\cdots}$ for $m \geq 1$ will vanish as $\beta \to \infty$, leaving only the β-independent terms. Thus, we have

$$G(x,\tau) = \sum_{n=0}^{\infty} \frac{e^{-\tilde{\eta}\, u|\tau|}}{2\, n!} \left(\frac{-\tilde{\eta}\, x^2}{2\, u\, |\tau|}\right)^n K_n\left[\tilde{\eta}\, u\, |\tau|\right], \tag{7.4.16}$$

where K_n is a modified Bessel function of the second kind, and we use the shorthand

$$\tilde{\eta} \equiv \eta\, K/2 \tag{7.4.17}$$

throughout. Unlike the closed Luttinger liquid, the correlation function G is not divergent in general. In most regimes, the sum over n converges rapidly; in all cases, G decays sharply to zero for $x, u\tau \gtrsim \tilde{\eta}^{-1}$.

The correlation function F is given straightforwardly from the above using the relation Eq. (7.4.15) and the derivation of $G(0,0)$ in Appendix D.3.2. We have at zero temperature $F(x,\tau) =$

$$-\gamma - \ln\frac{\tilde{\eta}\,\alpha}{2} - \sum_{n=0}^{\infty} \frac{e^{-\tilde{\eta}\, u|\tau|}}{n!} \left(\frac{-\tilde{\eta} x^2}{2u\, |\tau|}\right)^n K_n\left[\tilde{\eta} u\, |\tau|\right] \ , \tag{7.4.18}$$

where γ is the Euler-Mascheroni constant, and implicit is the limit $\alpha \to 0$.

Although these results are exact—in the sense that no approximations were necessary beyond those outlined in our formulation of the model in Sec. 7.4.2—it is worth considering approximate forms of Eq. (7.4.16) corresponding to various physical regimes. A handful of limits can be taken straightforwardly; however, some must be analyzed with additional care. For example, the limits of $\eta \to 0$ and $\tau \to 0$ should not be taken independently of any others, and the limit $x \to \infty$ can only be taken along with some limit of η or τ.

Long time limit.— Perhaps the most natural; in the limit of large argument, one has for the Bessel function in Eq. (7.4.16)

$$\lim_{z\to\infty} K_\nu(z) = \sqrt{\frac{\pi}{2z}} e^{-z}, \tag{7.4.19}$$

and inserting this into the definition of $G(x,\tau)$ Eq. (7.4.16) gives

$$G(x,\tau) \approx \sqrt{\frac{\pi}{8\tilde{\eta}\, u\, |\tau|}} \exp\left(-2\tilde{\eta} u\, |\tau| - \frac{\tilde{\eta}\, x^2}{2u\, |\tau|}\right), \tag{7.4.20}$$

where clearly the conformal invariance of the $\eta = 0$ Luttinger liquid has been destroyed. The exponential decay in t suppresses correlations for $\tilde{\eta} u\tau \gtrsim 1$; the remaining factors in Eq. (7.4.20) resemble a diffusion kernel, with diffusion constant $\propto u/\tilde{\eta}$. Thus, a non-zero density introduced at the origin, $x = 0$, at time $\tau = 0$ will spread diffusively under the combined system and bath dynamics Eq. (7.4.10), with exponential suppression on a time scale $1/u\tilde{\eta}$.

Auto-correlation limit.— Also of interest is the limit $x \to 0$, corresponding to a temporal auto-correlation function. Only the $n = 0$ term in the sum in Eq. (7.4.16) survives, i.e.

$$G(0,\tau) = \frac{e^{-\tilde{\eta}\, u|\tau|}}{2} K_0\left[\tilde{\eta}\, u\, |\tau|\right] \ . \tag{7.4.21}$$

For nonzero $x \ll 1$, we retain terms with $1 < n < n_*$, resulting in an expansion to order x^{2n_*}; we then expand in the Bessel function's argument for further insight.

The small argument limit is uninteresting: the result is parametrically close in x, τ to $G(0,0)$ Eq. (D.3.13). At $\tau = 0$, we reinstate the α-dependent convergence factor, per Appendix D.3.2, and expand in $z = \tilde{\eta}\, u\, |\tau|$

$$K_0(z) \to \sum_{k=0}^{\infty} \frac{(z/2)^{2k}}{(k!)^2} \left(\psi(k+1) - \ln\left(\frac{z}{2}\right) \right) , \tag{7.4.22}$$

where ψ is the DiGamma function. Higher order corrections can be found following Appendices D.3.2 and D.3.4.

The late time limit is unambiguous:

$$\lim_{\tau \to \infty} G(0,\tau) = 0 , \tag{7.4.23}$$

referred to as "seizing of the vacuum" [274, 317]. One can show that Eq. (7.4.23) holds for real time t starting from Eq. (7.4.14) with $\tau = it$, using contour integrals rotated 90° in the complex plane, or by analytic continuation of Eq. (7.4.16) to real time. This seizing signals localization of the fermion degrees of freedom [274, 317], and will be discussed in Sec. 7.4.7.

Various interaction limits.— Details of the bare interactions in the Luttinger liquid are encoded in the velocity, u, and Luttinger parameter, K, via the parameters $g_{2,4}$ in Eq. (7.4.2). The limit $K \to 1$ corresponds to free fermions; other limits, such as $K \to 0$ and $K \to \infty$, may be realized experimentally. Referring to the action Eq. (7.4.1), the Luttinger liquid may be described in terms of *either* the field ϕ or its dual, θ; the corresponding bare actions Eq. (7.4.1) have overall coefficient K^{-1} and K, respectively. The two-point functions of ϕ and θ correspond to the functions G, F, as the case may be, multiplied by K and K^{-1}, respectively. In the extreme limits $K \to 0$ and $K^{-1} \to 0$, one of these will be zero and the other infinite: naïvely, dissipation is unimportant in either limit; however, consideration of these scenarios likely requires a more careful treatment beyond the scope of this work.

Curiously, nothing in particular happens to Eq. (7.4.16) in the free fermion limit, $K = 1$. Rather, it seems any interesting interaction effects must be encoded in $\cos[\phi]$ terms of the type mentioned in Sec. 7.4.2, which we examine in Sec. 7.4.9. Otherwise, the non-interacting limit merely amounts to a specific value of $\tilde{\eta} = \eta/2$ and $u = v_F$, the Fermi velocity, with nothing remarkable at the level of density-density correlations.

Weak coupling regime.— Expansion of Eq. (7.4.16) to $O(\eta)$ is straightforward, as detailed in Appendix D.3.4. Let us consider $F(x,\tau)$ to order η^2: at lowest order we recover the dissipationless result (see Appendix D.3.3),

$$F(x,\tau) = \frac{1}{2} \ln\left[\frac{x^2 + u^2\tau^2}{\alpha^2} \right] , \tag{7.4.24}$$

then corrections from the factor $\exp(-\tilde{\eta} u |\tau|)$,

$$+ \left(\frac{1}{2}\tilde{\eta}^2 u^2 \tau^2 - \tilde{\eta} u |\tau| \right) \left(\gamma + \frac{1}{2} \ln\left[r^2\right] \right) , \tag{7.4.25}$$

and finally, from the Bessel function

$$+ \frac{\tilde{\eta}^2}{4} \left(x^2 + u^2\tau^2\right) \left(\gamma - 1 + \frac{1}{2} \ln \frac{x^2 + u^2\tau^2}{4\alpha^2} \right) , \tag{7.4.26}$$

and we note that to order $\tilde{\eta}^2 \propto \eta^2$, only the terms arising from expansion of the overall factor $\exp(-\tilde{\eta} u |\tau|)$ spoil the conformal invariance present for $\eta = 0$.

7.4.5 Finite temperature correlation functions

As shown in Appendix D.3.1, finite temperature correlations are no more difficult to obtain. For $T > 0$, $G(x,\tau)$ and $F(x,\tau)$ contain the respective terms Eq. (7.4.16) and Eq. (7.4.18) present at $T = 0$, i.e.

$$G(x,\tau;T) = G(x,\tau;0) + \sum_{m=1}^{\infty}\sum_{\pm} G(x, m\beta\hbar \pm |\tau|) \ , \tag{7.4.27}$$

with $G(x,\tau;0)$ given by Eq. (7.4.16). The dominant contribution at high temperature corresponds to $m = 1$.

By analogy, we obtain $F(x,\tau;T)$ by adding to $F(x,\tau;0)$ Eq. (7.4.18) the terms

$$\sum_{\substack{m=1,\\ \pm}}^{\infty}\left\{\frac{e^{-\tilde{\eta}um\beta\hbar}}{2}K_0\left[\tilde{\eta}um\beta\hbar\right] - 2G(x, m\beta\hbar \pm |\tau|)\right\}, \tag{7.4.28}$$

which is difficult to parse, even restricted to $m = 1$. Note that exponential factors in G and F that grow (rather than decay) in $|\tau|$ are at most unity, since $0 \le \tau < \beta\hbar$.

As for $T = 0$, one can evaluate a number of physical limits for $T > 0$; however, apart from the results of Sec. 7.4.4, which are still present for $T > 0$, little can be said about the finite temperature terms in the limits considered in Sec. 7.4.4 without expanding in T. Since the Luttinger liquid picture breaks down at high energies, only the low temperature limit is reasonable; that limit is well-captured by the results of Sec. 7.4.4.

Additionally, it is unclear how (or whether) to take the $\tau \to \infty$ limit of expressions involving $m\beta\hbar - |\tau|$, since our recovery of Bessel functions $K_n[z]$ is only valid if $\mathrm{Re}(z) > 0$. Given that $0 \le \tau \le \beta\hbar$, this does not pose an issue for the result itself; however, for finite β, the "long time" limit is more subtle. For the purposes of transport and "seizing", we are interested in the limit of *real time* $t \to \infty$, which we will address e.g. in Sec. 7.4.7.

7.4.6 Vertex operator correlations

In this section we consider two-point functions of "vertex operators", related, e.g., to the fermion creation/annihilation operators. These are exponential correlation functions of the form

$$C(x,\tau;m) = \frac{1}{(2\pi\alpha)^2}\langle e^{im\phi(x,\tau)}e^{-im\phi(0,0)}\rangle \tag{7.4.29}$$

$$= \frac{1}{(2\pi\alpha)^2}\exp\left\{-\frac{K\,m^2}{2}F(x,\tau)\right\} \ , \tag{7.4.30}$$

where F is given by Eq. (7.4.18) for $T = 0$ and Eq. (7.4.28) for $T > 0$.

Unlike the closed Luttinger liquid ($\eta = 0$), the absence of a constant, divergent term in $G(x,\tau)$ for $\eta > 0$ allows for vertex operator correlations of the form

$$\langle e^{i\sum_k A_j\,\phi(x_j,\tau_j)}\rangle$$

to be non-zero even for $\sum_k A_j \neq 0$. This will affect the use of standard techniques, e.g. Giamarchi-Schulz RG [318], for $\cos[m\phi]$ terms perturbing the action Eq. (7.4.1).

Let us compare $C(x,\tau)$ to its $\eta = 0$ form, $C_0(x,\tau)$; taking $T = 0$ and $m = 2$ for the first harmonic, to order η^2 (see Sec. 7.4.4 and App. D.3.4) one has

$$C_\eta(x,\tau) = C_0(x,\tau)\, e^{K\tilde{\eta}^2(x^2+u^2\tau^2)/2} \times \left(\frac{4e^{-2\gamma}}{x^2+u^2\tau^2}\right)^{\frac{K\tilde{\eta}^2}{4}\left(3u^2\tau^2+x^2-4u|\tau|/\tilde{\eta}\right)} , \tag{7.4.31}$$

where analysis of the behavior as $x, \tau \to \infty$ is complicated by competing terms.

However, we can see the limiting behavior at large distances [times] directly from Eq. (7.4.30). For $C(x,\tau)$ of the form Eq. (7.4.29), note that $F(x,\tau)$ vanishes as *either* $x, \tau \to \infty$ faster than x^{-2} or $(u\tau)^{-2}$. In contrast to the dissipationless case, $C(x,\tau) \to 1$, rather than zero, for large x or τ.

Because dissipation Eq. (7.4.8) destroys the conformal invariance of Eq. (7.4.1), we cannot simply read off RG relevance of $\cos[m\phi]$ terms perturbing Eq. (7.4.1) from the scaling dimension of their correlations, $C(x,\tau)$. Nevertheless, because $G(x,\tau)$ is finite as its arguments approach infinity, one expects that dissipation will generally render such cosine terms more relevant than for $\eta = 0$, since their correlations no longer vanish at long wavelengths.

7.4.7 Seizing of the vacuum

An earlier prediction for Luttinger liquids coupled to a CL bath [274] is a property termed *seizing of the vacuum* [317], corresponding to localization of the bare fermion degrees of freedom at $T = 0$. Quantitatively, this is indicated by

$$\lim_{t\to\infty} G(0,t) = 0 , \tag{7.4.32}$$

for real time, t, and G evaluated at $T = 0$. This effect was reported in Ref. 274 for a similar model; the exact solutions of Sec 7.4.3 confirm this property definitively.

It is easy to verify that the Euclidean time correlation function $G(0,\tau) \to 0$ as $\tau \to \infty$ without caveat. Using analytic continuation, i.e. $|\tau| = \tau \operatorname{sgn}\tau$, and thus $|\tau|^2 = \tau^2 = (it)^2 = -t^2$, we note that $|\tau|^{-n} K_n[\tilde{\eta}u|\tau|]$ has a series expansion involving only even powers of τ. Using this, we can take the limit $t \to \infty$ safely, finding that the summand in Eq. (7.4.16) goes to zero, even without the help of the exponential decay $\exp(-\tilde{\eta}u|\tau|)$. Additionally, it is possible to repeat the proceedings of Appendix D.3.1 for real time t, which requires the use of a rotated contour compared to Euclidean time derivation; nonetheless, taking $x \to 0$, one recovers an expression that unambiguously vanishes at large times, $t \to \infty$.

Surprisingly, this behavior is not limited to the vacuum: the "seizing" effect, characterized by Eq. (7.4.32), also holds for finite temperature $T > 0$, and thus is present in *excited states* as well. As for $T = 0$, this can be seen either by analytic continuation of $G(x,\tau)$ to real time, or by reproducing the calculation of G entirely for real time t. The latter requires taking $x = 0$ at the outset, and taking $t \to \infty$ when safe. At finite β, the t-dependence dominates, and we see that $G \to 0$; as $\beta \to \infty$, one recovers the $T = 0$ result, which also corresponds to seizing. Hence, we conclude that this effect is *not* limited to the ground state, but is present throughout the spectrum. However, at very high temperatures, one expects both a breakdown of the bosonization procedure itself, and for thermal fluctuations to outweigh this effect.

7.4.8 Conductivity

We can also see evidence of localization from a transport calculation using the Kubo formula. Restricting to $1d$ fermions with electron charge e, the charge density is $\rho = -\frac{e}{\pi}\nabla\phi + \ldots$; using the

continuity equation, $\partial_t \rho + \nabla j = 0$, we have

$$j(x,t) = \frac{e}{\pi}\partial_t \phi(x,t) \ , \tag{7.4.33}$$

in the limit of vanishing source, from which we can compute the current in the presence of a weak source using linear response. The source will be a weak electric field oriented along the wire, given by $E(t) = E_0 e^{-i(\omega+i\delta)t}$, where δ is a small, positive real number inserted for convergence purposes. Writing $E = -\partial_t A$, where A is the $1d$ vector potential, we invoke Ohm's law

$$j(q,\omega) = \sigma(q,\omega) E(q,\omega) \ , \tag{7.4.34}$$

where we will take $q \to 0$ to highlight the frequency dependence, and j on the LHS is given by the expectation value of the current operator Eq. (7.4.33), which we compute using the Kubo formula,

$$\langle j(x,t)\rangle = \langle j(x,t)\rangle_0 + \delta \langle j(x,t)\rangle \ . \tag{7.4.35}$$

The first term in Eq. (7.4.35) is proportional to the source, A_1,

$$\langle j(x,\tau)\rangle_0 = D A_1(x,\tau) = -\frac{e^2 u K}{\pi\hbar} A_1(x,\tau) \ , \tag{7.4.36}$$

known as the "diamagnetic" contribution. Going to Fourier space, the second term is given by

$$\delta j(q,\omega) = \chi(q;\omega) A_1(q,\omega) \ , \tag{7.4.37}$$

and we can write Ohm's law Eq. (7.4.34)

$$\sigma(q,\omega) = \frac{j(q,\omega)}{E(q,\omega)} = \frac{D + \chi(q,\omega)}{i(\omega + i\delta)} \ . \tag{7.4.38}$$

We next solve for χ, which is a current-current correlation function:

$$\chi(q,\omega_n) = -\frac{e^2\omega_n^2}{\pi^2\hbar}\langle \phi^*_{q,\omega_n}\phi_{q,\omega_n}\rangle - D \ , \tag{7.4.39}$$

and inserting this into Eq. (7.4.38), and analytically continuing $i\omega_n = \omega + i\delta$ with $\delta = 0^+$ one finds

$$\sigma(q,\omega) = \frac{e^2}{\pi^2 i\hbar}(\omega + i\delta)\langle \phi^*_{q,\omega_n}\phi_{q,\omega_n}\rangle \tag{7.4.40}$$

$$\sigma(q,\omega_n) = \frac{e^2\omega_n}{\pi^2\hbar}\frac{\pi u K}{u^2q^2 + \omega_n^2 + \eta u K|\omega_n|} \ , \tag{7.4.41}$$

and taking $q \to 0$, we recover the dc conductivity by further taking the limit $\omega \to 0$, i.e.

$$\begin{aligned}\sigma(\omega \to 0) &= \frac{e^2 u K}{\pi\hbar}\frac{1}{\delta - i\omega + \eta u K \operatorname{sgn}(\delta - i\omega)} \\ &= \frac{e^2}{\pi\hbar\eta\operatorname{sgn}(\delta)} = \frac{e^2}{\pi\hbar\eta} \ ,\end{aligned} \tag{7.4.42}$$

which is *finite*. We also note a relation between Eq. (7.4.42) and the condition for seizing, as discussed in Sec. 7.4.7.

This result Eq. (7.4.42) contrasts sharply with the infinite conductivity of the closed Luttinger liquid as $q, \omega \to 0$. This result does recover for $\eta \to 0$. Hence, we find further evidence that the dissipative bath localizes the underlying fermion excitations of the Luttinger liquid.

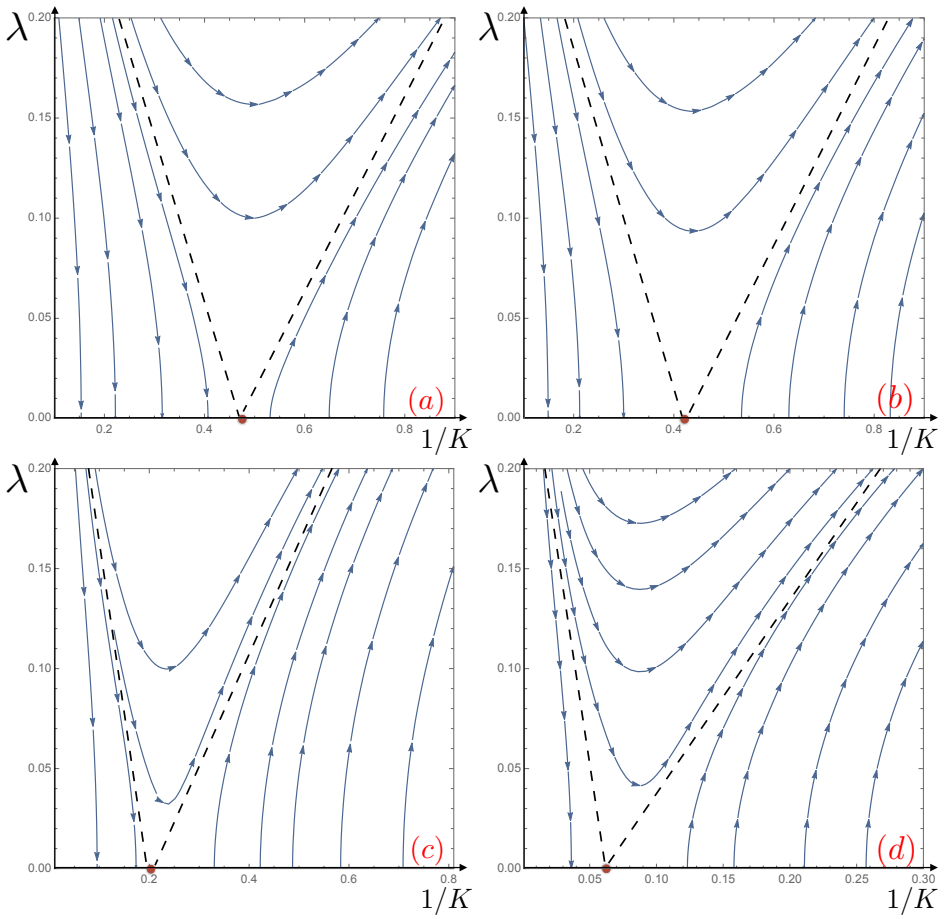

Figure 7.2: RG flow in the λ, $1/K$ plane, for various values of the dissipation strength, η; λ is the strength of the most relevant harmonic, corresponding to $m = 2$ in Eq. (7.4.43). We take the velocity u and the coefficient C in Eq. (7.4.53) to be unity; for $\eta = 0$, the Kosterlitz-Thouless transition corresponds to $1/K^* = 1/2$. The panels a through d correspond respectively to $\alpha\eta = 10^{-3}$, 10^{-1}, $1/2$, and 1, where $\alpha = 1/\Lambda$ is a UV cutoff; note horizontal axis is different in each panel, the critical values $1/K^*$ in each are roughly 0.47, 0.42, 0.2, and finally, 0.06 for $\eta = \Lambda$. Under the RG, η grows exponentially from its initial value, independent of λ and K; for η up to roughly one tenth the cutoff (panel b), the alteration to the dissipationless phase diagram is rather slight; for $\eta \gtrsim \Lambda/2$, we find a marked enhancement in the region of parameter space for which harmonic terms are relevant.

7.4.9 Relevance of harmonic terms

We now consider the relevance of generic cosine terms, omitted from Eq. (7.4.1), using standard momentum-shell RG. Our starting point is the action S_0, defined in Eq. (7.4.7) and Eq. (7.4.10), which contains the relevant, non-harmonic terms that one recovers after integrating out the bath degrees of freedom. We add to this a generic harmonic term of the form

$$S_1[\phi] = u\,\lambda_m \int_0^{\beta\hbar} d\tau \int_{-L/2}^{L/2} dx\, \cos\left[m\phi\left(x,\tau\right)\right] \ , \tag{7.4.43}$$

where $m \in \mathbb{N}$ specifies the harmonic: $m = 2$ is the first to appear in the density Eq. (7.4.3); an Umklapp (back-scattering) term corresponds to $m = 4$ (these will be multiples of two due to our convention). We defer analysis of multiple harmonics to future work.

We take $L, \beta \to \infty$ so the action Eq. (7.4.10) has an integral form in Fourier space as well,

$$S_0 = \int_{-\Omega}^{\Omega} \frac{d\omega}{2\pi} \int_{-\Lambda}^{\Lambda} \frac{dk}{2\pi} \frac{u^2k^2 + \omega^2 + \eta K u |\omega|}{2\pi u K} |\phi(k,\omega)|^2 , \tag{7.4.44}$$

where $\Omega = u/\alpha$ and $\Lambda = 1/\alpha$ are frequency and momentum cutoffs, respectively.

The RG is implemented by separating the field $\phi(k,\omega) = \phi_s(k,\omega) + \phi_f(k,\omega)$, with 'fast' modes living in an annulus in the momentum-frequency plane corresponding to $(b\alpha)^{-1} < q < \alpha^{-1}$, and all other modes 'slow'. Note $q = \sqrt{k^2 + \omega^2/u^2}$, α is our usual short-distance cutoff, and $b = e^{\ell} \geq 1$ quantifies the extent of the coarse graining. For a given term, we trace out the 'fast' modes, and then rescale frequency, momentum, and the fields themselves to obtain an effective theory of the slow degrees of freedom. The rescaling ($\tilde{\omega} = b\omega$, $\tilde{k} = bk$) is determined by the requirement that the 'fixed' part of the action, S_0 remain unchanged under the RG, which requires that ω and k have the same b, and results immediately in a rescaled coupling $\tilde{\eta} = b\eta$ and rescaled field $\tilde{\phi}$ given by $\tilde{\phi}(\tilde{k}, \tilde{\omega}) = b^{-2}\phi_s(k,\omega)$. In real space, one has $\tilde{x} = x/b$, $\tilde{\tau} = \tau/b$, and $\tilde{\phi}(\tilde{x}, \tilde{\tau}) = \phi_s(x,\tau)$.

We now have the scaling of η; the RG for all other terms follows from the usual, $\eta = 0$ case. We perform a cumulant expansion of S_1 to order λ_m^2, which for $\eta = 0$, gives rise to standard Kosterlitz-Thouless RG flow [308]. All other differences compared to the closed case arise from modification of the 'fast' two point function, taken with respect to S_0, which includes also the quadratic dissipation term. That function, $KG_{0,f} = \langle \phi_f^2(x,\tau) \rangle_{0,f}$ is given by

$$G_{0,f}(x,\tau) = \iint_{|\omega|,|k| \in f} \frac{d\omega}{2\pi} \frac{dk}{2\pi} \frac{\pi u \cos(kx + \omega\tau)}{u^2k^2 + \omega^2 + u\eta K |\omega|} , \tag{7.4.45}$$

which taking $x = r\cos\theta$, $u\tau = r\sin\theta$, $k = q\cos\psi$, $\omega = uq\sin\psi$, becomes

$$G_{0,f}(x,\tau) = \frac{1}{4\pi} \int_{\Lambda/b}^{\Lambda} dq \int_0^{\pi} d\psi \frac{\cos(qr\cos(\theta - \psi))}{q + \eta K |\sin\psi|} , \tag{7.4.46}$$

and details of the RG ensure that we need only consider $dG/d\ell$ as $\ell \to 0$ ($b \to 1$), i.e.

$$\frac{dG_{0,f}}{d\ell} = \frac{1}{4\pi} \int_0^{2\pi} d\psi \frac{\cos\left(\frac{r}{\alpha}\cos(\theta - \psi)\right)}{1 + \alpha\eta K |\sin\psi|} , \tag{7.4.47}$$

evaluated either at $r = 0$, or integrated directly over θ, which we can therefore shift by ψ. In either case, the numerator's dependence on ψ is eliminated, and we find a simple relation to the dissipationless result:

$$\frac{dG_{0,f}}{d\ell}(x,\tau,\eta) = \nu(\alpha\eta K) \frac{dG_{0,f}}{d\ell}(x,\tau,\eta = 0) , \tag{7.4.48}$$

where

$$\nu(z) = \frac{1}{2\pi} \int_0^{2\pi} d\psi \frac{1}{1 + z|\sin\psi|} \tag{7.4.49}$$

$$= \frac{1}{\sqrt{1 - z^2}} \left(1 - \frac{2}{\pi} \tan^{-1}\left[\frac{z}{\sqrt{1 - z^2}}\right]\right) , \tag{7.4.50}$$

which has important limits $\nu(0) = 1$, $\nu(1) = 2/\pi$, and $\nu(z) \to 0$ as $z \to \infty$.

Thus, the various couplings of this theory flow according to

$$\frac{d\eta}{d\ell} = \eta \tag{7.4.51}$$

$$\frac{d\lambda_m}{d\ell} = \left(2 - \frac{m^2 K}{4}\nu(\alpha\eta K)\right)\lambda_m \tag{7.4.52}$$

$$\frac{dK^{-1}}{d\ell} = \pi\nu(\alpha\eta K)\, C_0(K)\, m^2\lambda_m^2 \ , \tag{7.4.53}$$

where $C_0(K)$ is strictly positive function: it can be recovered from the $\eta = 0$ case, but its precise form is unimportant.

Compared to the usual RG flow with $\eta = 0$, here, we see that dissipation is strictly relevant, with η diverging exponentially as the RG is run. The other two couplings, the stiffness (Luttinger parameter) K and strength of the harmonic perturbation λ_m initially follow the usual Kosterlitz-Thouless flow until η approaches the cutoff, $\Lambda = 1/\alpha$, as can be seen in Fig. 7.2. For $\eta \gtrsim \Lambda/10$, the harmonic terms become relevant for increasing ranges of K. Throughout, the overall strength of the Luttinger liquid action Eq. (7.4.1), K^{-1} also grows, with the rate of growth slowed as η increases.

Referring to Eq. (7.4.50), for $\alpha\eta K = 1$, ν will only have decreased in value from unity to $2/\pi$ compared to the $\eta = 0$ value; this gives the impression that any interesting effect due to dissipation only occurs asymptotically late in the RG. However, due to the dependence of ν on K as well, dramatic changes occur when $\alpha\eta$ approaches unity, as depicted in the bottom right of Fig. 7.2, whereupon the critical value of K^{-1} for λ_m is suppressed tenfold compared to $\eta = 0$. If η is allowed to grow beyond the cutoff, only extremely large values of K can prevent harmonic terms from being relevant; for $\eta \gg 1/\alpha$, K ceases to flow entirely, and Eq. (7.4.52) becomes

$$\frac{d\lambda_m}{d\ell} \to 2\lambda_m \ , \tag{7.4.54}$$

such that *all* harmonic terms are relevant.

7.4.10 Discussion

In summary, we have investigated the effect of a dissipative bath on the properties of the Luttinger liquid. We argued that the effective contribution to the Luttinger liquid action corresponding to Ohmic dissipation captures the generic, relevant physics of CL baths. For this action, we computed two-point correlation functions non-perturbatively and for arbitrary temperature, finding evidence that dissipation makes the system vulnerable to localizing potentials. We later confirmed this using an RG analysis of generic harmonic terms, which we find to be more relevant under coarse-graining in the presence of dissipation, if not always relevant. For a wide range of parameters, the physics of the Luttinger liquid is altered substantially. Finally, a simple transport calculation reveals that dissipation destroys the perfect conductivity of the Luttinger liquid even in the absence of any spatial potentials or disorder, via Zeno localization. All of these findings show that the bath effectively *enhances* localization in this interacting quantum system, in contrast to the usual intuition from Markovian baths that decoherence ought to make a system less localized.

These surprising results invite follow-up study, which should be facilitated by the exact correlation functions presented here. Given the increased importance of harmonic terms in the presence of dissipation, one direction for follow-up work is to examine the temporally-nonlocal harmonic

terms generated by integrating out the bath. Also, consideration of higher-body correlations, specialization to physical applications, and higher dimensions may be of interest.

7.5 Summary and Outlook

In summary, we have found that a reasonable model for a dissipative quantum bath, i.e. that of Caldeira and Leggett, can enhance the effects and appearance of localization in a thermal quantum system. This result directly contradicts the standard intuition used to scrutinize the stability (or instability) of localized systems to thermalization: in such cases, the focus is generally on Markovian baths, which do not capture the most important feature of baths as relates to quantum thermalization, which is *entanglement*. Essentially, the mechanism by which the bath localizes the system is "Zeno localization": the bath effectively measures the particle(s) repeatedly, and in one-dimensional many-body systems and single particle systems in the presence of particular potential landscapes, the coherence necessary for the particle(s) to propagate freely is destroyed by this interaction with the bath. These results highlight the need for improved understanding of the role of a weak bath, e.g., as relates to ongoing cold atom experiments. This work suggests an intriguing possibility of designing *multicomponent* systems in such a way that the two components (i.e. species of particles) do not necessarily equilibrate; if the external bath then couples more strongly to the more thermal of the two components, it may be possible to localize that component, and prevent thermal decoherence of the less thermal component. Successfully engineering such systems would be extremely useful to the realization of robust quantum computers.

Appendix A

Supplementary Material for Random Unitary Circuits

A.1 Numerical Methods for the $U(1)$ Calculation

For $L = 10, 12, 14$, we find the eigenvalues of $\hat{W}$, given by Eq. (5.5.17) in Chapter 5, using exact diagonalization, and compute $\mathrm{Tr}[\hat{W}(t)] = \sum_n e^{it\theta_n}$ directly to obtain $K(t)$, which is then averaged. For $L = 16$ and 18, we sample the trace, computing an approximate version of $\mathrm{Tr}[\hat{W}(t)]$ via successive multiplication of $\hat{W}$ onto a number of 'sample states', which are superpositions of the basis states, with complex coefficients drawn from a Gaussian distribution with zero mean and unit variance. One can either sample the trace within a given realization of spatial disorder, or sample both disorder realizations and the trace concurrently. In either case, we expect the *total* number of samples required to reduce noise to a given degree to be the same for either method.

For the 12870 basis states comprising the trace for $L = 16$, we find that $\lesssim 100$ samples per disorder realization is sufficient to reproduce the correct behavior for $K(t)$, with $\gtrsim 10^4$ realizations of disorder. For $L = 18$, we use concurrent sampling of disorder and the trace; owing to the larger Hilbert space dimension, to obtain results with noise comparable to the $L = 16$ data would likely require $O(10^7)$ combined samples and realizations. The data shown in the main text correspond to 4×10^5 combined samples and realizations of disorder. As these data are noisier than those for smaller system sizes, we also average this data in windows of roughly 25 time steps to reduce noise further; we plot the average within each window, accompanied by error bars corresponding to the combination of disorder averaging and this temporal smoothing.

A.2 Large-time expansion

We consider the asymptotic behavior of $\psi(t, h)$ for large t and fixed h. Since $\psi(t, -h) = \psi(t, h)$, we take $h > 0$. The case $h = 0$ requires a different treatment. The functions $\eta_n(\lambda)$ admit the expansion:

$$\ln \eta_n(\lambda) = t\epsilon_n(\lambda) + 2nh + \sum_{k=0}^{\infty} t^{-k/2} q_{n,k}(\lambda/\sqrt{t}) \tag{A.2.1}$$

The following results are easily verified

$$\int_{-\infty}^{\infty} dx a_n(\lambda) = 1 \,, \qquad \lim_{t\to\infty} t a_n(\sqrt{t}z) = \frac{n}{\pi z^2} \,. \tag{A.2.2}$$

We have therefore

$$\sqrt{t}\,T_{nm}(z\sqrt{t}) \underset{t\gg 1}{=} \tau_{n,m}\delta(z) + \frac{2nm}{\pi\sqrt{t}z^2} + O(t^{-3/2}) \,, \tag{A.2.3}$$

$$\lim_{t\to\infty} \ln \eta_n(\sqrt{t}z) = \frac{4n}{z^2} + 2nh + q_{n,0}(z) \,, \tag{A.2.4}$$

where

$$\tau_{n,m} = \int dx\, T_{n,m}(\lambda) = 2\min(n,m) - \delta_{n,m}$$

Indeed, inserting Eq. (A.2.1) into the TBA equations of Chapter 2, we have at the leading order an equation for $q_{n,0}(z)$,

$$q_{n,0}(z) = \sum_{m=1}^{\infty} \tau_{n,m} \ln\left(1 + e^{-\frac{4m}{z^2} - 2mh - e_m^{(0)}(z)}\right) \,. \tag{A.2.5}$$

These equations can be mapped onto those describing the infinite temperature behavior of the Trotterized XXX model and admit an exact solution of the form

$$q_{n,0}(z) = -\frac{4m}{z^2} - 2mh + \log\left(\frac{\sinh(n(h+2z^{-2}))\sinh((n+2)(h+2z^{-2}))}{\sinh(h+2z^{-2})^2}\right) \,. \tag{A.2.6}$$

In particular, this implies $q_{n,0}(z\to 0) = 0$. At the next order, we have an equation for $q_{n,1}(z)$

$$q_{n,1}(z) = -\sum_{m=1}^{\infty} \frac{\tau_{nm} q_{m,1}(z)}{1 + e^{\frac{4m}{z^2} + 2mh + q_{m,0}(z)}} + \sum_{m=1}^{\infty} \int dz'\, \frac{2nm}{\pi(z-z')^2} \ln(1 + e^{-\frac{4m}{z'^2} - 2mh - q_{m,0}(z')}) \tag{A.2.7}$$

Using Eq. (2.4.40), one need only consider the case $n = 1$. Changing variables via $u = h + 2/z^2$, one obtains

$$\psi(t,h) \overset{t\gg 1}{=} -h - \frac{q_{1,1}(0)}{2\sqrt{t}} = -h - \sum_{m=1}^{\infty} \int_h^{\infty} du\, \frac{m \log\left(\frac{\sinh((m+1)u)^2}{\sinh(mu)\sinh((m+2)u)}\right)}{\sqrt{2\pi^2 t(u-h)}} \,. \tag{A.2.8}$$

Remarkably, exchanging the sum and integral allows for an explicit solution: setting $g_m = \log(\sinh(mu))$ and using

$$\sum_{m=1}^{M} m(2g_{m+1} - g_m - g_{m+1}) = (M+1)g_{M+1} - Mg_M - g_1 \,, \tag{A.2.9}$$

one recovers

$$\psi(t,h) = -h - \frac{\mathrm{Li}_{3/2}(e^{-2h})}{2\sqrt{\pi t}} + o(t^{-1/2}) \,. \tag{A.2.10}$$

The Legendre transform is obtained by observing that at large t, the maximum in Eq. (2.4.32) corresponds to $h \sim 0$. So one expands

$$\mathrm{Li}_{3/2}\left(e^{-2h}\right) = 2\sqrt{2\pi h} + \zeta(3/2) + O(h) \,, \tag{A.2.11}$$

and finds that Eq. (2.4.32) is maximal at $h^* \simeq 1/(2(1+2s)^2 t)$. Combining this with Eq. (2.4.32) recovers the main result, Eq. (5.5.13).

A.3 Alternative Approach: Quantum Transfer Matrix

The formulation presented in the previous section allows the calculation of the large-time expansion. However, the calculation of $\psi(t,h)$ at arbitrary values of t and h requires the solution of Eq. (2.4.36), i.e. an infinite set of coupled integral equations. One has to resort to truncation n up to when convergence is reached. A more numerically efficient procedure is based on the *quantum transfer matrix* approach [199]. We first note the relation

$$F_\delta(i-\delta)^{-1} = \lim_{x\to -i-\delta} \mathfrak{d}(x)^{-1} F_\delta(x) \ , \tag{A.3.1}$$

then using Eq. (2.3.24), one can write

$$\mathrm{Tr}[M_\delta^t e^{2hS^z}] = \lim_{x\to -i-\delta} \mathfrak{d}(x)^{-t} \mathrm{Tr}[\underbrace{F_\delta(x)F_\delta(i+\delta)\dots F_\delta(x)F_\delta(i+\delta)}_{t \text{ times}} e^{2hS^z}] = \mathrm{Tr}[\underbrace{\tilde{F}_1\tilde{F}_2\dots\tilde{F}_1\tilde{F}_2}_{L \text{ times}}] \ , \tag{A.3.2}$$

where $\tilde{F}_{1,2}$ are the dual transfer matrices defined on $2t$ sites, obtained via a 90° spacetime rotations (i.e. exchanging space and time), as clarified in Fig. A.1. The advantage of this transformation

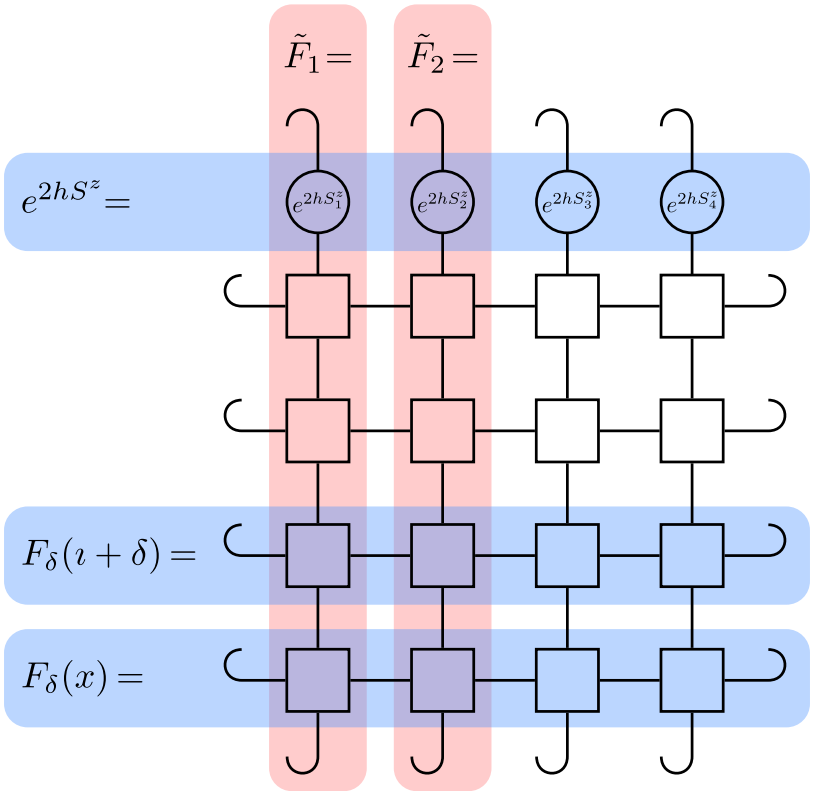

Figure A.1: Diagrammatic representation of $\mathrm{Tr}[M_\delta^t e^{2hS^z}]$. Blue (red) boxes group matrices that act in the time (space) direction. The curly legs at the boundary of the diagram represent the periodic boundary condition.

is that, in the limit $L\to\infty$, the last trace in Eq. (A.3.2) is dominated by the largest eigenvalue of the matrix $\tilde{F}_1\tilde{F}_2$. Moreover, integrability is preserved by the spacetime rotation, as can be checked explicitly from the Yang-Baxter relation, Eq. (2.3.3) (see also Ref. 200); therefore, the dual transfer matrices can be diagonalized as explained in Ch. 2. Using the general expressions

given by Eq. (2.3.15) and Eq. (2.3.17), we arrive at the equation

$$t\tilde{p}(\lambda_a) + \sum_{b=1}^{t} \tilde{\Theta}(\lambda_a - \lambda_b) + ih = \pi(a - (t-1)/2) \,, \qquad a = 0, \ldots, t-1 \tag{A.3.3a}$$

$$\tilde{p}(\lambda) = \arctan(2\lambda) - \arctan(2\lambda/3) \,, \quad \tilde{\Theta}(\lambda) = \arctan(\lambda) \tag{A.3.3b}$$

$$\psi(t,h) = -\frac{1}{2} \sum_{a=0}^{t-1} \log\Big(\frac{4\lambda_a^2 + 9}{16\lambda_a^2 + 4}\Big) \,. \tag{A.3.3c}$$

Note that Eq. (A.3.3a) can be solved efficiently using standard numerical tools for $t \lesssim 10^4$; by inserting the solutions $\{\lambda_a\}_{a=0}^{t-1}$ in Eq. (A.3.3c), one can efficiently obtain $\psi(t,h)$ for arbitrary values of t and h. Finally, $\phi(t,s)$ is recovered by Legendre transform. A comparison between the exact $\psi(t,h)$ obtained with this method and the expansion Eq. (A.2.10) is shown in Figure A.2.

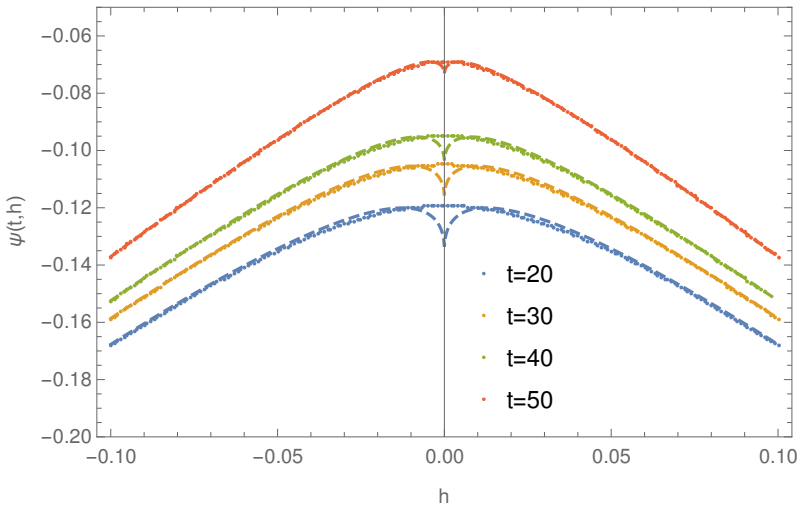

Figure A.2: The function $\psi(t,h)$ obtained via the QTM method, i.e. Eq. (A.3.3), as a function of h for different values of t. The dashed lines correspond to the expansion in Eq. (A.2.10). Such an expansion does not capture the quadratic behavior at $h = O(t^{-1/2})$ [202].

A.4 Free magnon scaling function

In order to derive the scaling function $\kappa(x,s)$ given by Eq. (5.5.15) of Chapter 5, we proceed as follows. First, since we are interested in the limit in which both $t, L \to \infty$, we can neglect the Trotterized structure of the matrix $\hat{M}$, and replace it with the de-Trotterized Hamiltonian via

$$K(t) = |t| \operatorname*{Tr}_s \left[\hat{M}^t\right] \approx |t| \operatorname*{Tr}_s \left[e^{-t\hat{H}}\right] \,, \tag{A.4.1}$$

where $\hat{H}$ is the XXX Hamiltonian. The scaling function is then defined by

$$\kappa(x,s) \equiv \ln\left[K(t)/t\right] \approx \ln \operatorname*{Tr}_s \left[e^{-t\hat{H}}\right] \,, \tag{A.4.2}$$

with $x = t/L^2$. This is essentially the free energy of the XXX model at "temperature" $1/t$.

The single-particle excitations of this effective $\hat{H}$ are *magnons*, which behave effectively as bosons with quadratic a dispersion relation given by $\varepsilon_k = Dk^2$ at small k. In a system of length L

with periodic boundary conditions, the momenta are quantized according to $k = 2\pi n/L$ for integer $n \in \{0, 1, \ldots, L-2, L-1\}$. At large t, the dominant contribution to κ comes configurations with only small-k magnons excited, and at low densities, we can ignore interactions between magnons. Starting from Eq. (A.4.2),

$$\kappa(x,s) = \ln \mathrm{Tr}\left[e^{-t\hat{H}}\right] = \ln \prod_{k\neq 0} \sum_{n_k=0}^{\infty} e^{-t\varepsilon_k n_k} \tag{A.4.3}$$

$$= \sum_{k\neq 0} \ln \frac{1}{1-e^{-tDk^2}} = -\sum_{n\neq 0} \ln\left[1-e^{-(2\pi n)^2 Dx}\right] , \tag{A.4.4}$$

where we ignore the $k = 0$ ($n = 0$) term as this corresponds to changes in the magnetization sector.

To reproduce the results of the main text, we note that the effective evolution $\hat{M}$ has dispersion $\varepsilon(\lambda) = -2 \ln \cos k(\lambda)$; to leading order, one has $\varepsilon(k) = k^2$, i.e. $D = 1$. The large x limit of Eq. (A.4.4) is dominated by the $n = 1$ term; expanding the logarithm reproduces the limit $\kappa(x) \sim e^{-4\pi^2 Dx}$ for $x \gg 1$. Small x corresponds to large L, as we are primarily interested in large t. In this case, we take the continuum limit, and the sum over momenta is replaced by an integral, which for either a $\cos k$ or k^2 dispersion gives $\kappa(x) \propto 1/\sqrt{x}$ for $x \ll 1$. Thus, the proposed scaling form Eq. (A.4.4) reproduces the two limits $x \ll 1$ and $x \gg 1$ recovered in the main text with *exactly* the same coefficients to leading order.

In comparing with the numerical data at finite q, we leave the diffusion constant D as a free parameter. In this case, Eq. (A.4.2) is also supported by its agreement with numerical study of $K(t)$, as depicted in Figure 5.13 in Chapter 5.

Appendix B

Supplementary Material for Disordered Clock and Potts Models

B.1 Renormalization Group for the S_3 Potts Model

The procedure of Real Space (or "Strong Disorder") Renormalization Group (RSRG) begins by locating the strongest bond and diagonalizing the corresponding term in the Hamiltonian. The next step is to incorporate the effect of the two bonds on either side of the strong bond as a perturbatively. Using the α parafermion description, it does not matter whether the strongest random coupling falls on a $\hat{\tau}_j$ or a $\hat{\sigma}_j^\dagger \hat{\sigma}_{j+1}$ term, we can simply write:

$$H_0 \equiv \omega^{-1} K_x \left(\alpha_x^\dagger \alpha_{x+1} + \alpha_x \alpha_{x+1}^\dagger \right), \tag{B.1.1}$$

and for simplicity, we will frequently call the site $x-1$ left of the strong bond "L," and the site $x+2$ to the right of the strong bond "R." Additionally, the value of the strong bond, $K_x \equiv \Omega$ will be divided out from all terms. The ratios $K_{L/R}/\Omega = \lambda_{L/R}$ will be the perturbing parameters.

B.1.1 Details of perturbation theory

For both Potts and Clock systems, the *many-body* eigenstates of H_0 are massively degenerate, since H_0 acts only on a three dimensional subspace of the Hilbert space. Let $\hat{Q}$ project onto all eigenstates that also have eigenvalue $\mathcal{E}_d$ under H_0, and $\hat{P}$ the projector onto all other states (so $\hat{P} + \hat{Q} = \hat{\mathbb{1}}$). We begin with the four parafermion Schrödinger equation,

$$(H_0 + \lambda V)\,|\varphi_k\rangle = E_k |\varphi_k\rangle, \tag{B.1.2}$$

where λV will be a shorthand for $\lambda_L V_L + \lambda_R V_R$. We insert the identity between the ket $|\varphi_k\rangle$ and the operators as a sum over the two projectors and left multiply by just one of the projectors, which commute with H_0, to obtain the equations:

$$E_k \hat{P}|\varphi_k\rangle = H_0 \hat{P}|\varphi_k\rangle + \left(\hat{P}\lambda V \hat{Q} + \hat{P}\lambda V \hat{P}\right)|\varphi_k\rangle \tag{B.1.3}$$

$$E_k \hat{Q}|\varphi_k\rangle = H_0 \hat{Q}|\varphi_k\rangle + \left(\hat{Q}\lambda V \hat{Q} + \hat{Q}\lambda V \hat{P}\right)|\varphi_k\rangle. \tag{B.1.4}$$

We next define $|\psi_k\rangle = \hat{Q}|\varphi_k\rangle$ and $|\chi_k\rangle = \hat{P}|\varphi_k\rangle$. The above two equations become the coupled equations

$$E_k|\chi_k\rangle = \left(H_0 + \hat{P}\lambda V \hat{P}\right)|\chi_k\rangle + \hat{P}\lambda V|\psi_k\rangle \tag{B.1.3}$$

$$E_k|\psi_k\rangle = \left(H_0 + \hat{Q}\lambda V \hat{Q}\right)|\psi_k\rangle + \hat{Q}\lambda V|\chi_k\rangle. \tag{B.1.4}$$

For the chiral clock model wherein none of the eigenvalues of H_0 are degenerate, we have that $\hat{Q}V\hat{Q} = 0$, and we combine the equations above into a single equation for $|\psi_k\rangle$, where we a

Looking at Eq. (B.1.3), we note that the operator $\left(E_k - H_0 - \hat{P}\lambda V\hat{P}\right)^{-1}$ is well defined when acting on kets projected by $\hat{P}$. Recognizing that acting on $|\chi_k\rangle$ with $\hat{P}$ does not change anything, we find

$$|\chi_k\rangle = \hat{P}\left(E_k - H_0 - \hat{P}\lambda V\hat{P}\right)^{-1}\hat{P}\lambda V|\psi_k\rangle, \tag{B.1.5}$$

and we can insert this into Eq. (B.1.4) to obtain in a suggestive form:

$$E_k|\psi_k\rangle = H_0|\psi_k\rangle + \hat{Q}\lambda V\hat{P}\left(E_k - H_0 - \hat{P}\lambda V\hat{P}\right)^{-1}\hat{P}\lambda V\hat{Q}|\psi_k\rangle. \tag{B.1.6}$$

We can obtain analogous equations for $|\chi_k\rangle$ as well, but let us focus on a particular model first.

B.1.2 Hamiltonian

The Potts Hamiltonian is given by

$$H = -\sum_{j=1}^{L} f_j\left(\hat{\tau}_j + \hat{\tau}_j^\dagger\right) - \sum_{j=1}^{L-1} J_j\left(\hat{\sigma}_j^\dagger\hat{\sigma}_{j+1} + \hat{\sigma}_j\hat{\sigma}_{j+1}^\dagger\right) \ , \tag{B.1.7}$$

and we will consider the case of dimerized random bonds,

$$f_j \equiv \lambda_j\left(\frac{1-\delta}{2}\right) \ , \qquad J_j \equiv \lambda_j'\left(\frac{1+\delta}{2}\right) \tag{B.1.8}$$

with λ_j, λ_j' drawn from the distribution

$$P(\lambda) = \frac{1}{W}\lambda^{1/W-1}, \tag{B.1.9}$$

where W parameterizes the disorder strength. The fully paramagnetic limit corresponds to $\delta = -1$, and the ferromagnetic limit at $\delta = +1$. We have left the overall algebraic sign common to clean systems, but the results should hold equally for either overall sign.

B.1.3 Second renormalization

The title derives from "second quantization," as we will treat the real space renormalization group's action on the theory of the effective spins half generated in the first step(s) of the standard RSRG. First, we provide an overview of the RG:

1. Identify the strongest bond in the Hamiltonian and diagonalize it. At the beginning, this will be a term with parafermion description $-K_x\omega^{-1}\alpha_x^\dagger\alpha_{x+1}$ and its Hermite conjugate, which will have eigenvalues $-2K_x, K_x, K_x$.

2. The decimation of parafermions into an inert singlet or an effective spin 1/2 is the most interesting step in the process. The fusion channel is $\sqrt{\mathbf{3}} \otimes \sqrt{\mathbf{3}} \to \mathbf{1} \oplus \mathbf{2}$. At this point, we populate the corresponding channels with probabilities 1/3 and 2/3, respectively.

   (a) For the nondegenerate $\mathbf{1}$ state with eigenvalue $-2K_x$, the parafermion modes at $x, x+1$ drop out of the chain, and the modes on either end are given a new effective coupling at second order perturbation theory. The Hamiltonian is self similar under this step, but with one site fewer.

(b) It is helpful to treat singlet formation as a site dropping out of the chain and creating an effective coupling between its neighbors because without this, we would have to keep track of terms of order $n+1$ in perturbation theory to describe two spins 1/2 separated by n. In the course of RG we will just update the new coupling.

(c) If we end up in the **2** space, we have an effective spin 1/2 degree of freedom. No subsequent step in the RG may tunnel to the trivial subspace. The spin 1/2 can be represented by an effective parafermion mode

$$\tilde{\alpha}_{x,x+1} = \frac{1}{3}\left(\alpha_x + \alpha_{x+1} + \omega\alpha_x^\dagger\alpha_{x+1}^\dagger\right), \tag{B.1.10}$$

which is equivalent to $\hat{s}_{\tilde{x}}^- = |1_{x,x+1}\rangle\langle 2_{x,x+1}|$. The conjugate of $\tilde{\alpha}_{x,x+1}$ is $\hat{s}_{\tilde{x}}^+$, and they obey all the properties of the Pauli matrices for a single site. They also respect the parafermion multiplication rules for parafermion operators of different sites.

(d) This RG step maintains interactions between the fused **2** mode and its neighbors, which can be regarded as first order corrections. There is also a term generated at second (and trivially[1], higher) orders. This expression can be solved exactly in Mathematica by considering two sites only, and a strong bond J between them, with on-site $\hat{\tau}$'s as perturbations, restricted to the 6×6 subspace of $\mathbf{2}\otimes\mathbf{3}$. However, it does not make sense to diagonalize this full thing in the case where nearby bonds might be strong.

(e) Depending on how dimerized the system is, we may see regions of just a single site [bond] forming a spin 1/2, or great extents of the chain with neighboring effective spins.

3. For cases where we find two neighboring on-site [link] terms, which are "strong," and fuse into neighboring spin 1/2 degrees of freedom, some RG step will eventually have us diagonalize a spin-spin interaction term.

(a) Perturbation theory tells us that the eigenstate of the full Hamiltonian will—at zeroth order—be an eigenstate of this first order correction (of XX form). This is just one reason that the order in which parafermions fuse into spins is of importance. Note that if the two neighboring spins 1/2 form into *singlet-type* states $|\pm\rangle = |\uparrow\downarrow\rangle \pm |\downarrow\uparrow\rangle$, they will be nondegenerate and "freeze in," dropping out of the chain. Strictly speaking, the RG process freezes in any states that form which are nondegenerate, forbidding nontrivial action on these states at higher order.

(b) In general, the strength of the first order correction between effective spins at sites $j, j+1$, given by J_j, will be roughly an order of magnitude larger than the second order corrections. This means the state of two or more spins will be dominated by eigenstates of pairs of spins under an XX interaction.

(c) Considering the case where $f_j > J_j$, the two site couplings for two spins 1/2 are, at first, second, and third order

$$J_j,\ \frac{J_j^2}{6\left(f_j + f_{j+1}\right)},\ \frac{J_j^3\left(f_j^2 + f_{j+1}^2\right)}{18 f_j^2 f_{j+1}^2} \tag{B.1.11}$$

[1]When decimating a single mode, the higher order terms are exactly the same as the second order term as far as operators.

with ratios to the first order coupling given by

$$1, \quad \frac{\lambda_j^{'}(1-\epsilon)}{6(\lambda_j+\lambda_{j+1})(1+\epsilon)} \lesssim \frac{1}{12}, \quad \frac{\lambda_j^2(1-\epsilon)^2\left(\lambda_j^2+\lambda_{j+1}^2\right)}{18\lambda_j^2\lambda_{j+1}^2(1+\epsilon)^2} \lesssim \frac{1}{9}, \tag{B.1.12}$$

where ϵ is a small, positive number specifying how deep in the paramagnetic phase we are. Any reasonable amount of disorder or greater depth in the paramagnetic phase will exaggerate this. Additionally, the first order correction is at least six times the three-site correction at second order. However, a nonrigorous calculation shows the third-order three-site terms may be nearly half the first order correction at weak disorder and near the transition...

4. The above shows us that we will be setting eigenstates of the XX model first. We will label this term

$$H_1^j = -J_j\left(\hat{s}_j^+\hat{s}_{j+1}^- + \hat{s}_j^-\hat{s}_{j+1}^+\right), \tag{B.1.13}$$

or H_{xx}^j. These terms are likely a factor of ten greater than higher order corrections. As mentioned above, the singlet-type states have unique energies $\mp J_j$, and will therefore drop out, though we will still calculate the exact form of the effective interactions due to high-order terms. The other two states are *super-spin states*, analogous to those obtained in RG for the random bond XXZ model.

5. Running the RG again for the *singlet-type states*, $|\pm\rangle$ generates the following corrections at first order:

   (a) The two-site correction at second order is simply a projector onto the $|+\rangle$ state:

$$\frac{2J_j^2}{3(f_j+f_{j+1})}\left(|+\rangle\langle+|\right)_{j,j+1}. \tag{B.1.14}$$

   (b) The two-site terms that overlap with only one of the spins give:

$$\frac{J_{j-1}^2}{6}\left(\frac{1}{f_j}+\frac{1}{f_{j-1}}+\frac{1}{f_j+f_{j-1}}\right)\hat{\mathbb{1}} \tag{B.1.15}$$

   (c) The three-site corrections at second order do not map the states $|\pm\rangle$ to themselves, so there are no corrections at first order.

   (d) The third order correction on both sites of the singlet is zero, while the corrections that intersect just one site give the correction

$$-\frac{J_{j-1}^3}{18}\left(\frac{1}{f_{j-1}^2}+\frac{1}{f_j^2}\right)\hat{\mathbb{1}} - \frac{J_{j+1}^3}{18}\left(\frac{1}{f_{j+1}^2}+\frac{1}{f_{j+2}^2}\right)\hat{\mathbb{1}} \tag{B.1.16}$$

   (e) The first order term from the three-site terms intersecting the full singlet is:

$$\mp J_j\left(\frac{J_{j-1}^2}{9f_{j-1}(f_{j-1}+f_j)}\frac{J_{j+1}^2}{9f_{j-1}(f_{j+1}+f_{j+2})}\right)\hat{P}_{j,j+1}^{(\pm)}. \tag{B.1.17}$$

(f) The terms that only intersect one spin in the singlet allow corrections to the hopping terms on the sides at first order

$$-\frac{J_{j-2}J_{j-1}^2}{9f_j\left(f_{j-1}+f_j\right)}\left(\hat{s}_{j-2}^+\hat{s}_{j-2}^- + h.c.\right) - \frac{J_{j+1}^2 J_{j+2}}{9f_{j+1}\left(f_{j+1}+f_{j+2}\right)}\left(\hat{s}_{j+2}^+\hat{s}_{j+3}^- + h.c.\right) \tag{B.1.18}$$

(g) The four site corrections contribute the following:

$$-\frac{J_{j-1}J_jJ_{j+1}}{9f_jf_{j+1}}\left(\hat{s}_{j-1}^+\hat{s}_{j+2}^- + \hat{s}_{j-1}^-\hat{s}_{j+2}^+ + \hat{\mathbb{P}}_{j-1,j,j+1,j+2}^{(\pm)}\right), \tag{B.1.19}$$

where $\hat{\mathbb{P}}_{j-1,j,j+1,j+2}^{(\pm)}$ projects onto the *super spin singlet state*

$$\frac{1}{\sqrt{2}}\left(|\uparrow\uparrow\downarrow\downarrow\rangle \pm |\downarrow\downarrow\uparrow\uparrow\rangle\right)_{j-1,j,j+1,j+2}, \tag{B.1.20}$$

where the sign is determined by the $\pm$ state of the inner two sites. Note that the nontrivial hopping term reveals that the first order perturbations to the singlet state allow both spins to drop out, preserving the form of the Hamiltonian.

6. We will only go to second order in the RG for the spins and just see what happens, bro:

(a) The terms that arise from an intermittent $|\mp\rangle$ state give rise to six terms proportional to the identity, and four terms proportional to $\hat{s}_{j-1}^z\hat{s}_{j+2}^z$, which restores the ZZ interaction as the singlet states drop out. The identity term is proportional to:

$$\begin{aligned}&\pm\frac{J_{j-1}^4}{72J_j}\left(\frac{1}{f_{j-1}}+\frac{1}{f_j}-\frac{1}{f_{j-1}+f_j}-\frac{J_{j-1}}{3f_{j-1}^2}-\frac{J_{j-1}}{3f_j^2}\right)^2\hat{\mathbb{1}}\\ &\pm\frac{J_{j+1}^2}{72J_j}\left(\frac{J_{j+1}}{3f_{j+1}^2}+\frac{J_{j+1}}{3f_{j+2}^2}+\frac{1}{f_{j-1}+f_{j+2}}-\frac{1}{f_{j-1}}-\frac{1}{f_{j+2}}\right)^2\hat{\mathbb{1}},\end{aligned} \tag{B.1.21}$$

and the ZZ interaction is

$$\begin{aligned}&\pm\frac{J_{j-1}^2J_{j+1}^2}{72J_j}\left(\frac{1}{f_{j-1}}+\frac{1}{f_j}-\frac{1}{f_{j-1}+f_j}-\frac{J_{j-1}}{3f_{j-1}^2}-\frac{J_{j-1}}{3f_j^2}\right)\times\\ &\left(\frac{J_{j+1}}{3f_{j+1}^2}+\frac{J_{j+1}}{3f_{j+2}^2}+\frac{1}{f_{j-1}+f_{j+2}}-\frac{1}{f_{j-1}}-\frac{1}{f_{j+2}}\right)\hat{s}_{j-1}^z\hat{s}_{j+2}^z,\end{aligned} \tag{B.1.22}$$

where in both cases the sign $\pm$ is that of the state of the singlet.

7. Now we will move on to the terms generated for the super-spin subspace

(a) The two-site correction $\propto J_j^2$ (H_2^j) acts diagonally on all states of the H_{xx}^j with energies

$$E_{2,\uparrow\uparrow}^j = E_{2,\downarrow\downarrow}^j = \frac{J_j^2}{3f_jf_{j+1}}\left(f_j+f_{j+1}\right), \tag{B.1.23}$$

which can act on all states. We could have incorporated this directly into H_{xx}^j, which would not change the degeneracy/ nondegeneracy of the eigenstates. This term has the opposite algebraic sign compared to the first order correction, meaning it would likely weaken overall the assertion that $H_1 > H_3^{j,j+1}$, a term that was already as close as half H_1. The strong disorder limit alleviates this concern.

(b) The three-site corrections at second order $H_2^{j-1,j}$ and $H_2^{j,j+1}$ all kill the singlet-type states. The effective terms from this are:

$$\frac{2J_{j-1}J_j}{3f_j}\left(\hat{s}^+_{j-1}\hat{s}^+_j\hat{s}^+_{j+1}+h.c.\right)+\frac{2J_jJ_{j+1}}{3f_{j+1}}\left(\hat{s}^+_j\hat{s}^+_{j+1}\hat{s}^+_{j+2}+h.c.\right), \tag{B.1.24}$$

i.e. in all cases, the next-nearest neighbor hopping dies, as it cannot map nontrivially between states in the same subspace.

(c) The two-site correction at third order acts diagonally on the XX states as well, giving

$$E^j_{3,\uparrow\uparrow}=E^j_{3,\downarrow\downarrow}=-\frac{J_j^2}{9f_j^2f_{j+1}^2}\left(f_j^2+f_{j+1}^2\right),\quad E^j_{3,\pm}=0, \tag{B.1.25}$$

analogous to the case at second order. Actually, in all likelihood we can get the two site correction to all orders via geometric sum.

(d) The three-site correction at third order, as with the correction at second order, is reduced simply to the triplet creation/annihilation operators in the super-spin subspace, and in the singlet subspace the energy is:

$$E_\pm=\mp\frac{J_j}{9}\left(\frac{J_{j-1}^2}{f_{j-1}\left(f_j+f_{j-1}\right)}+\frac{J_{j+1}^2}{f_{j+2}\left(f_{j+2}+f_{j+1}\right)}\right). \tag{B.1.26}$$

8. And beyond first order, we generate the new and interesting effective terms.

(a) For the singlet states on sites 1,2, the three-site effective corrections are:

i. For just the same term type:

$$\langle\pm_{12}|H_2^{(1,2)}\hat{Q}^{ss}_{12}\frac{1}{\mathcal{E}_\pm-H_1^{(1,2)}}\hat{Q}^{ss}_{12}H_2^{(1,2)}|\pm_{12}\rangle=\mp\frac{J_1}{2}\left(\frac{J_2}{3f_2}\right)^2\left(\hat{\mathbb{1}}+\hat{s}^x_3\right) \tag{B.1.27}$$

$$\langle\pm_{12}|H_2^{(0,1)}\hat{Q}^{ss}_{12}\frac{1}{\mathcal{E}_\pm-H_1^{(1,2)}}\hat{Q}^{ss}_{12}H_2^{(0,1)}|\pm_{12}\rangle=\mp\frac{J_1}{2}\left(\frac{J_0}{3f_1}\right)^2\left(\hat{\mathbb{1}}+\hat{s}^x_0\right) \tag{B.1.28}$$

ii. And when we have both $H_2^{(1,2)}$ and $H_2^{(0,1)}$, we get $-2J_0J_1J_2/9f_1f_2$ times a projector onto the 0123 states

$$\frac{1}{\sqrt{2}}\left(|\uparrow\uparrow\downarrow\downarrow\rangle\pm|\downarrow\downarrow\uparrow\uparrow\rangle\right), \tag{B.1.29}$$

which is a singlet of two super spins at sites $0,1$ and $2,3$, and the sign is determined by the type of singlet between sites $1,2$. The factor of two comes from the two orderings.

9. We will also encounter cases where one of the parafermion modes in the strong term for a given step $K_x\omega^{-1}\alpha_x^\dagger\alpha_{x+1}$ has not been incorporated into a spin 1/2. This can happen when a region of strong bonds meets the edge of the chain, or a region of strong on-site $\hat{\tau}$ terms, and can also happen when a strong field term is next to a field term that is weaker than the coupling between the sites, in which case we will diagonalize the bond before we have the chance to try projecting the weak site.

To summarize, the RG procedure in the non-Abelian case is far more complicated, and is generally not self-similar. Even in the strongly dimerized limits $f \gg J$ and $f \ll J$, one still must deal with the fact that the spin objects created by the RSRG are able to grow in size without bound. However, it is mostly clear that the resulting phase is MBL, and spontaneously breaks at least one of the constituent symmetries comprising $S_3 = D_3$. However, away from these harsh limits, one is likely to encounter scenarios in which at least one bond [site] is diagonalized before all of the sites [bonds]. In this case, unless the result of the RG step is a singlet, one will have to deal with awkward scenarios in which there are dangling parafermion modes, potentially separated by many sites. These modes complicate the RG even further; in general, the picture at intermediate dimerizations (i.e. near the transition) is murky due to the non-Abelian symmetry and lack of self-similarity under the RG. However, there may be evidence of a quantum critical glass [31] or other more exotic, nonergodic properties.

B.2 Special Effective Phases in the $n = 3$ Clock Model

One can make the following argument: suppose the phases are randomly distributed about zero, then after many RG steps the effective phase will be a sum over many random numbers with average value 0, leaving only a phase proportional to an integer (or half-integer, by factoring out -1) power of ω. When this happens, the procedure is that of the S_3 Potts model. If the system ends up in the nondegenerate ($\mathcal{E}_0 = \pm 2\Omega$) state, then the strong bond drops out per the typical second-order process. Sites L and R now have effective couplings given by:

$$\tilde{K}_{LR} = (-1)^n \frac{K_L K_R}{3\Omega} \ , \ \tilde{\varphi}_{LR} = \varphi_L + \varphi_R - \frac{2\pi n}{3}. \tag{B.2.1}$$

Although one might worry that a higher symmetry model is spawned, it is important to note that such a special value of the effective phase could only occur after *many* RG fusion steps, meaning the corresponding term would be a product of a very large number of small quantities. What's more, in order for any spin-1/2-type interactions to exist, there must be *two* such special-valued phases that emerge. The spin 1/2 behaves as though it has dropped out of the chain (as per the normal course of the $\mathbb{Z}_3$ RSRG) until it meets another spin 1/2 as a nearest neighbor. This means the Potts-type RG cannot be realized until enough RG steps have occurred to create two of these spins 1/2. Many RG steps will have occurred at this point, and the behavior of the couplings under renormalization should be clear. What's more, an overwhelming portion of the chain will be "frozen in" already.

It is worth noting that if only two spins 1/2 are generated, the interaction is exactly the XXZ model between them, which is easily solved for two spins. For three or more of these guys, we get the full ugliness of Potts, but with couplings that are quite weak compared to the energy scale of the frozen-in things. These processes will also be highly nonlocal.

B.3 Supplementary Numerical Evidence for the S_3 Potts Model

B.3.1 Supplementary numerics: weak disorder

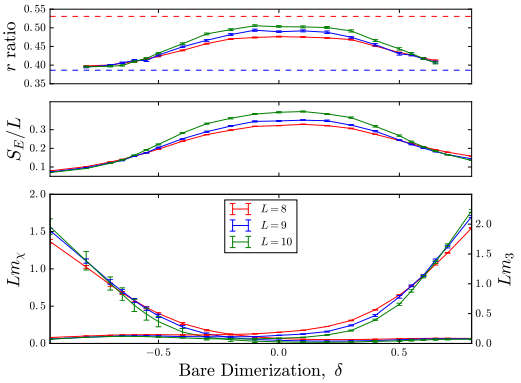

(a) $W = 0.5$ (Appears as Fig. 6.3a in Ch. 6.)

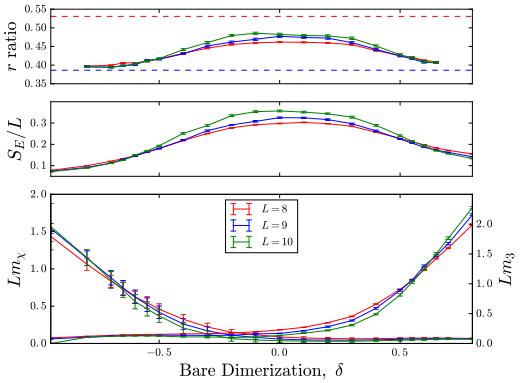

(b) Additional results for $W = 0.6$.

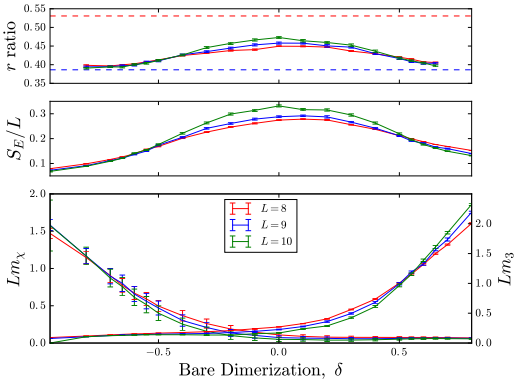

(c) Additional results for $W = 0.7$.

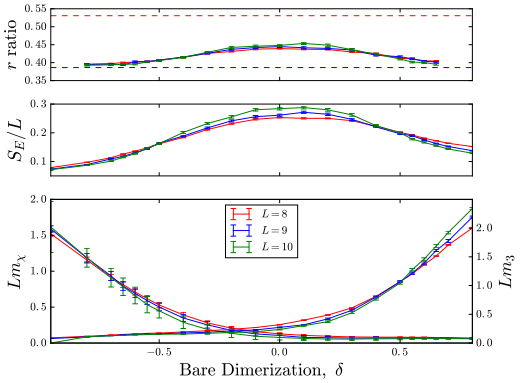

(d) Additional results for $W = 0.8$.

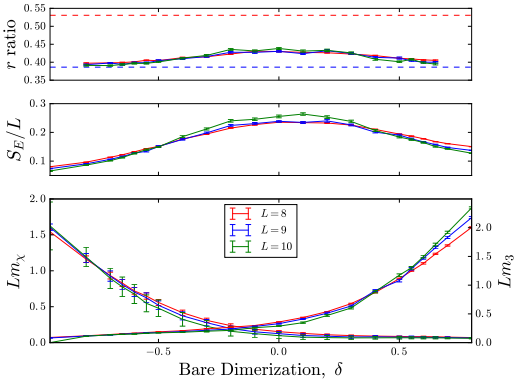

(e) Additional results for $W = 0.9$.

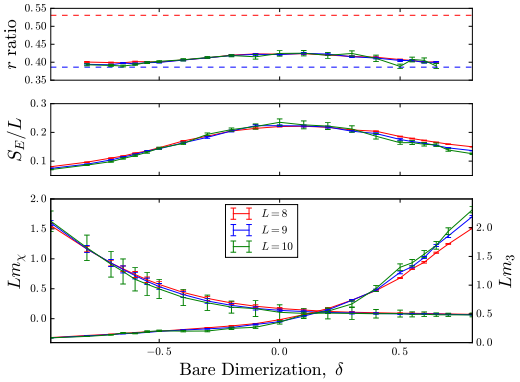

(f) $W = 1.0$ for comparison

Figure B.1: Weak disorder plots for the disordered S_3 Potts model.

B.3.2 Supplementary numerics: Strong disorder

Fig. B.2a-B.2d present additional data showing Poisson level statistics and area law entanglement as one moves toward strong disorder ($W \sim 2$), as well as finite-size scaling collapse predicated on a direct infinite-randomness transition. Note the improvement in the quality of collapse as we move to stronger disorder.

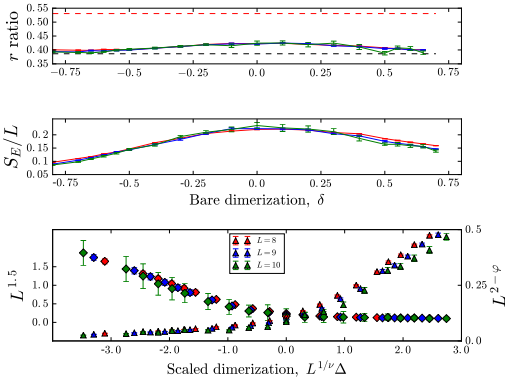

(a) "Strong Disorder" plot for $W = 1.0$.

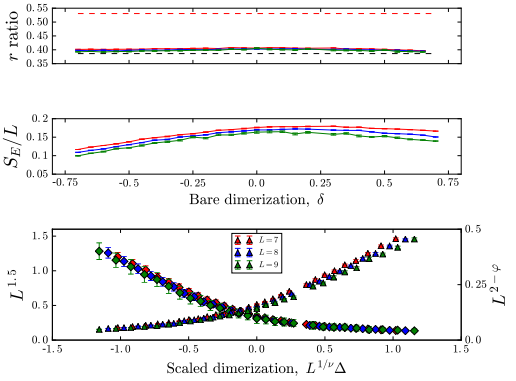

(b) Additional results for $W = 1.5$

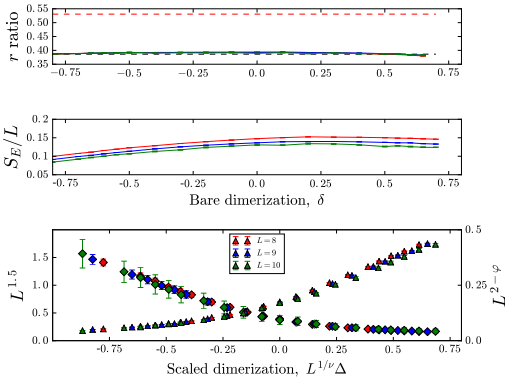

(c) $W = 2.0$ for comparison.

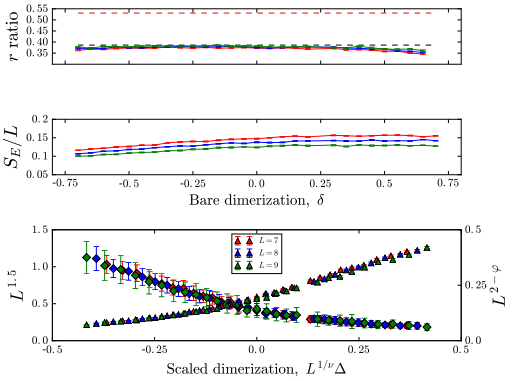

(d) Additional results for $W = 2.5$.

Figure B.2: Strong disorder plots for the disordered S_3 Potts model.

Appendix C

Supplementary Material for the Random Bond XXZ Model

C.1 Additional numerical results

C.1.1 Numerics and phase diagram

We compute the r ratio, entanglement entropy, and spin-glass order parameter, $m_{\mathrm{EA}} = \chi_{\mathrm{EA}}/L$, averaged over eigenstates at energy density $\epsilon = 0.5$ and disorder realizations for various values of the parameters W, Δ and L. The random couplings $J_i \in (0, 1]$ are drawn from the power-law distribution $P(J) = \frac{1}{W}\frac{1}{J^{1-1/W}}$ and we choose Δ_i to be uniformly distributed in the interval $[-\Delta, \Delta]$.

At sufficiently weak disorder (i.e., $0 \leq W \lessapprox 1.5$), we find evidence of an ergodic to MBL transition as a function of Δ, as depicted in Fig. C.1. For Δ smaller than a critical value $\Delta_c(W)$, the overall disorder strength is not enough to localize the system, and we observe clear signatures of a thermal phase (extensive entanglement entropy, GOE level statistics and $m_{\mathrm{EA}} = 0$). For $\Delta > \Delta_c(W)$, the system is localized with Poisson level statistics, sub-extensive entanglement entropy indicating a breaking of ergodicity and diverging spin glass parameter χ_{EA}. The entanglement entropy as a function of L shows a clear crossover from volume-law to sub-extensive behavior as a function of Δ (Fig. C.2). This MBL transition can also be observed at fixed Δ by tuning W, as depicted in Fig. C.3.

C.1.2 Uniform anisotropies $\Delta_i = \Delta$

Note that we took the anisotropy parameters Δ_i to be random since randomness in J_i generates randomness in Δ_i upon renormalization, so that we expect qualitatively similar conclusions for uniform $\Delta_i = \Delta$, except around the pathological $SU(2)$ symmetric point $|\Delta| = 1$ that is known to lead to thermalization for arbitrary disorder strength [31] (see also [209, 220]). To verify this numerically, we also considered the case of uniform anisotropies $\Delta_i = \Delta$ in the strong randomness regime $W = 2$ (Fig. C.4). We find that, away from the $SU(2)$-symmetric point $\Delta = 1$, the results are qualitatively similar to the random Δ_i case as expected, with a spin-glass MBL phase at all values of $\Delta \neq 1$. Precisely at the $SU(2)$-symmetric point $\Delta = 1$, the results are more intricate. Because of the different spin sectors $S^2 = j(j+1)$ that do not mix with each others, it is natural to expect Poisson statistics in the $S^z = 0$ sector even though the system should be thermalizing. We find numerically a r ratio below the Poisson value, suggesting a finite-size segmentation of the spectrum. This is consistent with the fact that we observe sub-extensive entanglement for $\Delta = 1$,

which suggests that the system has not yet reached the scaling regime which should be dominated by almost classical large superspins. We nevertheless observe that the point $\Delta = 1$ is much less localized than $\Delta \neq 1$ for the same disorder strength $W = 2$. Moreover, our numerical results indicate the absence of spin glass order precisely at $\Delta = 1$, also consistent with thermalization. We have also checked that taking $\Delta_i = \Delta$ does not modify the phase diagram shown in Fig. 6.5 quantitatively provided $\Delta \neq 1$. We leave a detailed numerical analysis of this interesting $SU(2)$-symmetric point for future work, and restrict ourselves to random anisotropies Δ_i which lead to qualitatively similar results but has the strong advantage of avoiding pathological features that are not the subject of interest for our study.

C.1.3 Additional numerical evidence

Included in this section are several additional plots based on numerical study of this system.

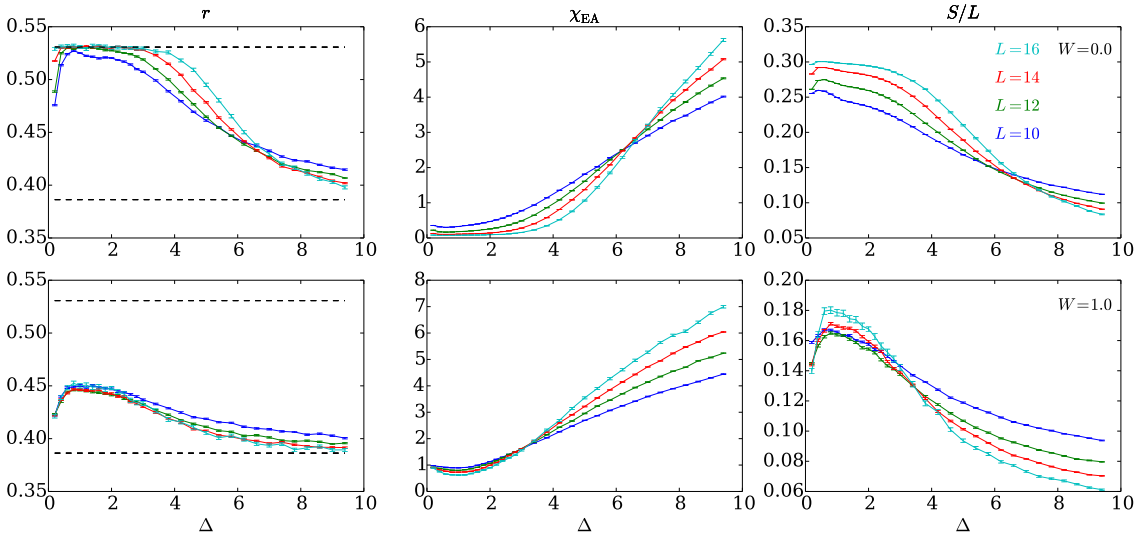

Figure C.1: Ergodic to spin glass (MBL) transition as a function of Δ, for $W = 0$ (top: uniform $J_i = 1$) and $W = 1$ (bottom). *Left:* Ratio of consecutive level spacings showing a transition from GOE to Poisson statistics. *Middle:* Scaling of χ_{EA} showing a divergence with system size in the localized phase. *Right:* Finite-size entanglement crossover.

C.2 Fermion Description and Symmetry-Protected Topological Phases

C.2.1 Mapping to fermions

To be self-contained and make contact with our discussion in the main text, we briefly review the equivalent descriptions of the XXZ chain in terms of spinless fermions, and its connection to symmetry protected topological phases (SPTs) for the case of dimerized couplings.

The XXZ spin chain, defined by Eq. (6.5.1), maps to an interacting fermion chain via the

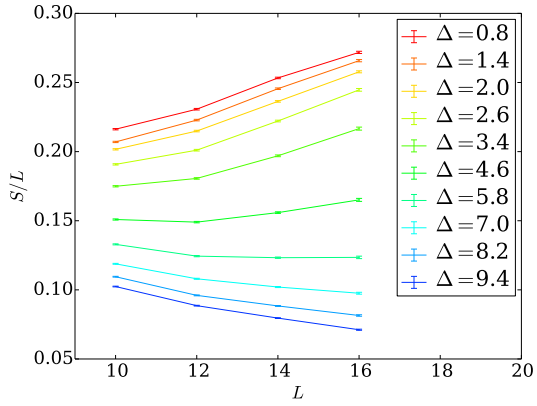

Figure C.2: Crossover between volume- and area-law scaling of the entanglement entropy as a function of Δ for $W = 0.5$.

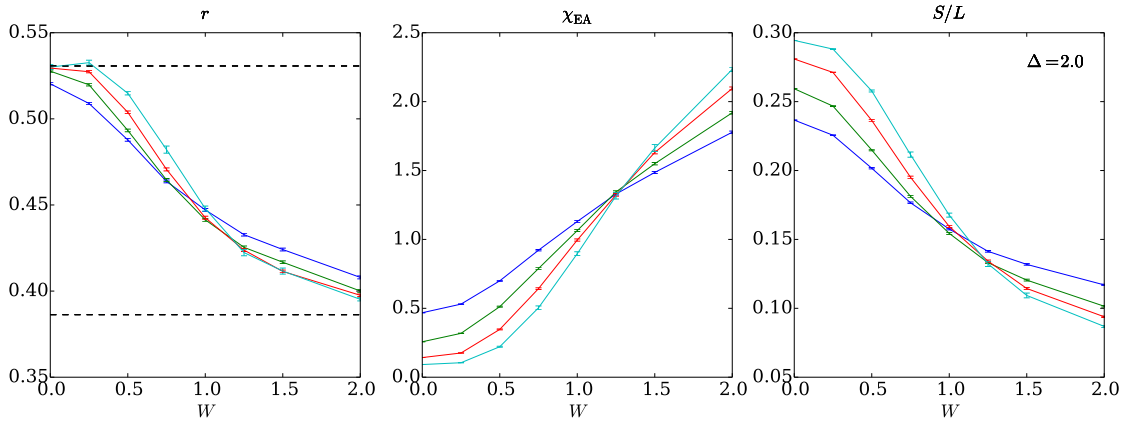

Figure C.3: Ergodic to spin glass (MBL) transition as a function of W at fixed $\Delta = 2.0$.

Jordan-Wigner mapping $S_i^z = c_i^\dagger c_i - \frac{1}{2}$, $S_i^+ = S_i^x + iS_i^y = \left(\prod_{j<i} \sigma_j^z\right) c_i^\dagger$:

$$H_{\text{spin}} = \sum_{i=1}^{2N-1} J_i \left(S_i^x S_{i+1}^x + S_i^y S_{i+1}^y + \Delta_i S_i^z S_{i+1}^z\right),$$
$$H_{\text{fermion}} = \sum_{i=1}^{2N-1} J_i \left[\frac{1}{2}\left(c_{i+1}^\dagger c_i + \text{h.c.}\right) + \Delta_i \left(n_i - \frac{1}{2}\right)\left(n_{i+1} - \frac{1}{2}\right)\right], \tag{C.2.1}$$

where we take $L = 2N$ even.

C.2.2 Symmetries

We now discuss the symmetries of the above model. We will first describe the symmetries in the spin language, and then use the Jordan-Wigner mapping to obtain their action on the fermion operators.

First, the spin chain has a $U(1)$ symmetry generated by S^z rotations $U_\phi = \prod_j e^{-i\phi\sigma_j^z/2}$, that corresponds to the conserved z-axis magnetization. The model also has $\mathbb{Z}_2$ time-reversal symmetry, implemented by $\mathcal{T} = K$, where K is the antilinear operator representing complex conjugation, and an Ising ($\mathbb{Z}_2$) symmetry generated by $\mathcal{C} = \prod_j \sigma_j^x$. Note that the action of this symmetry flips the axis of the conserved spin, $\mathcal{C}U_\phi\mathcal{C}^\dagger = U_{-\phi}$.

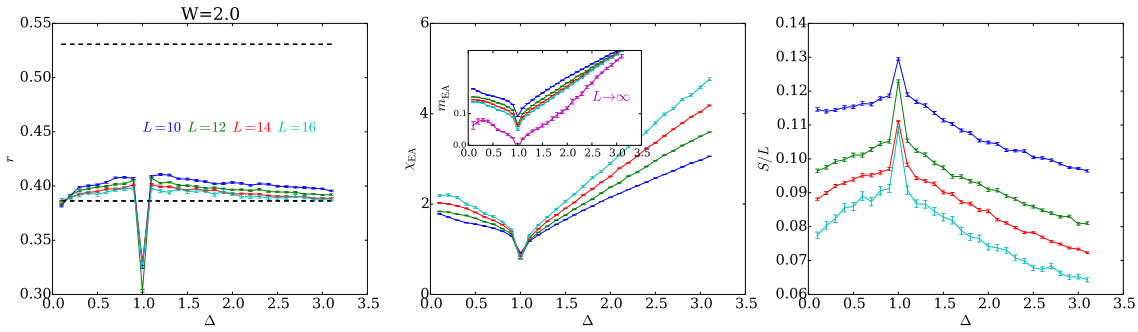

Figure C.4: Strong disorder regime ($W = 2.0$) with uniform anisotropy $\Delta_i = \Delta$. Away from the pathological $SU(2)$-symmetric point $\Delta = 1$, the results are qualitatively similar to the random Δ_i case, consistent with a many-body localized phase with spontaneously broken particle-hole symmetry at all values of $\Delta \neq 1$.

Turning to the fermions, we see that the symmetries act on the second-quantized fermion operators as follows:

$$U_\phi c_j U_\phi^\dagger = e^{-i\phi} c_j,$$
$$\mathcal{T} c_j \mathcal{T}^{-1} = c_j \quad \text{with} \quad \mathcal{T} i \mathcal{T}^{-1} = -i, \tag{C.2.2}$$
$$\mathcal{C} c_j \mathcal{C}^{-1} = (-1)^{j+1} c_j^\dagger. \tag{C.2.3}$$

Note that the time-reversal symmetry is antiunitary, while U_ϕ, $\mathcal{C}$ are unitary. In the fermionic language, $U(1)$ corresponds to the particle number conservation, while $\mathcal{C}$ corresponds to particle-hole symmetry. In addition, we can construct an antiunitary symmetry $\mathcal{S} \equiv \mathcal{C} \times \mathcal{T}$, usually termed "chiral" or "sublattice" symmetry,

$$\mathcal{S} c_j \mathcal{S}^{-1} = (-1)^{j+1} c_j^\dagger \quad \text{with} \quad \mathcal{S} i \mathcal{S}^{-1} = -i. \tag{C.2.4}$$

Note that $\mathcal{T}^2 = \mathcal{C}^2 = 1$ when acting on fermion operators, but that $\mathcal{S}^2$ has no well defined action on c_j, because we can redefine $\mathcal{S}^2$ by an arbitrary phase $e^{i\alpha}$ by combining it with a $U(1)$ rotation $\mathcal{S} \to \tilde{\mathcal{S}} = e^{i\alpha/2 \sum_j n_j} \mathcal{S}$.

A note on nomenclature. We caution that there is a potentially confusing alternative terminology frequently used for noninteracting fermion systems, wherein the particle-hole symmetry $\mathcal{C}$ is called "antiunitary" while $\mathcal{S}$ is called "unitary." The alternative convention arises because the traditional symmetry classification of free fermion systems considers the action of symmetries on the first-quantized Hamiltonian $\mathcal{H}$, where the noninteracting second-quantized Hamiltonian H is defined via $H = \sum_{i,j} c_i^\dagger \mathcal{H}_{ij} c_j$ (see also footnote on p.7 of [319]). Given a unitary symmetry, $\mathcal{C}$, that interchanges particles and holes, $\mathcal{C} c_i \mathcal{C}^{-1} = \sum_j (U_\mathcal{C}^*)_{ij} c_j^\dagger$, then $\mathcal{H}$ satisfies $U_\mathcal{C}^\dagger \mathcal{H}^* U_\mathcal{C} = -\mathcal{H}$.

Owing to the complex conjugation on the LHS of the preceding expression, the unitary symmetry $\mathcal{C}$ is sometimes termed "anti-unitary" in this context. Similarly, the anti-unitary symmetry $\mathcal{S}$ implies $U_\mathcal{S}^\dagger \mathcal{H} U_\mathcal{S} = -\mathcal{H}$, hence $\mathcal{S}$ "looks" unitary when acting on $\mathcal{H}$. When referring to operators as unitary or anti-unitary, we will *always* refer to the action on the second-quantized operators, which is more appropriate for the generic case of interacting systems. Hence we will refer to $\mathcal{C}$ as unitary, and $\mathcal{S}, \mathcal{T}$ as anti-unitary.

C.2.3 Ground-state SPT Order

When the hoppings in Eq. (C.2.1) are dimerized, $J_i \to \frac{J}{2}(1-\delta(-1)^i)$ with $1 > \delta > 0$, the ground-state realizes an SPT phase with symmetry protected topological (complex) fermion zero mode end states. The nontrivial edge structure is most easily seen by considering the limit of zero interactions ($\Delta_i = 0$) and strong dimerization, $\delta = 1$. Here, the fermion Hamiltonian possesses a strictly localized complex fermionic zero mode c_1 (c_{2N}) on the left (right) side of the chain respectively. Focusing just on the left side of the chain, the fermionic zero mode c_1 spans a degenerate two-state Hilbert space $\{|\pm\rangle\}$ with $c_1|-\rangle = 0$ and $|+\rangle = c_1^\dagger|-\rangle$.

It turns out that the protection of these edge states relies only on $U(1)$ and the $\mathbb{Z}_2^{\mathcal{S}}$ subgroup of $\mathbb{Z}_2^{\mathcal{C}} \times \mathbb{Z}_2^{\mathcal{T}}$, in the sense that we may break $\mathcal{T}$ and $\mathcal{C}$ separately so long as their product $\mathcal{S}$ remains a good symmetry. Then, the relevant symmetry group is $U(1) \times \mathbb{Z}_2^{\mathcal{S}}$, corresponding to class AIII in the Cartan notation [218, 219, 319]. A classic example of a problem in this symmetry class is the Su-Schrieffer-Heeger model [320]. In $d = 1$, free fermion problems in this class have a $\mathbb{Z}$ classification, which reduces to a $\mathbb{Z}_4$ classification upon including interactions [321].

This zero-energy edge mode has a projective implementation of the $U(1) \times \mathbb{Z}_2^{\mathcal{S}}$ symmetry group, which protects it from being gapped out by any interaction with local, bulk degrees of freedom, which all transform nonprojectively, and hence cannot couple in a symmetric fashion with the edge state. The projective action of symmetry on the edge state can be seen by considering just the $\mathbb{Z}_2$ subgroup of the $U(1)$ generated by the fermion number parity: $\mathcal{P}_F = e^{i\pi \sum_i n_i}$. For the full system (and for any set of bulk degrees of freedom), $\mathcal{P}_F$ commutes with charge conjugation, $[\mathcal{P}_F, \mathcal{S}] = 0$. However, acting within the low-energy subspace spanned by the zero-mode states $|\pm\rangle$ of one end of the chain, we see that $\pm$ have opposite eigenvalue of $\mathcal{P}_F$: $\langle +|\mathcal{P}_F|+\rangle = -\langle -|\mathcal{P}_F|-\rangle$. On the other hand, $\mathcal{S}$ changes $c_1 \to c_1^\dagger$, and hence exchanges $\mathcal{S}|\pm\rangle = |\mp\rangle$. Hence, the symmetry group is implemented projectively at the end of the chain: $\mathcal{P}_F\mathcal{S}\mathcal{P}_F\mathcal{S}|\pm\rangle = (-1)|\mp\rangle$. This projective action indicates that the zero-modes are topologically stable to any symmetry-respecting perturbation that does not close the bulk gap [321, 322]. In particular, this phase and topological edge states exist in the ground state over a finite range of parameters near the perfectlydimerized limit (though the zero modes are generically only exponentially localized to the edge).

The phase described above is the elementary, $n = 1$, "root" phase of the $1d$ AIII chains. Absent interactions, we may combine any integer number, n, of these phases to obtain a new, nontrivial phase. For $n = 2$ chains, we denote by $c_1^\dagger$ and $d_1^\dagger$ the fermionic edge modes acting on the left side of the two perfectly-dimerized chains: the ground-state Hilbert space can then be written as $\{|00\rangle, |10\rangle = c_1^\dagger|00\rangle, |01\rangle = d_1^\dagger|00\rangle, |11\rangle = c_1^\dagger d_1^\dagger|00\rangle\}$. Since $\mathcal{S}c_1\mathcal{S}^{-1} = c_1^\dagger$ and $\mathcal{S}d_1\mathcal{S}^{-1} = d_1^\dagger$, the sublattice symmetry $\mathcal{S}$ acts on the zero-mode states as $\mathcal{S}|00\rangle = |10\rangle$, $\mathcal{S}|11\rangle = -|00\rangle$, $\mathcal{S}|10\rangle = |01\rangle$, and $\mathcal{S}|01\rangle = -|10\rangle$. The $n = 2$ phase therefore has $\mathcal{S}^2 = -1$ when acting on the edge states, whereas $\mathcal{S}^2 = 1$ acting on any local bulk degree of freedom. Similarly, $n = 3$ has a combination of $\{\mathcal{P}_F, \mathcal{S}\} = 0$ and $\mathcal{S}^2 = -1$ on the edge states. However, there is no projective action of symmetry for phases with $n = 0$ mod 4, and hence, with interactions, these phases become equivalent to topologically trivial ones [321]. Our argument that the excited states of the $n = 1$ phase with strong randomness are unstable to spontaneous symmetry breaking also applies to the other members ($n = 2, 3$) of this AIII SPT family, and rules out the protection of SPT order.

Appendix D

Supplementary Material for Open Quantum Systems

D.1 Details of the Caldeira-Leggett model

D.1.1 Other forms of the spectral function, J

If we consider sub- and super-Ohmic forms of $J(\omega)$, we recover only mildly different results. In particular, we will take

$$J(\omega) = \eta_\gamma |\omega|^\gamma , \tag{D.1.1}$$

with $\gamma \neq 0$. Starting from the action given in Eq. (7.2.23) in Sec. 7.2 and plugging in the above form of $J(\omega)$, one has

$$S'_{\text{eff}}[q] = \frac{\eta_\gamma}{2} \int_0^{\beta\hbar} \mathrm{d}\tau \int_{-\infty}^{\infty} \mathrm{d}\tau' \left(q(\tau) - q(\tau')\right)^2 \int_0^{\infty} \frac{\mathrm{d}\omega}{2\pi} \omega^\gamma e^{-\omega|\tau-\tau'|} \tag{D.1.2}$$

$$= \frac{\eta_\gamma}{4\pi} \int_0^{\beta\hbar} \mathrm{d}\tau \int_{-\infty}^{\infty} \mathrm{d}\tau' \left(q(\tau) - q(\tau')\right)^2 \int_0^{\infty} \frac{\mathrm{d}\Omega\ \Omega^\gamma e^{-\Omega}}{|\tau-\tau'|^{\gamma+1}} \tag{D.1.3}$$

$$= \frac{\eta_\gamma \Gamma(\gamma+1)}{4\pi} \int_0^{\beta\hbar} \mathrm{d}\tau \int_{-\infty}^{\infty} \mathrm{d}\tau' \frac{\left(q(\tau) - q(\tau')\right)^2}{|\tau-\tau'|^{\gamma+1}}. \tag{D.1.4}$$

It is worth noting that any integer $\gamma \leq -1$ is forbidden, resulting in a divergent value of the above expression ($1/\Gamma(n) = 0$ for n a nonpositive integer).

Now, as with the Ohmic case, we will Fourier transform Eq. (D.1.4):

$$S'_{\text{eff}}[q] = \frac{\eta_\gamma \Gamma(\gamma+1)}{4\pi} \int_0^{\beta\hbar} \mathrm{d}\tau \int_{-\infty}^{\infty} \mathrm{d}\tau' \frac{\left(q(\tau) - q(\tau')\right)^2}{|\tau-\tau'|^{\gamma+1}} = \frac{\eta_\gamma \Gamma(\gamma+1)}{2\pi} \int_{-\infty}^{\infty} \mathrm{d}t \int_{-\infty}^{\infty} \mathrm{d}s \frac{\left(q(s+t) - q(s-t)\right)^2}{|2t|^{\gamma+1}} , \tag{D.1.5}$$

for which the Fourier transform is given by

$$= \frac{\eta_\gamma \Gamma(\gamma+1)}{2\pi} \int_{-\infty}^{\infty} \mathrm{d}t \int_{-\infty}^{\infty} \mathrm{d}s \int_{-\infty}^{\infty} \frac{\mathrm{d}\omega}{2\pi} \int_{-\infty}^{\infty} \frac{\mathrm{d}\omega'}{2\pi} \frac{\tilde{q}^*(\omega')\tilde{q}(\omega)}{|2t|^{\gamma+1}} \times$$
$$\left[e^{i(\omega-\omega')(s+t)} + e^{i(\omega-\omega')(s-t)} - e^{i\omega(s+t)} e^{-i\omega'(s-t)} - e^{i\omega(s-t)} e^{-i\omega'(s+t)} \right] \tag{D.1.6}$$

$$= \frac{\eta_\gamma \Gamma(\gamma+1)}{2\pi} \int_{-\infty}^{\infty} \frac{\mathrm{d}\omega}{2\pi} \int_{-\infty}^{\infty} \frac{\mathrm{d}\omega'}{2\pi} \tilde{q}^*(\omega')\tilde{q}(\omega) \int_{-\infty}^{\infty} \mathrm{d}s e^{i(\omega-\omega')s} \int_{-\infty}^{\infty} \frac{\mathrm{d}t}{|2t|^{\gamma+1}} \left[e^{i(\omega-\omega')t} - e^{i(\omega+\omega')t} + h.c. \right] \tag{D.1.7}$$

$$= \frac{\eta_\gamma \Gamma(\gamma+1)}{2\pi} \int_{-\infty}^{\infty} \frac{\mathrm{d}\omega}{2\pi} \int_{-\infty}^{\infty} \frac{\mathrm{d}\omega'}{2\pi} \tilde{q}^*(\omega')\tilde{q}(\omega) \left(2\pi\delta(\omega-\omega')\right) \int_{-\infty}^{\infty} \frac{\mathrm{d}t}{|2t|^{\gamma+1}} \left[e^{i(\omega-\omega')t} - e^{i(\omega+\omega')t} + h.c. \right] \tag{D.1.8}$$

$$= \frac{\eta_\gamma \Gamma(\gamma+1)}{2\pi} \int_{-\infty}^{\infty} \frac{\mathrm{d}\omega}{2\pi} |\tilde{q}(\omega)|^2 \int_{-\infty}^{\infty} \frac{\mathrm{d}t}{|2t|^{\gamma+1}} \left[2 - e^{2i\omega t} - e^{-2i\omega t} \right], \tag{D.1.9}$$

where the integral of the constant term "2" in the square braces vanishes for $\gamma > 0$. *Thus, we restrict to* $\gamma > 0$ *henceforth.* Continuing onward,

$$S'_{\text{eff}}[q] = -\frac{\eta_\gamma}{2\pi} \frac{\Gamma(\gamma+1)}{2^{\gamma+1}} \int_{-\infty}^{\infty} \frac{\mathrm{d}\omega}{2\pi} |\tilde{q}(\omega)|^2 \int_{-\infty}^{\infty} \mathrm{d}t \frac{e^{2i\omega t}}{|t|^{\gamma+1}} + h.c., \tag{D.1.10}$$

which, for $\gamma > 0$ and γ not an even integer, this Fourier transform becomes

$$S'_{\text{eff}}[q] = -\frac{\eta_\gamma}{2\pi} \frac{\Gamma(\gamma+1)}{2^\gamma} \int_{-\infty}^{\infty} \frac{\mathrm{d}\omega}{2\pi} |\tilde{q}(\omega)|^2 \left\{ 2^{\gamma+1} |\omega|^\gamma \cos(\pi\gamma/2) \Gamma(-\gamma) \right\} \tag{D.1.11}$$

$$= -\frac{\eta_\gamma}{\pi} \left(\Gamma(\gamma+1)\Gamma(-\gamma) \right) \cos(\pi\gamma/2) \int_{-\infty}^{\infty} \frac{\mathrm{d}\omega}{2\pi} |\omega|^\gamma |\tilde{q}(\omega)|^2 \tag{D.1.12}$$

$$= \eta_\gamma \frac{\cos(\pi\gamma/2)}{\sin(\pi\gamma)} \int_{-\infty}^{\infty} \frac{\mathrm{d}\omega}{2\pi} |\omega|^\gamma |\tilde{q}(\omega)|^2 \tag{D.1.13}$$

where we used the fact that $\Gamma(1+z)\Gamma(-z) = -\pi/\sin(\pi z)$, and now further simplify with a double-angle formula:

$$= \frac{\eta_\gamma}{2\sin(\pi\gamma/2)} \int_{-\infty}^{\infty} \frac{\mathrm{d}\omega}{2\pi} |\omega|^\gamma |\tilde{q}(\omega)|^2, \tag{D.1.14}$$

which, despite the illegality of using the γ product identity above for integer arguments, nonetheless works out exactly for odd $\gamma \in \mathbb{Z}$.

Inserting dimensionless parameters as usual, along with a cutoff frequency Λ, we have

$$S'_{\text{eff}}[\theta] = \frac{\hbar}{2} \int_{-\Lambda}^{\Lambda} \frac{\mathrm{d}\omega}{2\pi} K'(\omega) \left|\tilde{\theta}(\omega)\right|^2, \tag{D.1.15}$$

where the Gaussian Kernel

$$K'(\omega) = \frac{\alpha_\gamma |\omega|^\gamma}{2\pi \sin(\pi\gamma/2)}. \tag{D.1.16}$$

If we assume that this temporal self-interaction term is relevant, as for $\gamma = 1$, and that the kinetic term is irrelevant by power counting, then when we calculate the zeroth order correction, we find

$$\langle S_0[\theta_s, \theta_f]\rangle_{0,f} = S_0[\theta_s] \tag{D.1.17}$$

$$= \frac{\hbar}{2}\int_{-\Lambda/b}^{\Lambda/b} \frac{\mathrm{d}\omega}{2\pi} K'(\omega)\left|\tilde{\theta}(\omega)\right|^2, \tag{D.1.18}$$

and rescaling to restore the original bounds of integration, $\pm\Lambda$, we have $\omega' = b\omega$, giving

$$= \frac{\hbar}{2} b^{-1-\gamma}\int_{-\Lambda}^{\Lambda} \frac{\mathrm{d}\omega'}{2\pi} K'(\omega')\left|\tilde{\theta}(\omega'/b)\right|^2, \tag{D.1.19}$$

where now, in contrast to the $\gamma = 1$ case, we will need to rescale the field $\theta(\tau)$ for S_0 to be self-similar. However, this will make our lives incredibly painful when inserting a rescaled field into the cosine potential, and so we instead maintain that $\theta'(\tau') = \theta(\tau)$, and instead renormalize the coupling α_γ,

$$\alpha'_\gamma = b^{1-\gamma}\alpha_\gamma. \tag{D.1.20}$$

Note that this is all predicated on dropping the kinetic (ω^2) term. Now, setting $b = e^\ell$, we recover the zeroth-order RG flow for the dissipative coupling α_γ:

$$\frac{d\alpha_\gamma}{d\ell} = (1-\gamma)\,\alpha_\gamma, \tag{D.1.21}$$

so the dissipation itself is irrelevant for $\gamma > 1$l. Thus, the function $J(\omega)$ must involve a power of $|\omega|^\gamma$ restricted to the interval $[0, 1]$. This result stems from our particular rescaling procedure, where we elected to preserve $\theta(\tau)$ to avoid complications with the cosine terms. We could instead have opted to preserve the form of the Gaussian dissipative term, and dealt with the fallout in the tight-binding and quasi-periodic perturbing potentials.

D.2 Supplementary Material for Quantum Brownian Motion

This section contains additional information and details pertaining to Sec. 7.3 in Ch. 7

D.2.1 RG procedure: integrating out fast modes, cumulants

Recognizing that the kinetic part of the bare action is proportional to ω^2 and therefore *irrelevant by power-counting* in $D = 0 + 1$, we can omit this term and restrict the bounds of integration over ω to $\pm\Lambda$:

$$S_0[\theta(\omega)] = \int_{-\Lambda}^{\Lambda} \frac{d\omega}{2\pi}\frac{\alpha|\omega|}{4\pi}|\theta(\omega)|^2. \tag{D.2.1}$$

We now *define* the slow and fast modes as $\theta(\omega) = \theta_f(\omega)$ for $\Lambda/b \le |\omega| \le \Lambda$ and $\theta(\omega) = \theta_s(\omega)$ for $0 \le |\omega| \le \Lambda/b$, where $b \ge 1$ is the parameter for rescaling of frequencies. We will always take the limit $b \to 1$ in the 'momentum shell' procedure, so that only an infinitesimal number of modes are

integrated out at each step. In general, the effective theory for the low energy modes is given by the action

$$\tilde{S}[\theta_s] = S_0[\theta_s] + \sum_\lambda \langle S_\lambda[\theta]\rangle_{0,f} - \frac{1}{2}\langle\left[\sum_\lambda \left(S_\lambda[\theta] - \langle S_\lambda[\theta]\rangle_{0,f}\right)\right]^2\rangle_{0,f} + \ldots, \tag{D.2.2}$$

where the $0, f$ subscript on the expectation values indicates that the expectation values apply to the fast fields only, and with respect to the bare action S_0. The $\ldots$ represent higher cumulant expressions, although we will find these do not contribute to the RG flow. Note that $S_0[\theta_s]$ is simply the same bare action, Eq. (D.2.1), with the bounds of integration restricted to the "slow modes."

D.2.2 Two point correlation function, $G_{0,f}(\tau, \tau')$

The two-point correlation function G, will be necessary in formulating the second and higher cumulants. Denoting by "f" integration over the range $\Lambda/b \le |\omega| \le \Lambda$, this is

$$G_{0,f}(\tau,\tau') = \langle\theta_f(\tau)\theta_f(\tau')\rangle_{0,f} = \int_f \frac{d\omega}{2\pi}\int_f \frac{d\omega'}{2\pi}\left\langle\theta_f^*(\omega')\theta_f(\omega)e^{i(\omega'\tau'-\omega\tau)}\right\rangle_{0,f} \tag{D.2.3}$$

$$= \int_f \frac{d\omega}{2\pi}\int_{\Lambda/b\le|\omega'|\le\Lambda} \frac{d\omega'}{2\pi}e^{i(\omega'\tau'-\omega\tau)}\left(\frac{2\pi}{\alpha|\omega|}\right)(2\pi\delta(\omega-\omega')) = \frac{2}{\alpha}\int_{\Lambda/b}^{\Lambda}\frac{d\omega}{\omega}\cos(\omega(\tau'-\tau)), \tag{D.2.4}$$

which can be computed to arbitrary precision via Taylor series about $\tau = \tau'$,

$$G_{0,f}(\tau,\tau') = \frac{2}{\alpha}\ln b + \frac{2}{\alpha}\sum_{l=1}^{\infty}\frac{(-1)^l(\tau-\tau')^{2l}}{2l\cdot(2l)!}\left(\Lambda^{2l} - (\Lambda/b)^{2l}\right) \tag{D.2.5}$$

$$= \frac{2}{\alpha}\ln b - \frac{\Lambda^2}{2\alpha}\left(1-b^{-2}\right)(\tau-\tau')^2 + \mathcal{O}((\tau-\tau')^4) \tag{D.2.6}$$

D.2.3 General form of expectation values of exponentials

The harmonic perturbations we consider can be rewritten

$$S_\lambda[\theta] = \sum_\pm \frac{V_\lambda}{2}\int_0^{\beta\hbar} d\tau\ e^{\pm i\lambda\theta(\tau)}, \tag{D.2.7}$$

and so the expectation value of n copies of the perturbative terms (i.e. the sum over non-S_0 terms) is given by

$$\langle S_{\lambda_1}\ldots S_{\lambda_n}\rangle_{0,f} = \prod_{j=1}^n\left(\sum_{\lambda_j}\frac{V_{\lambda_j}}{2}\sum_{\sigma_j=\pm1}\int_0^{\beta\hbar}d\tau_j\right)\langle\prod_{j=1}^n e^{i\sigma_j\lambda_j\theta(\tau_j)}\rangle_{0,f} \tag{D.2.8}$$

$$= \prod_{j=1}^n\left(\sum_{\lambda_j}\frac{V_{\lambda_j}}{2}\sum_{\sigma_j=\pm1}\int_0^{\beta\hbar}d\tau_j\ e^{i\sigma_j\lambda_j\theta_s(\tau_j)}\right)\langle\prod_{j=1}^n e^{i\sigma_j\lambda_j\theta_f(\tau_j)}\rangle_{0,f}, \tag{D.2.9}$$

where the slow terms have been factored out, as they do not participate in the expectation value. This leaves

$$\begin{aligned}\langle\prod_j e^{i\sigma_j\lambda_j\theta_f(\tau_j)}\rangle_{0,f} &= \langle\exp\left\{i\sum_j \sigma_j\lambda_j\theta_f(\tau_j)\right\}\rangle_{0,f} \\ &= \langle\exp\left\{i\sum_j \sigma_j\lambda_j\int_f\frac{d\omega}{2\pi}\theta_f(\omega)\,e^{-i\omega\tau_j}\right\}\rangle_{0,f},\end{aligned} \tag{D.2.10}$$

which is a standard Gaussian functional integral, which evaluates to

$$= \exp\left\{\int_{\Lambda/b\le|\omega|\le\Lambda}\frac{d\omega}{2\pi}\frac{4\pi}{\alpha|\omega|}\sum_{j,k}\left(\frac{i}{2}\sigma_j\lambda_j\right)\left(\frac{i}{2}\sigma_k\lambda_k\right)e^{i\omega(\tau_j-\tau_k)}\right\} \tag{D.2.11}$$

$$= \exp\left\{-\frac{1}{\alpha}\int_{\Lambda/b}^{\Lambda}\frac{d\omega}{\omega}\left(\sum_j\lambda_j^2+2\sum_{j<k}\sigma_j\sigma_k\lambda_j\lambda_k\cos\left(\omega\left(\tau_j-\tau_k\right)\right)\right)\right\} \tag{D.2.12}$$

$$= b^{-\frac{1}{\alpha}\sum_j\lambda_j^2}\exp\left\{-\sum_{j<k}\sigma_j\sigma_k\lambda_j\lambda_k G_{0,f}\left(\tau_j,\tau_k\right)\right\}. \tag{D.2.13}$$

Note that the j,k indices correspond to imaginary time integration variables, τ_j,τ_k. Integrating out the fast modes gives an overall cutoff-dependence (the leading factor of Eq. (D.2.13)), as well as the exponential of the sum of two-point correlation functions evaluated at pairs of time coordinates. The structure of the cumulants will subtract off terms with fewer time coordinates from the quantities above. In general, these results will be intractable, but noting that the RG procedure should preserve temporal locality, we will carefully invoke gradient expansions about the temporal coordinates being equal to a single time τ.

D.2.4 Fixed part of the action: rescaling

The cumulants are calculated with respect to the "fixed" part of the action, Eq. (D.2.2), which dictates how we ought to rescale our coordinates and fields. We choose this to be the term generated by integrating out the bath, and require it to be self-similar ("fixed") under the RG. Thus, as we integrate out the fast modes to obtain a low energy theory, we rescale the resulting effective action so that this term remains the same as we run the RG. We have

$$\tilde{S}_0[\theta] = \int_{-\Lambda/b}^{\Lambda/b}\frac{d\omega}{2\pi}\frac{\alpha|\omega|}{4\pi}\left|\theta_s(\omega)\right|^2, \tag{D.2.14}$$

and we can restore the original bounds of integration by introducing a rescaled frequency $\tilde{\omega}=b\omega$, and we then have

$$\tilde{S}_0[\theta] = \int_{-\Lambda}^{\Lambda}\frac{d\tilde{\omega}}{2\pi b}\frac{\alpha|\tilde{\omega}|}{4\pi b}\left|\theta_s(\tilde{\omega}/b)\right|^2, \tag{D.2.15}$$

which works out just fine if we have $\tilde{\theta}(\tilde{\omega}) = b^{-1}\theta_s(\omega)$, in which case

$$\tilde{S}_0[\theta] = \int_{-\Lambda}^{\Lambda}\frac{d\tilde{\omega}}{2\pi}\frac{\alpha|\tilde{\omega}|}{4\pi}\left|\tilde{\theta}(\tilde{\omega})\right|^2, \tag{D.2.16}$$

which is, indeed, self-similar. These new frequencies also suggest new temporal coordinates, $\tilde{\tau} = b^{-1}\tau$, and the scaling of the frequency-dependent field implies that the time-dependent version (i.e. Fourier transform) obeys $\tilde{\theta}(\tilde{\tau}) = \theta_s(\tau)$, which is also quite nifty for the sake of the cosine terms.

D.2.5 First cumulant: $\langle \delta S_\lambda[\theta] \rangle_{0,f}$

The first order ($\mathcal{O}(V)$)contribution to the low-energy action is given straightforwardly from Eq. (D.2.8) and Eq. (D.2.13) as

$$\tilde{S}^{(1)} \equiv \langle \sum_\lambda S_\lambda \rangle = \sum_\lambda \frac{V_\lambda}{2} \sum_\pm \int_0^{\beta\hbar} d\tau \; e^{\pm i\lambda\theta_s(\tau)} \langle e^{i\pm\lambda\theta_f(\tau)} \rangle_{0,f} \tag{D.2.17}$$

$$= \sum_\lambda \frac{V_\lambda}{2} \sum_\pm \int_0^{\beta\hbar} d\tau \; e^{\pm i\lambda\theta_s(\tau)} \left[b^{-\frac{\lambda^2}{\alpha}} \right] = \sum_\lambda b^{-\frac{\lambda^2}{\alpha}} V_\lambda \int_0^{\beta\hbar} d\tau \cos\left[\lambda\theta_s(\tau)\right], \tag{D.2.18}$$

which we immediately recognize is self-similar, and we implement the rescaling of coordinates and fields set by the fixed part of the action S_0 to recover

$$\sum_\lambda b^{-\frac{\lambda^2}{\alpha}} V_\lambda \int_0^{\beta\hbar/b} (b \; d\tilde{\tau}) \cos\left[\lambda\tilde{\theta}(\tilde{\tau})\right], \tag{D.2.19}$$

which suggests the renormalized couplings $\tilde{V}_\lambda = b^{1-\frac{\lambda^2}{\alpha}} V_\lambda$, and a rescaled temperature, $\tilde{\beta}\hbar = \beta\hbar/b$, and we now have full self-similarity to first order. Note that the rescaling of temperature will not affect our results.

These results agree with a previous study [271], however in our case, the presence of a second harmonic potential requires us to examine the second cumulant.

D.2.6 Second cumulant, $-\frac{1}{2}\left\langle \left(\sum_\lambda S_\lambda - \langle S_\lambda \rangle\right)^2 \right\rangle_{0,f}$

Here we consider the second cumulant,

$$\tilde{S}^{(2)} \equiv -\frac{1}{2} \sum_{\lambda,\lambda'} \left(\langle S_\lambda S_{\lambda'} \rangle - \langle S_\lambda \rangle \langle S_{\lambda'} \rangle \right), \tag{D.2.20}$$

which we know how to calculate from Eq. (D.2.13),

$$\begin{aligned}
\tilde{S}^{(2)} = &- \sum_{\lambda,\lambda'} \frac{V_\lambda V_{\lambda'}}{8} \sum_{\sigma,\sigma'=\pm1} \int_0^{\beta\hbar} d\tau \int_0^{\beta\hbar} d\tau' e^{i\sigma\lambda\theta_s(\tau)} e^{i\sigma'\lambda'\theta_s(\tau')} \\
&\times \left\{ \langle e^{i\sigma\lambda\theta_f(\tau)} e^{i\sigma'\lambda'\theta_f(\tau')} \rangle_{0,f} - \langle e^{i\sigma\lambda\theta_f(\tau)} \rangle_{0,f} \langle e^{i\sigma'\lambda'\theta_f(\tau')} \rangle_{0,f} \right\} \qquad \text{(D.2.21)} \\
= &- \sum_{\lambda,\lambda'} \frac{V_\lambda V_{\lambda'}}{8} \sum_{\sigma,\sigma'=\pm1} \int_0^{\beta\hbar} d\tau \int_0^{\beta\hbar} d\tau' e^{i\sigma\lambda\theta_s(\tau)} e^{i\sigma'\lambda'\theta_s(\tau')} b^{-\frac{\lambda^2}{\alpha}} b^{-\frac{\lambda'^2}{\alpha}} \left\{ e^{-\sigma\sigma'\lambda\lambda' G_{0,f}(\tau,\tau')} - 1 \right\} \qquad \text{(D.2.22)} \\
= &- \frac{1}{4} \sum_{\lambda,\lambda',\pm} b^{-\frac{\lambda^2}{\alpha}} V_\lambda b^{-\frac{\lambda'^2}{\alpha}} V_{\lambda'} \int_0^{\beta\hbar} d\tau \int_0^{\beta\hbar} d\tau' \cos\left[\lambda\theta_s(\tau) \pm \lambda'\theta_s(\tau')\right] \left\{ e^{\mp\lambda\lambda' G_{0,f}(\tau,\tau')} - 1 \right\} . \qquad \text{(D.2.23)}
\end{aligned}$$

We then relate this the terms allowed at bare level using a 'gradient expansion' about $\tau' = \tau$, motivated by the fact that the coarse-graining procedure should preserve temporal locality. The zeroth order term in the gradient expansion tells us that the second order cumulant's contribution to the RG is to generate new terms by adding and subtracting the existing wave numbers. When only a single harmonic is present at bare level (e.g., the case studied in Ref. **?**, or a typical boundary sine-Gordon theory), the only possibilities are to generate integer multiples of the original harmonic, which are less relevant at first order, and a correction to the kinetic term, which goes like ω^2 and is thus already irrelevant by power-counting. When an additional harmonic that is a nonintegral multiple of the first is also included, the second order processes can generate new harmonics smaller and more relevant than those present at bare level. When the second harmonic is an irrational multiple of the first, the generated harmonics can be arbitrarily small.

D.2.7 Two-point function contributions of higher cumulants

As mentioned in the previous section, higher cumulants will contain products of the form

$$b^{-\frac{1}{\alpha}\sum_j \lambda_j^2} \exp\left\{-\sum_{j<k} \sigma_j \sigma_k \lambda_j \lambda_k G_{0,f}\left(\tau_j, \tau_k\right)\right\} \equiv b^{-\frac{1}{\alpha}\sum_j \lambda_j^2} \prod_{j<k} z_{j,k},$$

where it will prove useful to define this quantity $z_{j,k}$, which depends on $\tau_{j,k}$ and ℓ. In general, these terms will be multiplied by factors $\exp\left(i\sigma_j \lambda_j \theta_s\left(\tau_j\right)\right)$ and some coefficients, and integrated over all the τ_j. The rescaling procedure will introduce factors of $b = e^\ell$ there as well. However, we point out a few things first.

For the second, third, and fourth cumulants, the factors that come from the two point functions will then have the respective forms

$$\frac{1}{2}\left\{1 - z_{1,2}\right\} \tag{D.2.24a}$$

$$\frac{1}{6}\left\{2 + z_{1,2}z_{1,3}z_{2,3} - z_{1,2} - z_{1,3} - z_{2,3}\right\} \tag{D.2.24b}$$

$$\begin{aligned}\frac{1}{24}\Big\{&6 - z_{1,2}z_{1,3}z_{1,4}z_{2,3}z_{2,4}z_{3,4} + z_{1,2}z_{1,3}z_{2,3} + z_{1,2}z_{1,4}z_{2,4} + z_{1,3}z_{1,4}z_{3,4} + z_{2,3}z_{2,4}z_{3,4} \\ &+ z_{1,2}z_{3,4} + z_{1,3}z_{2,4} + z_{1,4}z_{2,3} - 2\left(z_{1,2} + z_{1,3} + z_{1,4} + z_{2,3} + z_{2,4} + z_{3,4}\right)\Big\}.\end{aligned} \tag{D.2.24c}$$

These have the notable property that at $\ell = 0$, $z_{i,j} = 1$, and the contents of the curly braces in each case sum to zero. Therefore, in taking the derivative of everything with respect to ℓ for the RG flow equation, only the derivatives of these cumulants, given by Eq. (D.2.24), matter (in implementing the product rule), and we take $\ell = 0$ for all other terms.

What is especially interesting is that for the third and fourth cumulants, the derivative of the factors themselves with respect to ℓ, evaluated at $\ell = 0$, are precisely zero. Based on the way the various moments factorize for cumulants beyond the second, it appears that this will hold for all higher cumulants, and thus, to lowest order in $\Delta\ell$, there is no contribution to the RG flow equations beyond second order in the couplings V_λ.

D.2.8 Full RG flow equation

The full RG flow equation, to lowest order in ℓ, is given by

$$\frac{d}{d\ell}V_\lambda = \left(1 - \frac{\lambda^2}{\alpha}\right)V_\lambda + \sum_{\lambda',\lambda''} C^\lambda_{\lambda',\lambda''} V_{\lambda'} V_{\lambda''} + \mathcal{O}\left(\ell\right), \tag{D.2.25}$$

where $C^{\lambda}_{\lambda',\lambda''} = \frac{\lambda'\lambda''}{2\alpha}\left(\delta_{\lambda,\lambda'+\lambda''} - \delta_{\lambda,|\lambda'+\lambda''|}\right)$, and many terms will be counted twice by the sum.

The first order contribution to this equation, which comes from the first cumulant, is easily obtained by taking a derivative. The second order contribution follows from the standard procedure used for sine Gordon or Kosterlitz-Thouless RG: we perform a gradient expansion of Eq. (D.2.23) about $\tau' = \tau$, keeping only the lowest order term, and factor out a constant that spills over from dummy integration over τ' (i.e. in Eq. (D.2.25), all the Vs have been divided by this factor). In the sine Gordon case, there is only one λ, and the $\lambda + \lambda$ process generates a less relevant term, which we ignore, and the $\lambda - \lambda$ term generates a correction to the kinetic energy. In our case, we ignore the correction to the kinetic energy, as this term is already irrelevant by power coupling. Additionally, since we have two frequencies at the start of the RG, the second order processes also generate new harmonics by superposition. Hidden from Eq. (D.2.25) are terms that enter at higher order in ℓ, including $\mathcal{O}(V^3)$ terms, and higher order contributions from the gradient expansion.

D.2.9 Approximate solution of the RG flow equations

In general, we are interested in understanding the flow of couplings when both of the bare frequencies—which we include by hand—are irrelevant at first order, but some linear combination of the two is *relevant* for a given value of dissipation α. We will always take the smaller of the bare frequencies to be unity, by rescaling our fields, and work with the two frequencies $\lambda = 1$, with bare coupling u_0, and $\lambda = \gamma$, with bare coupling ϵu_0.

For γ rational, it is possible to simulate the RG flow equations numerically using iterative updates, truncating at some arbitrarily large frequency, which will be highly irrelevant. However, we wish to understand what happens when γ is *irrational*, in which case there will be no means by which to truncate the allowed frequencies from below. Here we will describe a means of approximately integrating the RG flow equations in a manner that is physically sensible, in which we take $\gamma = m/n$ with $m > n$ and $m, n \in \mathbb{Z}$, and importantly, $n^{-2} < \alpha < 1$. We will take

$$\frac{dV_1}{d\ell} = \left(1 - \frac{1}{\alpha}\right) V_1 + \dots \quad , \quad \frac{dV_\gamma}{d\ell} = \left(1 - \frac{m^2}{n^2\,\alpha}\right) V_\gamma + \dots, \tag{D.2.26}$$

and since these couplings are guaranteed to be irrelevant, we will ignore the higher-order corrections $\dots$ to their functional form, and integrate them directly to obtain

$$V_1(\ell) = e^{\ell\left(1-\frac{1}{\alpha}\right)} u_0 \quad , \quad V_\gamma = e^{\ell\left(1-\frac{m^2}{n^2\,\alpha}\right)} \epsilon u_0, \tag{D.2.27}$$

and now for simplicity, we will take $m = n + 1$ so that the relevant term $\lambda = 1/n$ is formed in a single iteration of the RG, seen from implementation of Eq. (D.2.25) :

$$\begin{aligned} \frac{dV_{1/n}}{d\ell} &= \left(1 - \frac{1}{n^2\,\alpha}\right) V_{1/n} - \frac{m}{n\alpha} V_1 V_\gamma \\ &= \left(1 - \frac{1}{n^2\,\alpha}\right) V_{1/n} - \frac{m\,\epsilon u_0^2}{n\alpha} e^{\ell\left(2-\frac{n^2+m^2}{n^2\,\alpha}\right)}, \end{aligned} \tag{D.2.28}$$

and a simple Ansatz for the form of $V_{1/n}$ yields an easy solution:

$$V_{1/n} = C(\ell)\, e^{\ell\left(1-\frac{1}{n^2\,\alpha}\right)} \Rightarrow V_{1/n} = \frac{m\,n\,\epsilon u_0^2}{n^2(\alpha-1) + 1 - m^2}\left(e^{\ell\left(\frac{1}{n^2\,\alpha}-1\right)} - e^{\ell\left(2-\frac{1}{\alpha}\left(1+\frac{m^2}{n^2}\right)\right)}\right). \tag{D.2.29}$$

We now wish to calculate ℓ^*, the RG time for which $V_{1/n}$, here assumed to be the *only* relevant term, grows to value unity. Since we will generally be interested in the limit where α is small, we will drop the latter term in Eq. (D.2.29), and recover the expression

$$\ell^* = \left(1 - \frac{1}{n^2\,\alpha}\right)^{-1} \left(\ln\left[\epsilon u_0^2\right] + \ln\left[\frac{m\,n}{n^2\,(\alpha-1)+1-m^2}\right]\right), \tag{D.2.30}$$

plus corrections due to the term we dropped. In general, we will be interested in the scenario where the second harmonic V_γ is initially quite weak, while the main harmonic is order one (or vice versa), in which case the logarithm of ϵ will dominate, and we have

$$\ell^* \to \left(\frac{1}{n^2\,\alpha} - 1\right)^{-1} \ln\left[\epsilon\right] = \frac{\alpha}{\alpha_c - \alpha} \ln\left[\epsilon\right], \tag{D.2.31}$$

where α_c for this rational case is n^{-2}, giving a straightforward scaling form for $b^* = e^{\ell^*}$ as a power of ϵ.

In general, more than a single iteration of the second order RG processes will be needed to generate a relevant coupling. However, we note from the form of Eq. (D.2.31) that the leading coefficient depends only on the relevant term itself, and not on any of the intermediate steps. Although this may add a somewhat complicated structure, following the procedure above will produce, at every step, additional powers of ϵ and u_0, factors resulting from integration as in Eq. (D.2.29), all of which multiply a sum of terms of the form $e^{A\ell}$. All of the complications arising from integration factors can be separated into a sub-leading contribution to Eq. (D.2.31), and the only way the number of steps required to generate the relevant term shows up is in the power of ϵ (and u_0, if we decided to retain it).

For an arbitrary second wave number γ, it would be quite cumbersome to determine the optimal sequence of second order processes to generate a given, relevant term. However, for the particular choice of $\gamma = \varphi = \frac{1}{2}\left(1+\sqrt{5}\right)$, this is quite simple. For a given value of α, the relevant term generated in the fewest number of RG iterations will be a Fibonacci wave number, the n^{th} of which is given by $\lambda_n \equiv (-1)^n \left(F_{n+1} - \varphi F_n\right) = \varphi^{-n}$. In the first step, the term $\lambda_1 = \varphi^{-1} = \varphi - 1$ is generated, and in general, λ_n is formed in n steps. Correspondingly, after n steps, there are F_n factors of ϵ, where F_n is the n^{th} Fibonacci number, and F_{n+2} factors of u_0. Thus, supposing n^* corresponds to the first Fibonacci potential with a coupling that grows to $O(1)$, then the RG time required to do so is given by

$$\ell^* \to \frac{\alpha\,F_{n^*}}{\varphi^{-2n^*} - \alpha} \ln\left[\epsilon\right], \tag{D.2.32}$$

plus sub-leading corrections. In the limit of large n^*, the parenthetical prefactor goes quickly to $-F_{n^*}$. For scenarios in which the first relevant λ_n is just barely relevant, it may be the case that λ_{n+1} or a subsequent Fibonacci potential grows to $O(1)$ faster than λ_n, despite being formed later in the RG, and thus we must always choose the minimal value of ℓ^* over the various relevant λs for a given value of α.

D.2.10 Localization length

While the RG time ℓ^* provides a useful cross-over scale for when the particle begins to "feel" localized due to the presence of a growing, relevant potential, we also note that it can take a substantial amount of RG time for this localization to take hold. Although the RG flow equations clearly show that, for any nonzero value of α, there will exist some potential generated by second

order processes that is relevant, it is also clear that as α is decreased, it will take longer and longer for this localization to take effect, and additionally, the potential well to which the particle is localized will be correspondingly larger. To give this physical meaning, we will extract a localization length from the crossover time, ℓ^*.

Although it is possible to associate a genuine time scale τ to the RG time ℓ^*, and then calculate how far the particle travels on such a time scale, the same result is more expediently obtained using the following definition:

$$\xi = \langle q^2(\tau)\rangle^{1/2} = \frac{q_0}{2\pi}\sqrt{\langle\theta^2(\tau)\rangle}, \tag{D.2.33}$$

and we perform the average by integrating out only the modes $\Lambda/b^* \leq \omega \leq \Lambda$, i.e. those corresponding to our RG time ℓ^*. Additionally, we make the assumption that, until the time ℓ^* is reached, the effect of the cosine terms may be ignored in evaluating the two-point function, and we have

$$\langle\theta^2(\tau)\rangle = 2\int_{\Lambda/b^*}^{\Lambda}\frac{d\omega}{2\pi}\left[\frac{\alpha\omega}{2\pi}+\ldots\right]^{-1} = \frac{2}{\alpha}\ln(\omega)\Big|_{\Lambda/b^*}^{\Lambda} = \frac{2}{\alpha}\ln b^* = \frac{2\ell^*}{\alpha}, \tag{D.2.34}$$

and from this we conclude that

$$\xi = \frac{q_0}{2\pi}\sqrt{\frac{2\ell^*}{\alpha}}. \tag{D.2.35}$$

We can compare to a previous prediction that the localization length diverges as $(\alpha-1)^{-1/2}$ for the case of integer harmonics by using the result for Eq. (D.2.31) for $n = 1$, which indeed gives $\xi \sim (\alpha-1)^{-1/2}$.

D.3 Supplementary Material for Dissipative Quantum Fluids

D.3.1 Derivation of correlation function

This section details the calculation of the correlation function $G(x,\tau)$ for the Luttinger liquid with dissipation, for any temperature. Starting from Eq. (7.4.13), we take $L \to \infty$ by necessity, and restricting to the *Ohmic* case $J(k,\omega) = \eta|\omega|$, we have

$$G(x,\tau) = \frac{iu}{4\pi}\int_{-\infty}^{\infty} dk \oint dz\, \frac{h_B(z)\cos(kx - i\tau z)}{z^2 - u^2k^2 - uK\eta|z|}, \tag{D.3.1}$$

where $z = i\omega$ as usual, and using the shorthand $\tilde{\eta} \equiv K\eta/2$ Eq. (7.4.17), the denominator of Eq. (D.3.1) has zeros at $z_\pm^* = \pm uZ_k$, with

$$Z_k = \tilde{\eta} + \sqrt{\tilde{\eta}^2 + k^2}\ , \tag{D.3.2}$$

which follows straightforwardly from setting $z = Re^{i\psi}$ and solving $z^2 = u^2k^2 + uK\eta|z|$, where the righthand side of that expression is real, constraining $\psi = n\pi/2$.

Contour integration over z returns the residues from poles of h_B, reproducing the sum over discrete Matsubara frequencies, as well as residues corresponding to the poles at $z_\pm^*$. This quantity vanishes when taken along the great circle $|z| \to \infty$, and thus the Matsubara sum is equal to minus

the contribution from the $z_\pm^*$ poles, as for the "closed" Luttinger liquid. However, in the "open" case, the poles of the denominator of Eq. (D.3.1) do not simply give Z_k^{-1}, as was the case for $\eta = 0$ whence $Z_k = k$. The result is

$$G(x,\tau) = \int_0^\infty dk \, \frac{\cos(kx)}{\sqrt{\tilde{\eta}^2 + k^2}} \times \left\{ n_B(uZ_k)\cosh(u\tau Z_k) + \frac{1}{2} e^{-u|\tau|Z_k} \right\} \tag{D.3.3}$$

where Z_k is strictly positive, and reduces to k as $\eta \to 0$. We can massage the term in braces, noting that $\cosh(u\tau Z_k) = \cosh(u|\tau| Z_k) = \frac{1}{2}\sum_\pm e^{\pm u|\tau|Z_k}$, and that

$$n_B(uZ_k) = \frac{1}{e^{\beta\hbar u Z_k} - 1} = \sum_{m=1}^\infty e^{-m\beta\hbar u Z_k} \tag{D.3.4}$$

meaning all of the terms in curly braces in Eq. (D.3.3) can be written in the form $e^{-A\cdot uZ_k}$. Explicitly, the braced term is

$$\frac{1}{2}\left\{ e^{-u|\tau|Z_k} + \sum_\pm \sum_{m=1}^\infty e^{-u(m\beta\hbar\pm|\tau|)Z_k} \right\}, \tag{D.3.5}$$

which simplifies the integration procedure substantially, as all of these terms have the same general form. For $T = 0$, i.e. $\beta \to \infty$, the latter term is simply zero. We rewrite Eq. (D.3.3) in the generic form

$$G(x,\tau) = \frac{1}{2}\sum_\sigma \int_0^\infty dk \, \frac{\cos(kx)}{\sqrt{\tilde{\eta}^2 + k^2}} e^{-A_\sigma^{(\tau)} Z_k}, \tag{D.3.6}$$

where the τ-dependent coefficients A_σ reproduce the terms in Eq. (D.3.5), indexed by σ.

We next invoke hyperbolic substitution, $k \equiv \tilde{\eta}\sinh(\lambda)$, and therefore $dk = \tilde{\eta}\cosh(\lambda)\, d\lambda$ and $Z_k \to \tilde{\eta}(1+\cosh(\lambda))$, and the integral in Eq. (D.3.6) becomes

$$\int_0^\infty d\lambda \, \cos(\tilde{\eta} x \sinh(\lambda)) \, e^{-\tilde{\eta} A_\sigma^{(\tau)}(1+\cosh(\lambda))}, \tag{D.3.7}$$

and we then invoke a Taylor expansion for the cosine, i.e.,

$$G(x,\tau) = \frac{1}{2}\sum_\sigma e^{-\tilde{\eta}A_\sigma^{(\tau)}} \sum_{n=0}^\infty \frac{(-1)^n (\tilde{\eta}x)^{2n}}{(2n)!} \times \int_0^\infty d\lambda \, \sinh^{2n}(\lambda) \, e^{-\tilde{\eta}A_\sigma^{(\tau)}\cosh(\lambda)}. \tag{D.3.8}$$

At this point, we make use of a particular integral representation of the modified Bessel function of the second kind,

$$K_n(z) = \frac{\pi^{1/2}(z/2)^n}{\Gamma\left(n+\frac{1}{2}\right)} \int_0^\infty dt \, \left[\sinh(t)\right]^{2n} e^{-z\cosh(t)}, \tag{D.3.9}$$

or written more usefully,

$$\frac{(2n)!}{(2z)^n n!} K_n(z) = \int_0^\infty dt \, \left[\sinh(t)\right]^{2n} e^{-z\cosh(t)}, \tag{D.3.10}$$

which we can use to express Eq. (D.3.8) exactly as

$$G(x,\tau) = \sum_{\sigma}\sum_{n=0}^{\infty} \frac{e^{-\tilde{\eta}A_{\sigma}^{(\tau)}}}{2\,n!}\left(\frac{-\tilde{\eta}\,x^2}{2\,A_{\sigma}^{(\tau)}}\right)^n K_n\left[\tilde{\eta}\,A_{\sigma}^{(\tau)}\right], \tag{D.3.11}$$

where $A_{\sigma}^{(\tau)}$ are summed over $A(\tau) = \alpha + u|\tau|$ and $A_{m,\pm}(\tau) = u\,(m\beta\hbar \pm |\tau|)$ for positive integers $m \geq 1$, and we have reinstated α as it would appear had we included the usual convergence factor $e^{-i\omega\alpha/u}$ starting from Eq. (D.3.1). Strictly, this convergence factor ought to be included, as is standard practice even in the dissipationless limit. Unlike the $\eta = 0$ case, for $\eta > 0$ all integrals converge, giving exact results, except at $\tau = 0$, necessitating the convergence factor in the ω integral. Finally, for $T = 0$, only the former, β-independent term appears in Eq. (D.3.11).

D.3.2 Evaluating $G(0,0)$

The evaluation of the more generic correlation function $F(x,\tau)$ requires knowledge of $G(0,0)$, which requires the α-dependent versions of $A_{\sigma}^{(\tau)}$ in the previous section. We will take $\alpha \to 0$ wherever safe. Regarding Eq. (D.3.11), note that the limit $x \to 0$ can be taken safely, and only the $n = 0$ term remains:

$$G(0,0) = \sum_{\sigma} \frac{e^{-\tilde{\eta}A_{\sigma}^{(0)}}}{2} K_0\left[\tilde{\eta}\,A_{\sigma}^{(0)}\right], \tag{D.3.12}$$

where now the sum over σ of the terms $A_{\sigma}^{(0)}$ corresponds to the terms $A = \alpha$ and $A_{m,\pm} = \alpha + um\beta\hbar \to um\beta\hbar$, i.e.

$$G(0,0) = \frac{1}{2}K_0[\tilde{\eta}\alpha] + \sum_{m=1}^{\infty} e^{-\tilde{\eta}um\beta\hbar} K_0(\tilde{\eta}um\beta\hbar), \tag{D.3.13}$$

where only the first term survives at $T = 0$, and we have already taken the $\alpha \to 0$ limit where safe. Referring to the exact series expansion for $K_0(z)$, we note that the limit $z = \tilde{\eta}\alpha \to 0$ can be taken safely in the majority of terms, resulting in

$$\lim_{z\to 0} K_0(z) = -\gamma - \lim_{z\to 0} \ln\left(\frac{z}{2}\right), \tag{D.3.14}$$

where $\gamma \approx 0.577216$ is the Euler-Mascheroni constant.

D.3.3 Matching the closed case for $\eta \to 0$

Also note that inserting the form of the expansion of K_n for arbitrary index n about zero argument into Eq. (D.3.11), and taking the limit $\tilde{\eta} \propto \eta \to 0$ of $\tilde{\eta}^n K_n$ recovers exactly the results for the closed case [308]. We recover from Eq. (D.3.11) in the limit $\tilde{\eta} \to 0$

$$\lim_{\tilde{\eta}\to 0} G(x,\tau) = -\frac{1}{2}\sum_{\sigma}\left\{\gamma + \ln\left(\frac{\tilde{\eta}}{2}\right) + \frac{1}{2}\ln\left(A_{\sigma}^2(\tau) + x^2\right)\right\}, \tag{D.3.15}$$

with $A_{\sigma}^{(\tau)}$ defined as before.

For $T = 0$, we have only one allowed configuration σ that corresponds to a nonvanishing term, with $A_\sigma^{(\tau)} \to \alpha + u\,|\tau|$. Thus, in this limit Eq. (D.3.15) becomes

$$\lim_{\tilde{\eta},T\to 0} G(x,\tau) = -\frac{1}{2}\lim_{\tilde{\eta}\to 0}\ln\left(\frac{\tilde{\eta}}{2}\right) - \frac{\gamma}{2} - \frac{1}{4}\ln\left[(\alpha + u\,|\tau|)^2 + x^2\right] , \tag{D.3.16}$$

which resembles the result i for the closed case [308], though matching divergent constants is murky at best. However, we note that

$$\lim_{\tilde{\eta},T\to 0} G(0,0) = -\frac{\gamma}{2} - \frac{1}{2}\lim_{\tilde{\eta}\to 0}\ln\left(\frac{\tilde{\eta}\,\alpha}{2}\right) , \tag{D.3.17}$$

and using now the formula for F Eq. (7.4.15) in combination with Eq. (D.3.15), we have for $T = 0$:

$$\lim_{\tilde{\eta},T\to 0} F(x,\tau) = \frac{1}{2}\ln\left[\frac{u^2\,|\tau|^2 + x^2}{\alpha^2}\right] , \tag{D.3.18}$$

in perfect agreement with the standard result [308]. At finite temperature, this procedure is more cumbersome, and we content ourselves with the benchmark given by Eq. (D.3.18) as ample validation of our results for $\eta \neq 0$.

D.3.4 Expansion for small η

Moving slightly beyond $\eta = 0$ may provide some insight. We restrict here to $T = 0$; while one can certainly repeat this procedure at finite temperature, it affords little insight beyond the exact results. Looking at the definition of $G(x,\tau)$, i.e. Eq. (7.4.16),

$$G(x,\tau) = \sum_{n=0}^{\infty} \frac{e^{-\tilde{\eta}\,u|\tau|}}{2\,n!}\left(\frac{-\tilde{\eta}\,x^2}{2\,u\,|\tau|}\right)^n K_n\left[\tilde{\eta}\,u\,|\tau|\right],$$

we can rewrite this as

$$\frac{e^{-z}}{2}\sum_{n=0}^{\infty}\frac{(-1)^n}{2^n\,n!}\left(\frac{x}{u\,\tau}\right)^{2n}\left[z^n\,K_n(z)\right], \tag{D.3.19}$$

where $z = \tilde{\eta}\,u\,|\tau|$ is a useful shorthand, as we will take the $z \to 0$ limit (recall $\tilde{\eta} \propto \eta$, per Eq. (7.4.17)). Note that the limit $\eta \to 0$ is unimportant to the evaluation of $G(0,0)$ in Appendix D.3.2.

Regarding Eq. (D.3.19), we now evaluate the summand to order z^2 as $z \to 0$ (ignoring for now the term e^{-z}), noting that the Modified Bessel function $K_n(x)$ has a well known Maclaurin series in z. We have at zeroth order the terms recovered Appendix D.3.3,

$$\frac{e^{-\tilde{\eta}u|\tau|}}{2}\left(-\gamma - \ln\left[\frac{\tilde{\eta}}{2}\right] - \frac{1}{2}\ln\left[x^2 + u^2\tau^2\right]\right) , \tag{D.3.20}$$

the latter obtaining from contributions for terms at all n. The lowest terms arising from the summand at nontrivial order are proportional to $\tilde{\eta}^2$, i.e.

$$\frac{\tilde{\eta}^2}{8}\left(x^2 + u^2\tau^2\right)\left\{1 - \gamma + \ln 2 - \frac{1}{2}\ln\left[x^2 + u^2\tau^2\right]\right\} , \tag{D.3.21}$$

where we have dropped the overall exponential term above, and γ is the Euler-Mascheroni constant in both Eq. (D.3.20) and Eq. (D.3.21). Notably, at low order, only the overall factor of $e^{-\tilde{\eta}u|\tau|}$ spoils the conformal invariance present without dissipation (the invariance is not present in each term in the summand of Eq. (D.3.19) individually, but is restored by the various contributions from different terms at a given order in η).

We have then for the correlation function $F(x,\tau)$ the following, expanding now the exponential decay term in η as well:

$$\begin{aligned} F(x,\tau) &= \frac{1}{2}\ln\left[\frac{x^2+u^2\tau^2}{\alpha^2}\right] \\ &+\left(\frac{\tilde{\eta}^2u^2\tau^2}{2}-\tilde{\eta}u|\tau|\right)\left(\gamma+\ln\left[\frac{\tilde{\eta}}{2}\right]+\frac{1}{2}\ln\left[x^2+u^2\tau^2\right]\right) \\ &+\frac{\tilde{\eta}^2}{4}\left(x^2+u^2\tau^2\right)\left(\gamma-1-\ln 2+\frac{1}{2}\ln\left[x^2+u^2\tau^2\right]\right)\ , \end{aligned} \tag{D.3.22}$$

where the term on the righthand side of the first line corresponds to $\eta = 0$, and we note that $\eta^z \ln\eta \to 0$ as $\eta \to 0$ for positive z, which eliminates the $\ln\tilde{\eta}$ term in the second line.

Bibliography

[1] H. Poincaré, "Sur le problème des trois corps et les équations de la dynamique," *Acta Math.* **13** (1890) 1–270.

[2] L. Cugliandolo, "Dynamics and disorder in quantum many body systems far from equilibrium," in *Dynamics of Glassy Systems*. August, 2019.

[3] D. Arovas, *Lecture Notes on Thermodynamics and Statistical Mechanics*. Online Notes, 2013. https://courses.physics.ucsd.edu/2010/Spring/physics210a/lectures.html.

[4] S. Sachdev and J. Ye, "Gapless spin-fluid ground state in a random quantum heisenberg magnet," *Phys. Rev. Lett.* **70** (May, 1993) 3339–3342. https://link.aps.org/doi/10.1103/PhysRevLett.70.3339.

[5] S. Sachdev, "Bekenstein-hawking entropy and strange metals," *Phys. Rev. X* **5** (Nov, 2015) 041025. https://link.aps.org/doi/10.1103/PhysRevX.5.041025.

[6] A. Kitaev, "A simple model of quantum holography," in *KITP Program: Entanglement in Strongly-Correlated Quantum Matter*.

[7] J. Maldacena and D. Stanford, "Remarks on the sachdev-ye-kitaev model," *Phys. Rev. D* **94** (Nov, 2016) 106002. https://link.aps.org/doi/10.1103/PhysRevD.94.106002.

[8] Y. Gu, X.-L. Qi, and D. Stanford, "Local criticality, diffusion and chaos in generalized sachdev-ye-kitaev models," *Journal of High Energy Physics* **2017** no. 5, (May, 2017) . http://dx.doi.org/10.1007/JHEP05(2017)125.

[9] D. Huse, "Dynamics and disorder in quantum many body systems far from equilibrium," in *Quantum Thermalization and Many-Body Localization*. August, 2019.

[10] P. W. Anderson, "Absence of diffusion in certain random lattices," *Phys. Rev.* **109** (Mar, 1958) 1492–1505. http://link.aps.org/doi/10.1103/PhysRev.109.1492.

[11] D. Basko, I. Aleiner, and B. Altshuler, "Metal-insulator transition in a weakly interacting many-electron system with localized single-particle states," *Annals of Physics* **321** no. 5, (2006) 1126 – 1205. http://www.sciencedirect.com/science/article/pii/S0003491605002630.

[12] R. Nandkishore and D. A. Huse, "Many-body localization and thermalization in quantum statistical mechanics," *Annual Reviews of Condensed Matter Physics* **6** no. 0, (2015) 15 – 38. http://dx.doi.org/10.1146/annurev-conmatphys-031214-014726.

[13] D. A. Huse, R. Nandkishore, and V. Oganesyan, "Phenomenology of fully many-body-localized systems," *Phys. Rev. B* **90** (Nov, 2014) 174202. http://link.aps.org/doi/10.1103/PhysRevB.90.174202.

[14] A. Pal and D. A. Huse, "Many-body localization phase transition," *Phys. Rev. B* **82** (Nov, 2010) 174411. http://link.aps.org/doi/10.1103/PhysRevB.82.174411.

[15] D. A. Huse, R. Nandkishore, V. Oganesyan, A. Pal, and S. L. Sondhi, "Localization-protected quantum order," *Phys. Rev. B* **88** (Jul, 2013) 014206. http://link.aps.org/doi/10.1103/PhysRevB.88.014206.

[16] P. Bocchieri and A. Loinger, "Quantum recurrence theorem," *Phys. Rev.* **107** (Jul, 1957) 337–338. http://link.aps.org/doi/10.1103/PhysRev.107.337.

[17] J. M. Deutsch, "Quantum statistical mechanics in a closed system," *Phys. Rev. A* **43** (Feb, 1991) 2046–2049. http://link.aps.org/doi/10.1103/PhysRevA.43.2046.

[18] M. Srednicki, "Chaos and quantum thermalization," *Phys. Rev. E* **50** (Aug, 1994) 888–901. http://link.aps.org/doi/10.1103/PhysRevE.50.888.

[19] M. Rigol, V. Dunjko, and M. Olshanii, "Thermalization and its mechanism for generic isolated quantum systems," *Nature* **452** no. 7189, (04, 2008) 854–858. http://dx.doi.org/10.1038/nature06838.

[20] M. Serbyn, Z. Papić, and D. A. Abanin, "Local conservation laws and the structure of the many-body localized states," *Phys. Rev. Lett.* **111** (Sep, 2013) 127201. link.aps.org/doi/10.1103/PhysRevLett.111.127201.

[21] J. Z. Imbrie, "On many-body localization for quantum spin chains," *arXiv preprint arXiv:1403.7837* (2014) .

[22] D. J. Luitz, N. Laflorencie, and F. Alet, "Many-body localization edge in the random-field heisenberg chain," *Phys. Rev. B* **91** (Feb, 2015) 081103. http://link.aps.org/doi/10.1103/PhysRevB.91.081103.

[23] D. J. Luitz, N. Laflorencie, and F. Alet, "Extended slow dynamical regime close to the many-body localization transition," *Phys. Rev. B* **93** (Feb, 2016) 060201. http://link.aps.org/doi/10.1103/PhysRevB.93.060201.

[24] S. R. White, "Density matrix formulation for quantum renormalization groups," *Phys. Rev. Lett.* **69** (Nov, 1992) 2863–2866. http://link.aps.org/doi/10.1103/PhysRevLett.69.2863.

[25] S. R. White and A. Feiguin, "Real-time evolution using the density matrix renormalization group," *Phys. Rev. Lett.* **93** (2004) 076401.

[26] V. Khemani, F. Pollmann, and S. L. Sondhi, "Obtaining highly excited eigenstates of many-body localized hamiltonians by the density matrix renormalization group approach," *Phys. Rev. Lett.* **116** (Jun, 2016) 247204. https://link.aps.org/doi/10.1103/PhysRevLett.116.247204.

[27] L. D'Alessio and M. Rigol, "Long-time behavior of isolated periodically driven interacting lattice systems," *Physical Review X* **4** no. 4, (Dec, 2014) . http://dx.doi.org/10.1103/PhysRevX.4.041048.

[28] D. A. Abanin, J. H. Bardarson, G. D. Tomasi, S. Gopalakrishnan, V. Khemani, S. A. Parameswaran, F. Pollmann, A. C. Potter, M. Serbyn, and R. Vasseur, "Distinguishing localization from chaos: challenges in finite-size systems," 2019.

[29] B. Swingle, "A simple model of many-body localization," *ArXiv e-prints* (July, 2013) , arXiv:1307.0507 [cond-mat.dis-nn].

[30] G. Refael and J. E. Moore, "Entanglement entropy of random quantum critical points in one dimension," *Phys. Rev. Lett.* **93** (Dec, 2004) 260602. http://link.aps.org/doi/10.1103/PhysRevLett.93.260602.

[31] R. Vasseur, A. C. Potter, and S. A. Parameswaran, "Quantum criticality of hot random spin chains," *Phys. Rev. Lett.* **114** (May, 2015) 217201. http://link.aps.org/doi/10.1103/PhysRevLett.114.217201.

[32] R. Vasseur, A. J. Friedman, S. A. Parameswaran, and A. C. Potter, "Particle-hole symmetry, many-body localization, and topological edge modes," *Phys. Rev. B* **93** (Apr, 2016) 134207. http://link.aps.org/doi/10.1103/PhysRevB.93.134207.

[33] A. J. Friedman, R. Vasseur, A. C. Potter, and S. A. Parameswaran, "Localization-protected order in spin chains with non-abelian discrete symmetries," *Physical Review B* **98** no. 6, (Aug, 2018) . http://dx.doi.org/10.1103/PhysRevB.98.064203.

[34] V. Alba and P. Calabrese, "Entanglement dynamics after quantum quenches in generic integrable systems," *SciPost Physics* **4** no. 3, (Mar, 2018) . http://dx.doi.org/10.21468/SciPostPhys.4.3.017.

[35] J. H. Bardarson, F. Pollmann, and J. E. Moore, "Unbounded growth of entanglement in models of many-body localization," *Phys. Rev. Lett.* **109** (Jul, 2012) 017202. http://link.aps.org/doi/10.1103/PhysRevLett.109.017202.

[36] M. Žnidarič, T. c. v. Prosen, and P. Prelovšek, "Many-body localization in the heisenberg xxz magnet in a random field," *Phys. Rev. B* **77** (Feb, 2008) 064426. http://link.aps.org/doi/10.1103/PhysRevB.77.064426.

[37] A. J. Friedman, S. Gopalakrishnan, and R. Vasseur, "Integrable many-body quantum floquet-thouless pumps," *Phys. Rev. Lett.* **123** (Oct, 2019) 170603. https://link.aps.org/doi/10.1103/PhysRevLett.123.170603.

[38] M. Vanicat, L. Zadnik, and T. c. v. Prosen, "Integrable trotterization: Local conservation laws and boundary driving," *Phys. Rev. Lett.* **121** (Jul, 2018) 030606. https://link.aps.org/doi/10.1103/PhysRevLett.121.030606.

[39] H. Bethe, "Zur theorie der metalle," *Zeitschrift für Physik* **71** no. 3, (Mar, 1931) 205–226. https://doi.org/10.1007/BF01341708.

[40] G. Schütz, "Exactly solvable models for many-body systems far from equilibrium," in *Phase Transitions and Critical Phenomena*, C. Domb and J. Lebowitz, eds., vol. 19. Academic Press, 2001.

[41] M. Gaudin, *The Bethe Wavefunction*. Cambridge University Press, 2014.

[42] F. Franchini, *An introduction to integrable techniques for one-dimensional quantum systems*, vol. 940. Springer.

[43] A. J. Friedman, A. Chan, A. De Luca, and J. T. Chalker, "Spectral statistics and many-body quantum chaos with conserved charge," *Phys. Rev. Lett.* **123** (Nov, 2019) 210603. https://link.aps.org/doi/10.1103/PhysRevLett.123.210603.

[44] V. E. Korepin, N. M. Bogoliubov, and A. G. Izergin, *Quantum inverse scattering method and correlation functions*, vol. 3. Cambridge university press, 1997.

[45] M. Takahashi, *Thermodynamics of one-dimensional solvable models*. Cambridge University Press, 2005.

[46] L. Faddeev, "How algebraic bethe ansatz works for integrable model," *arXiv preprint hep-th/9605187* (1996) .

[47] C.-N. Yang and C. P. Yang, "Thermodynamics of a one-dimensional system of bosons with repulsive delta-function interaction," *Journal of Mathematical Physics* **10** no. 7, (1969) 1115–1122.

[48] F. H. L. Essler and M. Fagotti, "Quench dynamics and relaxation in isolated integrable quantum spin chains," *Journal of Statistical Mechanics: Theory and Experiment* **2016** no. 6, (2016) 064002. http://stacks.iop.org/1742-5468/2016/i=6/a=064002.

[49] P. Calabrese, F. H. L. Essler, and G. Mussardo, "Introduction to 'quantum integrability in out of equilibrium systems'," *Journal of Statistical Mechanics: Theory and Experiment* **2016** no. 6, (2016) 064001. http://stacks.iop.org/1742-5468/2016/i=6/a=064001.

[50] L. Vidmar and M. Rigol, "Generalized gibbs ensemble in integrable lattice models," *Journal of Statistical Mechanics: Theory and Experiment* **2016** no. 6, (2016) 064007. http://stacks.iop.org/1742-5468/2016/i=6/a=064007.

[51] B. Pozsgay, E. Vernier, and M. A. Werner, "On Generalized Gibbs Ensembles with an infinite set of conserved charges," arXiv:1703.09516. http://arxiv.org/abs/1703.09516.

[52] L. Bonnes, F. H. L. Essler, and A. M. Läuchli, ""light-cone" dynamics after quantum quenches in spin chains," *Phys. Rev. Lett.* **113** (Oct, 2014) 187203. https://link.aps.org/doi/10.1103/PhysRevLett.113.187203.

[53] J.-S. Caux and F. H. L. Essler, "Time evolution of local observables after quenching to an integrable model," *Phys. Rev. Lett.* **110** (Jun, 2013) 257203. http://link.aps.org/doi/10.1103/PhysRevLett.110.257203.

[54] V. B. Bulchandani, R. Vasseur, C. Karrasch, and J. E. Moore, "Bethe-boltzmann hydrodynamics and spin transport in the xxz chain," *Phys. Rev. B* **97** (Jan, 2018) 045407. https://link.aps.org/doi/10.1103/PhysRevB.97.045407.

[55] B. Bertini, M. Collura, J. De Nardis, and M. Fagotti, "Transport in out-of-equilibrium xxz chains: Exact profiles of charges and currents," *Phys. Rev. Lett.* **117** (Nov, 2016) 207201. http://link.aps.org/doi/10.1103/PhysRevLett.117.207201.

[56] O. A. Castro-Alvaredo, B. Doyon, and T. Yoshimura, "Emergent hydrodynamics in integrable quantum systems out of equilibrium," *Phys. Rev. X* **6** (Dec, 2016) 041065. http://link.aps.org/doi/10.1103/PhysRevX.6.041065.

[57] B. Doyon, H. Spohn, and T. Yoshimura, "A geometric viewpoint on generalized hydrodynamics," *Nuclear Physics B* **926** (Jan, 2018) 570?583. http://dx.doi.org/10.1016/j.nuclphysb.2017.12.002.

[58] J. De Nardis, D. Bernard, and B. Doyon, "Hydrodynamic diffusion in integrable systems," *Phys. Rev. Lett.* **121** (Oct, 2018) 160603. https://link.aps.org/doi/10.1103/PhysRevLett.121.160603.

[59] B. Doyon and H. Spohn, "Drude Weight for the Lieb-Liniger Bose Gas," *SciPost Phys.* **3** (2017) 039. https://scipost.org/10.21468/SciPostPhys.3.6.039.

[60] J. D. Nardis, D. Bernard, and B. Doyon, "Diffusion in generalized hydrodynamics and quasiparticle scattering," *SciPost Phys.* **6** (2019) 49. https://scipost.org/10.21468/SciPostPhys.6.4.049.

[61] A. Eckardt, "Colloquium," *Rev. Mod. Phys.* **89** (Mar, 2017) 011004. https://link.aps.org/doi/10.1103/RevModPhys.89.011004.

[62] M. Bukov, L. D'Alessio, and A. Polkovnikov, "Universal high-frequency behavior of periodically driven systems: from dynamical stabilization to floquet engineering," *Advances in Physics* **64** no. 2, (2015) 139–226.

[63] F. Meinert, M. J. Mark, K. Lauber, A. J. Daley, and H.-C. Nägerl, "Floquet engineering of correlated tunneling in the bose-hubbard model with ultracold atoms," *Phys. Rev. Lett.* **116** (May, 2016) 205301. http://link.aps.org/doi/10.1103/PhysRevLett.116.205301.

[64] M. Holthaus, "Floquet engineering with quasienergy bands of periodically driven optical lattices," *Journal of Physics B: Atomic, Molecular and Optical Physics* **49** no. 1, (2016) 013001. http://stacks.iop.org/0953-4075/49/i=1/a=013001.

[65] N. Goldman and J. Dalibard, "Periodically driven quantum systems: Effective hamiltonians and engineered gauge fields," *Phys. Rev. X* **4** (Aug, 2014) 031027. http://link.aps.org/doi/10.1103/PhysRevX.4.031027.

[66] T. Kitagawa, E. Berg, M. Rudner, and E. Demler, "Topological characterization of periodically driven quantum systems," *Phys. Rev. B* **82** (Dec, 2010) 235114. http://link.aps.org/doi/10.1103/PhysRevB.82.235114.

[67] N. H. Lindner, G. Refael, and V. Galitski, "Floquet topological insulator in semiconductor quantum wells," *Nature Physics* **7** (03, 2011) 490 EP –. http://dx.doi.org/10.1038/nphys1926.

[68] M. S. Rudner, N. H. Lindner, E. Berg, and M. Levin, "Anomalous edge states and the bulk-edge correspondence for periodically driven two-dimensional systems," *Phys. Rev. X* **3** (Jul, 2013) 031005. http://link.aps.org/doi/10.1103/PhysRevX.3.031005.

[69] F. Nathan and M. S. Rudner, "Topological singularities and the general classification of floquet–bloch systems," *New Journal of Physics* **17** no. 12, (2015) 125014. http://stacks.iop.org/1367-2630/17/i=12/a=125014.

[70] T. Oka and H. Aoki, "Photovoltaic hall effect in graphene," *Phys. Rev. B* **79** (Feb, 2009) 081406. https://link.aps.org/doi/10.1103/PhysRevB.79.081406.

[71] F. Görg, M. Messer, K. Sandholzer, G. Jotzu, R. Desbuquois, and T. Esslinger, "Enhancement and sign change of magnetic correlations in a driven quantum many-body system," *Nature* **553** (01, 2018) 481 EP –. http://dx.doi.org/10.1038/nature25135.

[72] M. Bukov, M. Kolodrubetz, and A. Polkovnikov, "Schrieffer-wolff transformation for periodically driven systems: Strongly correlated systems with artificial gauge fields," *Phys. Rev. Lett.* **116** (Mar, 2016) 125301. https://link.aps.org/doi/10.1103/PhysRevLett.116.125301.

[73] F. Harper, R. Roy, M. S. Rudner, and S. L. Sondhi, "Topology and Broken Symmetry in Floquet Systems," *arXiv e-prints* (May, 2019) arXiv:1905.01317, arXiv:1905.01317 [cond-mat.str-el].

[74] T. c. v. Prosen, "Ergodic properties of a generic nonintegrable quantum many-body system in the thermodynamic limit," *Phys. Rev. E* **60** (Oct, 1999) 3949–3968. https://link.aps.org/doi/10.1103/PhysRevE.60.3949.

[75] T. Prosen, "Exact Time-Correlation Functions of Quantum Ising Chain in a Kicking Transversal Magnetic Field: Spectral Analysis of the Adjoint Propagator in Heisenberg Picture," *Progress of Theoretical Physics Supplement* **139** (05, 2000) 191–203, http://oup.prod.sis.lan/ptps/article-pdf/doi/10.1143/PTPS.139.191/5335503/139-191.pdf. https://doi.org/10.1143/PTPS.139.191.

[76] Y. Wang, H. Steinberg, P. Jarillo-Herrero, and N. Gedik, "Observation of floquet-bloch states on the surface of a topological insulator," *Science* **342** no. 6157, (2013) 453–457.

[77] M. Aidelsburger, M. Atala, M. Lohse, J. T. Barreiro, B. Paredes, and I. Bloch, "Realization of the hofstadter hamiltonian with ultracold atoms in optical lattices," *Phys. Rev. Lett.* **111** (Oct, 2013) 185301. https://link.aps.org/doi/10.1103/PhysRevLett.111.185301.

[78] H. Miyake, G. A. Siviloglou, C. J. Kennedy, W. C. Burton, and W. Ketterle, "Realizing the harper hamiltonian with laser-assisted tunneling in optical lattices," *Phys. Rev. Lett.* **111** (Oct, 2013) 185302. https://link.aps.org/doi/10.1103/PhysRevLett.111.185302.

[79] G. Jotzu, M. Messer, R. Desbuquois, M. Lebrat, T. Uehlinger, D. Greif, and T. Esslinger, "Experimental realization of the topological haldane model with ultracold fermions," *Nature* **515** no. 7526, (2014) 237.

[80] Z. Gu, H. A. Fertig, D. P. Arovas, and A. Auerbach, "Floquet spectrum and transport through an irradiated graphene ribbon," *Phys. Rev. Lett.* **107** (Nov, 2011) 216601. https://link.aps.org/doi/10.1103/PhysRevLett.107.216601.

[81] T. Kitagawa, T. Oka, A. Brataas, L. Fu, and E. Demler, "Transport properties of nonequilibrium systems under the application of light: Photoinduced quantum hall insulators without landau levels," *Phys. Rev. B* **84** (Dec, 2011) 235108. https://link.aps.org/doi/10.1103/PhysRevB.84.235108.

[82] V. Khemani, A. Lazarides, R. Moessner, and S. L. Sondhi, "Phase structure of driven quantum systems," *Phys. Rev. Lett.* **116** (Jun, 2016) 250401. https://link.aps.org/doi/10.1103/PhysRevLett.116.250401.

[83] C. W. von Keyserlingk, V. Khemani, and S. L. Sondhi, "Absolute stability and spatiotemporal long-range order in floquet systems," *Phys. Rev. B* **94** (Aug, 2016) 085112. http://link.aps.org/doi/10.1103/PhysRevB.94.085112.

[84] D. V. Else, B. Bauer, and C. Nayak, "Floquet Time Crystals," *Phys. Rev. Lett.* **117** no. 9, (Aug., 2016) 090402. http://link.aps.org/doi/10.1103/PhysRevLett.117.090402.

[85] D. V. Else, B. Bauer, and C. Nayak, "Prethermal phases of matter protected by time-translation symmetry," *Phys. Rev. X* **7** (Mar, 2017) 011026. https://link.aps.org/doi/10.1103/PhysRevX.7.011026.

[86] W. W. Ho, S. Choi, M. D. Lukin, and D. A. Abanin, "Critical time crystals in dipolar systems," *Phys. Rev. Lett.* **119** (Jul, 2017) 010602. https://link.aps.org/doi/10.1103/PhysRevLett.119.010602.

[87] J. Zhang, P. W. Hess, A. Kyprianidis, P. Becker, A. Lee, J. Smith, G. Pagano, I. D. Potirniche, A. C. Potter, A. Vishwanath, N. Y. Yao, and C. Monroe, "Observation of a discrete time crystal," *Nature* **543** (03, 2017) 217 EP –. http://dx.doi.org/10.1038/nature21413.

[88] S. Choi, J. Choi, R. Landig, G. Kucsko, H. Zhou, J. Isoya, F. Jelezko, S. Onoda, H. Sumiya, V. Khemani, C. von Keyserlingk, N. Y. Yao, E. Demler, and M. D. Lukin, "Observation of discrete time-crystalline order in a disordered dipolar many-body system," *Nature* **543** (03, 2017) 221 EP –. http://dx.doi.org/10.1038/nature21426.

[89] P. Titum, N. H. Lindner, M. C. Rechtsman, and G. Refael, "Disorder-induced floquet topological insulators," *Phys. Rev. Lett.* **114** (Feb, 2015) 056801. https://link.aps.org/doi/10.1103/PhysRevLett.114.056801.

[90] P. Titum, E. Berg, M. S. Rudner, G. Refael, and N. H. Lindner, "Anomalous floquet-anderson insulator as a nonadiabatic quantized charge pump," *Phys. Rev. X* **6** (May, 2016) 021013. https://link.aps.org/doi/10.1103/PhysRevX.6.021013.

[91] D. J. Thouless, "Quantization of particle transport," *Phys. Rev. B* **27** (May, 1983) 6083–6087. https://link.aps.org/doi/10.1103/PhysRevB.27.6083.

[92] N. H. Lindner, E. Berg, and M. S. Rudner, "Universal chiral quasisteady states in periodically driven many-body systems," *Phys. Rev. X* **7** (Feb, 2017) 011018. https://link.aps.org/doi/10.1103/PhysRevX.7.011018.

[93] T. Kuwahara, T. Mori, and K. Saito, "Floquet–magnus theory and generic transient dynamics in periodically driven many-body quantum systems," *Annals of Physics* **367** (2016) 96 – 124. http://www.sciencedirect.com/science/article/pii/S0003491616000142.

[94] D. A. Abanin, W. De Roeck, and F. m. c. Huveneers, "Exponentially slow heating in periodically driven many-body systems," *Phys. Rev. Lett.* **115** (Dec, 2015) 256803. https://link.aps.org/doi/10.1103/PhysRevLett.115.256803.

[95] V. Oganesyan and D. A. Huse, "Localization of interacting fermions at high temperature," *Phys. Rev. B* **75** (Apr, 2007) 155111. http://link.aps.org/doi/10.1103/PhysRevB.75.155111.

[96] E. Altman and R. Vosk, "Universal dynamics and renormalization in many-body-localized systems," *Annual Review of Condensed Matter Physics* **6** no. 1, (2015) 383–409, http://dx.doi.org/10.1146/annurev-conmatphys-031214-014701. http://dx.doi.org/10.1146/annurev-conmatphys-031214-014701.

[97] R. Vasseur and J. E. Moore, "Nonequilibrium quantum dynamics and transport: from integrability to many-body localization," *Journal of Statistical Mechanics: Theory and Experiment* **2016** no. 6, (2016) 064010. http://stacks.iop.org/1742-5468/2016/i=6/a=064010.

[98] D. A. Abanin, E. Altman, I. Bloch, and M. Serbyn, "Ergodicity, Entanglement and Many-Body Localization," *ArXiv e-prints* (Apr., 2018) , arXiv:1804.11065 [cond-mat.dis-nn].

[99] A. Lazarides, A. Das, and R. Moessner, "Fate of many-body localization under periodic driving," *Phys. Rev. Lett.* **115** (Jul, 2015) 030402. http://link.aps.org/doi/10.1103/PhysRevLett.115.030402.

[100] Y. Bahri, R. Vosk, E. Altman, and A. Vishwanath, "Localization and topology protected quantum coherence at the edge of hot matter," *Nat Commun* **6** (07, 2015) . http://dx.doi.org/10.1038/ncomms8341.

[101] B. Bauer and C. Nayak, "Area laws in a many-body localized state and its implications for topological order," *Journal of Statistical Mechanics: Theory and Experiment* **2013** no. 09, (2013) P09005. http://stacks.iop.org/1742-5468/2013/i=09/a=P09005.

[102] T. c. v. Prosen, "Time evolution of a quantum many-body system: Transition from integrability to ergodicity in the thermodynamic limit," *Phys. Rev. Lett.* **80** (Mar, 1998) 1808–1811. https://link.aps.org/doi/10.1103/PhysRevLett.80.1808.

[103] P. Ponte, Z. Papić, F. m. c. Huveneers, and D. A. Abanin, "Many-body localization in periodically driven systems," *Phys. Rev. Lett.* **114** (Apr, 2015) 140401. http://link.aps.org/doi/10.1103/PhysRevLett.114.140401.

[104] C. W. von Keyserlingk and S. L. Sondhi, "Phase structure of one-dimensional interacting floquet systems. i. abelian symmetry-protected topological phases," *Phys. Rev. B* **93** (Jun, 2016) 245145. https://link.aps.org/doi/10.1103/PhysRevB.93.245145.

[105] C. W. von Keyserlingk and S. L. Sondhi, "Phase structure of one-dimensional interacting floquet systems. ii. symmetry-broken phases," *Phys. Rev. B* **93** (Jun, 2016) 245146. https://link.aps.org/doi/10.1103/PhysRevB.93.245146.

[106] D. V. Else and C. Nayak, "Classification of topological phases in periodically driven interacting systems," *Phys. Rev. B* **93** (May, 2016) 201103. http://link.aps.org/doi/10.1103/PhysRevB.93.201103.

[107] A. C. Potter, T. Morimoto, and A. Vishwanath, "Classification of Interacting Topological Floquet Phases in One Dimension," *Phys. Rev. X* **6** no. 4, (Oct., 2016) 041001. http://link.aps.org/doi/10.1103/PhysRevX.6.041001.

[108] R. Roy and F. Harper, "Abelian floquet symmetry-protected topological phases in one dimension," *Phys. Rev. B* **94** (Sep, 2016) 125105. https://link.aps.org/doi/10.1103/PhysRevB.94.125105.

[109] S. Roy and G. J. Sreejith, "Disordered chern insulator with a two-step floquet drive," *Phys. Rev. B* **94** (Dec, 2016) 214203. https://link.aps.org/doi/10.1103/PhysRevB.94.214203.

[110] R. Roy and F. Harper, "Floquet topological phases with symmetry in all dimensions," *Phys. Rev. B* **95** (May, 2017) 195128. https://link.aps.org/doi/10.1103/PhysRevB.95.195128.

[111] H. C. Po, L. Fidkowski, T. Morimoto, A. C. Potter, and A. Vishwanath, "Chiral floquet phases of many-body localized bosons," *Phys. Rev. X* **6** (Dec, 2016) 041070. https://link.aps.org/doi/10.1103/PhysRevX.6.041070.

[112] M. H. Kolodrubetz, F. Nathan, S. Gazit, T. Morimoto, and J. E. Moore, "Topological floquet-thouless energy pump," *Phys. Rev. Lett.* **120** (Apr, 2018) 150601. https://link.aps.org/doi/10.1103/PhysRevLett.120.150601.

[113] T. Kinoshita, T. Wenger, and D. Weiss, "A quantum newton's cradle," *Nature* **440** (2006) 900.

[114] S. Hild, T. Fukuhara, P. Schauß, J. Zeiher, M. Knap, E. Demler, I. Bloch, and C. Gross, "Far-from-equilibrium spin transport in heisenberg quantum magnets," *Phys. Rev. Lett.* **113** (Oct, 2014) 147205. https://link.aps.org/doi/10.1103/PhysRevLett.113.147205.

[115] A. Lazarides, A. Das, and R. Moessner, "Equilibrium states of generic quantum systems subject to periodic driving," *Phys. Rev. E* **90** (Jul, 2014) 012110. https://link.aps.org/doi/10.1103/PhysRevE.90.012110.

[116] A. Lazarides, A. Das, and R. Moessner, "Periodic thermodynamics of isolated quantum systems," *Phys. Rev. Lett.* **112** (Apr, 2014) 150401. https://link.aps.org/doi/10.1103/PhysRevLett.112.150401.

[117] V. Gritsev and A. Polkovnikov, "Integrable Floquet dynamics," *SciPost Phys.* **2** (2017) 021. https://scipost.org/10.21468/SciPostPhys.2.3.021.

[118] A. C. Cubero, "Integrable Floquet QFT: Elasticity and factorization under periodic driving," *SciPost Phys.* **5** (2018) 25. https://scipost.org/10.21468/SciPostPhys.5.3.025.

[119] P. W. Claeys, S. De Baerdemacker, O. E. Araby, and J.-S. Caux, "Spin polarization through floquet resonances in a driven central spin model," *Phys. Rev. Lett.* **121** (Aug, 2018) 080401. https://link.aps.org/doi/10.1103/PhysRevLett.121.080401.

[120] A. Bobenko, M. Bordemann, C. Gunn, and U. Pinkall, "On two integrable cellular automata," *Communications in mathematical physics* **158** no. 1, (1993) 127–134.

[121] T. Prosen and C. Mejía-Monasterio, "Integrability of a deterministic cellular automaton driven by stochastic boundaries," *Journal of Physics A: Mathematical and Theoretical* **49** no. 18, (2016) 185003.

[122] S. Gopalakrishnan, "Operator growth and eigenstate entanglement in an interacting integrable floquet system," *Phys. Rev. B* **98** (Aug, 2018) 060302. https://link.aps.org/doi/10.1103/PhysRevB.98.060302.

[123] T. Prosen and B. Buča, "Exact matrix product decay modes of a boundary driven cellular automaton," *Journal of Physics A: Mathematical and Theoretical* **50** no. 39, (Sep, 2017) 395002. https://doi.org/10.1088%2F1751-8121%2Faa85a3.

[124] S. Gopalakrishnan and B. Zakirov, "Facilitated quantum cellular automata as simple models with non-thermal eigenstates and dynamics," *Quantum Science and Technology* **3** no. 4, (Oct, 2018) 044004, arXiv:1802.07729 [cond-mat.stat-mech].

[125] S. Gopalakrishnan, D. A. Huse, V. Khemani, and R. Vasseur, "Hydrodynamics of operator spreading and quasiparticle diffusion in interacting integrable systems," *Phys. Rev. B* **98** (Dec, 2018) 220303. https://link.aps.org/doi/10.1103/PhysRevB.98.220303.

[126] K. Klobas, M. Medenjak, T. Prosen, and M. Vanicat, "Time-dependent matrix product ansatz for interacting reversible dynamics," *arXiv preprint arXiv:1807.05000* (2018) .

[127] B. Buča, J. P. Garrahan, T. Prosen, and M. Vanicat, "Exact large deviation statistics and trajectory phase transition of a deterministic boundary driven cellular automaton," *arXiv e-prints* (Jan, 2019) arXiv:1901.00845, arXiv:1901.00845 [cond-mat.stat-mech].

[128] V. Alba, J. Dubail, and M. Medenjak, "Operator Entanglement in Interacting Integrable Quantum Systems: the Case of the Rule 54 Chain," *arXiv e-prints* (Jan, 2019) arXiv:1901.04521, arXiv:1901.04521 [cond-mat.stat-mech].

[129] M. A. Nielsen and I. L. Chuang, *Quantum Computation and Quantum Information: 10th Anniversary Edition*. Cambridge University Press, New York, NY, USA, 10th ed., 2011.

[130] A. Larkin and Y. N. Ovchinnikov, "Quasiclassical method in the theory of superconductivity," *Sov Phys JETP* **28** no. 6, (1969) 1200–1205.

[131] J. Maldacena, S. H. Shenker, and D. Stanford, "A bound on chaos," *Journal of High Energy Physics* **2016** no. 8, (2016) 106.

[132] C.-J. Lin and O. I. Motrunich, "Out-of-time-ordered correlators in a quantum ising chain," *Phys. Rev. B* **97** (Apr, 2018) 144304. https://link.aps.org/doi/10.1103/PhysRevB.97.144304.

[133] V. Khemani, D. A. Huse, and A. Nahum, "Velocity-dependent lyapunov exponents in many-body quantum, semiclassical, and classical chaos," *Phys. Rev. B* **98** (Oct, 2018) 144304. https://link.aps.org/doi/10.1103/PhysRevB.98.144304.

[134] B. Doyon and T. Yoshimura, "A note on generalized hydrodynamics: inhomogeneous fields and other concepts," *SciPost Phys.* **2** (2017) 014. https://scipost.org/10.21468/SciPostPhys.2.2.014.

[135] E. Ilievski and J. De Nardis, "Microscopic origin of ideal conductivity in integrable quantum models," *Phys. Rev. Lett.* **119** (Jul, 2017) 020602. https://link.aps.org/doi/10.1103/PhysRevLett.119.020602.

[136] B. Doyon, T. Yoshimura, and J.-S. Caux, "Soliton gases and generalized hydrodynamics," *Phys. Rev. Lett.* **120** (Jan, 2018) 045301. https://link.aps.org/doi/10.1103/PhysRevLett.120.045301.

[137] L. Piroli, J. De Nardis, M. Collura, B. Bertini, and M. Fagotti, "Transport in out-of-equilibrium xxz chains: Nonballistic behavior and correlation functions," *Phys. Rev. B* **96** (Sep, 2017) 115124. https://link.aps.org/doi/10.1103/PhysRevB.96.115124.

[138] E. Ilievski and J. De Nardis, "Ballistic transport in the one-dimensional hubbard model: The hydrodynamic approach," *Phys. Rev. B* **96** (Aug, 2017) 081118. https://link.aps.org/doi/10.1103/PhysRevB.96.081118.

[139] M. Collura, A. De Luca, and J. Viti, "Analytic solution of the domain-wall nonequilibrium stationary state," *Phys. Rev. B* **97** (Feb, 2018) 081111. https://link.aps.org/doi/10.1103/PhysRevB.97.081111.

[140] V. Alba and P. Calabrese, "Entanglement and thermodynamics after a quantum quench in integrable systems," *Proceedings of the National Academy of Sciences* **114** no. 30, (2017) 7947–7951.

[141] A. De Luca, M. Collura, and J. De Nardis, "Nonequilibrium spin transport in integrable spin chains: Persistent currents and emergence of magnetic domains," *Phys. Rev. B* **96** (Jul, 2017) 020403. https://link.aps.org/doi/10.1103/PhysRevB.96.020403.

[142] B. Bertini and L. Piroli, "Low-temperature transport in out-of-equilibrium xxz chains," *Journal of Statistical Mechanics: Theory and Experiment* **2018** no. 3, (2018) 033104.

[143] V. B. Bulchandani, R. Vasseur, C. Karrasch, and J. E. Moore, "Solvable hydrodynamics of quantum integrable systems," *Phys. Rev. Lett.* **119** (Nov, 2017) 220604. https://link.aps.org/doi/10.1103/PhysRevLett.119.220604.

[144] V. B. Bulchandani, "On classical integrability of the hydrodynamics of quantum integrable systems," *Journal of Physics A: Mathematical and Theoretical* **50** no. 43, (2017) 435203. http://stacks.iop.org/1751-8121/50/i=43/a=435203.

[145] B. Doyon, J. Dubail, R. Konik, and T. Yoshimura, "Large-scale description of interacting one-dimensional bose gases: Generalized hydrodynamics supersedes conventional hydrodynamics," *Phys. Rev. Lett.* **119** (Nov, 2017) 195301. https://link.aps.org/doi/10.1103/PhysRevLett.119.195301.

[146] J.-S. Caux, B. Doyon, J. Dubail, R. Konik, and T. Yoshimura, "Hydrodynamics of the interacting Bose gas in the Quantum Newton Cradle setup," *arXiv e-prints* (Nov, 2017) arXiv:1711.00873, arXiv:1711.00873 [cond-mat.stat-mech].

[147] X. Cao, V. B. Bulchandani, and J. E. Moore, "Incomplete thermalization from trap-induced integrability breaking: Lessons from classical hard rods," *Phys. Rev. Lett.* **120** (Apr, 2018) 164101. https://link.aps.org/doi/10.1103/PhysRevLett.120.164101.

[148] B. Doyon, "Exact large-scale correlations in integrable systems out of equilibrium," *SciPost Physics* **5** no. 5, (2018) 054.

[149] M. Schemmer, I. Bouchoule, B. Doyon, and J. Dubail, "Generalized hydrodynamics on an atom chip," *Phys. Rev. Lett.* **122** (Mar, 2019) 090601. https://link.aps.org/doi/10.1103/PhysRevLett.122.090601.

[150] M. Bruschi, P. Santini, and O. Ragnisco, "Integrable cellular automata," *Physics Letters A* **169** no. 3, (1992) 151–160.

[151] B. Grammaticos, Y. Ohta, A. Ramani, D. Takahashi, and K. Tamizhmani, "Cellular automata and ultra-discrete painlevé equations," *Physics Letters A* **226** no. 1-2, (1997) 53–58.

[152] J. Preskill, "Quantum computing in the nisq era and beyond," *Quantum* **2** (2018) 79.

[153] K. X. Wei, P. Peng, O. Shtanko, I. Marvian, S. Lloyd, C. Ramanathan, and P. Cappellaro, "Emergent prethermalization signatures in out-of-time ordered correlations," *Phys. Rev. Lett.* **123** (Aug, 2019) 090605. https://link.aps.org/doi/10.1103/PhysRevLett.123.090605.

[154] P. Roushan, C. Neill, J. Tangpanitanon, V. Bastidas, A. Megrant, R. Barends, Y. Chen, Z. Chen, B. Chiaro, A. Dunsworth, *et al.*, "Spectroscopic signatures of localization with interacting photons in superconducting qubits," *Science* **358** no. 6367, (2017) 1175–1179.

[155] A. J. Friedman, S. Gopalakrishnan, and R. Vasseur, "Diffusive hydrodynamics from integrability breaking," *arXiv preprint (forthcoming)* (2019) .

[156] J. De Nardis and M. Panfil, "Exact correlations in the lieb-liniger model and detailed balance out-of-equilibrium," *SciPost Physics* **1** no. 2, (Dec, 2016) . http://dx.doi.org/10.21468/SciPostPhys.1.2.015.

[157] M. Rigol, V. Dunjko, V. Yurovsky, and M. Olshanii, "Relaxation in a completely integrable many-body quantum system: An ab initio study of the dynamics of the highly excited states of 1d lattice hard-core bosons," *Phys. Rev. Lett.* **98** (Feb, 2007) 050405. http://link.aps.org/doi/10.1103/PhysRevLett.98.050405.

[158] V. Alba, "Eigenstate thermalization hypothesis and integrability in quantum spin chains," *Phys. Rev. B* **91** no. 15, (2015) 155123.

[159] Y. Tang, W. Kao, K.-Y. Li, S. Seo, K. Mallayya, M. Rigol, S. Gopalakrishnan, and B. L. Lev, "Thermalization near integrability in a dipolar quantum newton's cradle," *Phys. Rev. X* **8** (May, 2018) 021030. https://link.aps.org/doi/10.1103/PhysRevX.8.021030.

[160] P. Calabrese and J. Cardy, "Evolution of entanglement entropy in one-dimensional systems," *Journal of Statistical Mechanics: Theory and Experiment* **2005** no. 04, (Apr, 2005) P04010. http://dx.doi.org/10.1088/1742-5468/2005/04/P04010.

[161] P. Calabrese and J. Cardy, "Quantum quenches in 1??+??1 dimensional conformal field theories," *Journal of Statistical Mechanics: Theory and Experiment* **2016** no. 6, (Jun, 2016) 064003. http://dx.doi.org/10.1088/1742-5468/2016/06/064003.

[162] V. Alba and P. Calabrese, "Entanglement and thermodynamics after a quantum quench in integrable systems," *Proceedings of the National Academy of Sciences* **114** no. 30, (Jul, 2017) 7947?7951. http://dx.doi.org/10.1073/pnas.1703516114.

[163] V. Alba, P. Calabrese, and E. Tonni, "Entanglement spectrum degeneracy and the cardy formula in 1+1 dimensional conformal field theories," *Journal of Physics A: Mathematical and Theoretical* **51** no. 2, (Dec, 2017) 024001. http://dx.doi.org/10.1088/1751-8121/aa9365.

[164] B. Doyon, T. Yoshimura, and J.-S. Caux, "Soliton gases and generalized hydrodynamics," *Phys. Rev. Lett.* **120** (Jan, 2018) 045301. https://link.aps.org/doi/10.1103/PhysRevLett.120.045301.

[165] M. Rigol and A. Muramatsu, "Fermionization in an expanding 1d gas of hard-core bosons," *Phys. Rev. Lett.* **94** (Jun, 2005) 240403. http://link.aps.org/doi/10.1103/PhysRevLett.94.240403.

[166] O. Bohigas, M.-J. Giannoni, and C. Schmit, "Characterization of chaotic quantum spectra and universality of level fluctuation laws," *Phys. Rev. Lett.* **52** no. 1, (1984) 1.

[167] T. Guhr, A. Müller-Groeling, and H. A. Weidenmüller, "Random-matrix theories in quantum physics: common concepts," *Physics Reports* **299** no. 4-6, (1998) 189–425.

[168] M. Berry, "Mv berry, j. phys. a 10, 2083 (1977)." *J. Phys. A* **10** (1977) 2083.

[169] J. M. Deutsch, "Quantum statistical mechanics in a closed system," *Phys. Rev. A* **43** (Feb, 1991) 2046–2049. http://link.aps.org/doi/10.1103/PhysRevA.43.2046.

[170] M. Srednicki, "Chaos and quantum thermalization," *Phys. Rev. E* **50** (Aug, 1994) 888–901. http://link.aps.org/doi/10.1103/PhysRevE.50.888.

[171] F. Borgonovi, F. M. Izrailev, L. F. Santos, and V. G. Zelevinsky, "Quantum chaos and thermalization in isolated systems of interacting particles," *Physics Reports* **626** (2016) 1–58.

[172] M. Rigol, "Breakdown of thermalization in finite one-dimensional systems," *Physical Review Letters* **103** no. 10, (2009) 100403.

[173] L. F. Santos and M. Rigol, "Onset of quantum chaos in one-dimensional bosonic and fermionic systems and its relation to thermalization," *Physical Review E* **81** no. 3, (2010) 036206.

[174] G. Biroli, C. Kollath, and A. M. Läuchli, "Effect of rare fluctuations on the thermalization of isolated quantum systems," *Physical Review Letters* **105** no. 25, (2010) 250401.

[175] M. Rigol and M. Srednicki, "Alternatives to eigenstate thermalization," *Phys. Rev. Lett.* **108** no. 11, (2012) 110601.

[176] D. J. Luitz and Y. B. Lev, "Anomalous thermalization in ergodic systems," *Physical review letters* **117** no. 17, (2016) 170404.

[177] A. Dymarsky, "Bound on eigenstate thermalization from transport," *arXiv preprint arXiv:1804.08626* (2018) .

[178] L. Foini and J. Kurchan, "Eigenstate thermalization hypothesis and out of time order correlators," *Physical Review E* **99** no. 4, (2019) 042139.

[179] L. Foini and J. Kurchan, "Eigenstate thermalization and rotational invariance in ergodic quantum systems," *arXiv preprint arXiv:1906.01522* (2019) .

[180] A. Chan, A. De Luca, and J. T. Chalker, "Eigenstate Correlations, Thermalization and the Butterfly Effect," *arXiv e-prints* (Oct, 2018) arXiv:1810.11014, arXiv:1810.11014 [cond-mat.stat-mech].

[181] G. Brandino, A. De Luca, R. Konik, and G. Mussardo, "Quench dynamics in randomly generated extended quantum models," *Physical Review B, 2012* **85** no. 21, (2011) 214435.

[182] W. Beugeling, R. Moessner, and M. Haque, "Off-diagonal matrix elements of local operators in many-body quantum systems," *Phys. Rev. E* **91** (Jan, 2015) 012144. https://link.aps.org/doi/10.1103/PhysRevE.91.012144.

[183] H. Kim, T. N. Ikeda, and D. A. Huse, "Testing whether all eigenstates obey the eigenstate thermalization hypothesis," *Physical Review E* **90** no. 5, (2014) 052105.

[184] A. Nahum, J. Ruhman, S. Vijay, and J. Haah, "Quantum entanglement growth under random unitary dynamics," *Phys. Rev. X* **7** (Jul, 2017) 031016. https://link.aps.org/doi/10.1103/PhysRevX.7.031016.

[185] A. Nahum, S. Vijay, and J. Haah, "Operator spreading in random unitary circuits," *Phys. Rev. X* **8** (Apr, 2018) 021014. https://link.aps.org/doi/10.1103/PhysRevX.8.021014.

[186] C. W. von Keyserlingk, T. Rakovszky, F. Pollmann, and S. L. Sondhi, "Operator hydrodynamics, otocs, and entanglement growth in systems without conservation laws," *Phys. Rev. X* **8** (Apr, 2018) 021013. https://link.aps.org/doi/10.1103/PhysRevX.8.021013.

[187] A. Chan, A. De Luca, and J. T. Chalker, "Solution of a minimal model for many-body quantum chaos," *Phys. Rev. X* **8** (Nov, 2018) 041019. https://link.aps.org/doi/10.1103/PhysRevX.8.041019.

[188] A. Chan, A. De Luca, and J. T. Chalker, "Spectral statistics in spatially extended chaotic quantum many-body systems," *Phys. Rev. Lett.* **121** (Aug, 2018) 060601. https://link.aps.org/doi/10.1103/PhysRevLett.121.060601.

[189] T. Rakovszky, F. Pollmann, and C. W. von Keyserlingk, "Diffusive hydrodynamics of out-of-time-ordered correlators with charge conservation," *Phys. Rev. X* **8** (Sep, 2018) 031058. https://link.aps.org/doi/10.1103/PhysRevX.8.031058.

[190] V. Khemani, A. Vishwanath, and D. A. Huse, "Operator spreading and the emergence of dissipative hydrodynamics under unitary evolution with conservation laws," *Phys. Rev. X* **8** (Sep, 2018) 031057. https://link.aps.org/doi/10.1103/PhysRevX.8.031057.

[191] C. Sünderhauf, D. Pérez-García, D. A. Huse, N. Schuch, and J. I. Cirac, "Localization with random time-periodic quantum circuits," *Phys. Rev. B* **98** (Oct, 2018) 134204. https://link.aps.org/doi/10.1103/PhysRevB.98.134204.

[192] P. Kos, M. Ljubotina, and T. c. v. Prosen, "Many-body quantum chaos: Analytic connection to random matrix theory," *Phys. Rev. X* **8** (Jun, 2018) 021062. https://link.aps.org/doi/10.1103/PhysRevX.8.021062.

[193] H. Gharibyan, M. Hanada, S. H. Shenker, and M. Tezuka, "Onset of random matrix behavior in scrambling systems," *Journal of High Energy Physics* **2018** no. 7, (Jul, 2018) 124. https://doi.org/10.1007/JHEP07(2018)124.

[194] B. Bertini, P. Kos, and T. Prosen, "Exact spectral form factor in a minimal model of many-body quantum chaos," *Physical review letters* **121** no. 26, (2018) 264101.

[195] D. J. Thouless, "Maximum metallic resistance in thin wires," *Phys. Rev. Lett.* **39** (Oct, 1977) 1167–1169. https://link.aps.org/doi/10.1103/PhysRevLett.39.1167.

[196] B. L. Altshuler and B. I. Shklovskii, "Repulsion of energy levels and conductivity of small metal samples," *JETP* **64** (1986) 127–135. http://www.jetp.ac.ru/cgi-bin/dn/e_064_01_0127.pdf.

[197] P. Braun, D. Waltner, M. Akila, B. Gutkin, and T. Guhr, "Transition from quantum chaos to localization in spin chains," *ArXiv e-prints* (2019) , arXiv:1902.06265 [cond-mat.stat-mech].

[198] P. W. Brouwer and C. W. J. Beenakker, "Diagrammatic method of integration over the unitary group, with applications to quantum transport in mesoscopic systems," *Journal of Mathematical Physics* **37** no. 10, (1996) 4904–4934. https://doi.org/10.1063/1.531667.

[199] M. Suzuki, "Quantum transfer-matrix method and thermo-quantum dynamics," *Physica A: Statistical Mechanics and its Applications* **321** no. 1-2, (2003) 334–339.

[200] A. Klmper, "Integrability of quantum chains: Theory and applications to the spin-1/2 xxz chain," *Lecture Notes in Physics* (2004) 349379. http://dx.doi.org/10.1007/BFb0119598.

[201] P. Schlottmann, "Critical behavior of the isotropic ferromagnetic quantum heisenberg chain," *Physical review letters* **54** no. 19, (1985) 2131.

[202] M. Takahashi, "Quantum heisenberg ferromagnets in one and two dimensions at low temperature," *Progress of Theoretical Physics Supplement* **87** (1986) 233–246.

[203] J. Šuntajs, J. Bonča, T. Prosen, and L. Vidmar, "Quantum chaos challenges many-body localization," *arXiv e-prints* (May, 2019) arXiv:1905.06345, arXiv:1905.06345 [cond-mat.str-el].

[204] T. Rakovszky, P. Sala, R. Verresen, M. Knap, and F. Pollmann, "Statistical localization: from strong fragmentation to strong edge modes," 2019.

[205] S. A. Parameswaran and R. Vasseur, "Many-body localization, symmetry and topology," *Reports on Progress in Physics* **81** no. 8, (Jul, 2018) 082501. https://doi.org/10.1088%2F1361-6633%2Faac9ed.

[206] D. Pekker, G. Refael, E. Altman, E. Demler, and V. Oganesyan, "Hilbert-glass transition: New universality of temperature-tuned many-body dynamical quantum criticality," *Phys. Rev. X* **4** (Mar, 2014) 011052. http://dx.doi.org/10.1103/PhysRevX.4.011052.

[207] J. A. Kjäll, J. H. Bardarson, and F. Pollmann, "Many-body localization in a disordered quantum ising chain," *Phys. Rev. Lett.* **113** (Sep, 2014) 107204. http://link.aps.org/doi/10.1103/PhysRevLett.113.107204.

[208] S. A. Parameswaran, A. C. Potter, and R. Vasseur, "Eigenstate phase transitions and the emergence of universal dynamics in highly excited states," *Annalen der Physik* (2017) 1600302–n/a. http://dx.doi.org/10.1002/andp.201600302. 1600302.

[209] R. Vosk and E. Altman, "Many-body localization in one dimension as a dynamical renormalization group fixed point," *Phys. Rev. Lett.* **110** (Feb, 2013) 067204. http://link.aps.org/doi/10.1103/PhysRevLett.110.067204.

[210] R. Vosk and E. Altman, "Dynamical quantum phase transitions in random spin chains," *Phys. Rev. Lett.* **112** (May, 2014) 217204. http://link.aps.org/doi/10.1103/PhysRevLett.112.217204.

[211] Y.-Z. You, X.-L. Qi, and C. Xu, "Entanglement holographic mapping of many-body localized system by spectrum bifurcation renormalization group," *Phys. Rev. B* **93** (Mar, 2016) 104205. https://link.aps.org/doi/10.1103/PhysRevB.93.104205.

[212] C. Monthus, "Many-body localization: construction of the emergent local conserved operators via block real-space renormalization," *Journal of Statistical Mechanics: Theory and Experiment* **2016** no. 3, (Mar, 2016) 033101. https://doi.org/10.1088%2F1742-5468%2F2016%2F03%2F033101.

[213] D. S. Fisher, "Critical behavior of random transverse-field ising spin chains," *Phys. Rev. B* **51** (Mar, 1995) 6411–6461. https://link.aps.org/doi/10.1103/PhysRevB.51.6411.

[214] A. C. Potter, R. Vasseur, and S. A. Parameswaran, "Universal properties of many-body delocalization transitions," *Phys. Rev. X* **5** (Sep, 2015) 031033. http://link.aps.org/doi/10.1103/PhysRevX.5.031033.

[215] D. S. Fisher, "Random transverse field ising spin chains," *Phys. Rev. Lett.* **69** (Jul, 1992) 534–537. http://link.aps.org/doi/10.1103/PhysRevLett.69.534.

[216] D. S. Fisher, "Random antiferromagnetic quantum spin chains," *Phys. Rev. B* **50** (Aug, 1994) 3799–3821. http://link.aps.org/doi/10.1103/PhysRevB.50.3799.

[217] A. C. Potter and R. Vasseur, "Symmetry constraints on many-body localization," *Phys. Rev. B* **94** (Dec, 2016) 224206. https://link.aps.org/doi/10.1103/PhysRevB.94.224206.

[218] A. P. Schnyder, S. Ryu, A. Furusaki, and A. W. W. Ludwig, "Classification of topological insulators and superconductors," *AIP Conference Proceedings* **1134** no. 1, (2009) 10–21.

[219] A. Kitaev, "Periodic table for topological insulators and superconductors," *AIP Conference Proceedings* **1134** no. 1, (2009) 22–30.

[220] A. Chandran, V. Khemani, C. R. Laumann, and S. L. Sondhi, "Many-body localization and symmetry-protected topological order," *Phys. Rev. B* **89** (Apr, 2014) 144201. http://link.aps.org/doi/10.1103/PhysRevB.89.144201.

[221] K. Slagle, B. Zhen, Y.-Z. You, and C. Xu, "Many-body localization of symmetry protected topological states," *arXiv:1505.05147* (2015) .

[222] A. C. Potter and A. Vishwanath, "Protection of topological order by symmetry and many-body localization," *arXiv:1506:00592* (2015) .

[223] J. Alicea and P. Fendley *Annual Review of Condensed Matter Physics* **7** (2016) 119–139. http://dx.doi.org/10.1146/annurev-conmatphys-031115-011336.

[224] E. Fradkin and L. P. Kadanoff, "Disorder variables and para-fermions in two-dimensional statistical mechanics," *Nuclear Physics B* **170** no. 1, (1980) 1 – 15. http://www.sciencedirect.com/science/article/pii/0550321380904721.

[225] P. Fendley, "Parafermionic edge zero modes in z n -invariant spin chains," *Journal of Statistical Mechanics: Theory and Experiment* **2012** no. 11, (2012) P11020. http://stacks.iop.org/1742-5468/2012/i=11/a=P11020.

[226] A. Prakash, S. Ganeshan, L. Fidkowski, and T.-C. Wei, "Eigenstate phases with finite on-site non-abelian symmetry," *Phys. Rev. B* **96** (Oct, 2017) 165136. https://link.aps.org/doi/10.1103/PhysRevB.96.165136.

[227] S. Ostlund, "Incommensurate and commensurate phases in asymmetric clock models," *Phys. Rev. B* **24** (Jul, 1981) 398–405. https://link.aps.org/doi/10.1103/PhysRevB.24.398.

[228] D. A. Huse, "Simple three-state model with infinitely many phases," *Phys. Rev. B* **24** (Nov, 1981) 5180–5194. https://link.aps.org/doi/10.1103/PhysRevB.24.5180.

[229] J. Motruk, E. Berg, A. M. Turner, and F. Pollmann, "Topological phases in gapped edges of fractionalized systems," *Phys. Rev. B* **88** (Aug, 2013) 085115. https://link.aps.org/doi/10.1103/PhysRevB.88.085115.

[230] R. Bondesan and T. Quella, "Topological and symmetry broken phases of z n parafermions in one dimension," *Journal of Statistical Mechanics: Theory and Experiment* **2013** no. 10, (2013) P10024. http://stacks.iop.org/1742-5468/2013/i=10/a=P10024.

[231] W. Li, S. Yang, H.-H. Tu, and M. Cheng, "Criticality in translation-invariant parafermion chains," *Phys. Rev. B* **91** (Mar, 2015) 115133. https://link.aps.org/doi/10.1103/PhysRevB.91.115133.

[232] A. Alexandradinata, N. Regnault, C. Fang, M. J. Gilbert, and B. A. Bernevig, "Parafermionic phases with symmetry breaking and topological order," *Phys. Rev. B* **94** (Sep, 2016) 125103. https://link.aps.org/doi/10.1103/PhysRevB.94.125103.

[233] Y. Zhuang, H. J. Changlani, N. M. Tubman, and T. L. Hughes, "Phase diagram of the Z_3 parafermionic chain with chiral interactions," *Phys. Rev. B* **92** (Jul, 2015) 035154. https://link.aps.org/doi/10.1103/PhysRevB.92.035154.

[234] A. S. Jermyn, R. S. K. Mong, J. Alicea, and P. Fendley, "Stability of zero modes in parafermion chains," *Phys. Rev. B* **90** (Oct, 2014) 165106. https://link.aps.org/doi/10.1103/PhysRevB.90.165106.

[235] T. Senthil and S. N. Majumdar, "Critical properties of random quantum potts and clock models," *Phys. Rev. Lett.* **76** (Apr, 1996) 3001–3004. https://link.aps.org/doi/10.1103/PhysRevLett.76.3001.

[236] J. Chayes, L. Chayes, D. Fisher, and T. Spencer, "Finite-size scaling and correlation lengths for disordered systems," *Phys. Rev. Lett.* **57** (Dec, 1986) 2999–3002. http://link.aps.org/doi/10.1103/PhysRevLett.57.2999.

[237] W. De Roeck and F. m. c. Huveneers, "Stability and instability towards delocalization in many-body localization systems," *Phys. Rev. B* **95** (Apr, 2017) 155129. https://link.aps.org/doi/10.1103/PhysRevB.95.155129.

[238] W. De Roeck and J. Z. Imbrie, "Many-Body Localization: Stability and Instability," *arXiv:1705.00756* (May, 2017) .

[239] F. Pollmann, V. Khemani, J. I. Cirac, and S. L. Sondhi, "Efficient variational diagonalization of fully many-body localized hamiltonians," *Phys. Rev. B* **94** (Jul, 2016) 041116. https://link.aps.org/doi/10.1103/PhysRevB.94.041116.

[240] X. Yu, D. Pekker, and B. K. Clark, "Finding matrix product state representations of highly excited eigenstates of many-body localized hamiltonians," *Phys. Rev. Lett.* **118** (Jan, 2017) 017201. https://link.aps.org/doi/10.1103/PhysRevLett.118.017201.

[241] D. Pekker and B. K. Clark, "Encoding the structure of many-body localization with matrix product operators," *Phys. Rev. B* **95** (Jan, 2017) 035116. https://link.aps.org/doi/10.1103/PhysRevB.95.035116.

[242] L. Fleishman and P. Anderson, "Interactions and the anderson transition," *Phys. Rev. B* **21** (Mar, 1980) 2366–2377. http://link.aps.org/doi/10.1103/PhysRevB.21.2366.

[243] I. Gornyi, A. Mirlin, and D. Polyakov, "Interacting electrons in disordered wires: Anderson localization and low-t transport," *Phys. Rev. Lett.* **95** (Nov, 2005) 206603. http://link.aps.org/doi/10.1103/PhysRevLett.95.206603.

[244] M. Serbyn, M. Knap, S. Gopalakrishnan, Z. Papić, N. Y. Yao, C. R. Laumann, D. A. Abanin, M. D. Lukin, and E. A. Demler, "Interferometric probes of many-body localization," *Phys. Rev. Lett.* **113** (Oct, 2014) 147204. http://link.aps.org/doi/10.1103/PhysRevLett.113.147204.

[245] R. Vasseur, S. A. Parameswaran, and J. E. Moore, "Quantum revivals and many-body localization," *Phys. Rev. B* **91** (Apr, 2015) 140202. http://link.aps.org/doi/10.1103/PhysRevB.91.140202.

[246] B. Bauer and C. Nayak, "Analyzing many-body localization with a quantum computer," *Phys. Rev. X* **4** (Nov, 2014) 041021. http://link.aps.org/doi/10.1103/PhysRevX.4.041021.

[247] S. Choi, N. Y. Yao, S. Gopalakrishnan, and M. D. Lukin, "Quantum Control of Many-body Localized States," *ArXiv e-prints* (Aug., 2015) , arXiv:1508.06992 [quant-ph].

[248] K. Slagle, Z. Bi, Y.-Z. You, and C. Xu, "Many-Body Localization of Symmetry Protected Topological States," *ArXiv e-prints* (May, 2015) , arXiv:1505.05147 [cond-mat.str-el].

[249] A. C. Potter and A. Vishwanath, "Protection of topological order by symmetry and many-body localization," *ArXiv e-prints* (June, 2015) , arXiv:1506.00592 [cond-mat.dis-nn].

[250] R. Nandkishore and D. A. Huse, "Many-body localization and thermalization in quantum statistical mechanics," *Annual Review of Condensed Matter Physics* **6** no. 1, (2015) 15–38. http://dx.doi.org/10.1146/annurev-conmatphys-031214-014726.

[251] J. A. Kjäll, J. H. Bardarson, and F. Pollmann, "Many-body localization in a disordered quantum ising chain," *Phys. Rev. Lett.* **113** (Sep, 2014) 107204. http://link.aps.org/doi/10.1103/PhysRevLett.113.107204.

[252] S. Gopalakrishnan and R. Nandkishore, "Mean-field theory of nearly many-body localized metals," *Phys. Rev. B* **90** (Dec, 2014) 224203. http://link.aps.org/doi/10.1103/PhysRevB.90.224203.

[253] R. Vosk, D. A. Huse, and E. Altman, "Theory of the many-body localization transition in one-dimensional systems," *Phys. Rev. X* **5** (Sep, 2015) 031032. http://link.aps.org/doi/10.1103/PhysRevX.5.031032.

[254] L. Balents and M. P. A. Fisher, "Delocalization transition via supersymmetry in one dimension," *Phys. Rev. B* **56** (Nov, 1997) 12970–12991. http://link.aps.org/doi/10.1103/PhysRevB.56.12970.

[255] R. Nandkishore and A. C. Potter, "Marginal anderson localization and many-body delocalization," *Phys. Rev. B* **90** (Nov, 2014) 195115. http://link.aps.org/doi/10.1103/PhysRevB.90.195115.

[256] Y. Huang and J. E. Moore, "Excited-state entanglement and thermal mutual information in random spin chains," *Phys. Rev. B* **90** (Dec, 2014) 220202. http://link.aps.org/doi/10.1103/PhysRevB.90.220202.

[257] Y. Y. Atas, E. Bogomolny, O. Giraud, and G. Roux, "Distribution of the ratio of consecutive level spacings in random matrix ensembles," *Phys. Rev. Lett.* **110** (Feb, 2013) 084101. http://link.aps.org/doi/10.1103/PhysRevLett.110.084101.

[258] F. Nathan and M. S. Rudner, "Topological singularities and the general classification of Floquet-Bloch systems," *ArXiv e-prints* (June, 2015) , arXiv:1506.07647 [cond-mat.mes-hall].

[259] V. Khemani, A. Lazarides, R. Moessner, and S. L. Sondhi, "On the phase structure of driven quantum systems," *ArXiv e-prints* (Aug., 2015) , arXiv:1508.03344 [cond-mat.dis-nn].

[260] D. Abanin, W. De Roeck, and F. Huveneers, "A theory of many-body localization in periodically driven systems," *ArXiv e-prints* (Dec., 2014) , arXiv:1412.4752 [cond-mat.dis-nn].

[261] I. Bloch, J. Dalibard, and W. Zwerger, "Many-body physics with ultracold gases," *Rev. Mod. Phys.* **80** (Jul, 2008) 885–964. http://link.aps.org/doi/10.1103/RevModPhys.80.885.

[262] H. P. Lüschen, S. Scherg, T. Kohlert, M. Schreiber, P. Bordia, X. Li, S. Das Sarma, and I. Bloch, "Single-particle mobility edge in a one-dimensional quasiperiodic optical lattice," *Phys. Rev. Lett.* **120** (Apr, 2018) 160404. https://link.aps.org/doi/10.1103/PhysRevLett.120.160404.

[263] H. P. Lüschen, P. Bordia, S. S. Hodgman, M. Schreiber, S. Sarkar, A. J. Daley, M. H. Fischer, E. Altman, I. Bloch, and U. Schneider, "Signatures of many-body localization in a controlled open quantum system," *Phys. Rev. X* **7** (Mar, 2017) 011034. https://link.aps.org/doi/10.1103/PhysRevX.7.011034.

[264] R. Nandkishore, S. Gopalakrishnan, and D. A. Huse, "Spectral features of a many-body-localized system weakly coupled to a bath," *Phys. Rev. B* **90** (Aug, 2014) 064203. http://link.aps.org/doi/10.1103/PhysRevB.90.064203.

[265] R. Nandkishore and S. Gopalakrishnan, "Many body localized systems weakly coupled to baths," *Annalen der Physik* **529** no. 7, 1600181. https://onlinelibrary.wiley.com/doi/abs/10.1002/andp.201600181.

[266] R. Nandkishore, S. Gopalakrishnan, and D. A. Huse, "Spectral features of a many-body localized system weakly coupled to a heat bath," *ArXiv e-prints* (Feb., 2014) , arXiv:1402.5971 [cond-mat.stat-mech].

[267] K. Hyatt, J. R. Garrison, A. C. Potter, and B. Bauer, "Many-body localization in the presence of a small bath," *Phys. Rev. B* **95** (Jan, 2017) 035132. https://link.aps.org/doi/10.1103/PhysRevB.95.035132.

[268] A. O. Caldeira and A. J. Leggett, "Influence of dissipation on quantum tunneling in macroscopic systems," *Phys. Rev. Lett.* **46** (Jan, 1981) 211–214. https://link.aps.org/doi/10.1103/PhysRevLett.46.211.

[269] A. Caldeira and A. Leggett, "Quantum tunnelling in a dissipative system," *Annals of Physics* **149** no. 2, (1983) 374 – 456. http://www.sciencedirect.com/science/article/pii/0003491683902026.

[270] F. Guinea, "Low-temperature properties of a quantum particle coupled to dissipative environments," *Phys. Rev. B* **67** (Jan, 2003) 045103. https://link.aps.org/doi/10.1103/PhysRevB.67.045103.

[271] M. P. A. Fisher and W. Zwerger, "Quantum brownian motion in a periodic potential," *Phys. Rev. B* **32** (Nov, 1985) 6190–6206. https://link.aps.org/doi/10.1103/PhysRevB.32.6190.

[272] A. Caldeira and A. Leggett, "Path integral approach to quantum brownian motion," *Physica A: Statistical Mechanics and its Applications* **121** no. 3, (1983) 587 – 616. http://www.sciencedirect.com/science/article/pii/0378437183900134.

[273] A. J. Leggett, S. Chakravarty, A. T. Dorsey, M. P. A. Fisher, A. Garg, and W. Zwerger, "Dynamics of the dissipative two-state system," *Rev. Mod. Phys.* **59** (Jan, 1987) 1–85. https://link.aps.org/doi/10.1103/RevModPhys.59.1.

[274] A. H. Castro Neto, C. de C. Chamon, and C. Nayak, "Open luttinger liquids," *Phys. Rev. Lett.* **79** (Dec, 1997) 4629–4632. https://link.aps.org/doi/10.1103/PhysRevLett.79.4629.

[275] A. J. Friedman, R. Vasseur, A. Lamacraft, and S. A. Parameswaran, "Quantum brownian motion in a quasiperiodic potential," *Phys. Rev. B* **100** (Aug, 2019) 060301. https://link.aps.org/doi/10.1103/PhysRevB.100.060301.

[276] A. Kamenev, "Many-body theory of non-equilibrium systems," *arXiv preprint arXiv:cond-mat/0412296* (Dec, 2004) . https://arxiv.org/abs/cond-mat/0412296.

[277] D. A. Huse, R. Nandkishore, F. Pietracaprina, V. Ros, and A. Scardicchio, "Localized systems coupled to small baths: From anderson to zeno," *Phys. Rev. B* **92** (Jul, 2015) 014203. https://link.aps.org/doi/10.1103/PhysRevB.92.014203.

[278] C. G. Callan and D. Freed, "Phase diagram of the dissipative hofstadter model," *Nuclear Physics B* **374** no. 3, (1992) 543 – 566. http://www.sciencedirect.com/science/article/pii/0550321392904006.

[279] C. G. Callan, A. G. Felce, and D. E. Freed, "Critical theories of the dissipative hofstadter model," *Nuclear Physics B* **392** no. 3, (1993) 551 – 592. http://www.sciencedirect.com/science/article/pii/055032139390517S.

[280] U. Weiss and H. Grabert, "Quantum diffusion of a particle in a periodic potential with ohmic dissipation," *Physics Letters A* **108** no. 2, (1985) 63 – 67. http://www.sciencedirect.com/science/article/pii/0375960185905171.

[281] H. Yi and C. L. Kane, "Quantum brownian motion in a periodic potential and the multichannel kondo problem," *Phys. Rev. B* **57** (Mar, 1998) R5579–R5582. https://link.aps.org/doi/10.1103/PhysRevB.57.R5579.

[282] C. Aslangul, N. Pottier, and D. Saint-James, "Quantum ohmic dissipation: Particle on a one-dimensional periodic lattice," *Physics Letters A* **111** no. 4, (1985) 175 – 178. http://www.sciencedirect.com/science/article/pii/0375960185905705.

[283] P. Werner, K. Völker, M. Troyer, and S. Chakravarty, "Phase diagram and critical exponents of a dissipative ising spin chain in a transverse magnetic field," *Phys. Rev. Lett.* **94** (Jan, 2005) 047201. https://link.aps.org/doi/10.1103/PhysRevLett.94.047201.

[284] C. L. Kane and M. P. A. Fisher, "Transport in a one-channel luttinger liquid," *Phys. Rev. Lett.* **68** (Feb, 1992) 1220–1223. https://link.aps.org/doi/10.1103/PhysRevLett.68.1220.

[285] C. L. Kane and M. P. A. Fisher, "Transmission through barriers and resonant tunneling in an interacting one-dimensional electron gas," *Phys. Rev. B* **46** (Dec, 1992) 15233–15262. https://link.aps.org/doi/10.1103/PhysRevB.46.15233.

[286] A. H. Castro Neto and M. P. A. Fisher, "Dynamics of a heavy particle in a luttinger liquid," *Phys. Rev. B* **53** (Apr, 1996) 9713–9718. https://link.aps.org/doi/10.1103/PhysRevB.53.9713.

[287] F. Guinea, V. Hakim, and A. Muramatsu, "Diffusion and localization of a particle in a periodic potential coupled to a dissipative environment," *Phys. Rev. Lett.* **54** (Jan, 1985) 263–266. https://link.aps.org/doi/10.1103/PhysRevLett.54.263.

[288] H. P. Lüschen, P. Bordia, S. S. Hodgman, M. Schreiber, S. Sarkar, A. J. Daley, M. H. Fischer, E. Altman, I. Bloch, and U. Schneider, "Signatures of many-body localization in a controlled open quantum system," *Phys. Rev. X* **7** (Mar, 2017) 011034. https://link.aps.org/doi/10.1103/PhysRevX.7.011034.

[289] S. Aubry and G. André *Ann. Isr. Phy.* **3** (1980) 133.

[290] S. Iyer, V. Oganesyan, G. Refael, and D. A. Huse, "Many-body localization in a quasiperiodic system," *Phys. Rev. B* **87** (Apr, 2013) 134202. https://link.aps.org/doi/10.1103/PhysRevB.87.134202.

[291] A. Chandran and C. R. Laumann, "Localization and symmetry breaking in the quantum quasiperiodic ising glass," *Phys. Rev. X* **7** (Sep, 2017) 031061. https://link.aps.org/doi/10.1103/PhysRevX.7.031061.

[292] S. Gopalakrishnan, K. Agarwal, D. A. Huse, E. Demler, and M. Knap, "Griffiths effects and slow dynamics in nearly many-body localized systems," *arXiv preprint arXiv:1511.06389* (2015) .

[293] H. P. Lüschen, P. Bordia, S. Scherg, F. Alet, E. Altman, U. Schneider, and I. Bloch, "Observation of slow dynamics near the many-body localization transition in one-dimensional quasiperiodic systems," *Phys. Rev. Lett.* **119** (Dec, 2017) 260401. https://link.aps.org/doi/10.1103/PhysRevLett.119.260401.

[294] M. Schreiber, S. S. Hodgman, P. Bordia, H. P. Lüschen, M. H. Fischer, R. Vosk, E. Altman, U. Schneider, and I. Bloch, "Observation of many-body localization of interacting fermions in a quasirandom optical lattice,". http://science.sciencemag.org/content/349/6250/842.

[295] K. Singh, K. Saha, S. A. Parameswaran, and D. M. Weld, "Fibonacci optical lattices for tunable quantum quasicrystals," *Phys. Rev. A* **92** (Dec, 2015) 063426. https://link.aps.org/doi/10.1103/PhysRevA.92.063426.

[296] S. Li, I. I. Satija, C. W. Clark, and A. M. Rey, "Exploring complex phenomena using ultracold atoms in bichromatic lattices," *Phys. Rev. E* **82** (Jul, 2010) 016217. https://link.aps.org/doi/10.1103/PhysRevE.82.016217.

[297] K. He, I. I. Satija, C. W. Clark, A. M. Rey, and M. Rigol, "Noise correlation scalings: Revisiting the quantum phase transition in incommensurate lattices with hard-core bosons," *Phys. Rev. A* **85** (Jan, 2012) 013617. https://link.aps.org/doi/10.1103/PhysRevA.85.013617.

[298] A. M. Rey, I. I. Satija, and C. W. Clark, "Noise correlations of fermions and hard core bosons in a quasi-periodic potential," *Laser Physics* **17** no. 2, (Feb, 2007) 205–210. https://doi.org/10.1134/S1054660X07020260.

[299] R. Feynman and F. Vernon, "The theory of a general quantum system interacting with a linear dissipative system," *Annals of Physics* **24** (1963) 118 – 173. http://www.sciencedirect.com/science/article/pii/000349166390068X.

[300] See supplementary material for details of RG procedure and plots of flow of couplings under the RG.

[301] A. Lamacraft, "Dispersion relation and spectral function of an impurity in a one-dimensional quantum liquid," *Phys. Rev. B* **79** (Jun, 2009) 241105. https://link.aps.org/doi/10.1103/PhysRevB.79.241105.

[302] A. J. Friedman, "Dissipative luttinger liquids," arXiv:1910.06371 [cond-mat.quant-gas].

[303] J. M. Luttinger, "An exactly soluble model of a manyfermion system," *Journal of Mathematical Physics* **4** no. 9, (1963) 1154–1162, https://doi.org/10.1063/1.1704046. https://doi.org/10.1063/1.1704046.

[304] D. C. Mattis and E. H. Lieb, "Exact solution of a manyfermion system and its associated boson field," *Journal of Mathematical Physics* **6** no. 2, (1965) 304–312, https://doi.org/10.1063/1.1704281. https://doi.org/10.1063/1.1704281.

[305] A. Luther and I. Peschel, "Single-particle states, kohn anomaly, and pairing fluctuations in one dimension," *Phys. Rev. B* **9** (Apr, 1974) 2911–2919. https://link.aps.org/doi/10.1103/PhysRevB.9.2911.

[306] F. D. M. Haldane, "Effective harmonic-fluid approach to low-energy properties of one-dimensional quantum fluids," *Phys. Rev. Lett.* **47** (Dec, 1981) 1840–1843. https://link.aps.org/doi/10.1103/PhysRevLett.47.1840.

[307] F. D. M. Haldane, "'luttinger liquid theory' of one-dimensional quantum fluids. i. properties of the luttinger model and their extension to the general 1d interacting spinless fermi gas," *Journal of Physics C: Solid State Physics* **14** no. 19, (1981) 2585. http://stacks.iop.org/0022-3719/14/i=19/a=010.

[308] T. Giamarchi, *Quantum physics in one dimension*. Clarendon Oxford, 2004.

[309] J. von Delft and H. Schoeller, "Bosonization for beginners ? refermionization for experts," *Annalen der Physik* **7** no. 4, 225–305. https://onlinelibrary.wiley.com/doi/abs/10.1002/%28SICI%291521-3889%28199811%297%3A4%3C225%3A%3AAID-ANDP225%3E3.0.CO%3B2-L.

[310] S. Sachdev, P. Werner, and M. Troyer, "Universal conductance of nanowires near the superconductor-metal quantum transition," *Phys. Rev. Lett.* **92** (Jun, 2004) 237003. https://link.aps.org/doi/10.1103/PhysRevLett.92.237003.

[311] K. Le Hur and M.-R. Li, "Unification of electromagnetic noise and luttinger liquid via a quantum dot," *Phys. Rev. B* **72** (Aug, 2005) 073305. https://link.aps.org/doi/10.1103/PhysRevB.72.073305.

[312] M. A. Cazalilla, F. Sols, and F. Guinea, "Dissipation-driven quantum phase transitions in a tomonaga-luttinger liquid electrostatically coupled to a metallic gate," *Phys. Rev. Lett.* **97** (Aug, 2006) 076401. https://link.aps.org/doi/10.1103/PhysRevLett.97.076401.

[313] Z. Ristivojevic and T. Nattermann, "Transport in a dissipative luttinger liquid," *Phys. Rev. Lett.* **101** (Jul, 2008) 016405. https://link.aps.org/doi/10.1103/PhysRevLett.101.016405.

[314] E. G. Dalla Torre, E. Demler, T. Giamarchi, and E. Altman, "Quantum critical states and phase transitions in the presence of non-equilibrium noise," *Nature Physics* **6** (Aug, 2010) 806. https://doi.org/10.1038/nphys1754http://10.0.4.14/nphys1754https://www.nature.com/articles/nphys1754{#}supplementary-information.

[315] E. G. Dalla Torre, E. Demler, T. Giamarchi, and E. Altman, "Dynamics and universality in noise-driven dissipative systems," *Phys. Rev. B* **85** (May, 2012) 184302. https://link.aps.org/doi/10.1103/PhysRevB.85.184302.

[316] Z. Cai, U. Schollwöck, and L. Pollet, "Identifying a bath-induced bose liquid in interacting spin-boson models," *Phys. Rev. Lett.* **113** (Dec, 2014) 260403. https://link.aps.org/doi/10.1103/PhysRevLett.113.260403.

[317] J. Kogut and L. Susskind, "How quark confinement solves the $\eta \to 3\pi$ problem," *Phys. Rev. D* **11** (Jun, 1975) 3594–3610. https://link.aps.org/doi/10.1103/PhysRevD.11.3594.

[318] T. Giamarchi and H. J. Schulz, "Anderson localization and interactions in one-dimensional metals," *Phys. Rev. B* **37** (Jan, 1988) 325–340. http://link.aps.org/doi/10.1103/PhysRevB.37.325.

[319] S. Ryu, A. P. Schnyder, A. Furusaki, and A. W. W. Ludwig, "Topological insulators and superconductors: tenfold way and dimensional hierarchy," *New Journal of Physics* **12** no. 6, (2010) 065010. http://stacks.iop.org/1367-2630/12/i=6/a=065010.

[320] W. P. Su, J. R. Schrieffer, and A. J. Heeger, "Solitons in polyacetylene," *Phys. Rev. Lett.* **42** (Jun, 1979) 1698–1701. http://link.aps.org/doi/10.1103/PhysRevLett.42.1698.

[321] L. Fidkowski and A. Kitaev, "Effects of interactions on the topological classification of free fermion systems," *Phys. Rev. B* **81** (Apr, 2010) 134509. http://link.aps.org/doi/10.1103/PhysRevB.81.134509.

[322] A. M. Turner, F. Pollmann, and E. Berg, "Topological phases of one-dimensional fermions: An entanglement point of view," *Phys. Rev. B* **83** (Feb, 2011) 075102. http://link.aps.org/doi/10.1103/PhysRevB.83.075102.